

Monitoring Snow and Glaciers of Himalayan Region

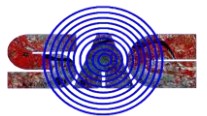
Space Applications Centre (ISRO)
Ahmedabad – 380 015

Front Cover shows debris covered ablation zone near snout of Batal glacier in Lahaul and Spiti district, Himachal Pradesh. Back cover upper panel shows IRS AWiFS FCC and RISAT-1 MRS images over Moraine dammed lake (buried under snow during winter season) of Samudra Tapu glacier in Chandra Basin (Himachal Pradesh). Lower panel shows GPR survey over bare ice ablation zone of Chota Shigri glacier in Chandra basin.

Monitoring Snow and Glaciers of Himalayan Region



Space Applications Centre, ISRO
Ahmedabad 380 015





Published by: Space Applications Centre, ISRO, Ahmedabad, India
www.sac.gov.in

Copyright: © Space Applications Centre, ISRO, 2016

This publication may be produced in whole or in part and in any form for education or non-profit uses, without special permission from the copyright holder, provided acknowledgement of source is made. SAC will appreciate a copy of any publication which uses this publication as a source.

Citation: SAC (2016) Monitoring Snow and Glaciers of Himalayan Region, Space Applications Centre, ISRO, Ahmedabad, India, 413 pages, ISBN: 978 – 93 – 82760 – 24 – 5

ISBN: ISBN: 978 – 93 – 82760 – 24 – 5



Available from: Space Applications Centre, ISRO, Ahmedabad - 380015, India

Publications: SAC carried out the work in collaboration with State Remote Sensing Applications Centers, Academic Institutes and Government Organisations. This project is sponsored by Ministry of Environment, Forest and Climate Change and Department of Space, Government of India.

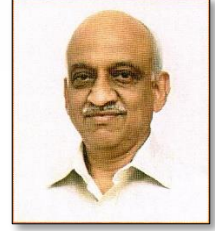
Printed by: Chandrika Corporation, Ahmedabad

भारतीय अन्तरिक्ष अनुसंधान संगठन
अन्तरिक्ष विभाग
भारत सरकार
अन्तरिक्ष भवन
न्यू बी ई एल रोड, बेंगलूर – 560 231, भारत
दूरभाष : +91-80-2341 5241 / 2217 2333
फैक्स : +91-80-2341 5328



Indian Space Research Organisation
Department of Space
Government of India
Antariksh Bhavan
New BEL Road, Bangalore - 560 231, India
Telephone: +91-80-2341 5241 / 2217 2333
Fax : +91-80-2341 5328
e-mail : chairman@isro.gov.in

आ. सी. किरण कुमार / A. S. Kiran Kumar
अध्यक्ष / Chairman



Preamble

Himalayan Cryosphere plays an important role as a sensitive indicator of climate change. Melt water from Himalayan snow and glaciers is perennial source for irrigation, hydropower, domestic water requirements and sustainability of bio-diversity & environment in particular. Monitoring Himalayan snow and glaciers is important in view of the associated natural hazards such as, avalanches, bursting of glacial lakes, floods and landslides.

This volume is the outcome of a national project on “Monitoring Snow and Glaciers of Himalayan Regions”, providing details of the current status of Himalayan snow and glaciers based on the analysis of time series multi-sensor data from Indian Earth Observation satellite supported by field based observations. It covers details about the types of satellite sensors used, methodology developed and salient findings related to snow cover, glaciers and Himalayan Glacier Information System. Studies have been carried out using Ground Penetrating Radar (GPR), hyperspectral data, SAR Interferometry and Photogrammetry for glacier ice thickness, snow pack characterization, glacier flow determination and glacier mass balance estimation. Development of advance technique using INSAT-3D, RISAT-1, Gravity Recovery and Climate Experiment (GRACE), ICESat/GLAS laser altimetry data for snow cover, detection of glacial lakes buried under snow, estimation of regional water mass variations and monitoring ice thickness changes have been well documented in the document.

I am sure that the information generated in the document will be extremely useful to the Ministry of Environment, Forest and Climate Change, representing India in various international forums related to Climate Change, concerned policy makers, planners, managers and researchers.

I congratulate the team behind this information compilation for their valuable contributions.

आ सी किरण कुमार
(A. S. Kiran Kumar)

Bangalore
September 21, 2016

अजय नारायण झा
AJAY NARAYAN JHA, IAS



सचिव
भारत सरकार
पर्यावरण, वन एवं जलवायु परिवर्तन मंत्रालय
Secretary
Government of India
Ministry of Environment, Forest and Climate Change



Preface

Himalayas possess one of the largest resources of snow and ice outside the Polar Regions. It is the snow and glacier melt runoff from the Himalayan region which sustains the perennial flow of the Indus, Ganga and Brahmaputra river systems. These river systems receive almost 30-50% of the annual flow from snow and glacier melt runoff. The runoff from the Himalayan rivers support domestic, irrigational and industrial water demand of a very large population residing in the Himalayas and the Indo-Gangetic alluvial plains. Melt water from the Himalayan region is required for generation of hydropower and sustainability of Himalayan bio-diversity and environment.

There are increasing concerns by scientific community that global warming caused by increase in concentration of greenhouse gases in atmosphere can cause significant impact on the snow and glacier melt runoff in the river systems. In view of the importance and significance of snow fields and glaciers for water security of the nation and assessing climatic impact in Indian sub-continent, these cryosphere elements need to be regularly mapped and monitored. Sensitivity of snow and glaciers to variations in temperature makes them a key indicator of climate change.

Himalayan region is difficult to study using conventional field based methods due to rugged topography, high altitude and extreme weather conditions. Satellite data due to its synoptic view, distinct spectral properties of snow and glaciers, high temporal frequency aided by advanced digital image processing and analysis techniques provide accurate and reliable observations.

This document provides details of the salient findings of a national project entitled, "Monitoring Snow and Glaciers of Himalayan region (Phase-II)", taken up under National Natural Resources Management (NNRMS) Program and jointly sponsored by the Ministry of Environment, Forest and Climate Change (MoEF&CC) and Department of Space (DOS). The project has been successfully completed by Space Applications Centre, Indian Space Research Organisation (ISRO), Ahmedabad as a nodal agency along with eighteen partner institutes. A large geospatial database on changes in the Himalayan Snow and Glaciers based on space based observations has been generated. Field data has been collected through various glacier expeditions and utilised for development of analysis techniques and validation. Recent advanced techniques of satellite data interpretation and future trends are also highlighted.

I am sure that findings of the present work would be extremely useful to various national and International Programs of the Ministry as well to concerned scientific and academic community. I appreciate the efforts made by the national team and recommend that monitoring Himalayan Cryosphere using various current and planned Earth Observation Space Missions should be continued.

New Delhi
September 21, 2016


(Ajay Narayan Jha)



तपन मिश्रा

निदेशक

Tapan Misra
Director



भारत सरकार GOVERNMENT OF INDIA
अंतरिक्ष विभाग DEPARTMENT OF SPACE
अंतरिक्ष उपयोग केंद्र
SPACE APPLICATIONS CENTRE
अहमदाबाद AHMEDABAD - 380 015
(भारत) (INDIA)

दूरभाष PHONE : +91-79-26913344, 26928401

फैक्स /FAX : +91-79-26915843

ई-मेल E-mail : director@sac.isro.gov.in



Foreword

Monitoring of the Himalayan snow and glaciers is important in view of water security of the nation, hydroelectric power generation, understanding impact of climate change, assessing disaster vulnerability and protection of the biodiversity and environment.

Snow and Glacier Studies of the Himalayan region are one of the major thrust area identified by the Ministry of Environment, Forest & Climate Change, Government of India. Snow and glaciers of Himalayan region are difficult to study using conventional field based methods due to rugged topography, high altitude and extreme weather conditions. Space Applications Centre (SAC) has been developing tools and techniques of space based observations from various EO Missions for past few decades.

The present Final Technical Report provides salient results and analysis of the Project on "Monitoring Snow and Glaciers of Himalayan Region – Phase-II", jointly funded by MoEF&CC and DOS. Himalayan snow cover monitoring has been carried out for the time frame 2008-14 using AWiFS data of Resourcesat-2 satellite from October to June (Hydrological year) at every five day interval. Around 2018 glaciers for time frame 2000-2010 have been monitored using multi-date satellite data and the analysis depicted that 87% of the glaciers showed no change, 12% retreated and 1 % glaciers have advanced. The geospatial database of glacier inventory carried out on 1:50,000 scale using Resourcesat-1 satellite data contains 34919 glaciers covering 75, 779 sq km area. A Himalayan Glacier Information System (HGIS) has been developed. Some of the advanced techniques of satellite data analysis for snow and glacier studies are also demonstrated.

I compliment the entire team of scientists from both ISRO and other organizations for carrying out this task diligently. I do hope, the findings of the project presented in this documents shall be extremely useful to the MoEF&CC which represents India in key International forums of climate change and also to the researchers working in the field of environment, glaciology, hydrology and climate change.

Tapan Misra
(Tapan Misra)

भारत सरकार
अंतरिक्ष विभाग
अंतरिक्ष उपयोग केन्द्र
आंबावाडी विस्तार डाक धर,
अहमदाबाद-380 015. (भारत)

दूरभाष : +91-79-26914132
फैक्स : +91-79-26915825



Government of India
Department of Space
SPACE APPLICATIONS CENTRE
Ambawadi Vistar P.O.
Ahmedabad - 380 015. (INDIA)
Telephone : +91-79-26914132
Fax : +91-79-26915825



Acknowledgements

Ministry of Environment, Forest & Climate Change (MoEF&CC), Govt. of India has identified Himalayan glaciers and snow cover as one of the thrust area under NNRMS Standing Committee on Bio-resources and Environment (NNRMS SC-B). Based on the recommendations of NNRMS SC-B, a project on "Monitoring Snow and Glaciers of Himalayan Region (Phase-II)" was taken up by Space Applications Centre at the behest of MoEF&CC with joint funding by DOS and MoEF&CC, in continuation of generating long term space based database created earlier under Phase-I.

We would like to place on record our deep sense of gratitude to Shri A.S. Kiran Kumar, Secretary DOS and Chairman ISRO and Shri Tapan Misra, Director, SAC for their encouragement and guidance in carrying out this national project. We are very much thankful to Shri Lalit Kapur, Advisor, RE, Dr. T. Chandni, former Advisor, RE, Dr. G.V. Subrahmanyam, former Advisor, RE, Dr. Jag Ram, Director, Dr. Harendra Kharkwal, Deputy Director and Shri Pankaj Verma, Joint Director, MoEF&CC for their continuous support in executing this project.

We express our thanks to the Dr. B. S. Gohil, Deputy Director, EPSA, Dr. J. S. Parihar, and Dr P. K. Pal, former Deputy Directors, Dr. Rajkumar, Group Director, GHGAG and Dr. M. Chakraborty, former Group Director, GSAG for providing technical guidance and necessary support in carrying out this project. We are thankful to SAC Committee on "Space Applications: Projects Monitoring and review, Outsourcing and Inter Agency Document Review Committee", in particular Shri R.M. Parmar, Deputy Director & Committee Chairman and Shri Vivek Pandey, Member Secretary for their comments and suggestions. We are grateful to Dr. S. Bandyopadhyay, Scientist, EOS, ISRO HQ for providing necessary support.

We extend our gratitude to Directors/Heads of the Institute/Vice-Chancellors of eighteen collaborating research organizations/academic institutions of the country for their support in executing this project.


(Dr. A.S. Rajawat)
Project Director

National Team

Project Director

Dr. A.S. Rajawat

Dr. Ajai (upto October, 2013)

Deputy Project Directors

Dr. I.M. Bahuguna

Mr. A.K. Sharma

Space Applications Centre, ISRO, Ahmedabad Mr. B.P. Rathore Dr. Sushil Kumar Singh Ms. Gunjan Rastogi Mr. Ritesh Agrawal Dr. Sreejith, K.M. Mr. Manish Parmar Mr. J.G. Patel Mr. Anish Mohan Ms. Sandhya Rani Pattnaik	Department of Geology, M G Science Institute, Ahmedabad Prof. R.D. Shah Dr. Rupal Brahmhatt Mr. Mann Chaudhary
Centre for Environment and Planning Technology (CEPT) University, Ahmedabad Prof. Anjana Vyas Ms. Darshana Rawal Mr. Purnesh Jani Mr. Utkarsh Shah Mr. Kaivalya Pathak Mr. Anand Paleja Mr. Ashish Upadhyay	Department of Geography, University of Jammu, Jammu Prof. M.N. Koul Prof. V.S. Manhas Mr. Devinder Manhas Mr. Sadiq Ali
H.P. State Centre on Climate Change, State Council of Science, Technology and Environment, Himachal Pradesh, Shimla Dr. S.S. Randhawa Ms. Anjana Sharma Mr. Arvind Bhardwaj	Department of Geology, Government Post Graduate College, Dharamshala, Himachal Pradesh Dr. Sunil Dhar Mr. Dinesh Kumar Mr. Vikas Pathania
National Bureau of Plant Genetic Resources (NBPGR), Regional Station, Phagli, Shimla Dr. J.C. Rana Mr. Rameshwar Singh Ms. Supriyanka Rana	Uttarakhand Space Application Centre, Department of Science & Technology, Dehradun Dr. M.M. Kimothi Dr. Asha Thapliyal Ms. Anju Panwar Prof. Durgesh Pant

<p>Remote Sensing Applications Center, Uttar Pradesh, Lucknow Dr. A.K. Tangri Mr. S.K.S. Yadav Mr. Ramchandra Mr. Rupendra Singh Mr. Diwakar Pandey Mr. Dhanendra Kumar Singh</p>	<p>Department of Earth Sciences, University of Kashmir, Srinagar Prof. Shakil Ahmed Romshoo Mr. Irfan Rashid Mr. Gowhar Meraj Ms. Midhat Fayaz Mr. Obaidullah Mr. Khalid Omar</p>
<p>Centre for the Study of Regional Development, (UGC-Centre for Advance Studies in Geography), Jawaharlal Nehru University, New Delhi Dr. Milap Chand Sharma Mr. Ishwar Singh Mr. Sanjay Deswal Mr. Rakesh Saini Mr. Rakesh Arya Mr. Satya Prakash</p>	<p>CSRE, Indian Institute of Technology-Bombay, Mumbai Prof. G. Venkataraman Prof. Avik Bhattacharya Ms. Fajana Sikandar Birajdar</p>
<p>Divecha Centre of Climate Change, Indian Institute of Science, Bangalore Dr. A.V. Kulkarni Ms. Enakshi Bhar</p>	<p>G.B. Pant National Institute of Himalayan Environment & Sustainable Development (formerly known as G.B. Pant Institute of Himalayan Environment & Development), Almora Er. Kireet Kumar Mr. Kavindra Upreti Ms. Joyeeta Poddar Mr. Jagdish Pande Mr. Chanchal Singh</p>
<p>Sikkim State Remote Sensing Applications Centre, Department of Science & Technology and Climate Change, Government of Sikkim, Gangtok Mr. D.G. Shrestha Mr. Narpati Sharma Mr. Pranay Pradhan</p>	<p>State Remote Sensing Applications Centre, Arunachal Pradesh State Council for Science and Technology, Department of Science and Technology, Government of Arunachal Pradesh, Itanagar Er. T. Ronya Dr. Swapna Acharjee Mr. Jutsam Katang Mr. Saumitra Deb</p>
<p>School of Environmental Science, Jawaharlal Nehru University, New Delhi Prof. A.L. Ramanathan Mr. Mohd. Soheb</p>	<p>Department of Remote Sensing, Birla Institute of Technology, Mesra, Ranchi Dr. V.S. Rathore Dr. M.S. Nathawat Dr. A.C. Pandey</p>
<p>Department of Geology, University of Jammu, Jammu Prof. R.K. Ganjoo Ms. Sunita Chahar</p>	

Contents

1. Introduction.....	1
2. Snow Cover Monitoring	7
3. Glacier Monitoring	81
4. Glacier Mass Balance.....	151
5. Himalayan Glacier Information System	194
6. Effect of Black Carbon Soot and Contamination on Snow and Glacier Ice.....	206
7. Effect of Debris Cover on Glacier Ice Melt.....	214
8. Use of Ground Penetrating Radar	221
9. Use of Hyperspectral Data for Snowpack Characterization	229
10. Use of SAR Interferometry and Photogrammetry in Glacier Flow Determination and Glacier Mass Balance.....	238
11. Development of Algorithm for Auto Extraction of Debris Cover on Glaciers	264
12. Glacier Expeditions and Installation of AWS for Field Validation	270
13. Geospatial Modeling for Glacier Health Assessment.....	280
14. Impact of Climate Change on Flora of Spiti Valley	288
15. Development of Algorithm for Snow Cover/ Snow Depth Products using INSAT-3D Data	296
16. Development of Techniques for RISAT-1 SAR Data Analysis for Glacier Studies and Detection of Glacial Lakes Buried under Snow.....	307
17. Monitoring of Moraine-Dammed Lakes for Outburst Potential Assessment	317
18. Estimation of Regional Water Mass Variations from Gravity Recovery and Climate Experiment (GRACE) over Himalayan region	330
19. Snow and Glacier Melt Runoff Modeling	338
20. Development of Energy Balance Modeling.....	346
21. Analysis of ICESAT/GLAS LASER Altimetry Data for Monitoring Ice Thickness Changes	357
22. Future Plan	367
References.....	369

1. Introduction

Himalayas possess one of the largest resources of snow and ice outside the Polar Regions. Himalayan region due to its geo-climatic setting, arcuate length of approx. 2400 km, high altitude of its mountain ranges, proximity to Indian Ocean and sub-polar regions undergoes annually a cycle of snow precipitation and melting.

It is the snow and glacier melt runoff from the Himalayan region which sustains the perennial flow of the Indus, the Ganga and the Brahmaputra river systems. These river systems receive almost 30-50% of the annual flow from snow and glacier melt runoff. The runoff from the Himalayan rivers support domestic, irrigational and industrial water demand of a very large population residing in the Himalayas and the Indo-Gangetic alluvial plains. Melt water from the Himalayan region is also required for generation of hydropower and sustainability of Himalayan bio-diversity and environment. Monitoring of the Himalayan snow and glaciers is important in view of its hydrological significance and also the associated natural hazards like avalanches, bursting of high altitude lakes and consequent flooding downstream, mass wasting and debris flow etc. leading to several disasters in the region.

The importance of snow fields and glaciers of the Himalaya also lies in their interaction with atmosphere. Albedo from snow is one of the important components of the Earth's radiation balance. The difference in temperature between the Himalayan cryosphere and the Indian Ocean pulls SW monsoon towards the Indian landmass during summer. So collectively, snow fields and glaciers govern the climate system of the Indian land mass at regional and global scales. Sensitivity of snow and glaciers to variations in temperature makes them a key indicator of climate change.

There are increasing concerns by scientific community that global warming caused by increase in concentration of greenhouse gases in atmosphere can cause dramatic impact on the snow melt runoff in the river systems. In view of the importance and significance of snow fields and glaciers for water security of the nation and assessing climatic variations in Indian sub-continent, these cryosphere elements need to be regularly mapped and monitored.

Himalayan region is difficult to study using conventional field based methods due to rugged topography, high altitude and extreme weather conditions. Satellite data due to its synoptic view, distinct spectral properties of snow and glaciers, high temporal frequency aided by advanced digital image processing and analysis techniques provide accurate and reliable observations. Therefore, methods based on remote sensing (RS) coupled with Geographical Information System (GIS) techniques have become very useful tools to carry out accurate, quick inventory, mapping and monitoring of the inaccessible Himalayan terrain. Remote sensing methods are developed in the country since past two and a half decades to monitor the Himalayan

snow and glaciers by Space Applications Centre (SAC) along with concerned Central/State government Departments and academic institutions (SAC & MoEF, 2010).

Ministry of Environment, Forest and Climate Change (MoEF&CC) is the nodal Ministry which represents India in key International forums of climate change. Therefore, in view of the role and importance of the Himalayan snow and glaciers as sensitive indicator of climate change and likely impact on fresh water resources of the Indo-Gangetic plains, the National Natural Resources Management Standing Committee on Bio-Resources (NNRMS SC-B) Chaired by Secretary, MoEF&CC had identified “Snow and Glacier Studies”, as one of the thrust area where space based observations can be effectively utilized.

Accordingly, a project on “Snow and Glacier Studies” was taken up and completed by Space Applications Centre (SAC) along with 13 concerned Central/State government Departments and Academic Institutes using remote sensing and GIS techniques. The project was jointly funded by the MoEF&CC and the Department of Space (DOS), Government of India. The project has been completed during the time frame March 2005 to October 2010. The project aimed at i) Inventory of all Himalayan glaciers on 1,50,000 scale, ii) monitoring of seasonal snow cover (every 5 days) in hydrological years 2004-2008 for entire Indian Himalayan region, iii) monitoring of retreat/advance of the glaciers in fourteen glaciated basins representing different climatic zones of the Indian Himalayas and iv) estimation of mass balance of glaciers based on monitoring of snow line on glaciers at the end of ablation period in ten glaciated basins of the Himalaya (SAC, 2010; SAC, 2011a).

This project had generated large amount of geospatial database using primarily multirate satellite data in GIS environment of glacier inventory, snow cover mapping, changes in glacier retreat/advance and estimation of glacier mass balance. The information generated under the project provided accurate and reliable information on Himalayan snow cover and glaciers based on space based observations. It provided up-to-date information on the state of the Himalayan cryosphere and could be utilized in climate change research, snow and glacier melt runoff modeling, hydropower potential estimation and glacial lakes monitoring (SAC, 2010; SAC, 2011a; SAC, 2011b).

It was recommended by the NNRMS SC-B that snow and glacier resources of the Himalayan region need to be monitored continuously using satellite data for usage in climate change and hydrological applications and research.

Accordingly, the project entitled, “Monitoring Snow and Glaciers of Himalayan region (Phase-II)”, has been taken up by Space Applications Centre, ISRO, Ahmedabad and is jointly funded by the MoEF&CC and DOS, Government of India. The project has been completed during the time frame December 2010 to March 2015.

Monitoring the Himalayan Snow and Glaciers:

There are four major work elements completed in the project for monitoring the Himalayan Snow and Glaciers using satellite data viz.,

- I) Snow Cover Monitoring (2008-2014)
- II) Monitoring Glacier Retreat/Advance (2000-2010)
- III) Monitoring Glacier Mass Balance (2008-2013)
- IV) Development of Himalayan Glacier Information System

R&D Studies:

Apart from the above mentioned work, several R&D studies were carried out. These studies are as follows:

- i. Effect of black carbon soot and contamination on snow and glacier ice
- ii. Effect of debris cover on glacier ice-melt
- iii. Use of Ground Penetrating Radar (GPR) for determining glacier ice thickness
- iv. Use of hyperspectral data in snow pack characterization
- v. Use of SAR Interferometry and photogrammetry in glacier flow determination and glacier mass balance
- vi. Development of algorithm for auto extraction of debris cover on glaciers and moraine dammed lakes
- vii. Installation of AWS for field validation of data
- viii. Geospatial modeling for glacier health assessment
- ix. Impact of climate change on flora of Spiti valley
- x. Development of algorithm for snow cover/snow depth products using INSAT-3D Data
- xi. Development of techniques for RISAT SAR data analysis for glacier studies and detection of glacial lakes buried under snow

- xii. Monitoring of Moraine-Dammed Lakes for Outburst Potential Assessment
- xiii. Estimation of regional mass anomalies from Gravity Recovery and Climate Experiment (GRACE) over Himalayan region
- xiv. Snow and glacier melt runoff Modelling
- xv. Development of energy balance modeling
- xvi. Analysis of ICESat/GLAS laser altimetry data for monitoring ice thickness changes

The project has been executed by Space Applications Centre, ISRO, Ahmedabad as a nodal agency along with eighteen partner institutes. Table-1 provides list of participating organisations and their work responsibility.

Table 1: Participating Organisations and Work Responsibility

Sr. No.	Participating Organisations	Work Responsibility
1	Department of Geology, M G Science Institute, Ahmedabad	Glacier monitoring and mass balance estimation in Bhut and Warwan sub-basins of Chenab basin
2	Centre for Environment and Planning Technology (CEPT) University, Ahmedabad	Snow cover monitoring (Chandra, Bhaga, Miyar, Bhut, Warwan & Ravi sub-basins of Chenab basin), Develop Himalayan Glacier Information System (HGIS), Glacier Health Assessment
3	Department of Geography, University of Jammu, Jammu	Glacier monitoring (Drass sub-basin), mass balance studies of Machoi glacier based on field expeditions
4	H.P. State Centre on Climate Change, State Council of Science, Technology and Environment, Himachal Pradesh, Shimla	Snow cover monitoring (Spiti, Pin, Baspa, Jiwa, Parbati & Beas sub-basins of Satluj basin), Glacier Monitoring and Mass Balance (Spiti sub-basin)
5	Department of Geology, Government Post Graduate College, Dharamshala, Himachal Pradesh	Glacier monitoring (Chenab sub-basin, Lahaul-Spiti district, Himachal Pradesh) and field expeditions

6	National Bureau of Plant Genetic Resources (NBPGR), Regional Station, Phagli, Shimla	Understand impact of snow line on floral distribution and societal impacts in Spiti valley
7	Uttarakhand Space Application Centre, Department of Science & Technology, Dehradun	Snow cover monitoring (Alaknanda, Bhagirathi and Yamuna sub-basins), Glacier monitoring (Alaknanda & Bhagirathi sub-basins)
8	Remote Sensing Applications Center, Uttar Pradesh, Lucknow	Snow cover monitoring (Nubra, Shyok, Shigar, Hanza, Gilgit & Sasgan sub-basins), Glacier monitoring (Satopanth and Bhagirath Kharak glaciers in Alaknanda and Bhagirathi sub-basins) and field expeditions
9	Department of Earth Sciences, University of Kashmir, Srinagar	Glacier monitoring in Suru and Jhelum sub-basins, Field expeditions Kolhoi glacier
10	Centre for the Study of Regional Development, (UGC-Centre for Advance Studies in Geography), Jawaharlal Nehru University, New Delhi	Glacier monitoring in Miyar sub-basin and field expeditions
11	CSRE, Indian Institute of Technology-Bombay, Mumbai	Glacier monitoring and mass balance estimation (Bhaga sub-basin), Develop SAR Interferometry approaches for mass balance estimation and snow pack studies using hyperspectral data
12	Divecha Centre of Climate Change, Indian Institute of Science, Bangalore	Glacier mass balance in Chandra sub-basin and improve existing model for mass balance estimation
13	G.B. Pant National Institute of Himalayan Environment & Sustainable Development (formerly known as G.B. Pant Institute of Himalayan Environment & Development), Almora	Glacier monitoring (Dhauliganga, Goriganga & Kaliganga sub-basins), field expeditions in Dhauliganga sub-basin
14	Sikkim State Remote Sensing Applications Centre, Department of	Snow cover and glacier monitoring (Tista, Ranjit sub-basins)

	Science & Technology and Climate Change, Government of Sikkim, Gangtok	
15	State Remote Sensing Applications Centre, Arunachal Pradesh State Council for Science and Technology, Department of Science and Technology, Government of Arunachal Pradesh, Itanagar	Snow cover monitoring (Subansiri, Tawang & Diwang sub-basins of Brahamaputra basin), Glacier Monitoring (Tawang sub-basin of Brahmmaputra basin)
16	School of Environmental Science, Jawaharlal Nehru University, New Delhi	Glacier mass balance estimation of Patsio glacier, and energy balance modelling (Bhaga sub-basin)
17	Department of Remote Sensing, Birla Institute of Technology, Mesra, Ranchi	Snow cover monitoring, Glacier monitoring and mass balance estimation (Zanskar sub-basins)
18	Department of Geology, University of Jammu, Jammu	Glacier monitoring in Nubra sub-basin, Glacier mass balance Rulung glacier based on field expeditions
19	Space Applications Centre, ISRO, Ahmedabad	Project conceptualization, formulation, overall coordination, geospatial database design and organisation, training, quality checking, All activities defined under R&D Components, analysis of outcome and report/Atlas preparation.

2. Snow Cover Monitoring

2.1. Objective

To map, create and analyze geospatial database for snow cover monitoring (every 5 days and 10 days) in hydrological year 2008 to 2014 of Himalayan region covering Indus, Ganga and Brahmaputra river basins using IRS (Resourcesat-1 and 2) AWiFS data. List of basins / sub-basins is given in Table 2. Figure 1 shows locations of sub-basins taken up for snow cover monitoring.

Table 2: Sub-basins taken up for snow cover monitoring

Sr. No.	Basin	Sub-basin
1	Indus	Gilgit
2		Hanza
3		Shigar
4		Shasgan
5		Nubra
6		Shyok
7		Astor
8		Kishanganga
9		Shigo
10		Drass
11		Jhelum
12		Suru
13		Zanskar
14	Chenab	Warwan
15		Bhut
16		Miyar
17		Bhaga
18		Chandra
19		Ravi
20	Satluj	Beas
21		Parbati
22		Jiwa
23		Baspa
24		Pin
25		Spiti
26	Ganga	Bhagirathi
27		Yamuna
28		Alaknanda
29	Tista	Tista
30		Rangit
31	Brahmaputra	Tawang
32		Subansiri
33		Dibang

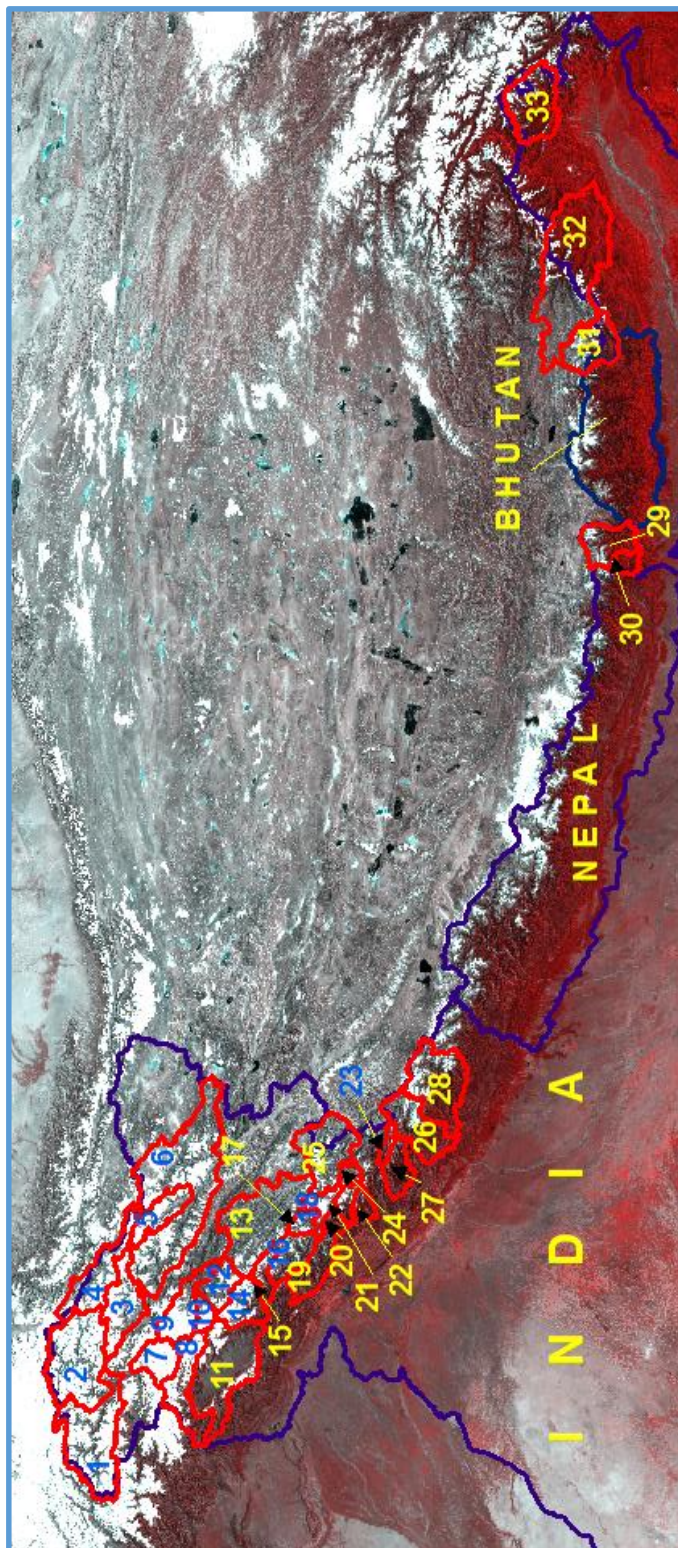


Figure 1: Location of sub-basins in Himalayan region taken up for snow cover monitoring shown on IRS AWiFS FCC

2.2. Scientific Rationale

Snow is a type of precipitation in the form of crystalline ice, consisting of a multitude of snowflakes that fall from clouds. Snow is composed of small ice particles. It is a granular material. The process of this precipitation is called snowfall. The density of snow when it is fresh is 30-50 kg/m³. When it becomes firn the density becomes about 400-830 kg/m³. Snow becomes glacier ice when density is 830-910 kg/m³. Snow becomes firn when it survives for minimum one summer and becomes glacier ice in many years. Density increases due to remelting and recrystallization and reduction in air spaces within the ice crystals.

The required atmospheric conditions for snow fall are met at higher latitudes and altitudes of the earth. There are three major classes of snow cover i.e. temporary, seasonal and permanent. Temporary and seasonal snow-cover occurs in winters while permanent snow cover is retained for many years. Permanent snow cover occurs principally in Antarctica, Greenland and above permanent snow line in mountainous areas. Monitoring accumulation and ablation of seasonal snow cover is an important requirement for various applications.

In terms of the spatial extent, snow cover is second largest component of the cryosphere and covers approximately 40–50% of the Earth's land surface during Northern Hemisphere winter (Hall et al., 1995; Pepe et al., 2005). Extent of the snow cover is considered as an important parameter for numerous climatological and hydrological applications.

Snow keeps Earth's radiation budget in balance as it reflects a large portion of the insolation (Foster and Chang, 1993; Klein et al., 2000; Jain et al, 2008; Zhao et al., 2009). The thermal insulation provided by snow protects plants from low winter temperatures (Rees, 2006). Several fundamental physical properties of snow modulate energy exchanges between the snow surface and the atmosphere (Armstrong and Brun, 2008). The surface reflection of incoming solar radiation is important for the surface energy balance (Wiscombe and Warren, 1981). The higher albedo for snow causes rapid shifts in surface reflectivity in autumn and spring in high latitudes. The high reflectivity of snow generates positive feedback to surface air temperature. Snow cover exhibits the greatest influence on the Earth radiation balance in spring (April to May) when incoming solar radiation is greatest over snow cover areas (Groisman et al., 1994a, 1994b).

The second role which snow precipitation plays is in feeding the glaciers of the world. Annual precipitation of snow feeds the accumulation zone of the glaciers and is considered as an important parameter for glacier mass balance studies. The third major importance of snow lies in its melt runoff. Snowmelt is the source of freshwater

required for drinking, domestic, agricultural and industrial sectors especially in middle and high latitudes (Jain et al., 2008; Akyurek and Sorman, 2002).

Himalayas being the loftiest mountains of the world are abode of snow and glaciers. The mountains are drained by three major rivers, i.e. Indus, Ganga and Brahmaputra and their tributaries. The higher altitudes of these three major rivers situated in temperate climate receive heavy snowfall during winters. The snowfall feeds glaciers of Himalayas and almost 30–50% of annual flow of all the rivers originating from higher Himalayas comes from its melt run-off (Agarwal et al., 1983; Jain et al., 2010). Increase in atmospheric temperature can influence snowmelt and stream runoff pattern which is considered as crucial for determining hydropower potential (Kulkarni et al., 2002a; Kulkarni et al., 2011; Rathore et al., 2009; Rathore et al., 2011). Information on snow cover is also needed for strategic application, as arrival of snow can significantly affect mobility of man and machine.

Mapping and monitoring of seasonal snow cover using conventional methods is a challenging task especially in harsh climatic conditions and rugged terrain of Himalayas. The ground measurements are point measurements and need high density of weather stations. Moreover, weather stations require telemetry of the data through satellites. In rugged mountainous regions, ground instruments do not survive for a longer period. Mapping and monitoring of seasonal snow cover can be best done by remote sensing because a large area is covered, high temporal frequency data are available and snow has distinct signatures in optical remote sensing data which makes it easily identifiable (Figure 2 and Figure 3).

Snow cover monitoring using satellite images started from TIROS-1 in April 1960 (Singer and Popham, 1963). Since then, the potential for operational satellite-based mapping has been enhanced by the development of sensors with higher temporal frequency and higher spatial resolution. Sensors with better radiometric resolutions, such as MODIS and AWiFS, have been used for generating the snow products (Hall et al., 1995; Kulkarni et al., 2006b; SAC, 2011, Singh et al., 2014; Nolin, 2010) and improvements over vegetation (Klein et al., 1998). Characteristics of the snow cover in the Hindukush, Karakoram and Himalaya region using satellite data have been studied (Butt, 2012; Gurung et al., 2011). An analysis of snow cover changes in the Himalayan region using MODIS snow products and in-situ temperature data has been made (Maskey et al., 2011).

Snow cover extracted from earlier data and snow products prepared using recent satellite images by auto extraction approaches have been analysed to know the trends in the snow cover variability in many other studies. A decrease in snow-covered areas has been observed globally since the 1960s (Brown, 2000). In some region such as China, a trend of increasing snow cover has been observed from 1978 to 2006 (Che et al., 2008) based on utilization of SMMR/SMMI data. Snow cover for the Indian

Himalaya has been monitored using AWiFS data for the period 2004-2007 and accumulation and ablation patterns studied (SAC, 2011).

There are difficulties in mapping of snow cover under mountain shadow. This makes snow cover mapping cumbersome and time consuming. To overcome this problem normalized difference snow index method has been developed. In optical region snow reflectance is higher as compared to other land features as grass, rock and water. However, in SWIR region snow reflectance is lower than rock and vegetation (Figure 4 and Figure 5). Therefore, snow on satellite images appears white in visible and black in SWIR region. This characteristic has been effectively used to develop Normalized Difference Snow Index (NDSI) for snow cover mapping. It is a useful technique in the Himalayan region, as it can be applied under mountain shadow condition (Kulkarni et al. 2002c; Hall et al. 1995). This is possibly due to reflectance from diffuse radiation in shadow areas. It also overcomes the problem of cloud and snow under mountain shadow.

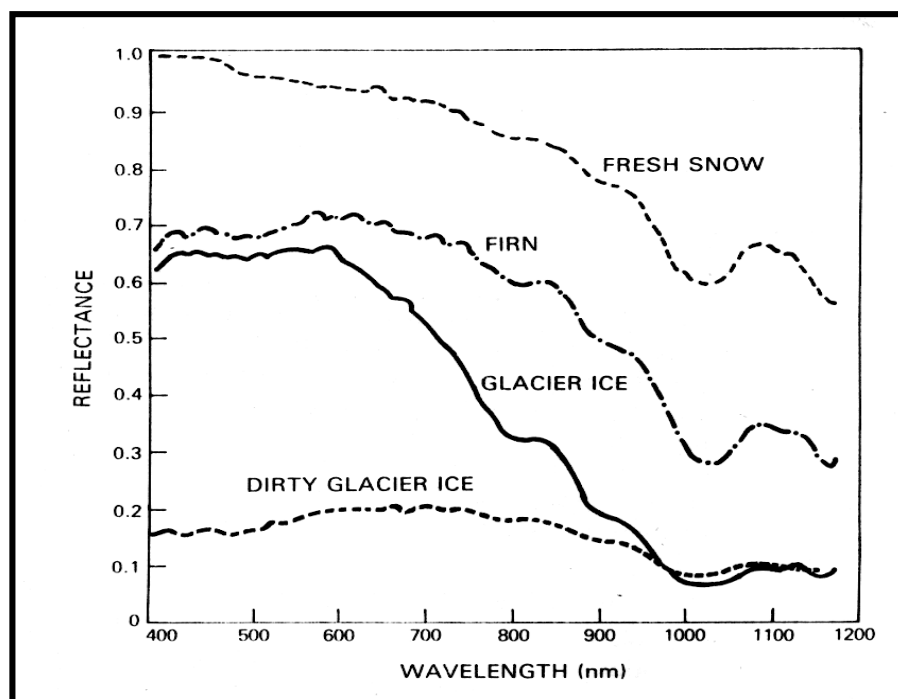


Figure 2: Spectral reflectance of fresh snow, firn, glacier ice and dirty glacier ice. Note changes in reflectance as fresh snow changes into glacier ice (Source: Hall and Martinec, 1985)

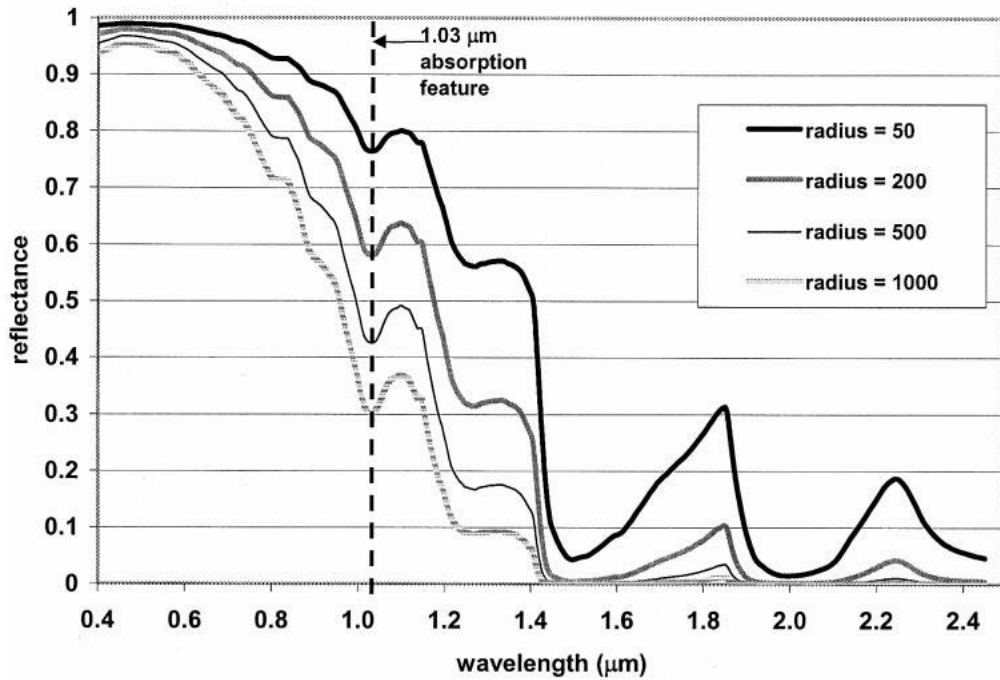


Figure 3: The spectral directional hemispherical reflectance of snow as calculated using the DISORT model. Each curve represents the spectrum for a different snow grain radius. The dashed line indicates the location of the 1.03- μm absorption feature (Source: Anne W. Nolin and Jeff Dozier, 2000)

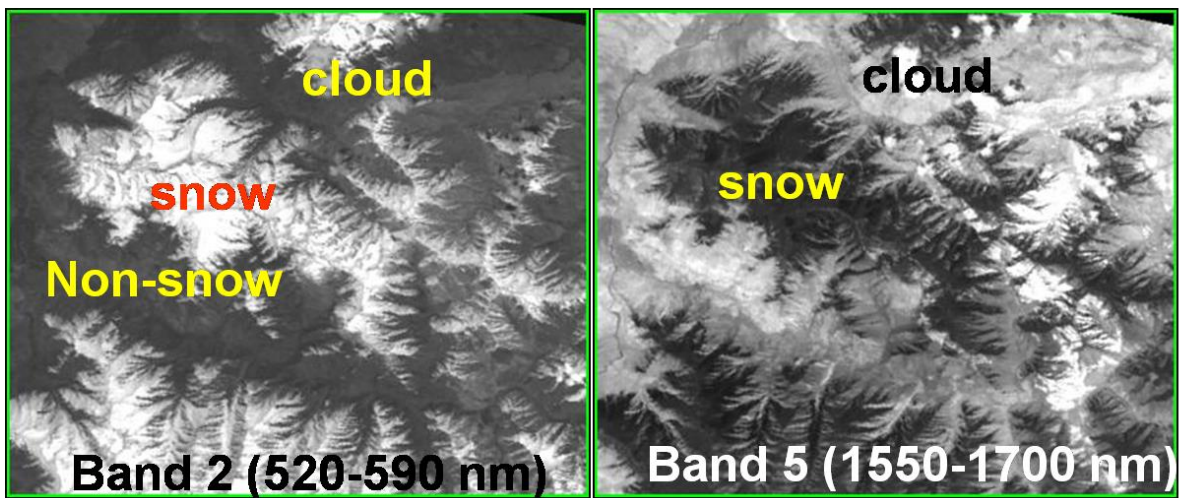


Figure 4: Discrimination of snow and cloud using SWIR channel (1.55 – 1.75 μm) of AWiFS. The band 2 shows snow and cloud in white tone and non-snow in dark tone whereas the band 5 shows snow in dark tone and cloud in white tone

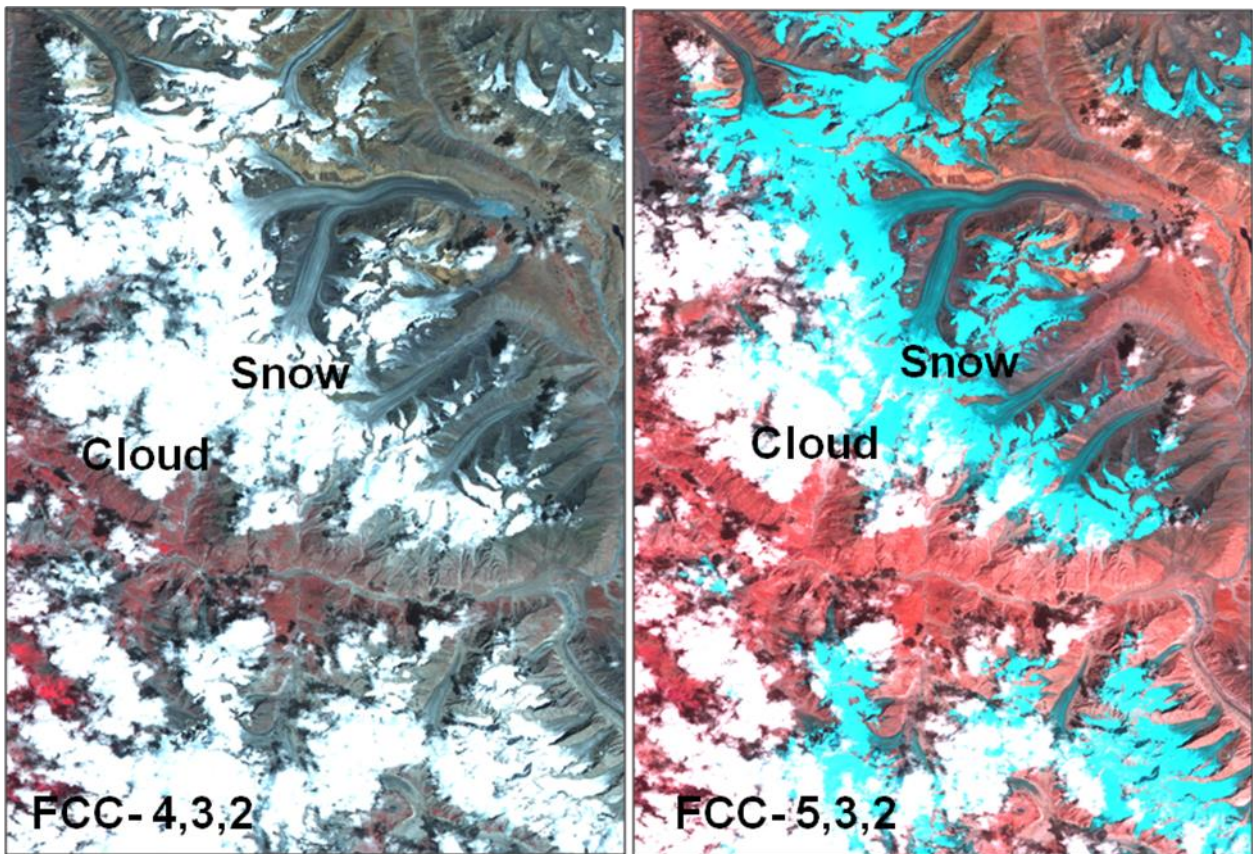


Figure 5: Discrimination of snow and cloud using FCC with SWIR channel (1.55 – 1.75 μm) of AWiFS

As snow reflects strongly in visible region and absorbs in SWIR, an NDSI image is prepared to delineate snow and non-snow features with the help of difference ratio of visible and SWIR channel, as given below;

$$\text{NDSI} = \frac{\text{Green Reflectance (B2)} - \text{SWIR Reflectance (B5)}}{\text{Green Reflectance (B2)} + \text{SWIR Reflectance (B5)}}$$

Polar orbiting sensors such as MODIS, AWiFS etc. have been routinely used to map and monitor snow cover at regular interval (Hall et al., 1995; Kulkarni et al., 2006b; SAC, 2011; Singh et al., 2014; Rathore et al., 2015a). Snow being very dynamic in nature, high temporal frequency is essential requirement in snow cover monitoring.

The Advanced Wide Field Sensor (AWiFS) camera is one of the three imaging instruments onboard IRS-P6 satellite also known as Resourcesat-1. AWiFS was also put on subsequent follow on Resourcesat-2 satellite. AWiFS provides a significant enhancement of imaging capabilities over WiFS of IRS 1C/D. AWiFS comprises a set of two identical cameras, each housing four lens assemblies, detectors and associated

electronics pertaining to the four spectral bands in visible, NIR and SWIR region at 56 m spatial resolution. Two cameras are used to achieve 750 km swath. The imaging concept is based on the push broom scanning scheme. The data from this sensor is available since 2004 onboard Resourcesat-1 and Resourcesat-2 satellites at 5 days interval. The reflected energy is converted into radiance and reflectance images using sensor calibration coefficients. Various parameters needed for estimating spectral reflectance are maximum and minimum band pass spectral radiances and mean solar exo-atmospheric spectral irradiances in the satellite sensor bands, satellite data acquisition time, solar declination, solar zenith and solar azimuth angles, mean Earth-Sun distance etc. (Markham and Barker, 1987; Srinivasulu and Kulkarni, 2004). A threshold value of ≥ 0.4 has been found suitable for AWiFS sensor using sensitivity analysis. AWiFS data has been used extensively for snow cover mapping in Himalayas using an algorithm based on NDSI approach.

2.3. Methodology

(i) Georeferencing of data for each sub-basin

The data obtained from NRSC, Hyderabad has undergone the basic geometric and radiometric corrections. This data (band 2, band 3, band 4, and band 5) is georeferenced with master images already archived. This is a second order correction applied to data. The georeferencing with master images is carried out by identifying a set of ground control points on the maps and images. The ERDAS imagine version 9.1 is used for this work.

(ii) Snow product generation

Snow products are generated at an interval of 5-days and 10-days, depending upon availability of AWiFS data. In 10-daily product, three scenes are analyzed, if available. For example, in generating snow cover product of 10th March, AWiFS data of 5, 10 and 15 March were used. If any pixel is identified as snow on any one date, then this pixel will be classified as snow on final product. This provides snow cover at an interval of 10 days, an important requirement in hydrological applications. Since this product is using three scenes, probability becomes high that at least in one scene, pixel may be cloud-free and this helps in overcoming problem associated with snow under cloud cover. If three consecutive scenes are not available, then all available scenes in 10 days interval were used in the analysis. To differentiate water and snow, water bodies were marked in pre-winter season and then masked in the final products during winter. Flow diagram of the algorithm is given in Figure 6. Few examples of various sub-basin wise AWiFS images and corresponding 10 daily snow products for the years 2014 and 2013 are shown in Figure 7 to Figure 16.

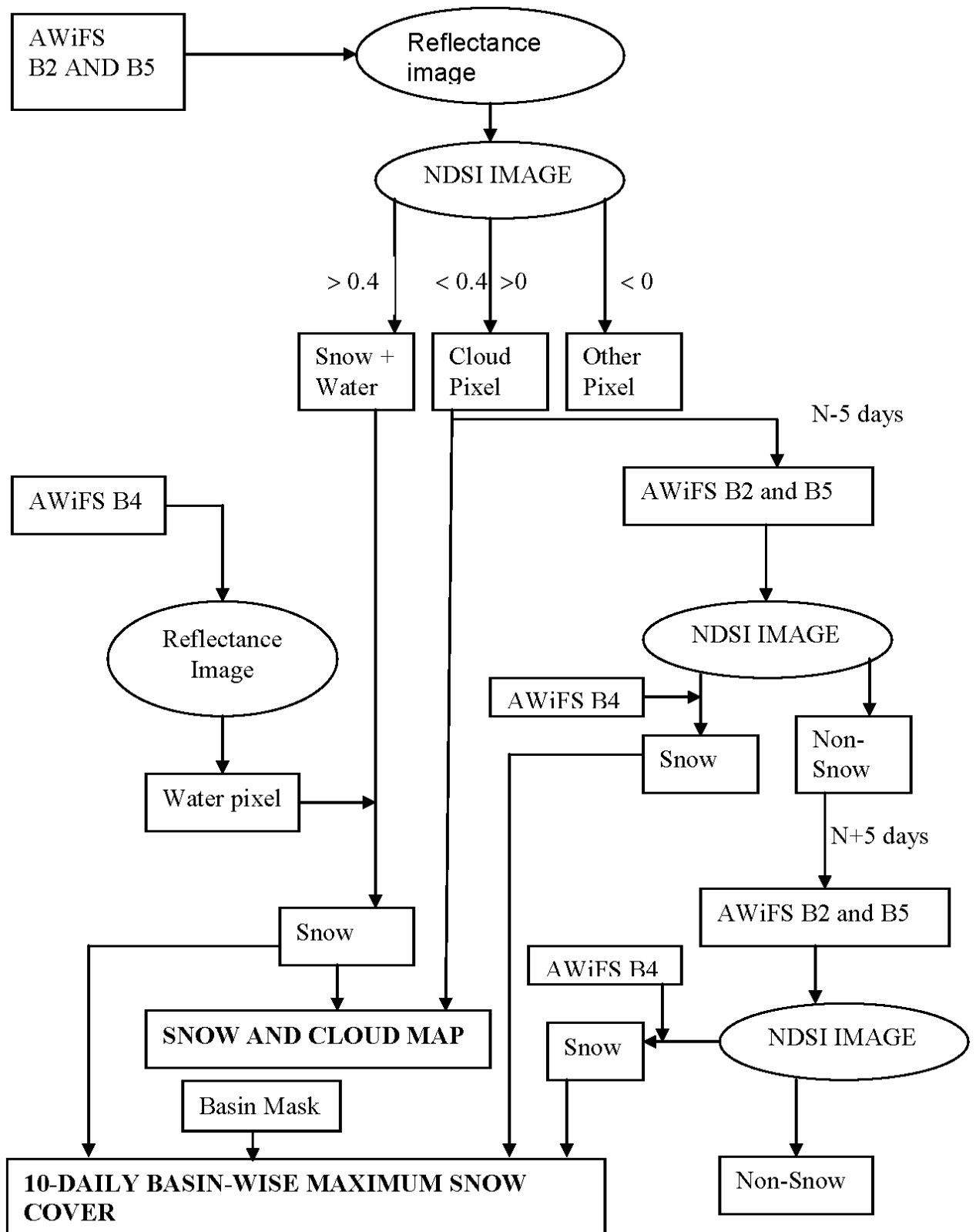


Figure 6: Flow chart showing NDSI algorithm (Source: Kulkarni et al., 2006b)

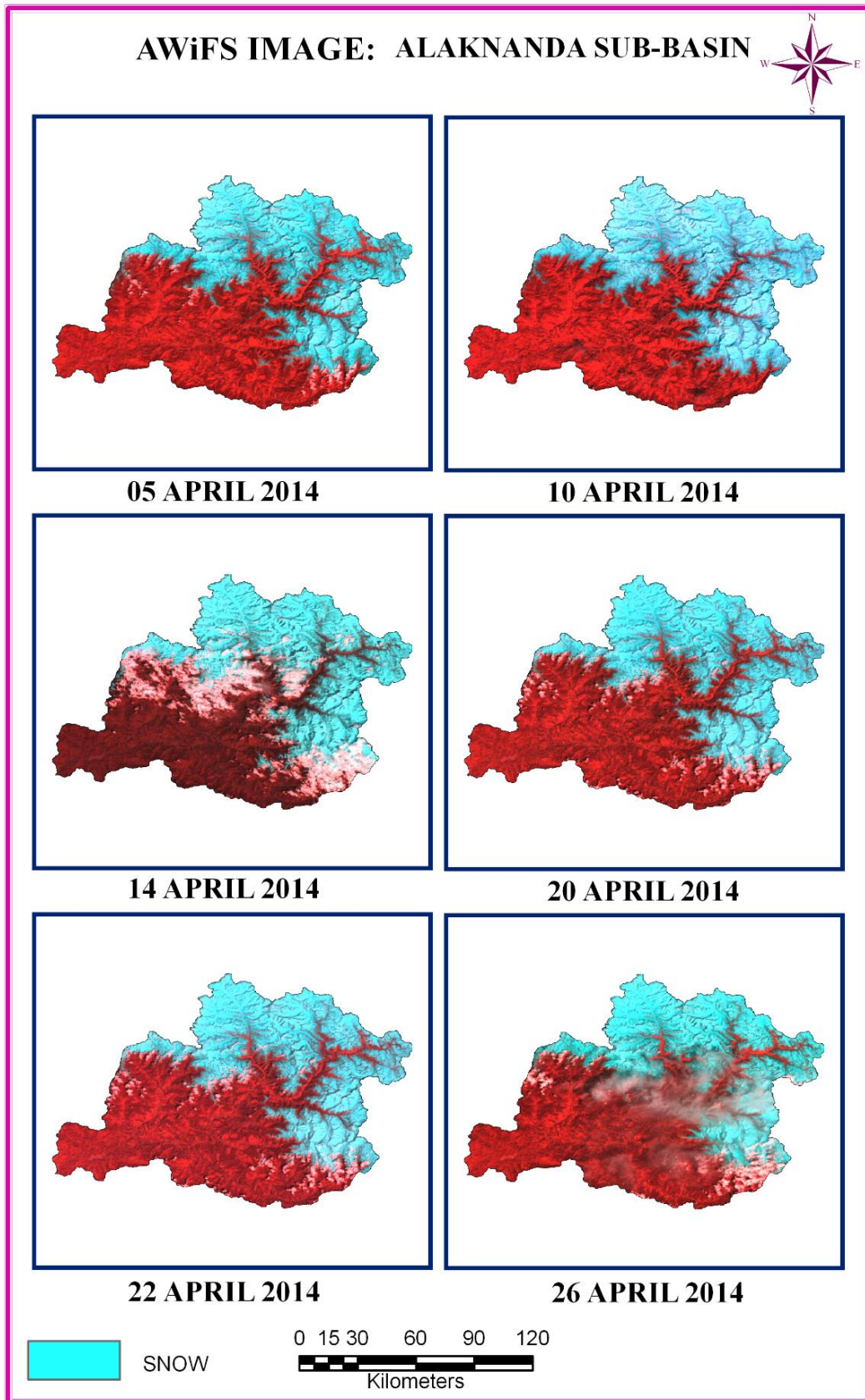
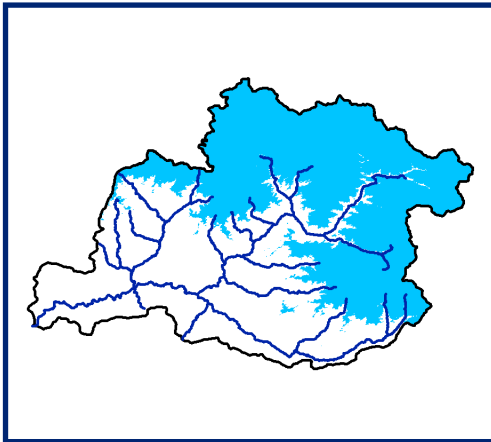
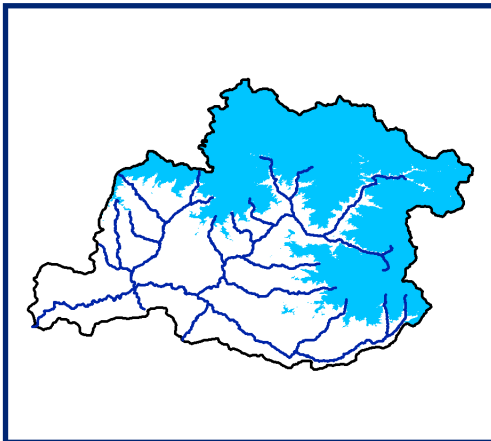


Figure 7: Snow cover products of Alaknanda sub-basin prepared using IRS AWiFS data of April, 2014

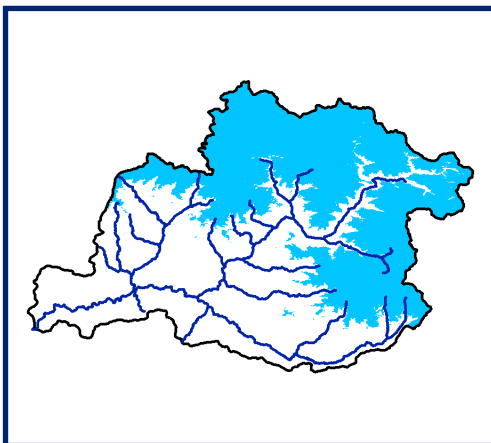
10 DAILY SNOW COVER MAP : ALAKNANDA SUB-BASIN



05 APRIL 2014
10 APRIL 2014



14 APRIL 2014
20 APRIL 2014



22 APRIL 2014
26 APRIL 2014

 SNOW

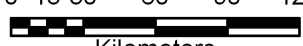
0 15 30 60 90 120

Kilometers

Figure 8: 10 Daily Snow cover maps of Alaknanda sub-basin basin prepared using IRS AWiFS data of April, 2014

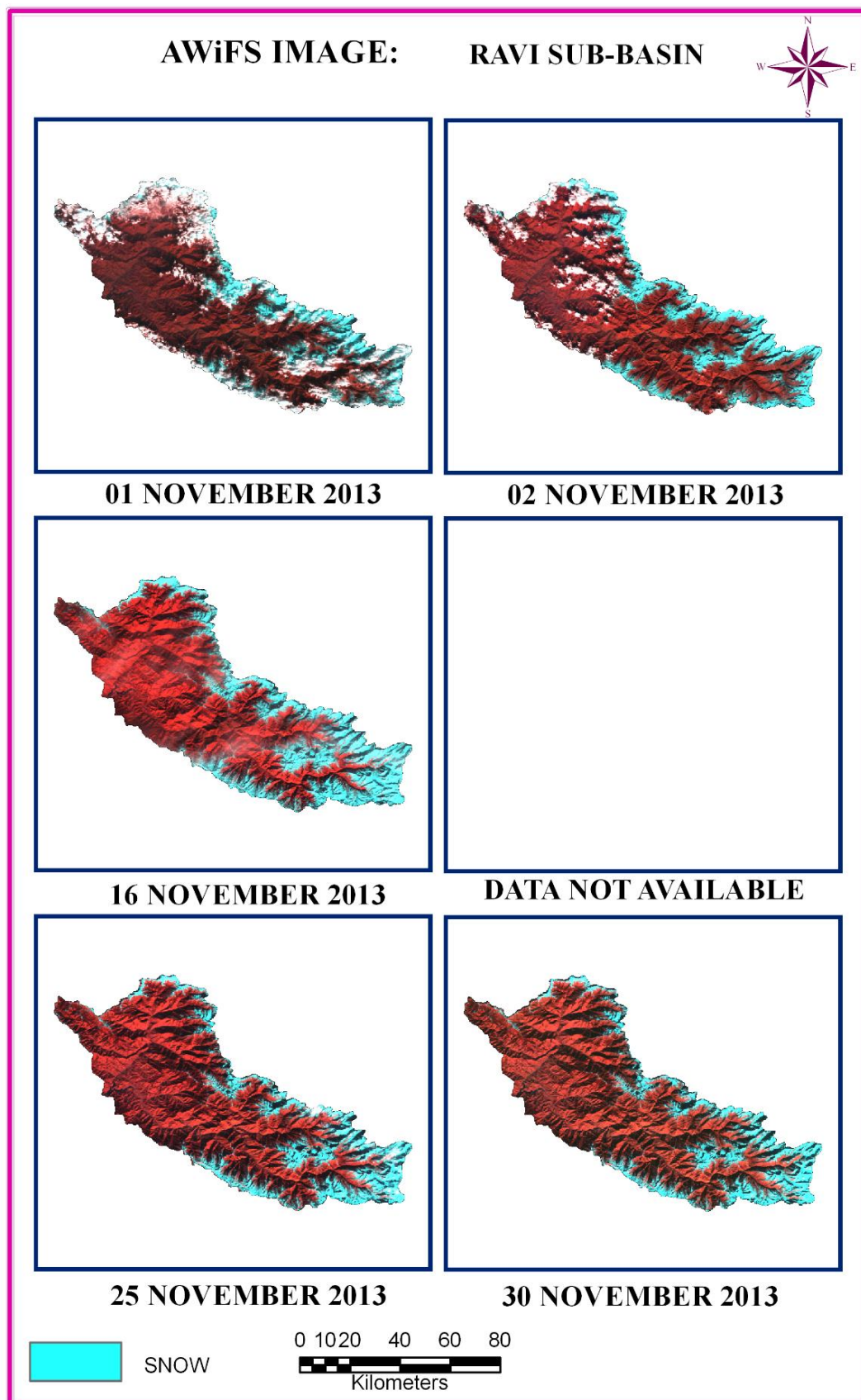
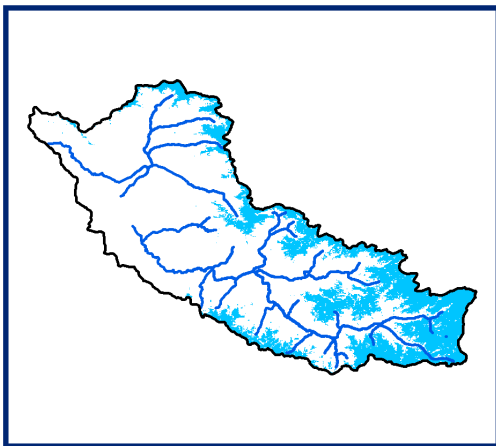


Figure 9: Snow cover products of Ravi sub-basin prepared using IRS AWiFS data of November, 2013

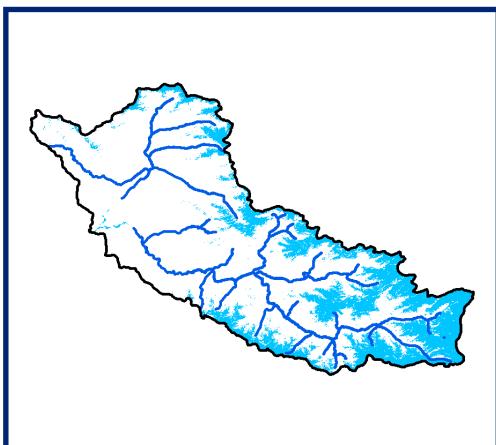
10 DAILY SNOW COVER MAP : RAVI SUB-BASIN



01 NOVEMBER 2013
02 NOVEMBER 2013



16 NOVEMBER 2013



25 NOVEMBER 2013
30 NOVEMBER 2013

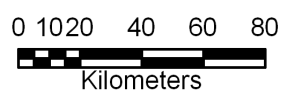


Figure 10: 10 Daily Snow cover maps of Ravi sub-basin Ravi sub-basin prepared using IRS AWiFS data of November, 2013

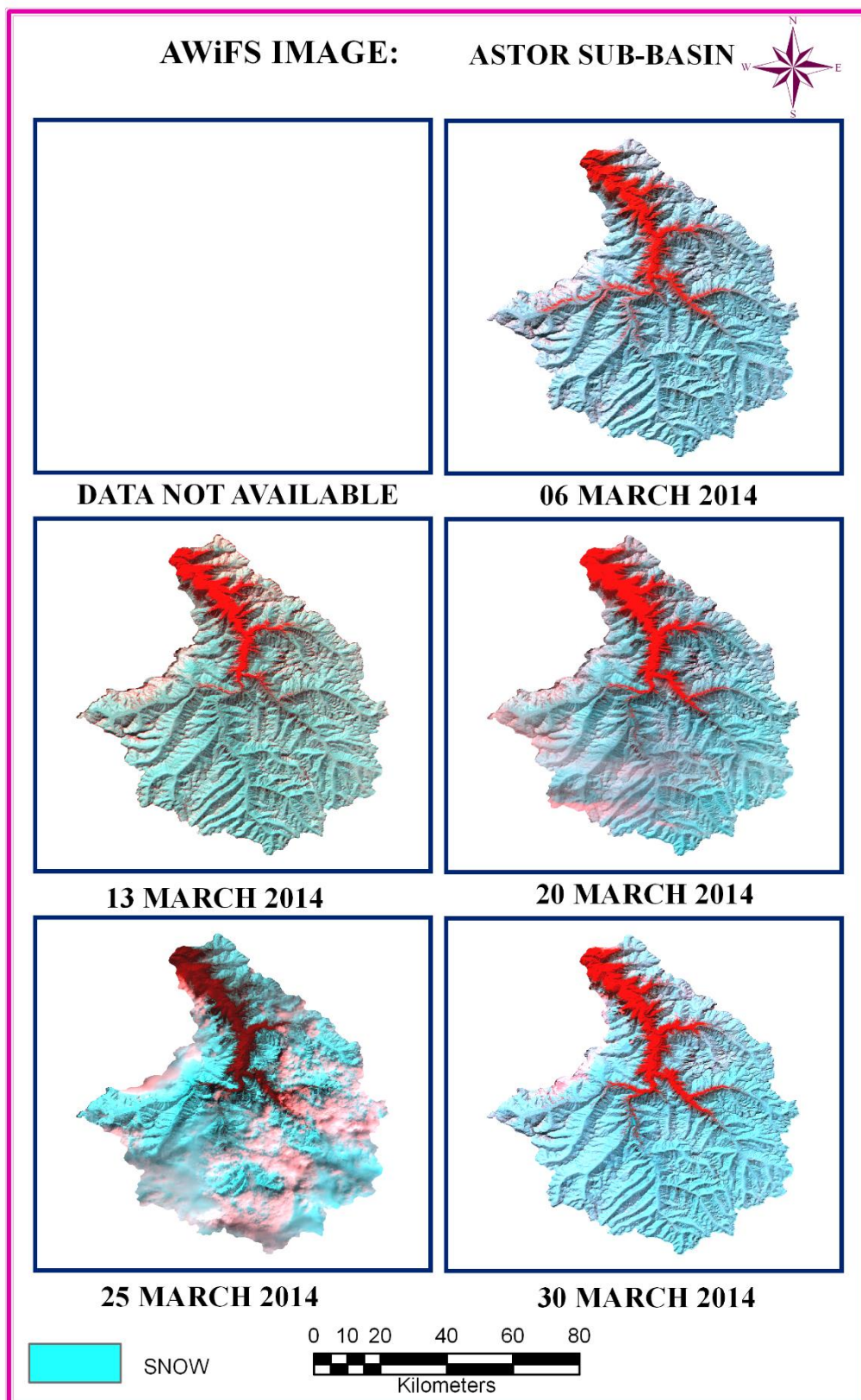
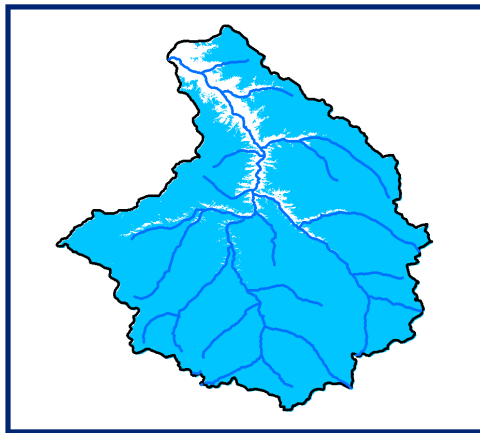
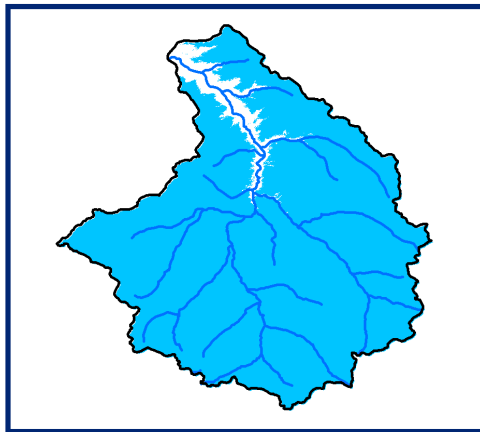


Figure 11: Snow cover products of Astor sub-basin prepared using IRS AWiFS data of March, 2014

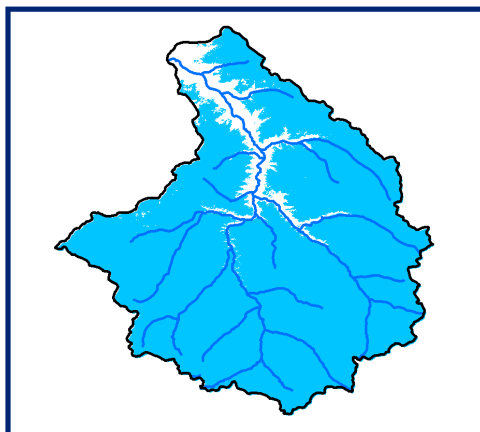
10 DAILY SNOW COVER MAP : ASTOR SUB-BASIN



06 MARCH 2014



**13 MARCH 2014
20 MARCH 2014**



**25 MARCH 2014
30 MARCH 2014**



SNOW

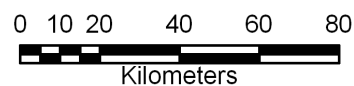


Figure 12: 10 Daily Snow cover maps of Astor sub-basin prepared using IRS AWiFS data of March, 2014

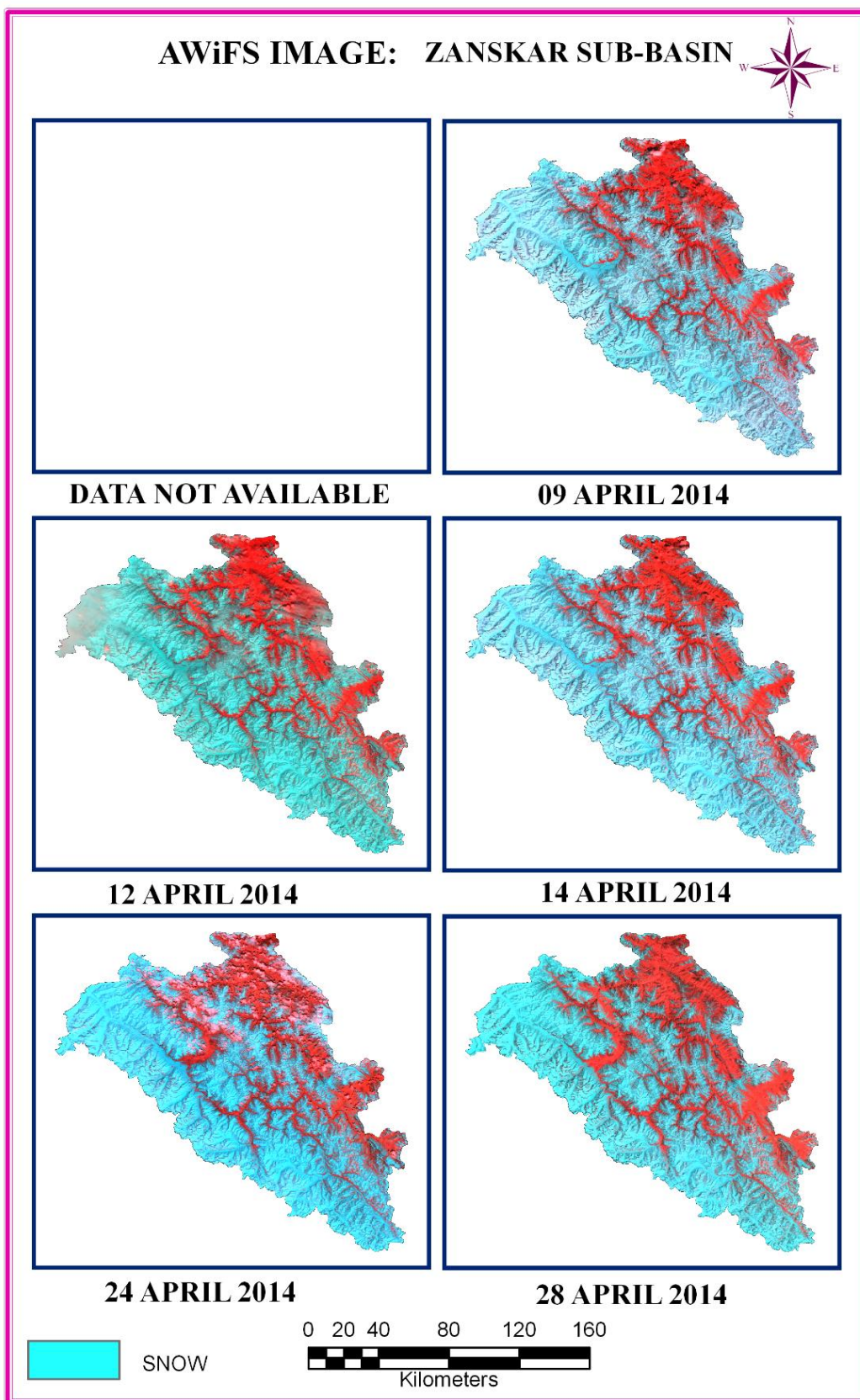
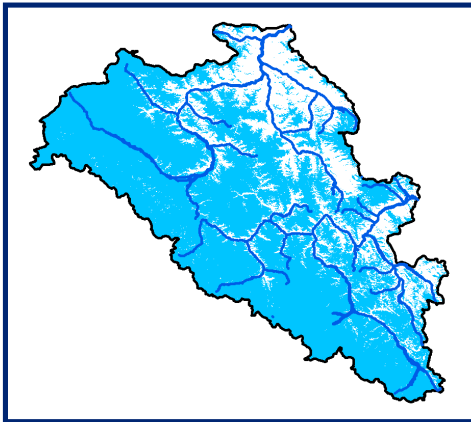
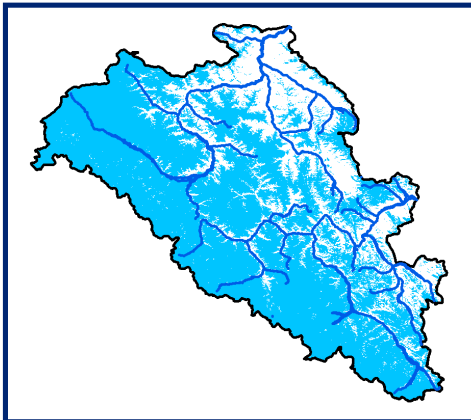


Figure 13: Snow cover products of Zaskar sub-basin prepared using IRS AWiFS data of April, 2014

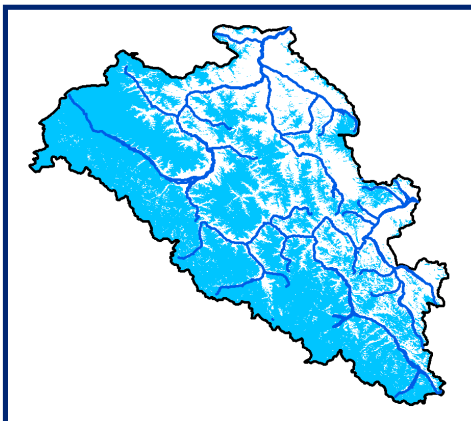
10 DAILY SNOW COVER MAP : ZANSKAR SUB-BASIN



09 APRIL 2014



**12 APRIL 2014
14 APRIL 2014**



**24 APRIL 2014
28 APRIL 2014**



SNOW

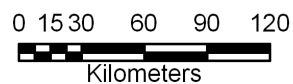


Figure 14: 10 Daily Snow cover maps of Zanskar sub-basin prepared using IRS AWiFS data of April, 2014

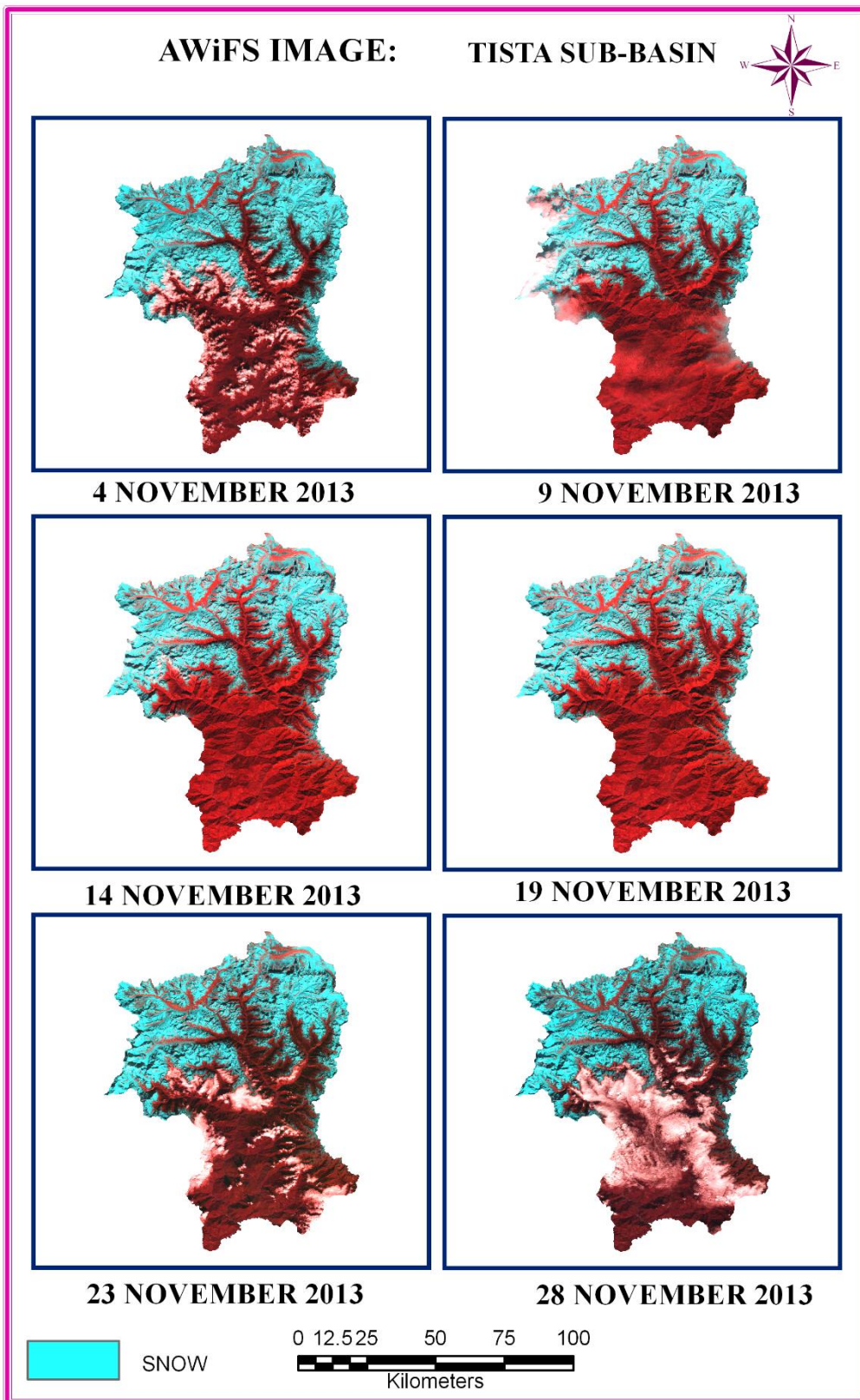


Figure 15: Snow cover products of Tista sub-basin prepared using IRS AWiFS data of November, 2013

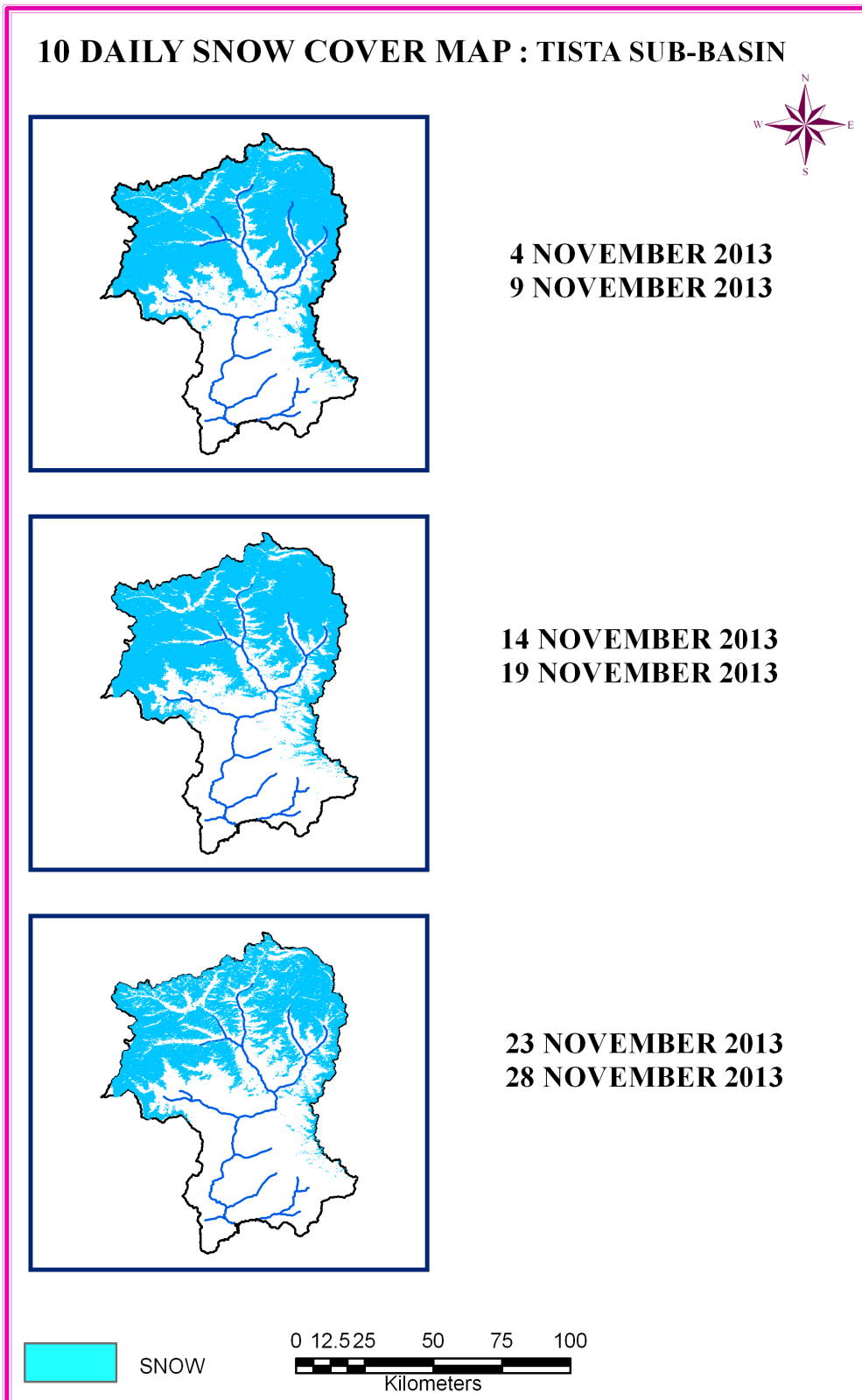


Figure 16: 10 Daily Snow cover maps of Tista sub-basin prepared using IRS AWiFS data of November, 2013

2.4. Results and Discussion

The spatial and temporal pattern of accumulation and ablation of snow cover within each basin varies from one sub-basin to other. It is governed by several factors such as temperature, wind velocity, humidity, latitude, aspect, altitude etc. The aim of presenting the results is to establish a unique pattern for each sub-basin which will help in snow-melt runoff behavior and any anomalous pattern will lead to understand the anomaly in weather system. As shown in earlier sections that snow cover has been mapped for each sub-basin and its variation has been measured as percentage of snow cover area to total sub-basin area. Absolute quantity of snow cover in each sub-basin is converted into percentage and plotted against time. The ascending part of snow cover is said to be accumulation and descending part is called the ablation. Intra-annual patterns are clubbed to get inter-annual patterns. The significance of these patterns lies in the snow melt runoff, glacier mass balance and climate change studies. Snow cover atlases prepared under this project is being provided in Annexure as soft copy in the form of CD.

i) Indus basin

Indus basin comprises thirteen sub-basins covering 125009 sq. km area. Six sub-basins i. e Gilgit, Hanza, Shigar, Shasgan, Nubra and Shyok are located in the North and seven sub-basins i.e. Astor, Kisan Ganga, Shigo, Drass, Jhelum, Suru and Zaskar are located in the South of Indus river. Although Shasgan sub-basin is draining towards China but is situated within the Indian territory.

Minimum and maximum snow cover

For each sub-basin of Indus basin, the minimum and maximum snow cover in each hydrological year from 2004-05 to 2013-14 has been compiled in the Tables 3 to 15. The snow cover in the tables has been represented in absolute value and in percentage as well. Mean and Standard Deviations (SD) are also mentioned in the tables.

It is observed that the mean of minimum snow cover is highest in Nubra sub basin and lowest in Jhelum sub-basin. The mean of maximum snow cover is high in Shigo, Astor, Suru, Zaskar and low in Jhelum sub-basins. It is observed that maximum variation of minimum snow cover is seen in Gilgit Astor and Suru sub-basins and minimum variation is seen in Jhelum sub-basin among all the sub-basins. The variation in maximum snow cover is seen more in Jhelum sub-basin. The values of SD of maximum snow cover suggests less variability in snow cover. Otherwise the SD values of rest of the sub-basins indicate less variability of maximum snow cover in the period of ten years.

The maximum and minimum amount of minimum snow cover also varies in each sub-basin. For example, the maximum % of minimum snow cover in Gilgit sub-basin is 57 in 2008-09 and 2010-11 and lowest of minimum snow cover is 9 % in 2013-14. But this figure is different for other sub-basins and in different years. This suggests that within Indus basin also the different sub-basins experience different amount of precipitation in different years due to variations in governing factors.

Table 3: Minimum and maximum snow cover in Gilgit sub-basin during 2004-14

Gilgit sub-basin (13615 sq. km)				
Year	Minimum snow cover		Maximum snow cover	
	Sq. km	%	Sq. km	%
2004-05	3268	24	13070	96
2005-06	4221	31	11845	87
2006-07	2859	21	11573	85
2007-08	2859	21	11981	88
2008-09	7761	57	12662	93
2009-10	5582	41	12117	89
2010-11	2451	18	12934	95
2011-12	7761	57	12254	90
2012-13	4085	30	12526	92
2013-14	1225	9	11437	84
Mean	4207	31	12240	90
SD	2203	16	554	4

Table 4: Minimum and maximum snow cover in Hanza sub-basin during 2004-14

Hanza sub-basin (13711 sq. km)				
Year	Minimum snow cover		Maximum snow cover	
	Sq. km	%	Sq. km	%
2004-05	6856	50	13025	95
2005-06	5759	42	10969	80
2006-07	4936	36	11243	82
2007-08	4250	31	11106	81
2008-09	6993	51	12888	94
2009-10	7678	56	12340	90
2010-11	4113	30	12203	89
2011-12	7541	55	11791	86
2012-13	5073	37	12888	94
2013-14	6581	48	11654	85
Mean	5978	44	12011	88
SD	1330	10	773	6

Table 5: Minimum and maximum snow cover in Shigar sub-basin during 2004-14

Shigar sub-basin (4258 sq. km)				
Year	Minimum snow cover		Maximum snow cover	
	Sq. km	%	Sq. km	%
2004-05	2470	58	4258	100
2005-06	2086	49	3832	90
2006-07	1661	39	3790	89
2007-08	2129	50	3790	89
2008-09	2555	60	3917	92
2009-10	2555	60	3832	90
2010-11	1874	44	4173	98
2011-12	2427	57	4003	94
2012-13	2427	57	4173	98
2013-14	2086	49	4088	96
Mean	2227	52	3986	94
SD	307	7	178	4

Table 6: Minimum and maximum snow cover in Shasgan sub-basin during 2004-14

Shasgan sub-basin (7613 sq. km)				
Year	Minimum snow cover		Maximum snow cover	
	Sq. km	%	Sq. km	%
2004-05	3730	49	7537	99
2005-06	3654	48	6776	89
2006-07	3121	41	5634	74
2007-08	3121	41	5405	71
2008-09	3426	45	6014	79
2009-10	2817	37	5557	73
2010-11	3045	40	6090	80
2011-12	2208	29	6243	82
2012-13	3121	41	6090	80
2013-14	2893	38	6319	83
Mean	3114	41	6167	81
SD	439	6	628	8

Table 7: Minimum and maximum snow cover in Nubra sub-basin during 2004-14

Nubra sub-basin (7050 sq. km)				
Year	Minimum snow cover		Maximum snow cover	
	Sq. km	%	Sq. km	%
2004-05	4724	67	7050	100
2005-06	3455	49	6416	91
2006-07	3666	52	6275	89
2007-08	3455	49	5993	85
2008-09	4089	58	6557	93
2009-10	3314	47	6698	95
2010-11	3948	56	6698	95
2011-12	4019	57	6557	93
2012-13	3878	55	6909	98
2013-14	3737	53	6275	89
Mean	3829	54	6543	93
SD	408	6	317	4

Table 8: Minimum and maximum snow cover in Shyok sub-basin during 2004-14

Shyok sub-basin (27120 sq. km)				
Year	Minimum snow cover		Maximum snow cover	
	Sq. km	%	Sq. km	%
2004-05	11390	42	26035	96
2005-06	5695	21	22781	84
2006-07	6238	23	18442	68
2007-08	6509	24	17086	63
2008-09	9221	34	25222	93
2009-10	5424	20	24137	89
2010-11	5695	21	23594	87
2011-12	7322	27	23323	86
2012-13	7594	28	24679	91
2013-14	7865	29	20882	77
Mean	7295	27	22618	83
SD	1863	7	2935	11

Table 9: Minimum and maximum snow cover in Astor sub-basin during 2004-2014

Astor sub-basin (4008 sq. km)				
Year	Minimum snow cover		Maximum snow cover	
	Sq. km	%	Sq. km	%
2004-05	1723	43	3968	99
2005-06	401	10	3808	95
2006-07	281	7	3928	98
2007-08	401	10	3888	97
2008-09	1002	25	3968	99
2009-10	2044	51	3968	99
2010-11	441	11	3928	98
2011-12	1042	26	3968	99
2012-13	882	22	3928	98
2013-14	200	5	3888	97
Mean	842	21	3924	98
SD	629	16	51	1

Table 10: Minimum and maximum snow cover in Kisanganga sub-basin during 2004-14

Kisanganga sub-basin (7451 sq km)				
Year	Minimum snow cover		Maximum snow cover	
	Sq. km	%	Sq. km	%
2004-05	1043	14	7451	100
2005-06	224	3	7078	95
2006-07	149	2	6855	92
2007-08	224	3	6929	93
2008-09	745	10	6706	90
2009-10	2161	29	6557	88
2010-11	224	3	7227	97
2011-12	1937	26	7004	94
2012-13	373	5	7004	94
2013-14	75	1	6929	93
Mean	716	10	6974	94
SD	765	10	251	3

Table 11: Minimum and maximum snow cover in Shigo sub-basin during 2004-14

Shigo sub-basin (5539 sq. km)				
Year	Minimum snow cover		Maximum snow cover	
	Sq. km	%	Sq. km	%
2004-05	1329	24	5539	100
2005-06	886	16	5484	99
2006-07	111	2	5539	100
2007-08	166	3	5539	100
2008-09	1274	23	5539	100
2009-10	554	10	5539	100
2010-11	222	4	5539	100
2011-12	554	10	5539	100
2012-13	222	4	5539	100
2013-14	55	1	5539	100
Mean	537	10	5534	100
SD	476	9	17	0

Table 12: Minimum and maximum snow cover in Drass sub-basin during 2004-14

Drass sub-basin (1683 sq. km)				
Year	Minimum snow cover		Maximum snow cover	
	Sq. km	%	Sq. km	%
2004-05	589	35	1683	100
2005-06	168	10	1649	98
2006-07	168	10	1683	100
2007-08	252	15	1649	98
2008-09	555	33	1683	100
2009-10	421	25	1666	99
2010-11	303	18	1666	99
2011-12	404	24	1683	100
2012-13	370	22	1649	98
2013-14	151	9	1683	100
Mean	338	20	1669	99
SD	158	9	16	1

Table 13: Minimum and maximum snow cover in Jhelum sub-basin during 2004-14

Jhelum sub-basin (14472 sq. km)				
Year	Minimum snow cover		Maximum snow cover	
	Sq. km	%	Sq. km	%
2004-05	579	4	10275	71
2005-06	289	2	6223	43
2006-07	724	5	11867	82
2007-08	145	1	10420	72
2008-09	434	3	6512	45
2009-10	434	3	11433	79
2010-11	145	1	13748	95
2011-12	1158	8	14038	97
2012-13	289	2	13314	92
2013-14	145	1	9407	65
Mean	434	3	10724	74
SD	320	2	2762	19

Table 14: Minimum and maximum snow cover in Suru sub-basin during 2004-14

Suru sub-basin (3575 sq. km)				
Year	Minimum snow cover		Maximum snow cover	
	Sq. km	%	Sq. km	%
2004-05	1287	36	3575	100
2005-06	787	22	3504	98
2006-07	644	18	3575	100
2007-08	679	19	3539	99
2008-09	1001	28	3575	100
2009-10	536	15	3539	99
2010-11	751	21	3539	99
2011-12	930	26	3575	100
2012-13	1394	39	3575	100
2013-14	536	15	3575	100
Mean	855	24	3557	100
SD	298	8	25	1

Table 15: Minimum and maximum snow cover in Zanskar sub-basin during 2004- 14

Zanskar sub-basin (14914 sq km)				
Year	Minimum snow cover		Maximum snow cover	
	Sq. km	%	Sq. km	%
2004-05	3281	22	14914	100
2005-06	1641	11	14467	97
2006-07	1193	8	14616	98
2007-08	1342	9	14467	97
2008-09	3878	26	14467	97
2009-10	1939	13	14914	100
2010-11	1641	11	14914	100
2011-12	1790	12	14914	100
2012-13	2535	17	14765	99
2013-14	1939	13	14168	95
Mean	2118	14	14661	98
SD	863	6	263	2

Monthly accumulation and ablation patterns (2008-2014) and Annual changes (2004-2014) of snow cover

Figures 17 to 28 show the curves of accumulation and ablation of snow plotted against time for each sub-basin of Indus basin. The curves have been generated from the snow cover data generated from 2008-09 to 2013-14. It is observed from these curves that for each sub-basin snow accumulation in each hydrological year differs from one sub-basin to other. Within each sub-basin also the part of curve is not similar for each hydrological year. This indicates high variability of snow accumulation in different sub-basins. The unevenness in accumulation indicate precipitation and subsequent melting of snow. But broadly it is observed that the sub-basins located at northern side of Indus river are showing moderate slope of accumulation pattern in comparison to sub-basins located at southern side. The slope of accumulation indicates rate of precipitation. The point of initiation of accumulation also varies. The accumulation pattern of Shasgan sub-basin is distinct as the accumulation starts from about 50 % snow but does not reach more than 80 %. In all northern sub-basins, the snow cover does not reach 100 % of the sub-basin area though the point of initiation is higher in northern sub-basins. In southern sub-basins the point of initiation are much lower but the maximum snow cover reaches near 100%. There are instances of sharp rise of accumulation as seen in year 2009-10 and 2012-13. There is close similarity of ablation pattern of snow cover for each sub-basin in different hydrological years. All sub-basins behave in a similar manner. The slopes of northern sub-basins are gentler than southern sub-basins. This indicates a contrast in the temperature regime of northern and southern sub-basins. The accumulation and ablation of snow in Jhelum sub-basin is different than of other sub-basins.

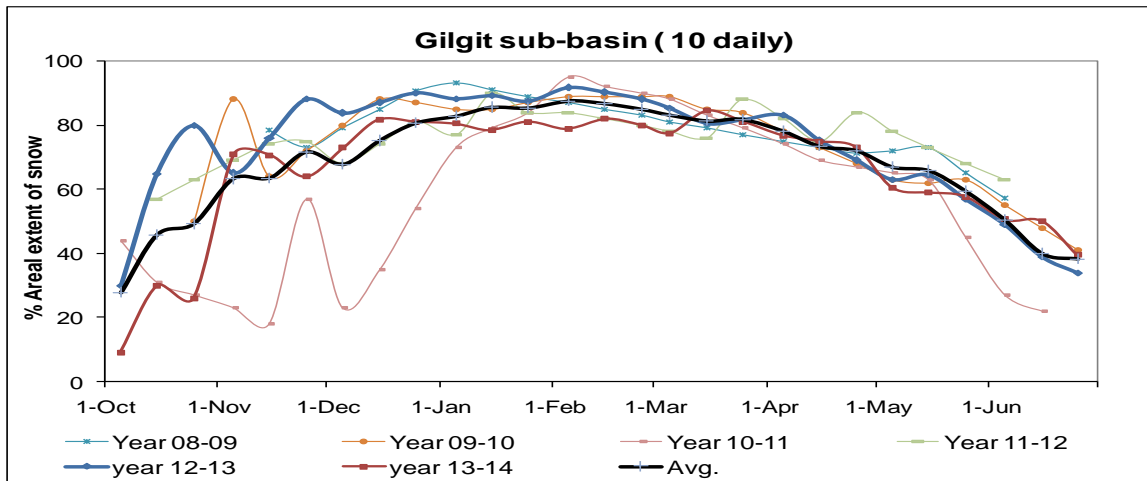


Figure 17: Accumulation and ablation pattern of snow cover for Gilgit sub-basin (Indus basin) between 2008 and 2014

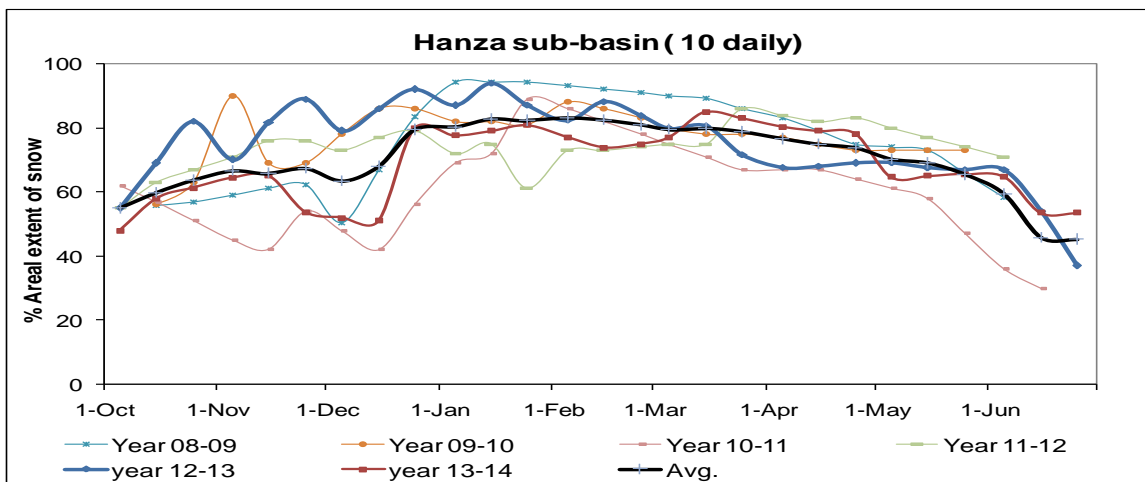


Figure 18: Accumulation and ablation pattern of snow cover for Hanza sub-basin (Indus basin) between 2008 and 2014

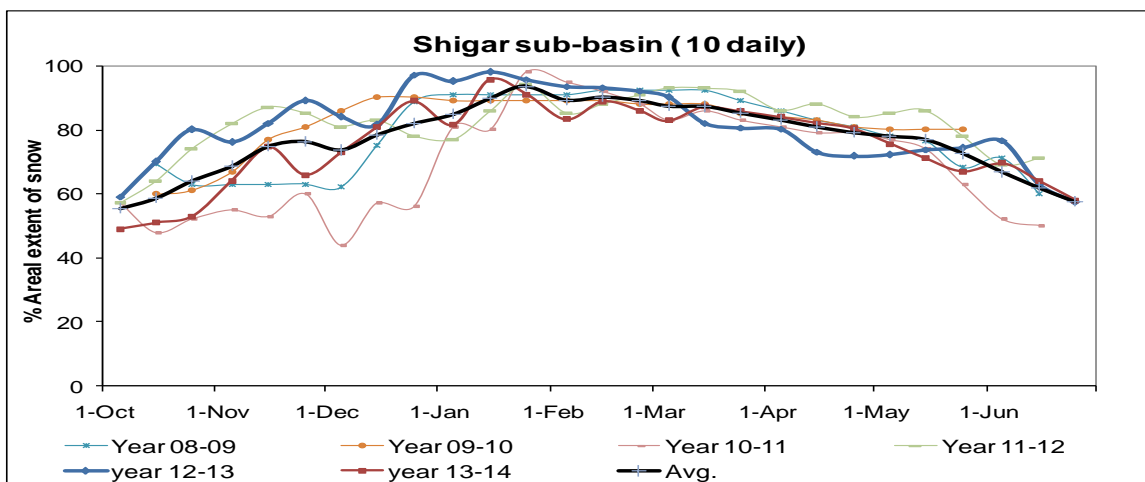


Figure 19: Accumulation and ablation pattern of snow cover for Shigar sub-basin (Indus basin) between 2008 and 2014

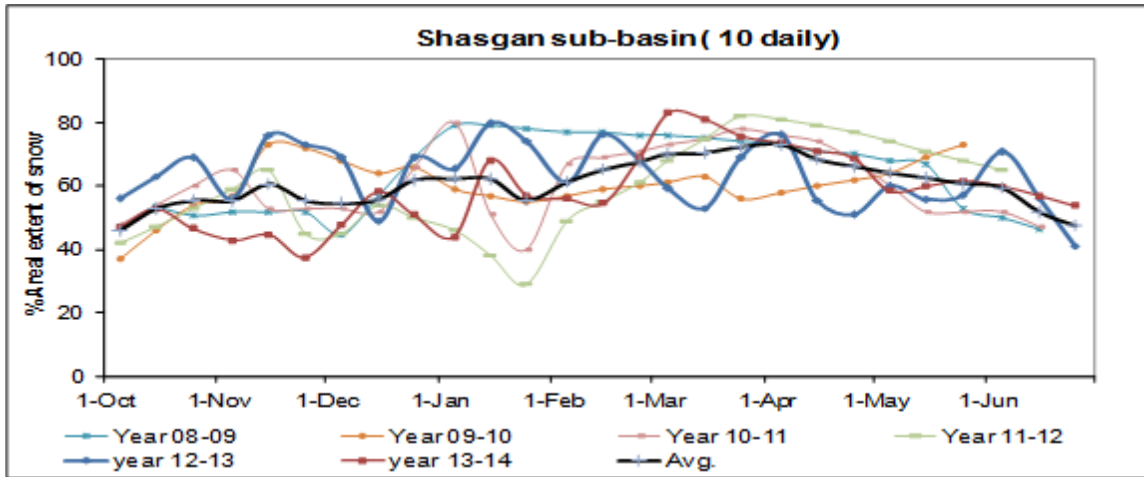


Figure 20: Accumulation and ablation pattern of snow cover for Shasgan sub-basin (Indus basin) between 2008 and 2014

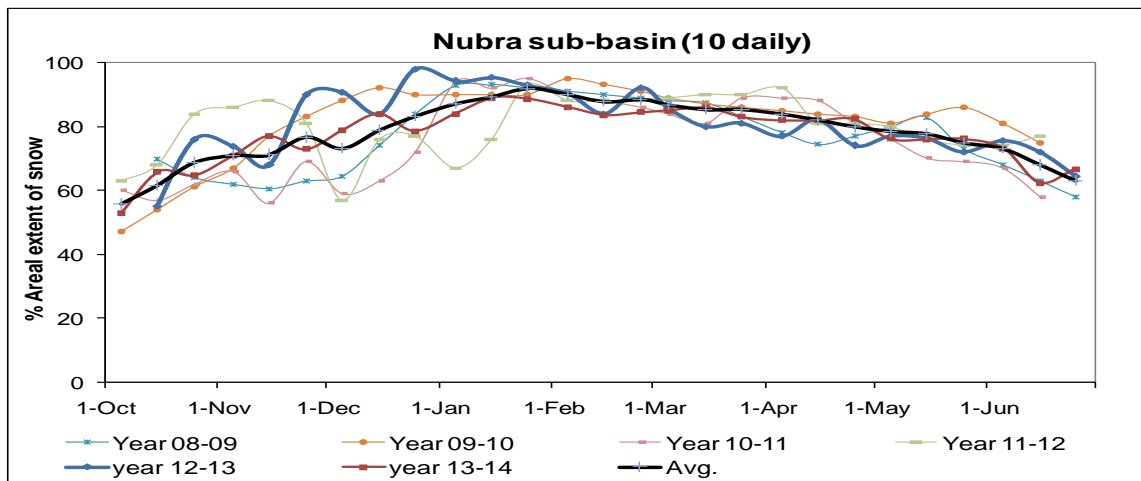


Figure 21: Accumulation and ablation pattern of snow cover for Nubra sub-basin (Indus basin) between 2008 and 2014

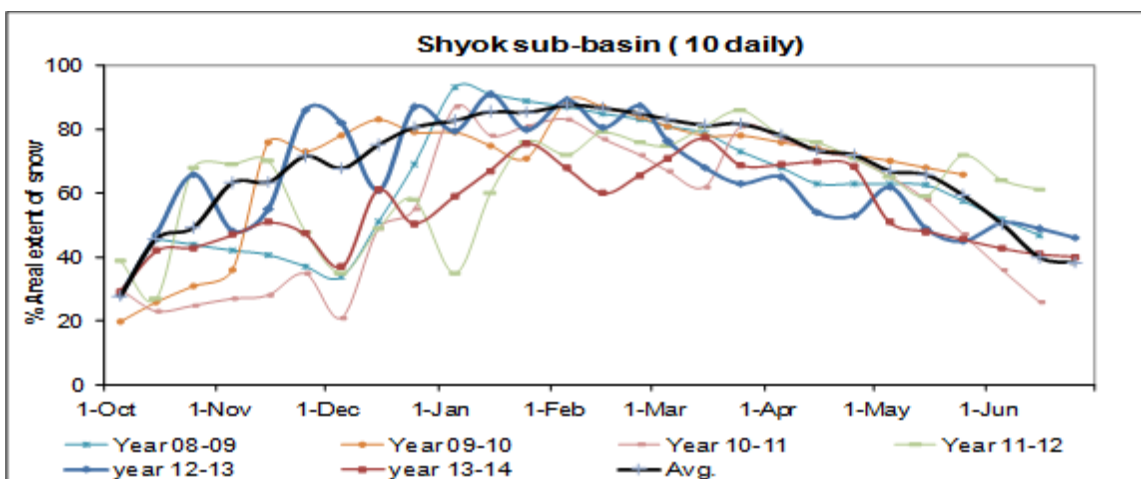


Figure 22: Accumulation and ablation pattern of snow cover for Shyok sub-basin (Indus basin) between 2008 and 2014

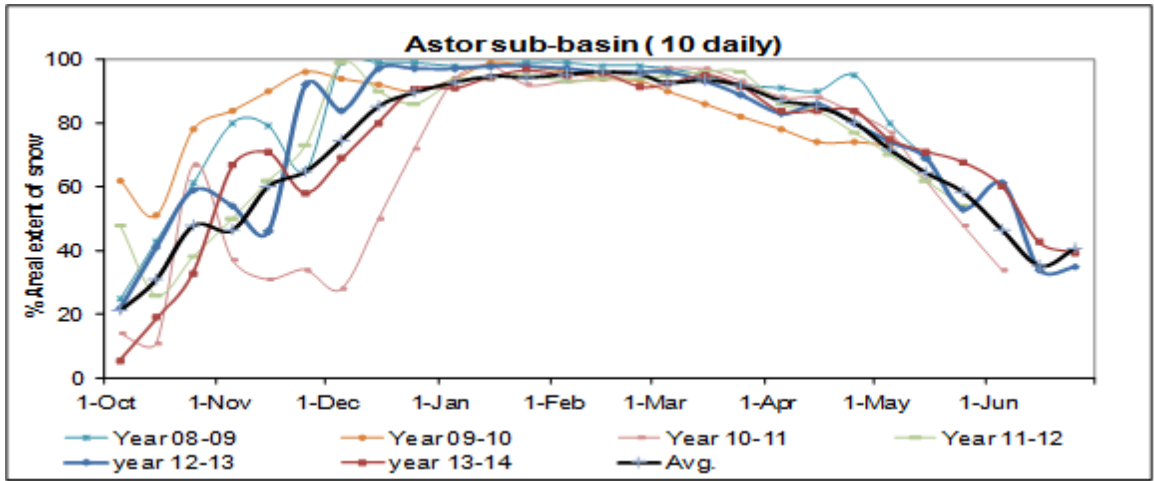


Figure 23: Accumulation and ablation pattern of snow cover for Astor sub-basin (Indus basin) between 2008 and 2014

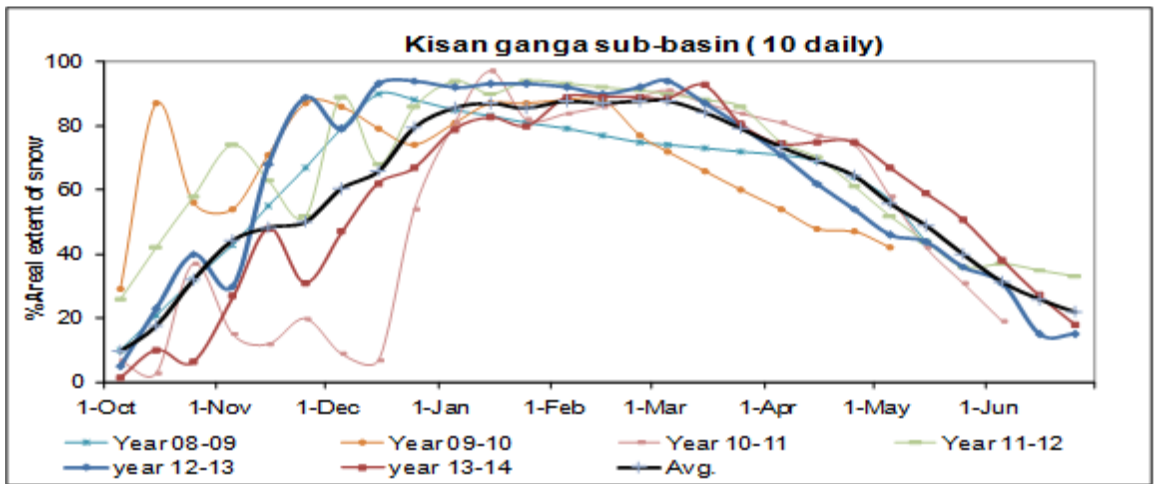


Figure 24: Accumulation and ablation pattern of snow cover for Kisanganga sub-basin (Indus basin) between 2008 and 2014

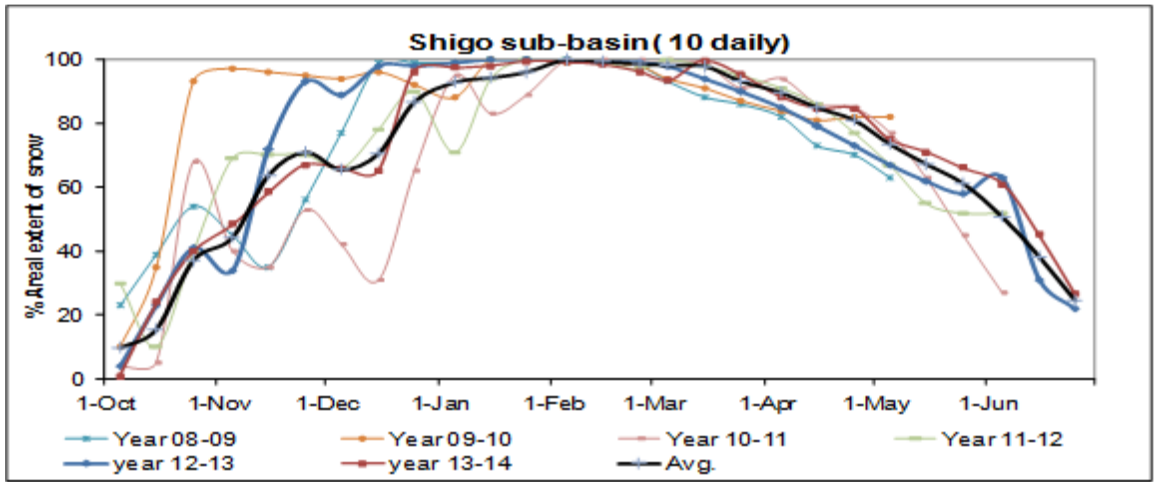


Figure 25: Accumulation and ablation pattern of snow cover for Shigo sub-basin (Indus basin) between 2008 and 2014

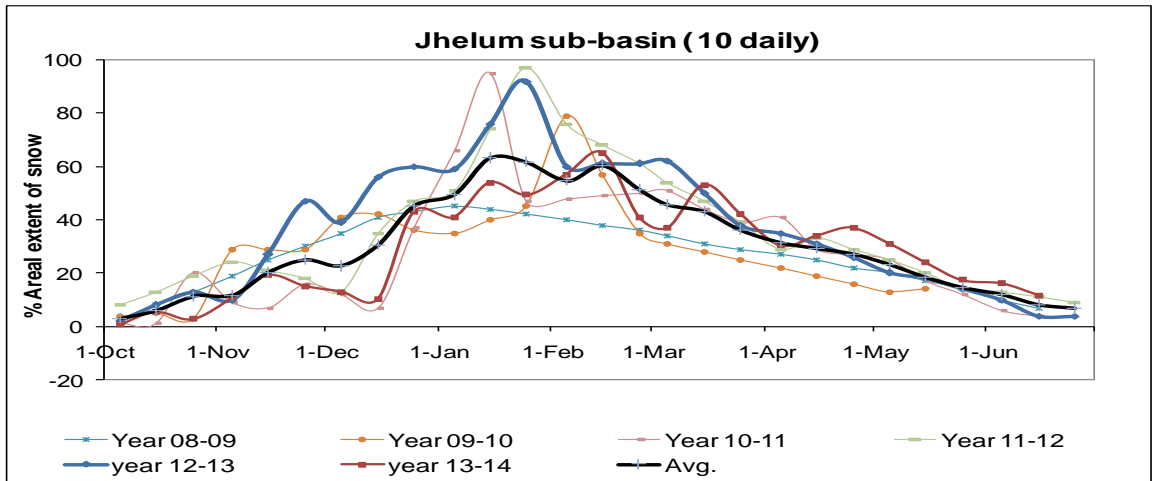


Figure 26: Accumulation and ablation pattern of snow cover for Jhelum sub-basin (Indus basin) between 2008 and 2014

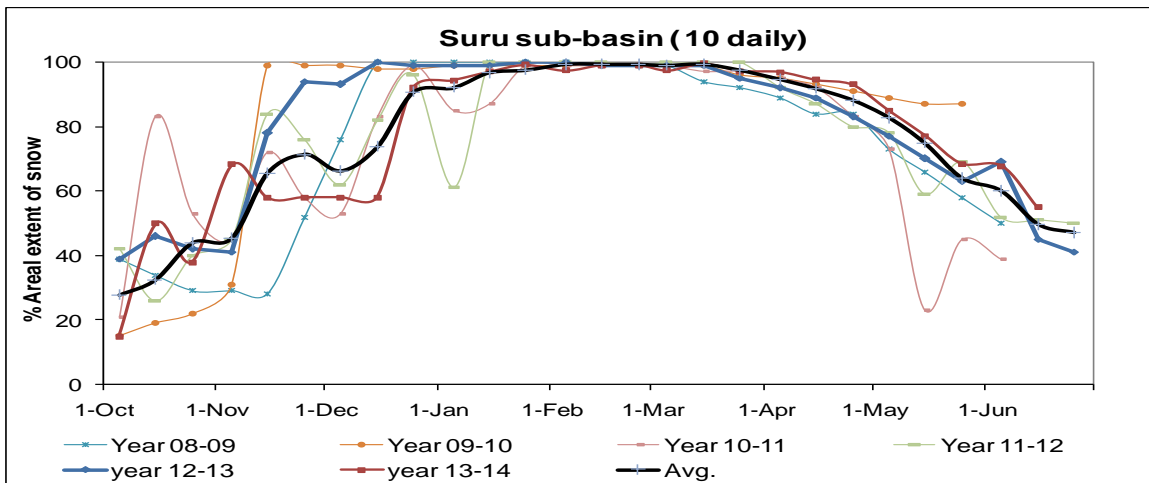


Figure 27: Accumulation and ablation pattern of snow cover for Suru sub-basin (Indus basin) between 2008 and 2014

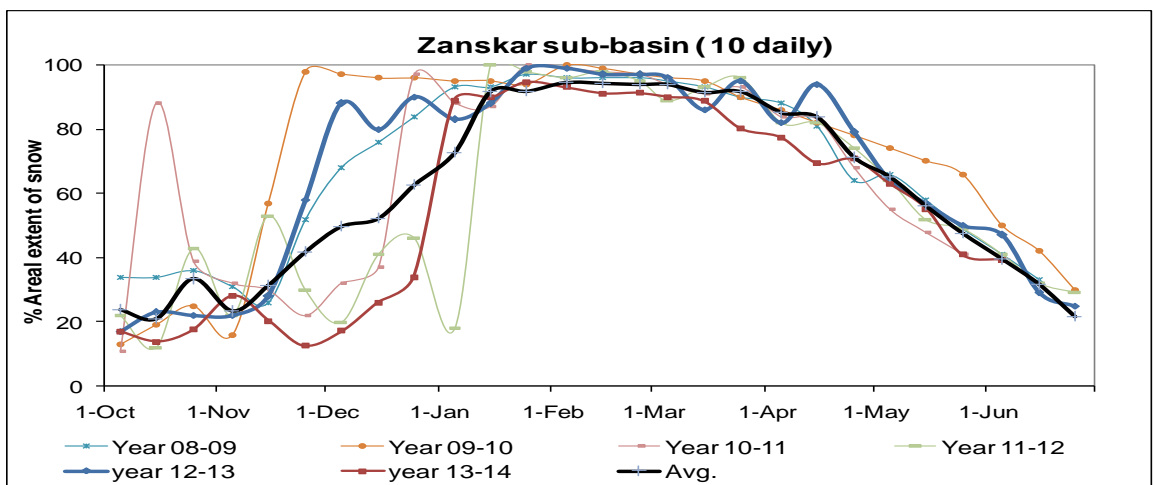


Figure 28: Accumulation and ablation pattern of snow cover for Zaskar sub-basin (Indus basin) between 2008 and 2014

Snow cover variations from 2004 to 2014 for different sub-basins are shown in Figures 29 to 41. These trends also depend on intra-annual variability but represent an overall trend of increase or decrease of snow cover. In all the 13 sub-basins there is no increase or decrease of snow cover beyond 5% of Mean. This indicates that snow precipitation within 10-year period has been almost stable. There is no difference in the northern or southern basins across Indus river. Though the pattern of accumulation and ablation in each year is different in different sub-basins but there is not much change within 10-year period (Figure 4.1.29 to 4.1.41).

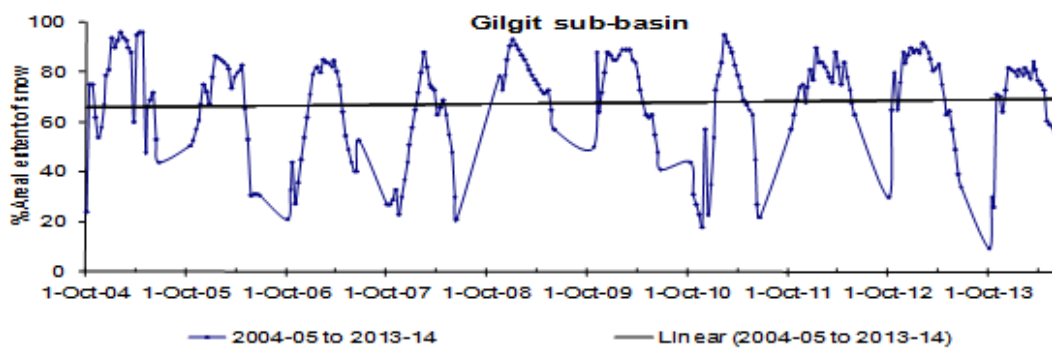


Figure 29: Changes in snow cover area and its trend during time frame 2004 to 2014 for Gilgit sub-basin of the Indus basin

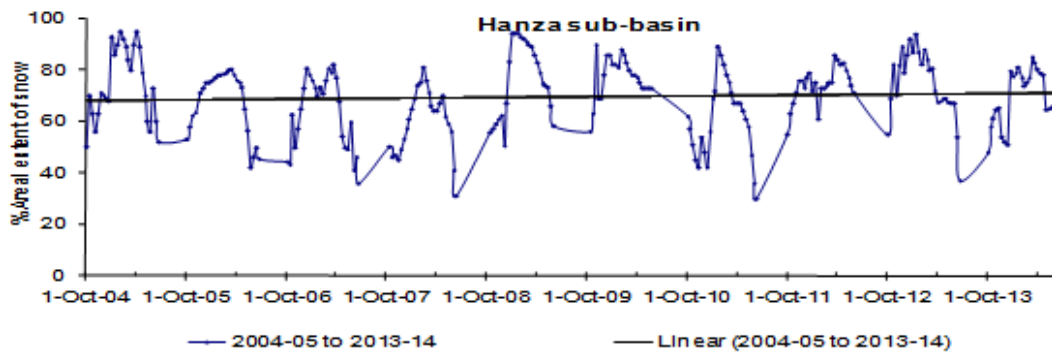


Figure 30: Changes in snow cover area and its trend during time frame 2004 to 2014 for Hanza sub-basin of the Indus basin

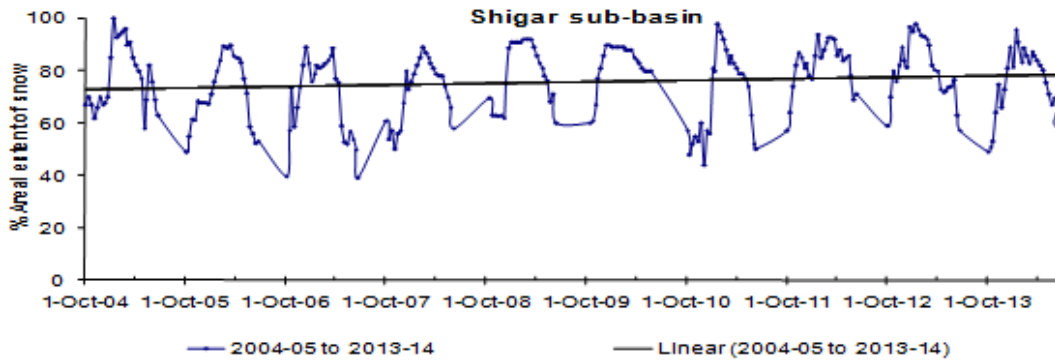


Figure 31: Changes in snow cover area and its trend during time frame 2004 to 2014 for Shigar sub-basin of the Indus basin

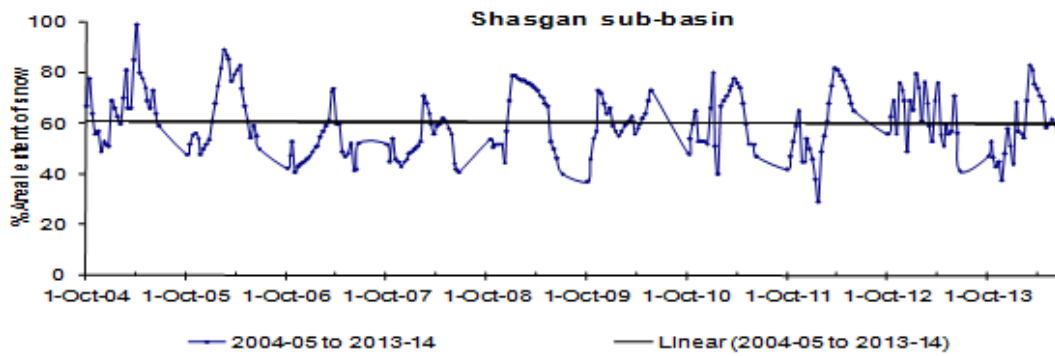


Figure 32: Changes in snow cover area and its trend during time frame 2004 to 2014 for Shasgan sub-basin of the Indus basin

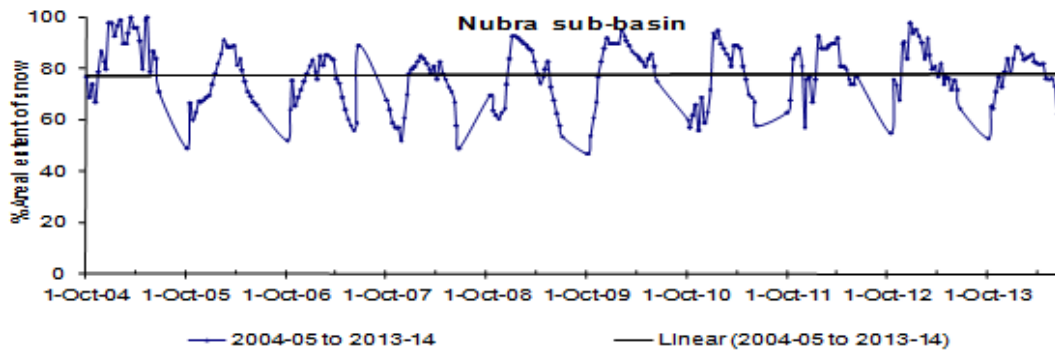


Figure 33: Changes in snow cover area and its trend during time frame 2004 to 2014 for Nubra sub-basin of the Indus basin

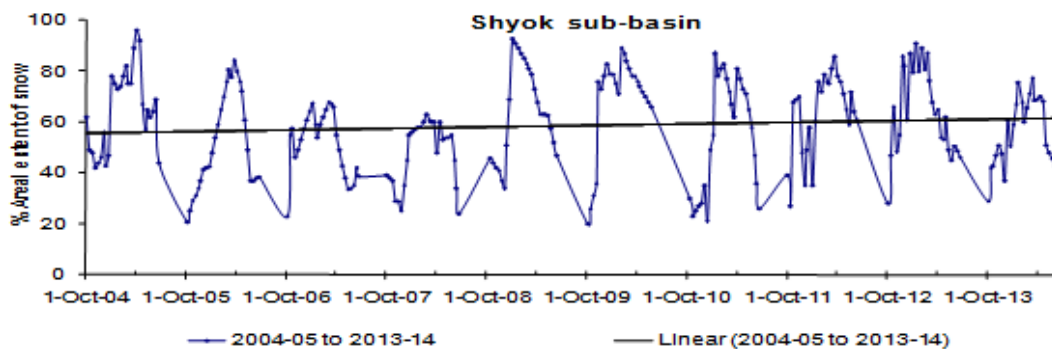


Figure 34: Changes in snow cover area and its trend during time frame 2004 to 2014 for Shyok sub-basin of the Indus basin

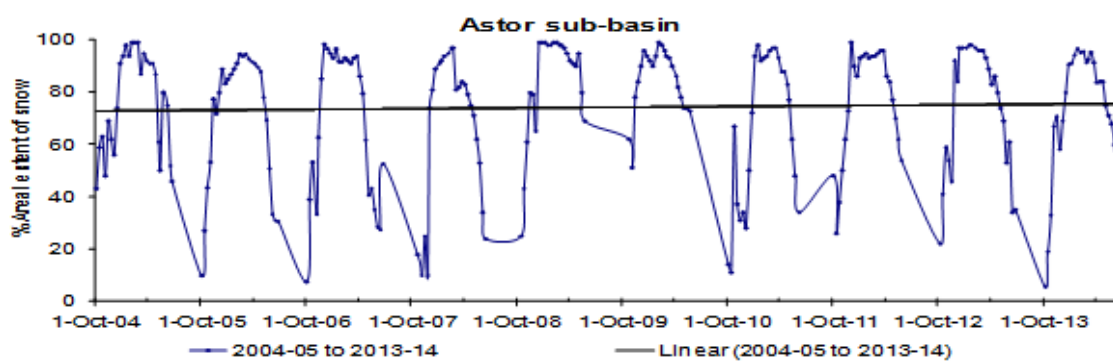


Figure 35: Changes in snow cover area and its trend during time frame 2004 to 2014 for Astor sub-basin of the Indus basin

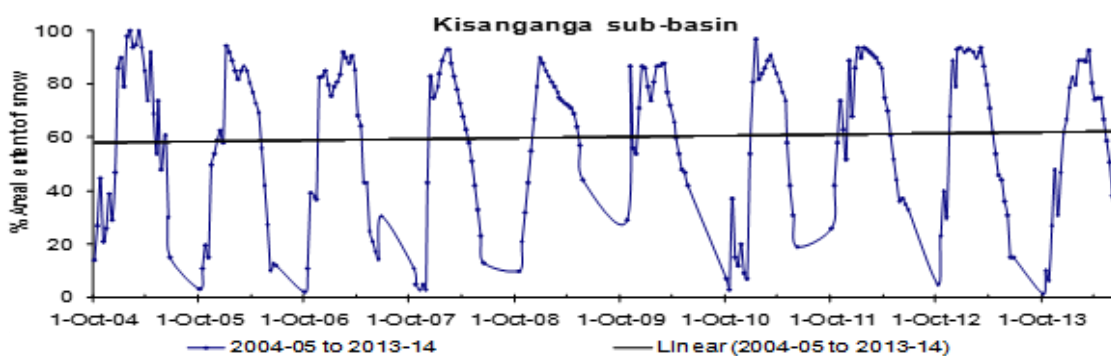


Figure 36: Changes in snow cover area and its trend during time frame 2004 to 2014 for Kisanganga sub-basin of the Indus basin

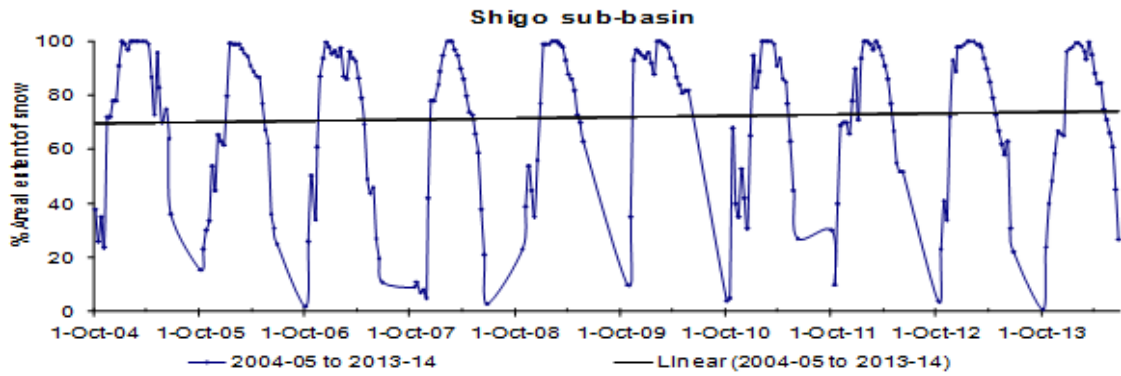


Figure 37: Changes in snow cover area and its trend during time frame 2004 to 2014 Shigo sub-basin of the Indus basin

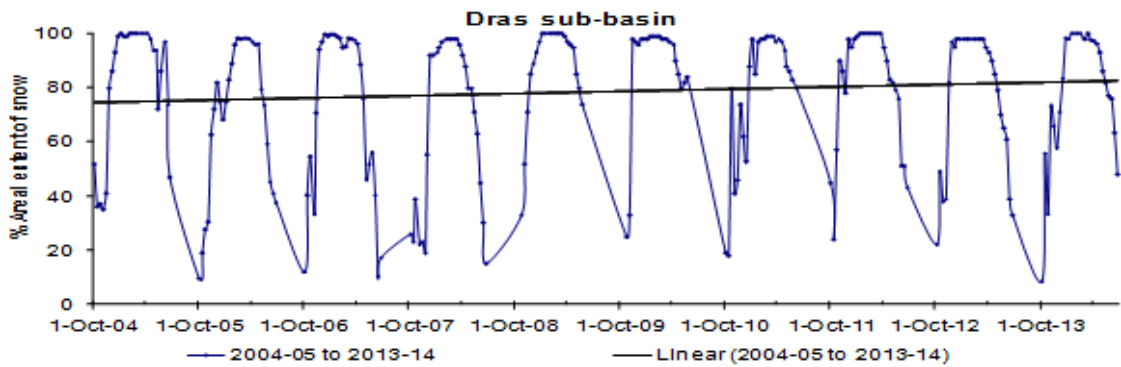


Figure 38: Changes in snow cover area and its trend during time frame 2004 to 2014 Drass sub-basin of the Indus basin

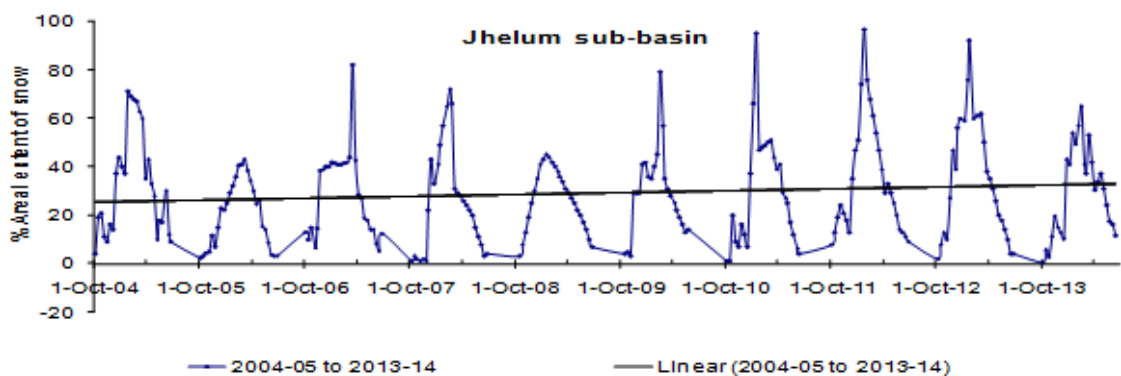


Figure 39: Changes in snow cover area and its trend during time frame 2004 to 2014 for Jhelum sub-basin of the Indus basin

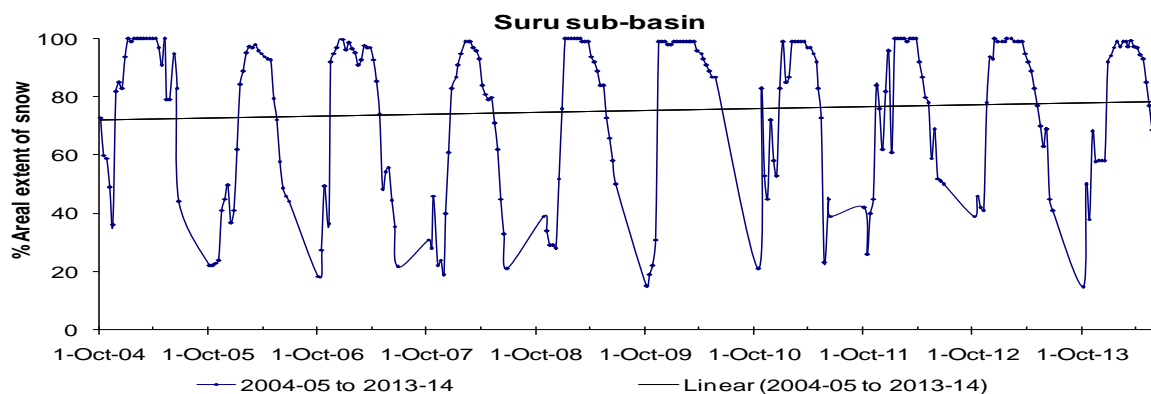


Figure 40: Changes in snow cover area and its trend during time frame 2004 to 2014 for Suru sub-basin of the Indus basin

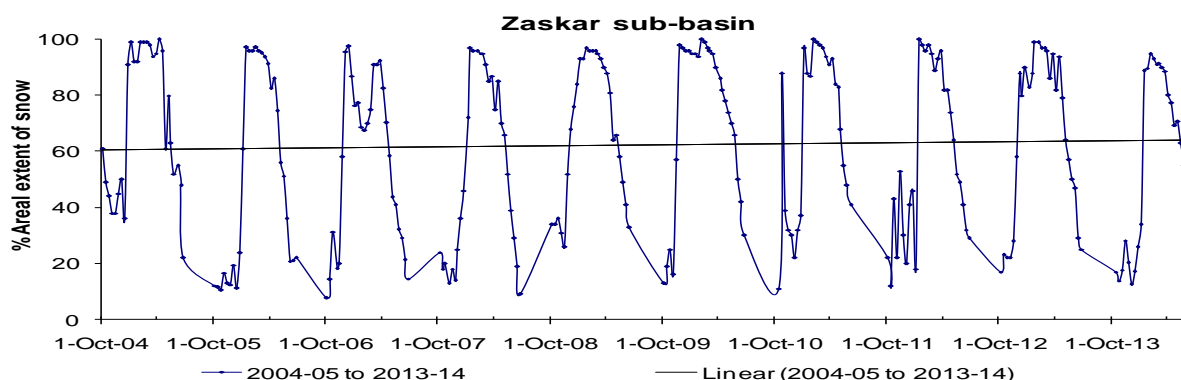


Figure 41: Changes in snow cover area and its trend during time frame 2004 to 2014 for Zaskar sub-basin of the Indus basin

ii) Chenab basin

Chenab basin comprises six sub-basins. The sub-basins are Miyar, Bhaga, Chandra, Warwan, and Bhut and Ravi. The following paragraphs describe temporal and spatial variability of snow cover in the sub-basins of Chenab basin.

Minimum and maximum snow cover

For each sub-basin of Chenab basin, the minimum and maximum snow cover in each hydrological year from 2004-05 to 2013-14 has been compiled in the Tables from 16 to 21. Referring to data compiled in these tables, it is observed that mean of minimum snow cover is highest in Chandra sub-basin and lowest in Ravi sub-basin. There is a large variation of minimum snow cover in each hydrological year and in each sub-basin. The SD values of minimum snow cover indicate a large variation in minimum snow cover. The mean values of maximum snow cover show 95 to 100 % snow cover each year except in Ravi sub-basin. The SD values of maximum snow cover show relatively less variation in maximum snow cover except in Ravi sub-basin.

The maximum and minimum amount of minimum snow cover also varies in each sub-basin. Overall the minimum snow cover was lowest in Chenab basin in the 2013-14 year. The quantity of minimum snow cover varies in each year for different sub-basins and is not uniformly same. This suggests that within Chenab basin also the different sub-basins experience different amount of precipitation in different years.

Table 16: Minimum and maximum snow cover in Warwan sub-basin during 2004- 14

Warwan sub-basin (4670 sq. km)				
Year	Minimum snow cover		Maximum snow cover	
	Sq. km	%	Sq. km	%
2004-05	1868	40	4670	100
2005-06	747	16	4110	88
2006-07	1401	30	4203	90
2007-08	887	19	4483	96
2008-09	1074	23	4063	87
2009-10	1354	29	4670	100
2010-11	701	15	4483	96
2011-12	747	16	4623	99
2012-13	1261	27	4530	97
2013-14	607	13	4483	96
Mean	1065	23	4432	95
S D	402	9	226	5

Table 17: Minimum and maximum snow cover in Bhut sub-basin during 2004-14

Bhut sub-basin (2218 sq km)				
Year	Minimum snow cover		Maximum snow cover	
	Sq km	%	Sq km	%
2004-05	976	44	2218	100
2005-06	488	22	1952	88
2006-07	399	18	2018	91
2007-08	555	25	2174	98
2008-09	466	21	1930	87
2009-10	421	19	2218	100
2010-11	444	20	2107	95
2011-12	444	20	2196	99
2012-13	665	30	2151	97
2013-14	421	19	2151	97
Mean	528	24	2112	95
S D	176	8	107	5

Table 18: Minimum and maximum snow cover in Miyar sub-basin during 2004-14

Miyar sub-basin (4449 sq km)				
Year	Minimum snow cover		Maximum snow cover	
	Sq km	%	Sq km	%
2004-05	1913	43	4449	100
2005-06	845	19	4405	99
2006-07	578	13	4360	98
2007-08	890	20	4449	100
2008-09	1335	30	4360	98
2009-10	756	17	4449	100
2010-11	667	15	4449	100
2011-12	756	17	4449	100
2012-13	1290	29	4449	100
2013-14	534	12	4449	100
Mean	956	22	4427	100
S D	431	10	38	1

Table 19: Minimum and maximum snow cover in Bhaga sub-basin during 2004-14

Bhaga sub-basin (1680 sq km)				
Year	Minimum snow cover		Maximum snow cover	
	Sq km	%	Sq. km	%
2004-05	1159	69	1680	100
2005-06	638	38	1663	99
2006-07	420	25	1680	100
2007-08	504	30	1680	100
2008-09	840	50	1680	100
2009-10	672	40	1680	100
2010-11	622	37	1680	100
2011-12	470	28	1680	100
2012-13	907	54	1680	100
2013-14	353	21	1680	100
Mean	659	39	1678	100
S D	249	15	5	0

Table 20: Minimum and maximum snow cover in Chandra sub-basin during 2004-14

Chandra sub-basin (2433 sq km)				
Year	Minimum snow cover		Maximum snow cover	
	Sq. km	%	Sq. km	%
2004-05	1825	75	2433	100
2005-06	925	38	2433	100
2006-07	706	29	2433	100
2007-08	1362	56	2433	100
2008-09	1484	61	2433	100
2009-10	1435	59	2433	100
2010-11	1241	51	2433	100
2011-12	754	31	2433	100
2012-13	1314	54	2433	100
2013-14	633	26	2433	100
Mean	1168	48	2433	100
S D	394	16	0	0

Table 21: Minimum and maximum snow cover in Ravi sub-basin during 2004-14

Ravi sub-basin (4907 sq. km)				
Year	Minimum snow cover		Maximum snow cover	
	Sq. km	%	Sq. km	%
2004-05	785	16	4465	91
2005-06	294	6	3091	63
2006-07	196	4	3827	78
2007-08	245	5	3827	78
2008-09	491	10	3190	65
2009-10	442	9	4220	86
2010-11	245	5	4760	97
2011-12	147	3	4564	93
2012-13	196	4	4024	82
2013-14	294	6	4171	85
Mean	334	7	4014	82
S D	192	4	551	11

Monthly accumulation and ablation patterns (2008-2014) and Annual changes (2004-2014) of snow cover

As also observed earlier section in Indus basin there is large unevenness in the accumulation pattern of snow cover in Chenab basin. The accumulation and ablation pattern of snow cover in sub-basins of Chenab basin are shown in Figures 42 to 47. One common observation during the accumulation is that there is sharp rise of snow fall in year 2012-13 in middle of November. The pattern of snow fall and subsequent

melting of snow up to middle of January is common in all the sub-basins. There is quite similarity in melting of snow cover from early march onwards. The slopes of ablation are also gentle. This indicates that there is no sudden rise of temperature up to end of June. In some of the sub-basins the snow cover becomes 100 % but in the sub-basins located in lower altitude such as Ravi sub-basin the snow cover does not reach 100 %. The slopes of accumulation and ablation in Ravi sub-basin are sharper as compared to her sub-basins. In Chandra basin the minimum snow cover before and after ablation season more or less remains same. Chandra and Bhaga sub-basins behave more or less in similar way as they are located near to each other. Warwan and Bhut sub-basins behave in a similar way as they are closer to each other geographically but quite away from Chandra and Bhaga sub-basins. Miyar sub-basin is located north of Chandra and Bhaga. Ravi sub-basin mainly drains in Kangra district and is climatically located much away from Chandra and Bhaga basin and thus respond differently to snow precipitation and melting.

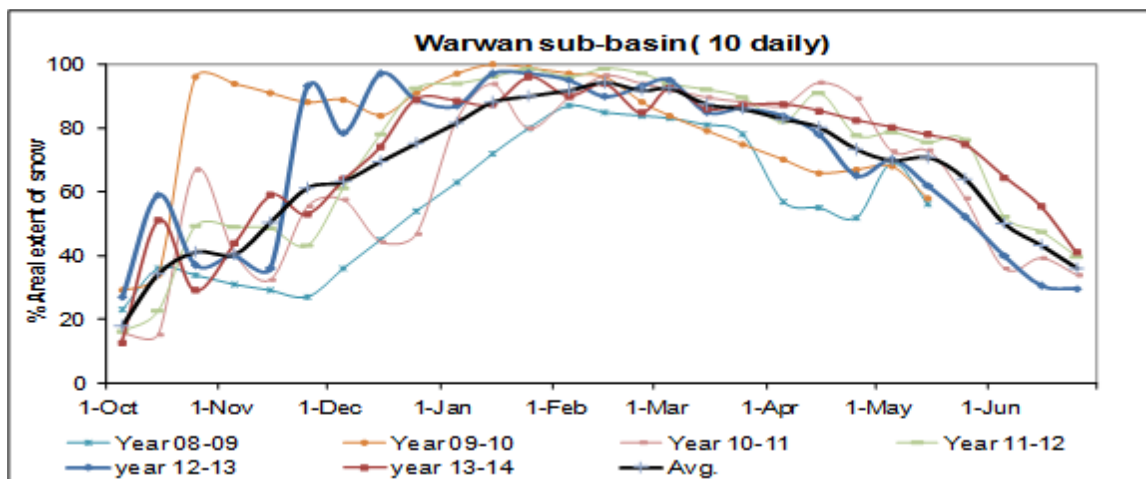


Figure 42: Accumulation and ablation pattern of snow cover for Warwan sub-basin (Chenab basin) between 2008 and 2014

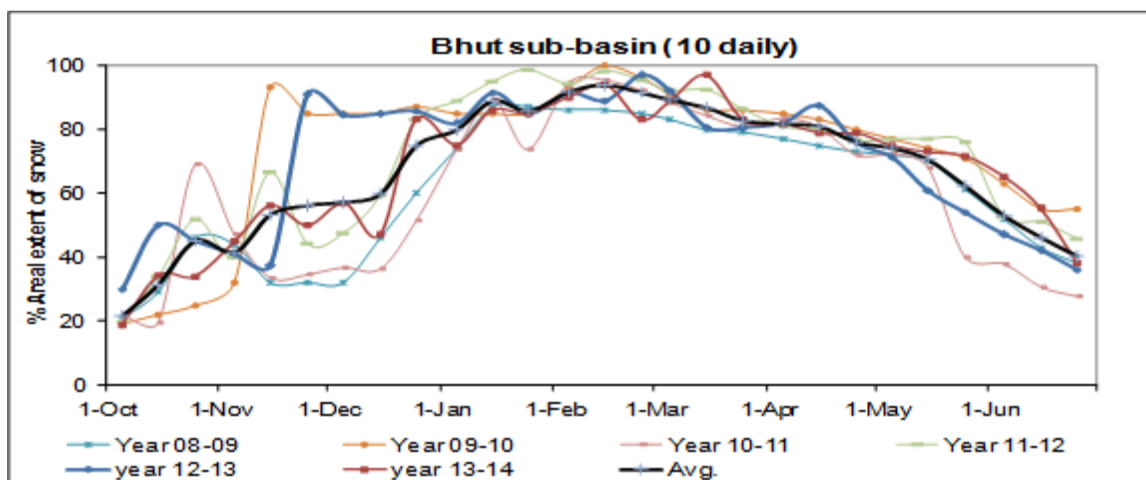


Figure 43: Accumulation and ablation pattern of snow cover for Bhut sub-basin (Chenab basin) between 2008 and 2014

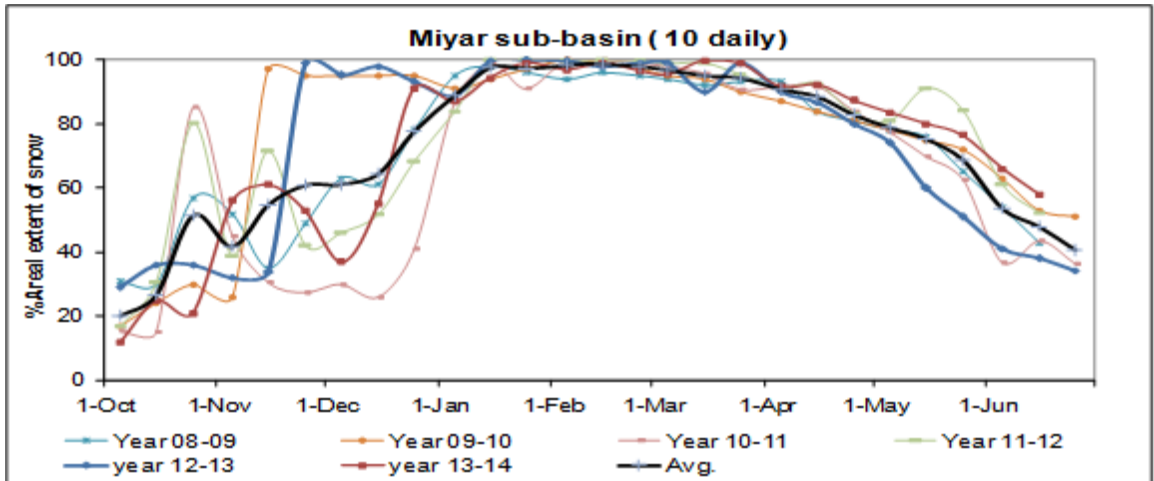


Figure 44: Accumulation and ablation pattern of snow cover for Miyar sub-basin (Chenab basin) between 2008 and 2014

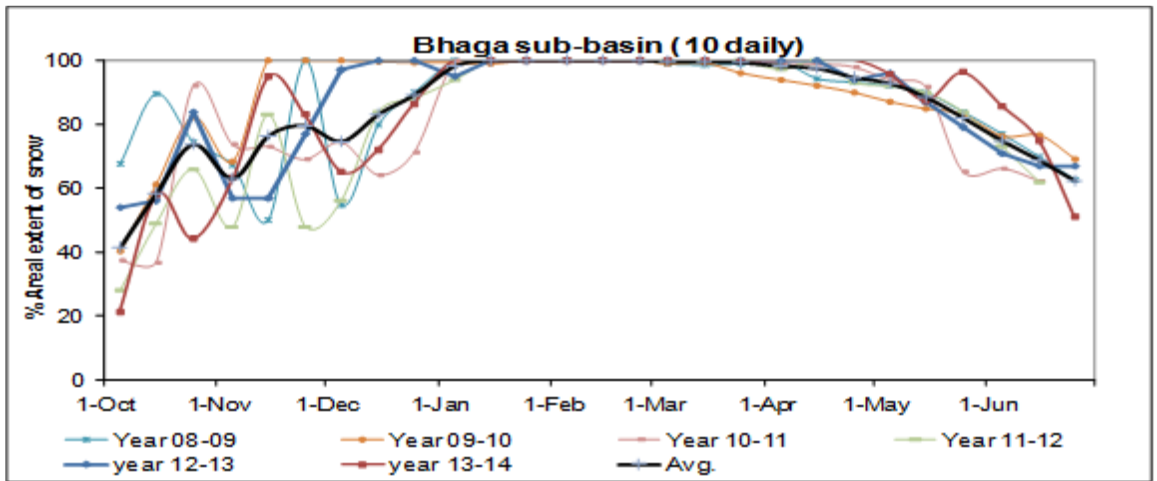


Figure 45: Accumulation and ablation pattern of snow cover for Bhaga sub-basin (Chenab basin) between 2008 and 2014

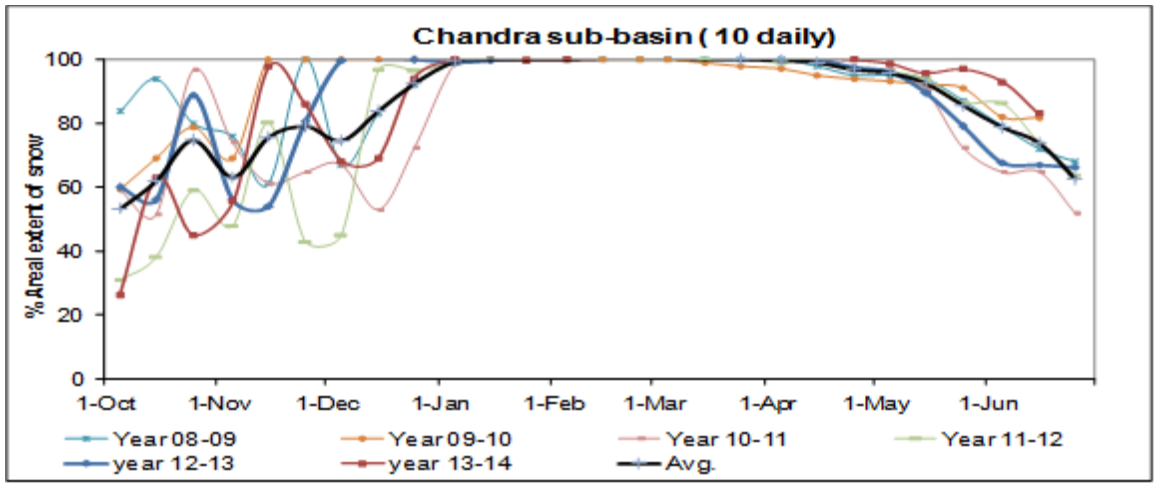


Figure 46: Accumulation and ablation pattern of snow cover for Chandra sub-basin (Chenab basin) between 2008 and 2014

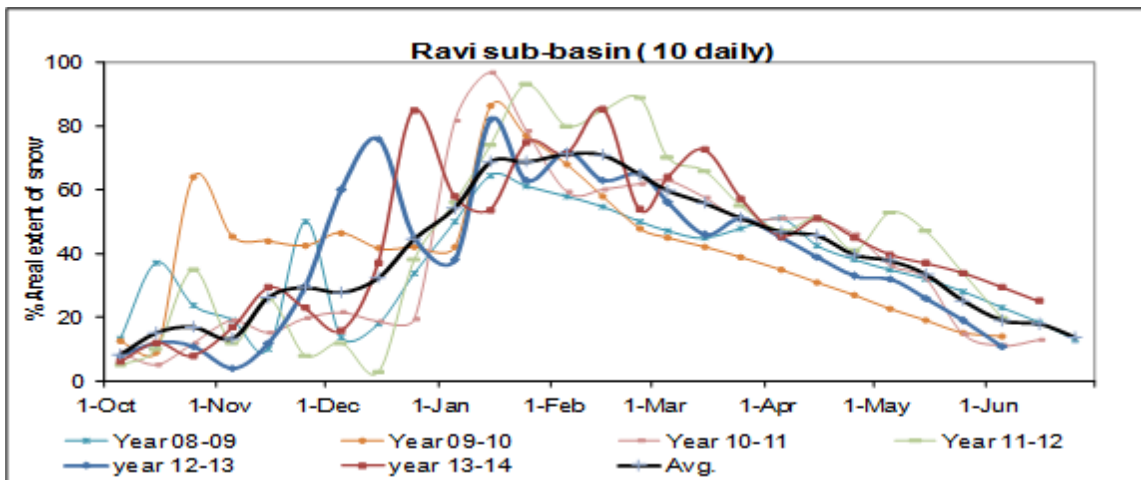


Figure 47: Accumulation and ablation pattern of snow cover for Ravi sub-basin (Chenab basin) between 2008 and 2014

Changes in snow cover for the duration 2004-2014 in sub-basins of the Chenab basin are shown in Figure 48 to Figure 53. It is observed that Ravi sub-basin shows minimum snow cover (5 to 70%), while remaining sub-basins show snow cover changes ranging 20 to 100% annually. All the sub-basins are showing a marginal increasing trend of snow cover during 2004-2014 time frame.

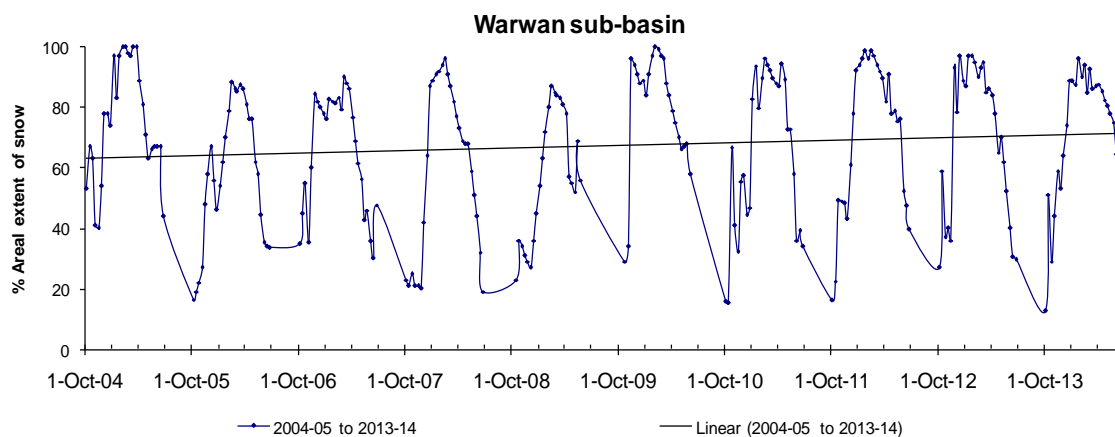


Figure 48: Changes in snow cover area and its trend during time frame 2004 to 2014 for Warwan sub-basin of the Chenab basin

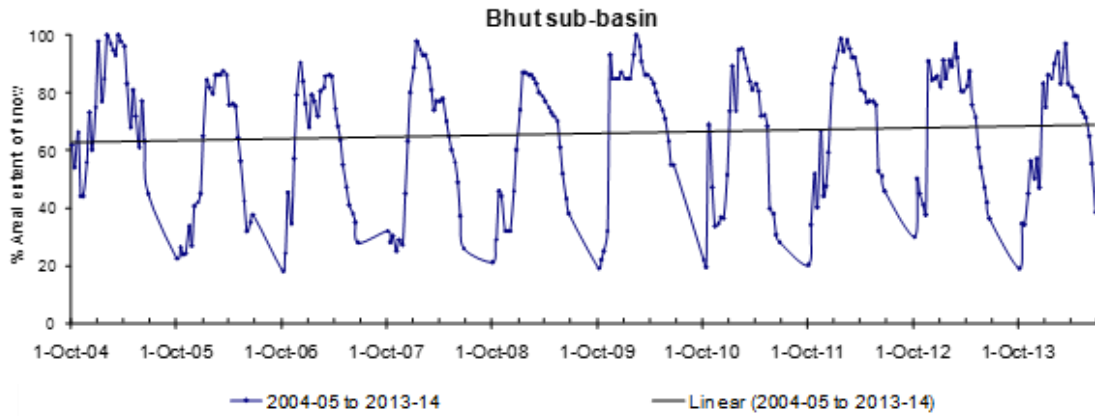


Figure 49: Changes in snow cover area and its trend during time frame 2004 to 2014 for Bhut sub-basin of the Chenab basin

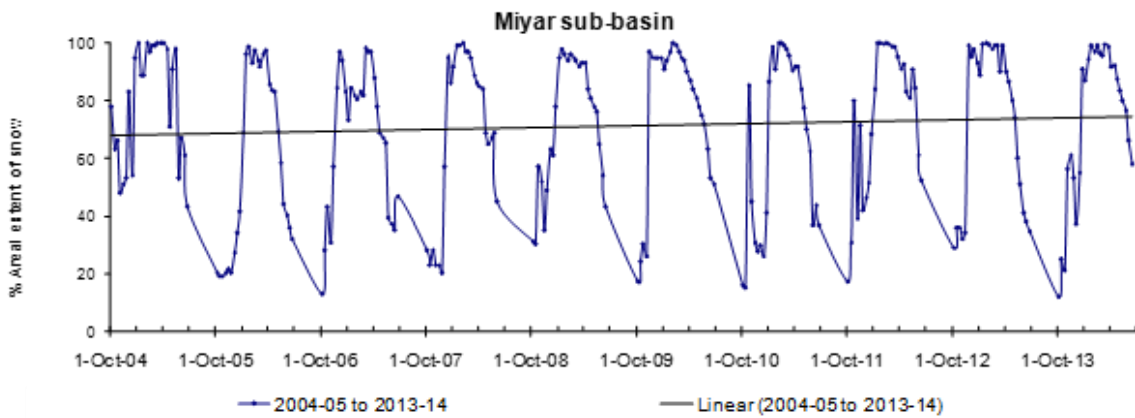


Figure 50: Changes in snow cover area and its trend during time frame 2004 to 2014 for Miyar sub-basin of the Chenab basin

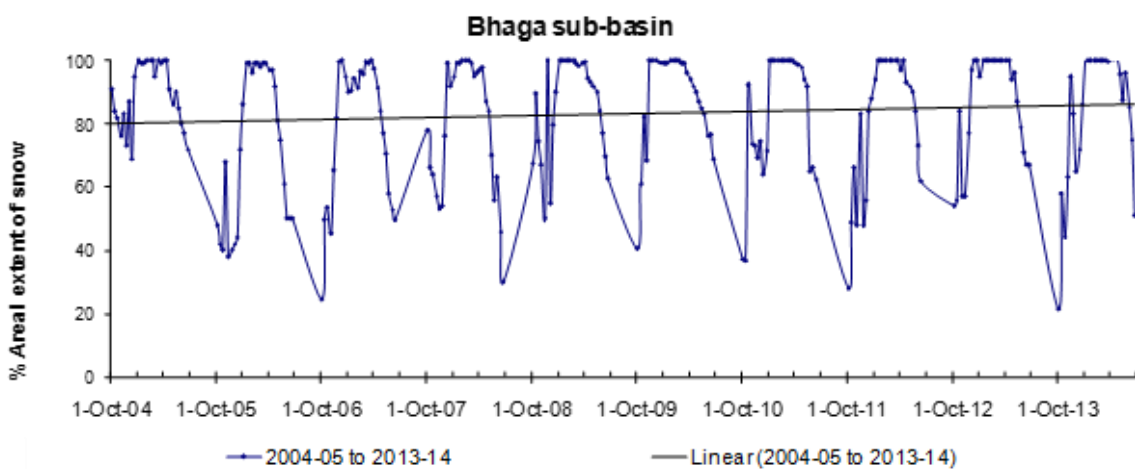


Figure 51: Changes in snow cover area and its trend during time frame 2004 to 2014 for Bhaga sub-basin of the Chenab basin

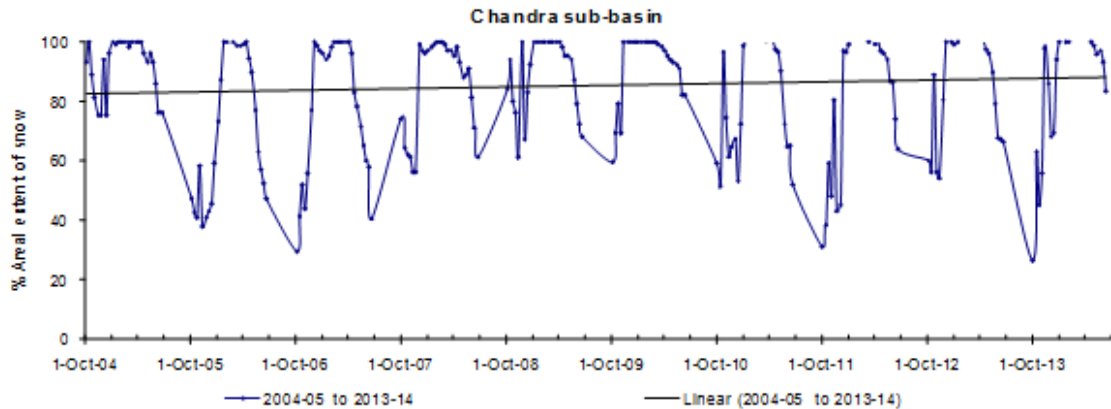


Figure 52: Changes in snow cover area and its trend during time frame 2004 to 2014 for Chandra sub-basin of the Chenab basin

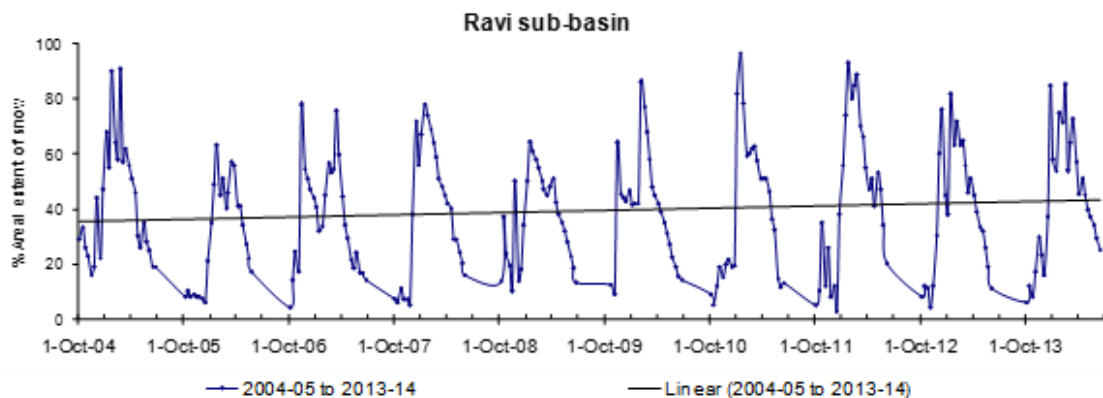


Figure 53: Changes in snow cover area and its trend during time frame 2004 to 2014 for Ravi sub-basin of the Chenab basin

iii) Satluj basin

Satluj basin comprises six sub-basins covering 15583 sq km area. The sub-basins are Beas, Parbati, Jiwa, Baspa, Pin and Spiti sub-basins. Parbati and Jiwa river are tributary of Beas river. Beas, Baspa, Pin & Spiti are tributary of Satluj river.

Maximum and minimum snow cover

For each sub-basin of Satluj basin the minimum and maximum snow cover in each hydrological year from 2004-05 to 2013-14 has been compiled in the Tables 22 to 27. The snow cover has been represented in absolute value and in percentage. Mean and standard deviations (SD) of snow cover are also mentioned in the tables.

The mean of minimum snow cover in % varies from 9 to 37 for different sub-basins. The SD of minimum snow cover varies from 4 to 23. This is a large variation in snow cover in each year for different sub-basins. The mean of minimum snow cover is high in Pin, Basapa and Parbati sub-basins and very low in rest of sub-basins. The mean

of maximum snow cover is high in almost all the sub-basins except in Jiwa sub-basin. The variation in maximum snow cover is seen more in Jiwa sub-basin. The maximum and minimum amount of minimum snow cover also varies in each sub-basin. This suggests that within Satluj basin also the different sub-basins experience different amount of precipitation in different years.

Table 22: Minimum and maximum snow cover in Beas sub-basin during 2004-14

Beas sub-basin (1132 sq. km)				
Year	Minimum snow cover		Maximum snow cover	
	Sq. km	%	Sq. km	%
2004-05	204	18	996	88
2005-06	79	7	872	77
2006-07	45	4	928	82
2007-08	102	9	917	81
2008-09	158	14	804	71
2009-10	125	11	1109	98
2010-11	68	6	940	83
2011-12	45	4	1121	99
2012-13	79	7	1109	98
2013-14	102	9	1075	95
Mean	101	9	987	87
S D	50	4	112	10

Table 23: Minimum and maximum snow cover in Parbati sub-basin during 2004-14

Parbati sub-basin (1773 sq. km)				
Year	Minimum snow cover		Maximum snow cover	
	Sq. km	%	Sq. km	%
2004-05	904	51	1613	91
2005-06	479	27	1489	84
2006-07	426	24	1578	89
2007-08	638	36	1578	89
2008-09	851	48	1472	83
2009-10	762	43	1738	98
2010-11	656	37	1578	89
2011-12	426	24	1720	97
2012-13	638	36	1738	98
2013-14	372	21	1720	97
Mean	615	35	1622	92
S D	186	11	101	6

Table 24: Minimum and maximum snow cover in Jiwa sub-basin during 2004-14

Jiwa sub-basin (1445 sq. km)				
Year	Minimum snow cover		Maximum snow cover	
	Sq. km	%	Sq. km	%
2004-05	246	17	968	67
2005-06	116	8	751	52
2006-07	87	6	838	58
2007-08	173	12	983	68
2008-09	202	14	665	46
2009-10	173	12	1214	84
2010-11	101	7	910	63
2011-12	87	6	1344	93
2012-13	145	10	1344	93
2013-14	72	5	1199	83
Mean	140	10	1022	71
S D	57	4	242	17

Table 25: Minimum and maximum snow cover in Baspa sub-basin during 2004-14

Baspa sub-basin (1096 sq. km)				
Year	Minimum snow cover		Maximum snow cover	
	Sq. km	%	Sq. km	%
2004-05	504	46	1096	100
2005-06	274	25	1074	98
2006-07	175	16	1096	100
2007-08	219	20	1096	100
2008-09	406	37	1052	96
2009-10	449	41	1096	100
2010-11	449	41	1052	96
2011-12	197	18	1096	100
2012-13	252	23	1096	100
2013-14	252	23	1096	100
Mean	318	29	1085	99
S D	121	11	19	2

Table 26: Minimum and maximum snow cover in Pin sub-basin during 2004-14

Pin sub-basin (1266 sq. km)				
Year	Minimum snow cover		Maximum snow cover	
	Sq. km	%	Sq. km	%
2004-05	696	55	1266	100
2005-06	342	27	1266	100
2006-07	329	26	1266	100
2007-08	506	40	1266	100
2008-09	658	52	1266	100
2009-10	671	53	1266	100
2010-11	481	38	1266	100
2011-12	203	16	1266	100
2012-13	380	30	1266	100
2013-14	203	16	1266	100
Mean	447	35	1266	100
S D	186	15	0	0

Table 27: Minimum and maximum snow cover in Spiti sub-basin during 2004-14

Spiti sub-basin (8871 sq. km)				
Year	Minimum snow cover		Maximum snow cover	
	Sq. km	%	Sq. km	%
2004-05	2306	26	8782	99
2005-06	1419	16	8427	95
2006-07	444	5	8427	95
2007-08	1508	17	8427	95
2008-09	2306	26	8427	95
2009-10	2218	25	8516	96
2010-11	1952	22	8871	100
2011-12	532	6	8871	100
2012-13	976	11	8871	100
2013-14	710	8	8871	100
Mean	1437	16	8649	98
S D	741	8	218	2

Monthly accumulation and ablation patterns (2008-2014) and Annual changes (2004-2014) of snow cover

The accumulation or ablation pattern of snow cover in sub-basins of Satluj basin are shown in Figures 54 to 59. The pattern of accumulation in all the sub-basins are closely matching indicating sharp rise in slopes or precipitation and subsequent melting. The pattern of snow accumulation is similar in Parbati and Beas sub-basins. It is similar in Basapa, Pin and Spiti sub-basins. The precipitation in Jiwa sub-basin is different than in other sub-basins. This likely due to geographical and climatic similarity. Slopes of

accumulation are steeper than in ablation. This is commonly observed in all sub-basins of Himalaya except in North-Western region. In the pattern of accumulation there is an unevenness indicating precipitation followed by melting. The unevenness is more in Basapa, Pin and Spiti sub-basins than in Beas and Parbati sub-basins. There are certain anomalies too. Maximum snow cover is attained in middle of January. The slopes of accumulation and ablation are sharper. Those sub-basins which are at higher altitude, the maximum snow cover reaches to 100 % and remains there for at least two months. The lowest part of ablation curves indicates that by end of June the snow cover does not reach to a low value in certain sub-basins as observed in Parbati and Pin sub-basins. The slope of ablation of Beas and Spiti sub-basins is steeper indicating a rapid decline in snow or melting.

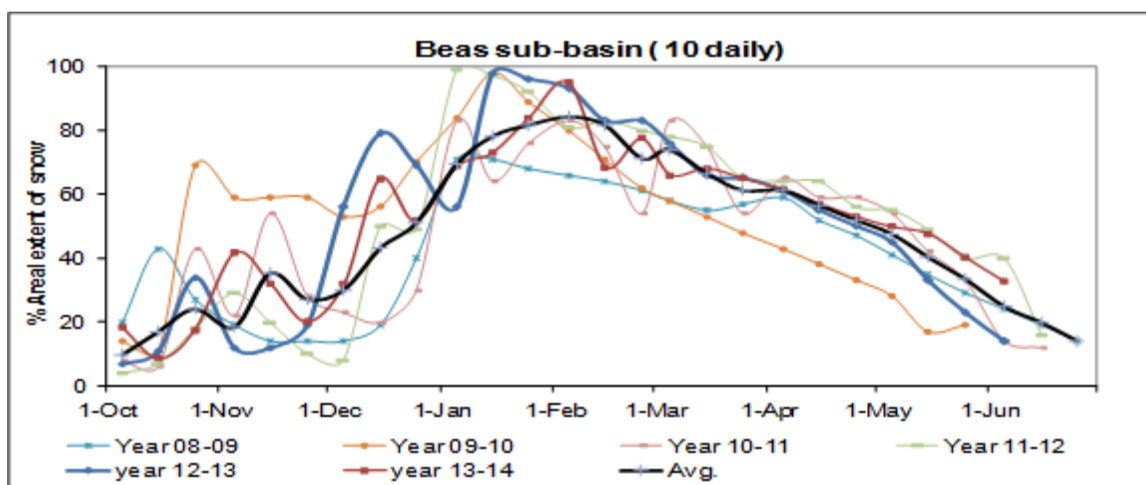


Figure 54: Accumulation and ablation pattern of snow cover for Beas sub-basin (Satluj basin) between 2008 and 2014

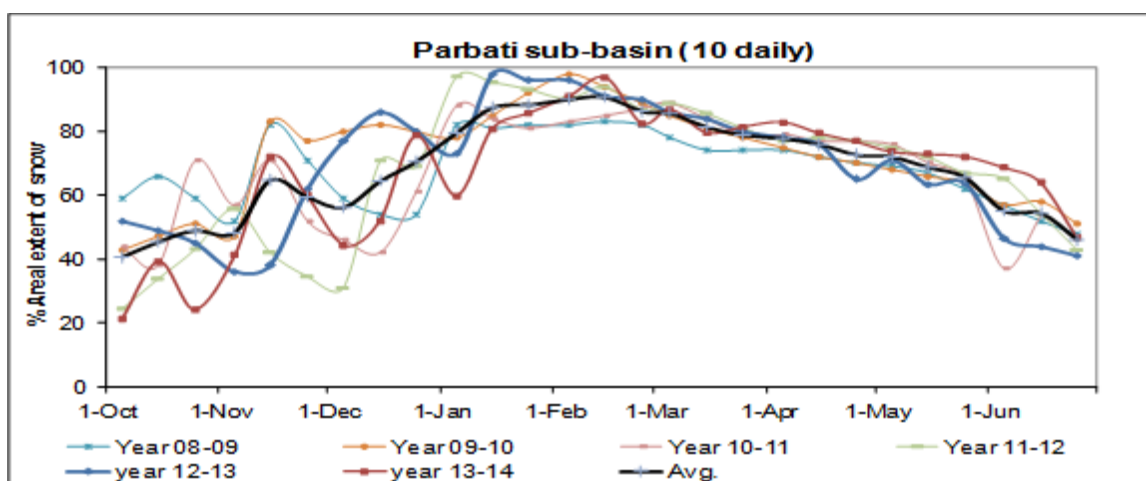


Figure 55: Accumulation and ablation pattern of snow cover for Parbati sub-basin (Satluj basin) between 2008 and 2014

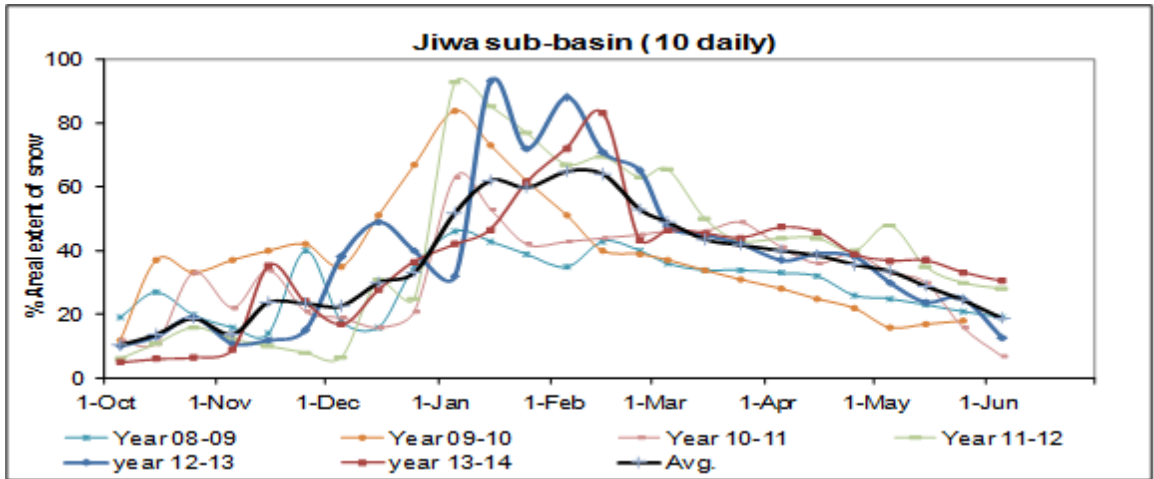


Figure 56: Accumulation and ablation pattern of snow cover for Jiwa sub-basin (Satluj basin) between 2008 and 2014

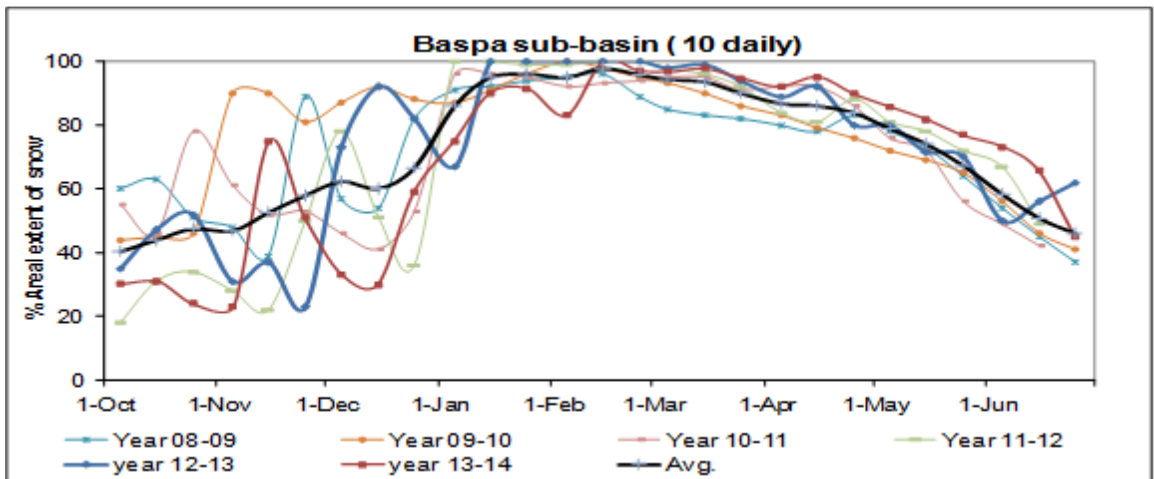


Figure 57: Accumulation and ablation pattern of snow cover for Baspa sub-basin (Satluj basin) between 2008 and 2014

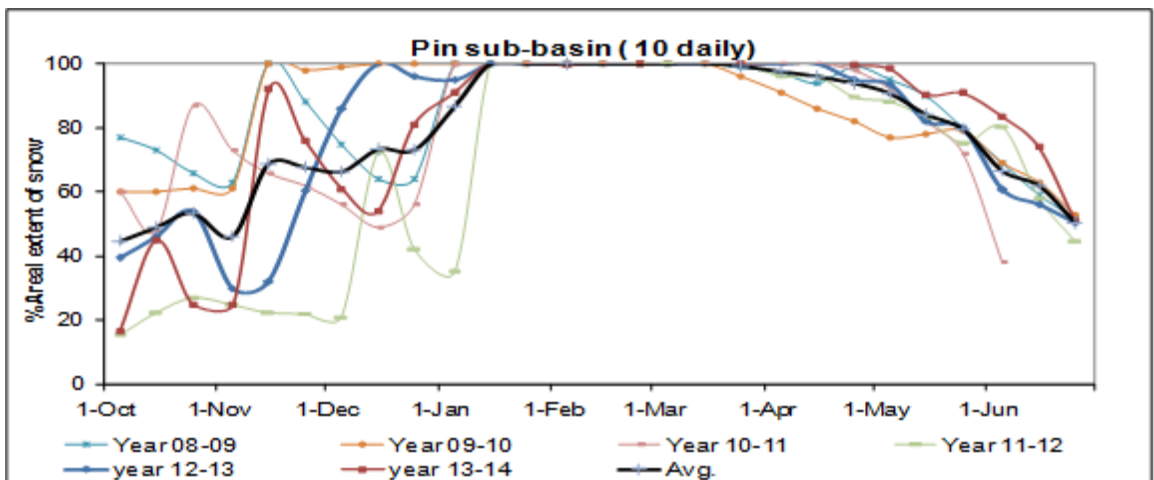


Figure 58: Accumulation and ablation pattern of snow cover for Pin sub-basin (Satluj basin) between 2008 and 2014

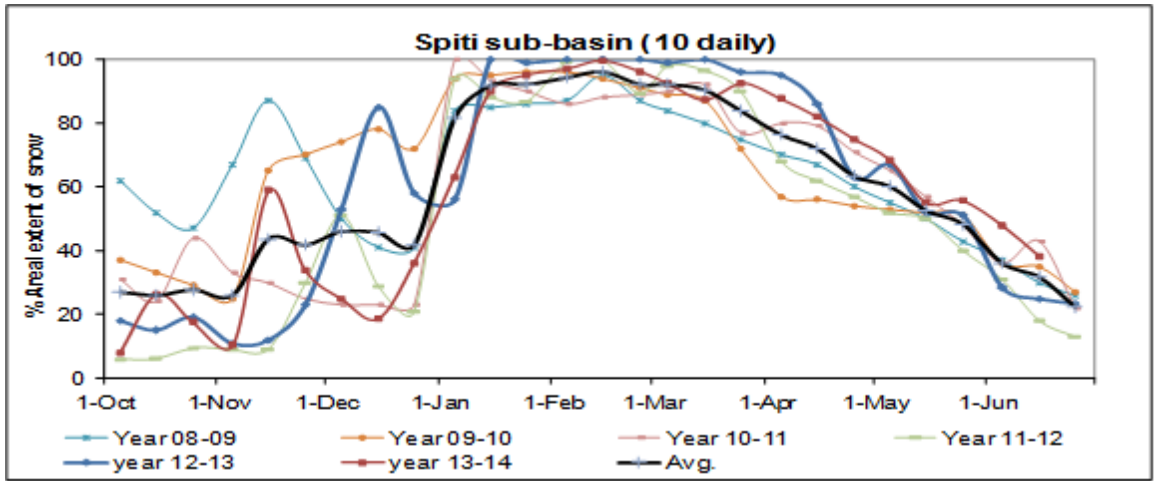


Figure 59: Accumulation and ablation pattern of snow cover for Spiti sub-basin (Satluj basin) between 2008 and 2014

Monthly accumulation and ablation patterns (2008-2014) and Annual changes (2004-2014) of snow cover

Figures 60 to 65 show trend of snow cover in each sub-basin from 2004 to 2014. There is slight increase in snow cover of the order of 0 to 10 % in Beas, Parbati and Jiwa sub-basin. But in Basapa, Pin and Spiti sub-basins, no trend of decrease or increase of snow cover is observed.

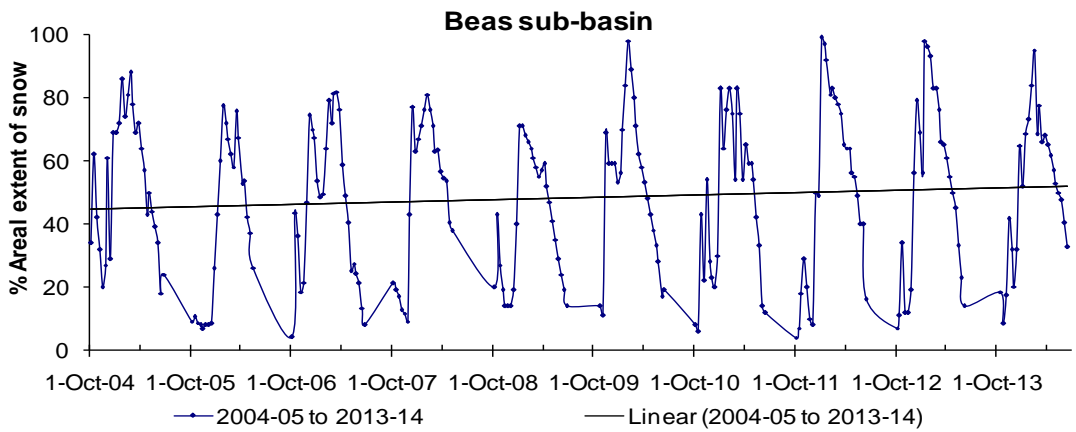


Figure 60: Changes in snow cover area and its trend during time frame 2004 to 2014 for Beas sub-basin of the Satluj basin

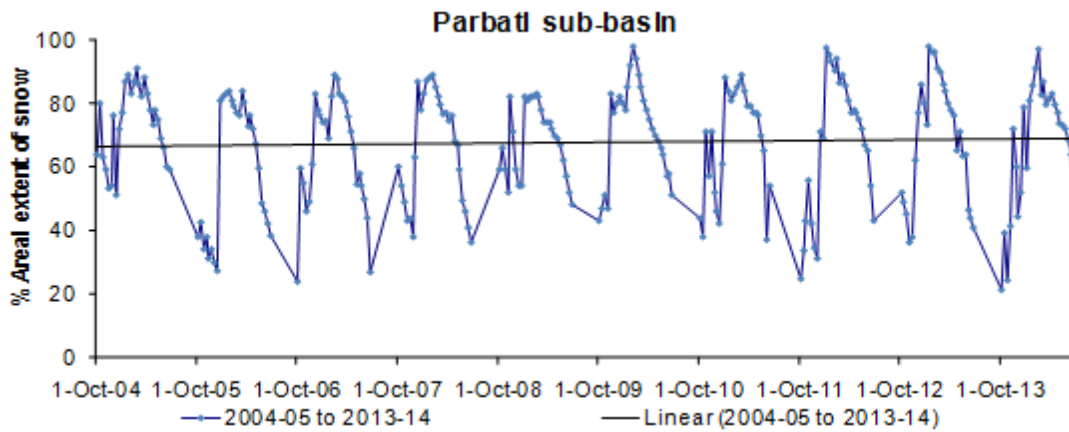


Figure 61: Changes in snow cover area and its trend during time frame 2004 to 2014 for Parbati sub-basin of the Satluj basin

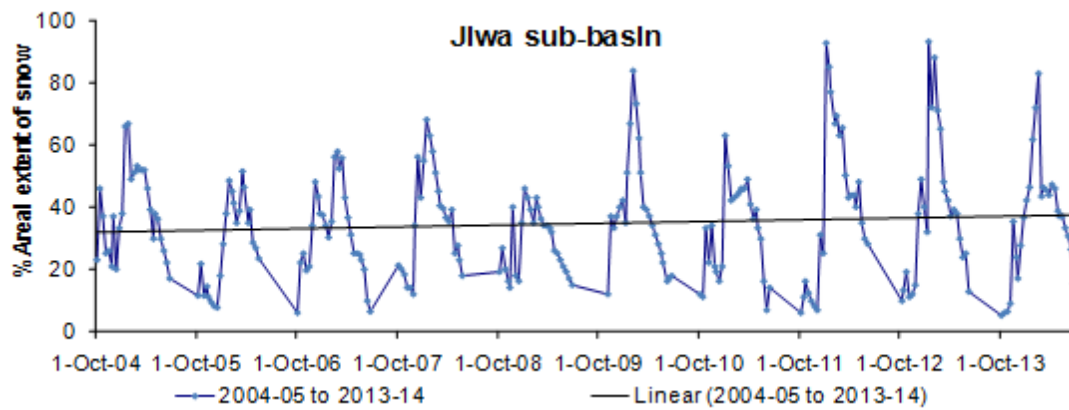


Figure 62: Changes in snow cover area and its trend during time frame 2004 to 2014 for Jiwa sub-basins of the Satluj basin

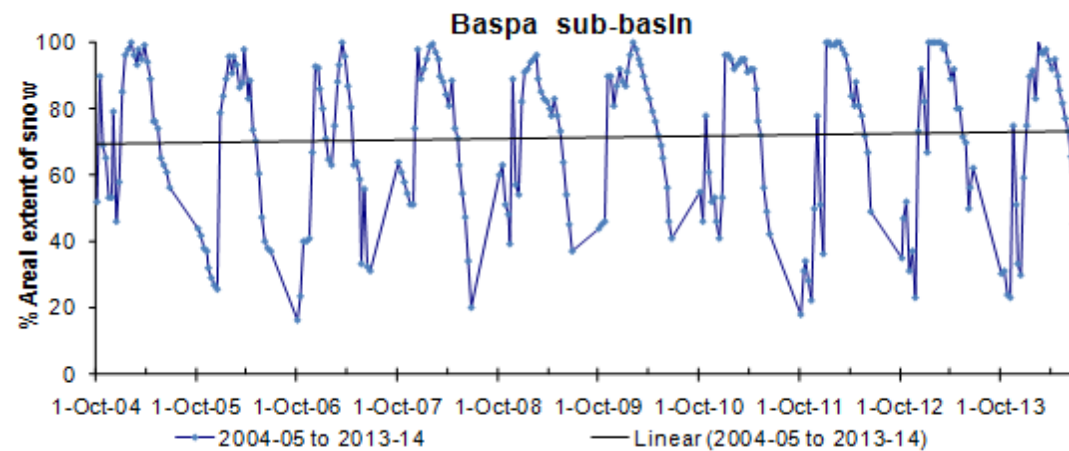


Figure 63: Changes in snow cover area and its trend during time frame 2004 to 2014 for Baspa sub-basins of the Satluj basin

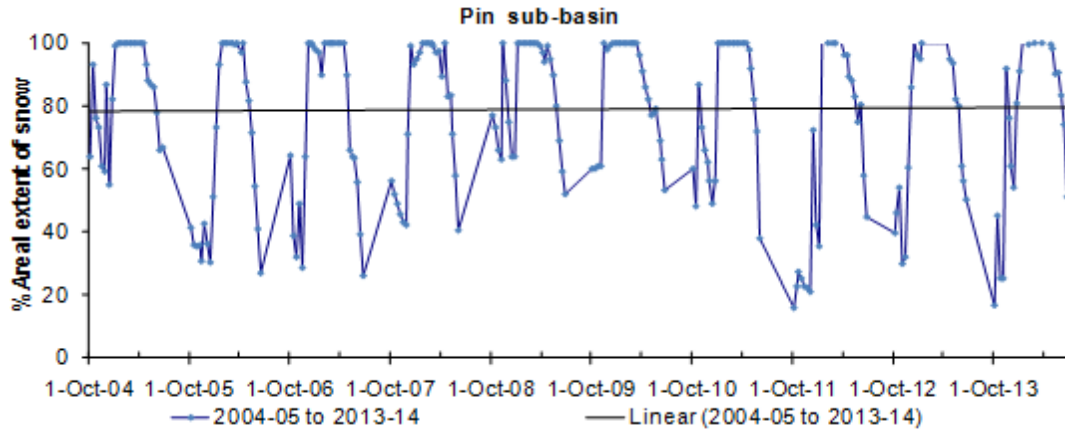


Figure 64: Changes in snow cover area and its trend during time frame 2004 to 2014 for Pin sub-basin of the Satluj basin

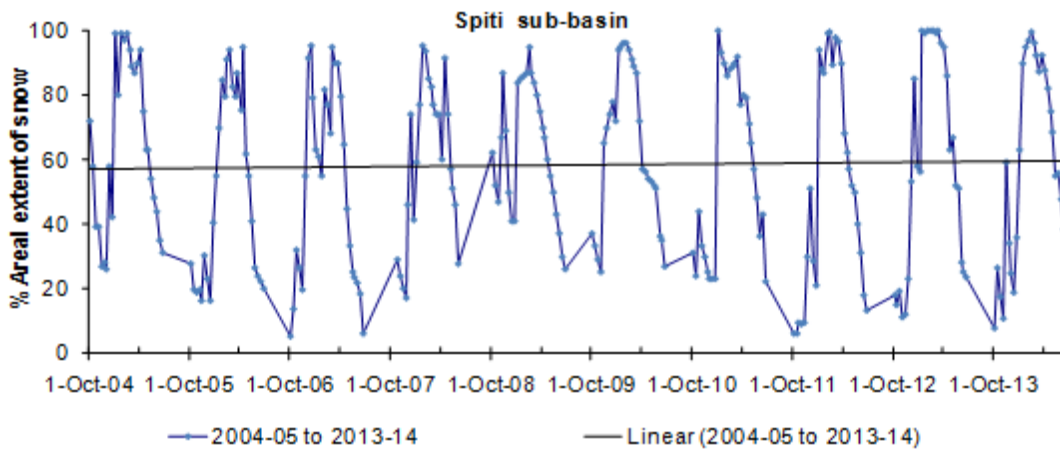


Figure 65: Changes in snow cover area and its trend during time frame 2004 to 2014 for Spiti sub-basins of the Satluj basin

iv) Ganga basin

Three sub-basins have been monitored in Ganga basin covering 22055 sq. km area viz., Bhagirathi, Yamuna and Alaknanda sub-basins. Alaknanda sub-basin is in east of Bhagirathi and Yamuna is in west of it.

Minimum and maximum snow cover

The following Tables 28-30 present the amount of minimum and maximum snow cover in three sub-basins. There is not much variation in mean of minimum snow cover as indicated by SD values. However, the variation of maximum snow cover is higher. The minimum snow cover varies between 9 to 21 %. It is very low in year 2005-06 and

2006-07. The maximum snow cover in Bhagirathi sub basin varies between 54 to 79 %. In most of the years it is below 70 % except in year 2011-12 and 2013-14. The SD values suggest low values for all three sub-basins. This suggest less variability of snow cover in Ganga basin in comparison to other basins.

Table 28: Minimum and maximum snow cover in Bhagirathi sub-basin during 2004-14

Bhagirathi sub-basin (7438 sq. km)				
Year	Minimum snow cover		Maximum snow cover	
	Sq. km	%	Sq. km	%
2004-05	1562	21	4909	66
2005-06	818	11	3942	53
2006-07	669	9	4165	56
2007-08	1339	18	4165	56
2008-09	1264	17	4017	54
2009-10	1190	16	4983	67
2010-11	1339	18	4017	54
2011-12	893	12	5876	79
2012-13	1041	14	4686	63
2013-14	818	11	5727	77
Mean	1093	15	4649	63
S D	289	4	716	10

Table 29: Minimum and maximum snow cover in Yamuna sub-basin during 2004-14

Yamuna sub-basin (3527 sq. km)				
Year	Minimum snow cover		Maximum snow cover	
	Sq. km	%	Sq. km	%
2004-05	459	13	2645	75
2005-06	212	6	1622	46
2006-07	141	4	1728	49
2007-08	388	11	2081	59
2008-09	353	10	1622	46
2009-10	353	10	2857	81
2010-11	317	9	1728	49
2011-12	282	8	3068	87
2012-13	353	10	2575	73
2013-14	317	9	3174	90
Mean	318	9	2310	66
S D	90	3	622	18

Table 30: Minimum and maximum snow cover in Alaknanda sub-basin during 2004-14

Alaknanda sub-basin (11090 sq km)				
Year	Minimum snow cover		Maximum snow cover	
	Sq. km	%	Sq. km	%
2004-05	2218	20	6765	61
2005-06	1996	18	5656	51
2006-07	1220	11	6321	57
2007-08	2551	23	5989	54
2008-09	1774	16	5545	50
2009-10	2107	19	7319	66
2010-11	2551	23	5878	53
2011-12	998	9	7874	71
2012-13	1553	14	6543	59
2013-14	1774	16	7985	72
Mean	1874	17	6588	59
S D	519	5	886	8

Monthly accumulation and ablation patterns (2008-2014) and Annual changes (2004-2014) of snow cover

In Bhagirathi sub-basin there is consistency in accumulation pattern except in one year. The snow cover varies between 20 to 80 % during accumulation period. The accumulation period is more uneven indicating precipitation and simultaneous melting. The maximum snow cover is observed in middle of February. Then there is a gradual decline in snow cover indicating gradual rise in temperature (Figure 66).

In Yamuna sub-basin snow cover varies from about 10 % to maximum 90 %. The decline in snow cover has higher slopes indicating sharp fall in snow cover. The peak of maximum snow cover is sharper in Yamuna sub-basin than in Bhagirathi basin (Figure 67).

In Alaknanda sub-basin the unevenness in accumulation is less than in Bhagirathi or Yamuna sub-basin. The maximum variation in accumulation is seen to vary between 20% to 70 %. The decline in snow cover is very gentle and similar to Bhagirathi sub-basin. Snow cover decline is consistent in all the years (Figure 68).

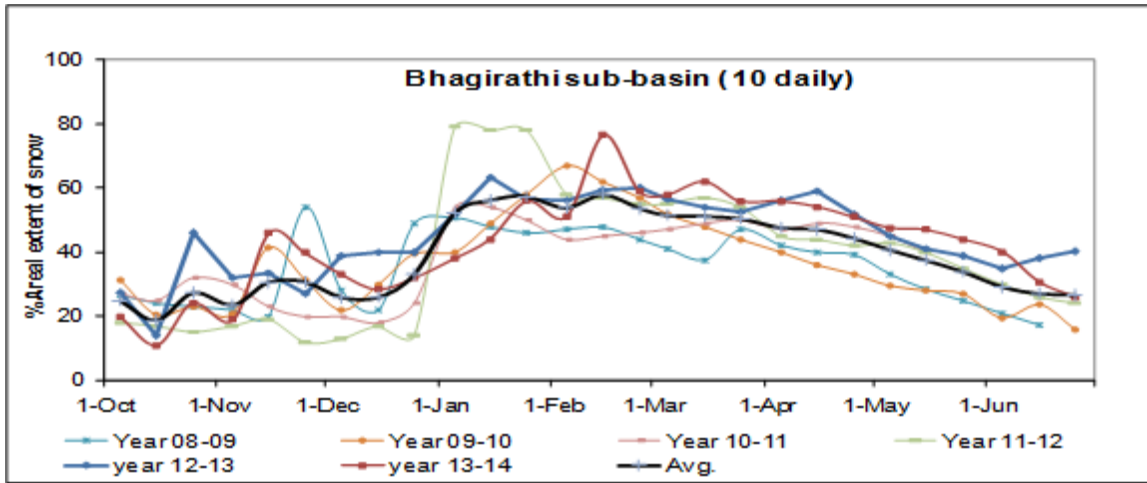


Figure 66: Accumulation and ablation pattern of snow cover for Bhagirathi sub-basin (Ganga basin) between 2008 and 2014

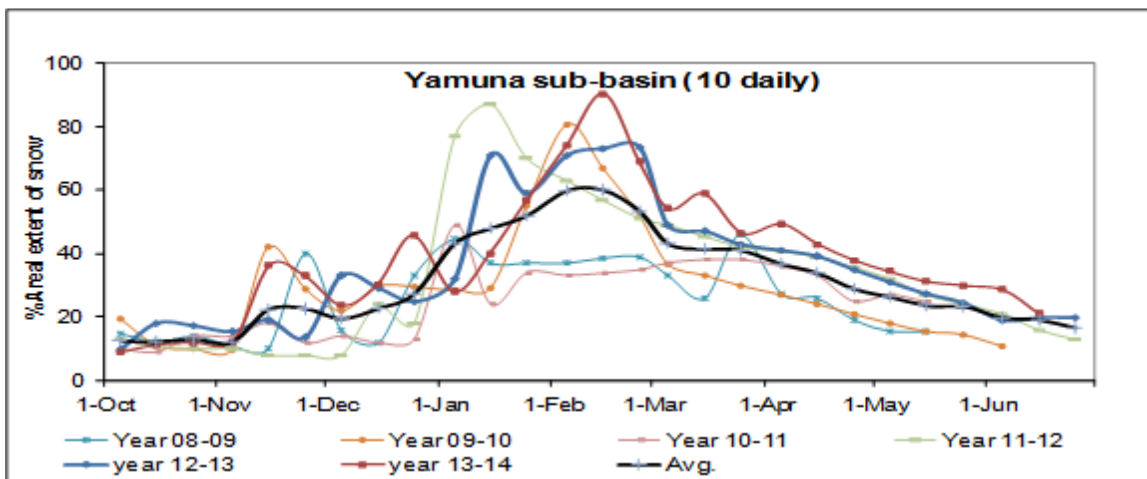


Figure 67: Accumulation and ablation pattern of snow cover for Yamuna sub-basin (Ganga basin) between 2008 and 2014

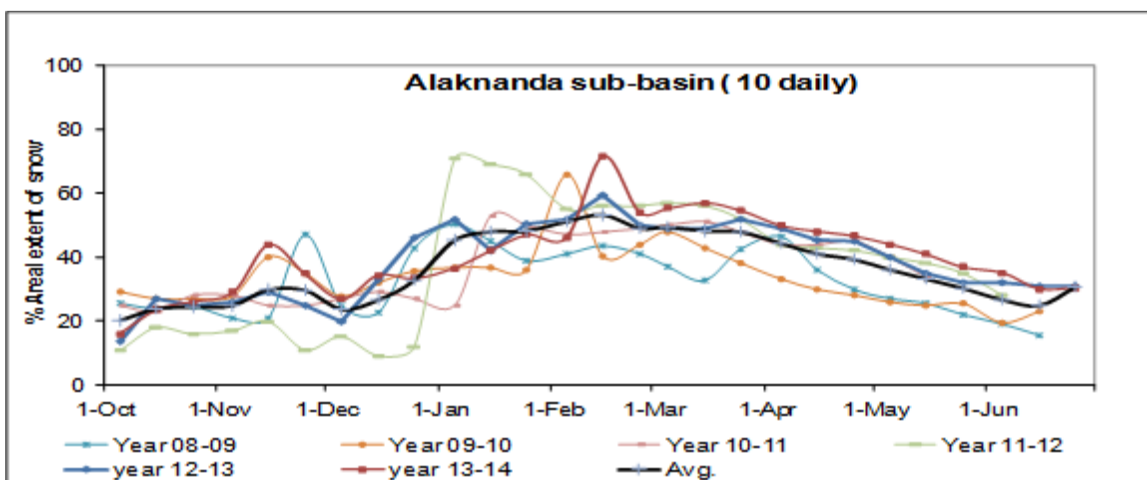


Figure 68: Accumulation and ablation pattern of snow cover for Alaknanda sub-basin (Ganga basin) between 2008 and 2014

Inter-annual variations indicate an increasing trend of snow cover in Bhagirathi sub-basin (Figure 69) and Yamuna sub-basins (Figure 70). The trend is consistent in Alaknanda basin (Figure 71).

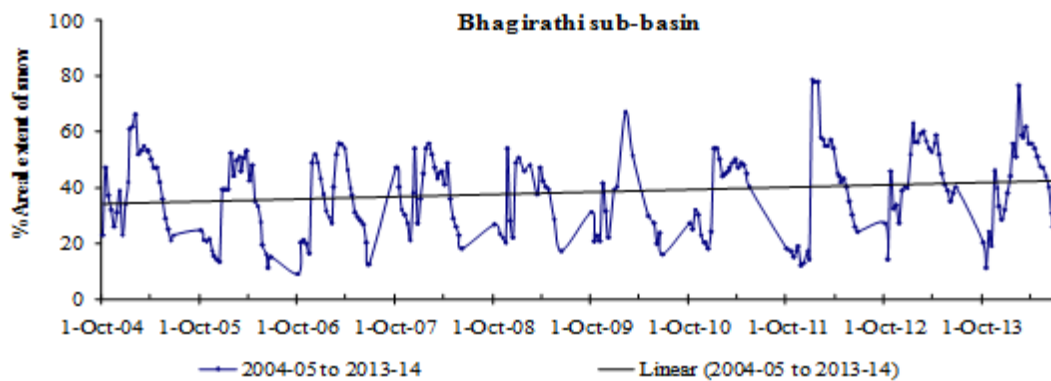


Figure 69: Changes in snow cover area and its trend during time frame 2004 to 2014 for Bhagirathi sub-basin of the Ganga basin

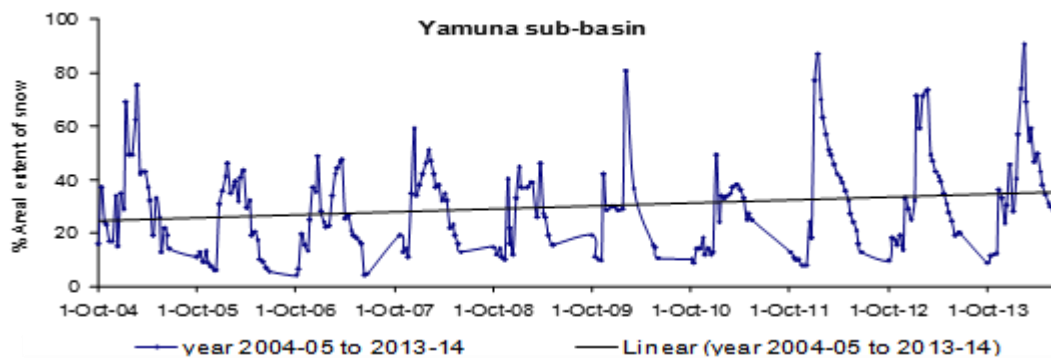


Figure 70: Changes in snow cover area and its trend during time frame 2004 to 2014 for Yamuna sub-basin of the Ganga basin

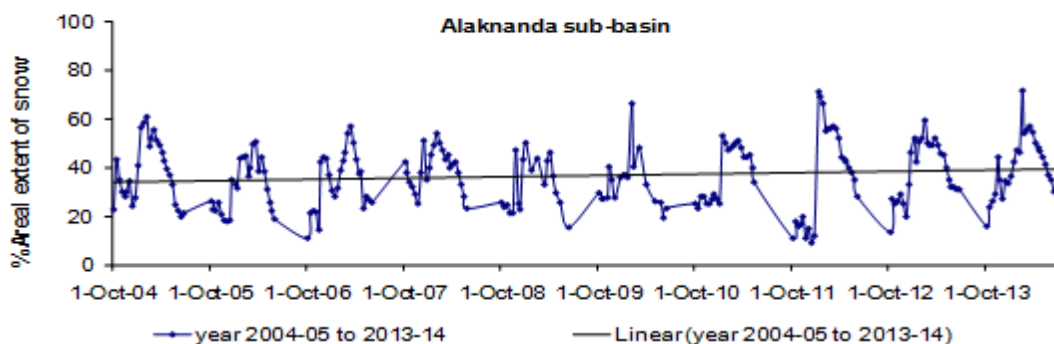


Figure 71: Changes in snow cover area and its trend during time frame 2004 to 2014 for Alaknanda sub-basin of the Ganga basin

v) Tista Basin

Tista basin has two sub-basins namely Tista and Rangit sub-basins covering 7096 sq. km area in Sikkim state. The spatial and temporal variability of these two sub-basins are discussed as following;

Minimum and maximum snow cover

The minimum and maximum snow cover in each hydrological year from 2004-05 to 2013-14 has been compiled in the Tables 31 and 32. It is observed from the data that Tista sub-basin gets more precipitation than Rangit sub-basin. The mean values of snow cover show that the minimum % of snow cover in Rangit sub-basin is much lesser than Tista sub-basin. The standard deviation of minimum snow cover suggests more temporal variability in Tista sub-basin than in Rangit sub-basin. and % of maximum snow cover is also less in Rangit. The data of maximum snow cover also shows higher % of snow cover in Tista sub-basin than in Rangit sub-basin. The SD values suggest close similarity in temporal variability of snow cover.

Table 31: Minimum and maximum snow cover in Tista sub-basin during 2004-14

Tista sub-basin (5466 sq km)				
Year	Minimum snow cover		Maximum snow cover	
	Sq. km	%	Sq. km	%
2004-05	1039	19	3280	60
2005-06	547	10	3006	55
2006-07	984	18	3662	67
2007-08	765	14	2569	47
2008-09	820	15	3006	55
2009-10	547	10	2733	50
2010-11	437	8	2842	52
2011-12	547	10	3389	62
2012-13	765	14	3772	69
2013-14	547	10	3498	64
Mean	700	13	3176	58
S D	206	4	406	7

Table 32: Minimum and maximum snow cover in Rangit sub-basin during 2004-14

Rangit sub-basin (1630 sq. km)				
Year	Minimum snow cover		Maximum snow cover	
	Sq. km	%	Sq. km	%
2004-05	82	5	310	19
2005-06	49	3	310	19
2006-07	65	4	489	30
2007-08	98	6	293	18
2008-09	49	3	310	19
2009-10	49	3	277	17
2010-11	33	2	228	14
2011-12	49	3	261	16
2012-13	33	2	440	27
2013-14	49	3	391	24
Mean	56	3	331	20
S D	21	1	83	5

Monthly accumulation and ablation patterns (2008-2014) and Annual changes (2004-2014) of snow cover

It is observed that in Tista sub-basin there is more unevenness in precipitation, however in ablation season there is gradual decline of snow cover. The time of highest snow cover in Tista sub-basin is late January (Figure 72). The pattern of Rangit sub-basin is unique among all the sub-basins in terms of accumulation and ablation. In Rangit sub-basin the accumulation and ablation curves in each year are more or less similar in pattern (Figure 73). Its near horizontal pattern indicates low precipitation and low ablation. In Rangit sub-basin the snow cover does not exceed more than 20 %.

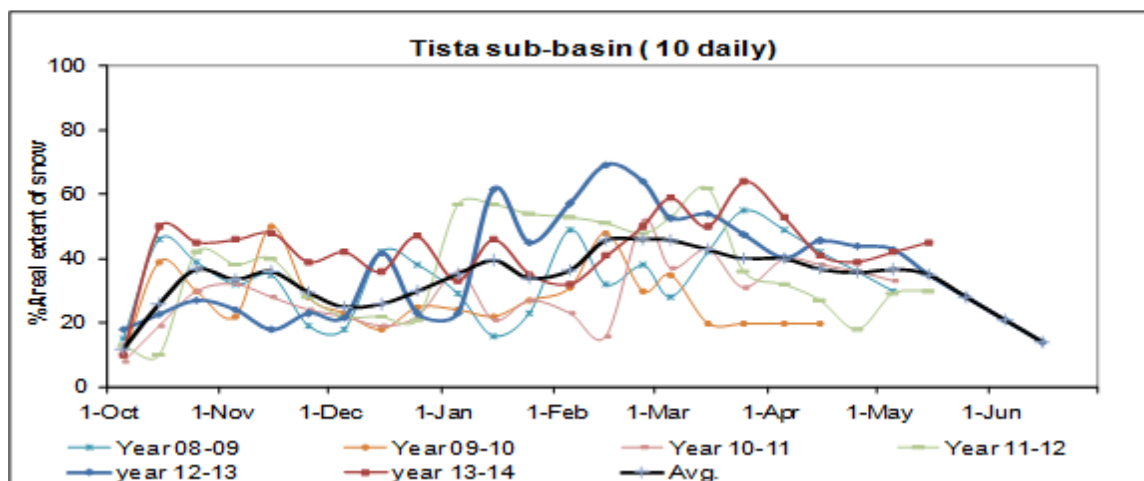


Figure 72: Accumulation and ablation pattern of snow cover for Tista sub-basin between 2008 and 2014

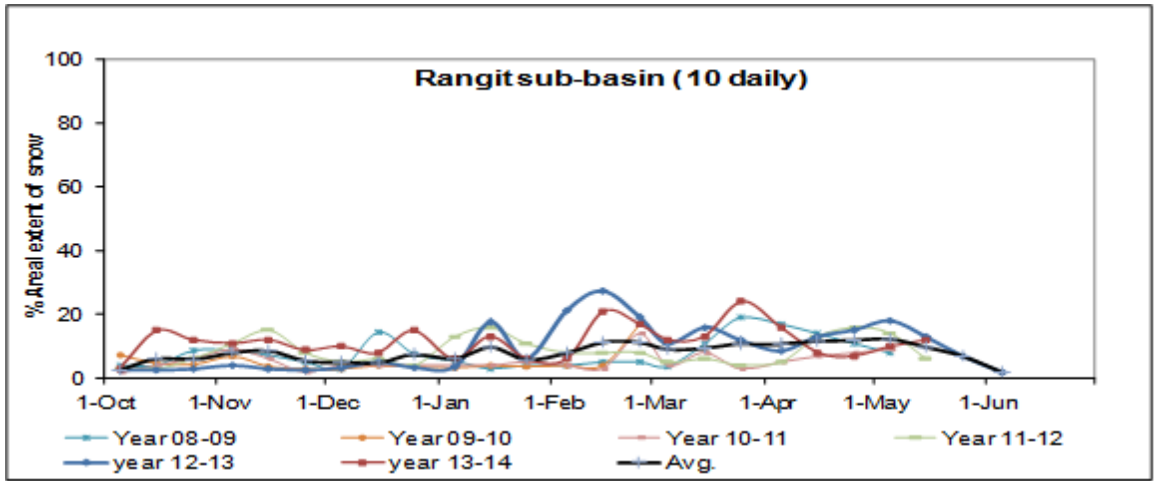


Figure 73: Accumulation and ablation pattern of snow cover for Rangit sub-basin between 2008 and 2014

In Tista sub-basin there is slight gain of snow cover of the order of 0 to 5 % over a period of 10 years (Figure 74). In Rangit sub-basin, in contrast, there is consistency of snow cover during this period (Figure 75). Tista sub-basin covers areas of high altitude and northern latitudes than the Rangit sub-basin. The trend of snow cover in Rangit sub-basin remains near horizontal.

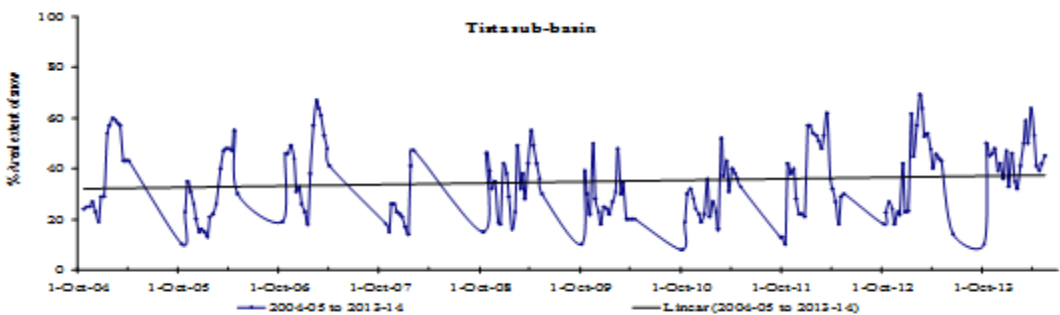


Figure 74: Changes in snow cover area and its trend during time frame 2004 to 2014 for Tista sub-basin of the Tista basin

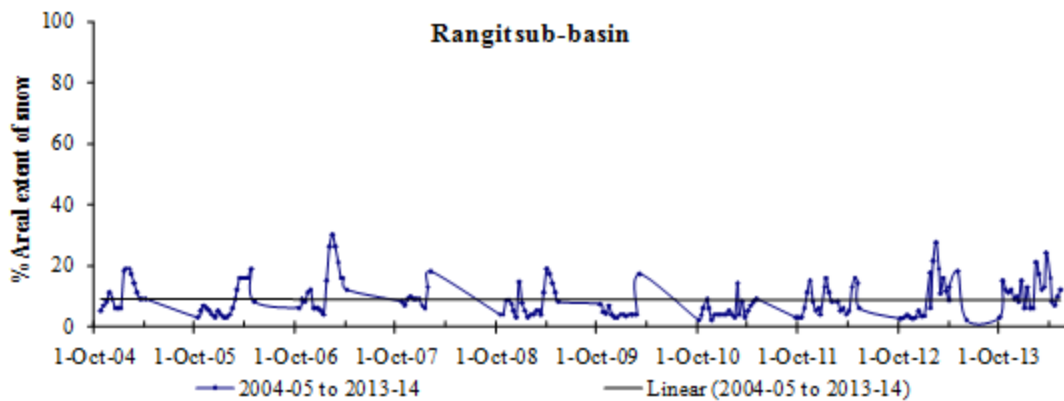


Figure 75: Changes in snow cover area and its trend during time frame 2004 to 2014 for Rangit sub-basin of the Tista basin

vi) Brahmaputra basin

Tawang, Subansiri and Dibang sub-basins are part of Brahmaputra basin and drain in Arunachal Pradesh in north-east of India. These sub-basins together cover 41224 sq. km area.

Minimum and maximum snow cover

The minimum and maximum snow cover in each hydrological year from 2004-05 to 2013-14 has been compiled in the Tables 33 to 35. It is observed that areal extent of snow in 2008-09, 2009-10, 2010-11 & 2011-12 were higher than the mean of all years of observations for all the sub-basins. It is observed that there is a not much variation of minimum snow covers in each hydrological year and in each sub-basin but the variation in maximum snow cover is relatively higher. The mean of maximum snow cover varies among three sub-basins. The SD values suggest low temporal variability in minimum snow cover. However, for all the three sub-basins there is contrast in minimum and maximum snow cover. This suggests that within Brahmaputra basin, different sub-basins experience different amount of precipitation in different years. The mean and standard deviation values suggest that variation is higher in Tawang sub-basin.

Table 33: Minimum and maximum snow cover in Tawang sub-basin during 2004-14

Tawang sub-basin (6721 sq. km)				
Year	Minimum snow cover		Maximum snow cover	
	Sq. km	%	Sq. km	%
2004-05	874	13	4839	72
2005-06	269	4	3764	56
2006-07	605	9	5780	86
2007-08	67	1	4839	72
2008-09	538	8	5175	77
2009-10	336	5	3965	59
2010-11	1075	16	4772	71
2011-12	403	6	6049	90
2012-13	336	5	5578	83
2013-14	538	8	3697	55
Mean	504	8	4846	72
SD	296	4	832	12

Table 34: Minimum and maximum snow cover in Subansiri sub-basin during 2004-14

Subansiri sub-basin (25345 sq. km)				
Year	Minimum snow cover		Maximum snow cover	
	Sq. km	%	Sq. km	%
2004-05	507	2	5576	22
2005-06	1267	5	5069	20
2006-07	2028	8	8110	32
2007-08	760	3	5576	22
2008-09	2535	10	9124	36
2009-10	1014	4	9124	36
2010-11	1267	5	6083	24
2011-12	760	3	7350	29
2012-13	1267	5	7604	30
2013-14	1267	5	4562	18
Mean	1267	5	6818	27
S D	609	2	1666	7

Table 35: Minimum and maximum snow cover in Dibang sub-basin during 2004-14

Dibang sub-basin (9158 sq. km)				
Year	Minimum snow cover		Maximum snow cover	
	Sq. km	%	Sq. km	%
2004-05	549	6	5953	65
2005-06	1832	20	3846	42
2006-07	824	9	5770	63
2007-08	458	5	6227	68
2008-09	1007	11	4762	52
2009-10	2564	28	4762	52
2010-11	458	5	5312	58
2011-12	1007	11	5312	58
2012-13	733	8	5128	56
2013-14	458	5	5220	57
Mean	989	11	5229	57
S D	693	8	682	7

Monthly accumulation and ablation patterns (2008-2014) and Annual changes (2004-2014) of snow cover

The analysis of accumulation and ablation patterns of snow cover show a distinct pattern in three sub-basins. In Tawang sub-basin the snow cover remains steady up to end of January followed by a sharp rise (Figure 76). Then it gradually decreases. In Subansiri sub-basin there is neither growth nor decay of snow cover. There remains a permanent snow cover of about less than 20% area of sub-basin (Figure 77). In Dibang sub-basin there is gentle rise of snow cover and gentle melting down (Figure 78). The pattern almost remains same in each year. These sub-basins are located adjacent each other, however snow precipitation and melting have a distinct contrast.

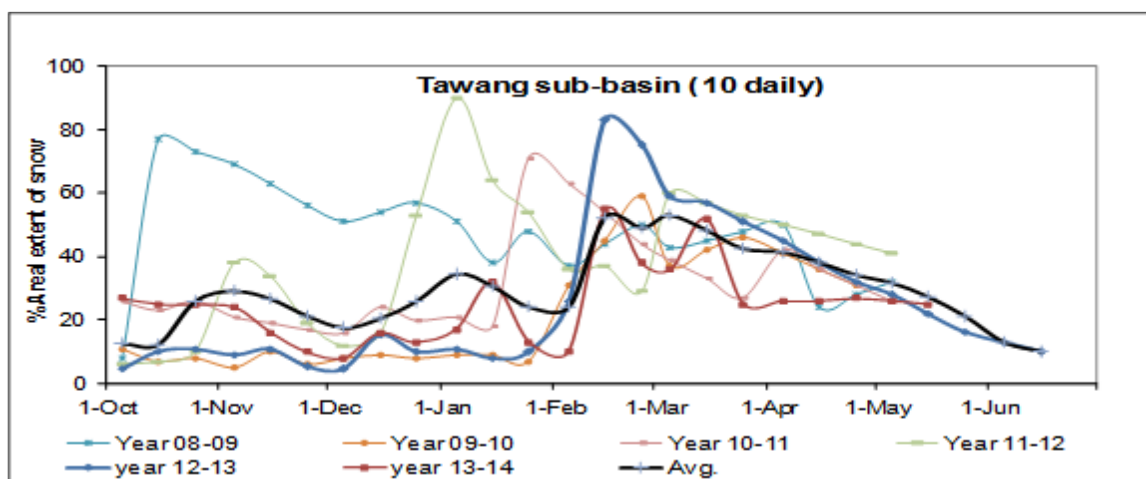


Figure 76: Accumulation and ablation pattern of snow cover for Tawang sub-basin (Brahmaputra basin) between 2008 and 2014

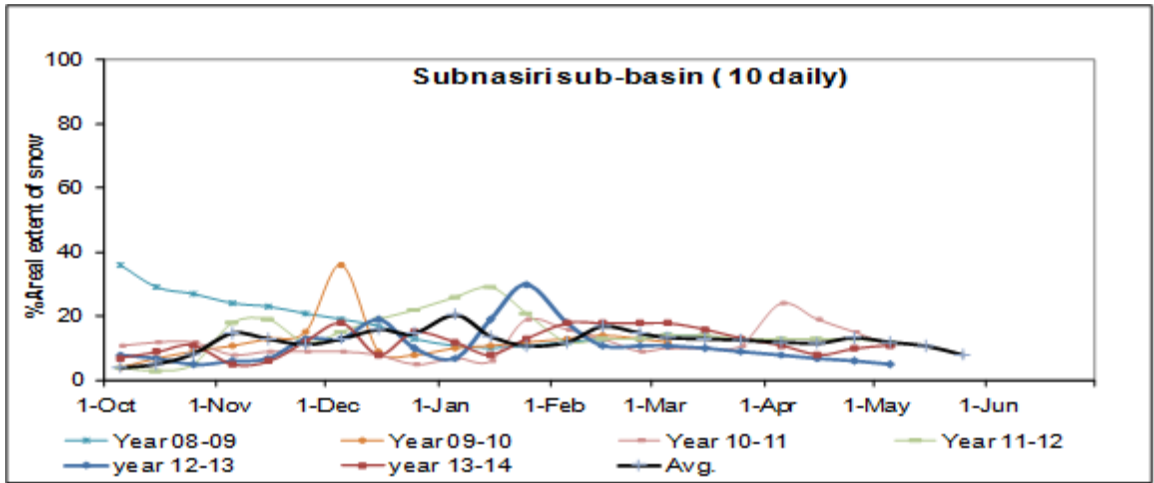


Figure 77: Accumulation and ablation pattern of snow cover for Subansiri sub-basin (Brahmaputra basin) between 2008 and 2014

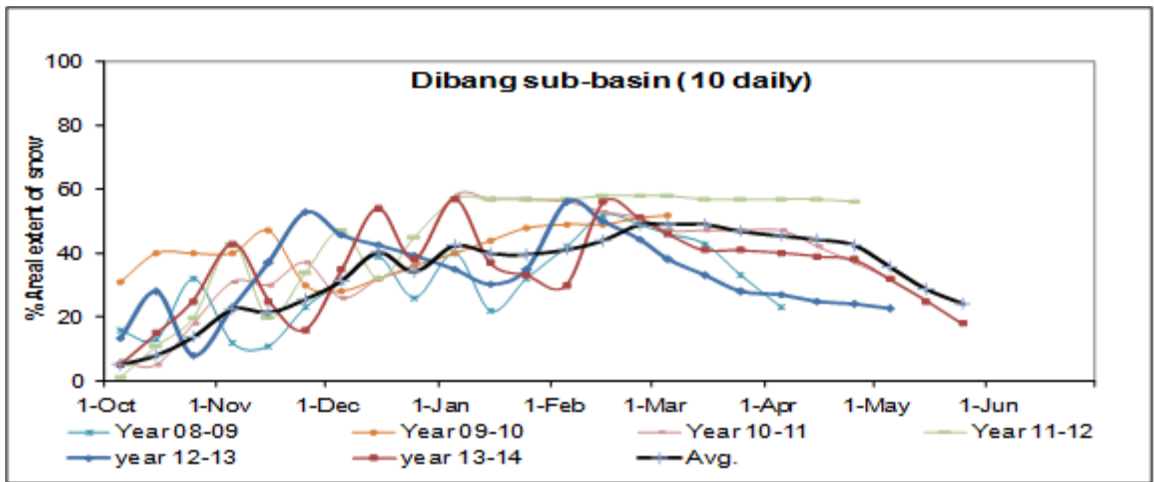


Figure 78: Accumulation and ablation pattern of snow cover for Dibang sub-basin (Brahmaputra basin) between 2008 and 2014

In Tawang and Subansiri sub-basins, a decrease in snow cover has been observed (Figure 79 and Figure 80). It is higher in Tawang i.e. less than 10%. In Subansiri sub-basin the decrease is much lesser. In Dibang sub basin there is 2-3 % rise in snow cover (Figure 81). The sub-basins in Arunachal Pradesh are influenced by climate of Bay of Bengal. The sub-basins are south facing and due to difference in altitude and geographic location respond differently to climatic variations.

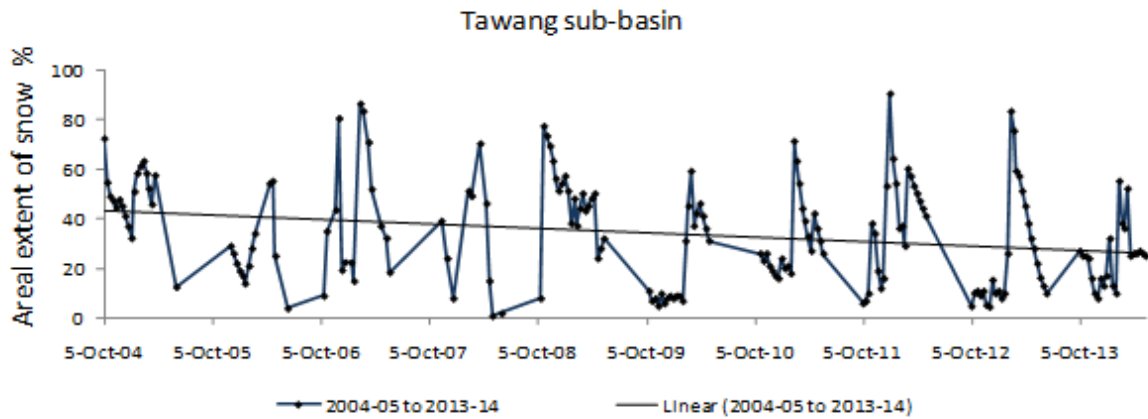


Figure 79: Changes in snow cover area and its trend during time frame 2004 to 2014 for Tawang sub-basin of the Brahmaputra basin

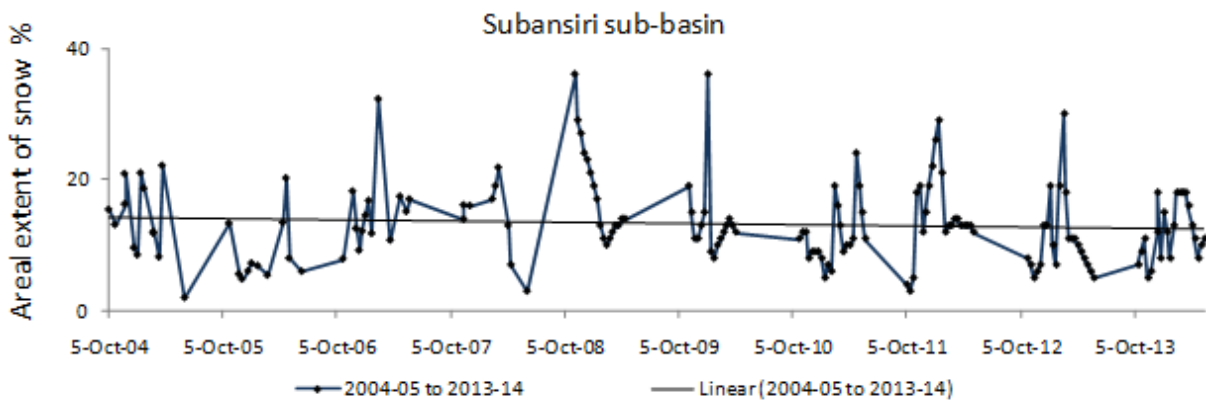


Figure 80: Changes in snow cover area and its trend during time frame 2004 to 2014 for Subansiri sub-basin of the Brahmaputra basin

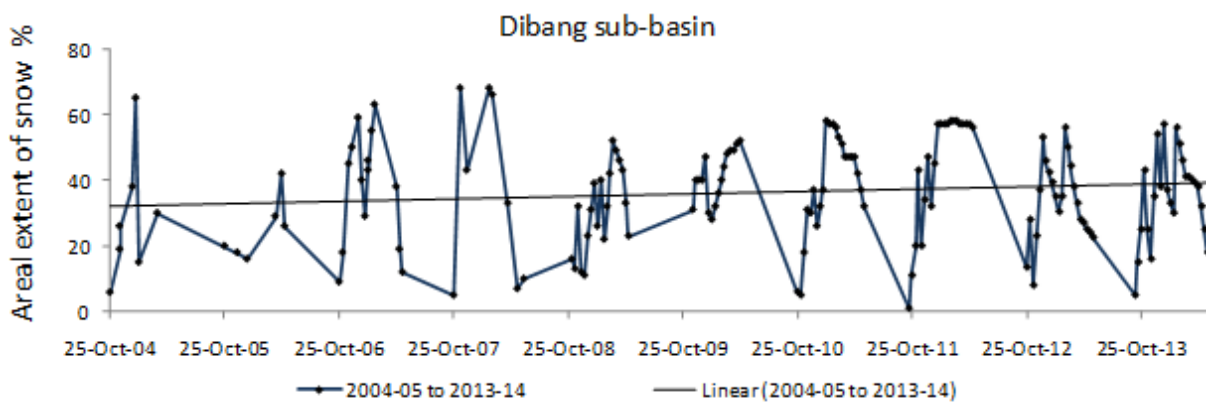


Figure 81: Changes in snow cover area and its trend during time frame 2004 to 2014 for Dibang sub-basin of the Brahmaputra basin

Overall, it is summarized that the analysis of snow cover data of 33 sub-basins for the period 2004-2014 shows 1-7 % increase in snow cover. It has been observed that snow line has come down to lower altitudes during the time frame 2010-2014 as compared to previous years. It is also observed that variation in snow cover changes are higher during October to February time frame.

Analysis of the mean maximum, mean minimum and mean variability ranges of snow cover area for 33 sub-basins of the Himalayan region during accumulation and ablations seasons of 2004-2014 time frame reveals that characteristics of snow cover extent in western (Indus, Chenab and Satluj), west-central (Ganga) and eastern (Tista and Brahamaputra) sub-basins are distinctly different i.e., western sub-basins (max. 71—100%, min. 3 – 54% and variability 39-90%), West-Central (max. 59-66%, min. 9-17% and variability 42-57%) and Eastern (max. 20-72%, min. 3-13% and variability 17-64%). The study indicated that the snow cover in the West-Central and Eastern Himalaya is around 30-40 % less as compared to sub-basins in the Western Himalaya during accumulation period.

During ablation season minimum snow cover has been observed in Jhelum (Indus), Rangit (Tista) and Subansiri (Brahamaputra) sub-basins (< 5%) and maximum snow cover has been observed in Shigar (Indus) and Nubra (Indus) Sub-basins (> 50%). During accumulation season Shigo (Indus), Suru (Indus), Miyar (Chenab), Bhaga (Chenab), Chandra (Chenab) and Pin (Satluj) sub-basins are observed to have 100% snow cover, whereas minimum snow cover is observed in the Rangit (Tista) and Subansiri sub-basins (Brahamaputra) (20-27%). The mean variability of maximum and minimum snow cover is observed in Shigo (Indus) sub-basin (90%) and minimum in Rangit sub-basin (Tista) (17%). The mean variability of maximum and minimum snow cover is observed to be low for sub-basins north of the Indus river i.e., Gilgit, Hanza, Shigar, Sasgan, Nubra and Shyok (39-59%) and high for sub-basins south of the Indus river i.e., Astor, Kisanganga, Shigo, Drass, Jhelum, Suru and Zaskar (71-90%). The temporal fluctuations of snow cover during accumulation season is higher in Jhelum (Indus), Jiwa (Satluj) and Yamuna sub-basins (Ganga) (17-19 %).

Analysis of the annual accumulation and ablation pattern of snow cover in 33 sub-basins during 2008-2014 time frame has shown that variability of snow cover changes is higher during accumulation period than in ablation period. This is probably due to the fact that during the accumulation period snow reaches to its lower altitudes where fluctuations are rapid due to variations in temperature.

vii) Detailed comparative analysis of spatial and temporal variability of snow cover in Alaknanda, Bhagirathi and Yamuna sub-basins of Ganga basin

A detailed comparative analysis of snow cover data of Alaknanda, Bhagirathi and Yamuna sub-basins of Ganga basin was carried out (Rathore et al., 2015a). Monthly average snow cover reached to its maximum in the month of January 2012 for all three sub-basins, corresponding to 71, 79 and 87 % (7874, 5876 and 3068 sq. km) of the total area for Alaknanda, Bhagirathi and Yamuna sub-basins respectively. The minimum was observed during October 2012 which corresponds to 9, 9 and 4 % (998, 669 and 141 sq. km) of the total area respectively. Monthly average snow cover for the period 2004-12 along with $\pm 1\sigma$ was analyzed (Figure 82). Most of the variations were observed during accumulation period especially in Yamuna sub-basin which is located at lower altitude ranging from 1000 to 6100 m. Alaknanda sub-basin has shown relatively low variation in standard deviation for monthly averaged snow cover for the period 2004-12 in comparison to other two sub-basins. However, Bhagirathi shows more snow cover area which could be due to coverage of more sub-basin area under high altitude region as shown in the hypsographic curve of all sub-basins (Figure 83).

If total snow cover over a year is considered in Ganga basin, then it is seen that areal extent of snow for the year 2004-05, 2007-08 and 2011-12 was higher than the mean of total snow cover over eight years (Figure 84). Snow cover area has shown slight increasing trend for all sub-basins from 2004 to 2014, however, it was found to be statistically insignificant using Mann-Kendall test. Minimum snow cover has not shown any variation which corresponds to negligible change in maximum snow line altitude, whereas maximum snow cover has shown an increasing pattern which corresponds to lowering of snow line altitude during the observed period that means snow fall reaches to lower region.

The pattern of accumulation and ablation also differs from one basin to other in Ganga basin. Annual accumulation and ablation pattern of snow cover of each sub-basins from 2004-2012 is shown in Figure 84. Frequent fluctuations of snow cover are observed during accumulation period. These fluctuations are being attributed to frequent snowfalls and continuous melting in the lower altitude regions. But this phenomenon is not true for ablation period. As the snow line progressively moves up during ablation months (April to June), fluctuations in snow cover on higher altitudes are not observed. Yamuna sub-basin has shown accumulation and ablation throughout the year in comparison to other two sub-basins as 77 % of the area falls below 4000-meter altitude. The gradient of ablation curves for all the years are similar indicating comparable time and rates of melting. Area-altitude distribution indicating the area covered in some definite altitude zones area was estimated for each sub-basin. The distribution is shown by hypsographic curves. Hypsographic curves of Yamuna sub-basin show gentle slope among all the three sub-basins which indicates

Yamuna sub-basin to be located in lower altitude zones than Bhagirathi or Alaknanda sub-basins.

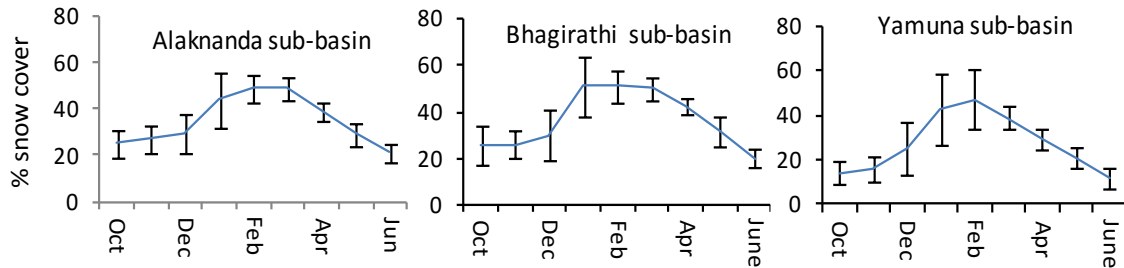


Figure 82: Monthly average snow cover for the period for 2004 to 2012 along with $\pm 1\sigma$ (Source: Rathore et al., 2015a)

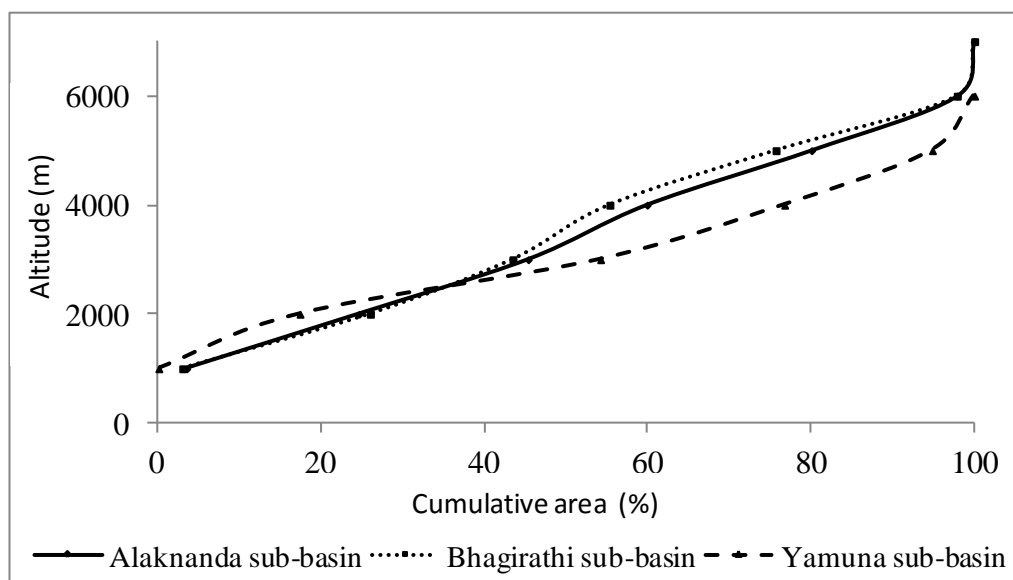


Figure 83: Hypsographic curve giving percentage cumulative area for Alaknanda, Bhagirathi and Yamuna sub-basins (Source: Rathore et al., 2015a)

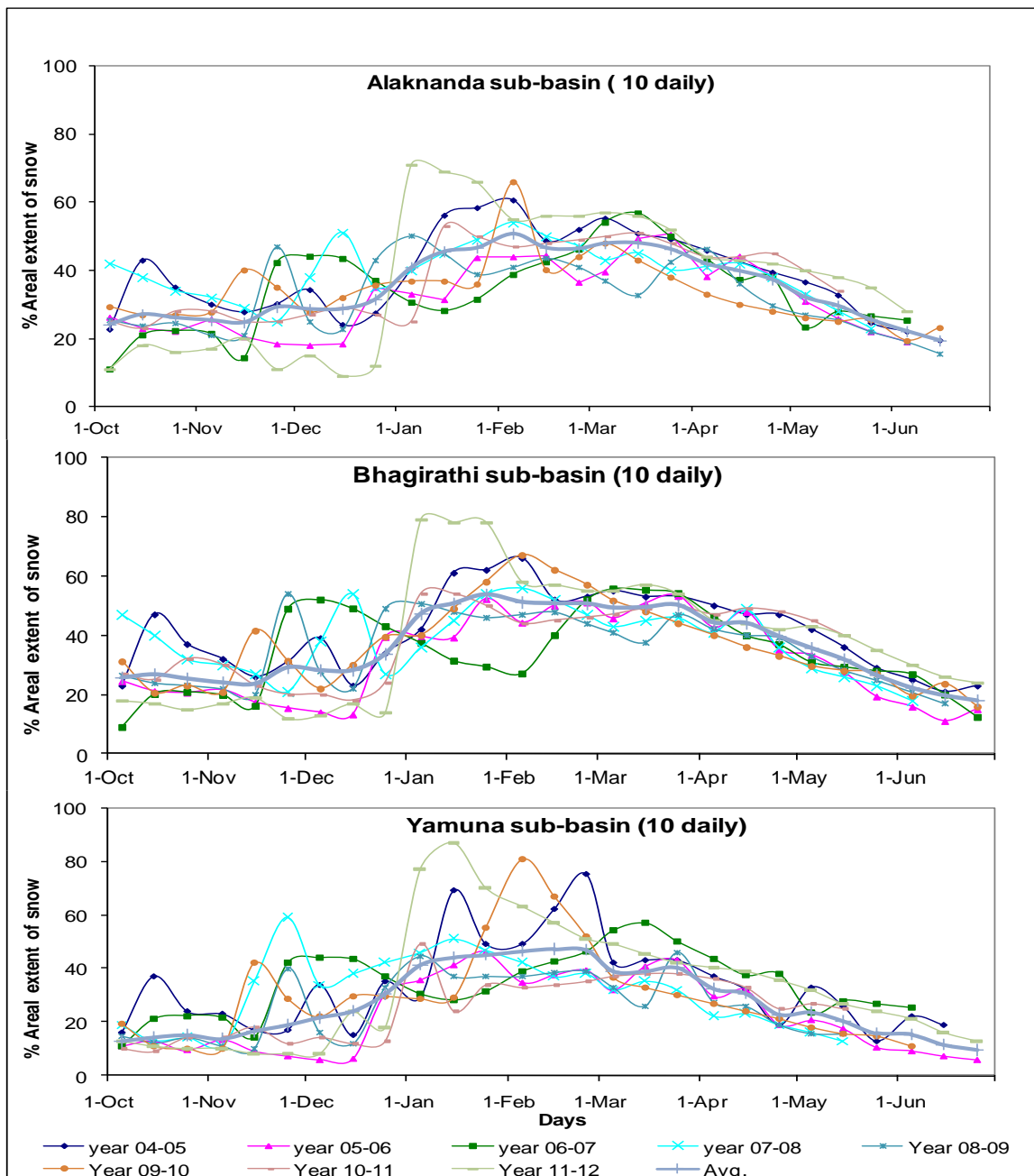


Figure 84: Snow accumulation and ablation pattern for Alaknanda, Bhagirathi and Yamuna sub-basins between 2004 and 2012 (Source: Rathore et al., 2015a)

However, it was observed that 60 % of the area of Bhagirathi sub-basin falls in higher altitudes in comparison to Alaknanda sub-basin. Mean monthly minimum and maximum snow cover was computed as 2329, 1488, 423 and 5434, 3793, 1658 sq. km for Alaknanda, Bhagirathi and Yamuna sub-basins respectively. Minimum and maximum snow line altitudes were determined as 3311, 3482, 2922 and 4924, 5232, 4362 m respectively (Table 36). This shows a variation of 3105, 2305 and 1235 sq. km in snow cover corresponding to 1613, 1770 and 1440 meter fluctuation in snow line altitudes. It has been observed that maximum variation takes place in 3000-4000

m altitude zone in all the three sub-basins corresponding to 0 to 95, 0 to 100 and 0 to 95 % change in snow cover respectively (Figure 85). It is probably due to high atmospheric temperature and heat conduction from ground in this altitude range. In 4000-5000 m zone, the snow cover varied from 4 to 100, 11 to 100 and 9 to 100 % for three sub-basins as this zone is characterized by occurrence of glacier ice, inducing low geothermal heat and moderately low air temperature. Snow cover does not vary much above 5000m amsl altitude. This zone remains mostly above permanent snow line throughout the year. Air temperature data of Dehradun (*TuTiempo.net*) is depicted in Figure 86 from year 2004 to 2012 which shows subtle increasing trend for both minimum and maximum 10 daily average temperatures. Rise in temperature and reduced snow cover was observed in the month of May and June 2012 which also gets reflected in high snow line for year 2012. Percent change in areal extent of snow in Alaknanda sub-basin had inverse correlation with temperature data (Figure 87). It is showing right angle pattern because of maximum variation during accumulation and minimum during ablation period.

Table 36: Mean monthly areal extent of snow and snow-line altitude from year 2004 to 2012 (Source: Rathore et al., 2015a)

Sub-basin	Alaknanda sub-basin		Bhagirathi sub-basin		Yamuna sub-basin	
	Area (sq. km)	Altitude (meter)	Area (sq. km)	Altitude (meter)	Area (sq. km)	Altitude (meter)
October	2773	4812	1934	4946	494	4262
November	2994	4740	1934	4946	564	4189
December	3216	4654	2231	4738	882	3958
January	4880	3683	3793	3482	1517	3174
February	5434	3311	3793	3482	1658	2922
March	5434	3311	3719	3548	1376	3408
April	4325	4053	3198	3995	1023	3846
May	3216	4654	2380	4634	741	4052
June	2329	4924	1488	5232	423	4362

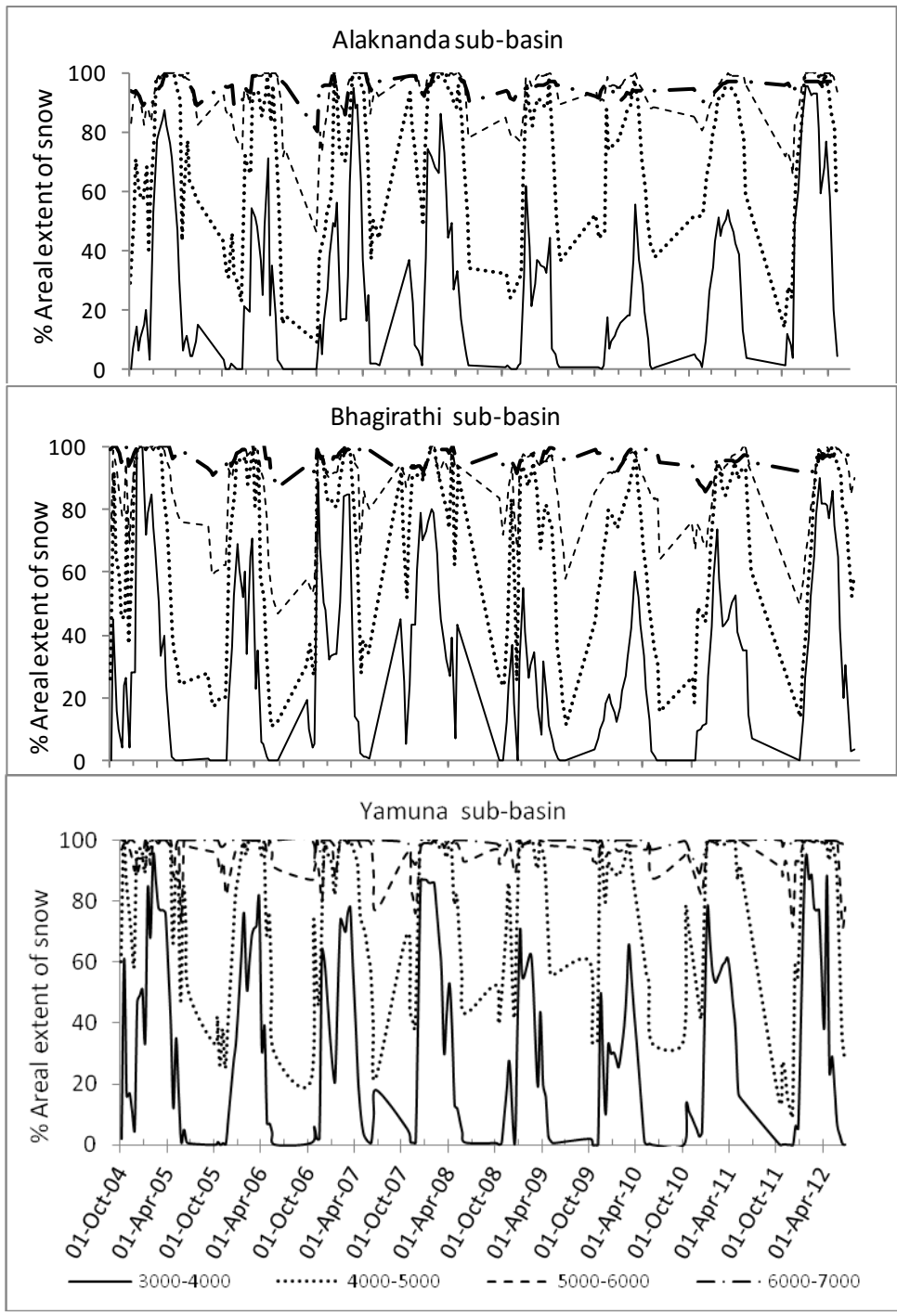


Figure 85: Snow cover variation for various altitude zones at 1000 m interval (Source: Rathore et al., 2015a)

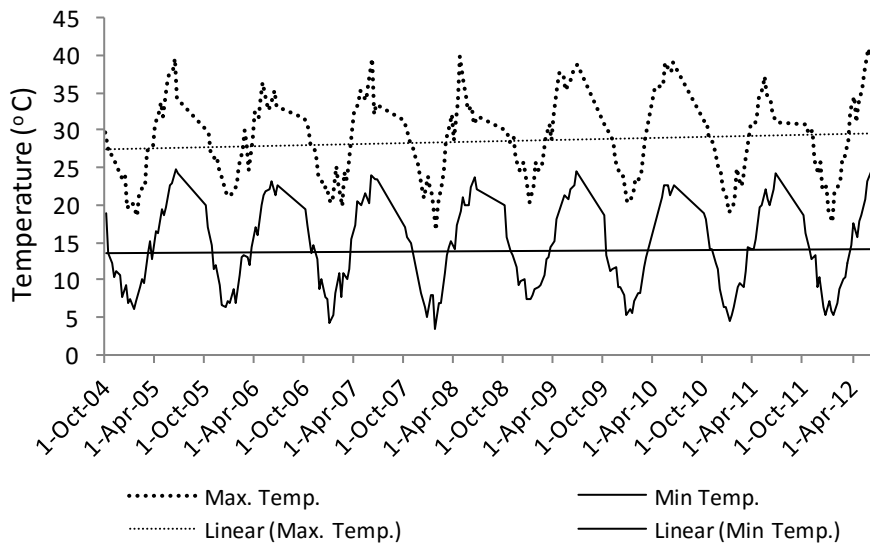


Figure 86: Air temperature (10 daily average) at Dehradun (Source: Rathore et al., 2015a)

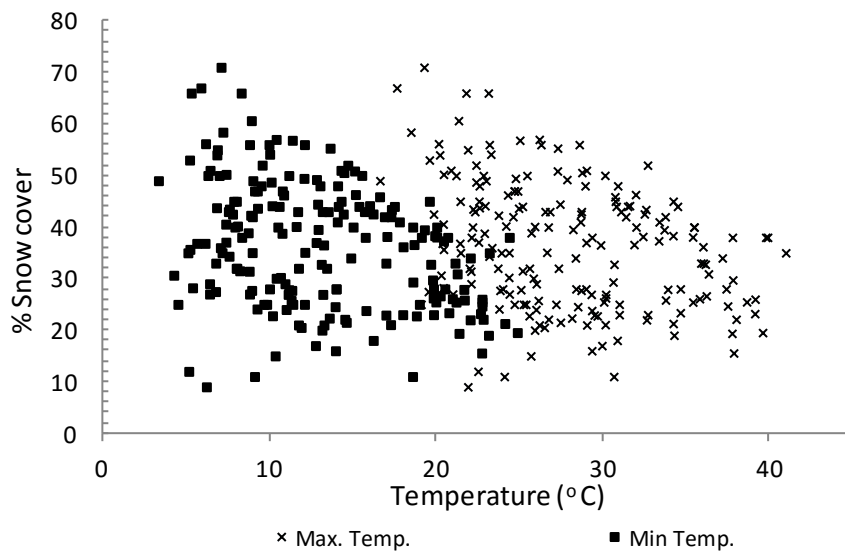


Figure 87 Scatter plot showing snow cover with air temperature for Alaknanda sub-basin (Source: Rathore et al., 2015a)

viii) Regional snow cover analysis for Indus, Ganga and Brahmaputra basins using MODIS data

Moderate Resolution Spectroradiometer (MODIS) is an imaging radiometer that acquires imagery of the Earth surface in 36 discrete spectral bands. MODIS (Terra/Aqua) provided regional to global information on land, ocean and atmosphere at spatial resolution of 250m, 500m and 1000m between 0.4 to 14.0 μm . In this investigation, monthly snow cover product of MODIS for time frame 2000-2011 were downloaded from <http://reverb.echo.nasa.gov>. and analysed to understand the changes in the extent of snow cover for the three major river basins of the Himalayas, namely the Indus, the Ganga and the Brahmaputra basins.

The analysis of MODIS snow cover products for the period 2000 to 2011 revealed that the maximum snow cover for the three basins altogether is 85.54 % of the total geographic area which reduces to 9.94 % during ablation (Table 37).

Table 37: Percentage snow cover area for Indus, Ganga and Brahmaputra Basins (Singh et al., 2014)

Basins	Maximum snow cover area %	Minimum snow cover area %
Indus	92.08	10.41
Ganga	77.30	11.32
Brahmaputra	84.23	8.10
Total	85.54	9.94

The analysed results are shown in Figure 88. Accumulation and ablation patterns of snow cover for all the three basins are very clearly depicted. Indus basin has the highest snow cover in comparison to Brahmaputra and Ganga basins. All the three basins have shown similar pattern of snow accumulation and ablation, but with different magnitudes. Accumulation period (October-June) has shown highest snow cover for Indus and lowest for Ganga whereas ablation period has shown lowest snow cover for Ganga basin. It is very clearly observed from Figure 88 that the ablation period for Ganga basin is prolonged upto the month of December. Indus basin shows minimum ablation period following high snow cover area whereas Brahmaputra basin behaves moderately. This makes snow and glacier system of the Ganga basin less nourished and non-replenishing in nature.

Overall, there is an increasing trend of snow cover in Indus Basin, whereas Ganga and Brahmaputra basins have shown subtle decreasing trend (Figure 89) during the same period. Indus basin has the highest snow cover in comparison to Brahmaputra and Ganga basins. A jump in peak during winter months was observed in all the three basins which shows initiation of snowfall. A smaller peak was also

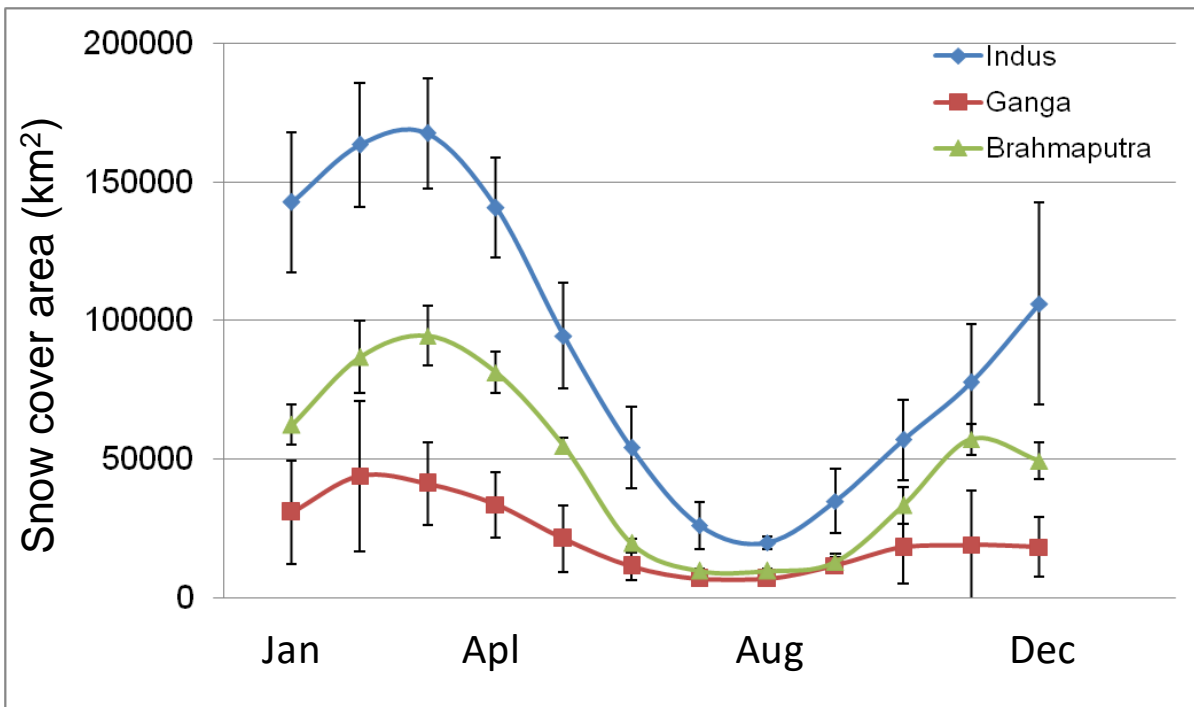


Figure 88: Monthly averaged accumulation and ablation snow cover of Indus, Ganga and Brahmaputra basins for the period 2000-2011 along with $\pm 1\sigma$ bar (Source: Singh et al., 2014)

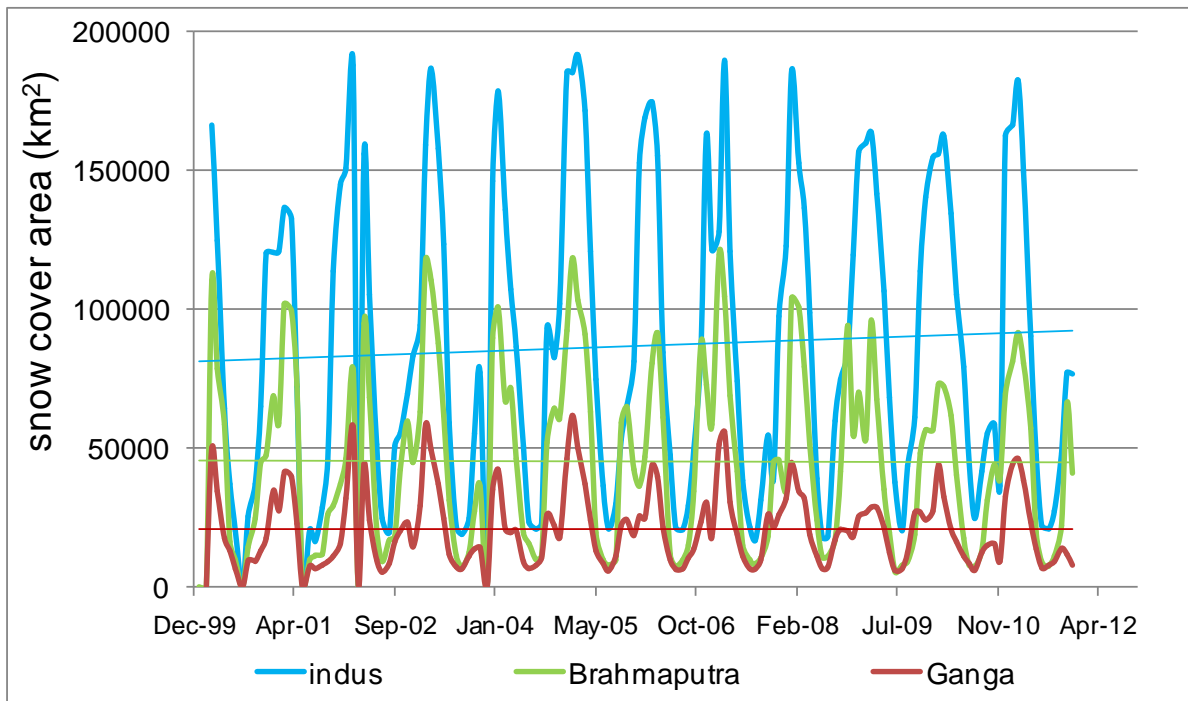


Figure 89: Monthly snow cover variability using MODIS product for Indus, Ganga and Brahmaputra basins (2000-2011). Indus snow cover shows an increasing trend; Ganga shows almost no change and Brahmaputra shows a decreasing trend (Source: Singh et al., 2014)

observed during October-November months followed by reduction in snow cover area due to melting. Indus basin has shown least ablation period whereas Ganga has shown prolonged ablation period. The present study shows that all the three major river basins may respond differently to changing climate (Singh et al., 2014).

The analysis of AWiFS derived snow cover products discussed in earlier sections also reveal that the snow accumulation and ablation in sub-basins of Western, West Central and Eastern Himalaya are observed to have distinct patterns. Mean value for minimum and maximum snow cover during the time frame 2004-05 to 2013-14 in Western Himalaya comprising of 13 sub-basins of Indus, 6 sub-basins of Chenab, 6 sub-basins of Satluj; West Central Himalaya comprising of 3 sub-basins of Ganga and Eastern Himalaya comprising of 5 sub-basins ranges from 3-100 %, 7-100 %, 9-100 %, 9-63 % and 3-72 % respectively. These observations show that the snow cover in the Ganga and Eastern Himalaya is around 30-40 % less as compared to basins in the Western Himalaya during accumulation period.

The findings indicated that the glaciers in the Indus basin are more stable than the other two basins and Ganga basin has the least snow cover area.

3. Glacier Monitoring

3.1. Objective

To monitor the changes (advance/retreat) in extent of glaciers in selected sub-basins representing different climatic zones of Himalayan region using satellite data and carry out change analysis in GIS environment for time frame 2000-2011 in particular using moderate to high resolution satellite images available from Indian satellites.

List of Basins and sub-basins selected for monitoring changes in glacier extent (retreat/advance) is given in the Table 4.2.1.

Table 38: Basins and Sub-basins selected for monitoring changes in glacier extent

Serial no.	Basin	Sub-basins
1	Indus	Nubra
2	Indus	Zaskar
3	Indus	Shasgan
4	Indus	Shigar
5	Indus	Shyok
6	Indus	Dras
7	Indus	Suru
8	Satluj	Spiti
9	Satluj	Parbati
10	Chenab	Chandra
11	Chenab	Bhaga
12	Chenab	Warwan
13	Chenab	Bhut
14	Chenab	Miyar
15	Chenab	Ravi
16	Ganga	Alaknanda
17	Ganga	Bhagirathi
18	Ganga	Dhauliganga
19	Ganga	Gauriganga
20	Ganga	Kosi
21	Brahmaputra	Tista

3.2. Scientific rationale

Glaciers are mass of snow, ice, water and rock debris slowly moving down a gradient under the influence of gravity. Glaciers are formed due to recrystallization and metamorphism of naturally fallen snow on land surface. It is permanent snow cover which gives rise to formation of glaciers. Glaciers are formed on the earth when rate of accumulation of snow is higher than rate of ablation and falling snow gets enough time and space to get metamorphosed to form ice. Nonetheless the glacier ice must move down under the influence of gravity to be called as glacier. Out of these ice is an essential component. Presently, glaciers are distributed either in Polar Regions of earth or in high mountainous regions. Two major zones of glaciers are normally identified i.e., accumulation and ablation zones separated by an equilibrium line. In the accumulation zone, the total accumulation from winter snowfall remains more than the summer ablation. Therefore, area above equilibrium line contains snow on the surface. In ablation zone, the total summer melting remains more than the winter snow accumulation. Therefore, the ablation zone contains the bare ice. Some part of ablation zone is also found to have partial or full debris cover. The part of ablation zone of the glacier from where river or stream appears on the surface is its terminus or snout. It is the part of the glacier which at its lowest altitude. Many Himalayan glaciers do not have clean surfaces and remain covered with varying amounts of moraine cover, consisting of dust, silts sands, gravel, cobbles and boulders. Moraine cover is one of the most important components of a glacier system in view of the control it exercises on rate of glacier melting. Its areal cover and thickness should be known in order to estimate effect of climate on retreat of glaciers.

The distribution of glaciers as what we see today is the result of last glaciation. Glaciation and deglaciation are the alternate cycles of cold and warm climate of earth. During Pleistocene, the earth's surface had experienced repeated glaciations over a large land mass. The most recent glaciations reached its maximum advance about 20,000 years ago due to fall of temperatures by 5° to 8° C. A Little ice age has been recognized during 1650-1850 AD. During peak of glaciations approximately 47 million km² area was covered by glaciers, three times more than the present ice cover of the earth. Based upon morphological characteristics of glaciers, the glaciers can be grouped into classes such as ice sheet, ice cap, and glacier constrained by topography. Ice sheet and ice cap are formed when underlying topography is fully submerged by ice and glacier flow is not influenced by topography. On the other hand, when glaciers are constrained by the surrounding topography and the shape of valley influences their flow, then such glaciers are classified as valley glaciers, cirque glaciers and ice fields. Mountain glaciers as in Himalayas, Alps, Andes are basically constrained by topography and are predominantly of valley type. In Himalayas glaciers are distributed from West in Kashmir to East in Arunachal Pradesh covering entire stretch of Himachal Pradesh, Uttarakhand, Nepal and Sikkim Bhutan. The distribution and intensity of glaciation is governed by latitude and altitude of the mountains.

Glaciers are very vital to human kind as these natural resources are (i) reservoirs of freshwater (ii) control global climate as the albedo over snow and glaciers is very high, (iii) sensitive indicators of climatic variations. Since Glaciers of Himalaya constitutes the largest concentration of freshwater reserve outside the polar region, a great significance is attached to the fact that these natural resources are the source of fresh water to almost all minor and major rivers of northern India and sustain the civilization for irrigation, hydroelectricity and drinking water.

Glacier inventory and changes in the Himalayan glaciers using remote sensing techniques have been reported in number of studies carried out by both global as well national community and the results are published (Sharma et al., 2013; Bahuguna et al., 2014; 2007; Bajracharya et al., 2014; 2006; Berthier et al., 2004; Bhambri et al., 2013; 2012; 2011; Bolch et al., 2012; 2010; Brahmabhatt et al., 2016; 2015a; 2015b; 2012a; Copland et al., 2012; Deota et al., 2011; Dobhal, 2010; Dobhal and Mehta, 2010; Dutta et al., 2012; Ganju, 2009; Kamp et al., 2011; Kasturirangan et al., 2013; Khalid and Romshoo, 2015; Koul et al., 2016; Kulkarni and Karyakarte, 2014; Kulkarni et al., 2011; 2007; 2006a; 2005; Kulkarni, 2010; Lama et al., 2015; Lamsal et al., 2011; Mir et al., 2014; Negi et al., 2013; 2012; Pandey et al., 2011a; 2011b; Racoviteanu et al., 2014; 2008; Raina et al., 2015; Raina, 2011; 2009; Raina and Srivastava, 2008; Rankl et al., 2014; SAC 2011a; 2011b; 2010; SAC and MoEF, 2010; Schimdt and Nusser, 2012; Srivastava, 2012; Tangri et al., 2004; Frey et al., 2012; Mir et al., 2014; Pfeffer et al., 2013; Racoviteanu et al., 2014b; Shroder and Bishop, 2010). Review of cryosphere research in India summarises salient observations and challenges (Ravindra and Laluraj, 2012).

The retreat or advance of glaciers depends upon static factors and dynamic factors. The static parameters are latitude, slope, orientation, width and size of the valley and altitude distribution of glaciers. The dynamic parameters are annual accumulation and ablation of snow and ice. These factors further depend upon daily and yearly variations in temperature, Solid/liquid precipitation, heat flow from earth crust, debris cover and cloud cover. Glacier snout fluctuations are considered to be highly reliable indicators of worldwide climatic trends. Change in snout position is a result of glacier mass balance. Climatic fluctuations cause variation in amount of accumulation of snow and ice of glaciers and its melting. Such changes in the mass initiate a complex series of change in the flow of glacier that ultimately results in a change of the position of terminus and area of glaciers. Thus advancement and retreat of glacier closely depend on the conditions of replenishment of an accumulation area and the intensity of ablation i.e. faster melting due to climatic changes and hence glaciers are considered as excellent indicators of global climatic changes.

3.3. Methodology

(i) Georeferencing of satellite images

The data obtained from NRSC has undergone the basic geometric and radiometric corrections. This data is (band 2, band 3, band 4, and band 5) georeferenced with master images already archived. This is a second order correction applied to data. The georeferencing with master images is carried out by identifying a set of ground control points on the maps and images. The ERDAS imagine version 9.1 is used for this work.

(ii) Delineation of glacial boundaries

A period of the year i.e. from July to end of September, when seasonal snow cover is at its minimum and permanent snow cover and glaciers are fully exposed, is selected for the glacier mapping using remote sensing data. Multi-temporal geocoded FCC's of standard band combination such as 2 (0.52-0.59 μm), 3 (0.62-0.68 μm) and 4 (0.77-0.86 μm) of IRS LISS III sensors at 1: 50,000 scale are used for interpretation. Most of the work carried out in phase I was done using survey of India topographical maps of 1962, IRS LISS III data of 2001 and in many cases of 2006/2007 and Landsat TM data of 1989. Spatial resolution of the Landsat and LISS III sensor is 30 m and 23.5 m respectively.

To extract glacial boundary from satellite image false color composite (FCCs) are viewed in different combination of band 1 to band 4. The SWIR band is used to discriminate cloud and snow because it might happen that clouds are observed on the upper boundary of the glaciers. The distinction of non-glaciated and glaciated region is sharper in SWIR band. The unique reflectance of snow-ice, shape of the valley occupied by the glacier, the flow lines of ice movement of glaciers, the rough texture of the debris on the ablation zone of the glaciers, the shadow of the steep mountain peaks and presence of vegetated parts of the mountains help in clear identification of a glacier on the satellite image. The understanding of reflectance curve of various glacier features helps to vectorize the glacial boundary on satellite data.

The snout of the glacier is a vital element of interpretation of glacial extents. The terminus is identified using multiple criterions for example:

- Sometimes the river originates from the snout and river can be easily identified on the image.
- The peri-glacier area downstream of the snout has distinct geomorphological set up then the glacier surface.
- In many instances the frontal portion of the glaciers which are retreating has convex shape therefore it helps identification of the terminus.
- When interpretation becomes more complex sometimes DEM is used in the background to confirm the snout as there is a chance of change in the slope of

glacier profile near the snout and 3d view help to identify the lateral and terminal boundary of glacial extent.

- Extreme care is taken while delineating glacier boundary that boundaries are marked in the inner side of the lateral moraines.

Snouts of a few selected glaciers for which Corona photographs (spatial resolution 4m) of 1965 were available were also compared with snouts seen on LISS III data of the corresponding year.

(iii) Estimating loss in area

To estimate change in glacial area the two sources of glacier extent are overlaid on each other. While matching of the boundary, it is seen that the scale of the map and image is kept at 1: 50,000 because the mapping depends on the scale. A map prepared at 1:50,000 scale and map prepared at larger scale might not match for their features. Increase or decrease in the evacuated area from glaciers can be measured. Mapping of glacial boundaries has been carried out using Landsat and LISS-III images. Images of July-September are normally used because during this period snow cover is at its minimum and glaciers are fully exposed.

(iv) Field verification

Field verification of location of snout using GPS observations has been conducted for a few glaciers. Normally ground verifications are carried out for those glaciers which are not easily interpreted.

3.4. Results and Discussion

(a) Himalayan region

In Himalayan region, 2018 glaciers were monitored. These glaciers represent six major climatic zones of Himalayan region; Kashmir Himalayas, Punjab Himalayas (Satluj Basin), Himachal Himalayas (Chenab Basin), Uttarakhand Himalayas, Nepal Himalayas and Sikkim Himalayas. Glaciers were monitored using IRS LISS III images of 2001 and 2011/12 (Bahuguna et al 2014). Table 39 summarises the findings of change in glaciers in 17 sub-basins of Himalaya. Figure 90 shows the location of glaciers monitored in different climatic zones of Himalayas. This number also includes a few glaciers of Nubra valley (Karakoram region). Area–frequency distribution of the monitored glaciers in the six regions is given in Table 40. Glaciers having area less than 1 sq. km constitutes 45% of the number monitored. Ninety-seven glaciers occupy area larger than 20 sq km.

Table 39: Changes in glacier extent studied for selected glaciers in 17 sub-basins of Himalayan region during 2000-2011 time frame

Serial no.	Sub-basins	No. of glaciers	Stable	Retreat	Advance	Glaciated Area (sq Km)		Area Change (Sq Km)
						Year	Year	
						2000/2001	2010/11	
1	Nubra	149	111	20	18	1686.22	1681.87	-4.35
2	Zaskar	188	180	8	0	102.49	102.21	-0.28
3	Suru	110	75	35	0	156.61	152.93	-3.68
4	Spiti	431	415	16	0	36.34	35.79	-0.55
5	Parbati	12	9	3	0	38.39	38.18	-0.21
6	Chandra	140	121	19	0	173.83	172.89	-0.94
7	Bhaga	69	53	16	0	100.58	97.35	-3.23
8	Warwan	77	56	21	0	170.68	167.4	-3.28
9	Bhut	167	158	9	0	64.5	63.54	-0.96
10	Miyar	59	52	7	0	111.77	111.61	-0.16
11	Ravi	36	33	3	0	11.61	11.47	-0.14
12	Alaknanda	20	13	7	0	132.29	131.43	-0.86
13	Bhagirathi	202	165	37	0	183.24	181.5	-1.74
14	Dhauliganga	68	64	4	0	7.66	7.42	-0.24
15	Gauriganga	63	57	6	0	130.08	129.8	-0.28
16	Kosi	195	168	27	0	326.4	322.5	-3.9
17	Tista	32	22	10	0	59.73	57.55	-2.18
Total		2018	1730	238	18	3432.69	3407.89	-24.8

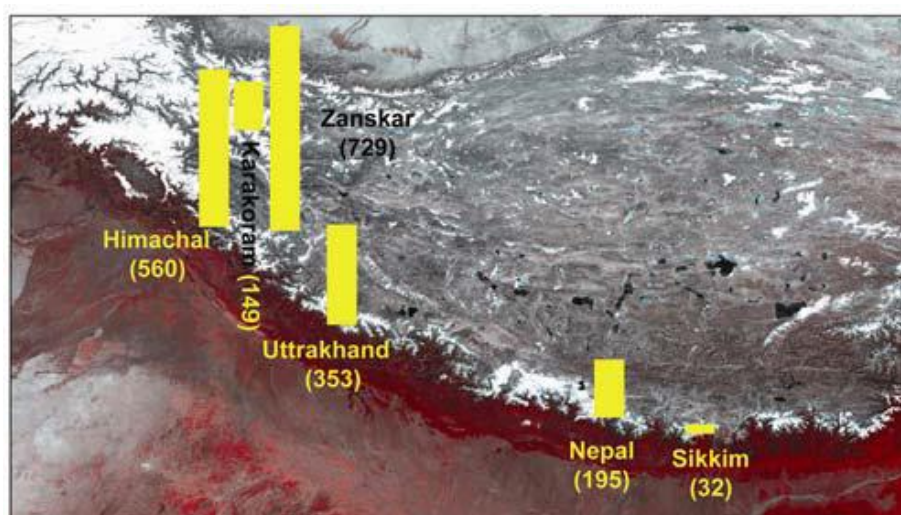


Figure 90: Locations of basins undertaken for glacier monitoring (Source: Bahuguna et al., 2014)

Table 40: The size-frequency distribution of glaciers in the six region (Source: Bahuguna et al., 2014)

Area (sq km)	Karakoram	Zaskar	Himachal	Uttarakhand	Nepal	Sikkim	Total
<1	8	436	261	184	21	4	914
1 to 3	46	197	139	90	59	8	539
3 to 5	30	43	54	23	32	7	189
5 to 10	17	31	51	26	37	8	170
10 to 20	21	9	33	18	25	3	109
>20	27	13	22	12	21	2	97
Total	149	729	560	353	195	32	2018

Monitoring of 2018 glacier snouts from the satellite data of 2000/01/02 shows that 1752 glaciers (86.8%) have been observed to be stable (no change in the snout position), 248 glaciers (12.3%) have exhibited retreat and 18 of them (0.9%) have experienced advancement (Figure 91).

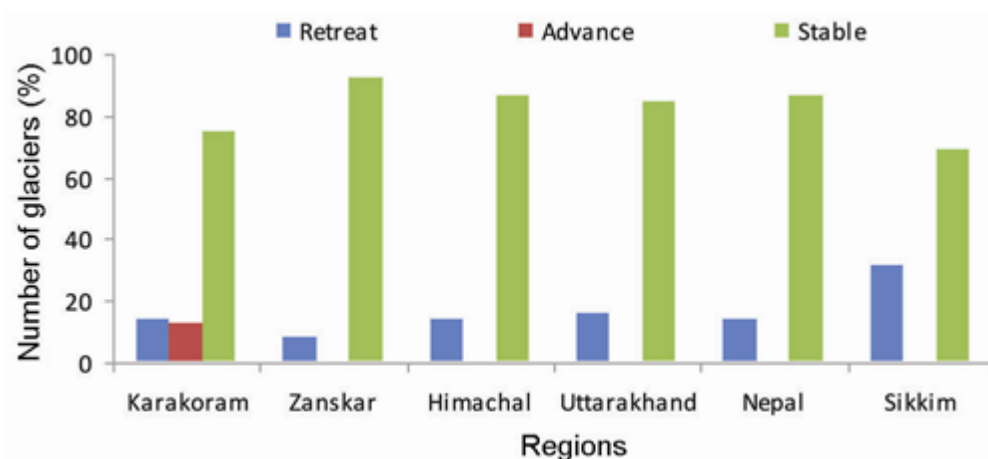


Figure 91: Number of glaciers showing No Change, retreat and advance (Source: Bahuguna et al., 2014)

Region-wise mean shift in snout position for the retreating glaciers is shown in Figure 92. It varies from 145 to 313 m for the 2000/01/02 period with a positional uncertainty of 11.5 m. Average movement of 300 m of snout was observed for advancing glaciers (18 glaciers) of Karakoram. Maximum retreat was observed in Sikkim region followed by Karakoram and Himachal region. The mean retreat of snout for 248 retreating glaciers was found to be 170 m (17 m annually approx.). However, by considering all the 2018 glaciers monitored, the mean retreat was found to be 21 m (2.1 m annually). No detachment of glaciers in the ablation zones in the study area was observed during the period of monitoring.

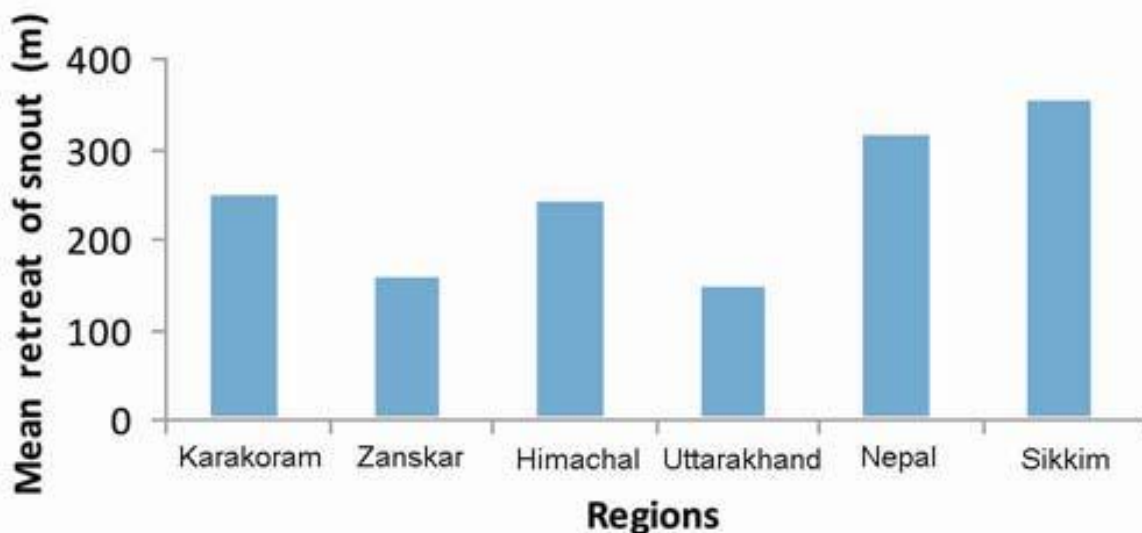


Figure 92: Mean retreat of snout in six regions (Source: Bahuguna et al., 2014)

Changes in area of glaciers were mapped and monitored in the ablation zones. The glaciers with stable snouts (1752 glaciers) have not exhibited any change in area of ablation zones. Glaciers with retreat of snout (248 glaciers covering 34% of total area in 2001) exhibited loss in area, whereas the glaciers having advancement (18 glaciers covering 6% of total area in 2001) exhibited increase in area. This gives a net loss of 20.94 sq. km ($0.2 \pm 2.5\%$ uncertainty) in the total area of 10,250.68 sq. km for all the monitored glaciers mapped in the year 2000/01. Net change in glaciated area varies from one region to another (Figure 93).

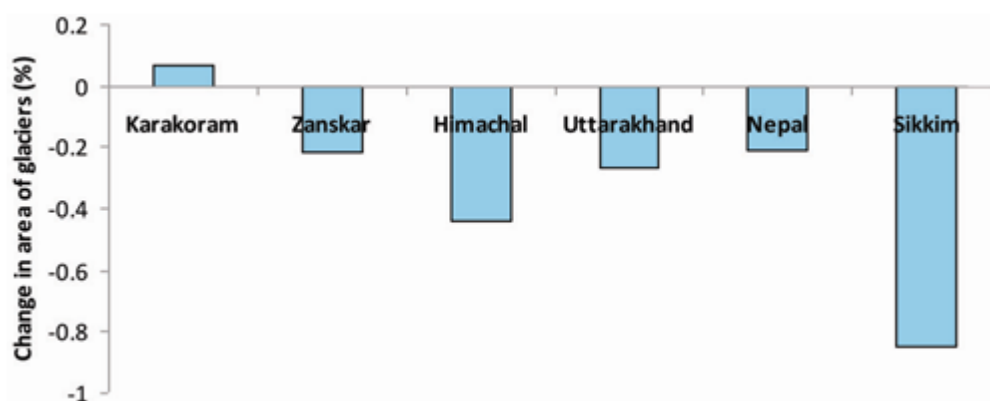


Figure 93: Percentage change in area of glaciers (Source: Bahuguna et al., 2014)

The uncertainty in the interpretation of mixed pixels at the margins of the extents of glaciers in the two datasets get nullified. However, there could be an uncertainty of about 2.5% in area due to half pixel error at the periphery of changed extents of

glaciers. The advancement of glaciers in Nubra valley region are probably because the Karakoram region is fed by mid-westerlies besides being influenced by the southwest monsoon. However, exceptionally high advance movement has not been noted in the glaciers of Nubra valley. Figures 94–97 show few examples of glaciers showing advancement, retreat and stable fronts as seen on IRS LISS III images. Field verifications were also carried out by visiting 15 glaciers during 2001–2011 to validate the snout positions. Overall, the results of the present study indicate that most of the glaciers show stable front or little loss in area during 2000/01/02/11.

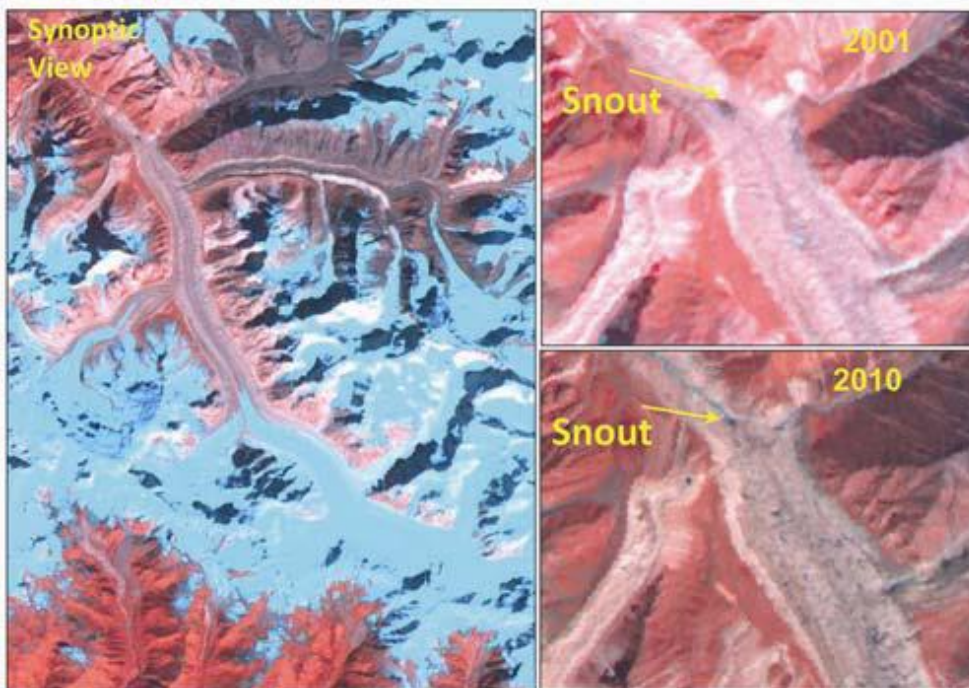


Figure 94: LISS III Images showing location of snout of Gangotri glacier in 2001 and 2010 (Source: Bahuguna et al., 2014)

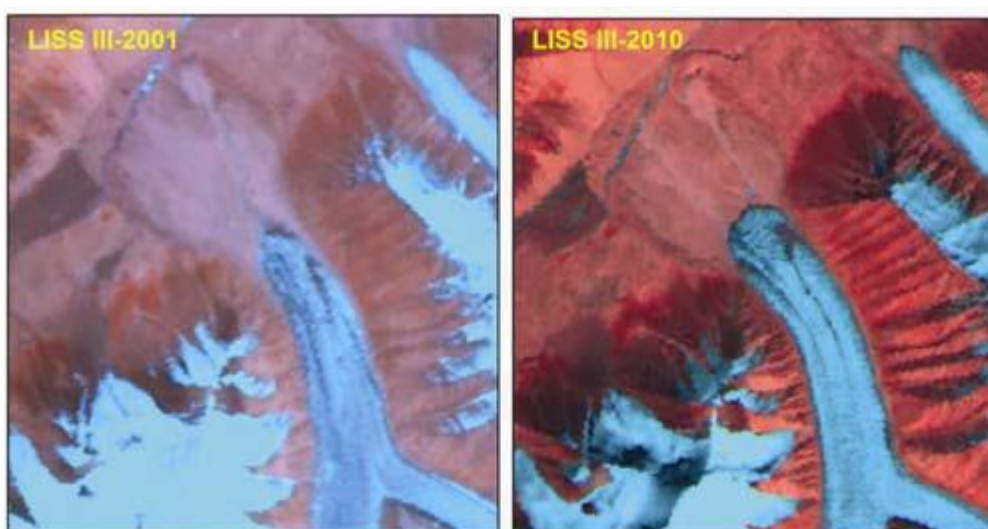


Figure 95: LISS III Images showing location of snout of a glacier in Western Himalaya in 2001 and 2010 (Source: Bahuguna et al., 2014)



Figure 96: LISS III Images showing location of snout of Siachen glacier in 2001 and 2010 (Source: Bahuguna et al., 2014)

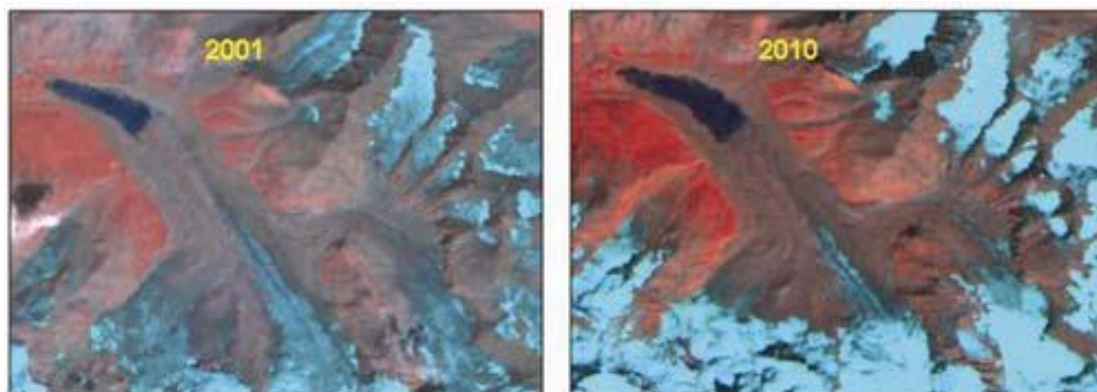


Figure 97: LISS III Images showing retreat of a glacier from 2001 to 2010 and increase in surface area of moraine-dammed lake (Source: Bahuguna et al., 2014)

In the Himalayan region, mean loss of 16% in area of glaciers was reported using topographical maps of 1962 and satellite images of 2001 (Kulkarni et al., 2007). However, present study show that the number and rate of glacier retreat have come down in the last decade compared to period prior to 2001. Most of the glaciers show no change during last decade. This period of monitoring almost corresponds to hiatus in global warming in the last decade. It is worthwhile to note that an interval of one decade could be smaller than the response time of glaciers to be reflected in terms of any significant change with 23.5 m spatial resolution of data. Therefore, further studies using high-resolution multitemporal satellite data are required. Few examples of IRS LISS III images and corresponding maps interpreted are shown in Figures 98 to 111.

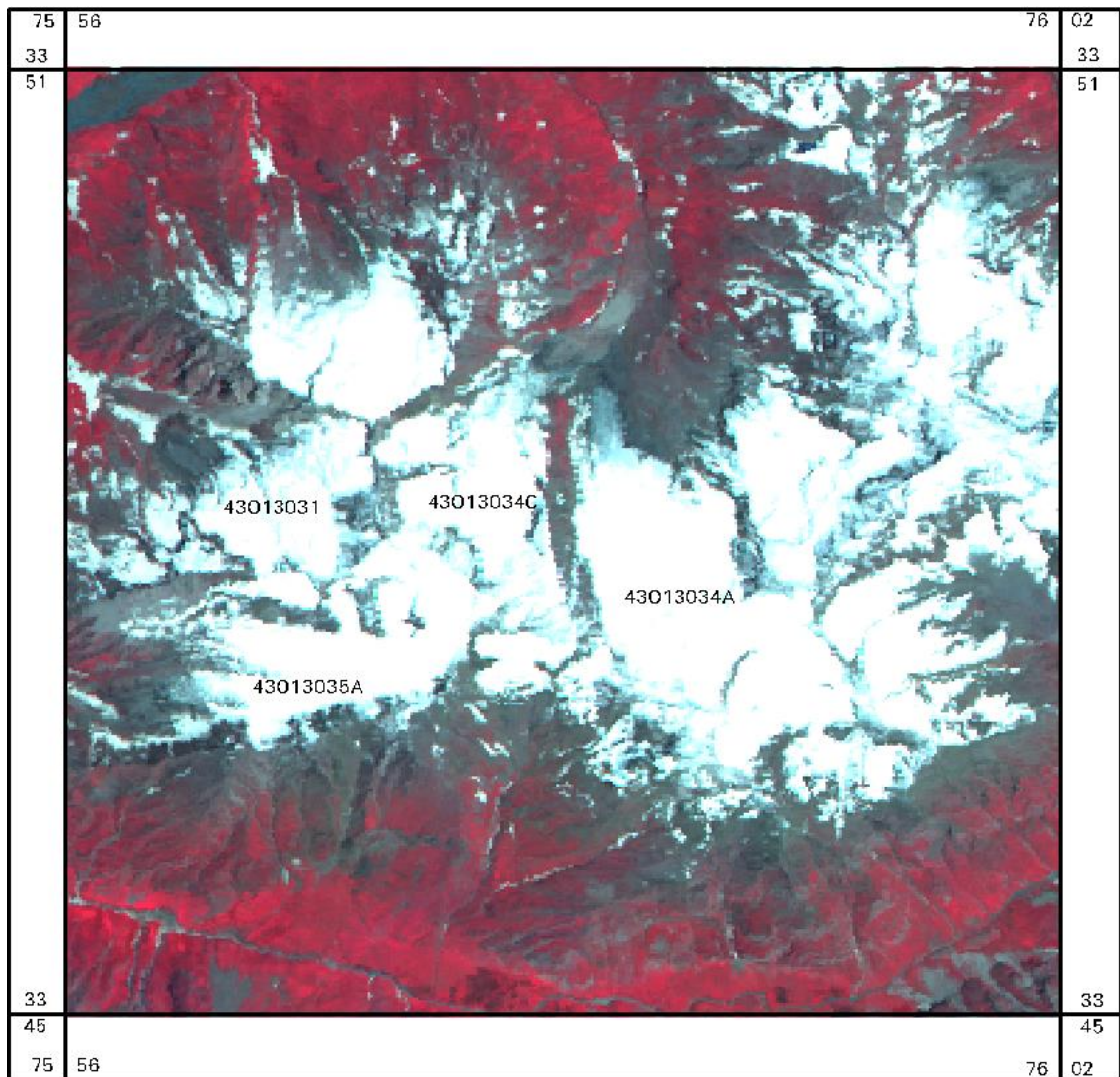


Figure 98: IRS P6 LISS III image of 2010, showing the glaciers of part of the Warwan sub-basin (Reference: Map No 43O/13)

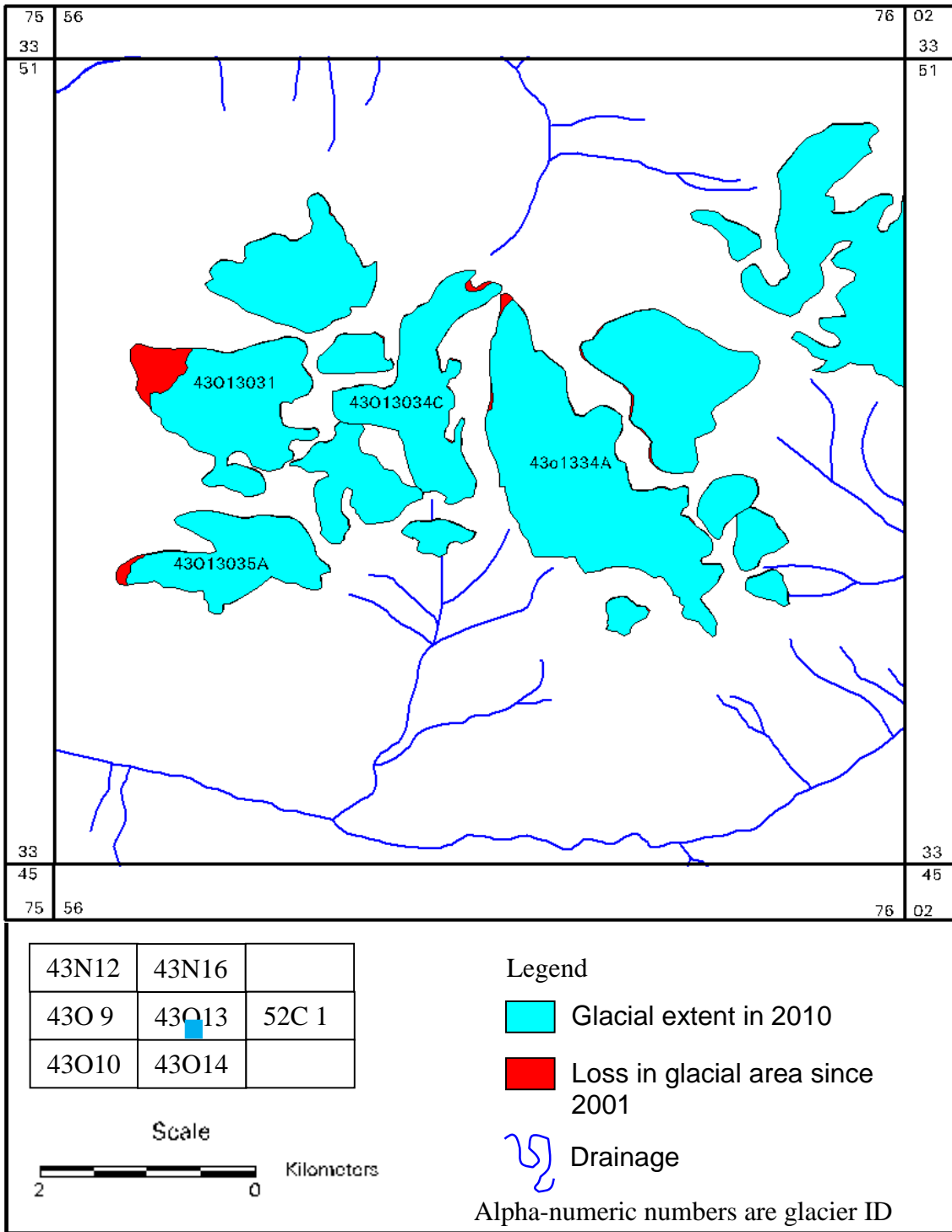


Figure 99: Map showing loss in area of the glaciers of a part of the Warwan sub-basin between 2001 and 2010 (Reference: Map No 43O/13)

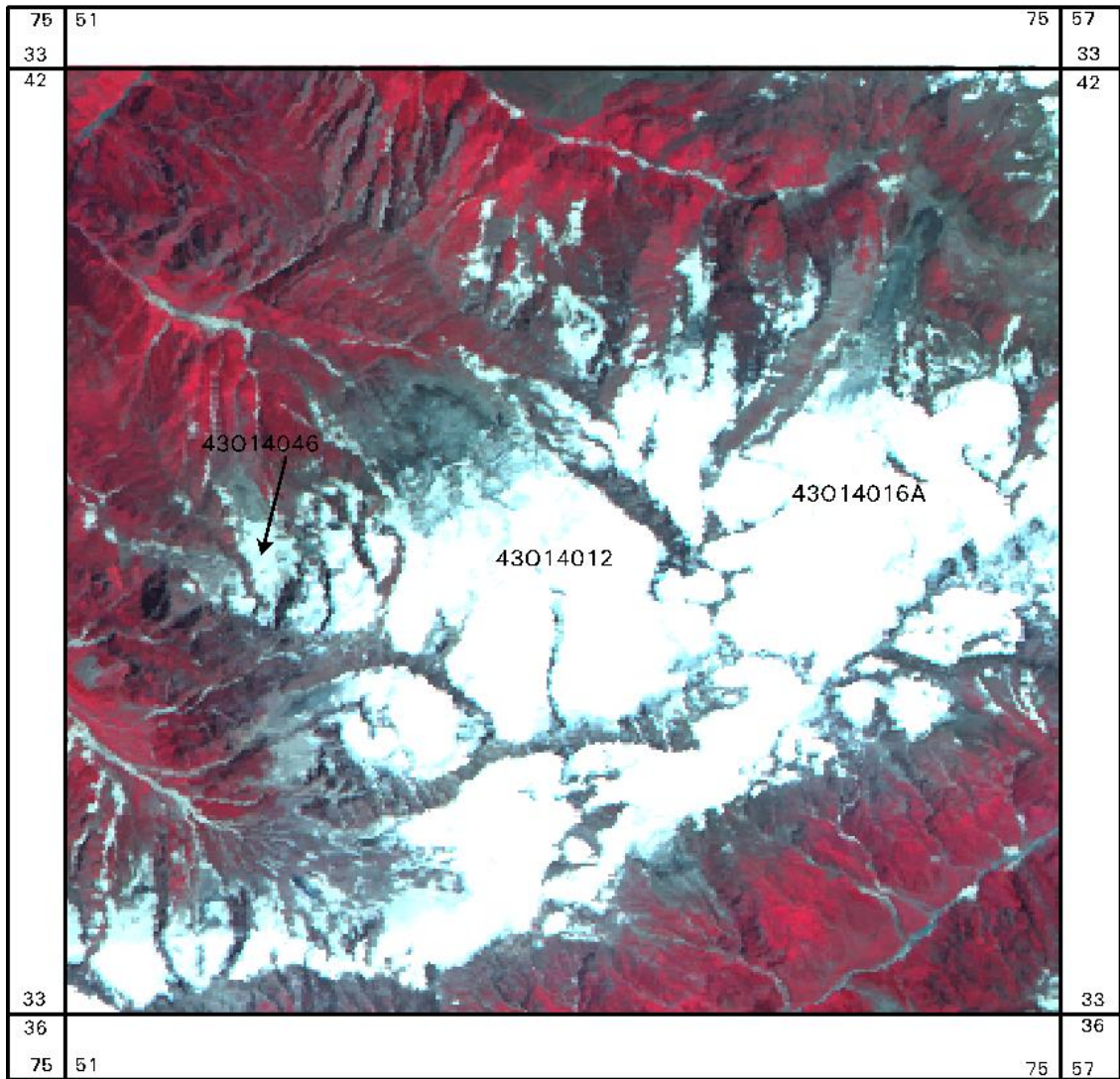


Figure 100: IRS P6 LISS III image of 2010, showing the glaciers of part of the Warwan sub-basin (Reference Map 43 O/14)

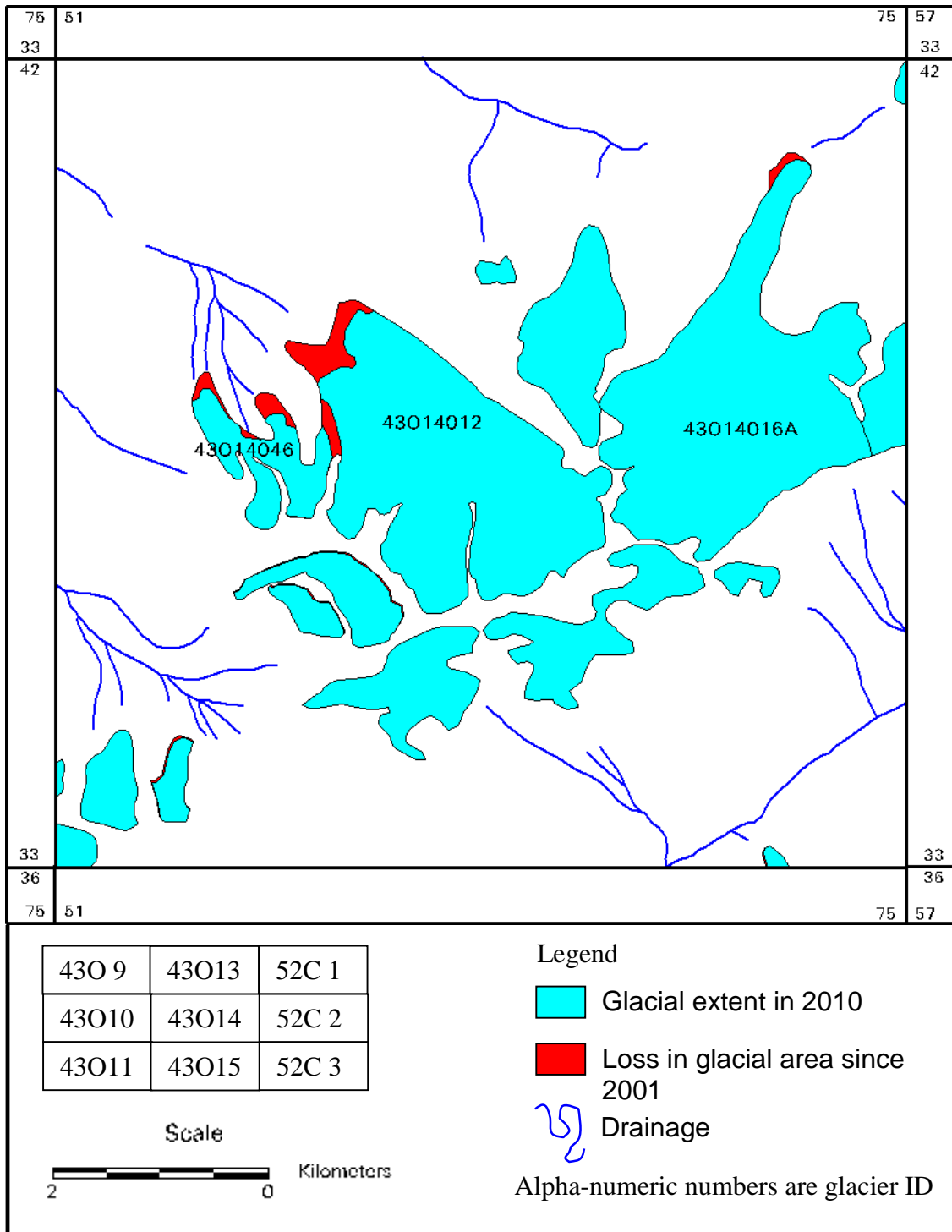


Figure 101: Map showing loss in area of the glaciers of a part of the Warwan sub-basin between 2001 and 2010 (Reference: Map No 430/14)

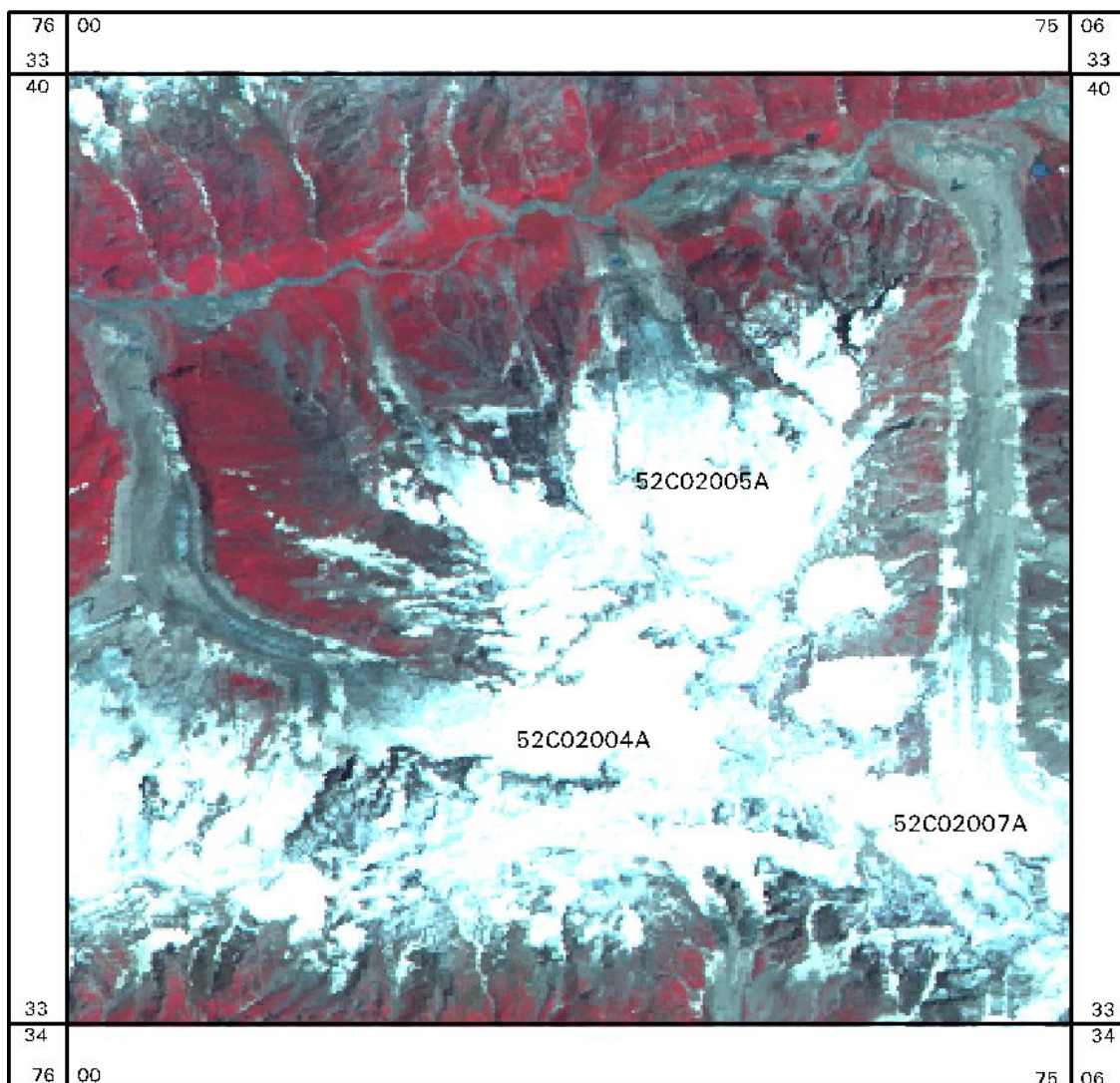


Figure 102: IRS P6 LISS III image of 2010, showing the glaciers of part of the Warwan sub-basin (Reference: Map No 52C / 02)

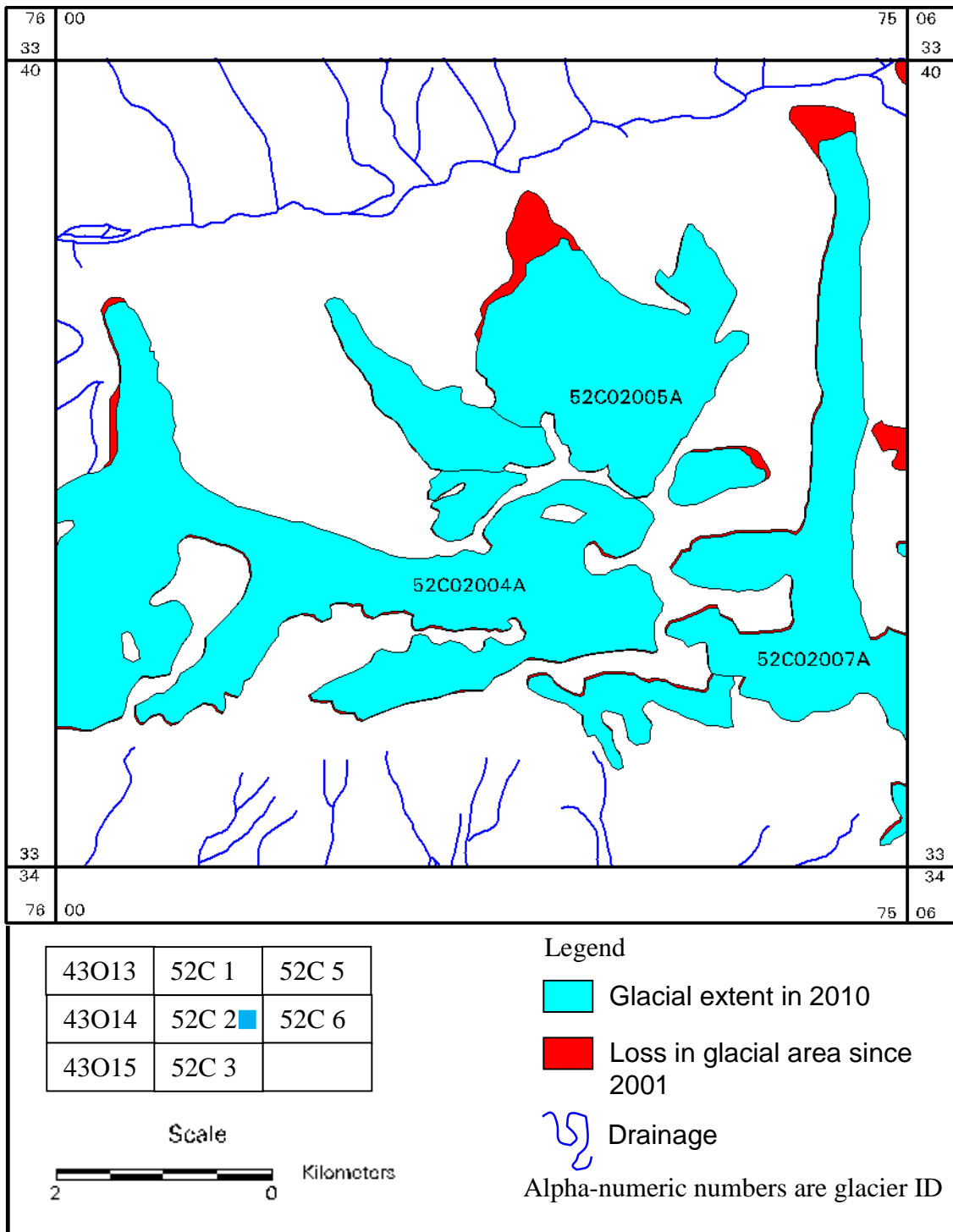


Figure 103: Map showing loss in area of the glaciers of a part of the Warwan sub-basin between 2001 and 2010 (Reference: Map No 52C / 02)

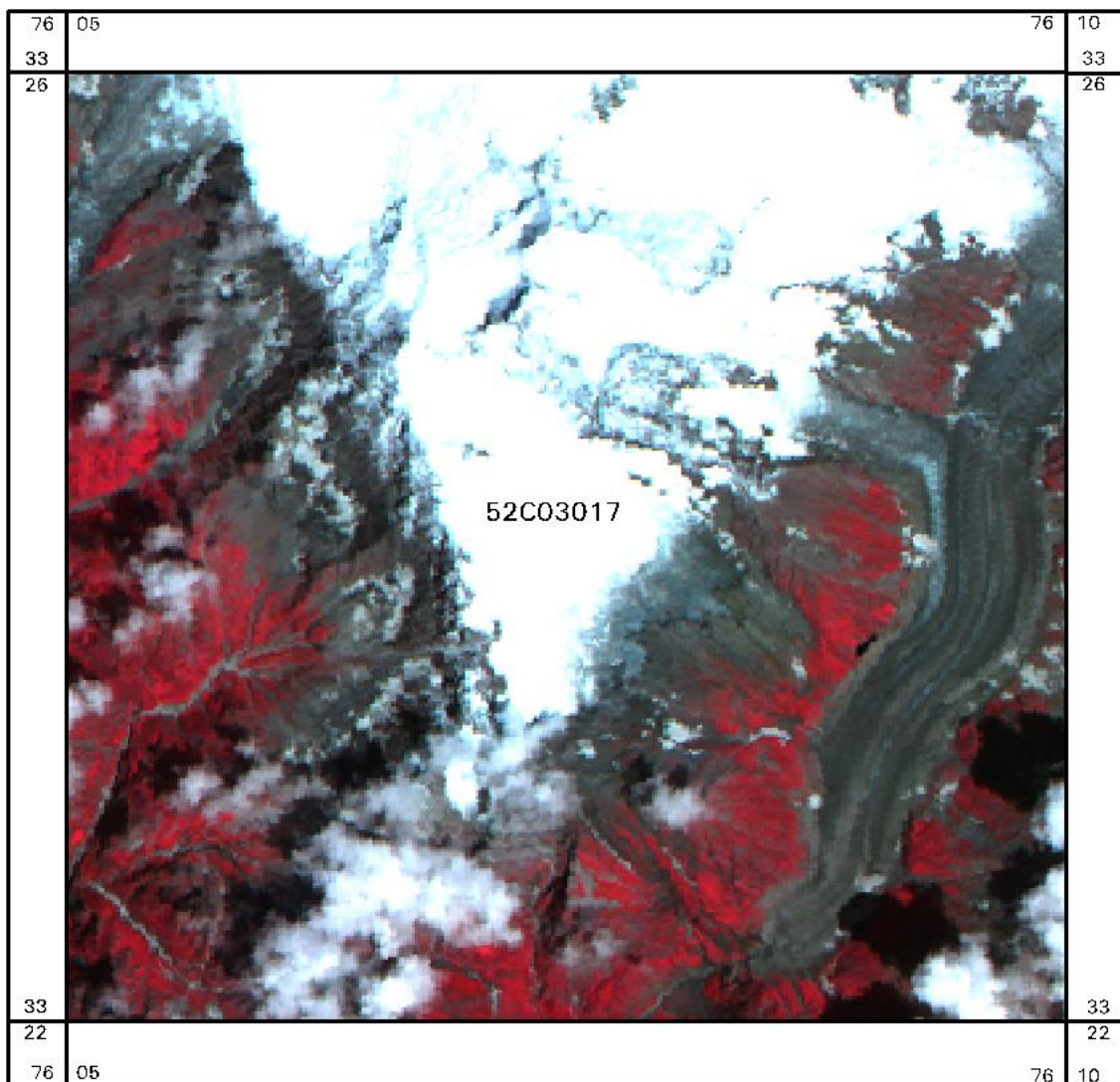


Figure 104: IRS P6 LISS III image of 2008, showing the glaciers of part of the Bhut sub-basin (Reference: Map No. 52C/3)

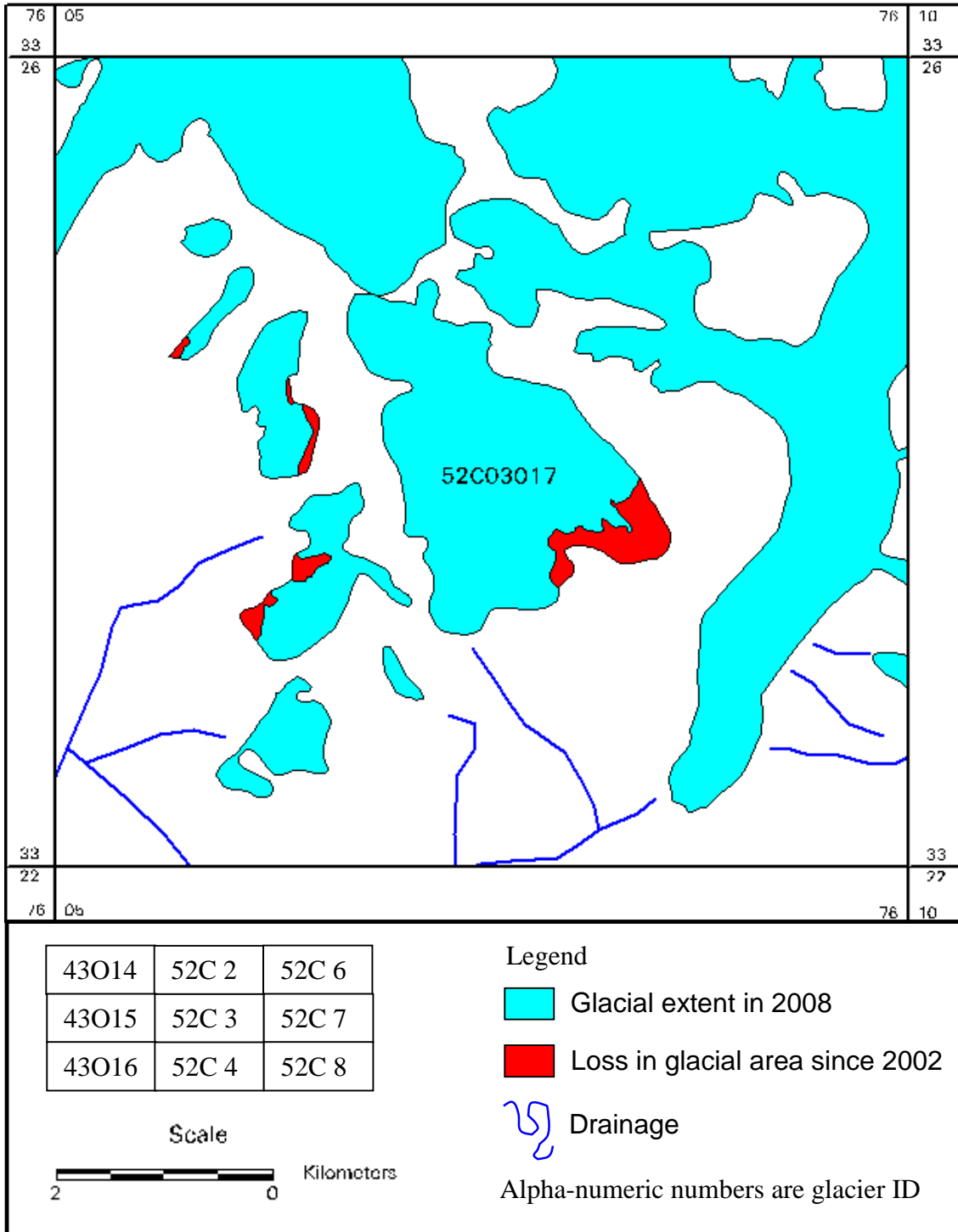


Figure 105: Map showing loss in area of the glaciers of a part of the Bhut sub-basin between 2002 and 2011 (Reference: Map No. 52C/3)

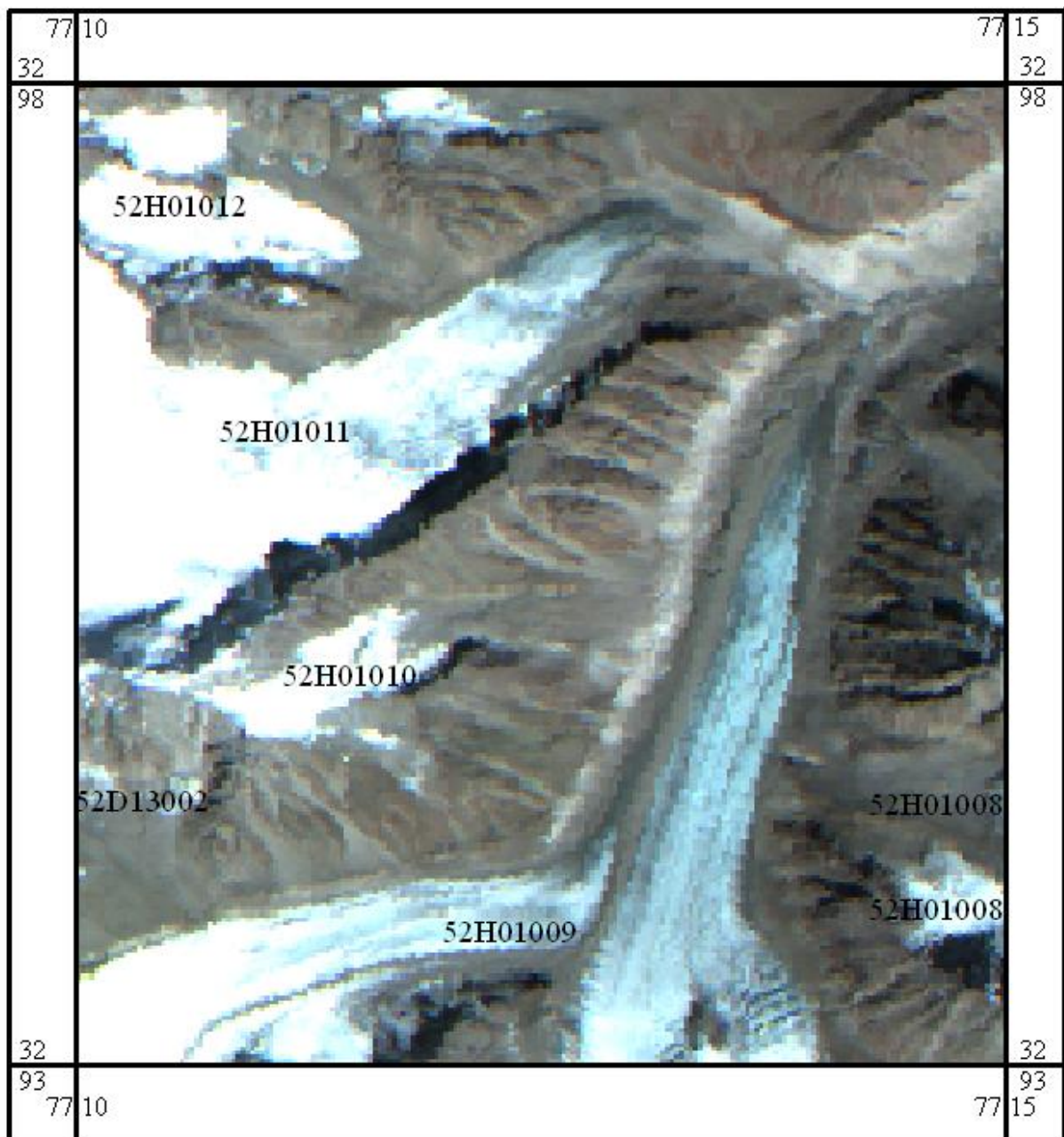


Figure 106: IRS 1C LISS III image of October, 2011 showing the Glaciers of part of the Bhaga sub-basin (Reference: Map No. 52H/1)

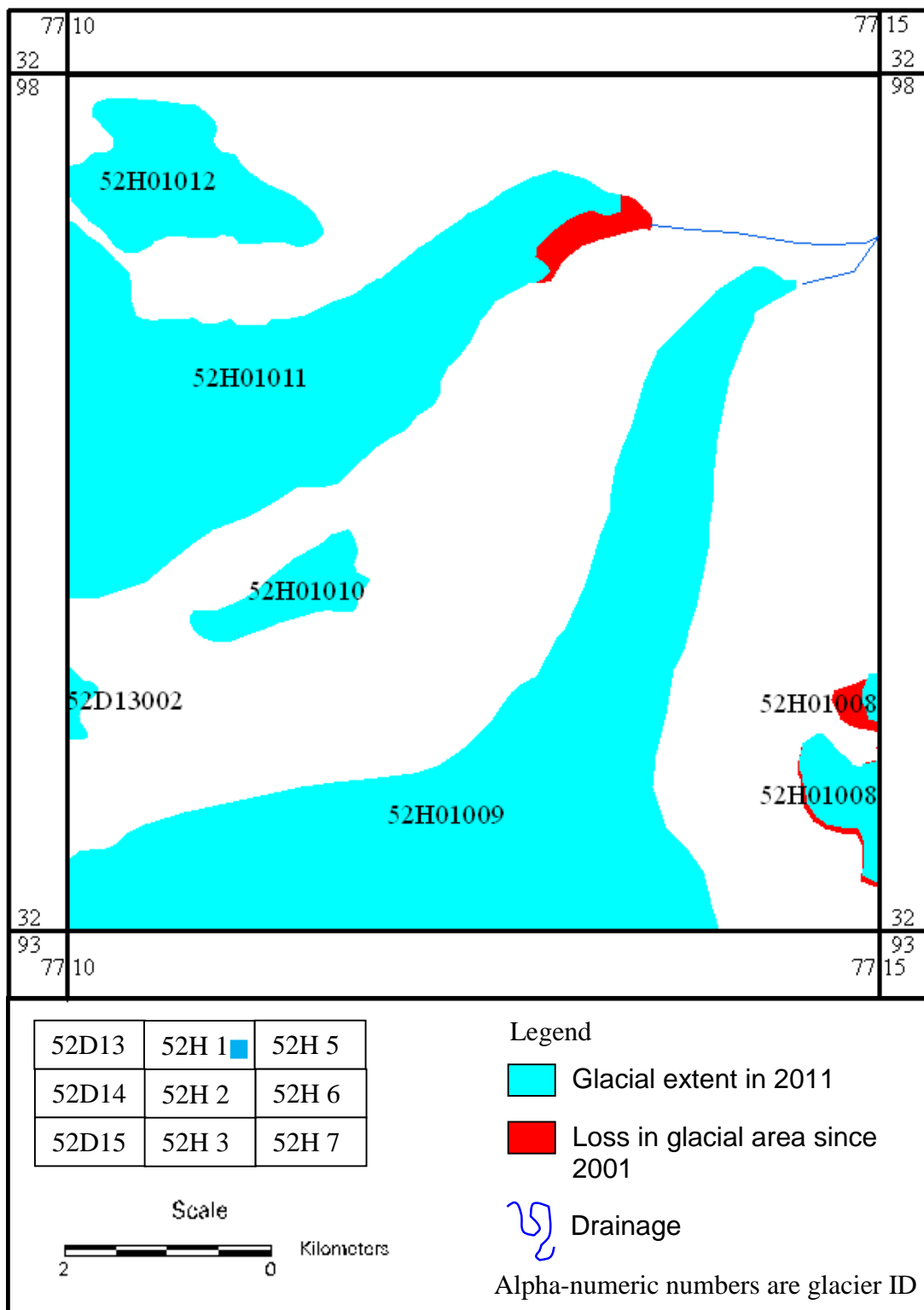


Figure 107: Map showing loss in area of the glaciers of a part of the Bhaga sub-basin between 2001 and 2011 (Reference map no.52H/1)

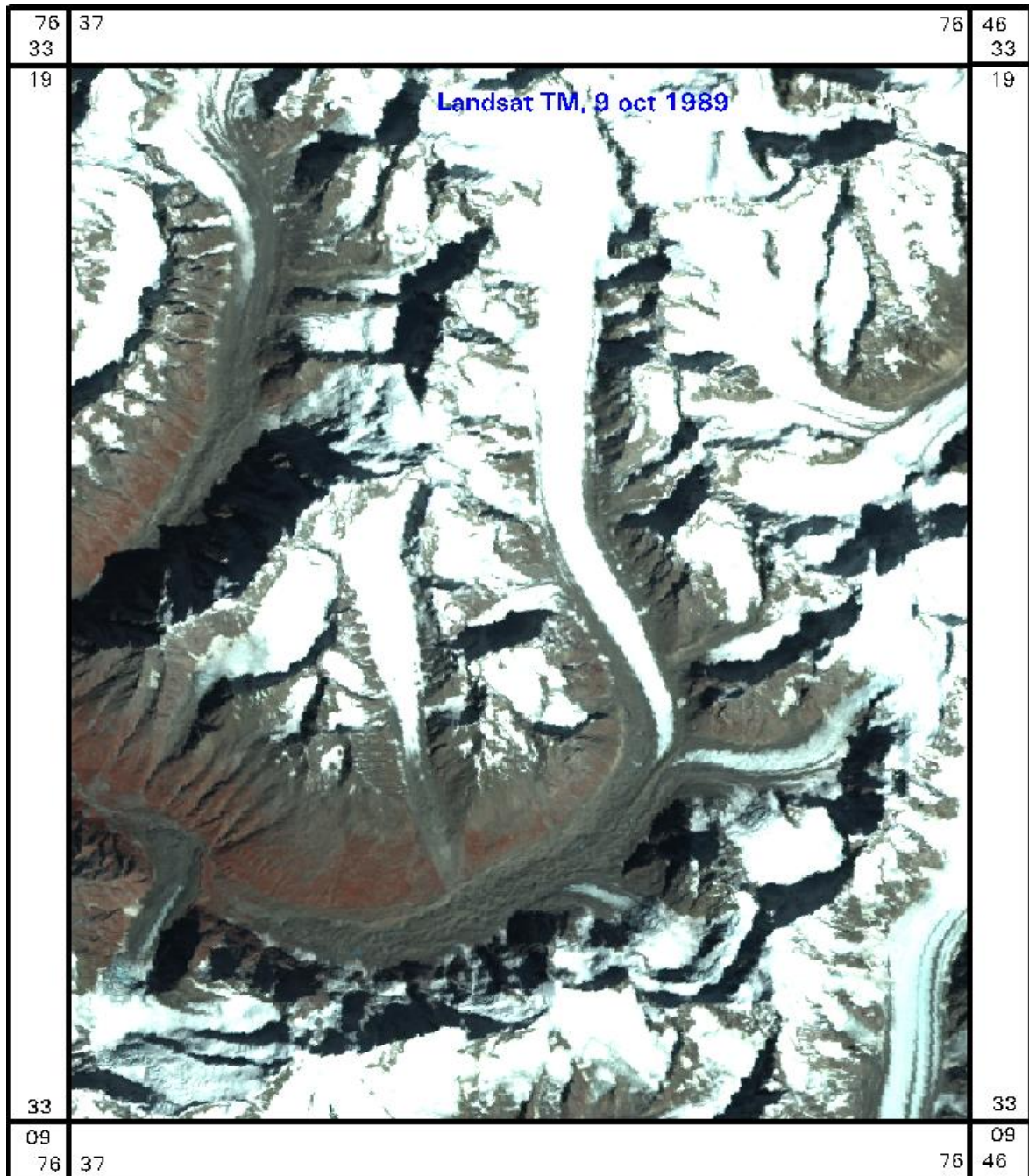


Figure 108: Landsat TM, image of October, 9 1989 showing the Glaciers of part of the Bhut sub-basin (Reference: Map No. 52H/7)

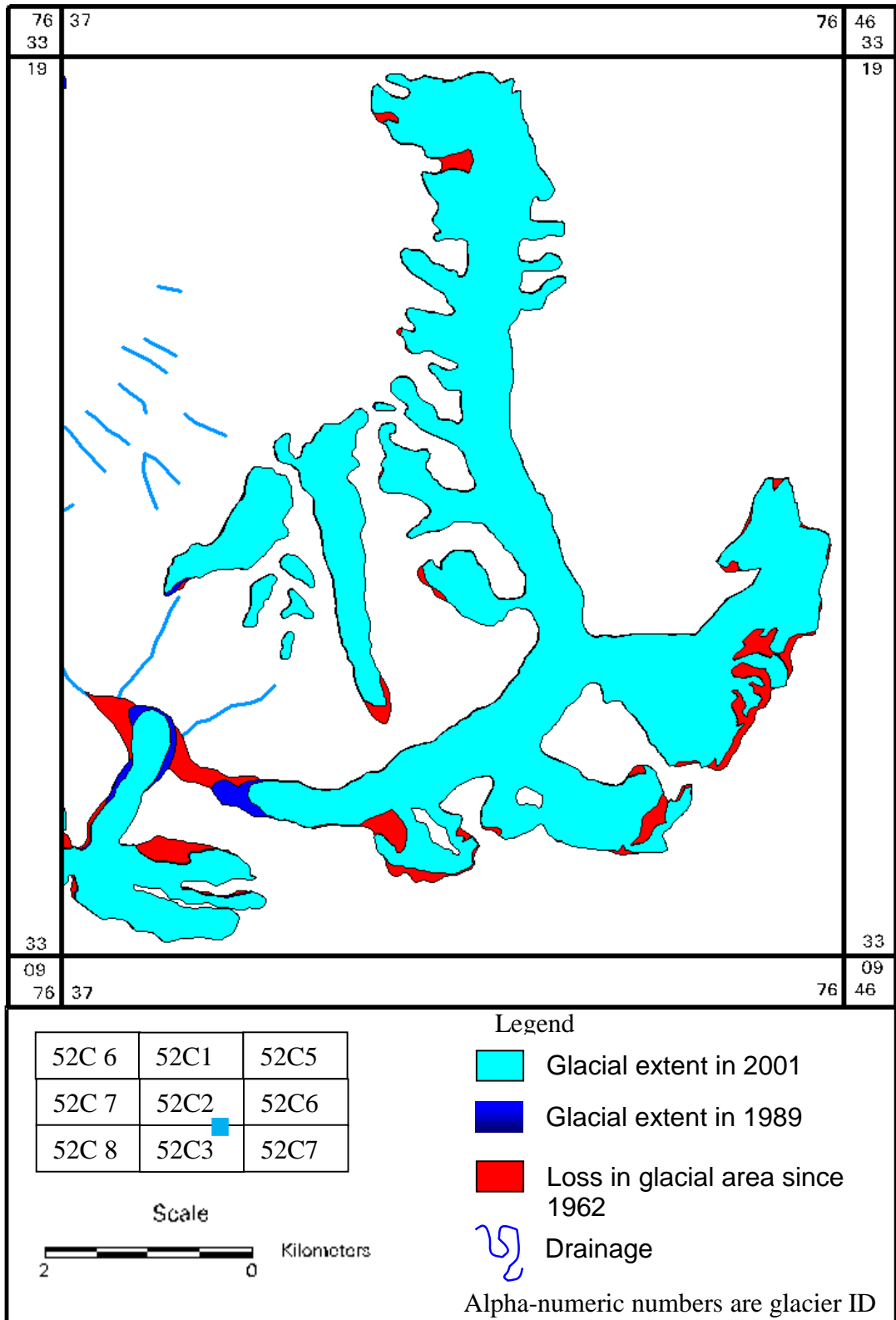


Figure 109: Map showing loss in area of the glaciers of a part of the Bhut sub-basin between 1989-2001-2011 (Reference map no.52H/7)

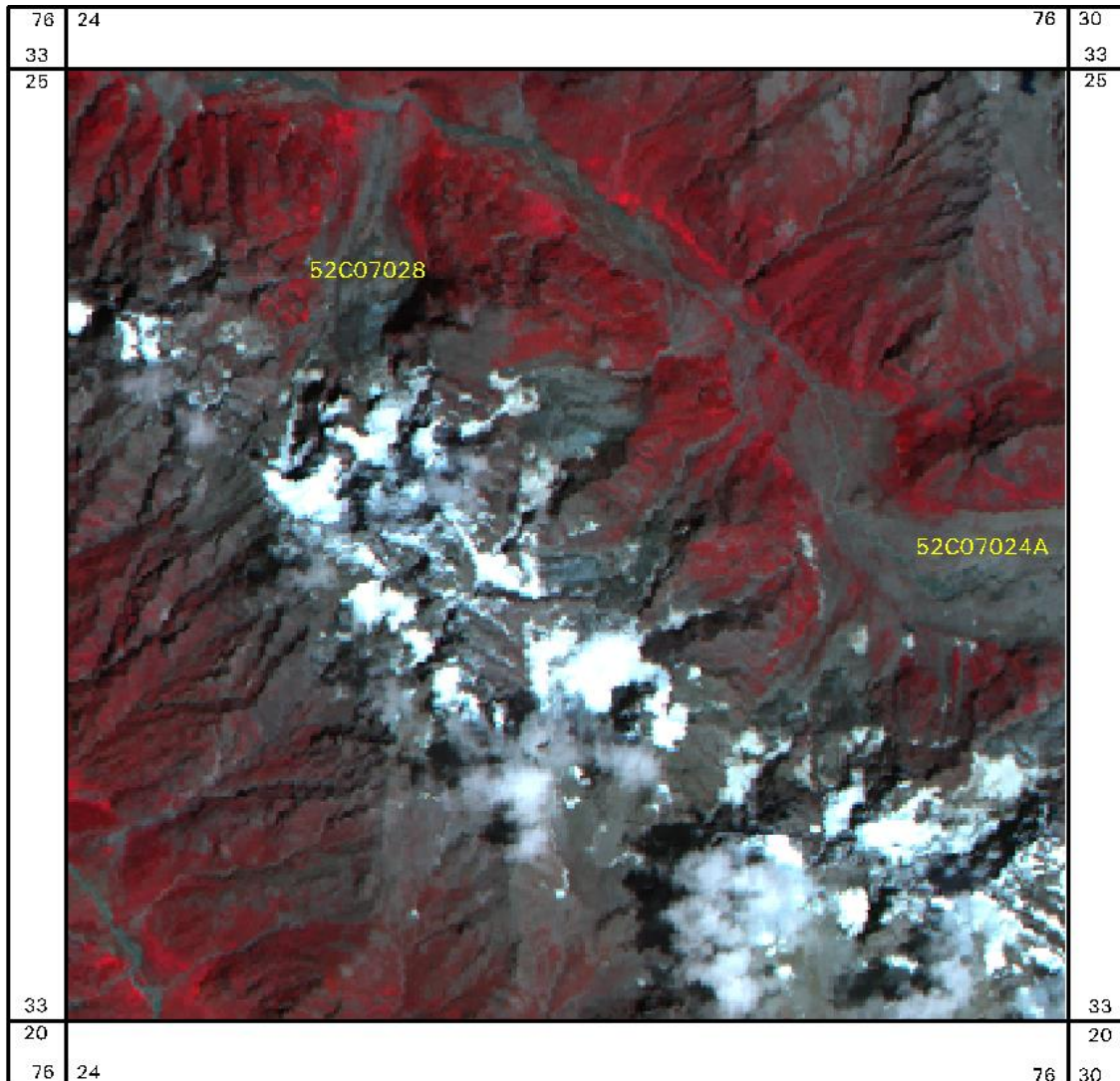


Figure 110: IRS P6 LISS III image of 2008, showing the glaciers of part of the Bhut sub-basin (Reference: Map No. 52C/7)

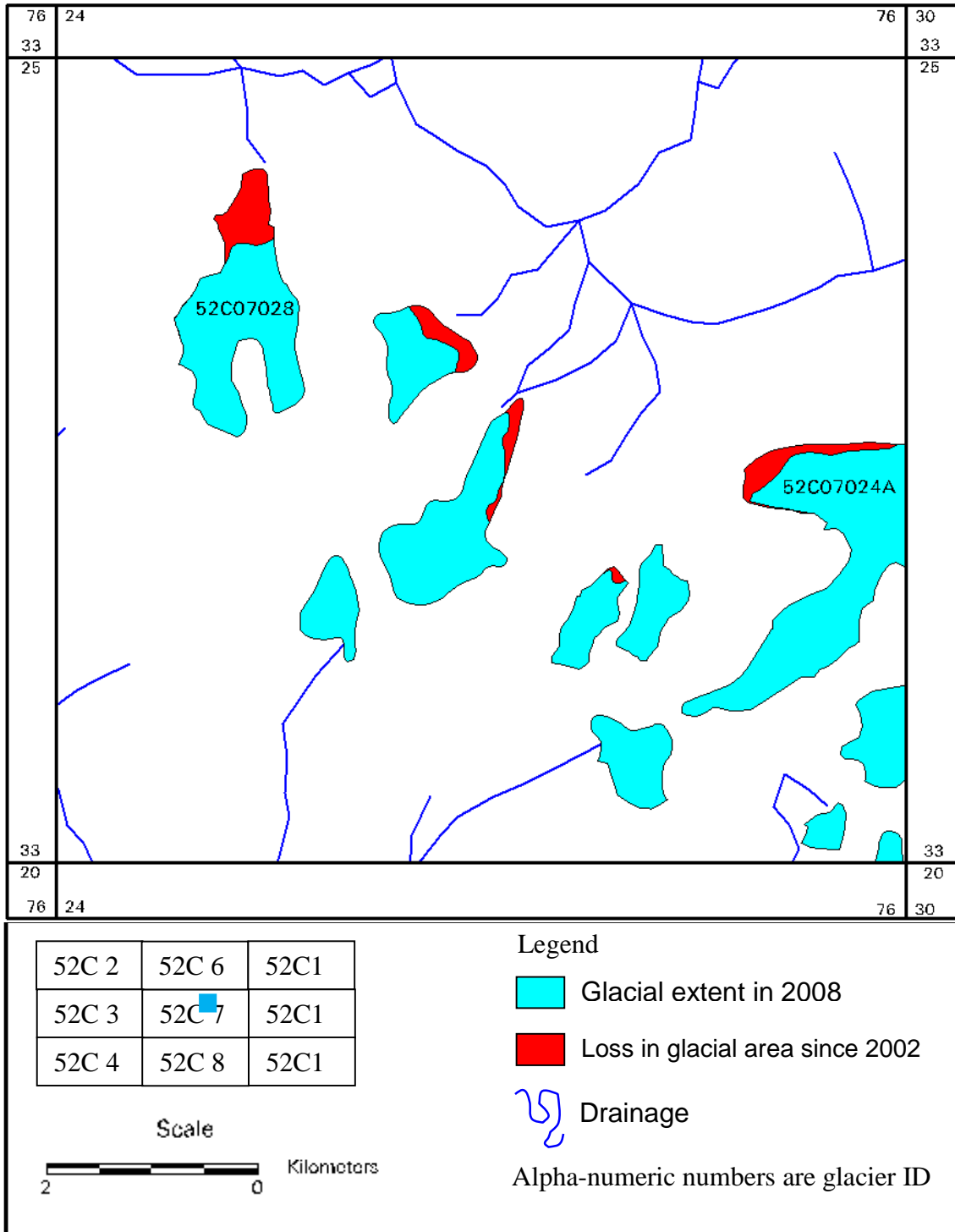


Figure 111: Map showing loss in area of the glaciers of a part of the Bhut sub-basin between 2002 and 2008 (Reference: Map No. 52C/7)

(b) Karakoram region

A detailed study has been carried out for 607 glaciers in the Shasgan, Shigar, Nubra and Shyok sub-basins of the Karakoram region. These glaciers were monitored for the period 1977 to 2013 using Landsat and IRS data (Brahmbhatt et al., 2015a; 2015b). This study shows a complete analysis of changes observed in the 607 glaciers during the time intervals 1977-1990, 1990-2000, 2000-2010 and 2010-2013. The location of glaciers in Karakoram region are shown in Figure 112.

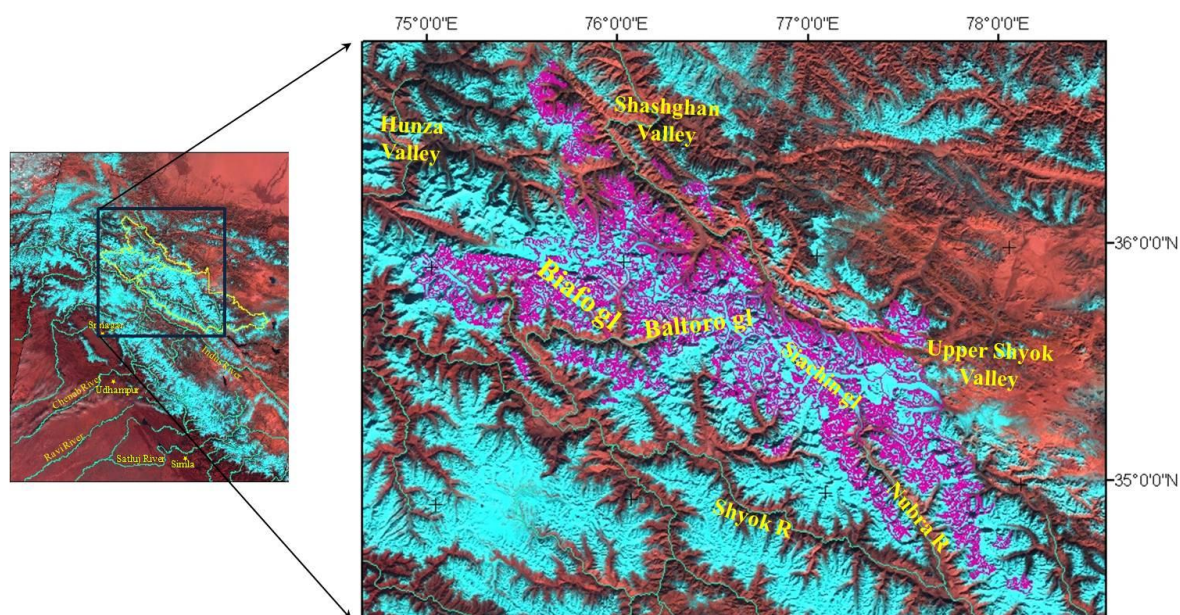


Figure 112: Locations of glaciers monitored in Karakoram region shown in satellite data (AWiFS image of year 2014 showing FCC of SWIR-NIR-Red) (Source: Brahmbhatt et al., 2015a)

The dynamics of glaciers in terms of stability, retreat or advance during 1977 to 2013 has been shown in the Figure 113 resembling like a tree. The glacier dynamics is discussed below:

1977-1990: Status of sub-basin wise changes in glaciers during 1977-1990 time frame is summarized in Table 41. It has been observed that out of 607 glaciers, 505 glaciers show no change, 79 glaciers show retreat and 23 glaciers show advance. Glaciers in all the four sub-basins viz., Shasgan, Shigar, Nubra and Shyok show loss in glaciated area. The total glaciated area of 607 glaciers in Karakoram region of 7894.95 sq. km. in 1977 has reduced to 7885.01 sq km in 1990. It is observed that net loss of glaciated area during 1977-1990 time frame is 9.94 sq km., indicating insignificant changes.

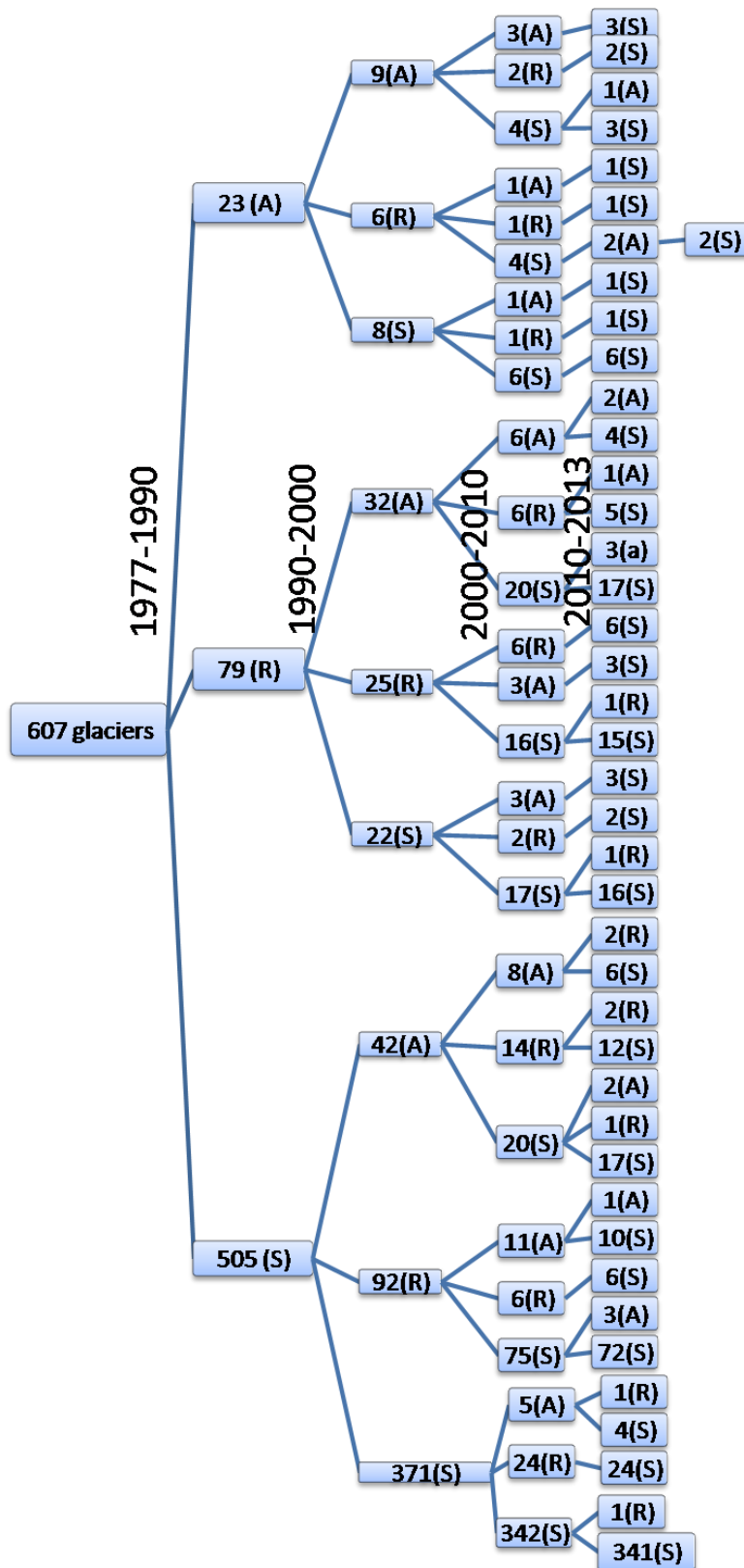


Figure 113: Glacier dynamics (S=Stable; R=Retreating; A=Advancing) of 607 glaciers of Karakoram during 1977-1990, 1990-2000, 2000-2010 and 2010-2013 time frames (Source: Brahmhatt et al., 2015a)

Table 41: Status of sub-basin wise changes in glaciers of Karakoram region during 1977 – 1990 time frame

Sub-basin	Glaciers studied (number)	Glaciers Stable (number)	Glaciers Retreating (number)	Glaciers Advancing (number)	Glaciated area in 1977 (km ²)	Glaciated area in 1990 (km ²)	Change in glaciated area (km ²)
Shasgan	291	263	21	7	2167.01	2165.35	-1.66
Shigar	139	123	12	4	2452.05	2449.15	-2.9
Nubra	135	86	41	8	1767.02	1764.68	-2.34
Shyok	42	33	5	4	1508.87	1505.83	-3.04
Total	607	505	79	23	7894.95	7885.01	-9.94

1990-2000: Status of sub-basin wise changes in glaciers during 1990-2000 time frame is summarized in Table 42. It is observed that out of 607 glaciers, 401 glaciers show no change, 123 glaciers show retreat and 83 glaciers show advance. Glaciers in Shigar and Shyok sub-basins show gain in area, whereas those in Shasgan and Nubra sub-basins show loss in glaciated area. However, the net glaciated area in Karakoram region of 7885.01 sq km in 1990 has reduced to 7882.18 sq km. It is observed that net loss of glaciated area during this time frame is 2.83 sq km., indicating insignificant changes.

Table 42: Status of sub-basin wise changes in glaciers of Karakoram region during 1990 – 2000 time frame

Sub-basin	Glaciers studied (number)	Glaciers Stable (number)	Glaciers Retreating (number)	Glaciers Advancing (number)	Glaciated area in 1990 (km ²)	Glaciated area in 2000 (km ²)	Change in glaciated area (km ²)
Shasgan	291	203	71	17	2165.35	2155.52	-9.83
Shigar	139	112	10	17	2449.15	2453.78	4.63
Nubra	135	84	31	20	1764.68	1762.34	-2.34
Shyok	42	2	11	29	1505.83	1510.54	4.71
Total	607	401	123	83	7885.01	7882.18	-2.83

Considering all the sub-basins together, Figure 113 show that 505 glaciers classified as stable during 1977-1990 time frame are observed to fall into three classes during 1990-2000 time frame viz., Stable - 371, Retreating - 92 and Advancing – 42. Glaciers observed to be retreating i.e., 79 glaciers during 1977-1990 time frame fall into three classes viz., Stable - 22, Retreating - 25 and Advancing - 32. Similarly, 23 glaciers classified as Advancing during 1977-1990 time frame show Stable – 8, Retreating – 6 and Advancing - 9 during 1990-2000 time frame. These observations indicate that behavior of glacier in one time frame may or may not be same during the subsequent time frames.

2000-2010: Status of sub-basin wise changes in glaciers during 2000-2010 time frame is summarized in Table 43. It is observed that out of 607 glaciers, 504 glaciers show no change, 62 glaciers show retreat and 41 glaciers show advance. Glaciers in Shyok sub-basin show gain in area, whereas those in Shasgan and Nubra have remained stable, while those in Shigar sub-basin have shown insignificant loss in area. However, the net glaciated area in Karakoram region of 7882.18 sq km in 2000 has increased to 7885.78 sq km. It is observed that net gain of glaciated area during this time frame is 3.6 sq km. Among advancing glaciers, 7 glaciers were observed to have sudden increase in their area. These glaciers are indicative of surging behavior.

Table 43: Status of sub-basin wise changes in glaciers of Karakoram region during 2000 – 2010 time frame

Sub-basin	Glaciers studied (number)	Glaciers Stable (number)	Glaciers Retreating (number)	Glaciers Advancing (number)	Glaciated area in 2000 (km ²)	Glaciated area in 2010 (km ²)	Change in glaciated area (km ²)
Shasgan	291	290	1	0	2155.52	2155.22	-0.3
Shigar	139	100	29	10	2453.78	2451.52	-2.26
Nubra	135	105	19	11	1762.34	1762.12	-0.22
Shyok	42	9	13	20	1510.54	1516.92	6.38
Total	607	504	62	41	7882.18	7885.78	3.6

Considering all the sub-basins together, Figure 113 show status of number of glaciers initially classed as Stable – 505, Retreating – 79, Advancing - 23 during 1977-1990 time frame in subsequent 1990-2000 and 2000-2010 time frames.

2010-2013: Status of sub-basin wise changes in glaciers during 2010-2013 time frame is summarized in Table 44. It is observed that out of 607 glaciers, 583 glaciers show no change, 9 glaciers show retreat and 15 glaciers show advance. Glaciers in Shasgan and Shyok sub-basin show gain in area, whereas those in Shigar and Nubra have remained stable. However, the net glaciated area in Karakoram region of 7885.78 sq km in 2010 has increased to 7888.63 sq km. It is observed that net gain of glaciated area during this time frame is 2.85 sq km.

Considering the overall changes in 607 glaciers of Karakoram region and also assessing the overall mapping accuracy, the salient findings are summarized in Table 45 and Figure 114, Figure 115, Figure 116 and Figure 117.

Table 44: Status of sub-basin wise changes in glaciers of Karakoram region during 2010 – 2013 time frame

Sub-basin	Glaciers studied (number)	Glaciers Stable (number)	Glaciers Retreating (number)	Glaciers Advancing (number)	Glaciated area in 2001 (km ²)	Glaciated area in 2010 (km ²)	Change in glaciated area (km ²)
Shasgan	291	275	4	12	2155.22	2157.75	2.53
Shigar	139	138	1	0	2451.52	2451.45	-0.07
Nubra	135	134	1	0	1762.12	1761.72	-0.4
Shyok	42	36	3	3	1516.92	1517.71	0.79
Total	607	583	9	15	7885.78	7888.63	2.85

Net glaciated area of advancing glaciers show increasing trend, retreating glaciers show a dip during 1977-1990 and since 1990 show increasing trend and stable glaciers remain stable during 1977-1990 and then a dip during 2000 and since 2000 show increasing trend. Some examples of advancing glaciers are shown in Figure 118, Figure 119 and Figure 120.

Table 45: Changes in glaciated area of 607 glaciers in Karakoram for time frame 1977-2013 (Source: Brahmabhatt et al., 2015a)

Year	Total Glacier Area (km ²)	Period	Change in total glacier area (km ²)	Change of area Advancing glacier (km ²)	Change of area of retreating glaciers (km ²)
1977	7895 ($\pm 8\%$)	-	-	-	-
1990	7885 ($\pm 3\%$)	1977-1990	(-)10 ($\pm 8\%$)	3.62 ($\pm 10\%$)	13.6 ($\pm 6\%$)
2000	7882 ($\pm 3\%$)	1990-2000	(-)3 ($\pm 1.7\%$)	20.2 ($\pm 1.8\%$)	23 ($\pm 1.5\%$)
2010	7885.8 ($\pm 3\%$)	2000-2010	(+)4 ($\pm 2.5\%$)	10.6 (± 2.1)	7.04 ($\pm 2.8\%$)
2013	7888.6 ($\pm 3\%$)	2010-2013	(+)3 ($\pm 3.8\%$)	5.5 (± 3.6)	2.7 ($\pm 4\%$)

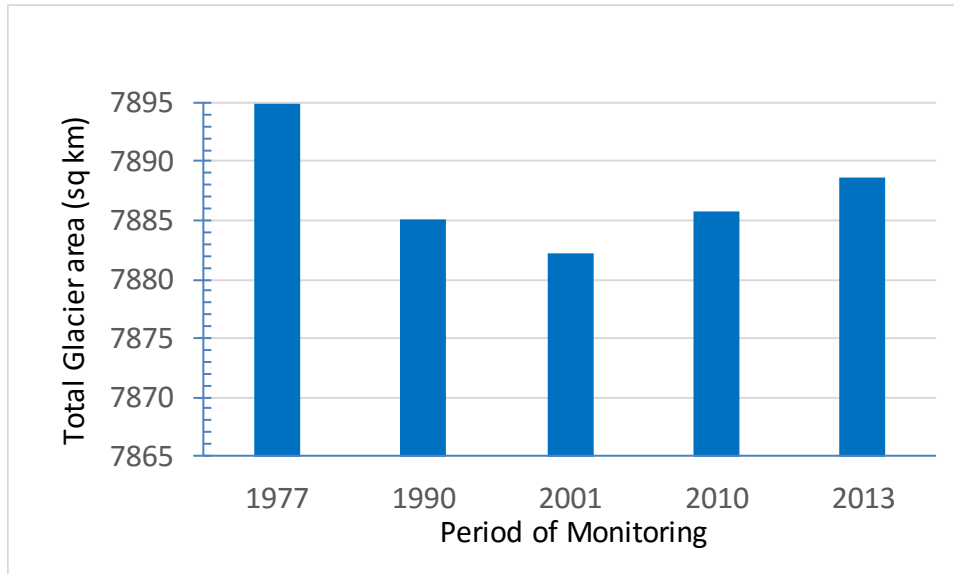


Figure 114: Total glaciated area of 607 glaciers in Karakoram during different time periods monitored using satellite data

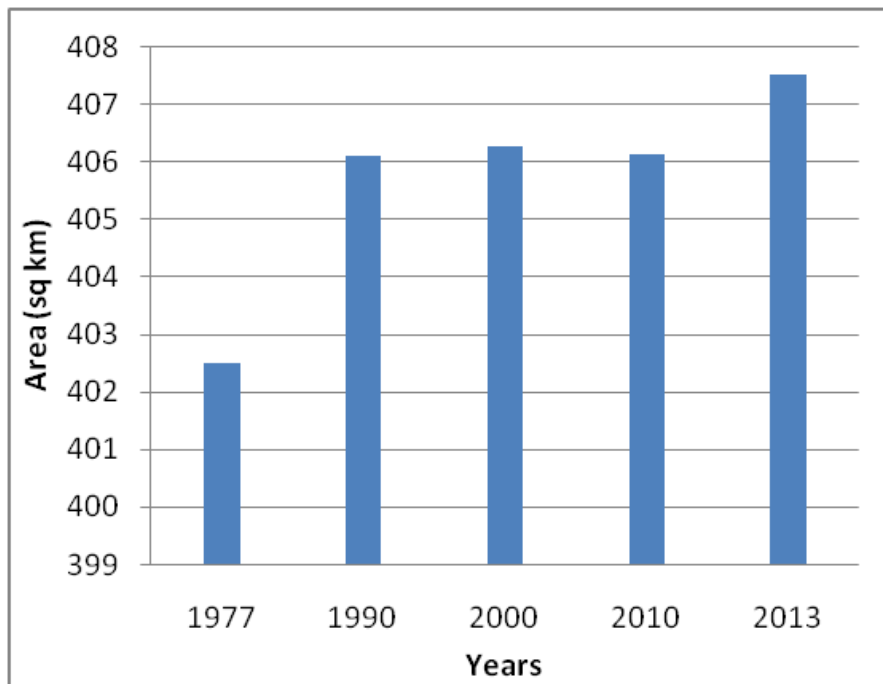


Figure 115: Total glaciated area of 23 advancing glaciers (as per changes observed during 1977-1990) in Karakoram during different time periods monitored using satellite data (Source: Brahmabhatt et al., 2015a)

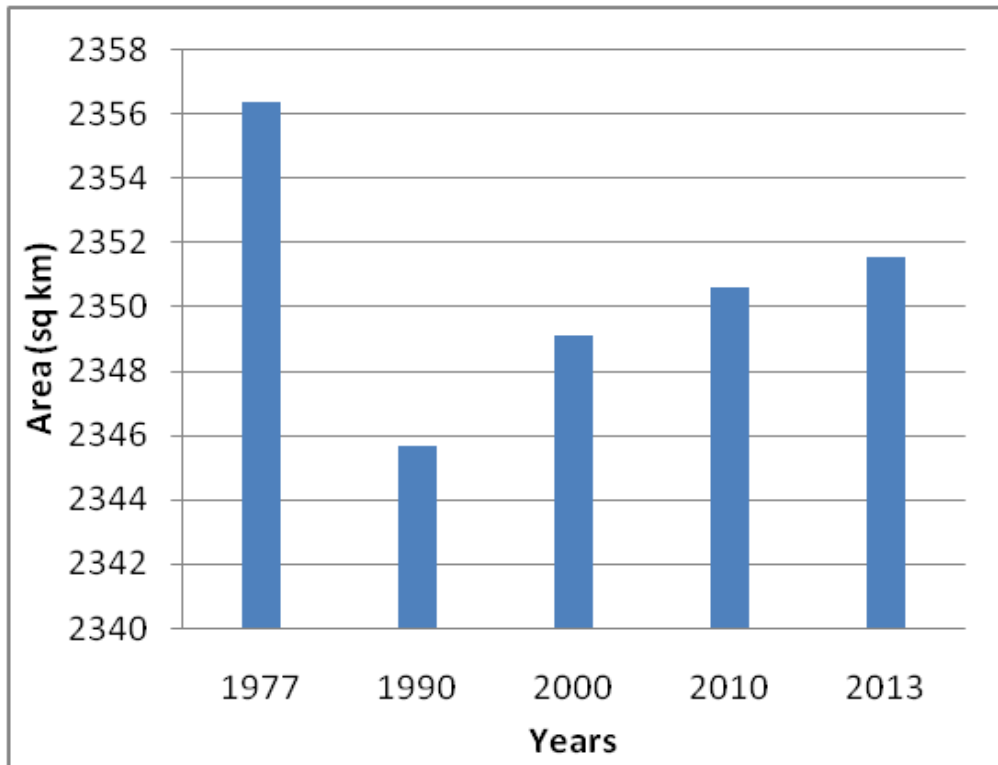


Figure 116: Total glaciated area of 79 retreating glaciers (as per changes observed during 1977-1990) in Karakoram during different time periods monitored using satellite data (Source: Brahmbhatt et al., 2015a)

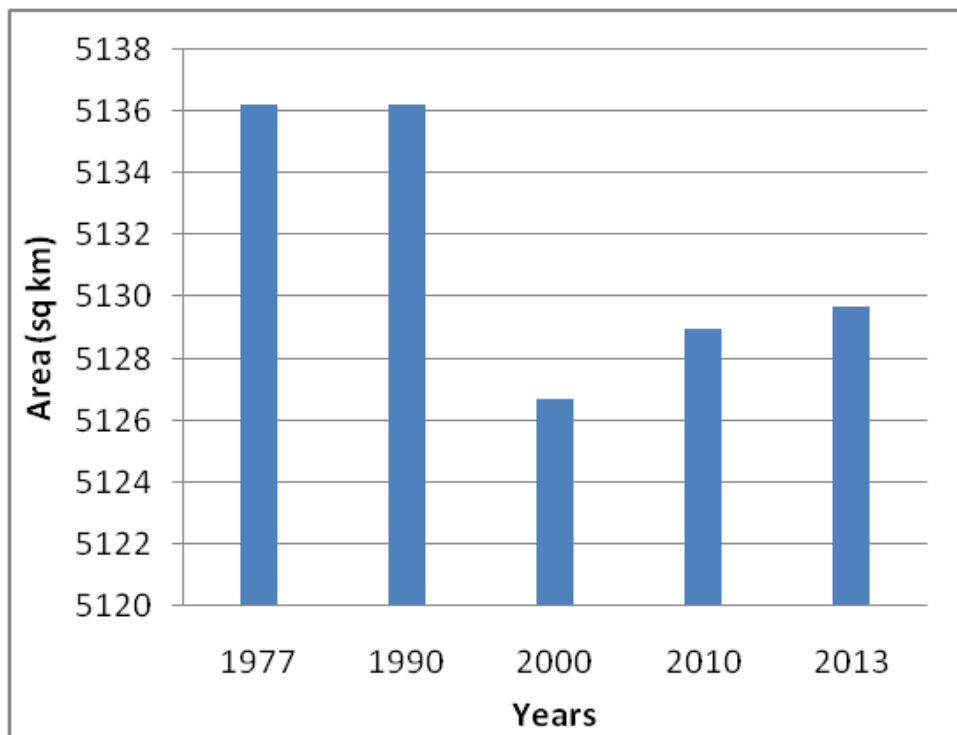


Figure 117: Total glaciated area of 505 stable glaciers (as per changes observed during 1977-1990) in Karakoram during different time periods monitored using satellite data (Source: Brahmbhatt et al., 2015a)

Spatial distribution of change in area of glaciers of Karakoram since 1977 is provided in Figure 118. Glaciers located at north-western and southeastern parts of the study area show tremendous variation in the advance and retreat for three time frames. Glaciers behaved very differently in each time frame, thus, no significant generalized trend was identified in changes of glaciers. In a few cases, glaciers have experienced advancement and overrode on other glacier and then gradually merged to main trunk glacier (Figure 119). In other cases, glaciers were advancing slowly and then stabilized (Figure 120). In a few cases, the tributary glaciers advanced and merged into main trunk glaciers, whereas the snout of main trunk glacier didn't show any considerable change (Figure 121).

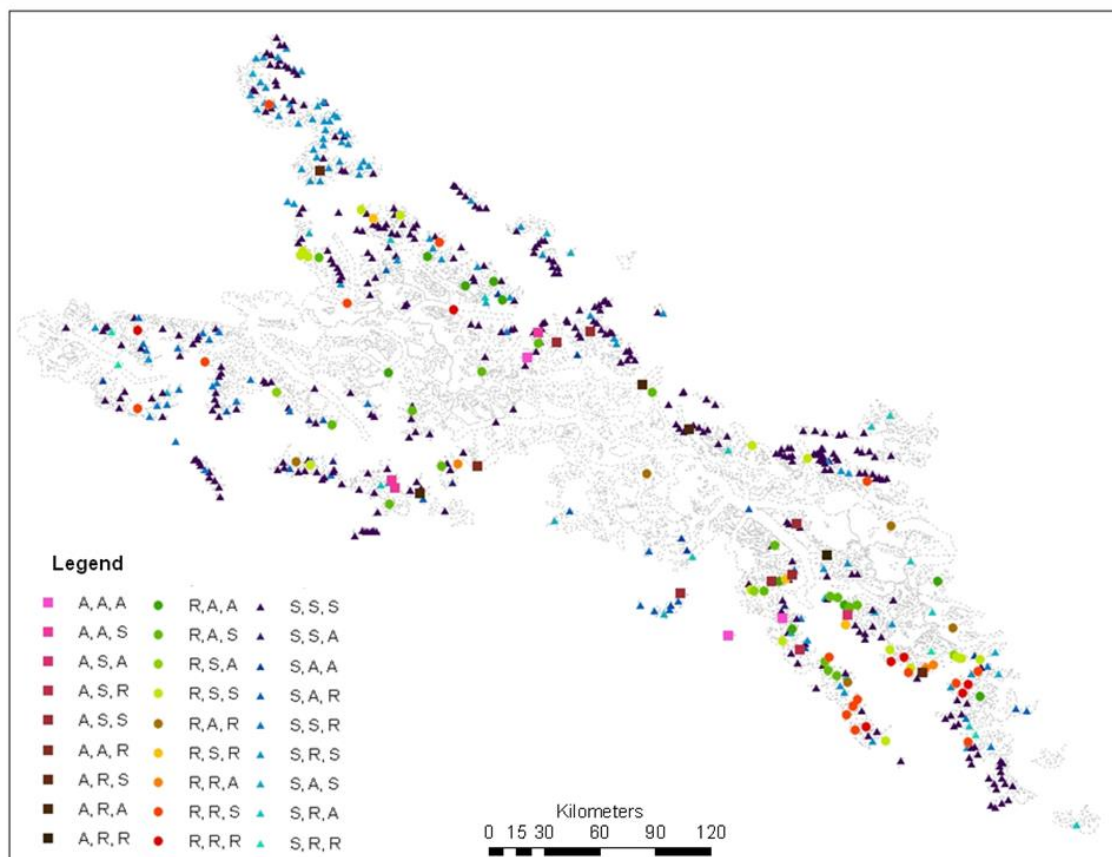


Figure 118: Spatial distribution of change in area of glaciers of Karakoram since 1977.

Note: R = Retreat, A= Advance and S = Stable E.g.: R-A-S = Retreat (in 1977-1990) – Advance (in 1990-2000) – Stable (in 2000-2013)
(Source: Brahmabhatt et al., 2015a)

Glaciers of the Karakoram have shown inconsistency in advance, retreat and no change during this period, and some examples of glacier surging have been observed. 341 glaciers exhibited no measured change throughout the 36 years of the study. Among other glaciers, no significant and sustained pattern of retreat or advance was observed. The overall changes in glacier area in the whole region are of small magnitudes (positive and negative values) in the various measured intervals.

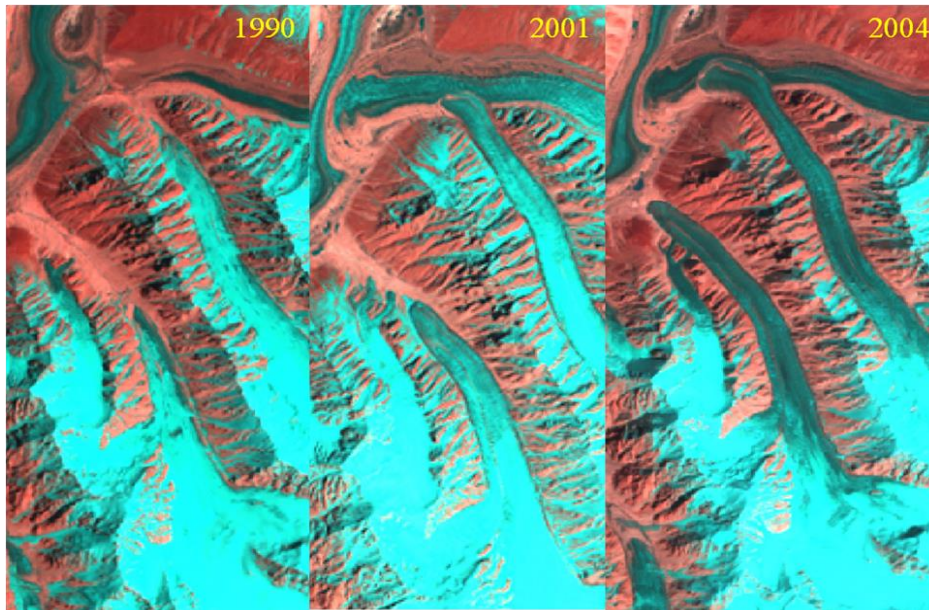


Figure 119: Landsat images of TM (1990), ETM (2001), ETM+ (2004) showing overriding and advancement of tributaries on main glacier (Panmah Glacier) (FCC in SWIR-NIR-Red) (Source: Brahmhatt et al., 2015a)

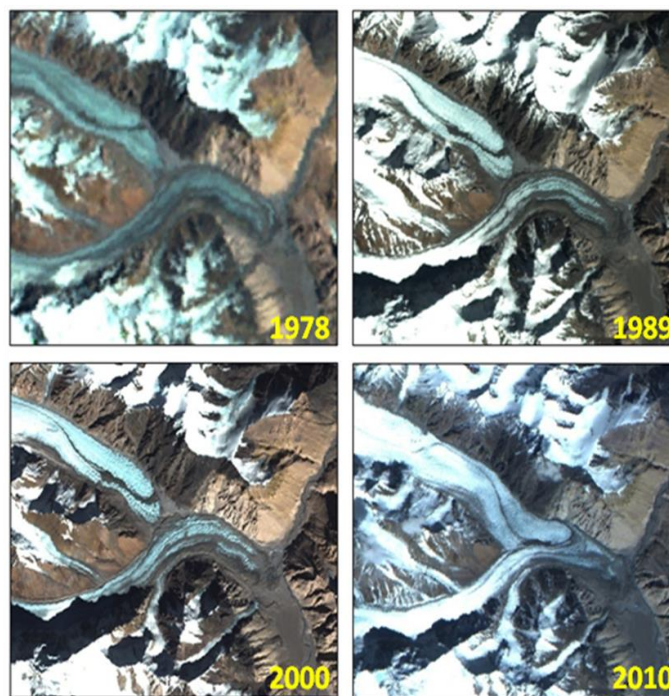


Figure 120: Landsat Images of MSS (1978), TM (1989), ETM (2001), ETM+ (2010) showing overriding and advancement of tributary glaciers (Chong Kumdan) (FCC in SWIR-NIR-Red). (Source: Brahmhatt et al., 2015a)

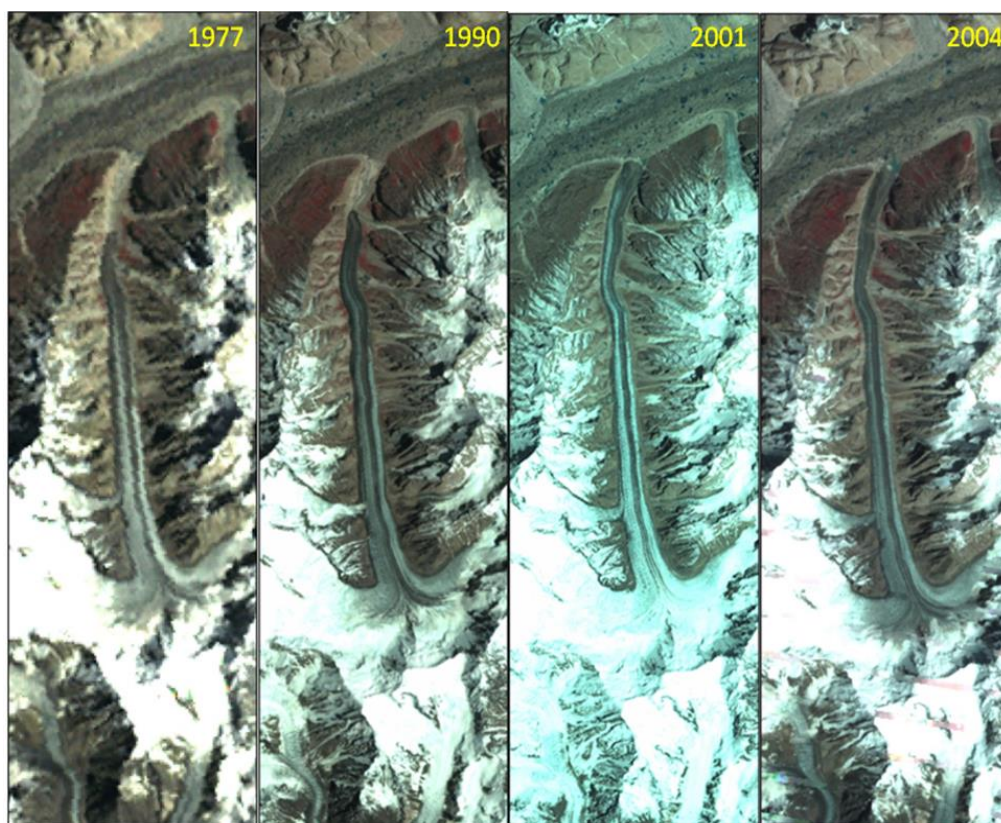


Figure 121: Images showing advancing of tributary glaciers up to bank of main trunk (Baltoro) glaciers. (Source: Brahmabhatt et al., 2015a)

Moreover, it is mostly disconnected glaciers in tributary valleys which have advanced, whereas the main former trunk glaciers have primarily not changed. The dynamical differences between disconnected former tributaries and trunks may be related to response time differences, with the smaller, perhaps steeper tributaries responding more rapidly than trunks to brief climatic fluctuations.

Precipitation system of Karakoram –Pamir region is different from other parts of Himalaya. Himalayas are influenced by SW and SE monsoon whereas Karakoram is nourished by western winds carrying moisture. The latitudinal differences account for difference in onset and longevity of winters and consequent impact on glacier dynamics of the Karakoram region, which is different than other parts of the Himalayas.

(c) Detail study of Kolahoi glacier in Kashmir valley, Himalayas

Four glaciations are evident in the Kolahoi valley on the basis of the detailed glacio-geomorphological features mapped in the field during the study. The oldest glaciation i.e., Pahalgam stage is represented by subglacial moraines which at present are overlain by bedded soil layers and vegetation identified and mapped during the field survey. The second glaciation (Aru Stage) is well represented by a 6 km long end moraine. The third glaciation (Lidderwat stage) is represented by well preserved end and lateral moraines. The fourth glaciation (Satlanjen stage), about 2.5 km downstream from the present snout position is represented by partially eroded end moraine and well preserved lateral moraines. Based on the presence of the moraines throughout the main valley, the present study proposes four glaciations witnessed in the region in the recent past. However, the number and timing of the major glacial advances in the region can be determined only by dating the moraines preserved in the valley.

Kolahoi glacier is the largest glacier (6 km long) in the Kashmir valley located in the Greater Himalayan range. A time series of satellite and other historical survey data was used for detecting recent changes in the snout, area and volume of Kolahoi glacier from 1857-2013. The analysis of the archived and remote sensing data revealed that the glacier has retreated 2.5 km from 1857 to 2013. On an average, the rate of retreat is 21.53 m/year during the period of observation. From 1887 till 1992 enhanced rate of snout retreat is observed. The glacier continued to melt at the average rate of 16.75 m/yr till 1992. The rate of retreat declined during 1992-2000 and was estimated as 5.55 m/year during the period (Figure 122 and 123). Though, low retreat of glacier tongue along its length is observed during 1992-2000, however, the glacier experienced relatively more recession across the width of its tongue during the period. The rate of retreat increased to its maximum between 2006 and 2014 receding at a rate of 56 m/yr during the period. This enhanced rate is partly attributed to the calving of the snout flowing over the steep bedrock. Though, the snout retreat is consistent with a number of glaciers studied across Himalayas including Milam in central Himalaya, Samandurtapu in western Himalaya and Gongotri in central Himalaya, however, a number of studies carried out in the neighboring Zaskar, Ladakh and Karakoram suggest that the snout retreat of Kolahoi glacier is quite high. The higher rate of retreat observed for the Kolahoi could be attributed to high temperatures observed in the region during the last century and comparatively low elevation of Kolahoi glacier snout

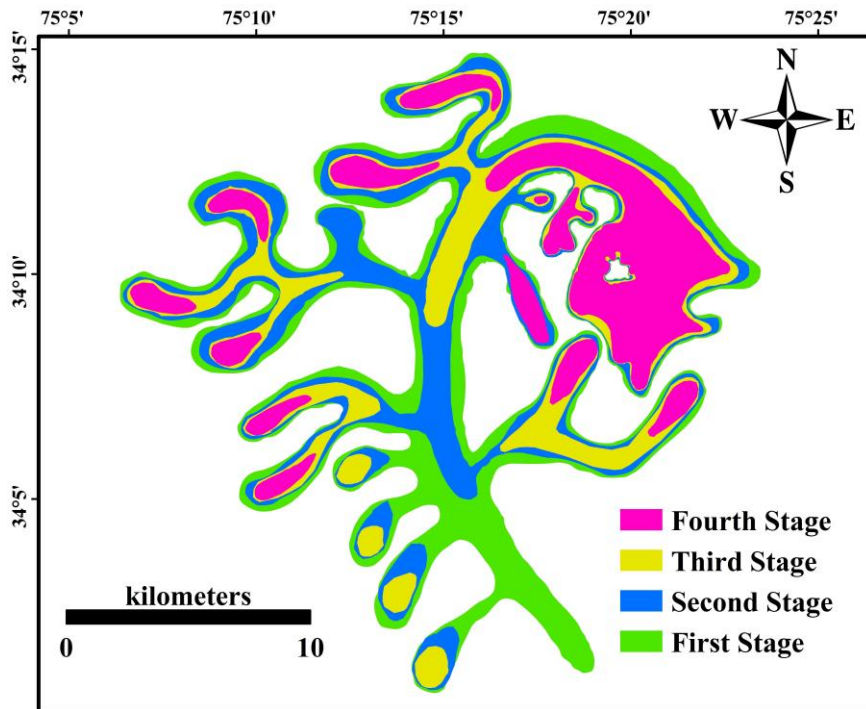


Figure 122: Deglaciation of Kolhoi valley (from field evidences)

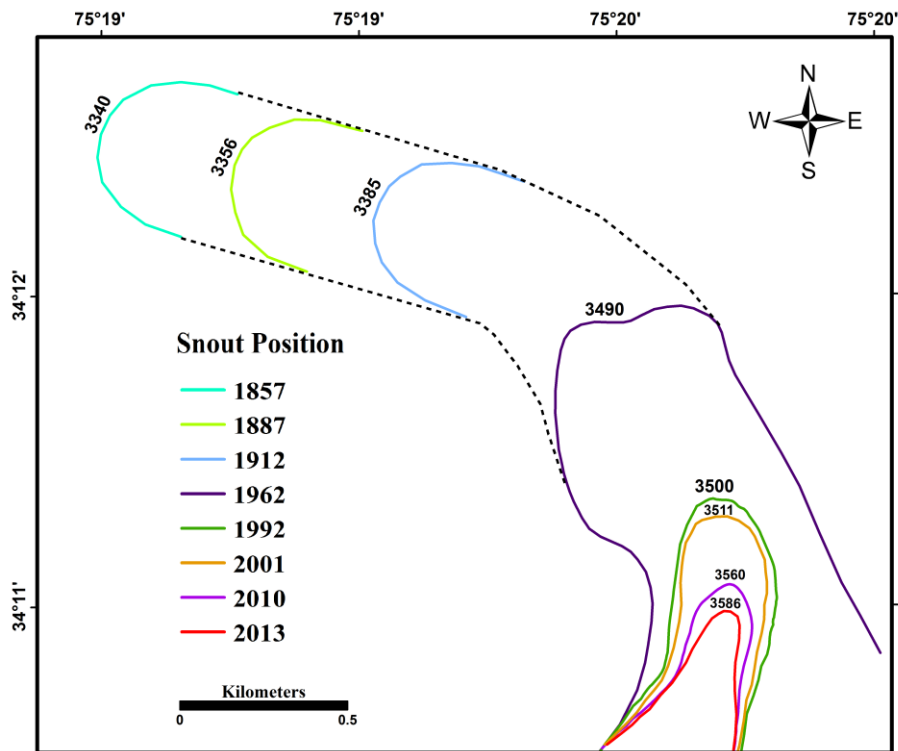


Figure 123: Position of Snout of Kolahoi at different points in time from 1857-2013

(d) Detailed study of glaciers of Miyar sub-basin

A detailed analysis of glaciers in the Miyar Basin, Lahaul & Spiti District of Himachal Pradesh (1963-2013) was carried out (Figure 124). Satellite images of post monsoon season i.e. September-October were selected for monitoring the glaciers, because this is the end of melting season. Since the basin is quite large in area and has a large number of glaciers, the satellite data of a particular year is not covering all glaciers and therefore every glacier has been monitored separately as per the availability of data. Corona images and Landsat images are freely downloadable from USGS earth explorer while the IRS PAN, IRS LISS III and IRS LISS IV images have been procured from NRSC, Hyderabad (Table 46).

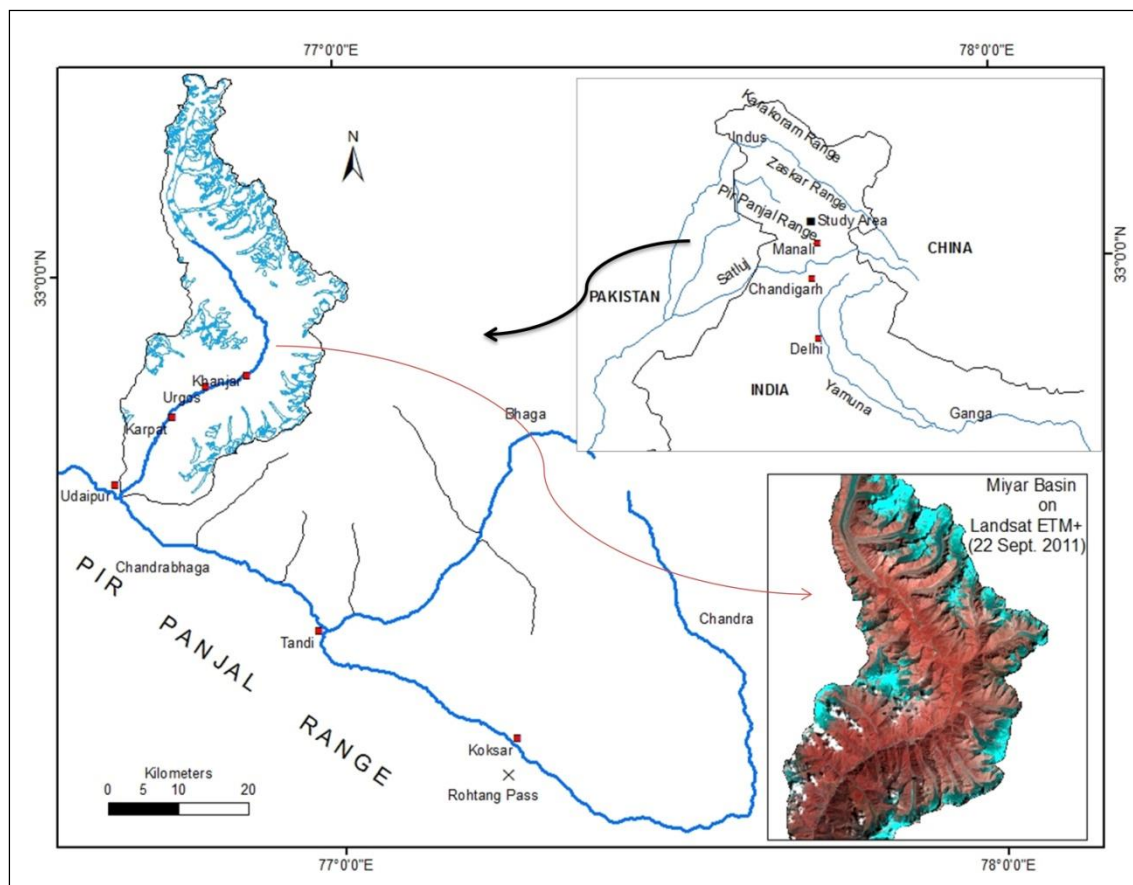


Figure 124: Location map of Miyar sub-basin

Corona images of Miyar basin are available for the years of 1965, 1971 and 1980. However, all glaciers of the basin could not be mapped using Corona because of the huge cloud cover. Therefore, Corona images have been used for a few glaciers only. Along with the remote sensing methods, field measurements have also been carried out for snout monitoring of the selected glaciers (Miyar, Pimu, Menthosa, Tharang and Uldhampu) with GPS in October 2006, June 2008, October 2010 (available archives), June 2011, June 2012 and June 2013.

Table 46: Satellite data used for monitoring of glaciers of Miyar basin

Sensor Type	Scene ID	Acquisition Date	Spatial Resolution (m × m)	Spectral Bands
Corona Forward	DS1024-1023DF102	24/09/1965	2	Pan
Corona Aft	DS1115-2282DA065	28/09/1971	2	Pan
Corona Aft	DS1115-2282DA064	28/09/1971	2	Pan
Corona KH-9	DZB1216-500361L008001	16/09/1980	2	Pan
Landsat MSS	p159r37_2m19751110	11/10/1975	79	4
Landsat TM	p147r37_5t19891009	09/10/1989	30	7
Landsat ETM+	p147r037_7t20000929	29/09/2000	30	7
IRS LISS III	142673600101	12/10/2000	23.5	4
IRS LISS III	142673600201	26/10/2001	23.5	4
IRS LISS III	142673600301	05/10/2006	23.5	4
IRS LISS III	142673711	15/10/2011	23.5	4
IRS PAN	142885900101	27/09/2002	5.8	Pan
IRS PAN	142673600701	05/10/2005	5.8	Pan
IRS PAN	142885900201	21/06/2007	5.8	pan
IRS LISS IV	7.890922 STUC00B234	04/10/2012	5.8	3
IRS LISS IV	7.447974 STUC00B234	23/10/2013	5.8	3
Aster GDEM	ASTGDEM2_0N32E076	17/10/2011	30	Pan
Aster GDEM	ASTGDEM2_0N33E076	17/10/2011	30	Pan

Miyar glacier is the largest in the basin with respect to length as well as area. Total number of glaciers in the basin is 76 as per the Survey of India Topographical Sheets of 1960. Total glacierised area in the basin as per SOI is 243.1 km², 25.22% (1960) of the total area of basin (963.85 km²). However, total number of glaciers in the basin is 92, delineated on the basis of satellite data of 2011 out of which 16 are valley glaciers and 76 are cirque glaciers. The total glacierised area is 230 km². The Aspect of the glaciers is found to be very important in this study with respect to the snout fluctuations of different glaciers in the basin. The major valley glacier in the basin, i.e. Miyar glacier is a south facing glacier. Dali, Chhudong and Takdung are the south-west facing glaciers, while Pimu and the other adjoining glaciers have north-east aspect. Dali, Chhudong and Takdung are opposite to Pimu on the right bank of Miyar River. Further down valley, all major glaciers on the left bank viz. Tharang, Uldhampu, Khanjar, Palbo, Gangpo and Karpat are north west facing while on the right, Menthosa having an aspect of south-east is just opposite to these glaciers (Figure 125). Changes in the glaciers of the Miyar sub-basin are mapped using topographical maps of 1963-1968 (Figure 125) and mutidate satellite data of 1965, 1975, 1989, 2000, 2002, 2007, 2008, 2010 and 2011 (Figure 126, Figure 127) supported by field measurements carried out for snout monitoring of the selected glaciers (Miyar, Pimu, Menthosa, Tharang and

Uldhampu) with GPS in June 2011, 2012 and 2013. Glaciological field evidences for changes in glacial extent were also studied.

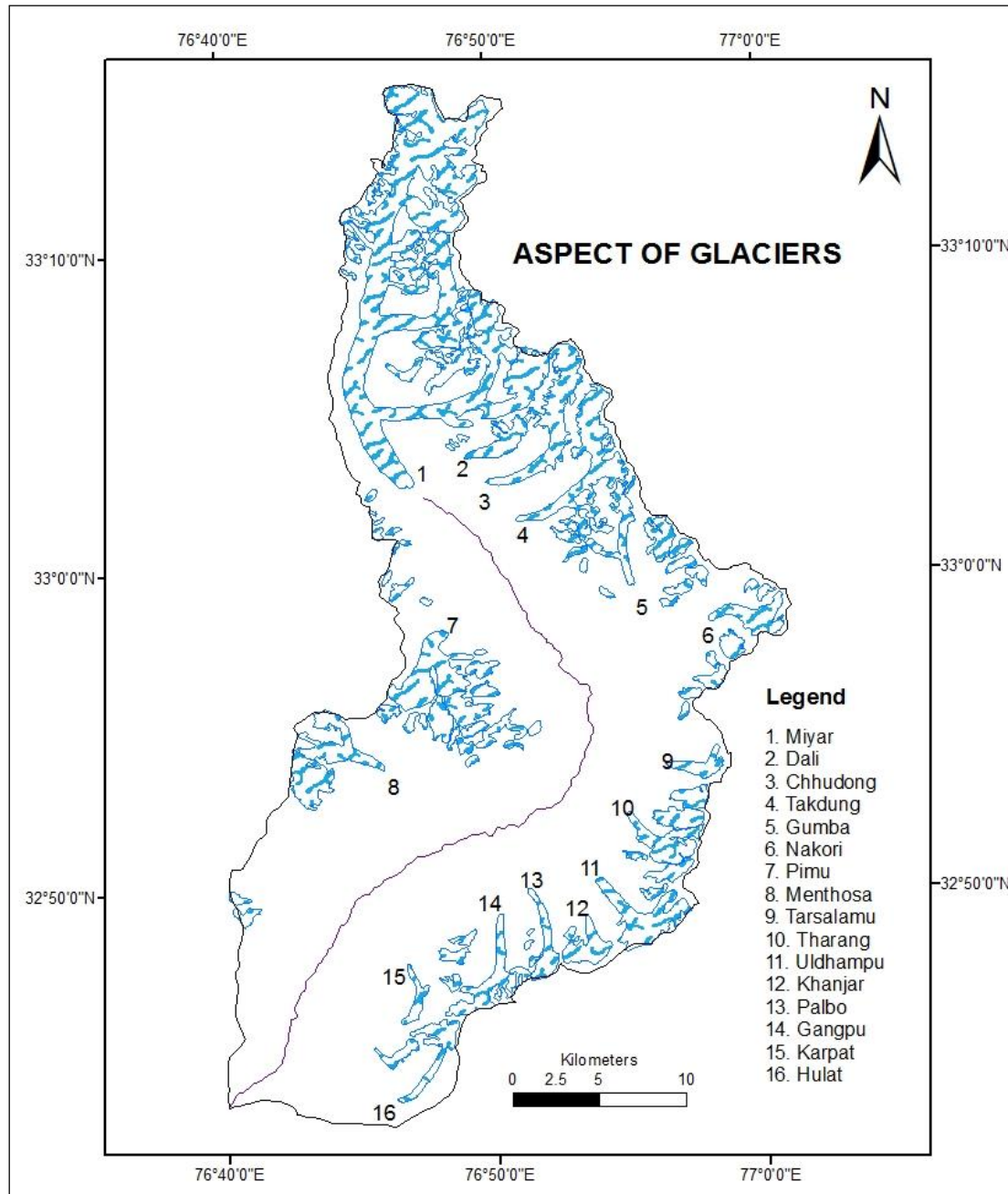


Figure 125: Glaciers in Miyar sub-basin as per topographical maps of 1963-1968

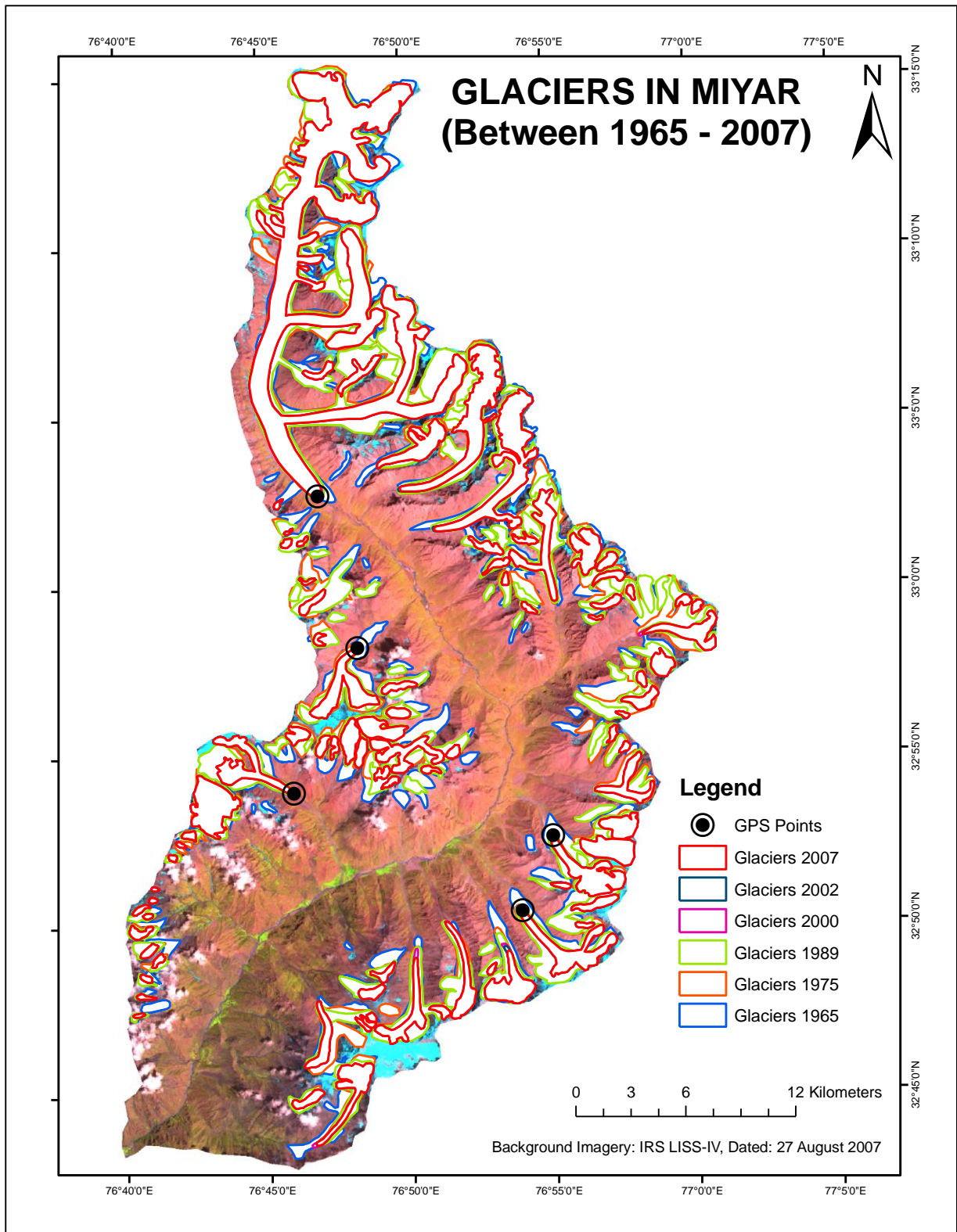


Figure 126: Changes in glaciers of Miyar sub-basin during 1965-2007

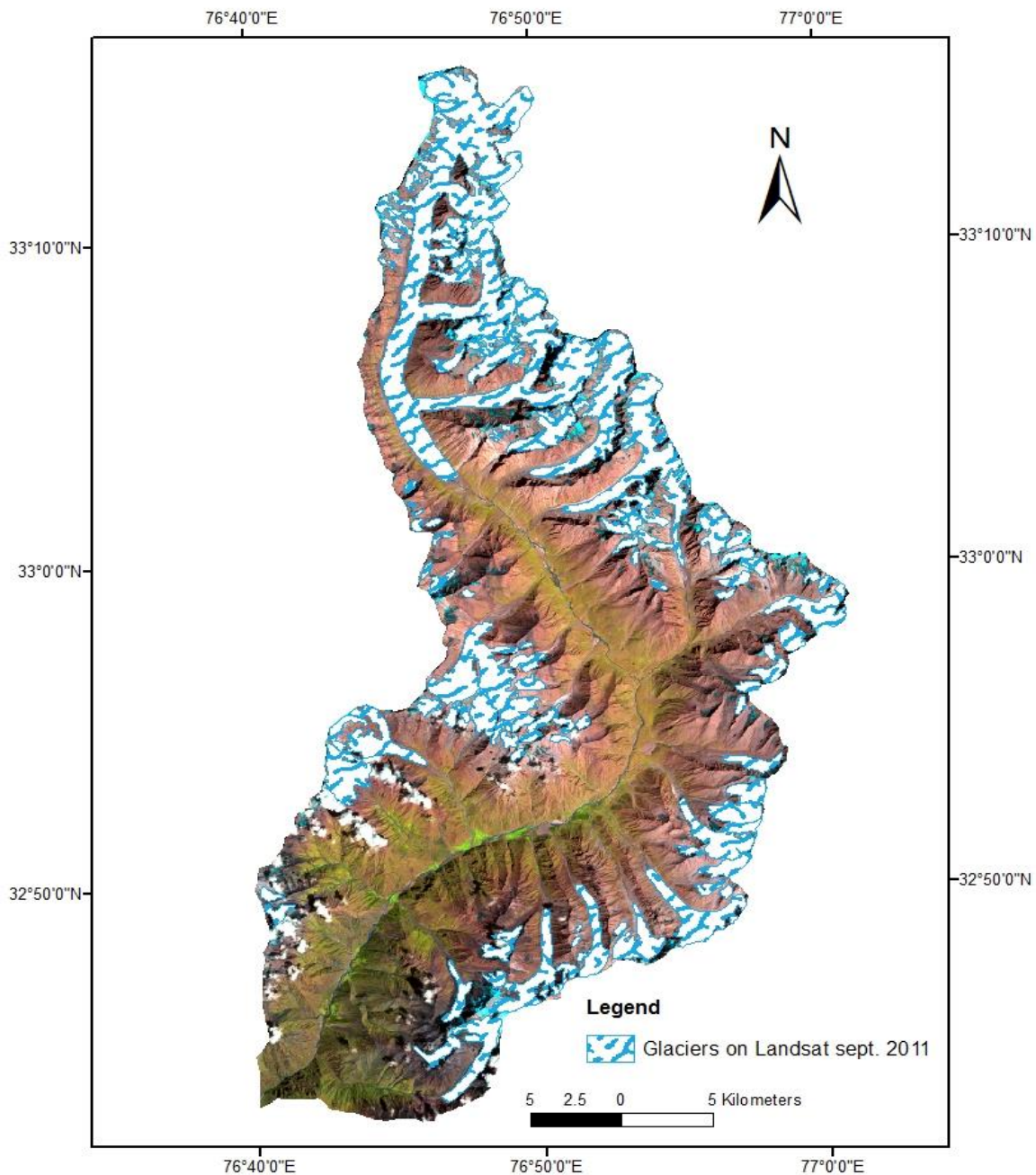


Figure 127: Extent of glaciers of Miyar sub-basin in 2011

It has been observed that the total glaciated area in the Miyar basin in 2007 has reduced to 169.60 km² from 243.12 km² in 1965, indicating a loss of 73.52 km² area during 42 years (Table 47). Total retreat and the rate of retreat of different glaciers viz., Miyar, Pimu, Menthosa, Hulat, Karpat, Gangpu, Palbo, Khanjar, Uldhampu, Tharang, Tarsalamu, Nakori, Gumba and Dali galciers (Total 14 glaciers) in Miyar sub-basin are given in Tables 48 to 61. Various data sets are used for various glaciers depending upon the availability of best scenes. A pattern of glacier recession can be observed from the Tables 48 to 61.

Table 47: Total and percent glacerised area in Miyar sub-basin

Year	Total glacerised area (km ²)	% glacerised area
1965	243.12	25.22
1975	170.87	17.72
1989	170.70	17.71
2000	170.13	17.65
2002	169.75	17.61
2007	169.60	17.59

Table 48: Monitoring of Miyar glacier

Miyar Glacier	Sol toposheet 1963	16 Sept. 1980 (Corona)	9 Oct.1989 (Landsat TM)	27 Sept. 2002 (IRS PAN)	5 Oct. 2005 (IRS PAN)	23 Oct. 2013 (IRS LISS IV)	Total Change
Linear retreat (meter)	Base year	1963-1980 627	1980-1989 58	1989-2002 128	2002-2005 33	2005-2013 121	1980-2013 340
Per year rate of retreat (meter)	_____	36.8	6.4	9.8	11	15.1	10

Table 49: Monitoring of Pimu glacier

Pimu Glacier	Sol toposheet 1963	28 Sept. 1971 (Corona)	16 Sept. 1980 (Corona)	9 Oct. 1989 (Landsat TM)	26 Oct. 2001 (IRS LISS III)	23 Oct. 2013 (IRS LISS IV)	Total Change
Linear retreat (meter)	Base year	1963-1971 1788	1971-1980 No Change	1980-1989 147	1989-2001 149	2001-2013 92	1971-2013 388
Per year rate of retreat (meter)	_____	223	----- -	16	12	7	9.2

Table 50: Monitoring of Menthosa glacier

Menthosa Glacier	Sol toposheet 1963	24 Sept. 1965 (Corona)	9 Oct. 1989 (Landsat TM)	26 Oct. 2001 (IRS LISS III)	23 Oct. 2013 (IRS LISS IV)	Total Change
Linear retreat (meter)	Base year	1963-1965	1965-1989	1989-2001	2001-2013	1965-2013
		Advance of 1260 meter	124	48	46	218
Per year rate of retreat (meter)	_____	630	5	4	3.8	4.5

Table 51: Monitoring of Hulat glacier

Hulat Glacier	28 Sept. 1971 (Corona)	9 Oct. 1989 (Landsat TM)	23 Oct. 2013 (IRS LISS IV)	Total Change
Linear retreat (meter)	Base year	1971-1989	1989-2013	1971-2013
		125	551	676
Per year rate of retreat (meter)	_____	6.9	22.9	16

Table 52: Monitoring of Karpát glacier

Karpát Glacier	Sol toposheet 1963	9 Oct. 1989 (Landsat TM)	12 Oct. 2000 (IRS LISS III)	27 Sept. 2002 (IRS PAN)	5 Oct. 2005 (IRS PAN)	23 Oct. 2013 (IRS LISS IV)	Total Change
Linear retreat (meter)	Base year	1963-1989	1989-2000	2000-2002	2002-2005	2005-2013	1989-2013
		300	No Change	No Change	No Change	No Change	No Change
Per year rate of retreat (meter)		11.5	-----	-----	-----	-----	-----

Table 53: Monitoring of Gangpu glacier

Gangpu Glacier	Sol toposheet 1963	28 Sept. 1971 (Corona)	23 Oct. 2013 (IRS LISS IV)	Total Change
Linear retreat (meter)	Base year	1963-1971 400	1971-2013 300	1971-2013 300
Per year rate of retreat (meter)	_____	50	7.1	7.1

Table 54: Monitoring of Palbo glacier

Palbo Glacier	Sol toposheet 1963	28 Sept. 1971 (Corona)	23 Oct. 2013 (IRS LISS IV)	Total Change
Linear retreat (meter)	Base year	1963-1971 Advance of 300 meter	1971-2013 122	1971-2013 122
Per year rate of retreat (meter)	_____	37.5	2.9	2.9

Table 55: Monitoring of Khanjar glacier

Khanjar Glacier	Sol toposheet 1963	28 Sept. 1971 (Corona)	12 Oct. 2000 (IRS LISSIII)	23 Oct. 2013 (IRS LISS IV)	Total Change
Linear retreat (meter)	Base year	1963-1971 1760	1971-2000 683	2000-2013 415	1971-2013 1098
Per year rate of retreat (meter)	_____	220	23.5	31.9	26.1

Table 56: Monitoring of Uldhampu glacier

Uldhampu Glacier	Sol toposheet 1963	28 Sept. 1971 (Corona)	9 Oct. 1989 (Landsat TM)	12 Oct. 2000 (IRS LISS III)	5 Oct. 2006 (IRS LISS III)	23 Oct. 2013 (IRS LISS IV)	Total Change
Linear retreat (meter)	Base year	1963-1971 908	1971-1989 30	1989-2000 50	2000-2006 234	2006-2013 65	1971-2013 379
Per year rate of retreat (meter)	_____	113.5	1.6	4.5	39	9.2	9

Table 57: Monitoring of Tharang glacier

Tharang Glacier	Sol toposheet 1963	28 Sept. 1971 (Corona)	9 Oct. 1989 (Landsat TM)	12 Oct. 2000 (IRS LISS III)	5 Oct. 2006 (IRS LISS III)	23 Oct. 2013 (IRS LISS IV)	Total Change
Linear retreat (meter)	Base year	1963-1971 880	1971-1989 128	1989-2000 No Change	2000-2006 110	2006-2013 310	1971-2013 548
Per year rate of retreat (meter)	_____	110	7.1	----- --	18.3	44.2	13

Table 58: Monitoring of Tarsalamu glacier

Tarsalamu Glacier	Sol toposheet 1963	28 Sept. 1971 (Corona)	9 Oct. 1989 (Landsat TM)	12 Oct. 2000 (IRS LISS III)	23 Oct. 2013 (IRS LISS IV)	Total Change
Linear retreat (meter)	Base year	1963-1971 Advance of 1610 meter	1971-1989 239	1989-2000 142	2000-2013 336	1971-2013 717
Per year rate of retreat (meter)	_____	201.2	13.2	12.9	25	17

Table 59: Monitoring of Nakori glacier

Nakori Glacier	Sol toposheet 1963	28 Sept. 1971 (Corona)	9 Oct. 1989 (Landsat TM)	12 Oct. 2000 (IRS LISS III)	23 Oct. 2013 (IRS LISS IV)	Total Change
Linear retreat (meter)	Base year	1963-1971	1971-1989	1989-2000	2000-2013	1971-2013
		Advance of 750 meter	105	102	101	308
Per year rate of retreat (meter)	_____	93.7	5.8	9.2	7.7	7.3

Table 60: Monitoring of Gumba glacier

Gumba Glacier	Sol toposheet 1963	28 Sept. 1971 (Corona)	9 Oct. 1989 (Landsat TM)	26 Oct. 2001 (IRS LISS III)	23 Oct. 2013 (IRS LISS IV)	Total Change
Linear retreat (meter)	Base year	1963-1971	1971-1989	1989-2001	2001-2013	1971-2013
		146	136	81	96	313
Per year rate of retreat (meter)	_____	18.5	7.5	6.7	8	7.4

Table 61: Monitoring of Dali glacier

Dali Glacier	Sol toposheet 1963	9 Oct. 1989 (Landsat TM)	23 Oct. 2013 (IRS LISS IV)	Total Change
Linear retreat (meter)	Base year	1963-1989	1989-2013	1989-2013
		1680	No Change	No Change
Per year rate of retreat (meter)	_____	64.6	_____	_____

Miyar glacier has retreated by 340 meters between 1980 and 2013 at a rate of about 10 meters per year. The rate of retreat is 15 meter/year since 2005, however, GPS positions and field photographs (Figure 128) of Miyar snout shows the similar position in 2012 and 2013.



Figure 128: Field photographs showing changes in snout position of Miyar glacier during 2008-2013

Pimu glacier on the other hand, shows a rate of retreat of 7 meter/year between 2001 and 2013 and a total rate of 9.1 meter/year, therefore indicating a diminishing rate.

Changes in the Minthosa glacier using multirate satellite data has been studied in detail. Figure 129 shows glacial extent on satellite data of 1971, 1980, 1989, 2000, 2005, 2013. Menthosa glacier has been studied extensively in the field in 2006, 2008, 2010, 2011, 2012 and 2013. As is the case of Pimu glacier, Menthosa glacier also shows a diminishing rate of retreat but interestingly it never had a rate of retreat more than 5 meter per year during last 48 years. Figures 130 and 131 are showing the field photographs of 2008 and 2013 and 3D views of Menthosa snout of 1965 and 2013 respectively. Figure 132 show field photographs for region around snout of Tharang glacier. One very important observation from the recession behaviour of glaciers is that the adjoining glaciers behave more or less similarly. Tarsalamu, Tharang, Uldhampu, Khanjar, Palbo, Gangpu and Karpat are situated in the parallel valleys with an aspect of North-West.

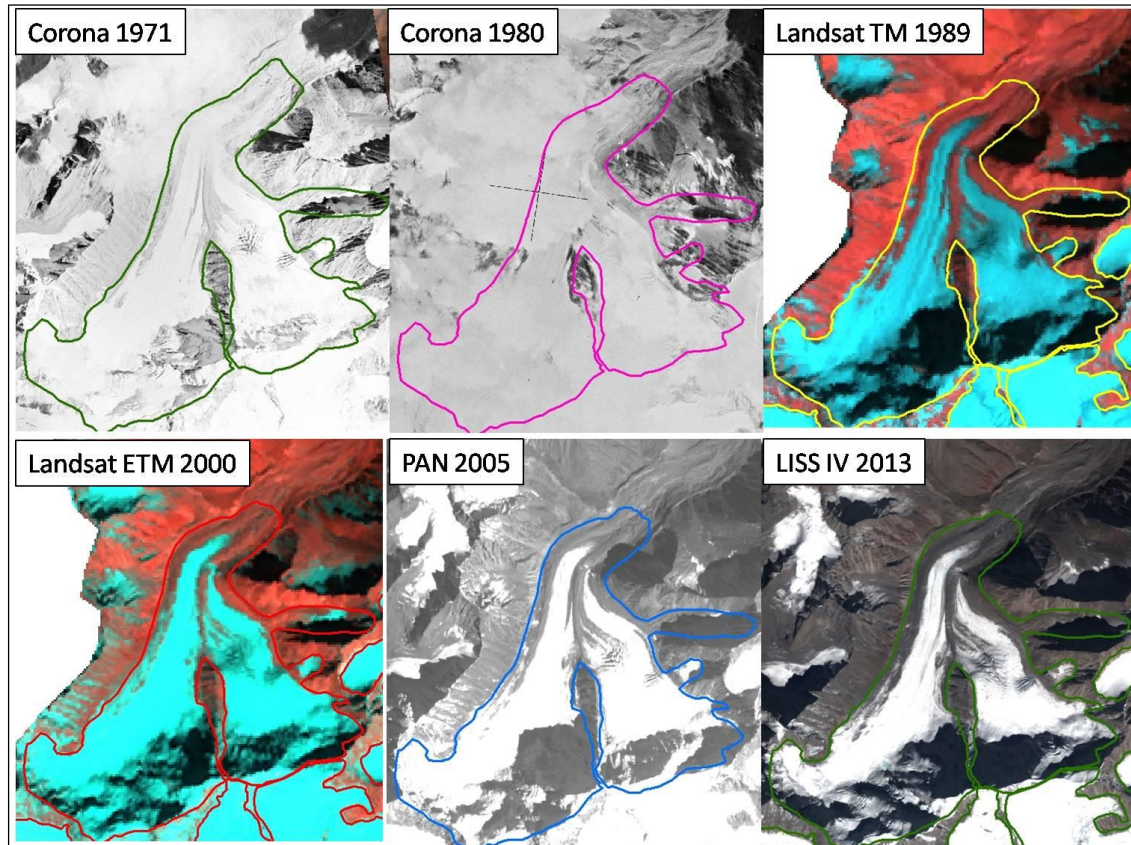


Figure 129: Changes in extent of Menthosa glacier as seen on satellite data of different time periods.

These glaciers can be grouped into two categories. While Karpat, Gangpu and Palbo have changed very little since earliest available images i.e. Corona of 1971 (Landsat TM 1989 in case of Karpat), other four glaciers (Khanjar, Uldhampu, Tharang and Tarsalamu) exhibit a recession behaviour which can be labelled as very fast since the turn of century. Exceptionally high rate of retreat (39 meter/year) in Uldhampu glacier between 2000 and 2006 can be attributed to the occurrence of a pro-glacial lake in this period, but the similar behaviour of Khanjar, Tharang and Tarsalamu glaciers can only be interpreted in terms of their micro-climate. In the similar fashion Dali, Chhudong and Takdung are in parallel valleys with an aspect towards south in upper parts and towards west in the lower zones. All these three glaciers have also exhibit a very little change since the 1980; however, change is not measurable because of intense shadow on the snout in all of the satellite images. Overall the study show that recessional pattern of glaciers in Miyar sub-basin is highly variable, where it is observed that some glaciers changed very little in last 40-50 years, and at the same time some glaciers have retreated rapidly during some time periods. The major glacier in the basin i.e., Miyar retreated by 340 meters since 1980 at the rate of 10 m/year. 10 glaciers out of 16 showed a retreat rate below 10 m/year



**Menthosa Snout:
A-June 2008
B-June 2013**



Figure 130: Field photograph of Menthosa glacier.

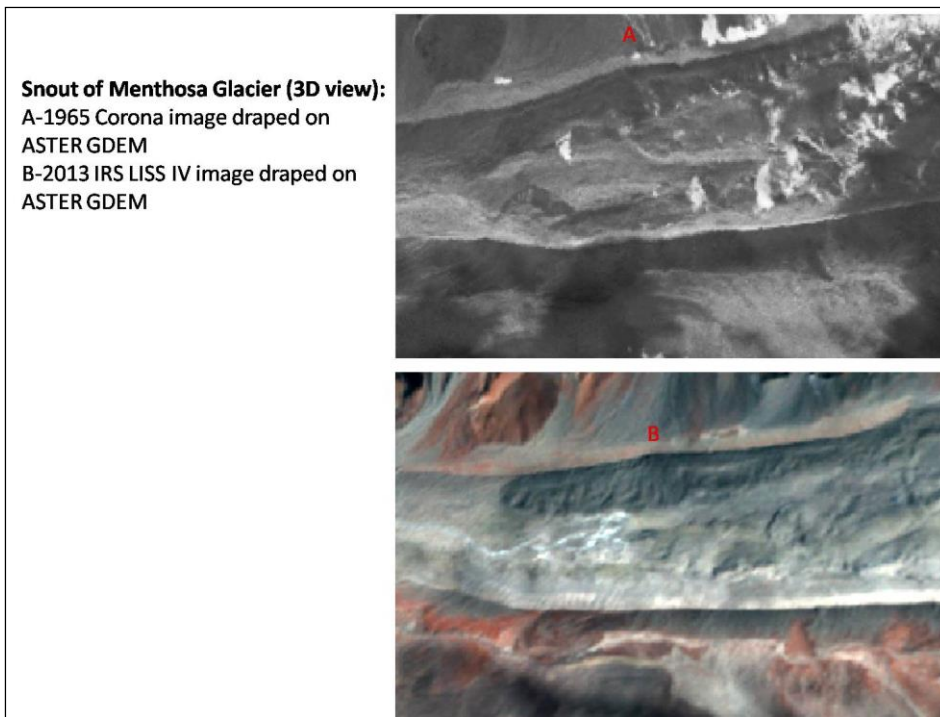


Figure 131: 3-D view of Menthosa glacier as seen in Corona (1965) and IRS LISS-IV (2013)

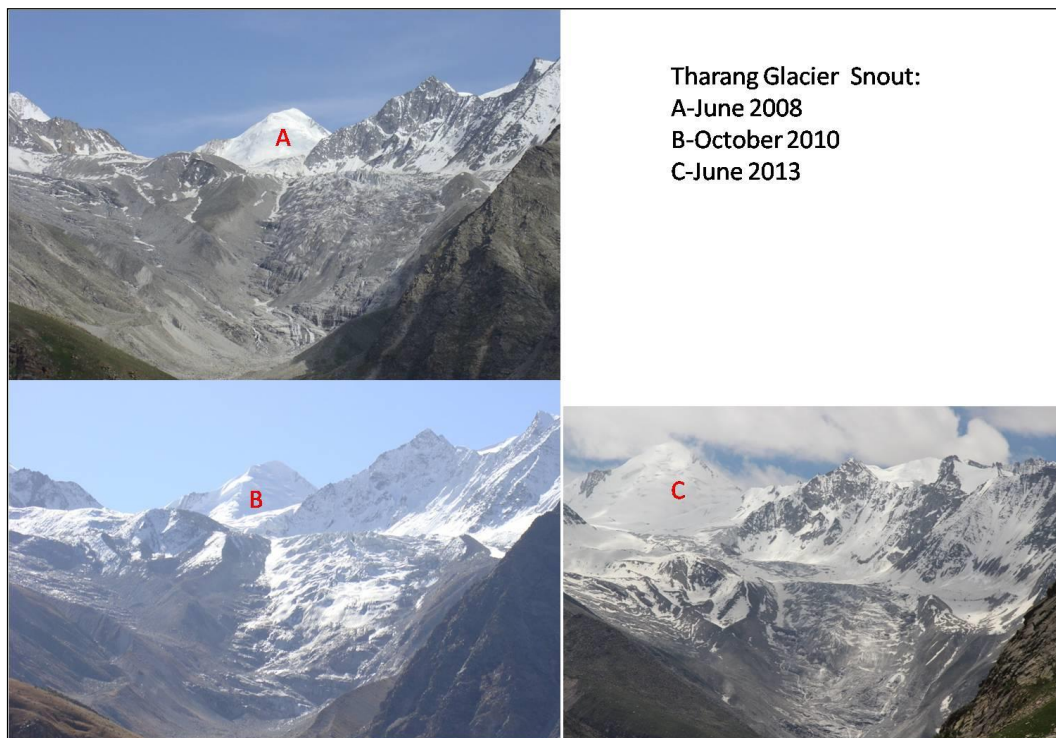


Figure 132: Field photographs showing region around snout of Tharang glacier

Equilibrium Line Altitude (ELA) estimation is very important aspect of glaciology because ELA is the altitude of the line of balance between accumulation and ablation of a glacier. A glacier is in equilibrium only if annual discharge through the equilibrium line cross section is equal to the net annual accumulation up-glacier and the net annual ablation down-glacier. Otherwise, it will grow or shrink. Rising ELAs indicate negative mass balance, while lowering ELA is a result of positive mass balance.

ELA in the Miyar sub-basin has been estimated using four different methods and the mean ELA has been worked out. These methods are Area Weighted Mean (A-WM), Area Accumulation Ratio (AAR), Toe to Headwall Ratio (THAR) and Maximum Elevation of Lateral Moraine (MELM)". ELA based on different methods and average ELA for selected glaciers in the Miyar basin are given in Table 62. Change in ELAs from Local Glacial Maximum (LGM) to the Present are provided in Table 63. The altitude of the LGM terminus has been taken as 3040 m (near Karpal village) on the basis of the geomorphic evidence of truncated spurs and trimlines. The position of the Holocene snouts of all the glaciers is well preserved by the end moraines. There are variations in the ELA values obtained from different methods, therefore average ELAs computed on the basis of ELAs obtained from all the four methods may help in reducing the error margin (Table 64).

Glacier retreat pattern in Miyar sub-basin during Last Glacial Maxima (LGM), Holocene and Recent (2011) is shown in Figure 133 and extent of Equilibrium Line Altitude (ELA) during Last Glacial Maxima (LGM), Holocene and Recent is shown in Figure 134. It shows that glaciers in the Miyar sub-basin are retreating since LGM, however impact of climate change may get reflected in accelerated retreat during past few decades.

Table 62: Equilibrium Line Altitude based on different methods and major characteristics of selected glaciers in the Miyar basin (based on the SOI topographical maps surveyed between 1963-1968)

Name of the glacier	Aspect	Length (km)	Size (sq km)	Headwall altitude (m)	Snout position (elevation in m)	ELA based on A-WM (0.44) (m amsl)	ELA based on AAR (0.44) (m amsl)	ELA based on AAR (0.48) (m amsl)	ELA based on THAR (m amsl)	Mean ELA (m amsl)
Tharang	NW	5.48	6	5560	4000	5027	5140	5100	4780	5012
Gumba	S	7	6.8	5680	4420	4926	4940	4900	5050	4954
Takdung	SW	12.55	15	5840	4200	5065	5240	5160	5020	5121
Miyar	S	27.43	85.6	6000	3980	5078	5240	5200	4990	5127
Chhudong	SW	11.26	10.7	5760	4500	5142	5200	5160	5130	5158
Pimu	NE	6.45	7.4	5480	4300	4871	4960	4920	4890	4910
Uldhampu	NW	8.1	7.5	5600	4340	4864	4960	4920	4870	4928
Khanjar	NW	5.88	4.9	5200	4200	4845	4940	4920	4700	4851
Menthosa	SE	3.86	3.3	5680	4480	4906	4720	4700	5080	4826
Karpat	NW	4.54	4.9	5720	4200	4990	5040	5000	4960	4997
Hulat	SW	7.86	5.4	5800	3940	4844	4880	4840	4870	4858
Other ice bodies			85.6							
Total Glacerised Area			243.1							
Total area of the basin			963.85							

Table 62: Equilibrium Line Altitude based on different methods and major characteristics of selected glaciers in the Miyar basin (based on the SOI topographical maps surveyed between 1963-1968)

Name of the glacier	Head wall	LGM Termini	Holocene Termini	Present Termini	Local Glacial Maximum ELA	Holocene ELA	Present ELA (THAR 0.5)	ELA Rise from LGM to Holocene	ELA Rise from Holocene to Present	Total Rise in ELA from LGM to present
Tharang	5560	3040	3600	4009	4300	4580	4785	280	205	485
Gumba	5450	3040	3900	4500	4245	4675	4975	430	300	730
Takdung	5570	3040	3950	4380	4305	4760	4975	455	215	670
Miyar	6000	3040	3970	4043	4520	4985	5021	465	36	501
Chhudong	5500	3040	3950	4558	4270	4725	5029	455	304	759
Pimu	5480	3040	3950	4604	4260	4715	5042	455	327	782
Uldhampu	5450	3040	3450	4346	4245	4450	4898	205	448	653
Khanjar	5380	3040	3450	4644	4210	4415	5012	205	597	802
Menthosa	5680	3040	3300	4380	4360	4490	5030	130	540	670
Miyar Basin	5563	3040	3724	4385	4302	4644	4974	342	330	672

Table 64: ELA by Maximum Elevation of Lateral Moraine (MELM) Method for selected glaciers of Miyar sub-basin

Name of the glacier	ELA based on MELM 2010	Average ELAs
Tharang	5085	5012
Gumba	4821	4954
Takdung	5000	5121
Miyar	4957	5157
Chhudong	5000	5158
Pimu	4933	4910
Uldhampu	4866	4928
Khanjar	4906	4851
Menthosa	4732	4826
Karpat	4750	4997
Hulat	5020	4858

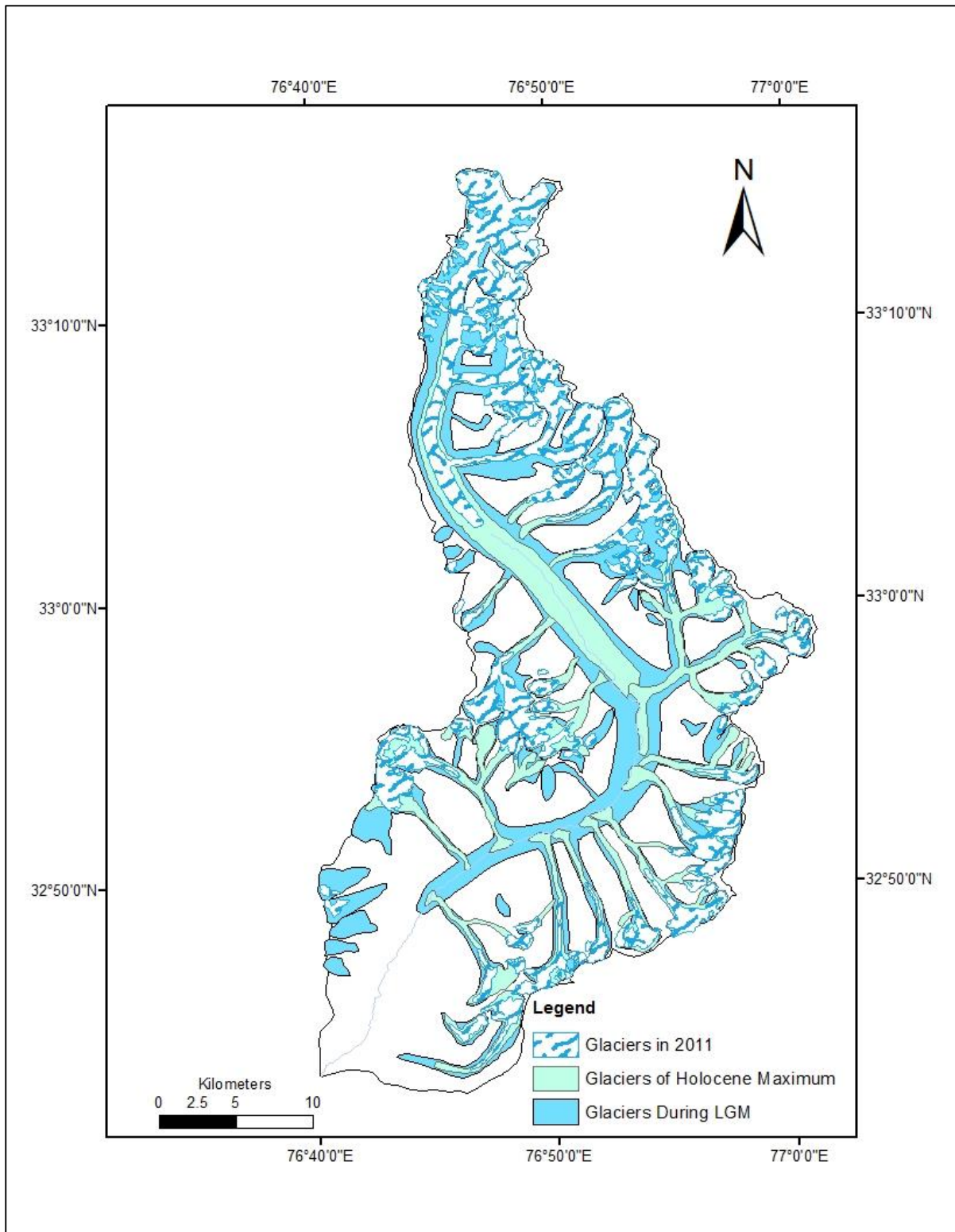


Figure 133: Glacier retreat pattern in Miyar sub-basin during Last Glacial Maxima (LGM), Holocene and Recent (2011) in Miyar sub-basin

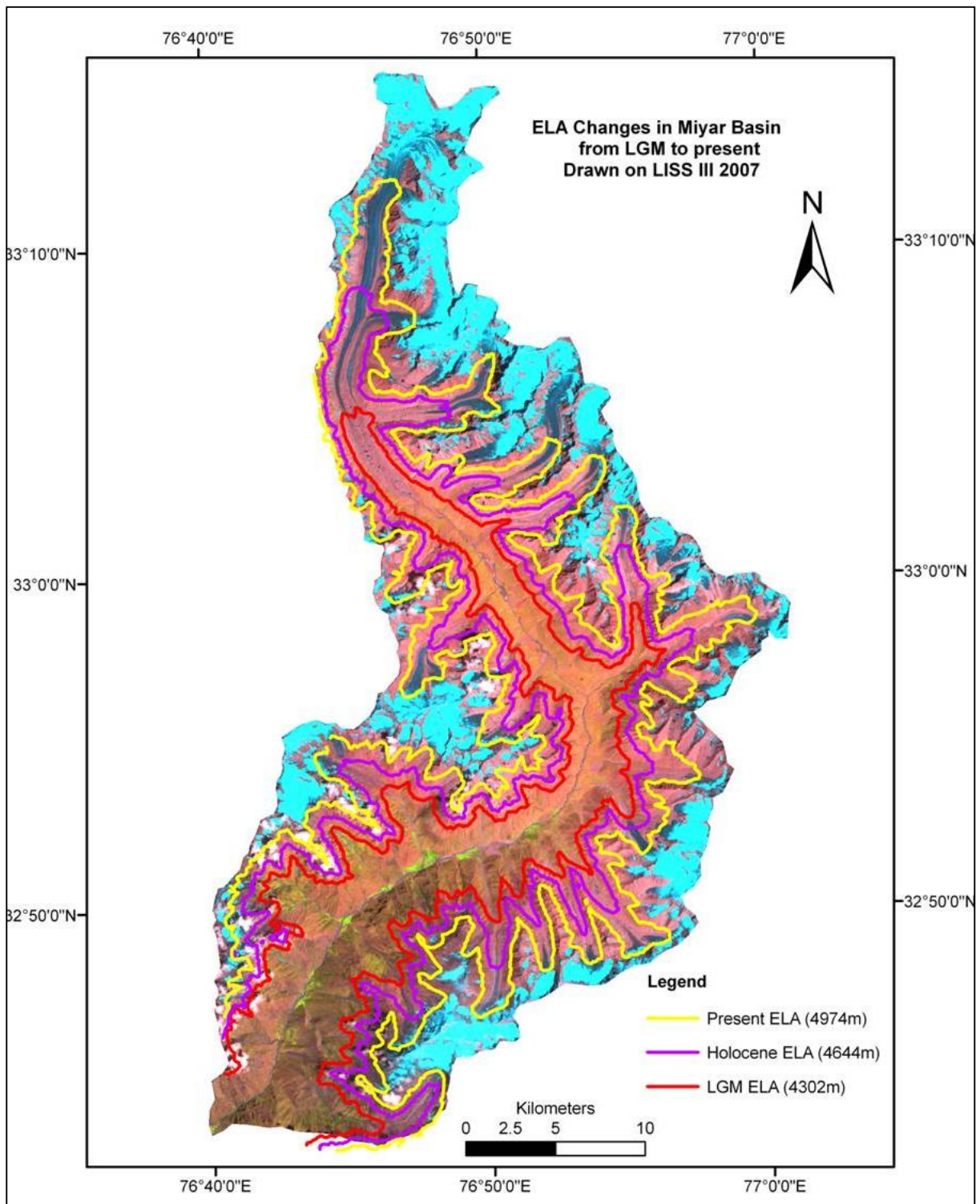


Figure 134: Extent of Equilibrium Line Altitude (ELA) during Last Glacial Maxima (LGM), Holocene and Recent in Miyar sub-basin

(e) Glaciers of Chandra Sub-basin

Chandra sub-basin is located between 32°10' to 32°85' North and 77 ° 00' to 77° 75' East in Lahaul and Spiti district of Himachal Pradesh. The Chandra river originates from the Great Himalayas and joins river Bhaga at Tandi in Lahaul and Spiti district. Changes in the glaciers of the Chandra basin were studied for the time frame 1980, 2001, 2007 and 2011 using multivariate satellite data. (Figure 135). The salient results are summarized in Table 65.

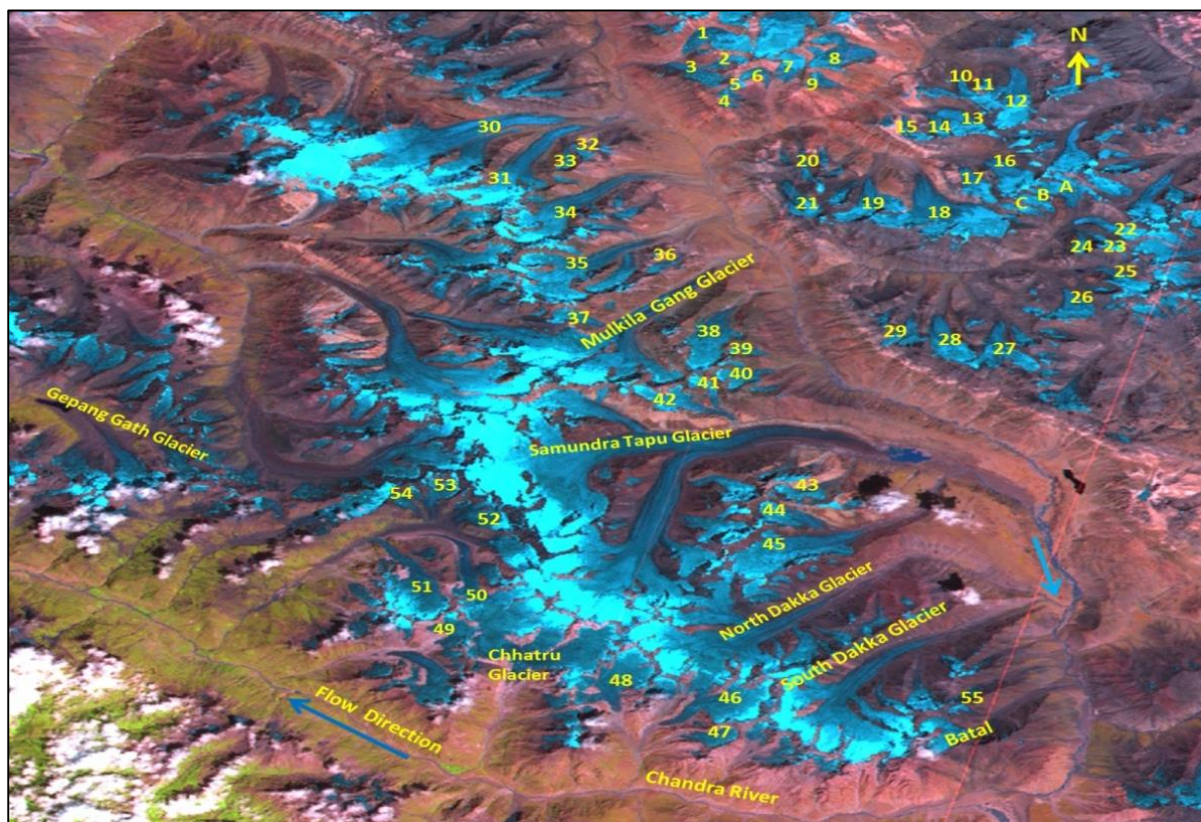


Figure 135: Location of glaciers studied in Chandra basin, Himachal Pradesh

Table 65: Changes in glaciers of the Chandra basin, Himachal Pradesh as per size frequency distribution during 1980-2011

Glacier Area (sq km)	1980		2001		2007		2011	
	No. of glaciers	Glaciated Area (sq km)	No. of glaciers	Glaciated Area (sq km)	No. of glaciers	Glaciated Area (sq km)	No. of glaciers	Glaciated Area (sq km)
0-1	16	11.95	20	12.83	20	10.44	20	9.78
1-3	17	35.10	20	39.03	23	45.28	24	44.72
3-5	09	34.17	07	25.63	03	11.98	04	16.45
5-10	08	61.45	10	72.49	09	63.33	10	68.13
>10	10	225.83	08	189.39	07	169.83	07	163.33
Total	60	368.50	65	339.71	62	300.67	65	302.09

It is observed that 10 larger glaciers i.e., with more than 10 sq km glaciated area in 1980 reduced to 7 in 2011 and smaller glaciers i.e. with glaciated area in category of 0-1 and 1-3 sq km have increased from 16 to 20 and 17 to 24 respectively in 2011. It indicates that glaciers have retreated as well fragmented into smaller glaciers.

Table 66 summarizes net change in glaciated area of glaciers in the Chandra basin, as per size frequency distribution during 2001-2011. It is observed that overall there has been net loss of 37.62 sq km glaciated area of the Chandra sub-basin during the time frame 2001-2011 for the 65 glaciers, which constitutes 11% net loss. Fragmentation of one glacier with >10 sq km glaciated area is also indicated by increase of 4 glaciers in the category of glaciers with 1-3 sq km area and 5.69 sq km gain in glaciated area, which is 14.6% net gain. Reduction in glaciated area of 3 glaciers in the category of glaciers with 3-5 sq km area is also indicated. It is also observed that glaciers upto 5 sq km area (upto 35.8%) have shown higher loss in glaciated area than glaciers greater than 5 sq km area (upto 13.7%). It may be due to their debris free nature as well steeper slope.

Table 66: Net change in glaciated area of glaciers in the Chandra basin, Himachal Pradesh as per size frequency distribution during 2001-2011

Glacier Area (sq km)	2001		2011		Net Change in glaciated area (sq km)	% change in glacial area
	No. of glaciers	Glaciated Area (sq km)	No. of glaciers	Glaciated Area (sq km)		
0-1	20	12.83	20	9.78	-3.05	-23.8
1-3	20	39.03	24	44.72	+ 5.69	+14.6
3-5	07	25.63	04	16.45	-9.18	-35.8
5-10	10	72.49	10	68.13	-4.36	-6
>10	08	189.39	07	163.33	-26.06	-13.7
Total	65	339.71	65	302.09	-37.62	-11

Changes in Samudra Tapu, Geepang Gath and Batal glaciers, Chandra basin
 Samudra Tapu, Geepang Gath and Batal glaciers (Figure 136) have been studied in detail by interpreting multirate satellite data as well collecting field based glaciological observations. The salient characteristics of these glaciers are given in Table 67. Samudra Tapu glacier is second largest glacier in Chandra sub-basin. It is east facing glacier with snout at 4160 m amsl (Figure 137). Geepang Gath glacier is NW facing glacier with largest moraine dammed lake in H.P. at its snout at 4088 m amsl. Batal glacier is a NE facing glacier with its snout at 4217 m amsl. Changes in glaciated area and retreat of Samudra Tapu, Geepang Gath and Batal glaciers are summarized in Table 68 and Table 69 respectively. It is observed that Samudra Tapu, Geepang Gath and Batal glaciers have retreated by 717 m, 507 m and 232.39 m during 31 years (1980-2011), with an average retreat of 23 m/year, 16 m/year and 7.50 m/year respectively. It is observed that loss in glaciated area of Samudra Tapu, Geepang Gath and Batal glaciers is 9.64 sq km, 2.86 sq km and 2.15 sq km during 31 years (1980-2011) respectively. However, % loss in glaciated area is highest for Batal (30.8%), followed by Geepang Gath (20.7%) and Samudra Tapu (11.5%) glaciers

respectively. Field photographs showing snout and adjoining parts of the Samudra Tapu, Geepang Gath and Batal glaciers are given in Figures 138 to Figure 145. It may be seen that there are distinct geomorphological evidences showing retreat of these glaciers and enlargement of the moraine dammed lakes of the Samudra Tapu as well Geepang Gath lakes.

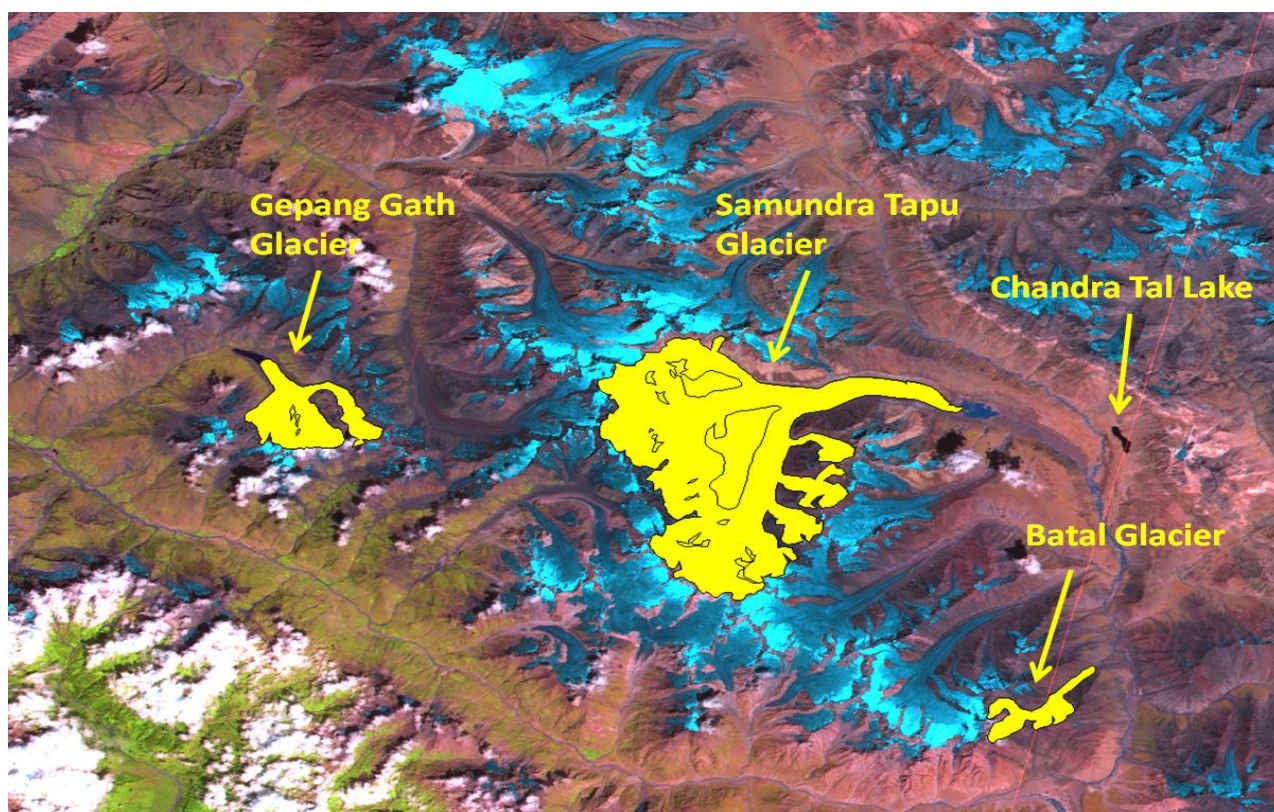


Figure 136: Geepang Gath, Samudra Tapu and Batal glaciers in the Chandra basin in Lahaul and Spiti district, Himachal Pradesh

Table 67: Salient Characteristics of Samudra Tapu, Geepang Gath and Batal glaciers

Parameters	Samudra Tapu Glacier	Geepang Gath Glacier	Batal Glacier
Length (km)	16 .2	5.5	6.3
Catchment Area (sq.km)	87.58	13.57	7.40
Snout Altitude (a.s.l)	4160 m (2001)	4088 m (2001)	4217 m (2001)
Orientation	E facing	NW facing	NE facing
Equilibrium Line Altitude (ELA)	5386 m (2001)	4860 m (2001)	5520 m (2001)

Table 68: Snout retreat of Samudra Tapu, Geepang Gath and Batal glaciers

Glacier Name	Snout retreat (m) 1980-1989	Snout retreat (m) 1989-1999	Snout retreat (m) 1999-2007	Snout retreat (m) 2007-2011	Snout retreat (m) 1980-2011	Average snout retreat m/yr 1980-2011
Samudra Tapu glacier	215	98	241	163	717	23
Geepang gath glacier	48	42	300	---	507	16
Batal Glacier	135 (1980-2001)	---	84 (2001-2007)	13.39	232.39	7.50

Table 69: Loss in glaciated area of Samudra Tapu, Geepang Gath and Batal glaciers

Glacier Name	Glaciated area in 1980 (sq km)	Glaciated area in 2001 (sq km)	Glaciated area in 2007 (sq km)	Glaciated area in 2011 (sq km)	Loss in glaciated area 1980-2011	% loss in glaciated area 1980-2011
Samudra Tapu glacier	84.06	80.41	77.28	74.42	9.64	11.5
Geepang gath glacier	13.80	12.23	11.63	10.94	2.86	20.7
Batal Glacier	6.97	5.28	5.25	4.82	2.15	30.8



Figure 137: Panoramic view of Samudra Tapu glacier, Chandra basin, Lahaul and Spiti district, Himachal Pradesh

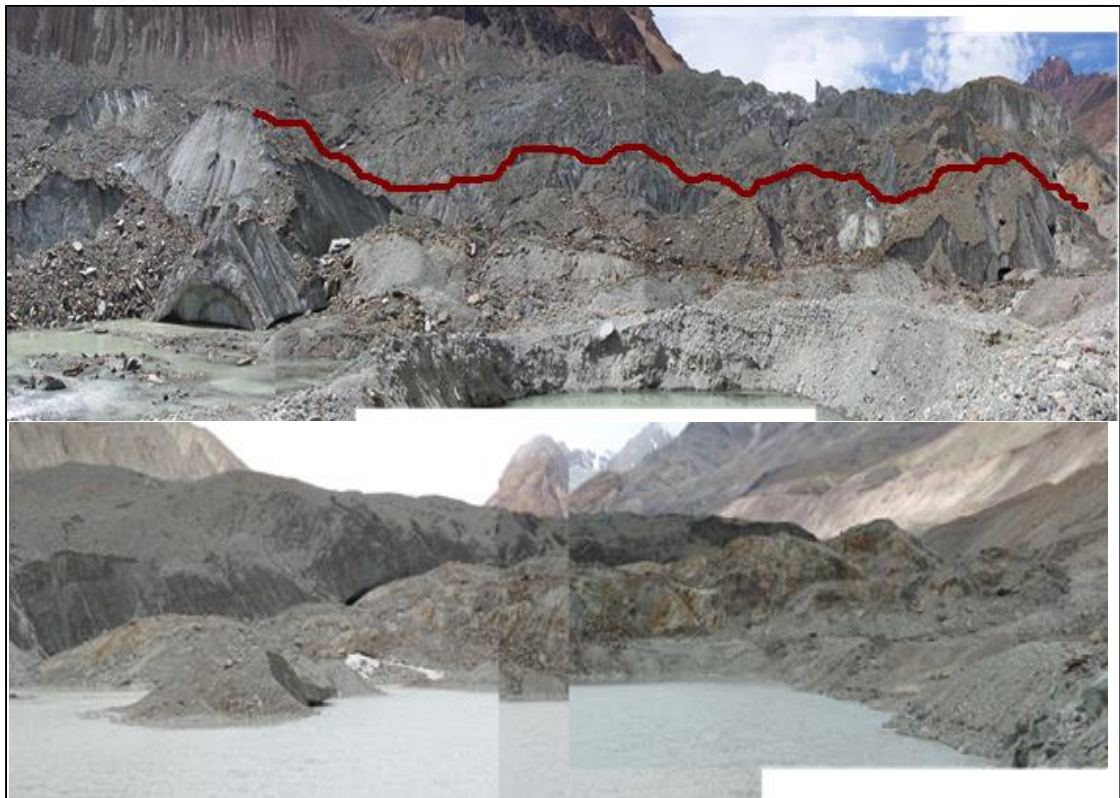


Figure 138: Field photograph showing glacial area evacuated by Samudra Tapu Glacier between eight years (2004 and 2012). Red line shows extent of glacier area vacated in 2012



Figure 139: Field photograph showing snout of Samudra Tapu glacier in 2004 (Upper) and the snout location submerged in lake (Lower) in subsequent years since 2007

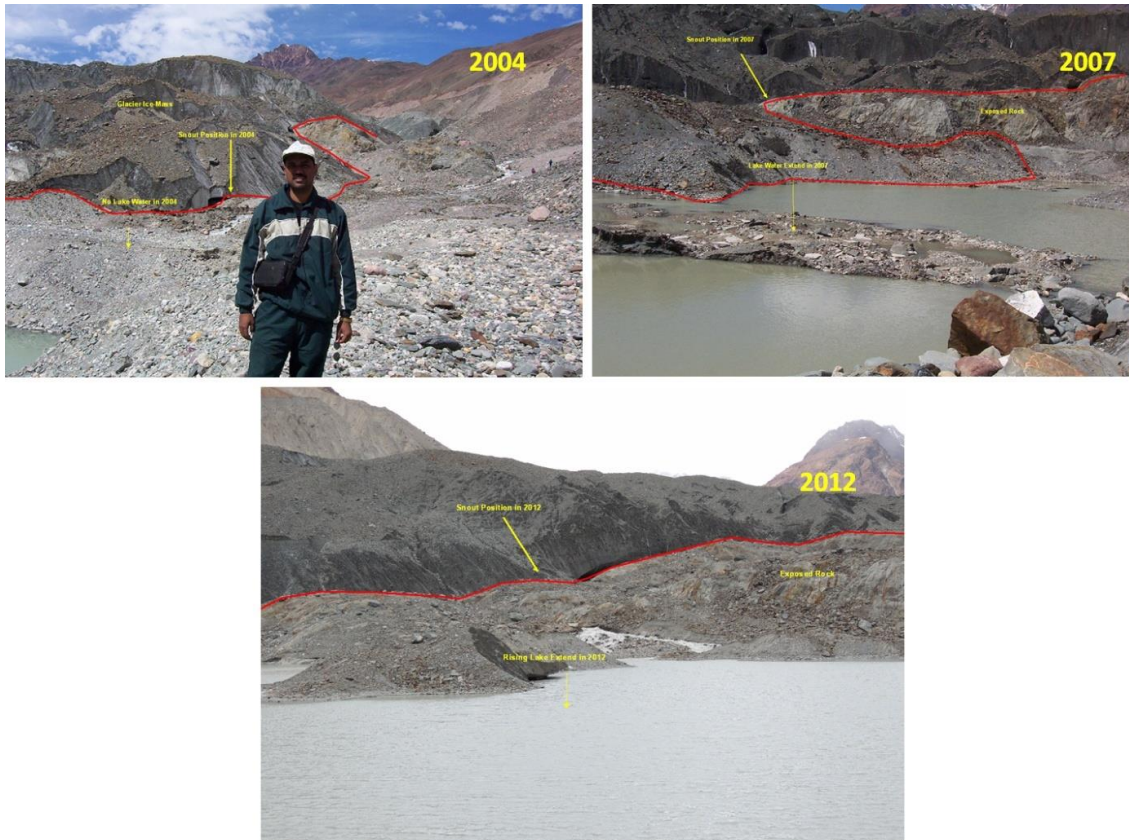


Figure 140: Field photograph showing enlargement of moraine dammed lake of Samudra Tapu glacier in different years. Red line indicates vacated area of the glacier



Figure 141: Field photograph showing Subterranean tunnels at snout of Samudra Tapu glacier



Figure 142: Field photograph showing snout of Geepang Gath glacier and moraine dammed lake



Figure 143: Field photograph showing accumulation area of Geepang Gath glacier



Figure 144: Field photograph showing retreating snout of Batal glacier



Figure 145: Field photograph showing moraine deposits exposed due to the retreat of Batal glacier

(f) Detailed Study of Satopanth and Bhagirath-Kharak glaciers, Alaknanda sub-basin, Uttarakhand

Changes in the Satopanth and Bhagirath-Kharak glaciers located at the head of Alaknanda river valley in Chamoli district, Uttarakhand were studied using old archived data, Corona satellite data of 1968 and Landsat as well IRS data of 1988, 2004, 2010 and 2013. Changes in the frontal parts of Bhagirath-Kharak and Satopanth glaciers as mapped using satellite data are shown in Figure 146 and Figure 147. The field photographs showing the frontal parts and snout are shown in Figure 148 and Figure 149. Table 70 summarises the retreat, rate of retreat/year and loss in glaciated area during 1968-1988, 1988-2004, 2004-2010 and 2010-2013 time frames for the Bhagirath-Kharak and Satopanth glaciers.

The earliest records have mentioned single glacier front for both these glaciers, however Corona photographs of 1968 show separate snouts. It is observed that for the entire time period between 1968 and 2013, Satopanth glacier shows an annual average retreat of 9.86 meters per year, whereas Bhagirath-Kharak glacier shows an average annual retreat of 8.13 meters per year. As a result of the retreat of the frontal parts of these glaciers, the area vacated by the Satopanth glacier between 1968 and 2013 is 0.39 sq km, while during the same period, the Bhagirath Kharak glacier has vacated an area of 0.24 sq km.

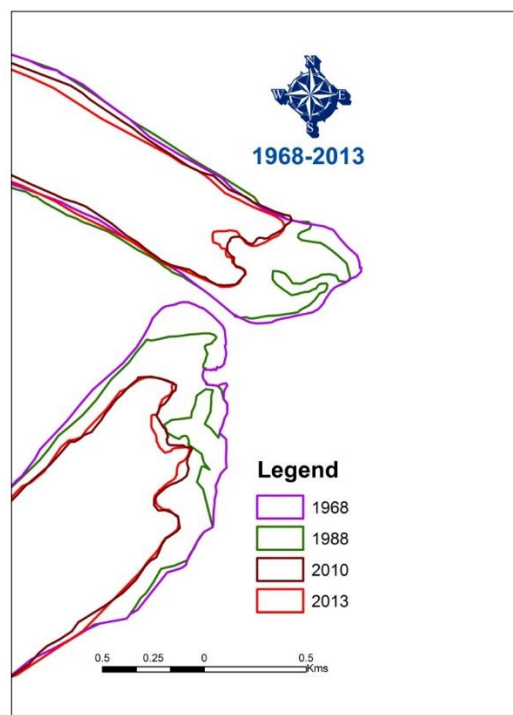


Figure 146: Changes in the frontal parts of Bhagirath-Kharak and Satopanth glaciers in Uttarakhand

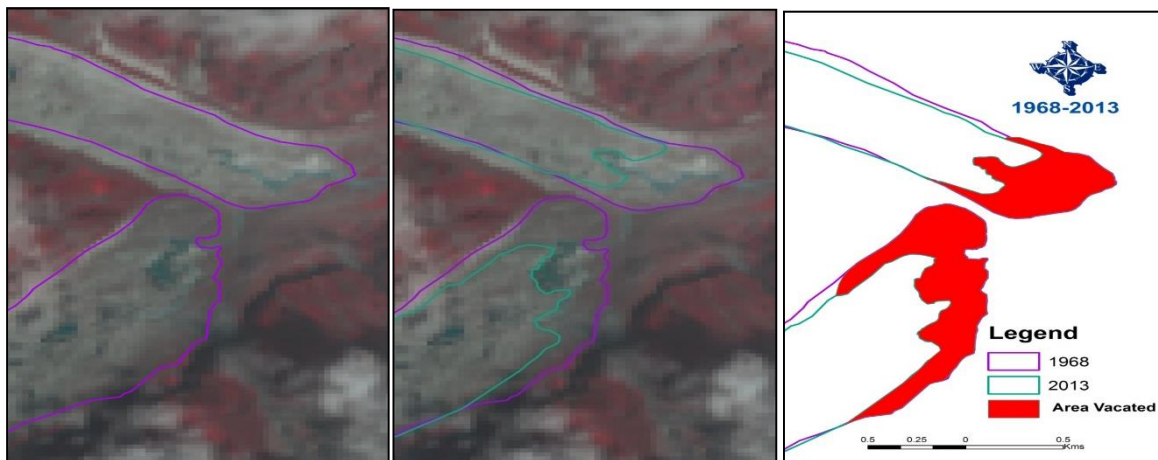


Figure 147: Changes in the frontal parts of Bhagirath-Kharak and Satopanth glaciers during 1968-2013



Figure 148: Field photograph of the frontal parts of the Satopanth glacier



Figure 149: Field photograph of the frontal parts of the Bhagirath Kharak glacier

Table 70: Changes in the frontal parts of Bhagirath-Kharak and Satopanth glaciers at the head of Alaknanda river, Chamoli district, Uttarakhand

YEAR/ PERIOD	BHAGIRATH-KHARAK GLACIER			SATOPANTH GLACIER		
	Total retreat in mts.	Average retreat In mts/year	Loss in area (sq km)	Total retreat in mts.	Average retreat In mts/year	Loss in area (sq km)
1968-1988	40.83	2.04	0.0565	37.51	1.87	0.1323
1988-2004	148.00	9.25	0.1143	294.00	18.37	0.1622
2004-2010	134.00	22.33	0.0618	070.00	11.66	0.0875
2010-2013	43.10	14.36	0.0080	42.50	14.16	0.0140
1968-2013	365.93	8.131	0.2426	444.01	9.86	0.3960

(g) Glaciers in Drass sub-basin

Drass is the sub-basin of Indus river. Drass river joins Indus near Kargil in Jammu and Kashmir. Drass sub basin is the Vth order basin of IVth order Indus and it extends between the Gumri (close to Zoji-La) in the west to Kargil in the east. Satellite data analysis revealed that there are 150 glaciers in Drass glacier sub-basin, whereas as per topographical maps of 1965, the basin occupied 115 glaciers and that the increased number in glaciers (115 to 150) is due to fragmentation (Koul et al., 2016). 150 glaciers cover an area of 152.68 km² with ice volume of 62.02 km³. Monitoring of 150 glaciers using satellite data for time frame 2001 to 2013 indicate that 120 glaciers show no change, 28 glaciers show loss and 2 glaciers show gain in glaciated area. The study show that larger glaciers above 5 km² has vacated a small area (0.64% to 2.64% of glacier area) in comparison to small glacier ranging in area 2 km² to 5 km² (1.68% to 9% of glacier) during 12 years period. There by indicating that glaciers of Drass valley in general retreat at slow pace. Two glaciers shows gain in area by 30% and 40% (Figure 150).

Eighty-one glaciers of Drass valley were selected for long-term monitoring for the period 1965-2001 and 2001-2013. It is observed that ten glaciers experienced gain in area, 13 glaciers a loss more than 50% of its area, 18 glaciers lost 25% - 50% of glacier area and the remaining glaciers lost marginal area during last 50 years period (Figure 151).

Out of the ten glaciers showing gain in area, four glaciers show gain in area during 1965 to 2001 but loss in area from 2001 to 2013 and remaining six glaciers of the category show gain in area from 1965 to 2001, and no change in their area between 2001 and 2013.

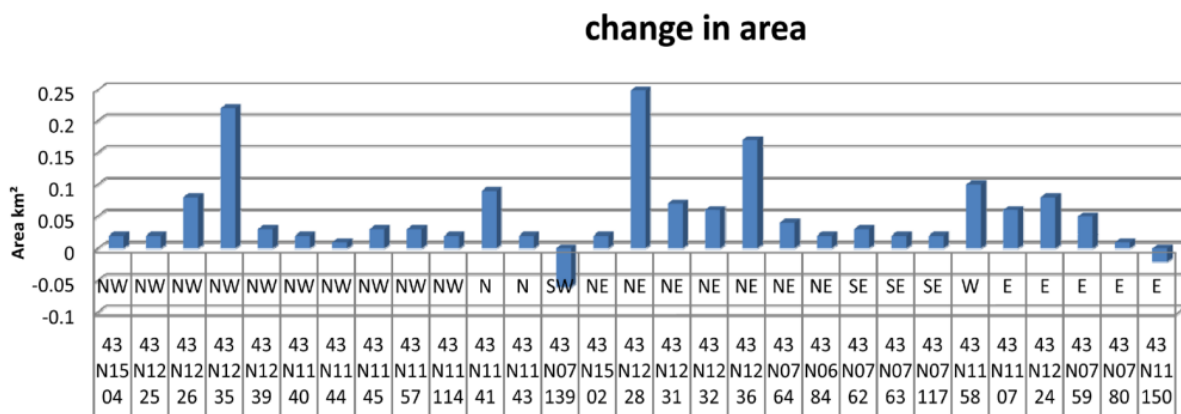


Figure 150: Glaciers in Drass valley showing changes in area 2001-2013 (Source: Koul et al., 2016)

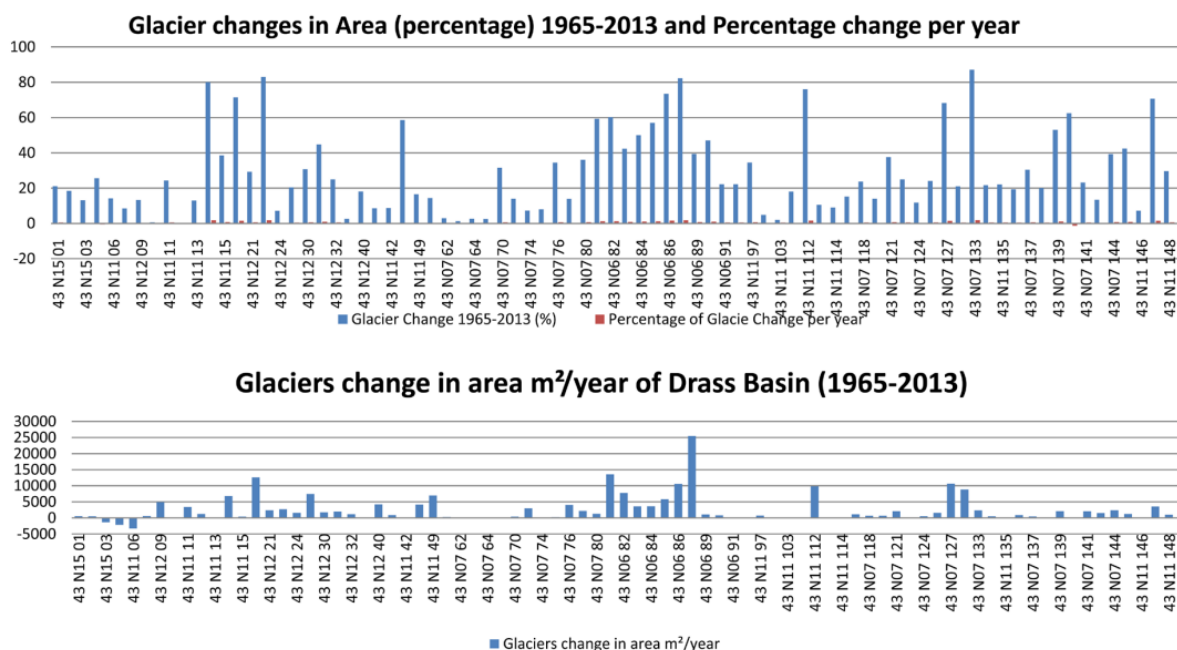


Figure 151: Glaciers in Drass valley showing change in area (1965-2013) (Source: Koul et al., 2016)

(h) Other glaciated areas

Detailed study of Bairpal Nai and Dhurlang glaciers in the Chenab basin, Jammu & Kashmir region show that the tributary glaciers are getting detached from the main trunk glacier causing fragmentation and interestingly, rate of retreat of main trunk glacier is higher than that of the tributary glacier (Brahmbhatt et al., 2015b). The causes of fragmentation and changes in rate of retreat are attributed to Accumulation Area Ratio (AAR), slope and altitude.

Changes in the glaciated area of the Warwan and Bhut basins of western Himalaya during the period 1962 and 2001/02 time frame have shown 19% and 9% loss respectively, which may be due to i) smaller size of glaciers of the Warwan basin (e.g., 164 glaciers having < 1 sq km area in comparison to 101 glaciers in Bhut basin), ii) lower percentage of debris cover in Warwan (18%) than in the Bhut basin (30%) and iii) higher percentage of glaciated area lying below 5100 m i.e., 80% in Warwan whereas 70% in the Bhut basin (Brahmbhatt et al., 2012a; Brahmbhatt, 2014; Brahmbhatt et al., 2016). Changes in debris free 13 glaciers in Warwan and Bhut sub-basins during time frame 2001 to 2007 studied using IRS LISS-III data show rate of retreat of the order 2 to 16 percent (Brahmbhatt et al., 2014).

Changes in glaciers in the Bhaga basin for the time frame 2001 and 2011 based on IRS LISS-III data show that the glacierised area of the 231 glaciers covering an area of $391.56 \pm 3.76 \text{ km}^2$ in 2001 has been reduced to $385.17 \pm 3.71 \text{ km}^2$ in 2011; a loss of $1.63 \pm 1.0\%$ in glacierized area within a period of 10 years (Birajdar et al., 2014).

4. Glacier Mass Balance

4.1. Objective

To determine the annual specific mass balance of glaciers of using AAR approach for four consecutive years (2010-2013) and analyze the variations in mass balance glaciers of identified sub-basins (Table 71) of Indus, Ganga and Brahmaputra river basins of Himalayan region based on their geographical and climatic diversity.

Table 71: Basins and sub-basins for glacial mass balance studies taken up under the project

Sr. No.	Basin	Sub-basins ↓
1	Indus	Nubra
2	Indus	Zaskar
3	Chenab	Warwan
4	Chenab	Bhut
5	Chenab	Chandra
6	Chenab	Bhaga
7	Chenab	Miyar
8	Beas	Parbati
9	Satluj	Basapa
10	Ganga	Alaknanda
11	Ganga	Bhagirathi
12	Ganga	Dhauliganga
13	Ganga	Goriganga

4.2. Scientific Rationale

The mass balance of the glacier is usually referred to as the total loss or gain in mass at the end of the hydrological year. It is estimated by measuring the total accumulation of seasonal snow and ablation of snow and ice. Mass balance has two components, accumulation and ablation. The accumulation (input) includes all forms of deposition, mainly precipitation, and ablation (output) means loss of snow and ice in the form of melting, evaporation and calving etc. from the glacier. The boundary at the end of ablation season between accumulation and ablation is known as Equilibrium line. The difference between net accumulation and net ablation for the whole glacier over a period of one year is Net balance. The net balance for each glacier is different in amount and depends upon the size/shape of the glacier and climatic condition of the area. The net balance per unit area of glacier is specific mass balance or SMB, expressed in cm of water equivalent. There is wide variation in mass changes from time to time and place to place on the glacier due to the various factors. The process of mass balance of the glaciers over an entire region is complex, as it is irregular in

amount, rate and time of occurrence. Therefore, the ultimate aim to monitor mass balance is to match it with the changes in various parameters of the glaciers. This change directly affects the flow of the glacier and its terminus position. i.e. advancement and recession of the frontal position of the glaciers. Generally mass balance studies are carried out using methods (Ben and Evans, 2010; Cuffley and Paterson, 2010; Gardelle et al., 2013) such as geodetic, glaciological, hydrological and AAR based.

Mass balance of a glacier determined annually is the most important parameter to assess the health of glaciers to understand the effect of climatic variations on the locked fresh water resource within a glacier. Trends of mass balances are direct indicator of climatic variations, however mass balance estimations require a large amounts of efforts in terms of resources, logistics and accuracy in any glaciated environment. Mountain glaciers in the Himalayan region are largely influenced by their climatic conditions and topographic undulations. This restricts field measurements using glaciological methods throughout the year (Wagnon et al., 2007; Dobhal et al., 2008). It is not feasible to study all the mountain glaciers in the field for every year, and hence it is important to replace the conventional methods by some cost effective, fast and reliable techniques so that a quick assessment of mass balance of individual glaciers could be done over a period of time. Remote sensing based methods have become an important alternative to conventional methods of mass balance estimation. These methods include monitoring of snow line at the end of ablation season, DEM differencing, LIDAR techniques, gravity measurements and GPR etc. Remote sensing has played a crucial role for mass balance estimation in the Himalayan region using Digital Elevation Model (DEM) (Bahuguna et al., 2007; Berthier et al., 2007) and Accumulation Area Ratio (AAR) approach (Kulkarni, 1992; Kulkarni et al., 2004b; Singh et al., 2013b).

Position of snow line at the end of ablation season is used to compute Accumulation Area Ratio (AAR). AAR is a ratio between accumulation area to total glacial area. Accumulation and ablation zone are defined as zones of glacier above and below snow line at the end of ablation season (melting season). It is a close approximation to the equilibrium line on glaciers in mountain glaciers. Snowline at the end of ablation season can be mapped using high temporal images in VNIR region. AAR is further used to compute specific mass balance based on empirical relationship between AAR and specific mass balance developed using field mass balance data of Shaune Garang and Gor Garang glaciers (Figure 152, Kulkarni 1992). The model has shown AAR representing zero mass balance as 0.48. On the basis of accumulation area ratio (area of accumulation divided by whole area of glacier) mass balance in terms of gain or loss can be estimated. This method is commonly used to assess mass balance at reconnaissance level. The approach based on satellite observations provide a quick regional assessment. However, to use AAR method, we are required to develop a relationship between mass balance and AAR for a particular glacier and a particular period. This relationship can be extended to many other glaciers of the basin.

4.3. Methodology

Data from AWiFS sensor onboard Resourcesat-1 and 2 satellites is main source of delineate the snow line at the end of ablation season. However, appropriate AWiFS data was not observed over few selected sub-basins and was identified cloudy in the ablation period. Therefore, AAR estimation was extended to six years instead of four years for those sub-basins for which the data was available. Thus, AAR estimation has been carried out for the hydrological years 2007-08, 2008-09, 2009-10, 2010-11, 2011-12 and 2012-13 for twelve sub-basins. The steps which are followed to extract AAR for each glacier under study have been enumerated as below.

- 1) AWiFS images of period from July to October were georeferenced with master images.
- 2) Basin boundaries were digitized and overlaid on the images. Image to map registration was carried out to match basin boundary.
- 3) All the glaciers boundaries were digitized on screen using IRS LISS III image to get area of glaciers. The LISS III scenes are used in order to ascertain the boundary of glaciers using higher resolution of the data. These boundaries are further confirmed using SOI maps. To match the boundary of glaciers from maps and satellite data, part of accumulation zone is matched on the ridges based on the shadows observed.
- 4) Glacier boundaries are overlaid on all AWiFS scenes sequentially. Snowline of the respective date is created for individual glacier.
- 5) The accumulation area is the area of glacier above equilibrium line or snow line at end of ablation season. Thus AAR is derived for each glacier based on location of snow line at the end of ablation season.
- 6) A table is generated for AAR of each glacier corresponding to each scene. The least AAR is considered for estimation of mass balance.
- 7) The mass balance for each glacier is estimated using relationship between AAR and mass balance.

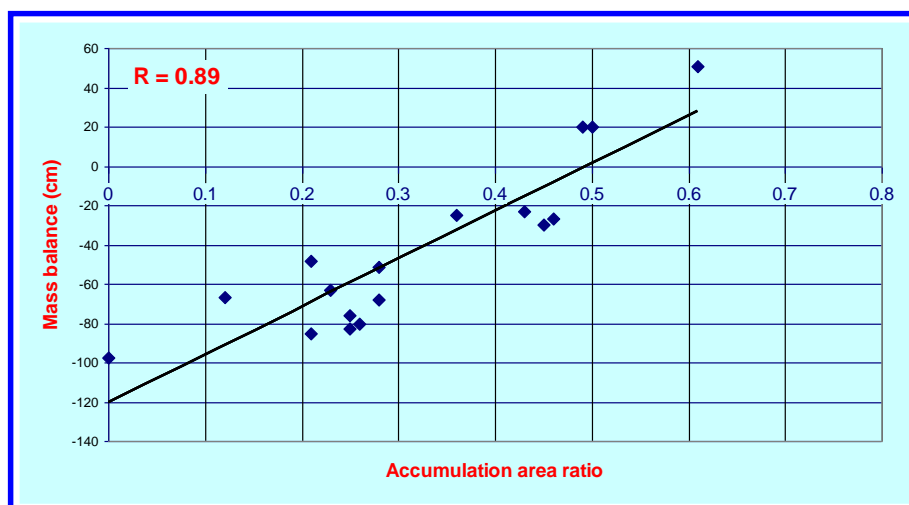


Figure 152: Relationship of AAR and Specific mass balance (Source: Kulkarni, 1992)

4.4. Results and Discussion

The mass balance was estimated for mainly valley glaciers and not for small glaciers /permanent snow fields (<3 sq. km) considering the accuracy in using 56 m spatial resolution AWiFS data.

Example of variation of snow line at the end of ablation season for an individual glacier are shown in Figure 153. Snow line fluctuates due to precipitation and melting and is observed to vary from one year to another as can be seen in the Figure for all respective years.

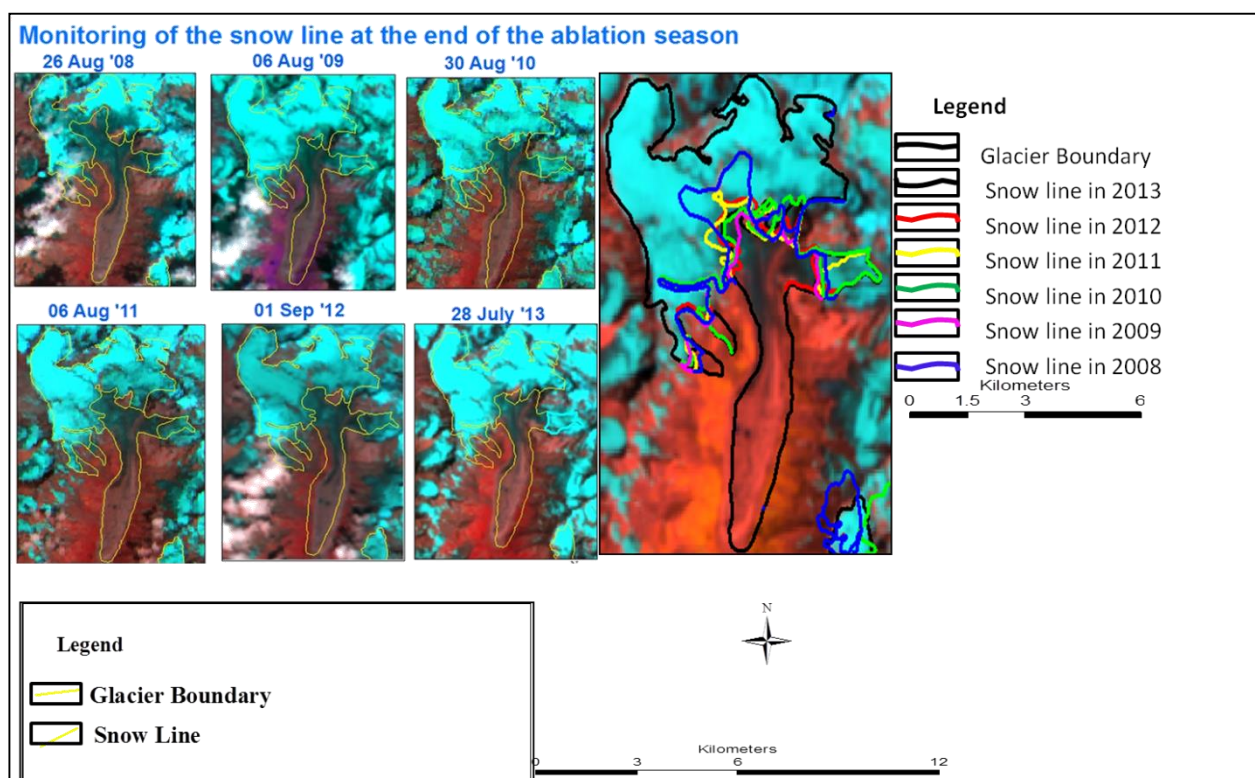


Figure 153: Variation of Snow line at the end of ablation season on glaciers for estimation of AAR.

(a) Sub-basin wise Glacier Mass Balance

The salient results of glacier mass balance for 13 sub-basins are summarized in Table 72 and Table 73. This data has been further analysed and salient results are discussed subsequently.

Table 72: Number of glaciers experiencing positive and negative specific mass balance using AAR approach during 2008 to 2013 in each sub-basin. C is cloudy data.

Basin	Sub-basin ↓	Years →	2008	2009	2010	2011	2012	2013
Indus	Nubra	Negative	42	3	3	6	10	20
		Positive	41	83	83	70	75	66
Indus	Zaskar	Negative	c	c	6	10	12	31
		Positive	c	c	46	68	24	62
Chenab	Warwan	Negative	37	2	14	11	7	13
		Positive	8	32	30	28	37	30
Chenab	Bhut	Negative	14	2	12	14	14	5
		Positive	15	12	32	32	32	33
Chenab	Chandra	Negative	40	16	1	0	16	14
		Positive	64	73	104	98	84	29
Chenab	Bhaga	Negative	7	3	20	5	64	0
		Positive	55	70	41	44	13	50
Chenab	Miyar	Negative	153	98	33	32	97	53
		Positive	47	50	177	203	63	19
Beas	Parbati	Negative	17	1	3	3	9	6
		Positive	14	17	35	25	16	22
Satluj	Basapa	Negative	13	11	4	8	9	c
		Positive	3	8	10	11	2	c
Ganga	Alaknanda	Negative	60	78	10	26	55	88
		Positive	24	21	48	94	66	12
Ganga	Bhagirathi	Negative	67	73	4	27	50	52
		Positive	11	16	10	114	54	21
Ganga	Dhauliganga	Negative	62	28	26	35	37	c
		Positive	40	11	21	45	6	c
Ganga	Goriganga	Negative	6	17	7	4	10	c
		Positive	23	6	3	23	14	c
	Total	Negative	518	332	143	181	390	282
		Positive	345	399	640	855	486	344
Grand Total			863	731	783	1036	876	626

Table 73: Average Accumulation Area Ratio (AAR) and Specific Mass Balance (SMB) in cm for selected glaciers studied in 13 sub-basins of Himalayan region during 2008 to 2013

C-cloudy data

Basin	Sub-basin		2008	2009	2010	2011	2012	2013
Indus	Nubra	AAR	0.5	0.85	0.77	0.78	0.67	0.62
		SMB	1.57	87.33	66.76	68.88	42.98	23.32
Indus	Zanskar	AAR	-	-	0.72	0.63	0.55	0.55
		SMB	-	-	54.59	32.61	13.57	13.05
Chenab	Warwan	AAR	0.36	0.77	0.55	0.6	0.74	0.61
		SMB	-32.3	66.51	14.21	25.61	58.93	28.55
Chenab	Bhut	AAR	0.48	0.65	0.56	0.54	0.56	0.67
		SMB	-2.43	37.12	16.22	10.84	14.9	41.77
Chenab	Chandra	AAR	0.53	0.68	0.83	0.94	0.68	0.61
		SMB	7.14	45.23	81.8	107.67	45.38	26.87
Chenab	Bhaga	AAR	0.7	0.84	0.58	0.83	0.71	0.81
		SMB	49.61	84.01	19.84	81.22	50.86	74.87
Chenab	Miyar	AAR	0.37	0.43	0.71	0.62	0.58	0.38
		SMB	-31.88	-17.25	51.44	30.03	20.01	-29.37
Beas	Parbati	AAR	0.5	0.7	0.73	0.73	0.53	0.73
		SMB	0.56	50.89	52.84	57.43	9.02	56.35
Satluj	Basapa	AAR	0.28	0.45	0.69	0.59	0.35	c
		SMB	-51.26	-11.3	48.12	5.49	-36.54	c
Ganga	Alaknanda	AAR	0.4	0.34	0.68	0.69	0.56	0.25
		SMB	-24.35	-38.83	44.95	46.88	15.13	-60.45
Ganga	Bhagirathi	AAR	0.31	0.33	0.9	0.71	0.55	0.38
		SMB	-45.18	-41.01	99.17	52.27	12.64	-28.34
Ganga	Dhauliganga	AAR	0.47	0.36	0.54	0.54	0.29	c
		SMB	-5.53	-33.84	9.95	1.44	-51.73	c
Ganga	Gauriganga	AAR	0.55	0.4	0.65	0.67	0.53	c
		SMB	12.85	-23.45	36.6	42.5	7.48	c

i) Indus Basin (Nubra and Zanskar Sub-basins)

Glacier mass balance has been estimated based on the shift of snow line to highest elevation during the ablation season as interpreted from IRS AWiFS data and AAR approach. Figure 154 shows the snow line fluctuation during ablation period in the Nubra sub-basin. This image shows gradual shift of snow line upwards reaching to highest elevation on August 30, 2010 and then downward shift of snowline due to fresh snowfall in the valley.

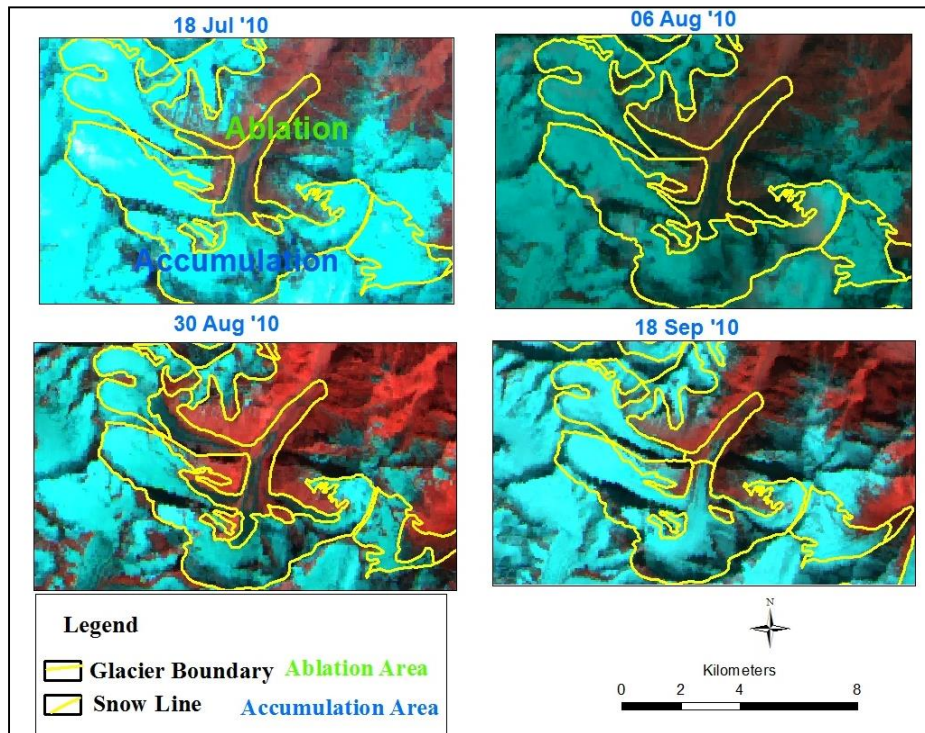


Figure 154: IRS AWiFS images showing fluctuation of snow line in a glacier of Nubra sub-basin during 2010

It is observed that number of glaciers having negative & positive mass balance in Nubra sub-basin are almost equal in year 2008, however in subsequent year 2009, the number of glacier with positive mass balance has doubled and remains same during 2010 and marginal reduction is observed during 2010-2013 (Figure 155). It is also observed that there is a continuous rise in number of glaciers having negative mass balance during 2009-2013 time frame. Specific Mass Balance has been observed to be close to zero in 2008 and maximum positive for year 2009 (Figure 156). This status is maintained during subsequent years with marginal reduction during year 2010 and 2011. There is further decreasing trend of SMB during 2011-2013. Glaciers in the Zaskar sub-basin show rise in number of glaciers showing negative mass balance during 2010-2013 (Figure 157), which is also reflected in decreasing trend of SMB (Figure 158). It may be noted that overall glaciers in Nubra and Zaskar sub-basins show positive mass balance for the entire period of observation i.e. 2008-2013, however the decreasing trend of SMB is also observed.

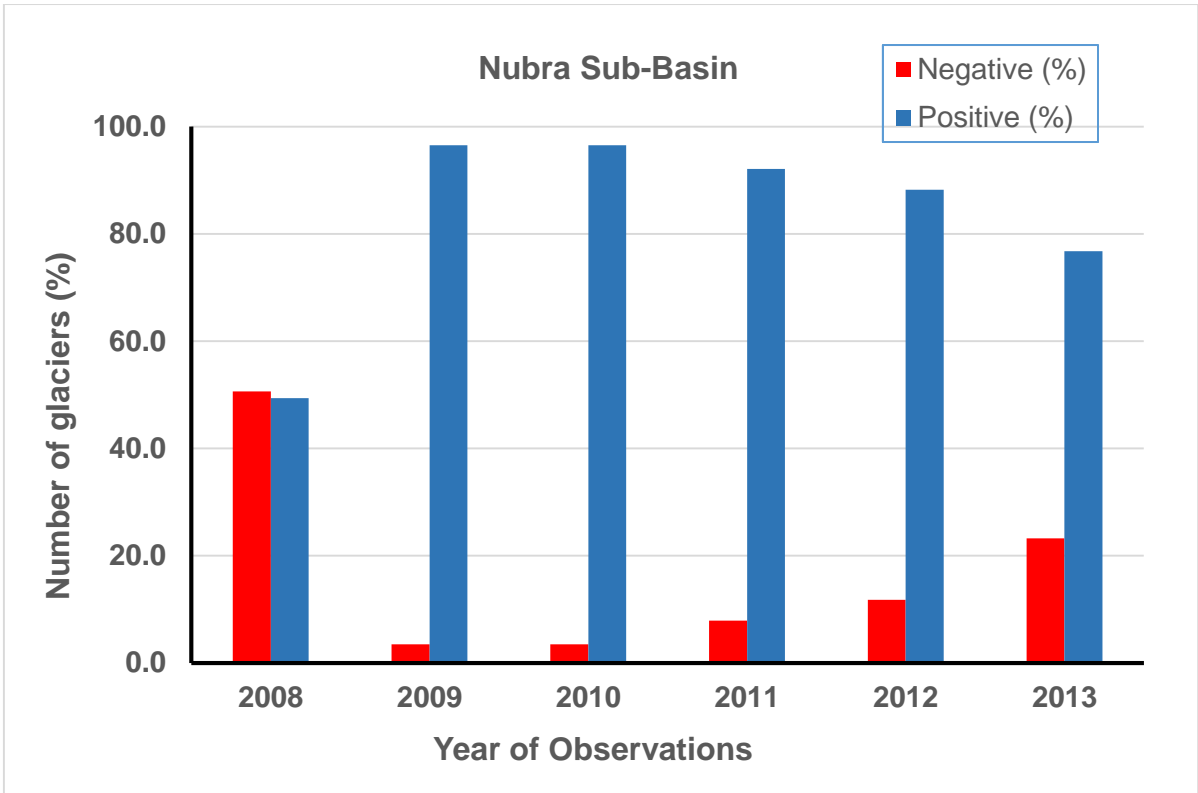


Figure 155: Number of glaciers experiencing negative or positive SMB in Nubra sub-basin based on location of snow line at the end of ablation season

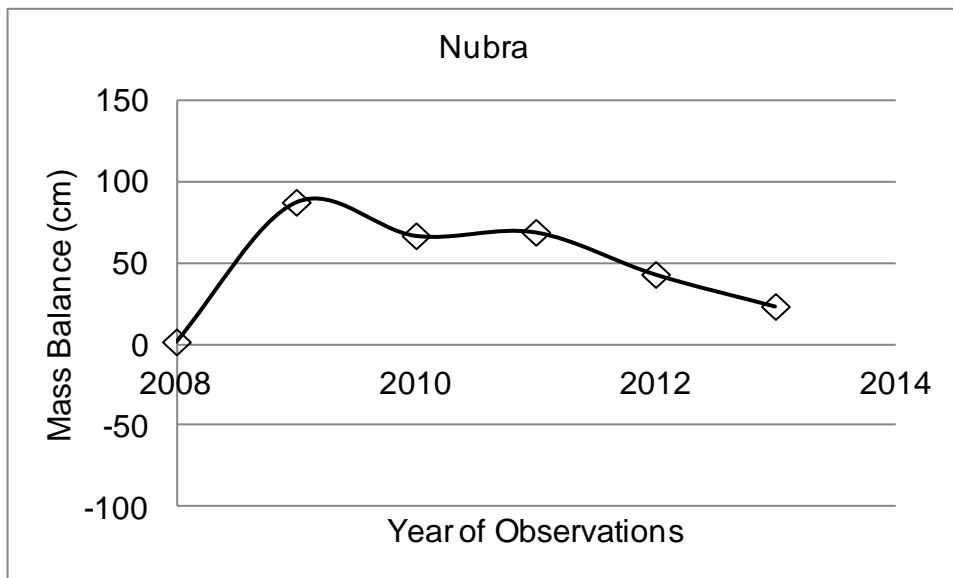


Figure 156: Mean Specific MB (in water equivalent or cm) for Nubra sub-basin based on Snow line at the end of ablation season

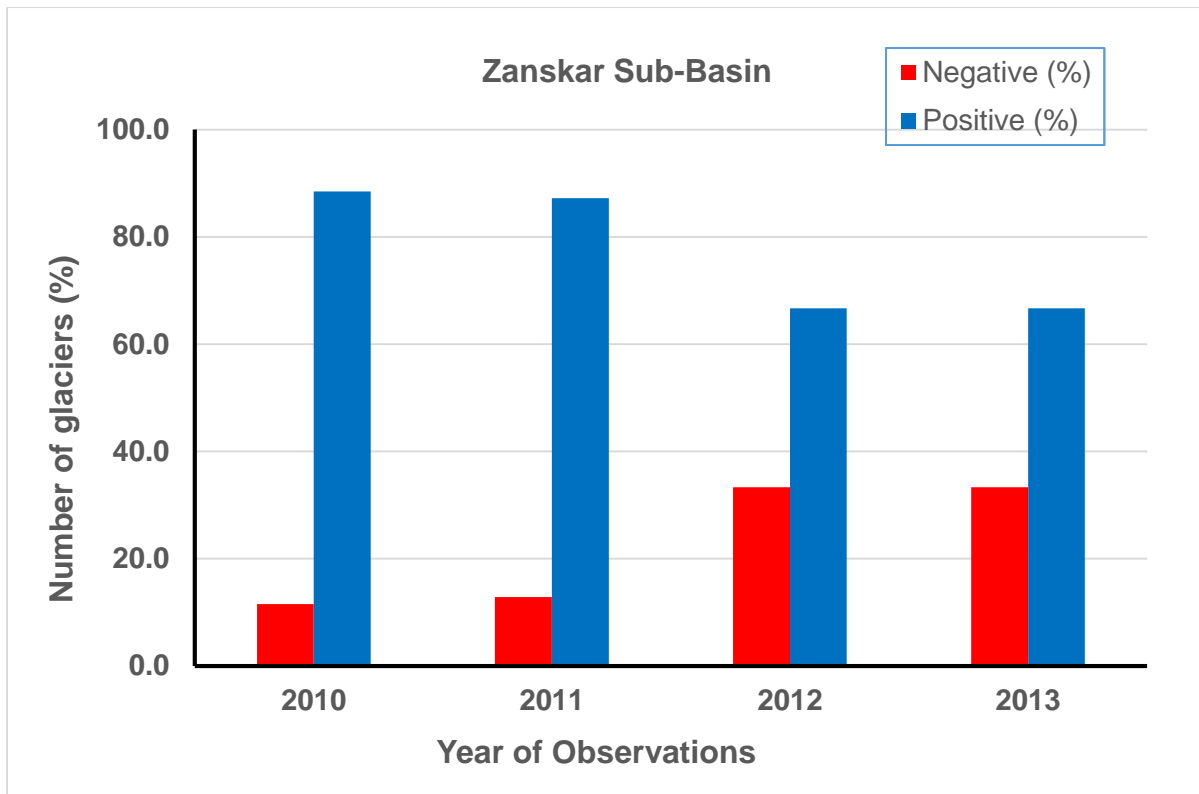


Figure 157: Number of glaciers experiencing negative or positive SMB in Zanskar sub-basin based on location of snow line at the end of ablation season

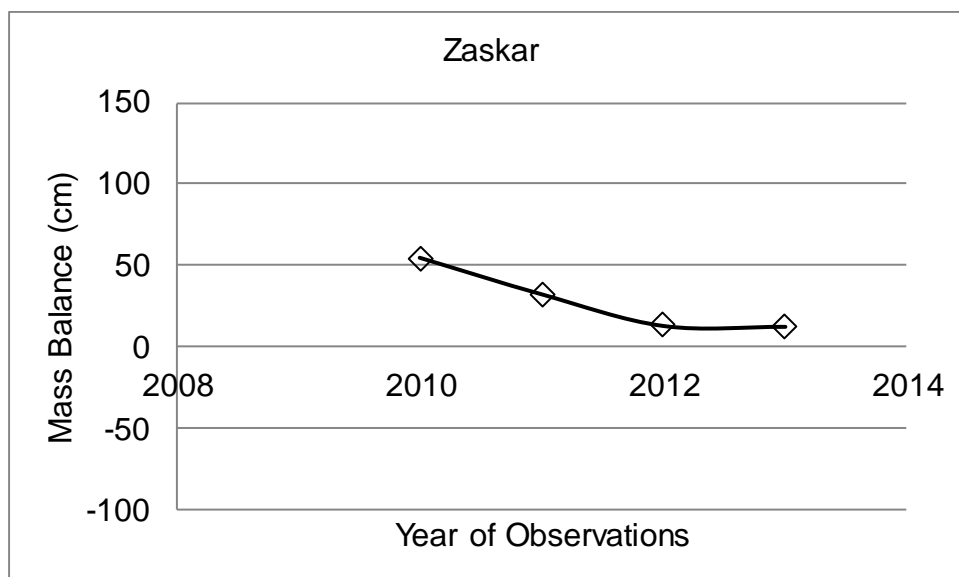


Figure 158: Mean Specific MB (in water equivalent or cm) for Zanskar sub-basin based on Snow line at the end of ablation season

ii) Chenab Basin (Warwan, Bhut, Chandra, Bhaga and Miyar Sub-basins)

Figure 159 shows the delineation of snow line of 28 July and 10 September 2013 for Warwan sub-basin. This depicts the upward movement of snow line in the month of September 2013 representing it as a suitable dataset for determining AAR and SMB respectively.

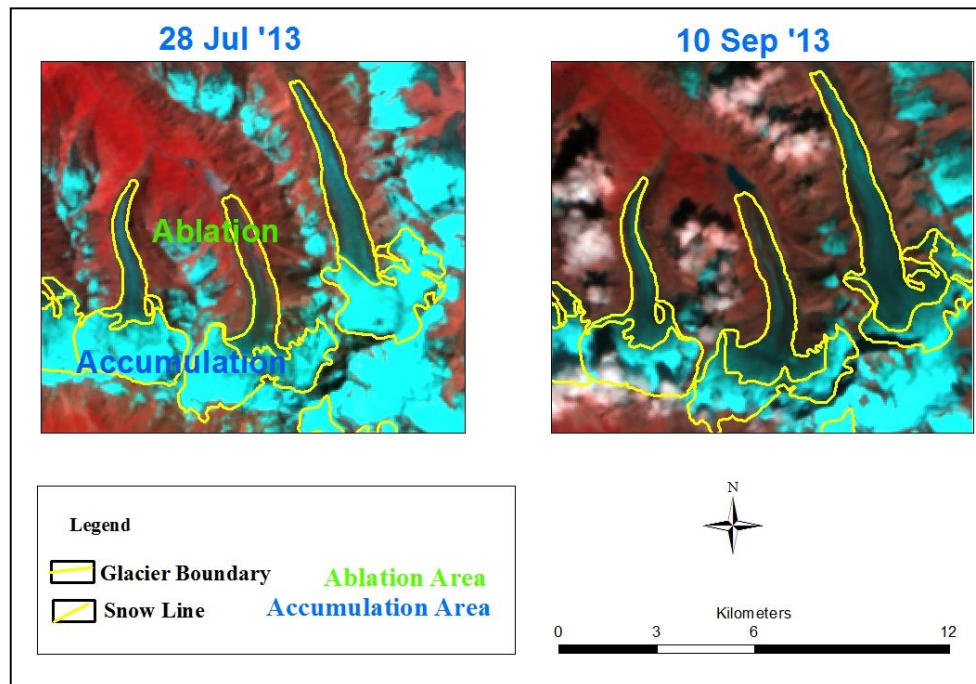


Figure 159: IRS AWiFS images showing fluctuation of snow line in a glacier of Warwan sub-basin during 2013

In Warwan sub-basin, number of glaciers having negative mass balance is high for year 2008 i.e., > 80%, whereas number of glaciers showing positive mass balance is > 68% in subsequent 2009-2013 time frame (Figure 160). SMB trend also clearly show negative mass balance during 2008 and positive mass balance subsequently (Figure 161). It is observed that ~ 30 % glaciers show negative mass balance during 2010, 2011 and 2013. However, fluctuations in SMB are observed indicating dynamic changes in glaciated region.

Bhut sub-basin has also shown similar pattern as Warwan sub-basin. Number of glaciers with positive mass balance i.e., > 69 % during 2009-2013 time frame are observed (Figure 162). Specific Mass Balance has been observed to be close to zero in 2008 (Figure 163). Overall, SMB in Bhut sub-basin is positive during the entire time frame 2009-2013, however, ~ 13-30 % glaciers show negative mass balance.

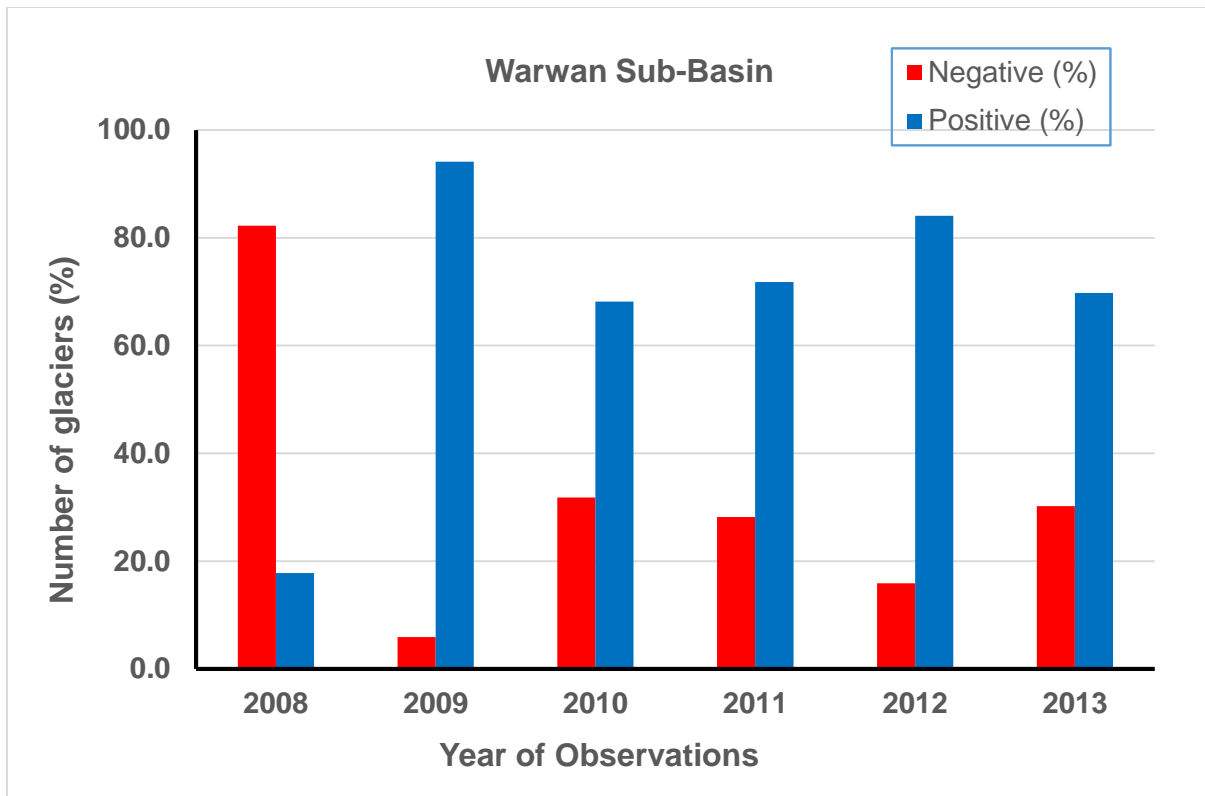


Figure 160: Number of glaciers experiencing negative or positive SMB in Warwan sub-basin based on location of snow line at the end of ablation season

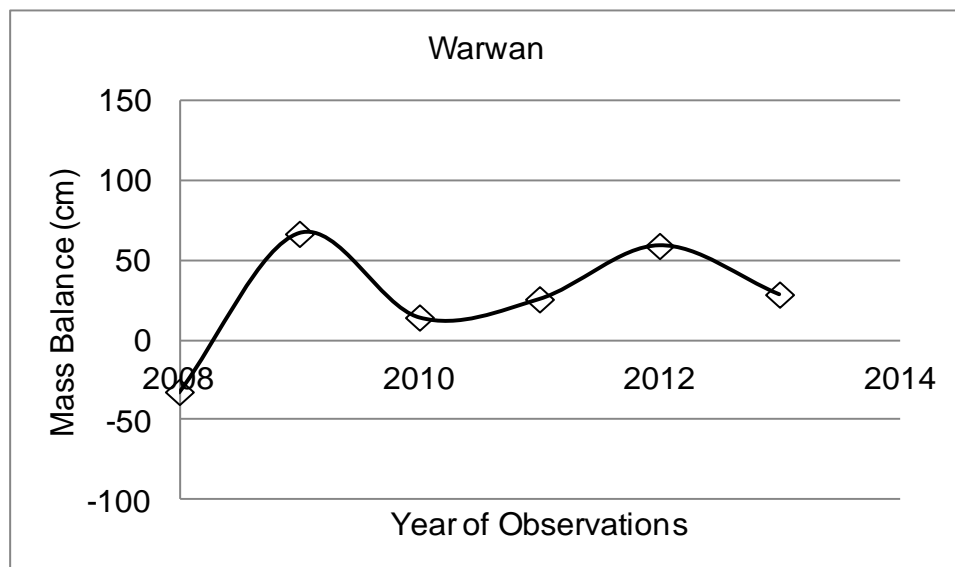


Figure 161: Mean Specific MB (in water equivalent or cm) for Warwan sub-basin based on Snow line at the end of ablation season

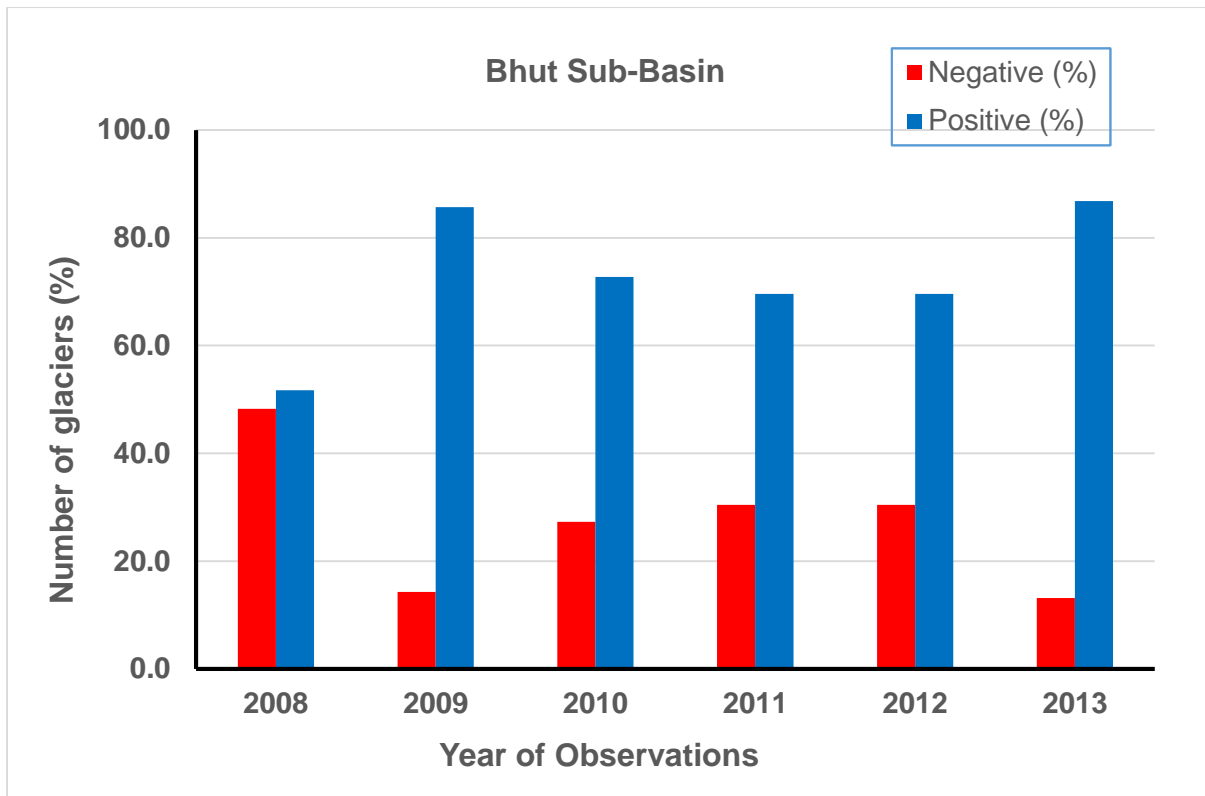


Figure 162: Number of glaciers experiencing negative or positive SMB in Bhut sub-basin based on location of snow line at the end of ablation season

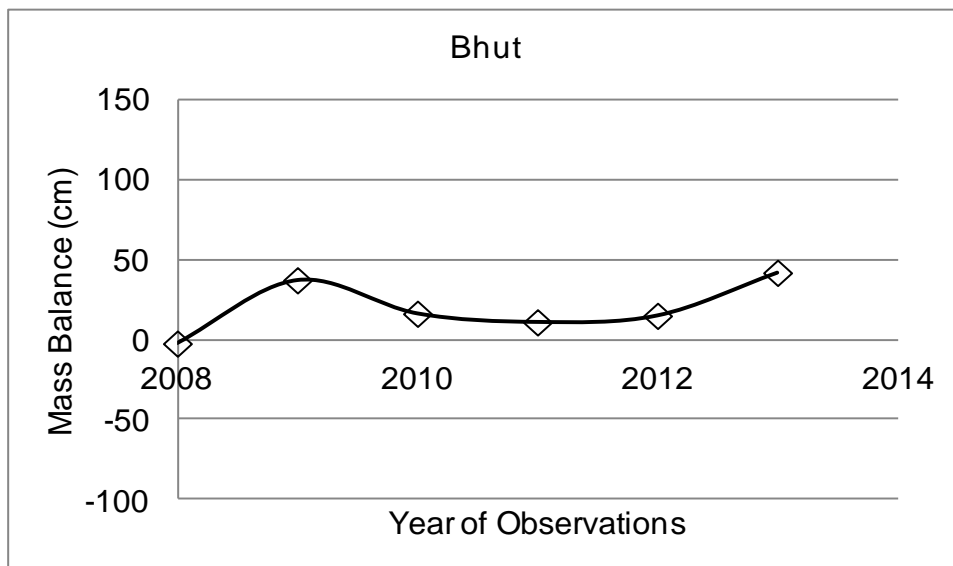


Figure 163: Mean Specific MB (in water equivalent or cm) for Bhut sub-basin based on Snow line at the end of ablation season.

Figure 164 shows the variability in snow line during ablation month from July to September 2012 in few glaciers of the Chandra sub-basin. It may be seen that the snow line recedes from July and reaches maximum elevation during September 10, 2012. The number of glaciers showing positive mass balance in Chandra sub-basin ranges between 61.5 to 100 % during 2008 to 2013 (Figure 165). Number of glaciers during 2008, 2009, 2012 and 2013 showing negative mass balance are 38.5%, 18%, 16% and 32.6%. During 2011 all the glaciers in Chandra sub-basin show positive mass balance. Overall glaciers in Chandra sub-basin show positive mass balance during 2008-2013 with increasing trend during 2008-2011 and decreasing trend during 2011-2013 (Fig. 166).

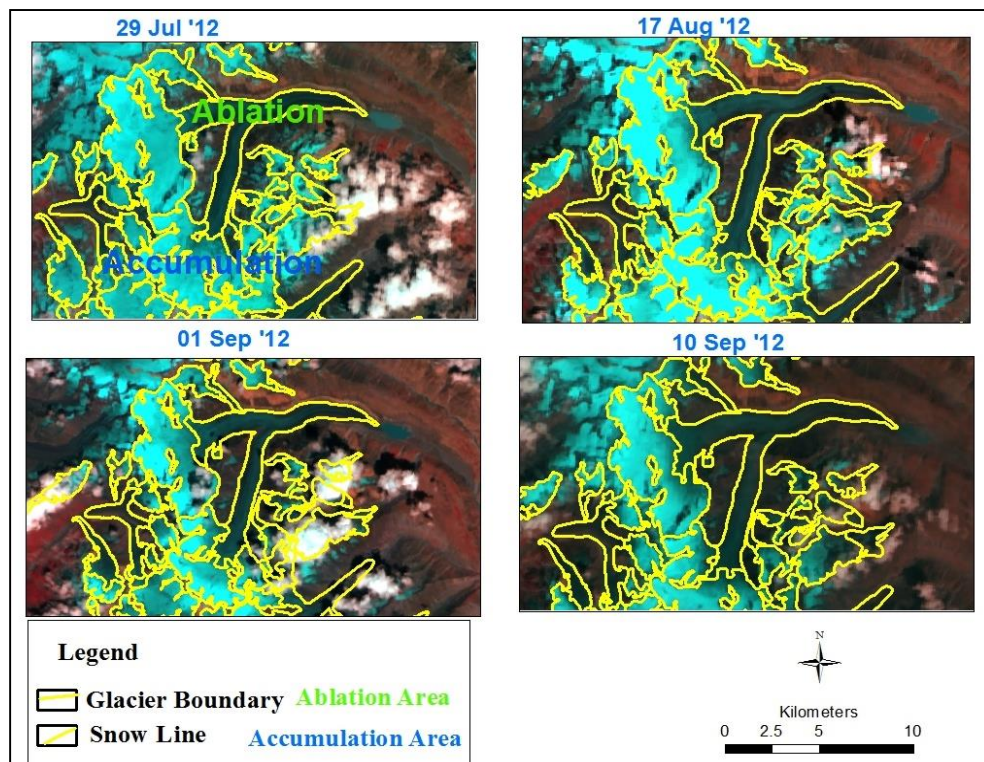


Figure 164: IRS AWiFS images showing fluctuation of snow line in few glaciers of Chandra sub-basin during 2012.

Bhaga sub-basin have shown similar pattern of positive mass balance except number of glaciers having negative mass balance were high in year 2012 (Figure 167 & Figure 168).

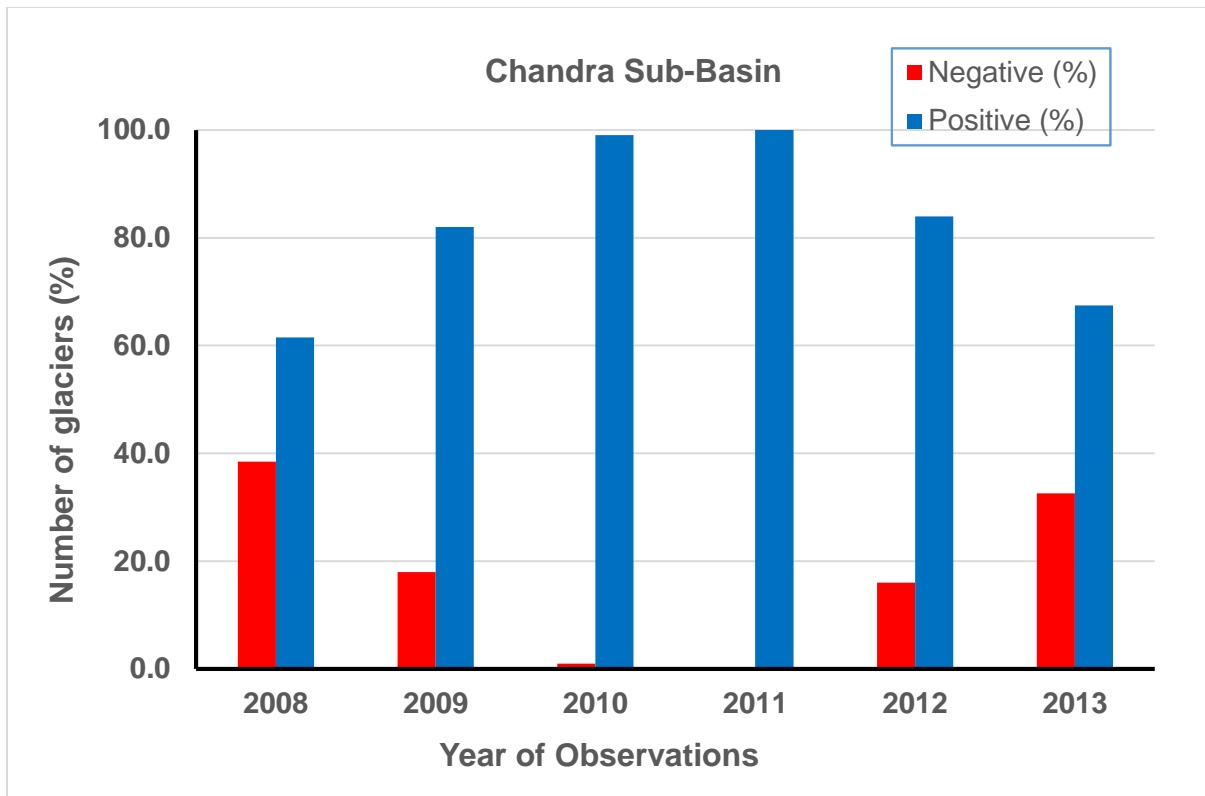


Figure 165: Number of glaciers experiencing negative or positive SMB in Chandra sub-basin based on location of snow line at the end of ablation season

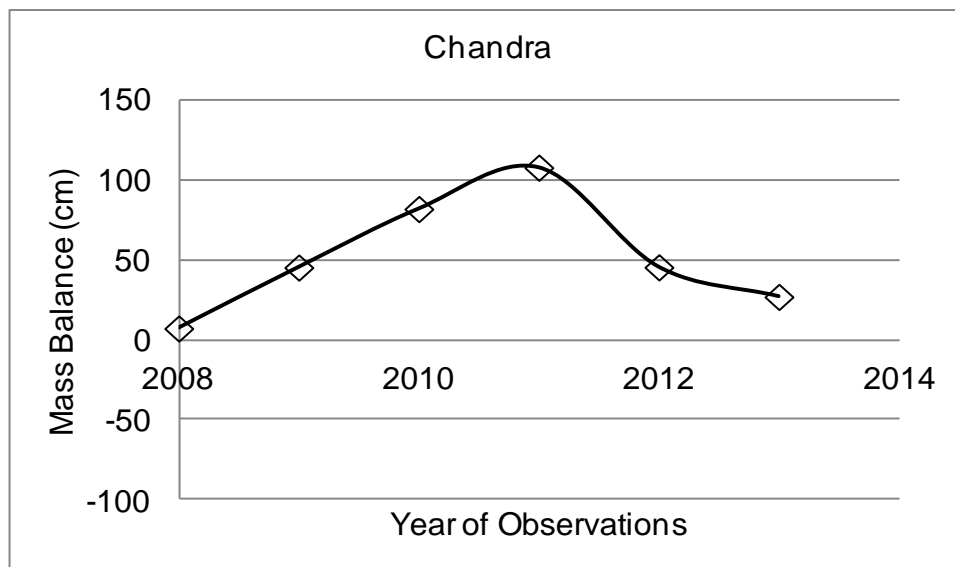


Figure 166: Mean Specific MB (in water equivalent or cm) for Chandra sub-basin based on Snow line at the end of ablation season

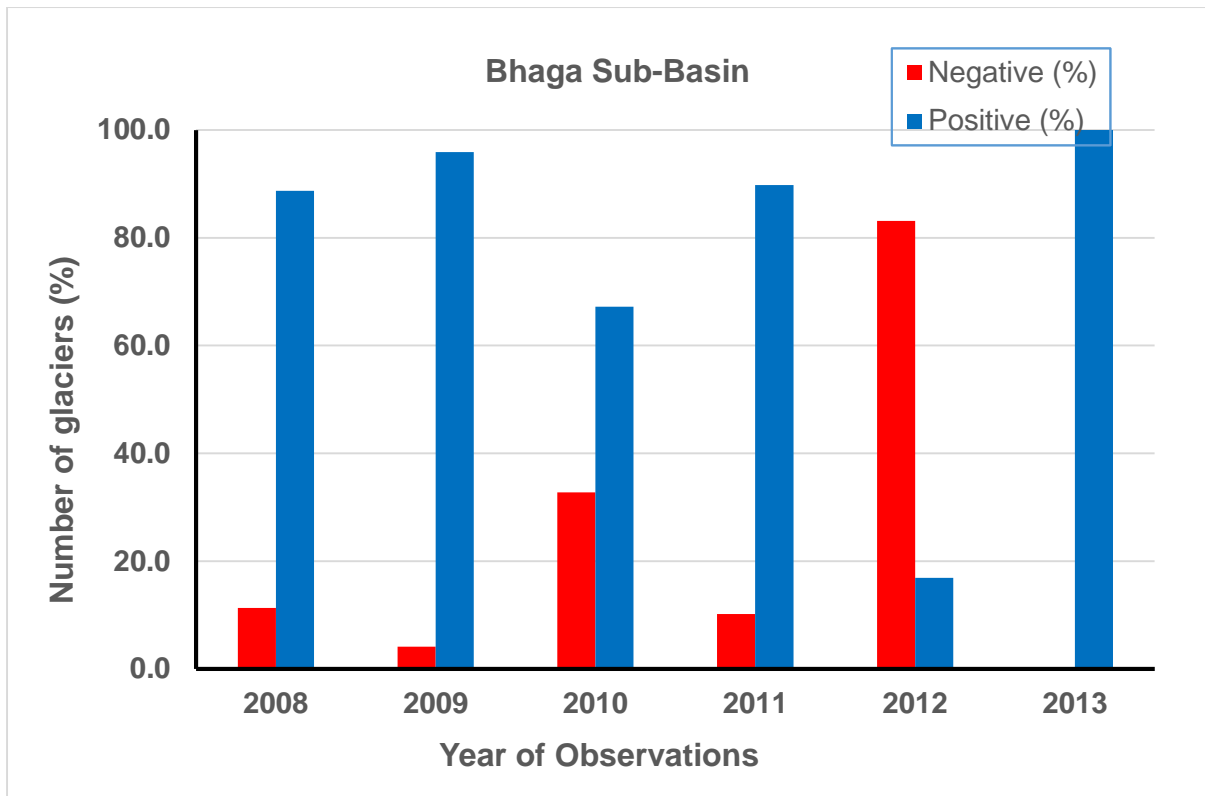


Figure 167: Number of glaciers experiencing negative or positive SMB in Bhaga sub-basin based on location of snow line at the end of ablation season

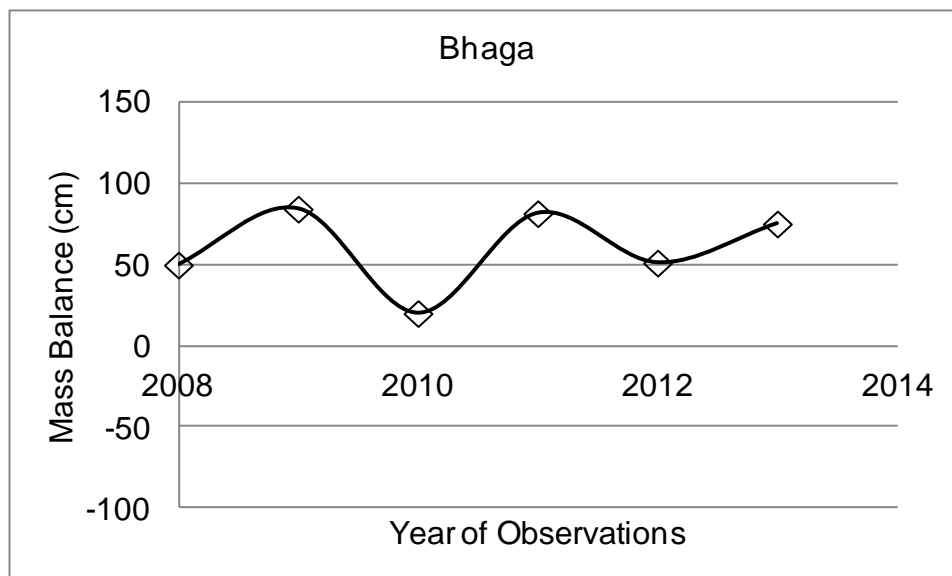


Figure 168: Mean Specific MB (in water equivalent or cm) for Bhaga sub-basin based on Snow line at the end of ablation season

Figure 169 shows the variability in snow line during ablation month from July to September 2011 in Miyar sub-basin. Snow line was observed to be minimum on 26 August 2011. It may be seen that the snow line recedes from July and reaches maximum elevation during August 26, 2011. AWiFS data has shown the presence of cloud during the observed period which sometimes severely affects the availability of suitable dataset for delineation of snow line and AAR derived mass balance.

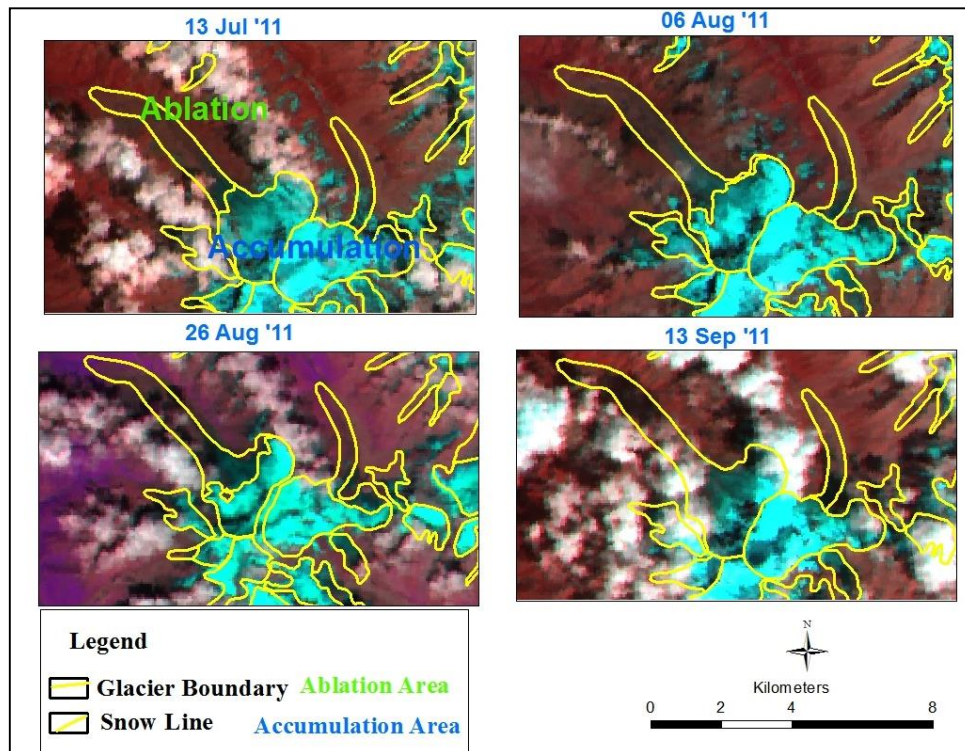


Figure 169: IRS AWiFS images showing fluctuation of snow line in few glaciers of Miyar sub-basin during 2011

In the Miyar sub-basin, number of glaciers having negative mass balance is observed to be higher than positive mass balance throughout the observed period except year 2010 and 2011 (Figure 170) which is also reflected in the trend of SMB (Figure 171). Maximum positive mass balance is observed in the year 2010, which reduces subsequently and reaches to negative mass balance in year 2013.

iii) Beas Basin (Parbati Sub-basin)

Glaciers in the Parbati sub-basin show zero mass balance during the year 2008 and subsequently positive mass balance during 2009 to 2013 (Figure 172 and Figure 173). SMB is positive from 2009 to 2013 consistently except a drop in year 2012.

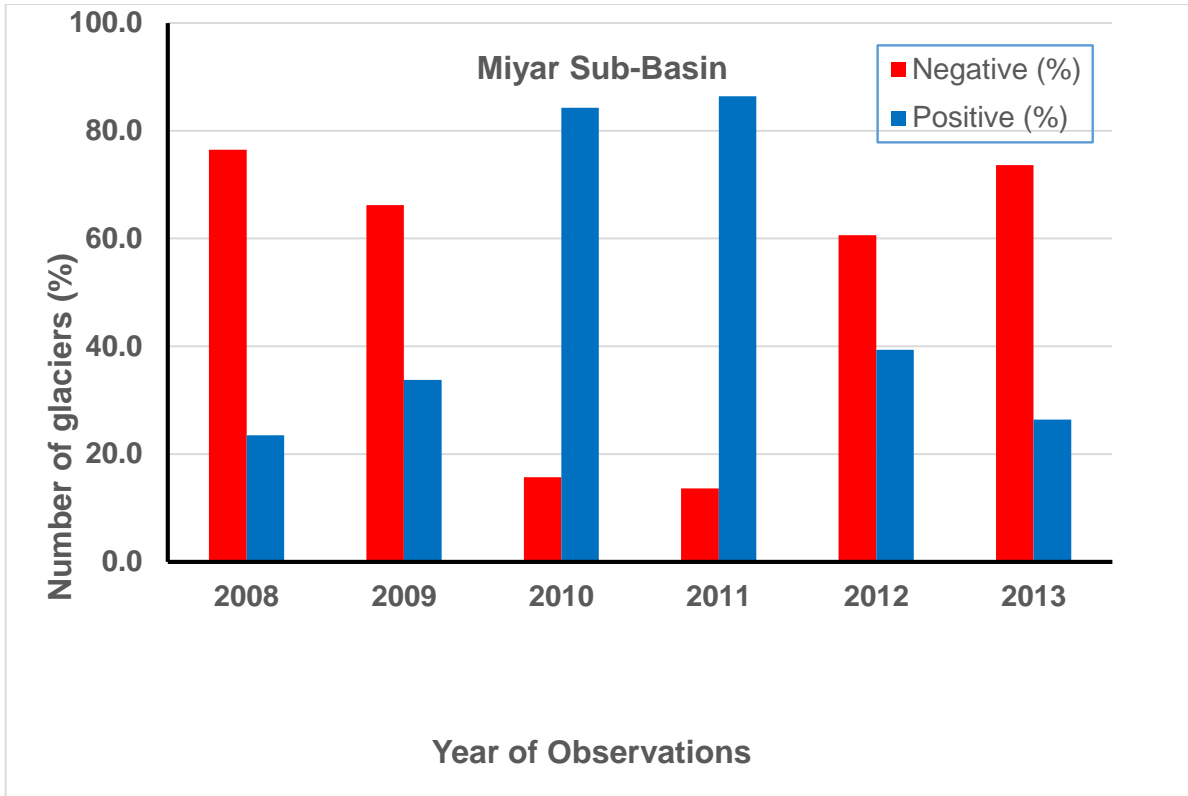


Figure 170: Number of glaciers experiencing negative or positive SMB in Miyar sub-basin based on location of snow line at the end of ablation season

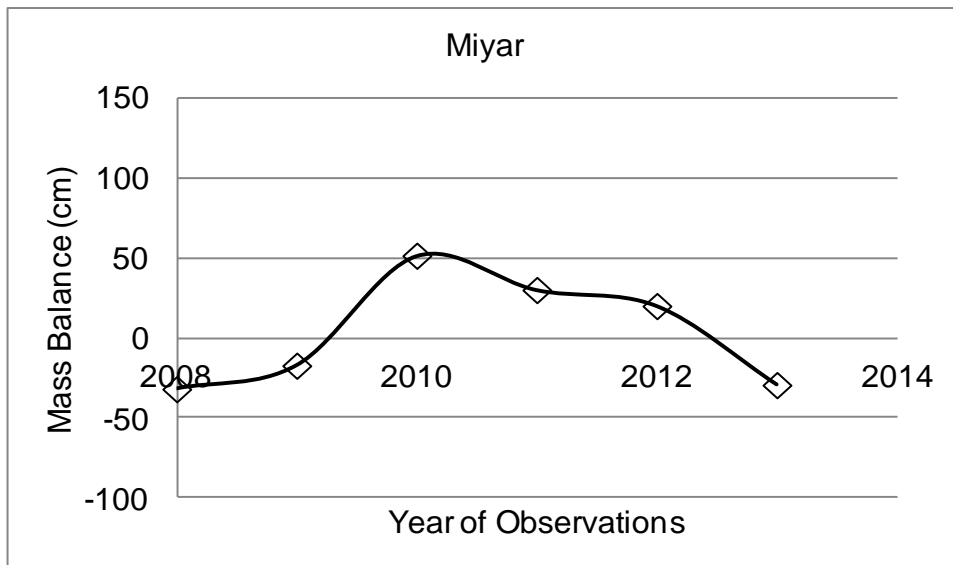


Figure 171: Mean Specific MB (in water equivalent or cm) for Miyar sub-basin based on Snow line at the end of ablation season

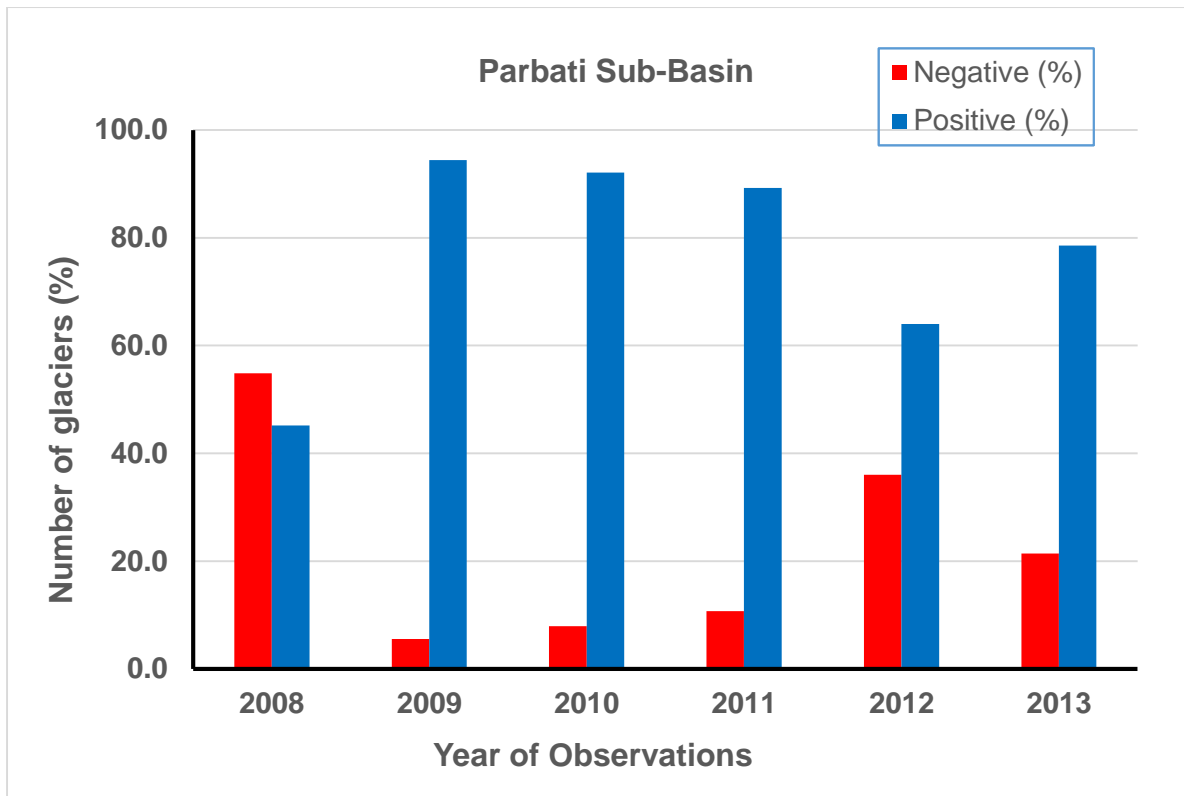


Figure 172: Number of glaciers experiencing negative or positive SMB in Parbati sub-basin based on location of snow line at the end of ablation season

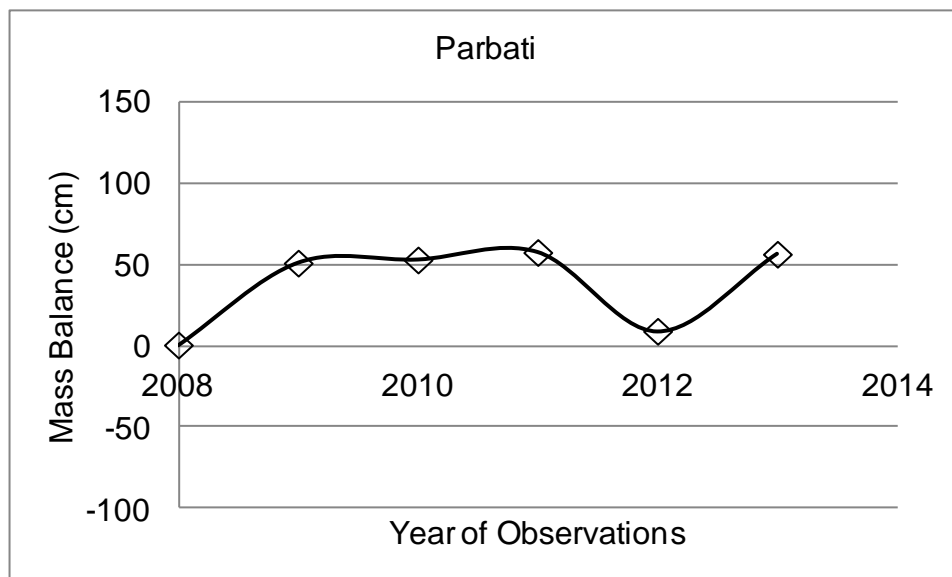


Figure 173: Mean Specific MB (in water equivalent or cm) for Parbati sub-basin based on Snow line at the end of ablation season

iv) Satluj Basin (Baspa Sub-basin)

Number of glaciers showed negative mass balance for all years of observations except year 2010 and 2011 and SMB was found to be negative throughout except year 2010 (Figure 174 & 175).

v) Ganga Basin (Bhagirathi, Alaknanda, Dhauliganga and Gauriganga sub-basins)

Bhagirathi sub-basin has shown number of glaciers having negative mass balance were high for observation period except 2010 & 2011 (Figure 176). SMB was observed to be negative for year 2008 & 2009 whereas it was observed to be positive for year 2010 & 2011 (Figure 177).

Alaknanda sub-basin has shown number of glaciers having negative mass balance were high for year 2010, 2011 & 2012 (Figure 178). SMB was observed to be negative for year 2008, 2009 & 2012 whereas it was observed to be positive for year 2010, 2011 & 2012 (Figure 179).

Gauriganga sub-basin has shown number of glaciers having negative mass balance were high for year 2008, 2011 & 2012 (Figure 180). SMB was observed to be negative only for year 2009 whereas it was observed to be slightly more positive for 2010 & 2011 (Figure 181). No suitable data was found for year 2013 due to cloudy conditions.

Dhauliganga sub-basin has shown number of glaciers having negative mass balance throughout the observed period except year 2011 where more number of glaciers having positive mass balance were observed (Figure 182). Overall mass balance was negative or close to zero for year 2010 & 2011 (Figure 183). No suitable data was found for year 2013 due to cloudy conditions.

Overall, it is summarized that the total number of glaciers studied during time frame 2008 – 2013 for 13 sub-basins and % of glaciers showing negative and positive mass balance year-wise are viz., 2008: 863 (-60%,+40%); 2009: 731 (-45%,+55%); 2010: 783 (-18%,+82%); 2011: 1036 (-17.5%,+82.5%); 2012: 876 (-44.5%,+55.5%); 2013: 626 (-45%,+55%). Only selected valley glaciers in each sub-basin were studied. The number of glaciers studied varied each year due to cloud cover in satellite data during ablation season. In addition, due to cloud cover problem, same glacier may not have been studied consecutively in few cases during the time frame 2008-2013.

Mean specific mass balance is observed to be negative for Alaknanda sub-basin (minimum – 60.45 cm in 2013), Bhagirathi, Dhauliganga, Basapa and Miyar sub-basin three times and Warwan, Bhut and Gauriganga sub-basins once during 2008-2013 time frame.

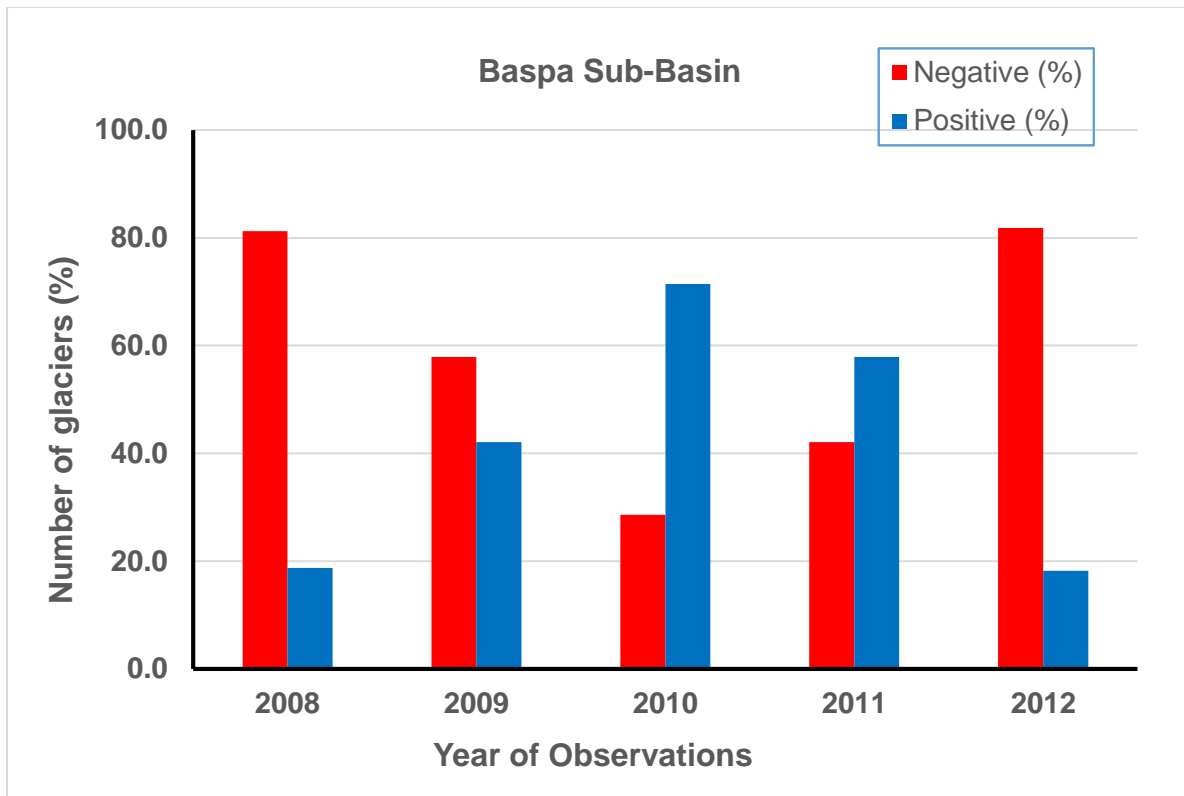


Figure 174: Number of glaciers experiencing negative or positive SMB in Baspa sub-basin based on location of snow line at the end of ablation season

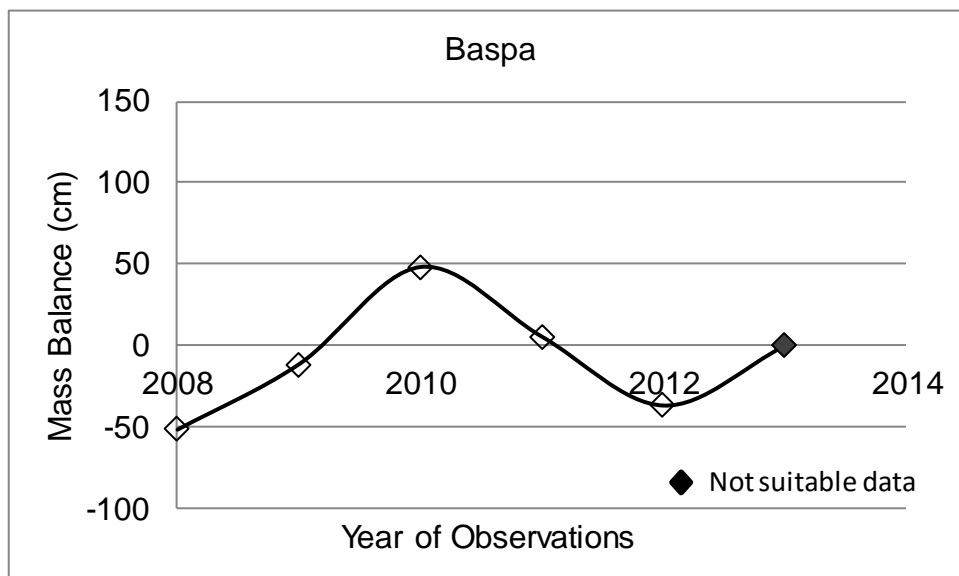


Figure 175: Mean Specific MB (in water equivalent or cm) for Baspa sub-basin based on Snow line at the end of ablation season

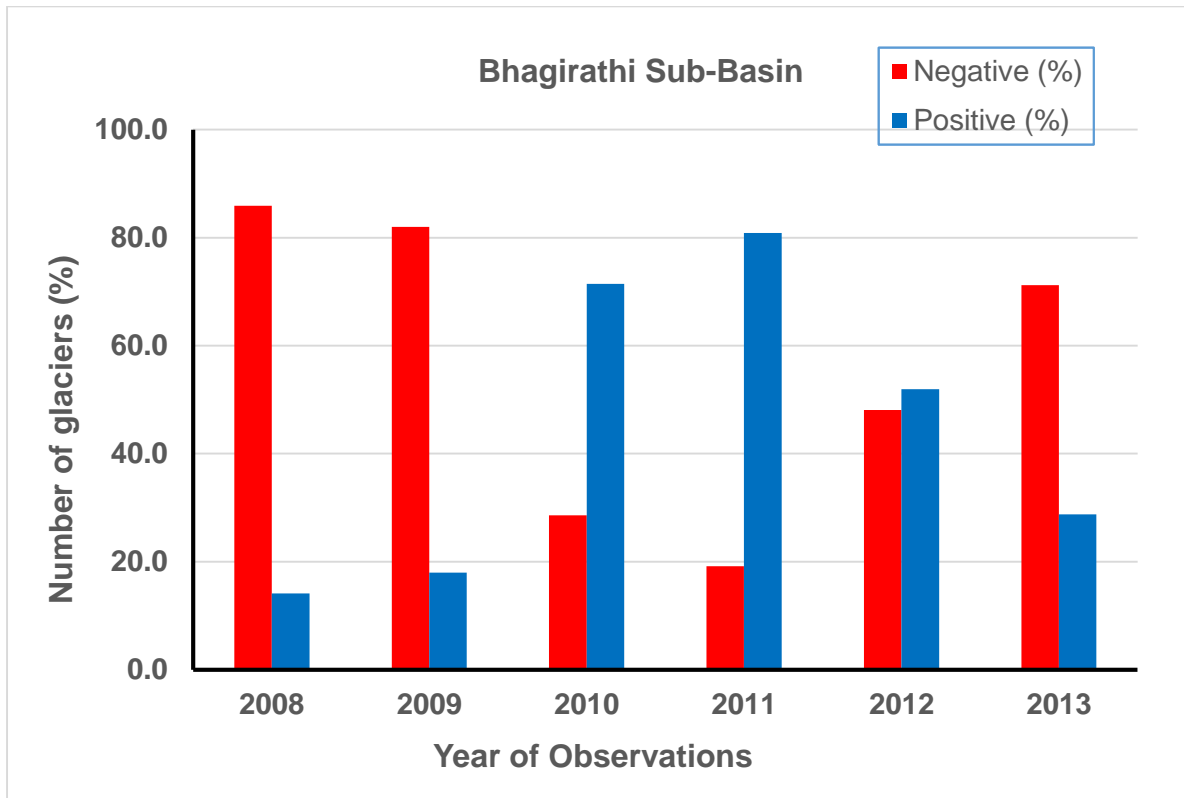


Figure 176: Number of glaciers experiencing negative or positive SMB in Bhagirathi sub-basin based on location of snow line at the end of ablation season

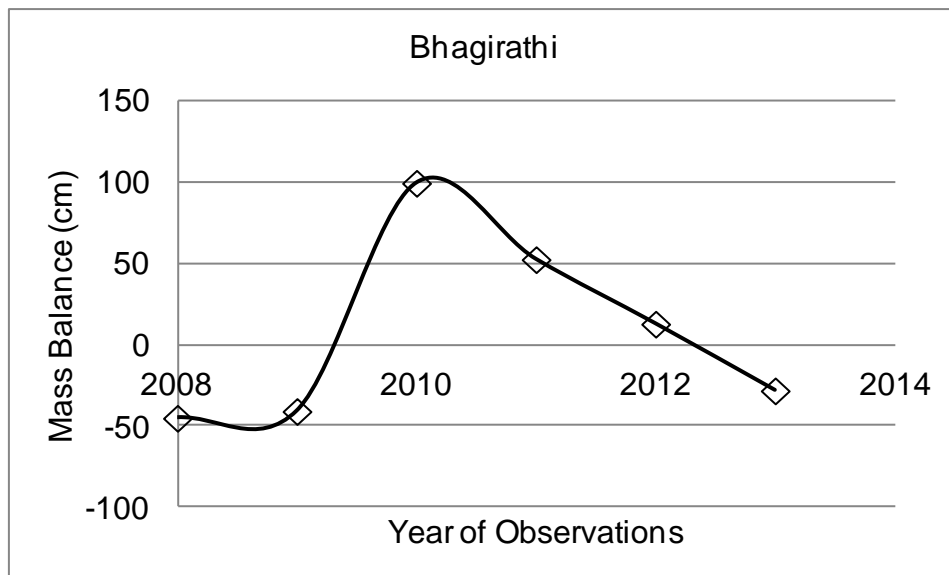


Figure 177: Mean Specific MB (in water equivalent or cm) for Bhagirathi sub-basin based on Snow line at the end of ablation season

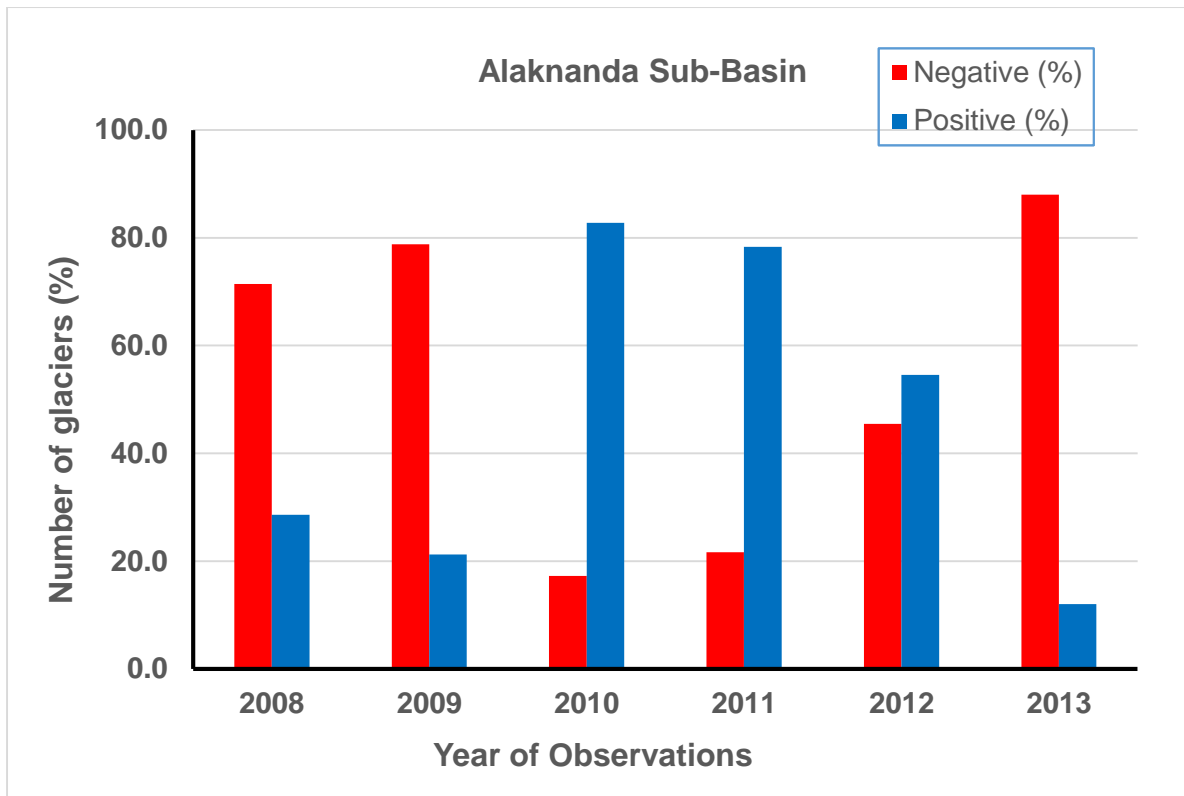


Figure 178: Number of glaciers experiencing negative or positive SMB in Alaknanda sub-basin based on location of snow line at the end of ablation season

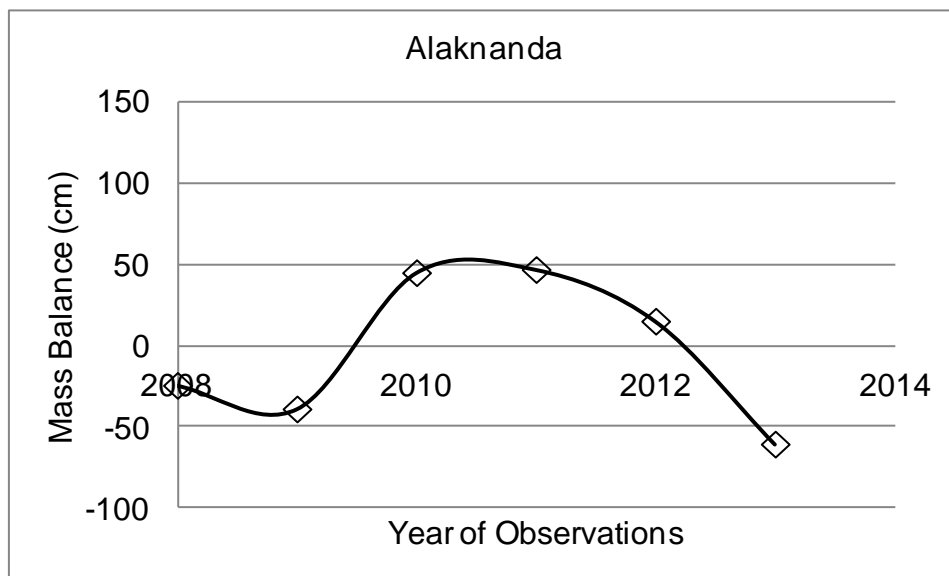


Figure 179: Mean Specific MB (in water equivalent or cm) for Alaknanda sub-basin based on Snow line at the end of ablation season

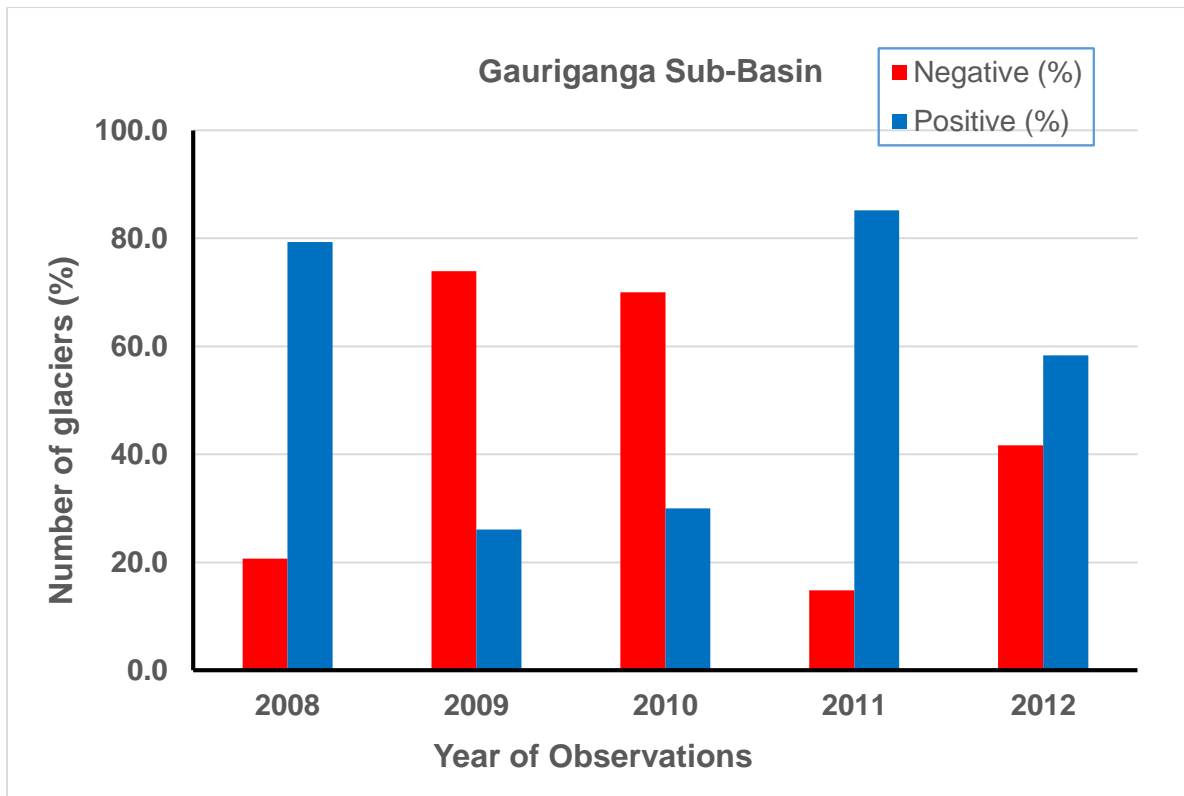


Figure 180: Number of glaciers experiencing negative or positive SMB in Gauriganga sub-basin based on location of snow line at the end of ablation season

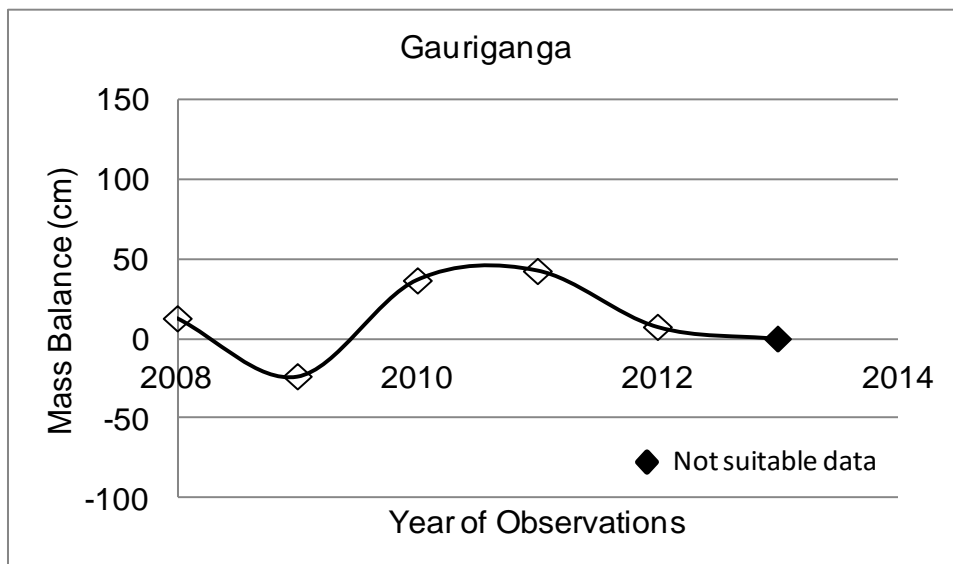


Figure 181: Mean Specific MB (in water equivalent or cm) for Gauriganga sub-basin based on Snow line at the end of ablation season

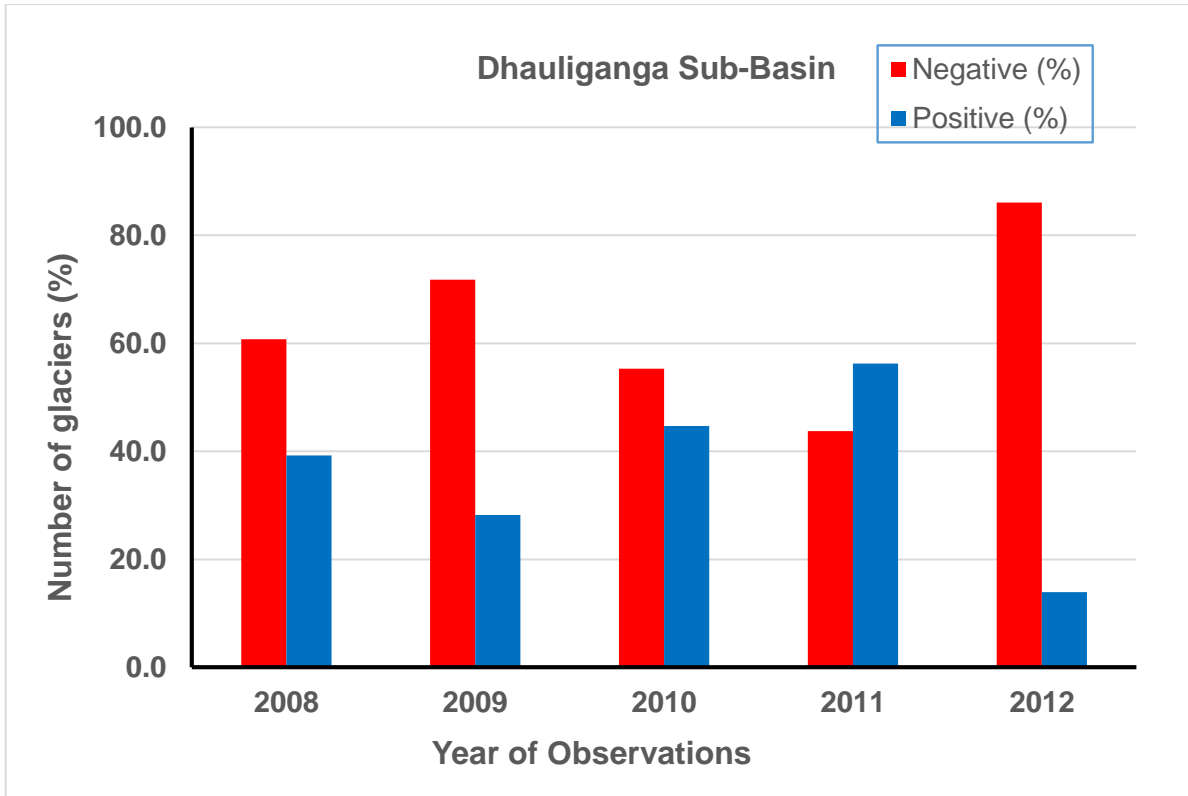


Figure 182: Number of glaciers experiencing negative or positive SMB in Dhauliganga sub-basin based on location of snow line at the end of ablation season

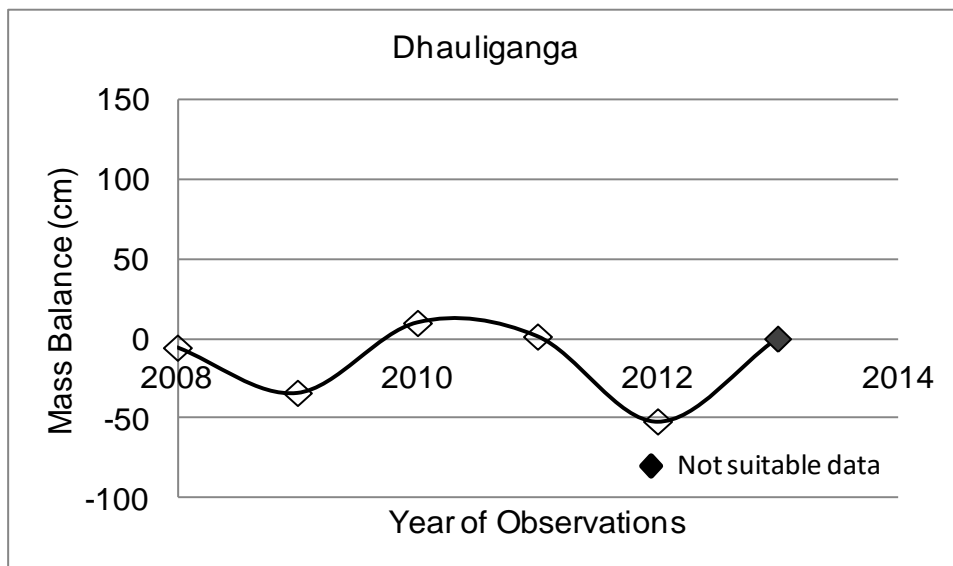


Figure 183: Mean Specific MB (in water equivalent or cm) for Dhauliganga sub-basin based on Snow line at the end of ablation season

All other sub-basins show mean specific mass balance positive during 2008-2013 (maximum +107.67 cm for Chandra sub-basin in the year 2011), however it varies and fluctuates during period of observation. In general, sub-basins of western Himalayan region show positive mass balance, whereas sub-basins of west-central Himalaya show negative mass balance.

The salient findings for glacier mass balance studied for 700 glaciers in 10 sub-basins for the year 2010 show that positive mass balance is indicated for 80% glaciers (Singh et al., 2013b). Specific mass balance for 43 glaciers of Warwan and 38 glaciers of Bhut sub-basins of Western Himalaya show negative mass balance for the year 2005 to 2007 and a loss of 4.3 and 0.83 km³ area of glaciated region respectively (Brahmbhatt et al., 2012b).

The purpose of monitoring snow line is to create a database of long term so that a pattern of snowline fluctuations could be understood. It is also desired that the database can be updated with a LISS III data and RISAT-1 SAR data for a better accuracy of snow line altitude. When this type of data is generated for entire Himalaya, it could give improved insight to draw conclusions on the nature of precipitation and melting across Himalayan region during ablation period. One of the limitations of this method is that it is based on the equation of 1992. If the size of the glaciers has reduced since then, the AAR of zero SMB might change. So there is a need to improve the relationship using more datasets for different climatic regions of Himalaya.

(b) Field based glacier mass balance studies for Machoi glacier, Drass sub-basin, Jammu & Kashmir

Machhoi glacier was selected as benchmark glacier in Drass sub-basin for detailed glacier mass balance studies. Machoi glacier is a transverse valley glacier situated 11 km east of Zoji La. The glacier basin is confined between the 34° 15'30" N to 34° 17' 40" N latitudes and 75° 31' to 75° 33' 30" E longitudes and is located in Drass Tehsil of Kargil District of Jammu and Kashmir State.

Systematic monitoring for mass balance of Machoi glacier was carried out during 2011-2012, 2012-2013 and 2013-2014. During this period the net annual accumulation and ablation measurement were carried out on the basis of winter and summer balance through pit study method (Figure 184). Snow densities were measured for estimating water equivalent mass.

Surface Ablation

The surface ablation measurement of Machoi glacier were carried out by monitoring 42 ablation stakes (graduated bamboo sticks with pointed metallic base) spread over glacier body from snout to 3650m to 4700m asl. The surface melting of the glacier result due to the high air temperature of summer season. Melt water plays an important role in lubricating the bed of the glacier. The surface ablation values of Machoi glacier

were measured during the month of August and September 2011 (1.53 cm/day); June, July, August and September, and October 2012 (1.71 cm/day), July, August, September and October 2013 (1.56 cm/day), July, August-September 2014 (1.43cm/day) field seasons by the stake measurements method. The surface ablation measurement of 38 stakes (graduated bamboo stick with pointed metallic base) of 3 meters length were fixed in the body of glacier with help of motor-operated drill spread over glacier body from snout (3652 m) to accumulation zone (4700m) at equal altitudinal interval of 100 meters, in three rows, one along the central part and two on the either sides (east and west) of the glacier. Hot water was poured around the stakes and snow and ice were packed around them so that they would freeze and remain in place during the field season of 2011 and 2012 (Figure 185).

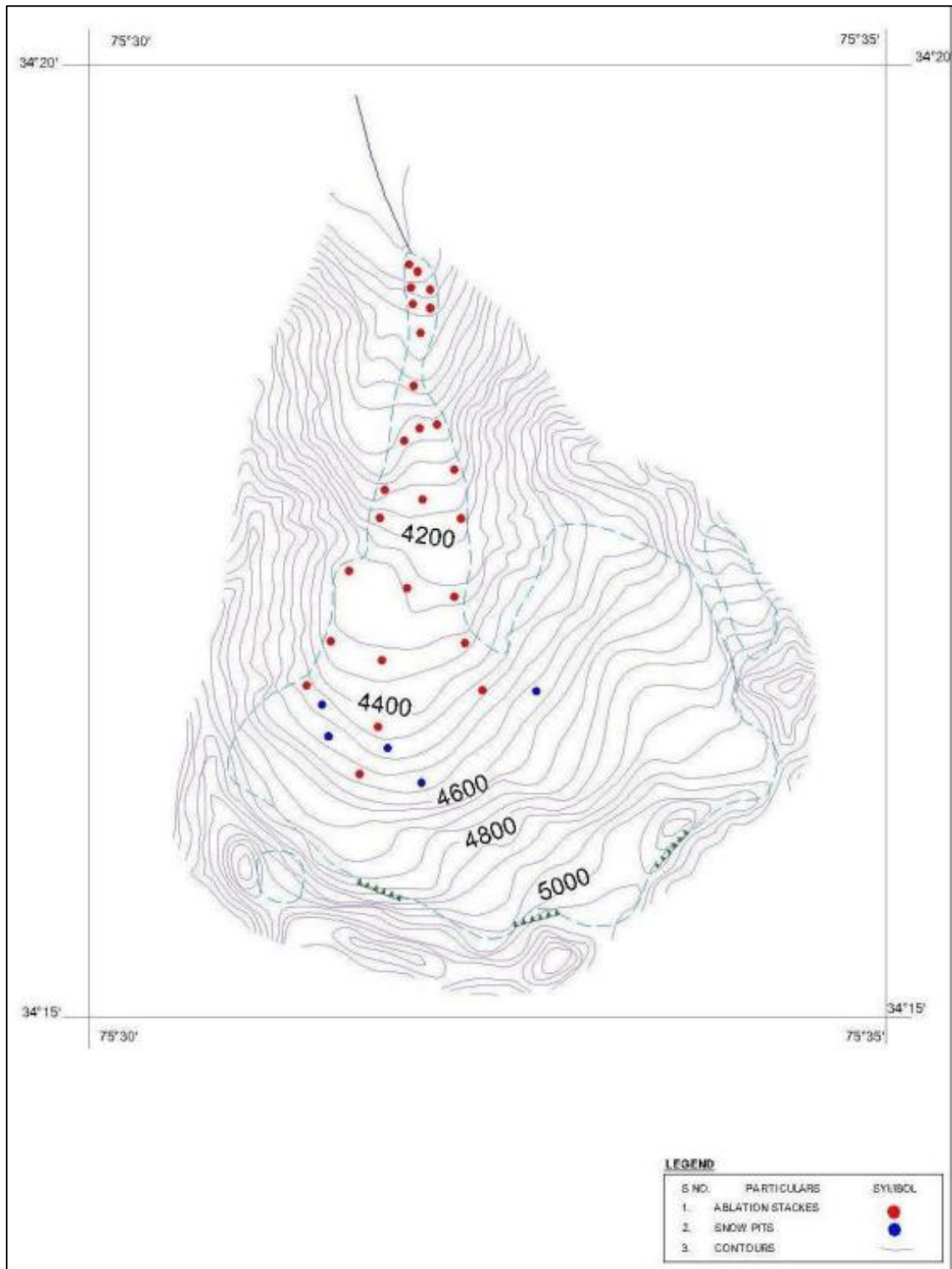


Figure 184: Location of ablation stakes and snow pits for estimating glacier mass balance of the Machoi glacier



Figure 185: Fixing of ablation stacks and measurements on Machoi glacier

Nearly 20 stakes were lost due to intense melting as well by high speed catabatic winds as observed in July 2013. Later 15 new mass balance stakes were installed deep up to 5 meters by newly acquired Heuck ice drill for the next year measurement. These stakes were planted in a linear form in ablation zone and as far as possible to the accumulation zone of the glacier. The stakes established for measuring the summer ablation were monitored in July, August, and, September months. The glacier melt during year 2012 was considerable as the stakes No. 23, 25 and 28 in altitude zone 4400m reported 2.22m of glacier ice loss in comparison 2013 and 2014.

The ablation data four years (2011, 2012, 2013, and 2014) show that average degree-day melting of three years is 1.54 cm/day during the peak melting season (July and August). The ablation rate varies, both way i.e. with respect to altitude and onset of summer. The gradual decrease in the melting of the glacier starts from the month of September (0.6 cm/day) till in October it reaches to zero. The degree-day melting of the Machoi glacier reaches maximum (1.24 to 5.1 cm/day) between the altitudes 4080 to 4480 meters asl during the summers of the years 2011 and 2012. Machoi glacier has a large ablation area lying between the snout and equilibrium line (3652-4620 meters). The ablation zone is sub-divided into lower zone with low melting (3652-3760), middle lower zone with moderate melting (3800-4080 meters), middle higher zone with high melting (4080-4400 meters) and upper zone with low melting (4400-4580 meters) according to their degree-day melting. The analysis of the ablation records of the glacier during the years 2011 to 2014 reveals that the melting of the glacier follows ablation pattern as per the altitude of the glacier. In the lower glacier zone the mean ablation measurements during the year 2011 is 1.5 cm/day with a standard deviation of 0.53; during 2012 (June, July, August, and September) it varies between 0.8 cm/day, 1.1 cm/day, 1.8 and 0.9 cm/day respectively with standard deviation. 0.95. In the year 2013 (June, July, August, and September), the mean melting range in lower glacier zone varies between 0.7 cm/day, 1.5 cm/day and 1.7 cm/day with standard deviation 0.78. In 2014 (July, August, September), it varies between 0.6 cm/day and 1.4 cm/day with standard deviation 0.56cm (Figure 186).

In the middle lower zone (3800 to 4080 m) the mean ablation measurements during the year 2011 is 1.9 cm/day with standard deviation of 0.35; during 2012 (June, July, August, September), it varies between 1.3 cm/day, 1.9 cm/day, 2.8/day and 2.1 cm/day with standard deviation. 0.79; during 2013 (July, August, September) it varies between 1.1 cm/day, 2.0 cm/day and 1.5 cm/day with standard deviation of 0.7. In the

Mean Monthly Ablations (cm/day)

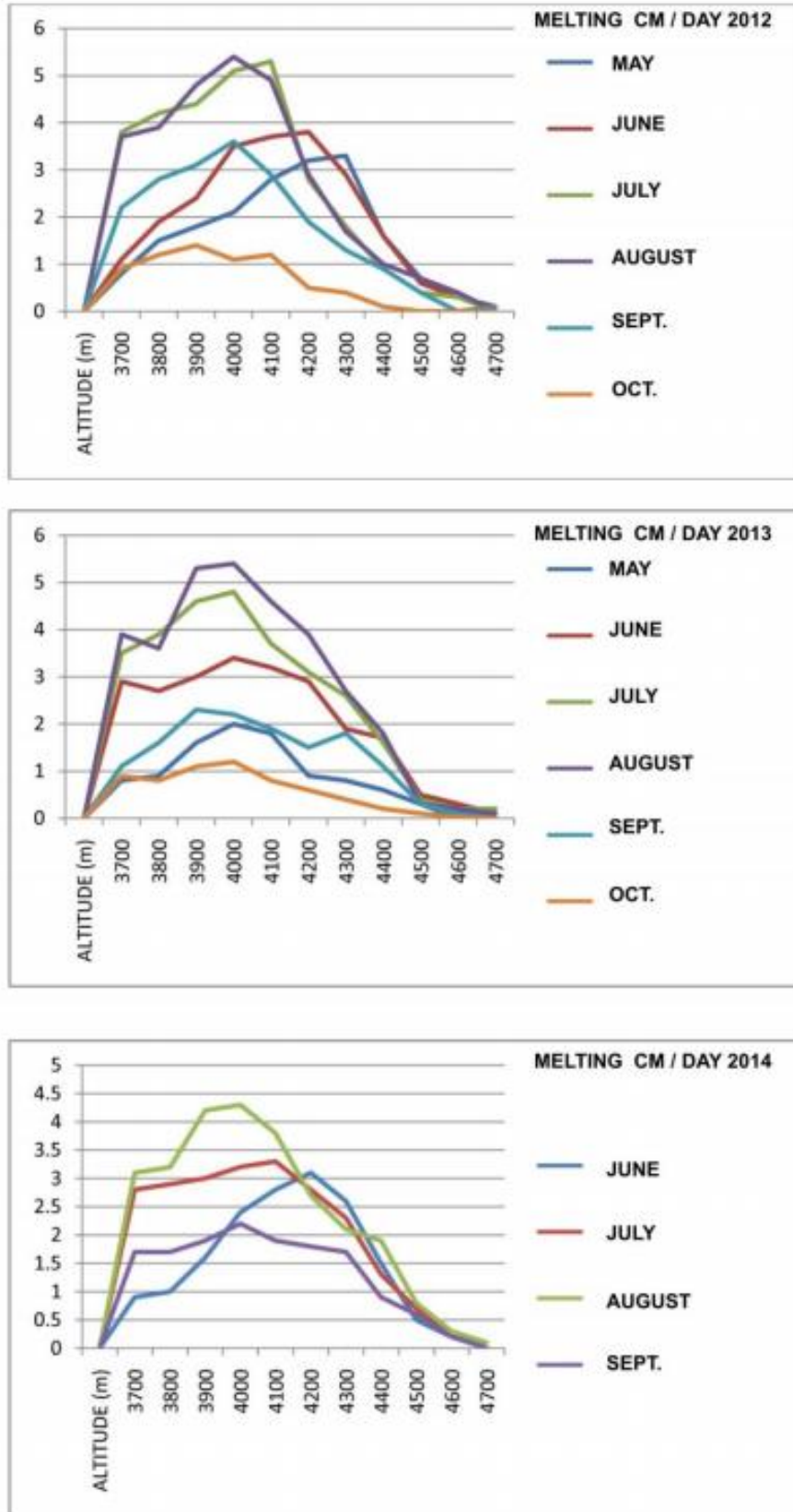


Figure 186: Mean monthly ablation pattern with respect to elevation changes of Machoi glacier during hydrological year 2011-2014

year 2014 (June, July, August, September), the mean melting range in middle zone ranges between 0.5cm/day to 1.8 cm/day with standard deviation of 0.49 (Figure 186).

In the middle upper zone (4080 to 4400 m) the mean ablation measurements during 2011 in August, September and October the melting rate varied 3.9cm/day, 2.8cm/day and 0.45cm/day respectively, In the year 2012 June, July, August, September, October the mean melting rate range between 2.7cm/day, 3.2cm/day, 3.8cm/day, 1.6cm/day and 0.46cm/day. During the year 2013 the melting rate varied between 1.8 cm/day, 2.9cm, 2.8cm/day, 1.9cm/day, and 0.34cm/day (Figure 186). In the year 2014 July, August, September the mean melting range varied 1.9cm/day, 2.9cm/day and 1.5cm/day respectively.

In the year 2011 July, August, September the mean melting in the upper zone ranges between 0.5 cm/day, 0.2 cm/day and 0.01 cm/day with a std.dev. of 0.36; during the 2012 June, July, August, September it varies between 0.5 cm/day and 0.01 cm/day with a std.dev. of 0.19 and during the year 2013 (July, August, September) it ranges between 0.3 cm/day, 0.4cm/day and 0.01 cm/day with a std.dev. 0.39. In the year 2014 June, July, August the mean melting rate ranged 0.2cm/day, 0.3cm/day, 0.01cm/day with a st.dev of 0.27.

The overall analysis reveals that the degree-day melting was higher in the middle lower zone as well middle upper zone (3880 to 4400 m) during the years 2011, and 2012 as compared to 2013 and 2014. This clearly reflects that years 2011, and 2012 has a warmer dry summer season as compared to the years 2013 and 2014, the cool and moist summer year being 2014 (Figure 186).

The melting of glacier in the lower zone is higher near front part of the snout area during the summer as it has a thin layer of debris on its body but along its margins (east and west) it has thick debris cover. The melting of glacier at its margins is very less due to which the height of the margins of the glacier and their extent is larger than the central part or clean part of the glacier. High rate of ablation in summer is due to high maximum temperature (17.23 °C). Further the high rate of melting is observed in the east part of the glacier as it has a very thin layer of dark colour debris (few centimeters) that absorbs and reflects more heat, and transfer heat to glacier body. The western part of the glacier is covered with somewhat thick debris, big boulders and angular rock fragments that prevent incoming of solar radiation from affecting the glacial surface and results in negligible melting. Further this side of glacier is confined in shadow zone hence the duration of incoming of the solar radiation is less as compared to the western and central part of the glacier. The presence of transverse as well as longitudinal crevasses in the snout further adds to variable rate of melting along the margin in comparison to the central part that leads to a tongue like outline of the snout. The variable rate of melting at different altitude levels of the glacier during the period 2011-2014 show that melting rate of glacier is comparatively maximum at <4080m asl to 4400m asl and minimum in the vicinity of equilibrium line (4509m asl

to 4540m asl) and nearly zero at equilibrium line altitude (4509masl, 4520m asl and 4540 masl) as seen in Figure 186. Mean monthly Maximum temperature and mean monthly ablation of Machoi glacier from 2011-2014 are summarized in Table 74.

Table 74: Mean monthly Maximum temperature and mean monthly ablation of Machoi glacier from 2011-2014

Month	2011		2012		2013		2014	
	Max. temp	Melting	Max.tem	Melting	Max.tem	Melting	Max.tem	Melting
	°C	cm/day	°C	cm/day	°C	cm/day	°C	cm/day
June			12.1	1.8	9.2	1.1	8.8	0.9
July			15.7	2.1	13.5	1.8	11.7	1.6
August	18.4	1.7	18.6	2.8	16.4	2	14.9	1.9
September	14.2	1.1	15.3	1.3	11.8	1	11.3	1.4

Accumulation Patterns

Snow accumulation responds to precipitation and temperature variation and forms an interesting climate index. These parameters integrate to influence during the entire late summer to spring period-September to July. Machoi glacier is cold glacier, where accumulation occurs both during winter as well in summer too in higher parts (4400m asl), and ablation during summer (June to September). While bulk of accumulation indeed occurs in winter which extends to June/July, often concentrated in short heavy snow fall events associated with western disturbances. Apart from its positive contribution to mass balance, the summer snow fall increases albedo. The effect of summer accumulation is especially remarkable around equilibrium line as low temperature reduces the melting rate appreciably and further helps to insulate snow and ice near equilibrium line and shifts it tens of meters. Change in timing of snow fall and periods of accumulation season from year to year in Machoi glacier has affected the position of equilibrium line. The annual measurement of net accumulation of snow is carried out at the end of each ablation season (September) of residual snow accumulated by opening pits in the vicinity of equilibrium line (4500m to 4600m). This altitudinal zone acts as transition between accumulation and ablation zone (Figure 187).

The thickness of winter snow pack was conducted during June 2012 on the accumulation stakes established at different elevations of the glacier and snow pack density was carried in snow pit. Snow pack density ranged from 0.39gm/cc to 0.49gm/cc and the specific winter mass balance of the glacier in 2012 is estimated to be 412mm w.e.v. The results closely corroborated with net accumulation snow carried out in September of residual snow. The residual snow measurements were carried during the field trips from 2011 to 2014 and it ranged between 1.5 to 2.5 meters. The average snow density in the

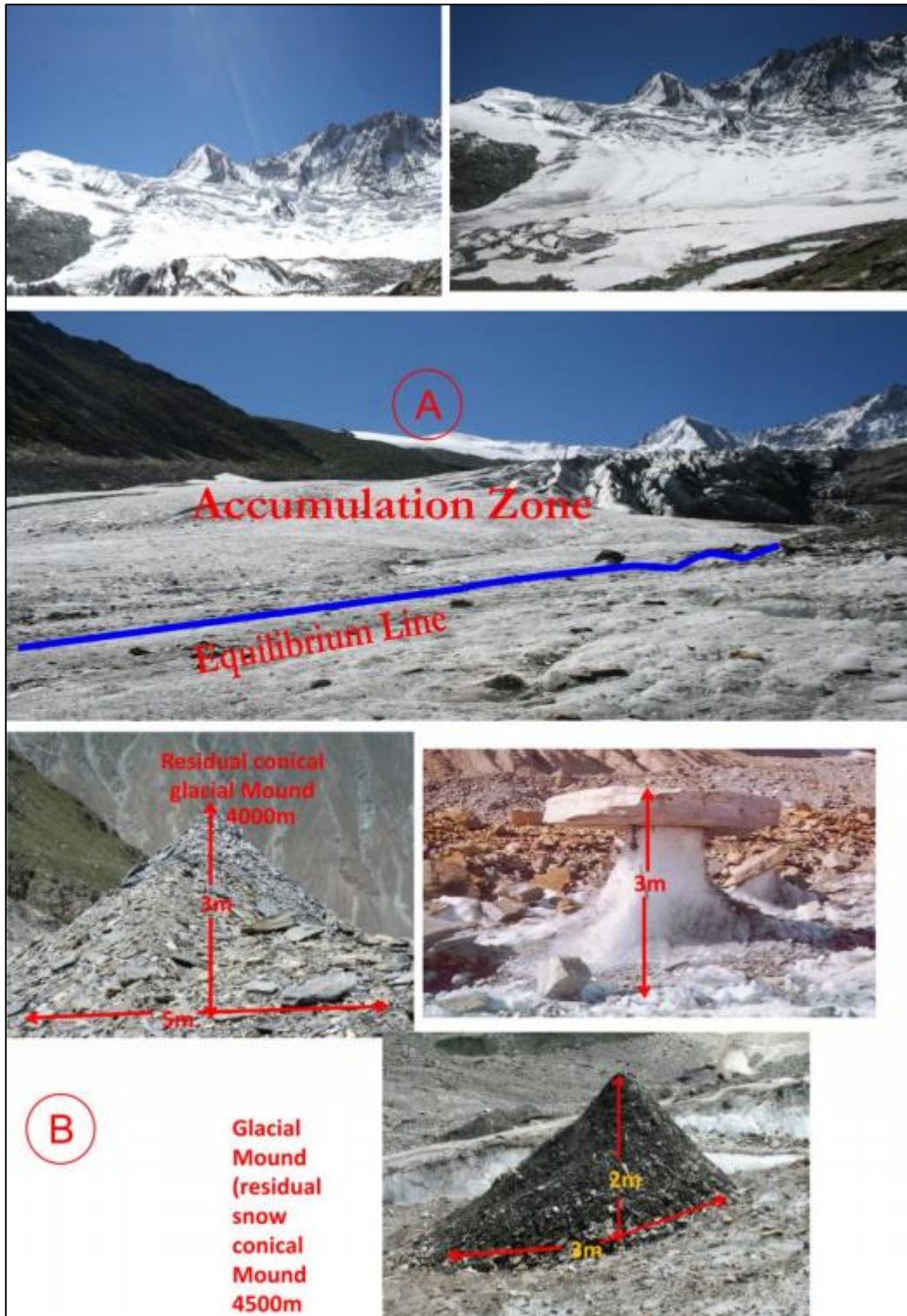


Figure 187: Accumulation zone of the Machoi glacier and associated field features

accumulation zone was 0.49 gm^3 in late summers. The accumulation zone encompasses nearly 65% of the total area out of which two altitudinal zones ranging between 4500 to 4800 meters, and 4800 to 5000 meters amounted for nearly 79% of the net accumulated area of the glacier. These accumulation zones are mainly cirque floors separated by stairs that encompasses near the 74% of the accumulation area.

The snow pits dug at different altitudinal levels between 4500m and 4700m in accumulation zone at the end of each melting season, September (2011-2012, 2012-2013, 2013-2014), displays somewhat little variations with maximum extent of accumulated residual snow (2.2m and 2m) during 2011-2012 and 2012-2013 and least (2 m-1.9m) during 2013-2014. These variations in snowfall effect the position of the firn line (equilibrium line). In course of a single year, the firn line oscillates tens of meters around a definite mean position (Figure 187).

Accumulation Area Ratio (AAR)

The Accumulation Area Ratio (AAR) is a ratio between snow accumulated area of the glacier and total area of the glacier. It is useful parameter in determining the general mass balance of the glacier and in defining the equilibrium line. In Machoi glacier the AAR value ranges between 0.65 and 0.615. It is highest (0.65) during the year 2013-2014, and shows descending trend from 2012-2013 to 2011-2012 (0.637, 0.615) respectively (Figure 188). The marginal increasing trends in AAR values indicate the increase of accumulation area and decrease of ablation area. This is supported by successive positive mass balance during 2011-2014. The analysis also suggests that AAR value is directly proportional to ELA. The ELA (Line of residual snow, separating accumulation zone from ablation zone) is observed to have descended from its position at 4540m asl during 2011-2012 to 4520m asl in 2012-2013 and to 4509m during 2013-2014 (Figure 188). During the balance years of 2011-2012, 2012-2013, and 2013-2014 the glacier had a positive net balance ($+0.9603 \times 10^6 \text{ m}^3$, $+0.7196 \times 10^6 \text{ m}^3$, and $+1.002 \times 10^6 \text{ m}^3$) (Figure 189). The marginal variation in net mass balance is attributed to low summer temperature leading low glacier melt.

Net Mass Balance

The estimates of net balance apparently reflect the trend of fluctuation in surface melting of ice in water equivalent. Machoi glacier being a cold dry type has a lesser ablation rate than those of accumulation rates. The glacier has net positive balance of $+0.960392 \times 10^6 \text{ m}^3$ in the year 2011-2012, $+0.719603 \times 10^6 \text{ m}^3$ in the year 2012-2013 and $+1.002060 \times 10^6 \text{ m}^3$ in the year 2013-2014 (Table 75). The increase in net positive balance during the year 2013-2014 than year 2012-2013, is due to cool and moist summer. In comparison, during 2011 -2012 the accumulation as well ablation is more (Table 75 and Figure 190). There is consistency in low temperature from June to September leading to less summer melting than the earlier reporting years.

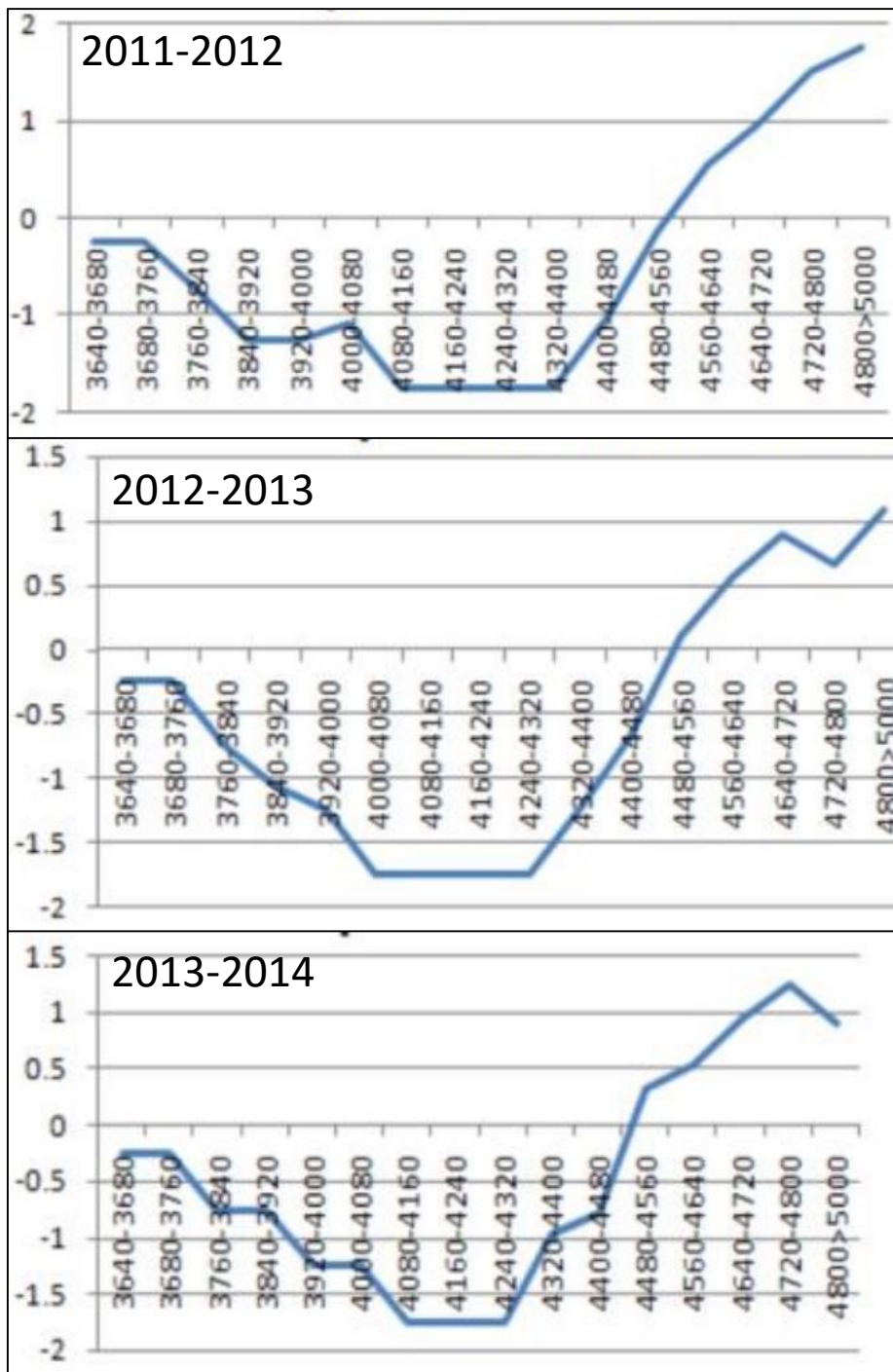


Figure 188: Specific Mass Balance of Machoi glacier during 2011-2014

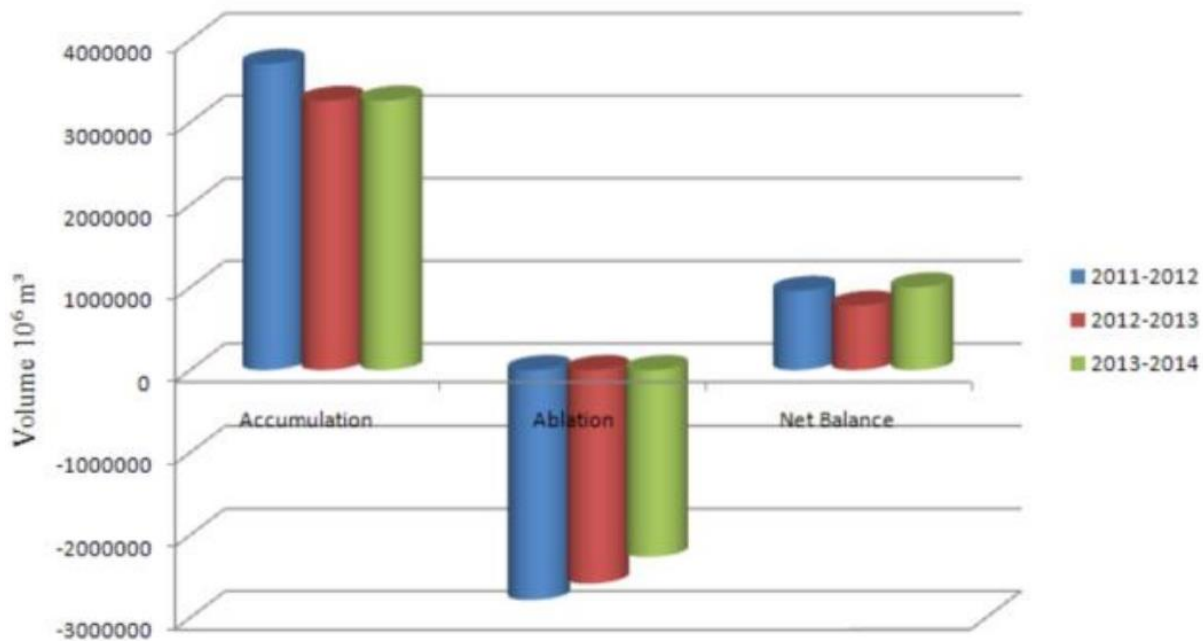


Figure 189: Specific Mass Balance of Machoi glacier during 2011-2014

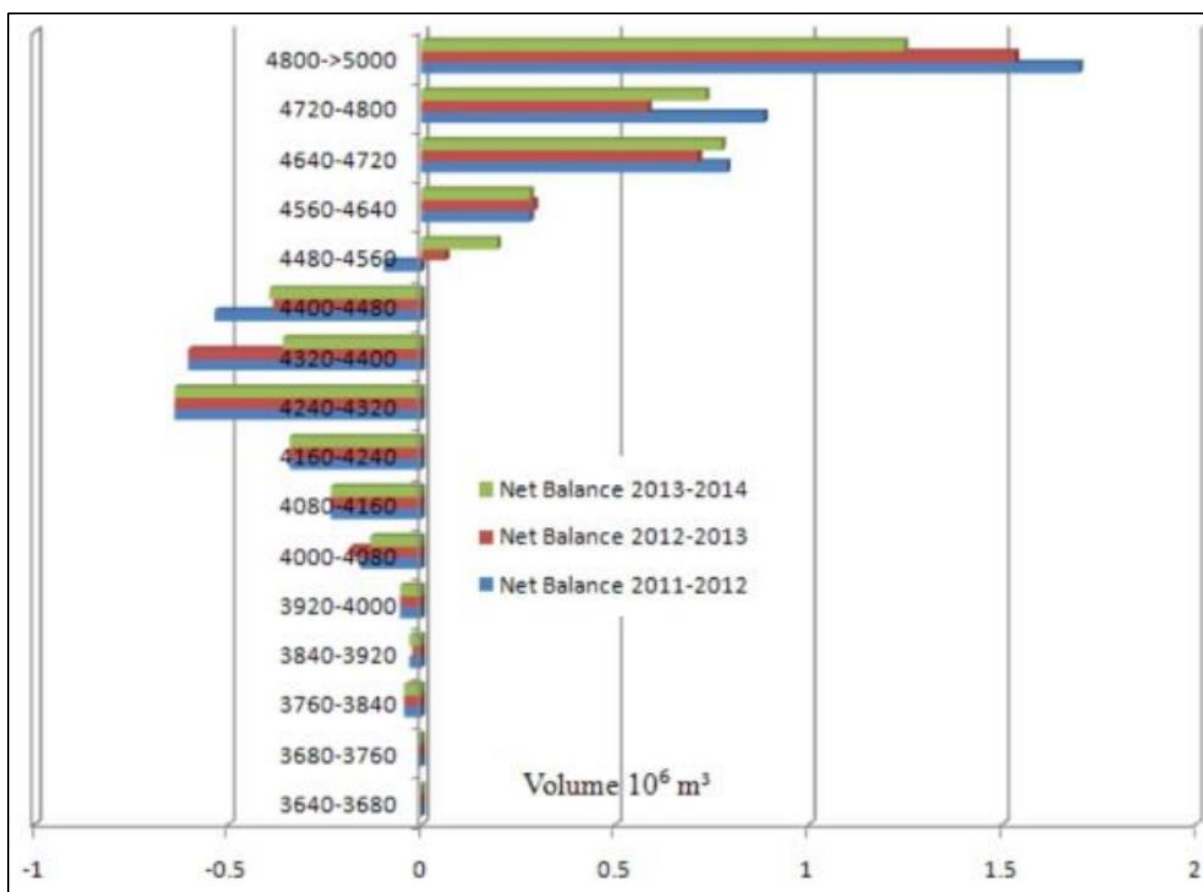


Figure 190: Net Mass Balance of Machoi glacier during 2011-2014

The fluctuation in net balance values is also attributed to variability in meteorological parameters particularly with respect to pattern of snowfall, amount of solar radiation and duration of sunshine hours during summer.

Table 75: Summary of Net Mass Balance estimates of Machoi glacier (2011-2014)
(Source: modified after Koul et al., 2016)

Year	Abl. area	Accu. Area	Net Abl.	Net Accu.	Net Bal.	AAR	ELA
	(Km ²)	(Km ²)	(Km ³)	(Km ³)	(Km ³)		(m)
2011-2012	2.219	3.54	-2.748	3.709	0.960	0.615	4540
2012-2013	2.100	3.62	-2.585	3.261	0.675	0.636	4520
2013-2014	1.933	3.83	-2.263	3.265	1.002	0.65	4509

The study shows positive net mass balance with cumulative specific balance of 0.16 m w.e./km/yr, resulting into shifting of Equilibrium Line Altitude (ELA) from 4540 m asl in the year 2011-2012 to 4509 m asl in 2013-14 for the Machoi glacier (Koul et al., 2016). The positive balance mass indicates about the stability phase of the glaciers.

(c) Field based glacier mass balance studies for Patsio glacier, Bhaga sub-basin, Himachal Pradesh

Patsio glacier is a valley type glacier, in the Bhaga river basin (Chandra-Bhaga River), located in the Lahaul valley, ~60 km from Keylong, headquarter of Lahaul & Spiti district, Himachal Pradesh (Figure 191). This glacier falls in the Great Himalayan range (western Himalaya). Patsio glacier is a compound glacier fed by two tributaries in the upper zone. Total area of the glacier is 2.25 km², with catchment area 7.82 km², mean orientation North-east, length approximately 2.7 km, maximum elevation 5741 m amsl, mean elevation 5298 m amsl and snout position at 4886 m amsl.

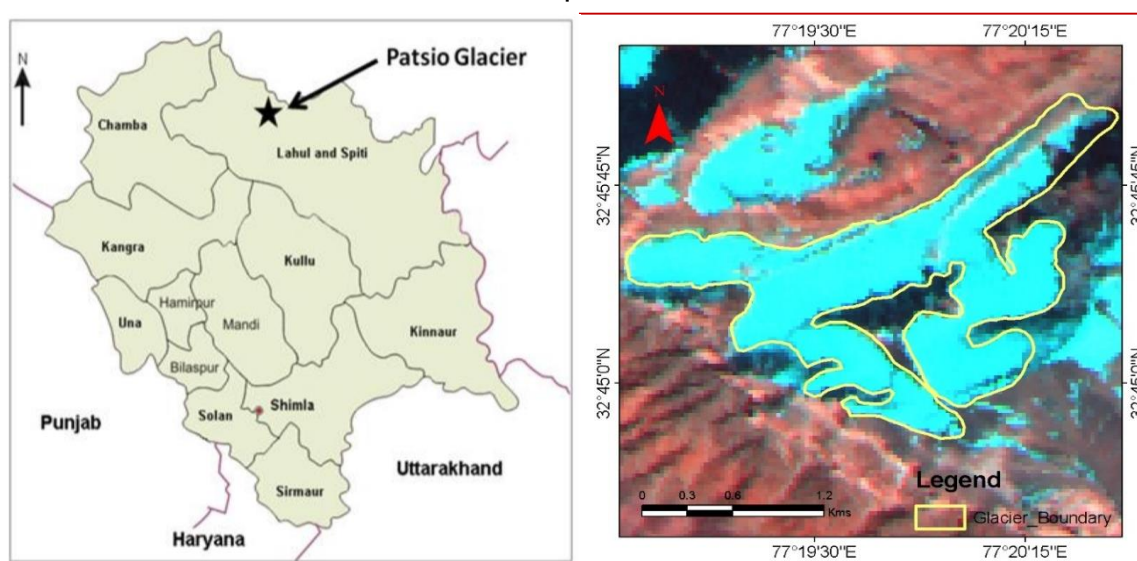


Figure 191: Glacier boundary of the Patsio glacier, H.P.

Glaciological observations and measurements were taken during various glacier expeditions organised during 2010-11, 2011-12, 2012-13 and 2013-14. Specific net mass (annual/summer and winter) balance of Patsio glacier was estimated. Winter mass balance has been calculated based on in-stu measured data on snow depth, snow core and snow pits. Summer ablation has been calculated based on ablation stakes, while accumulation was calculated by subtracting winter accumulation from annual accumulation. Twenty stakes have been put at various locations on the Patsio glacier. Location of various field measurement sites on Patsio glacier, H.P. are shown in Figure 192. Some of the field photographs during expeditions are shown in Figure 193. Specific net mass balance of Patsio glacier for 2011/12 and 2012/13 are presented in Figure 194. Maximum ablation was found in the lowermost part of the ablation zone in 2011/12 but in 2012/13 ablations were quite similar below the ELA at various altitudes. Annual mass balance Measurements were taken at end of the ablation season e.g. end of September. Specific net mass (annual/summer and winter) balance of Patsio glacier for 2012/13 is presented in Figure 195.

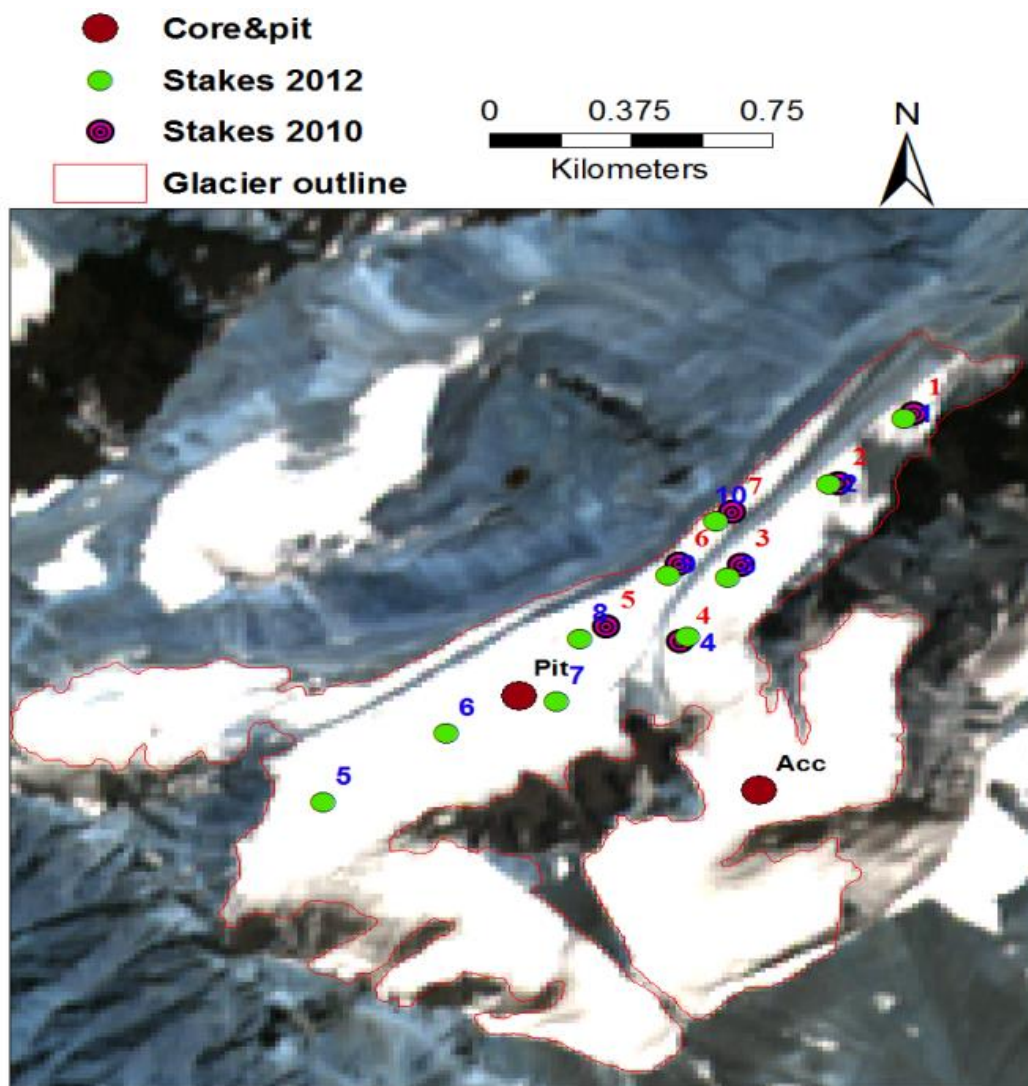


Figure 192: Locations of various field measurement sites on Patsio glacier, H.P.



Figure 193: Field photographs of Patsio glacier, H.P. during 2012-2013

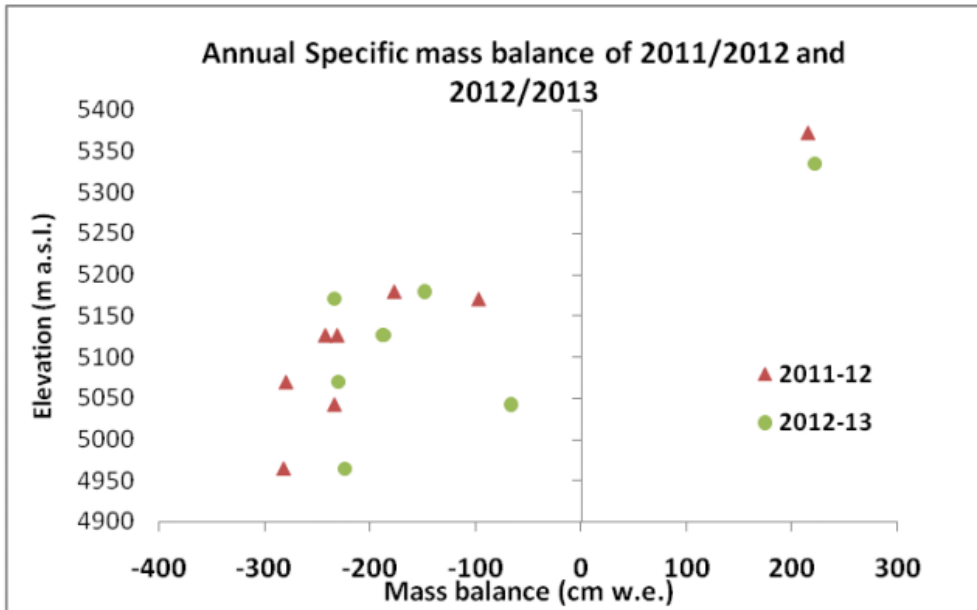


Figure 194: Annual Specific mass balance of the Patsio glacier during 2011-12 and 2012-13

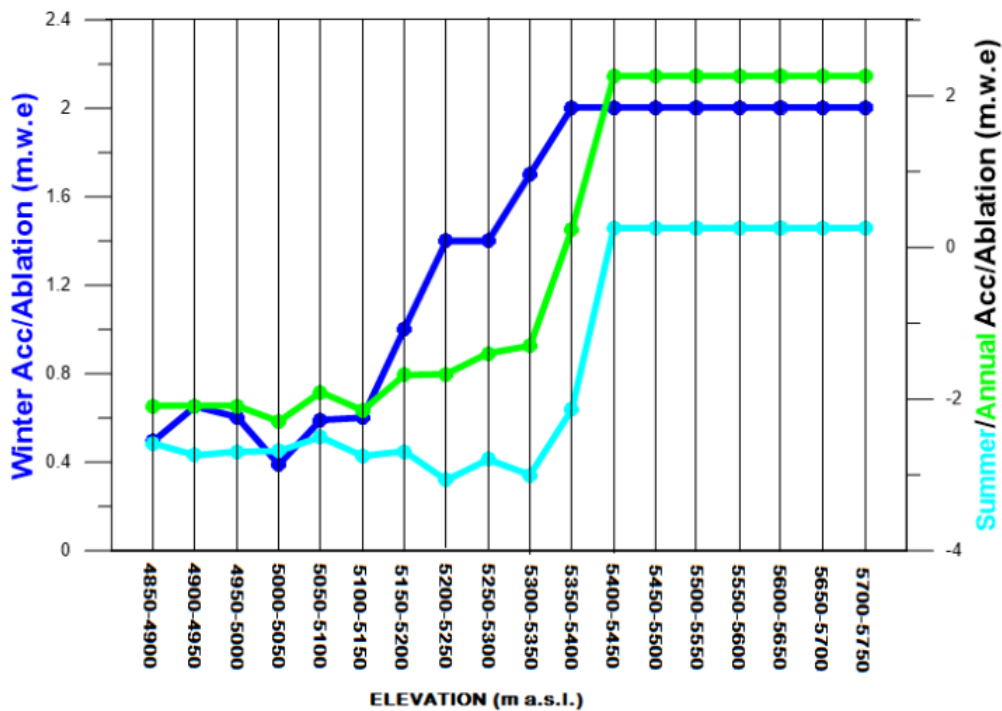


Figure 195: Specific net mass (annual/summer and winter) balance of Patsio glacier for 2012/13. Dark blue line represents the winter mass balance, calculated based on snow depth, snow core and pit. Light blue line represents the summer mass balance. Summer ablation was calculated based on ablation stakes, while accumulation was calculated by subtracting winter accumulation from annual accumulation. Green colour represents the annual mass balance measured from stakes and snow core

During the period 2012- 2013 the glacier wide annual mass balance of Patsio glacier was slightly negative at -0.04 ± 0.40 m w.e. The Equilibrium Line Altitude (ELA) was around 5350 m a.s.l. (based interpolation between ablation stake and the snow core measurement on the eastern flank) the Accumulation Area Ratio was found to be 47%. Changes in annual Specific Mass Balance of Patsio glacier during 2010-2011, 2011-12, 2012-13 and ablation at different elevations are shown in Figure 196.

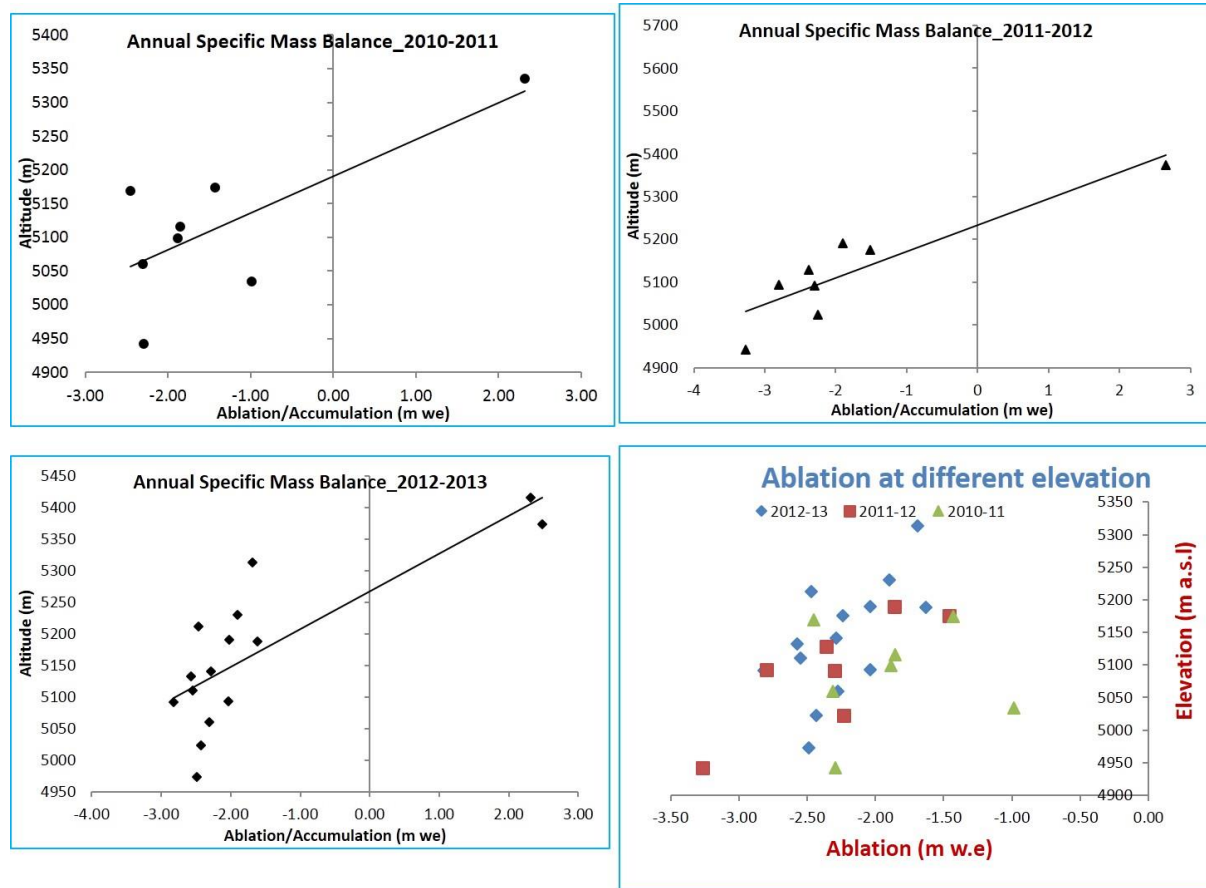


Figure 196: Changes in annual Specific Mass Balance of Patsio glacier during 2010-2011, 2011-12, 2012-13 and ablation at different elevations

In June 2014, a field expedition was carried out to monitor the winter mass balance of the Patsio glacier. Snow depths were measured at different elevations on the glacier, by using a snow probe between 4913 m and 5125 m a. s. l. (Figure 197). At higher elevations a snow pit and two snow cores were used to measure winter accumulation. One snow pit was made at 5158 m a. s. l., while two snow cores were extracted at 5235 m and 5375 m a. s. l. Table 76 is showing the detailed information of snow core take at 5375 m a.s.l. in 9th June 2014 for winter balance estimation. Salient results of the specific net ablation at various elevations of Patsio glacier for the balance year 2013-2014 (measured in end of September 2014) are shown in Figure 198.

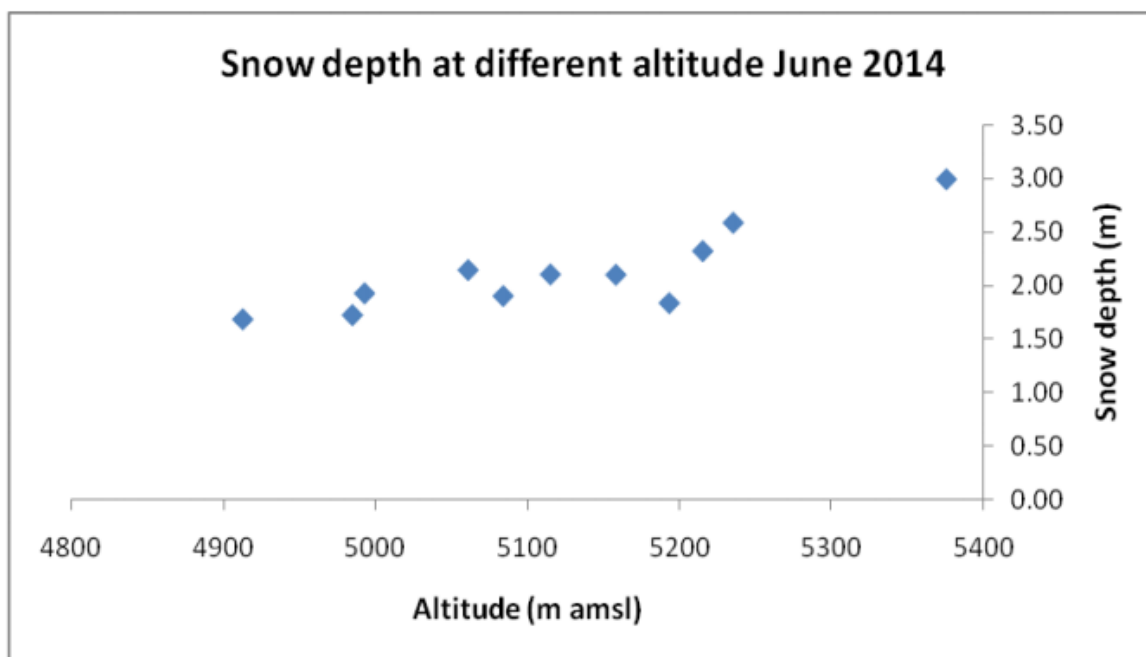


Figure 197: Snow depths at various elevations of Patsio glacier in June 2014

Table 76: Details of the core taken at 5375 amsl on 9th June 2014

Core Length (cm)	Mass (g)	Comments	Volume (cm ³)	Density (g/cm ³)
15-25	447	--	1004.8	0.444865
37-50	405	--	653.12	0.6201
60-78	364	--	904.32	0.402512
93-103	295	--	502.4	0.587182
130-150	602	Firn	1004.8	0.599124
170-180	330	Hard Firn	502.4	0.656847
188-210	306	Firn	602.88	0.507564
236-250	380	--	703.36	0.540264
263-270	257	~ 5 cm hard ice	351.68	0.730778
290-300	336	Dirt Layer	502.4	0.6687

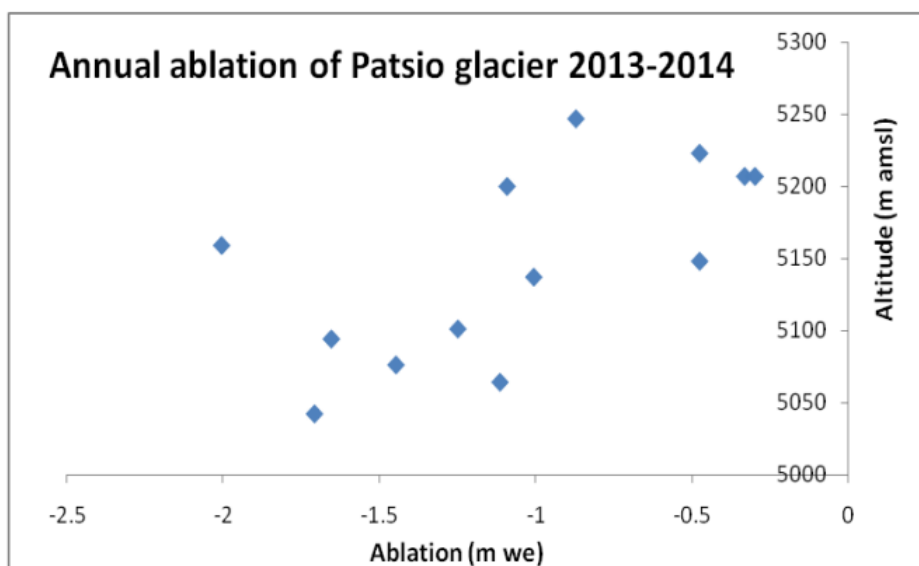


Figure 198: Specific net ablation at various elevations of Patsio glacier for the balance year 2013-2014 (measured in end of September 2014)

Overall mass balance for the study period was slight negative, which shows Patsio glacier is somewhat in equilibrium state.

5. Himalayan Glacier Information System

5.1. Objective

To develop a Web based Himalayan Glacier Information System (HGIS) using Open Source GIS tools.

5.2. Scientific Rationale

The web based information systems for snow and glaciers available in public domain (with certain restrictions) are from the World glacier inventory (WGI), the National Snow Data Centre, Global Land Ice Measurements from Space (GLIMS), and the International Centre for Integrated Mountain Development (*ICIMOD*). The GLIMS is used for glacier data preparation as per the GLIMS standards and imbibing into the GLIMS system.

A geospatial database has been created for the glacier inventory carried out in Phase-I (SAC, 2011a). The database contains inventory of all the glaciers in the Indus, Ganga and the Brahmaputra basins encompassing the Himalayas, Trans-Himalaya and Karakoram regions carried out on 1: 50,000 scale using Resourcesat-1 satellite data of 2004–2007 periods during Phase-I. The results show that there are 32, 392 glaciers covering 71,182 km² area in the Indus, Ganga and Brahmaputra basins draining into the Indian territory (Sharma et al., 2013). During Phase-II, the work was extended to map glaciers of West Indus basin which are draining into neighboring countries. Thus the total glacier inventory data for all the three Indus, Ganga and Brahmaputra basins show that there are 34919 glaciers covering 75, 779 sq. km area.

Such large repository of geospatial database of glacier inventory available at SAC has significant usage in Himalayan cryosphere studies and can be made available to researchers through a web-based geo-portal named as Himalayan Glacier Information System (HGIS). HGIS provides a platform for utilizing the glacier inventory data in various applications/studies related to climate change, water resource planning, hydropower site selection and assessment of glacial lake outburst flood (GLOF) hazards. A well designed, user friendly and robust Himalayan Glacier Information System (HGIS) would be helpful to researchers and encourage them to use the available information effectively.

5.3. Study area and Data Used

The study area (Figure 199) comprised of the glaciated parts of Indus, Ganga and Brahmaputra Basins over Himalayan, Trans Himalayan Karakoram region spread across India, Nepal, Bhutan, Tibet/China, Pakistan and Afghanistan.

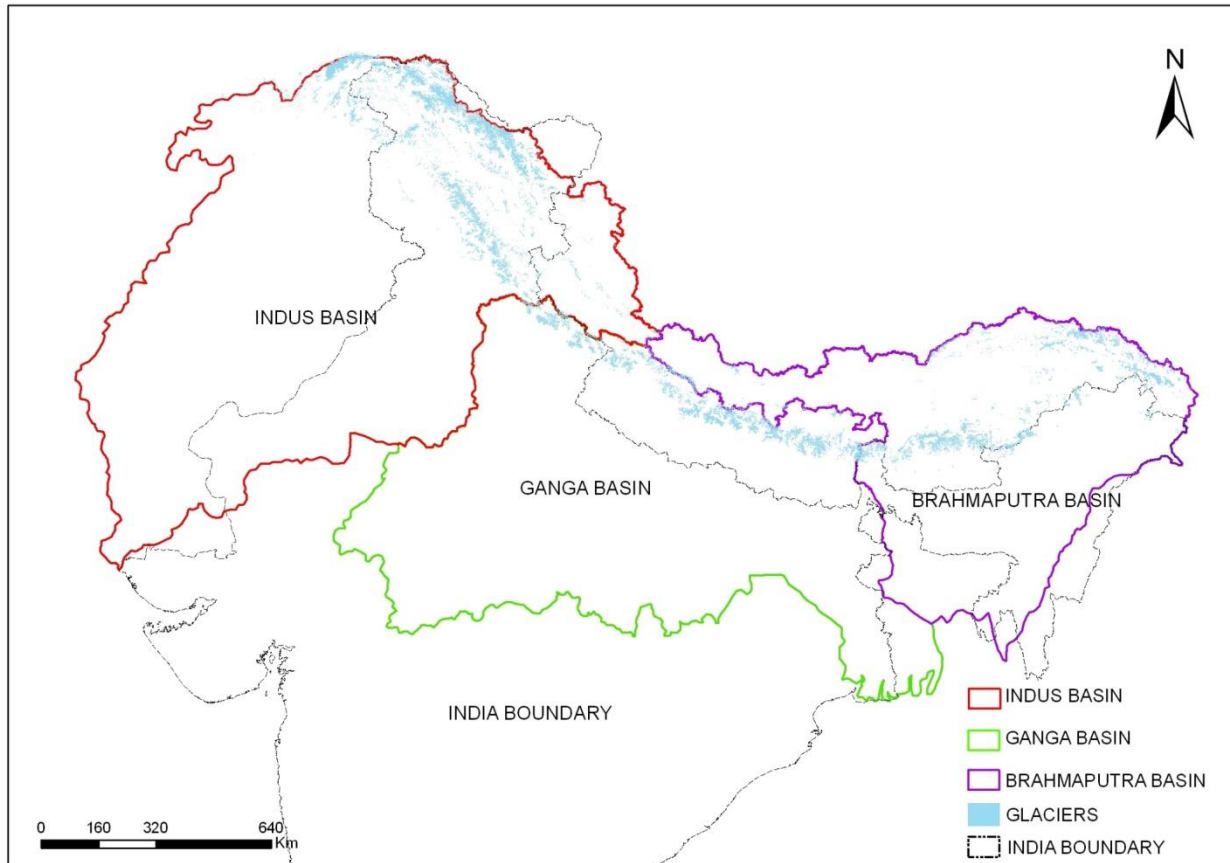


Figure 199: Study area – Indus, Ganga and Brahmaputra basins (Source: Sharma et al., 2013)

5.4. Methodology

Efforts were made to standardize and organize the available spatial and aspatial data in usable format in GIS. The HGIS information content comprises of 1) glacier inventory maps and 2) inventory data sheets. The map displays the glacier morphology features like accumulation zone and ablation (ice exposed and debris covered) zones, snout location, de-glaciated valleys, moraines and glacier lakes. The basin, sub-basin and administrative boundaries form the background. The inventory data sheet attributes for each glacier provides information on glacier Location, Identification, Dimension, Orientation, Elevation, Classification, etc.

The HGIS software design and development is carried out after making comprehensive review of existing information Systems / Decision Support System (DSS) like Glacier Land Ice Measurements from Space (GLIMS), International Centre for Integrated Mountain Development (ICIMOD) & Water Resources Information System (WRIS).

The spatial map and datasheet are linked by unique glacier identification number (glac_id) which is a key field present in all corresponding glacier related point, polygon

or line layers. All the glacier attribute is made amenable to query and analysis by users. The HGIS architecture is based on Open Geospatial Consortium (OGC) standards and utilizes OpenGeo Suite bundled software comprising of Postgresql (PostGIS), Geoserver, GeoWebCache and GeoExplorer each having a different function. The spatial and aspatial glacier data sets were stored in a pre-defined format and imbibed into spatially enabled database (PostGIS), having sophisticated functions for spatial data analysis and query.

HGIS development involved various components viz., i) Glacier Inventory, ii) HGIS software design and development, iii) Preparation of data for HGIS, base preparation and iv) Populating data in HGIS, installation and testing. The details are discussed below:

i) Glacier Inventory

Glacier inventory of the Himalayan region has been completed using IRS Satellite data on 1:50, 000 scale in Phase-I of the project (SAC, 2011a, Sharma et al., 2013). During the current project, all glaciers located in western parts of the Indus Basin (Pakistan-Afghanistan region) within the Kabul, Kunar, Swat and Indus sub-basins were mapped using Resourcesat-1&2 satellite data of 2007-2011 period following the methodology used in Phase-1 (SAC, 2011a, Sharma et al., 2013). Geocoded AWiFS data at the end of ablation season (July to September) were used to map the glaciological features using FCC with standard band combination 2 (0.52-0.59 μm), 3 (0.62-0.68 μm) and 4 (0.77-0.86 μm) and additional SWIR band 5 (1.55-1.70 μm). The SRTM DEM product, globally available at 90 m spatial resolution and vertical root mean square error of 16 m, has been used for generating the altitude information. The significant glaciological features extracted using satellite data comprised accumulation area, ablation area (both ice exposed and debris covered), glacieret & snow field, snout, ice divide, transient snow line, highest and lowest elevation points, deglaciated valley (DGV), glacial lakes, etc. Details required for generating the glacier data sheet such as glacier dimensions, orientations, elevation etc. were obtained and stored using GIS procedures. Inventory datasheets for all glaciers were prepared as per global standards. Thus the final glacier inventory data base for Indus, Ganga and Brahmaputra basins of the Himalayan-Karakoram region comprises of 34,919 glaciers covering 71,182 km² glaciated area.

ii) HGIS Software Design and Development

The HGIS software design and development comprised of review of existing information Systems / Decision Support System (DSS) like Glacier Land Ice Measurements from Space (GLIMS), International Centre for Integrated Mountain Development (ICIMOD) & Water Resources Information System (WRIS). The HGIS architecture was designed to use open source software and tools as broadly represented in Figure 200.

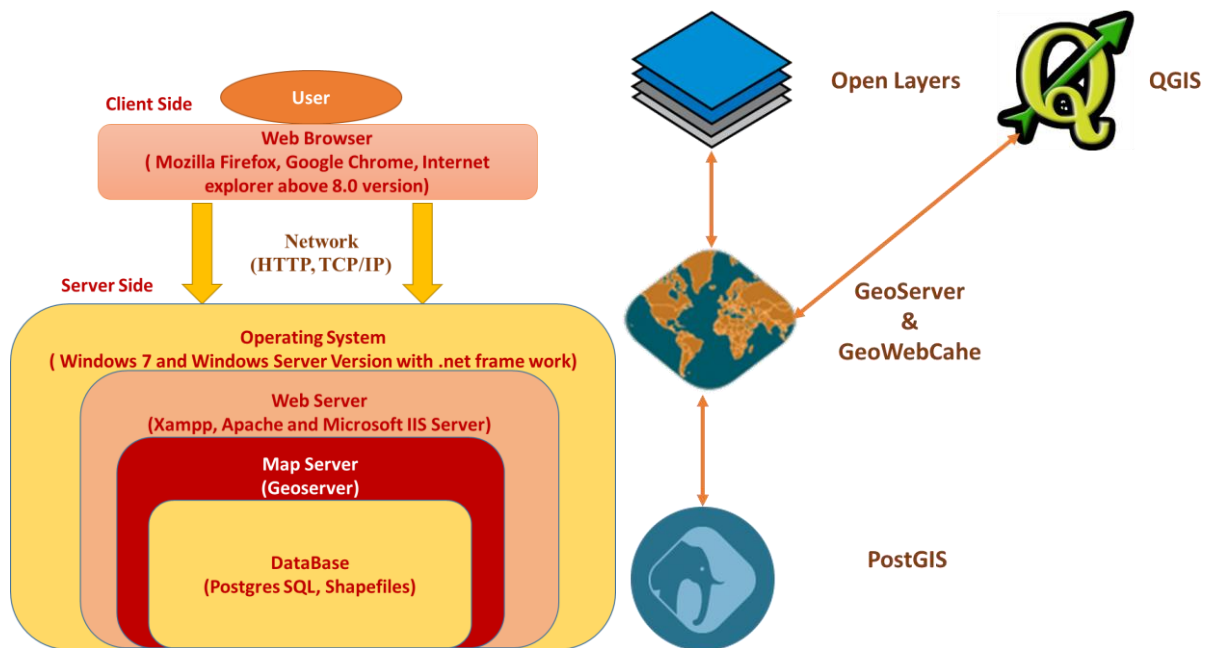


Figure 200: Basic HGIS Architecture

The HGIS Architecture comprises of OpenGeo Suite (Bundle) with PostgreSQL (PostGIS), Geoserver, Geocache and GeoExplorer.

- The Open-source software PostgreSQL is Database management system. The PostGIS extension enables PostgreSQL with Spatial capability
- The Geoserver is useful as web mapping server and enables user with functionalities like map sharing and web development.
- OpenLayers is a javascript library to enable web mapping support to the client over any modern browser.

Based on the above architecture and with a focus on available data sets and anticipated user requirements the HGIS was developed to meet the functional requirements a) Display and primary theme creation; b) multi-criteria based selective query and display through custom filters and c) Output generation (Outputs like map compositions, tables and graphs as per custom filters selection).

Elements for multi-parameter query are given in Table 77.

Table 77: Designed / Available HGIS elements for Filters/ Query

Sr. No.	Category	Sub-Category	Attribute
1	IDentification		GLAC_ID
			GLAC_NAME
			CONTINENT
			BASIN_CODE
2	Coordinates		LAT
			LON
3	Dimension	Area	TOTAL_AREA
			AREA_ACU
			AREA_EXP
			ARE_AB
			DGV_AREA
			LAKE_AREA
	Length	WID_ME_AB	
		LEN_ME_AB	
		LEN_MIN	
		LEN_MAX	
		MEAN_LEN	
		LEN_MAX_EX	
		LEN_MAX_AB	
DGV_LENT			
4	Elevation		MAX_ELEV
			MIN_ELEV
			MEAN_ELEV
			MIN_EL_AC
			MEAN_EL_AB
			LAKE_ELV
5	Orientation		ORIENT_AC
			ORIENT_AB
6	Classification		CLASS
			FORM

iii) Preparation of Data for HGIS

The information generated on glaciers in the form of spatial layers and aspatial tabular form were collected, prepared and compiled as input Glacier Datasets in GIS. This comprised editing for database, correction and standardization as per NRIS/NRDB Standards (Table 78). Further preparation of seamless mosaic and organizing data

sets at Sub-basin and Basin level in GIS was done. The database was made compatible for accessing through the Open Source Web Based HGIS software.

Table 78: Database Design Specifications (Based on NRIS/NRDB Standards)

Sr. No.	Element	Specification
A] Input Specifications		
1	Location reference	Latitude-longitude
2	Scale	1:50,000
3	Projection/Map standard	WGS84
4	Thematic Accuracy	
	Minimum Survey Unit	0.02 sq. km. or 2.0 ha
	Mapping Accuracy	90/90 (unverified)
B] Database Specifications		
1 Spatial framework		
	Registration scheme	Lat.-Long. Graticule 15' x 15'
	Projection / Coordinate system	WGS84 / UTM
	Coordinate units	Meters
2 Accuracy/Error limits		
	Registration accuracy (rms)	6.25 m
	Area	0.3%
	Weed tolerance	6.25

iv) Populating data in HGIS, installation and testing

The standardized spatial and aspatial data sets are populated into the HGIS. The HGIS is installed onto a server and tested and evaluated for its various designed functions. In case, there were errors in operating the HGIS, these were rectified. The HGIS is then demonstrated to users for its operational usage. The specifications for system requirements at server end (and client end) are given in Table 79.

Table 79: System Requirement (Server end)

Sr no	Item	Requirement/specification
1	Operating System	Vista, 7, 8, Server 2003 or newer, XP (client and dev tools only)
2	Memory	1GB minimum (2GB recommended)
3	Disk space	600MB minimum (plus extra space for data)
4	Browser (client end)	Any modern web browser is supported
5	Permissions	Administrative rights
6	Software	.NET Framework 4 (for windows, free downloadable)

5.5. Results and Discussion

Figure 201 shows the view of HGIS home page. The various installed capabilities of HGIS are discussed below:

- The HGIS displays the major Indus, Ganga and Brahmaputra Basin boundaries with international boundaries in the back ground (international boundaries are not authenticated) and allows one to choose any one major basin for display, query, graph generation (Figure 202).

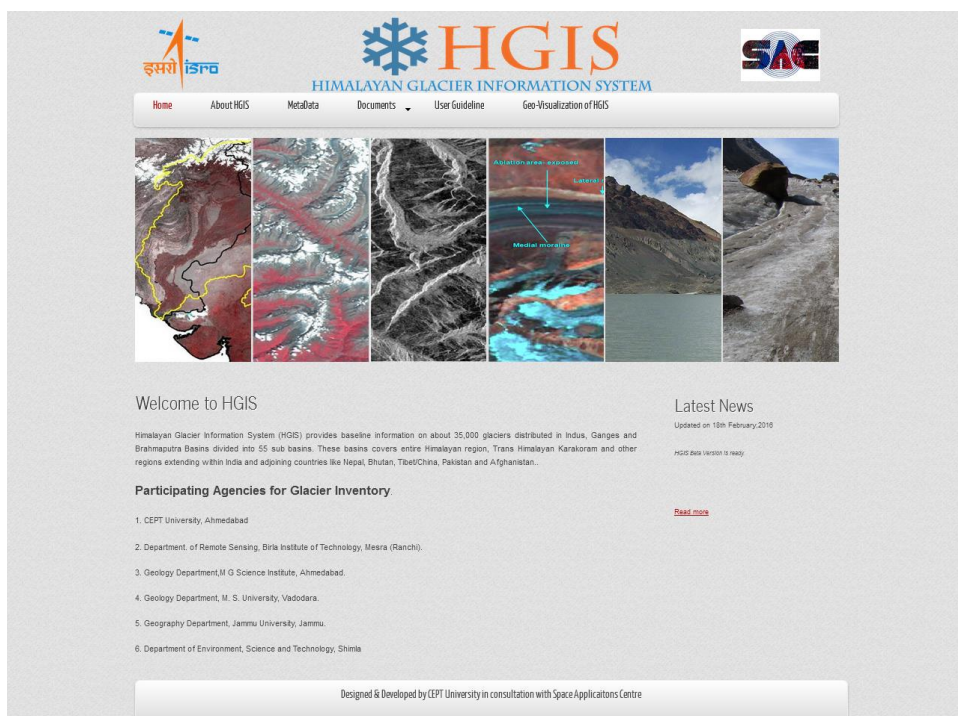


Figure 201: View of HGIS Home Page

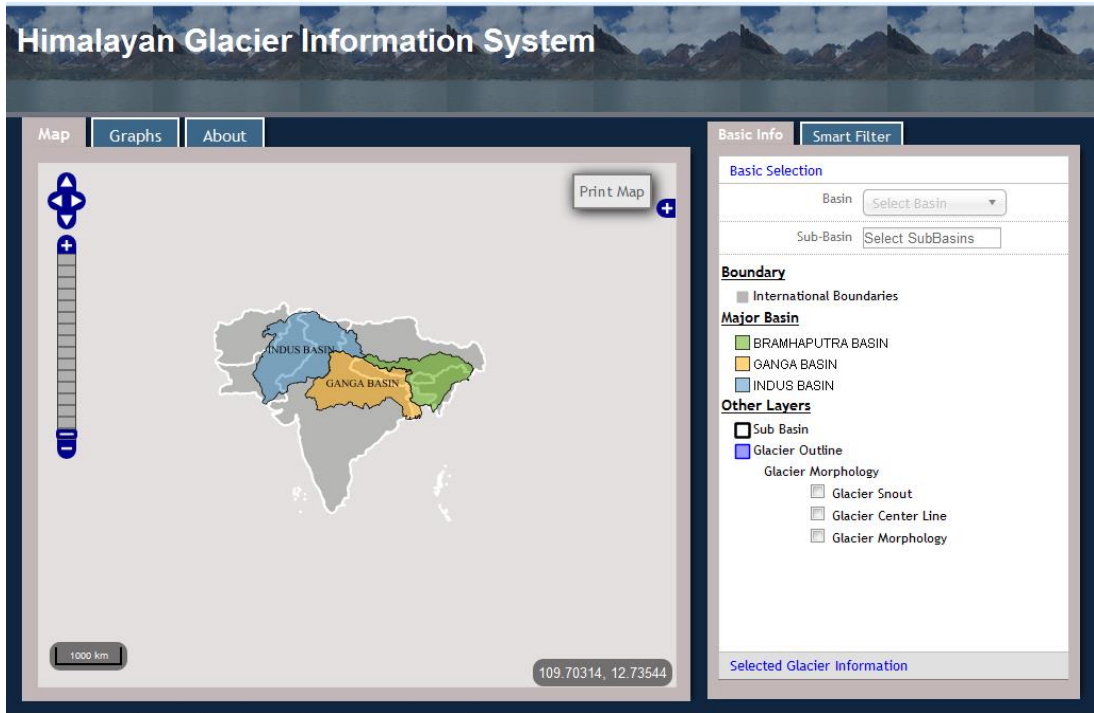


Figure 202: Display of three major basins of Himalayan Region (Indus, Ganga and Brahmaputra basins)

- For any one selected basin (say Ganga Basin) HGIS can display sub-basins with glaciers as a) glacier outlines b) glacier morphology with legend. (Figure 203, Figure 204 and Figure 205).

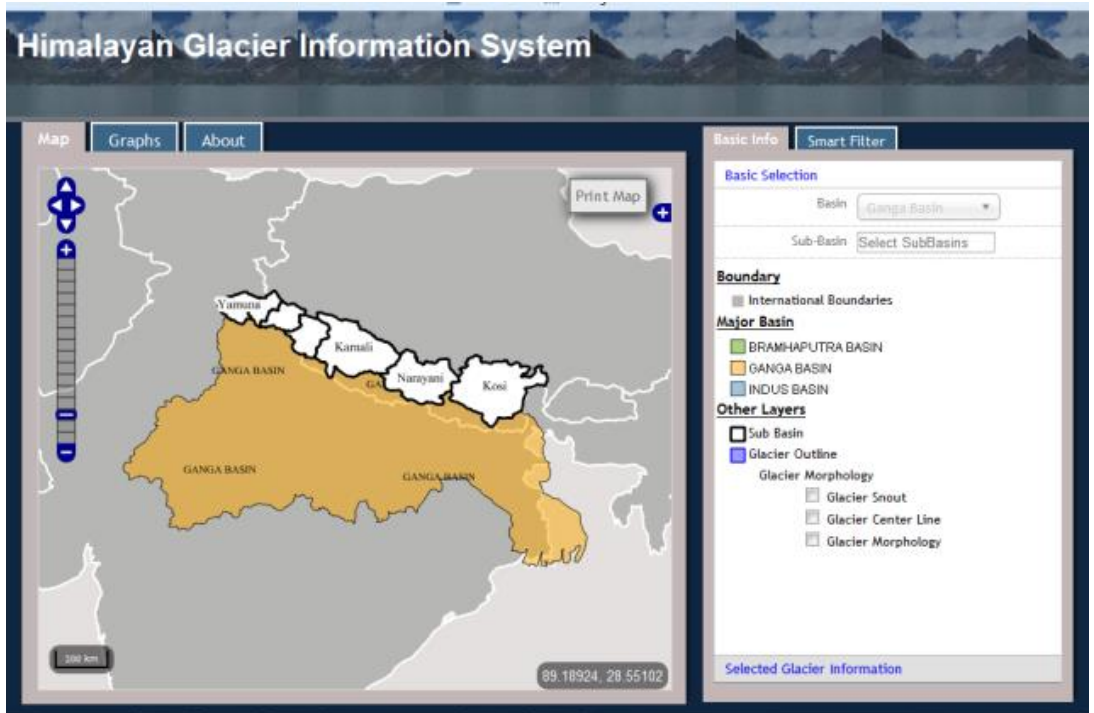


Figure 203: Display of the Ganga basin and its sub-basins

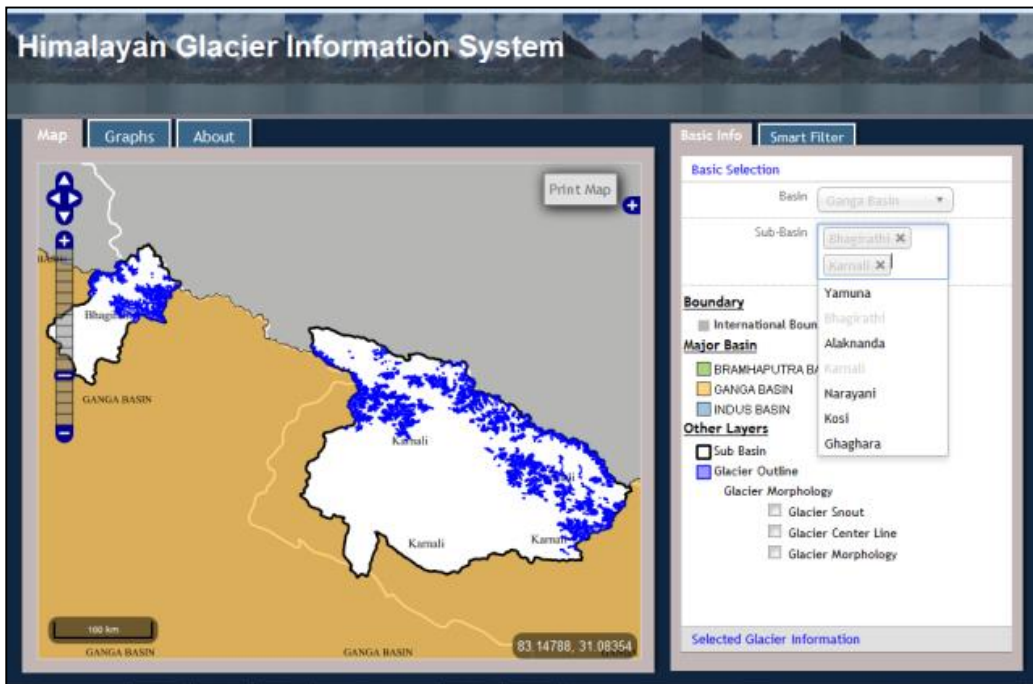


Figure 204: Display of glacier outlines in selected sub-basins

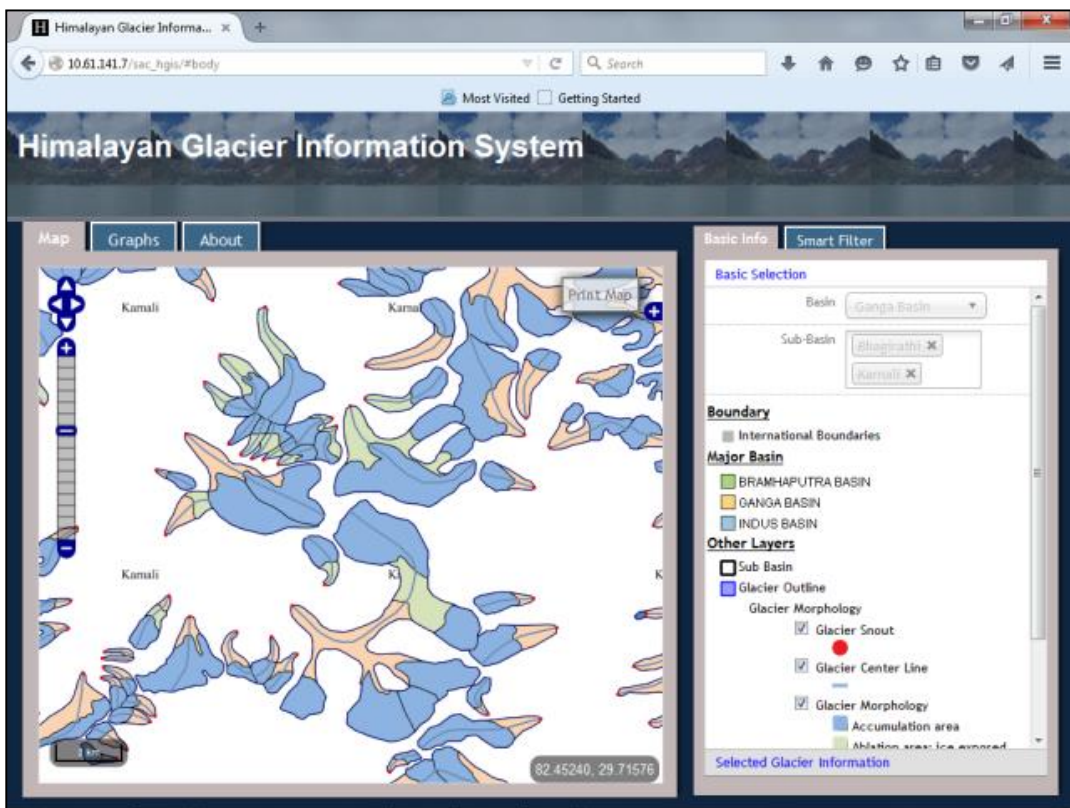


Figure 205: Glacier morphology within a sub-basin with Legend (Zoom view)

- The glacier morphology features like accumulation area, ablation area-ice exposed, ablation area debris covered, de-glaciated valley, supra glacier lakes and moraine dam / periglacial lakes can be displayed. An option for display glacier snout as point location and Centre line of glacier is also provided.
- On selecting any individual glacier by using the onscreen cursor, the five characteristic information about that specific glacier viz., glacier identification number, glacier total area, minimum elevation, maximum elevation and mean elevation are displayed on left display panel along the side of that glacier (Figure 205).
- The left panel also has a Layer display menu (ink blue, Figure 205)) which aids in switching on and off selective layers such as major basins with sub-basin boundary, glaciers outlines displayed in single colour, glacier morphology displayed in multi-colour colour as per legend.
- The detailed inventory information table for any one specific glacier can be assessed by selecting that glacier (Figure 206 and Figure 207).

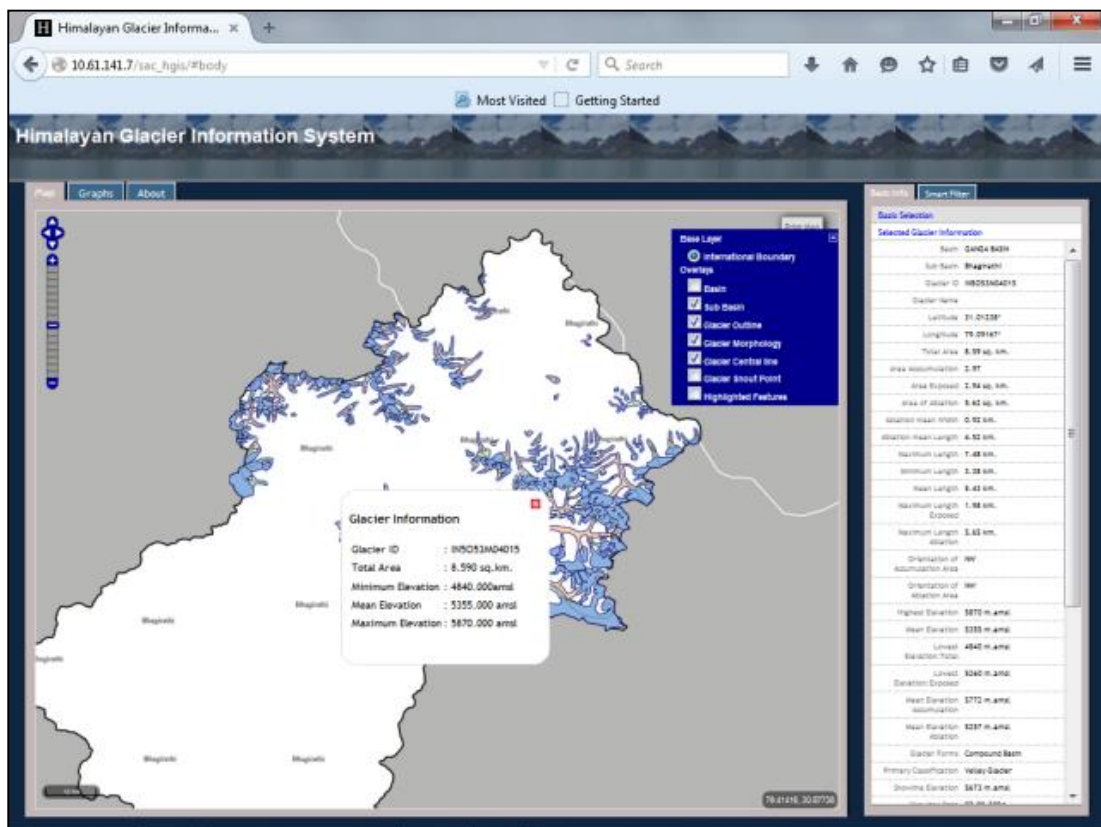


Figure 206: Glacier characteristics are displayed (Five major characteristics within the display screen in left) and detailed forty characteristics (Right scrollable panel)

Filter

Glacier ID	: IN5O62P11001	⊗
Total Area (sq km)	: Minimum <input type="text" value="0.02"/> - Maximum <input type="text" value="242.59"/> Minimum > 0.02 - Maximum < 242.59	
Accumulation Area (sq km)	: Minimum <input type="text" value="0.09"/> - Maximum <input type="text" value="168.91"/> Minimum > 0.09 - Maximum < 168.91	⊗
Ablation Area (sq km)	: Minimum <input type="text" value="0"/> - Maximum <input type="text" value="73.69"/> Minimum > 0 - Maximum < 73.69	⊗
Glacier Length (km)	: Minimum <input type="text" value="0.22"/> - Maximum <input type="text" value="35.04"/> Minimum > 0.22 - Maximum < 35.04	⊗
Ablation mean Width (km)	: Minimum <input type="text" value="0"/> - Maximum <input type="text" value="4.16"/> Minimum > 0 - Maximum < 4.16	⊗
Ablation Length (km)	: Minimum <input type="text" value="0"/> - Maximum <input type="text" value="12.59"/> Minimum > 0 - Maximum < 12.59	⊗
Maximum Elevation (m amsl)	: Minimum <input type="text" value="2912"/> - Maximum <input type="text" value="7601"/> Minimum > 2912 - Maximum < 7601	⊗
Mean Elevation (m amsl)	: Minimum <input type="text" value="2589"/> - Maximum <input type="text" value="6625"/> Minimum > 2589 - Maximum < 6625	⊗
Mean Elevation Accumulation (m amsl)	: Minimum <input type="text" value="0"/> - Maximum <input type="text" value="6990"/> Minimum > 0 - Maximum < 6990	⊗
Minimum Elevation Ablation (m amsl)	: Minimum <input type="text" value="0"/> - Maximum <input type="text" value="6417"/> Minimum > 0 - Maximum < 6417	⊗
Slow Line Elevation (m amsl)	: Minimum <input type="text" value="0"/> - Maximum <input type="text" value="6844"/> Minimum > 0 - Maximum < 6844	⊗
Supra-Glacier Lake Elevation (m amsl)	: Minimum <input type="text" value="0"/> - Maximum <input type="text" value="5884"/> Minimum > 0 - Maximum < 5884	⊗
Accumulation Orientation	: SE	⊗
Ablation Orientation	: SE	⊗

Figure 207: Multi-parameter query available as fifteen filters in HGIS

Thus a robust, user friendly Web based Himalayan Glacier Information System (HGIS), a first of its kind in the country is developed which facilitates any user to selectively display, query, analyze, compose maps and graphs and print, spatial and aspatial information on glaciers relevant to his interests (Sharma et al., 2015; Rajawat and Sharma, 2015). HGIS represents a significant step towards mapping and compiling individual glacier level inventory data in spatial form to fill the void in data and information on the status of Glaciers in the Himalaya and Trans-Himalayan Karakoram region. HGIS provides a basis for assessing the glacier inventory data which has applications in studies related to climate change, water resource planning, hydropower site selection and mitigation of glacial lake outburst flood (GLOF) hazards. Space Applications Centre, ISRO, Ahmedabad has developed a Web Portal <http://www.vedas.gov.in> for providing access to all thematic maps prepared for land applications under its recent efforts named as “Visualisation of Earth Data and Archival System (VEDAS)”. All the Himalayan glacier inventory maps have been ported into VEDAS for easy access by research community and it is planned to provide services of HGIS through SAC Web Portal VEDAS to user/research community.

6. Effect of Black Carbon Soot and Contamination on Snow and Glacier Ice

6.1. Objective

To measure the black carbon soot mass concentration on snow and glacier ice in representative glaciated regions of Himalayas using portable Aethalometer.

6.2. Scientific Rationale

Absorbing aerosols such as black carbon (BC) or dust over high-altitude Himalayan regions have potential implications on the regional climate and hydrological cycle. The black carbon also commonly referred to as “soot” comprises of microscopic particles of about 70 microns size that are released, but not broken down entirely, when burning fossil fuels. Soot consists primarily of elemental carbon that mostly comes from the consumption of fossil fuels particularly coal, diesel fuel, jet fuel, natural gas, kerosene and the burning of wood, animal dung, vegetable oil and other biomass fuels. In recent years scientists have begun to recognize soot as having the potential to cause changes in climate. Soot absorbs sunlight and, therefore, heats the surrounding air, also reducing the amount of sunlight that reaches the ground, resulting in a cooler surface. The heated air can create an unstable atmosphere resulting in rising air, forming clouds and bringing rainfall to areas heavily concentrated with soot. The rising air is often balanced by an increase in sinking air in neighboring regions, which tends to prevent cloud formation and rainfall. Black carbon soot is considered to be the second largest contributor to global warming next to the greenhouse gas carbon dioxide. Scientists propagate that a worldwide reduction in soot emissions and controlling biomass burning could quell the alarming pace of global warming and also reduce our reliance on soot-producing fuels. The International Global Panel on Climate Change (IGPCC) agreed that black carbon soot is a major contributor to global warming. It concluded that black carbon soot has a dire atmospheric warming effect. This was significant because soot had previously been unaddressed as a major contributor to global warming. Nor had the amplification of black carbon’s warming effect previously been taken into account when mixed with other aerosols, creating additional secondary fine particulates.

Soot also has been found to cause climate forcing in areas of higher latitude where ice and snow are more common. Typically, ice and snow reflect sunlight rather than absorb it due to having a white background, also known as an albedo effect. When snow and ice are covered in soot, the soot absorbs the sunlight warming the ice and snow and causing a faster than normal melt. As more melting occurs, the warming effect increases as the soot becomes more concentrated on the snow surface and the land surface is exposed. Monitoring of BC over fragile High altitude snow and glacier regions of Himalaya is thus very significant.

The reported work on BC monitoring for the Himalayan region is very limited. The Nepal Climate Observatory - PYRAMID established in 1990 at altitude of 5050 amsl in Mount Everest region in the north facing Nepal Himalayas is the only permanent station monitoring BC in high altitude mountainous region of Himalaya. The NCO-PYRAMID is joint experiment by scientific agencies from Nepal and Italy and over the years has participation from more than 180 other national and international scientific institutes from various parts of the world.

Absorbing aerosols such as black carbon (BC) or dust over high-altitude Himalayan regions have potential implications on the regional climate and hydrological cycle over South Asia. Deposition of black carbon (BC) soot on highly reflecting surfaces like snow or ice could reduce the surface albedo and result in a positive radiative forcing (warming) at the top of the atmosphere. A mean radiative forcing of $+0.1 \pm 0.1 \text{ W m}^{-2}$ for BC induced changes in snow albedo has been estimated (IPCC, 2007). Figure 208 shows the radiative forcing and efficacies of direct, semi-direct, and snow albedo effect of BC estimated based on the model simulations. It is seen that there exist large uncertainties in the estimates of all BC forcing. Also, snow albedo modification via BC has a very high efficacy compared to other BC forcing and most of the other climate forcing agents (Hansen et al., 2005, IPCC, 2013, Flanner et al., 2012, Flanner et al., 2011). For the range of 10-200 mg kg⁻¹ of BC in snow, the diurnally averaged forcing due to snow darkening has been found to vary from 0.87 to 10.2 W m⁻² for fresh snow and from 2.6 to 28.1 W m⁻² for the aged snow, which is significantly higher than the estimated direct radiative forcing of 1.67 W m⁻² (Nair et al 2013). Potentials of remote sensing for detecting black carbon in snow has been investigated (Warren, 2013).

Thus BC over Himalaya in general and glacier in particular has been a topic of prime scientific interest and several investigators have studied the BC over Himalayan region (Kulkarni et al., 2013, Das et al., 2010, Prasad et al., 2011, Lau et al., 2010) and few case studies based on the measurements from the northern (Nepal and Chinese regions) or Western (Pakistan) Himalaya (Yasunari et al., 2010, Ming et al., 2009). Aerosol Optical Depth (AOD) data of 2001-2008 from MODIS was studied to understand its impact on the Dokriani Glacier, Bhagirathi Valley, Garhwal Himalaya. An increase in AOD was observed after 2005, which is observed to be correlated with accelerated recession of the Dokriani glacier (Das et al., 2010). It is speculated that increased AOD has resulted in the enhanced aerosol induced heating and consequent accelerated recession of the Dokriani glacier. Modeling studies also predicted increase in Himalayan glacier melt and retreat due to the BC induced snow surface darkening.

In view of the above, investigation of snow, BC and albedo changes over Himalayan region has been taken up as a topic of research. Aerosol measurement of BC over Himalayan region was carried out in campaign mode using portable Aethalometer during expeditions to several valley glaciers spread in different climatic zones. The observations were carried out during ablation period of 2011 to 2014.

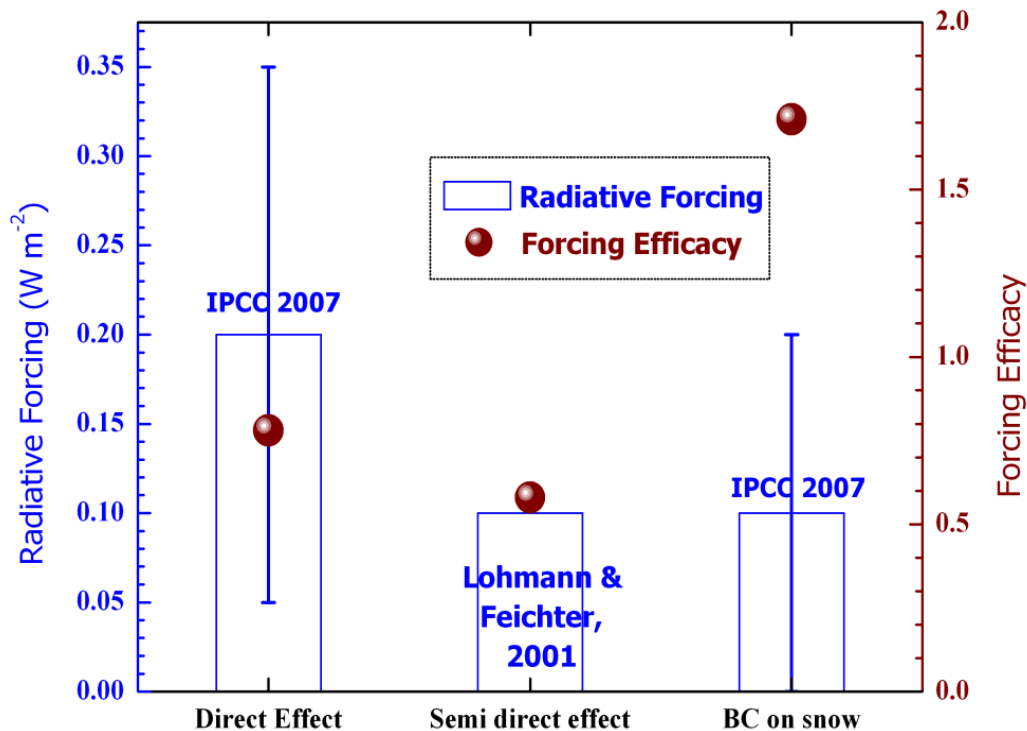


Figure 208: Radiative forcings and efficacies of direct effect, semi-direct effect and snow albedo effect of black carbon aerosols estimated based on global climate model simulations (Source: IPCC, 2007; Lohmann & Feichter, 2001)

6.3. Study Area

The study area comprised several valley glaciers occurring in different climatic zones of Himalayas in India. The glaciers are located in the states of Jammu & Kashmir, Himachal Pradesh, Uttarakhand and Sikkim. The location of glaciers is shown in Figure 209 and also given in Table 80.

6.4. Principle of Aethalometer

Multi-spectral portable Aethalometer (AE-42, Magee Scientific, USA) working on the principle of optical attenuation technique (Hansen et al., 1984) has been used for this study. The Aethalometer aspirate the ambient air at known flow rate (5 LPM for Himalayan conditions) and deposit on a quartz fiber filter tape to measure the change in optical attenuation due to aerosols deposited on the filter tape. The Aethalometer measures the black carbon soot at 370 nm (Ultra Violet) and 880 nm (Infra-Red) regions of the Electromagnetic spectrum. The quantity of black carbon measured is recorded in nano gram per cubic meter of air. The uncertainties associated with Aethalometer caused by the loading of aerosols on the filter tape and multiple scattering are well documented (Arnott et al., 2005; Nair et al., 2007).

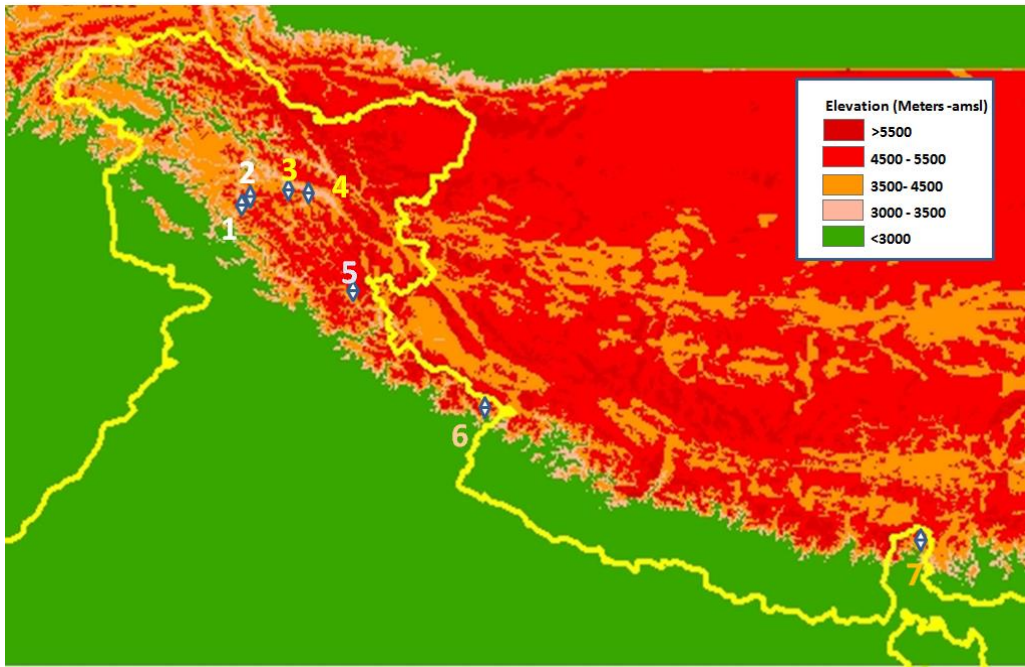


Figure 209: Locations of selected glaciers in different climatic zones of Himalayas taken up for monitoring of Black Carbon. (1. Thajwas, 2. Hoksar, 3. Machoi 4. Pensilumpa 5. Chhota Shigri 6. Satopanth 7. Changme Khanku)

Table 80: Details of Glacier locations selected for Black Carbon Soot studies in Himalayas

Sr. no.	Name of glacier	Sub-basin/ Glacier valley	State	Measurements at Elevation (m amsl)
1	Thajwas	Jhelum (Sind Nala)	Jammu & Kashmir	2850-2950
2	Hoksar	Jhelum (W. Liddar)	Jammu & Kashmir	3390-3660
3	Machoi	Drass	Jammu & Kashmir	3700-3750
4	Pensilumpa	Zaskar	Jammu & Kashmir	4100-4950
5	Chhota Shigri	Chandra	Himachal Pradesh	3750-4200
6	Satopanth	Alaknanda	Uttarakhand	3200-4400
7	Changme Khanku	Tista	Sikkim	4600

6.5. Methodology

- The Aethalometer is operated at various altitudes within glacier valley and on the glacier surface.
- Preferably the instrument is operated to obtain profile of BC mass variations along the track leading to glacier and on the glacier surface.
- The sites comprised the approachable regions like the de-glaciated valley, glacier snout, parts of ablation zone and accumulation zone of glacier sometimes in regions of fresh snowfall in vicinity of the glacier.
- The coordinates of the geographic location of BC observation site are recorded using hand held GPS instrument.
- The site is also identified on Resourcesat-1 satellite data. Some BC measurements were made at nearby settlement locations for understanding the altitude distribution of BC.
- The aerosol optical depth (AOD) at the site is measured by using a hand held Sun Photometer.
- The AOD information is related to the amount of solar radiation reaching the site and affecting the glacier melt.
- Aethalometer measurements during 1100-1500 hours when the dispersion of suspended particulate matter is maximum are recorded along the expedition track for a systematic profile of BC variations at different altitudes.
- Diurnal variations of BC are recorded by continuous Aethalometer recording at or near the camping sites.
- The local BC contributions can be observed during such long term diurnal recordings.
- On average, 5 to 10 measurements were made at each location.

6.6. Results and Discussion

BC measurements using portable Aethalometer are made at glacier locations in various climatic zones spread across Himalayas. The main focus was to obtain BC mass concentration data to fill the gaps in information content and understand the BC mass variation over snow and glacier region over India Himalayan region. The variation in BC mass distribution over Himalayan glaciers are analyzed. Following are major findings:

- Aerosol BC measurements depicts large spatio-temporal variations due to the heterogeneities in source and sink characteristics. In general the BC mass concentration and dispersion is affected by remoteness from human settlements & infrastructure, rapidly varying sky conditions, humidity, precipitation (rainfall or snowfall), wind direction and wind velocity.

- Diurnal variation showing increased BC concentration during peak human activity noon and evening time and fall in concentration during night time is observed (Figure 210).
- There is distinct latitudinal variation of BC mass concentration as seen through measurements across the Himalayas.
- High BC values observed at the lower altitudes decrease drastically as we move to higher altitudes. Steady BC concentration of about 200 ng m^{-3} is recorded in Himalayas above 4000 m amsl. Sample graph along with the observation locations marked on satellite data showing the altitudinal variation for Satopanth glacier in Uttarakhand are given in Figure 211. Results of altitudinal BC variations from several glacier located in J&K region are given in Figure 212. There exists a large temporal variability at the lower altitudes due to the proximity to the source regions and diurnal evolution of the boundary layer.
- The Zonal BC measurements from west to east in the Himalaya made at Jammu & Kashmir, Himachal Pradesh, Uttarakhand and Sikkim distinctly show that while the Leh-Ladhak & Drass region has relatively low BC mass concentration, the Kashmir valley glacier regions have relatively higher concentration of BC. The Sikkim region at 4600 m amsl has low BC as seen in Figure 213.
- The mean values of BC measurements of 200 ng m^{-3} recorded during the study at higher altitudes correspond well to the reported climatological mean of atmospheric BC over Hanle (Western Himalayas, 4500 m amsl) and Nepal Climate Observatory-Pyramid (Central Himalayas, 5000 m amsl) having BC values of $106 \pm 27 \text{ ng m}^{-3}$ and $190 \pm 95 \text{ ng m}^{-3}$ respectively.
- The direct and surface albedo radiative forcing due to BC (Nair et al., 2013) could contribute in warming effect over snow and glacier regions of the Himalayas.

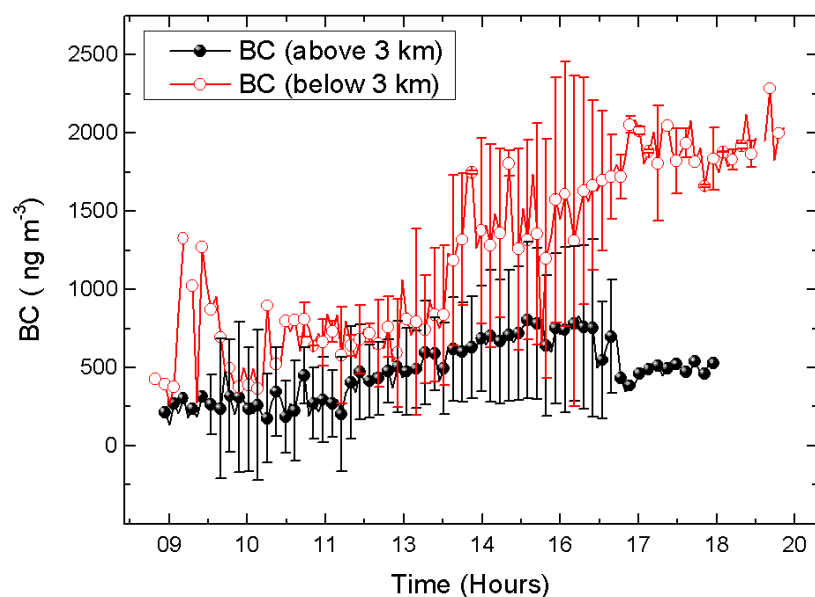


Figure 210: Diurnal variation of BC mass concentration above 3 km and below 3 km altitude regions over the Indus basin

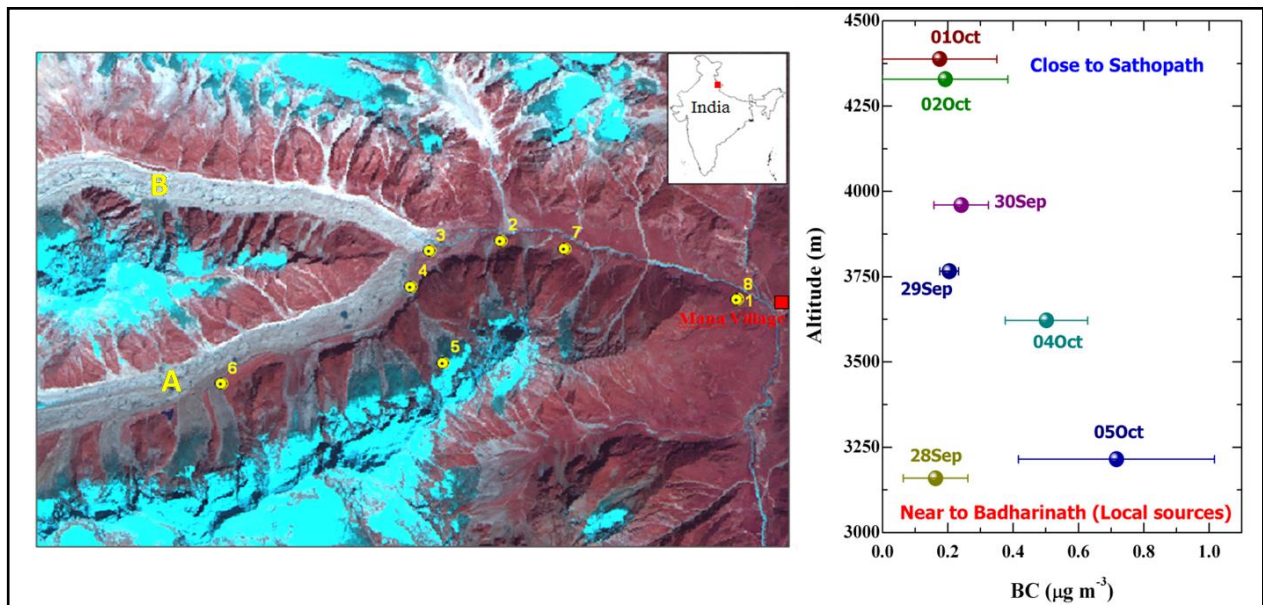


Figure 211: Vertical distribution of BC mass concentration inferred from the measurements at different altitudes for Satopanth glacier Uttarakhand. The BC measurement locations are marked on Resourcesat-1 satellite data

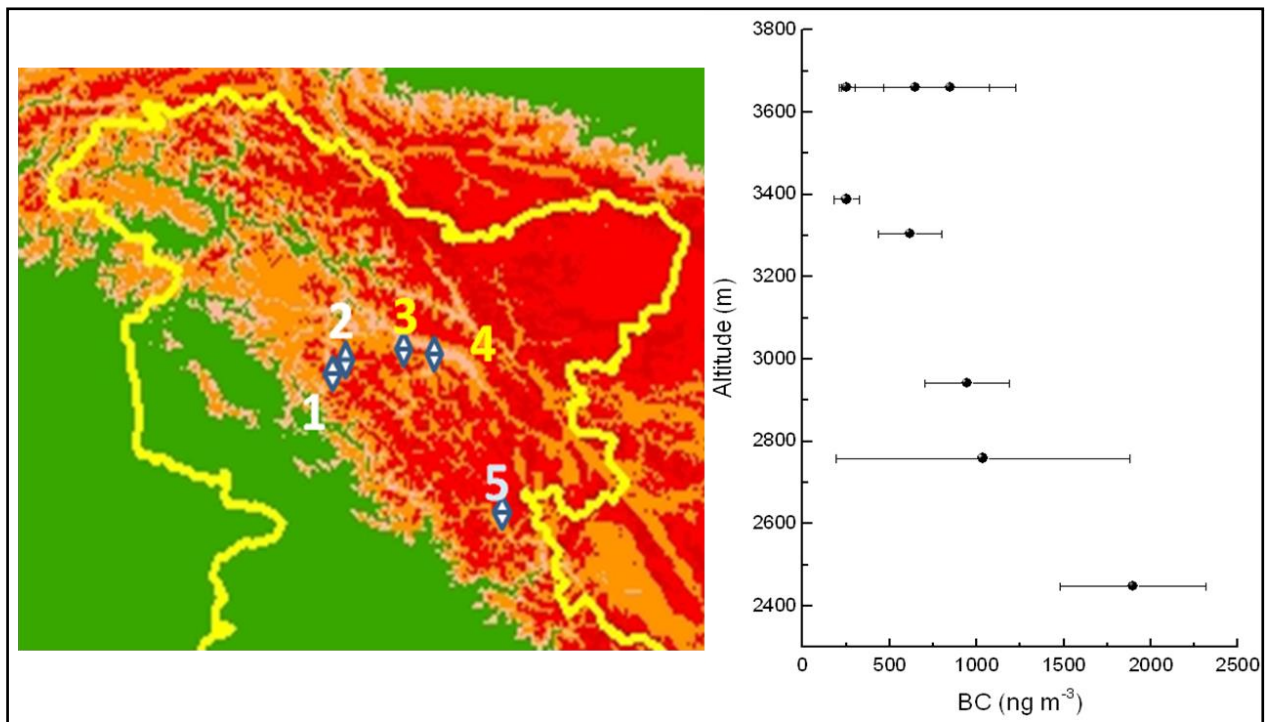


Figure 212: Vertical distribution of BC mass concentration inferred from the measurements at different altitudes for glaciers in Indus Basin (Jammu & Kashmir and Himachal Pradesh Himalayas). Legend: 1-Haskar, 2-Thajawas, 3-Machoi, 4-Pensilumpa and 5- Chhota Shigri

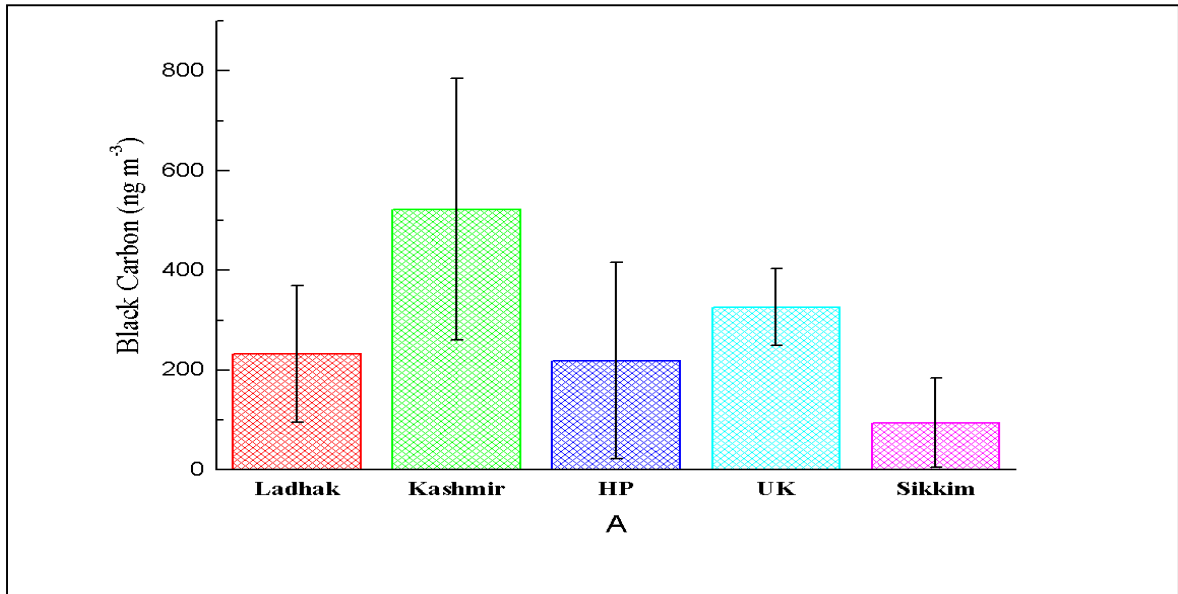


Figure 213: Variation in BC mass concentration across Himalayan region

7. Effect of Debris Cover on Glacier Ice Melt

7.1. Objective

To carry out studies to understand the effect of debris cover on glacier retreat.

7.2. Scientific Rationale

Most of the large glaciers in Himalayan region are covered with debris in their ablation areas. These glaciers are classified as debris covered glaciers. Debris is mainly confined to lower parts of ablation zones. The thickness, which may run sub-meters to meters, gradually increases down glaciers, and becomes maximum at the snout. The source of rock fragments is the surrounding high relief mountains which get shattered/broken due to frost action owing to high temperature extremities and gets deposited. The surface of a glacier is generally lower than the crest of the lateral side moraines. This difference gradually increases as one moves downward due to high probability of sliding of debris from the surroundings to the glacier surface. It is well established that the melting of glacier is influenced largely by the presence of dust or debris on the glacier body, because radiation balance is affected, which, in turn, influences the melt rate (Basnett et al 2013). An assessment of ablation rate under a dust or debris cover is needed for the studies of glacier mass balance, glacier dynamics, and artificial ablation control engineering and hydrological purpose. The ablation rate under the debris cover is governed by the radiation, air temperature and physical characteristics such as thickness, albedo, and thermal conductivity of the debris layer. There are two difficulties in estimating the mean value of ablation under a debris layer extending over a wide area (i) direct determination of thermal resistance of the layer in the field which is one of the essential parameter for estimation of ablation and (ii) detail information on meteorological variables necessary for estimation. Understandings the effect of debris cover on the ablation of glacier ice for predicting the water supply from mountain glacier is essential (Ben and Evans, 2010). Usually, the effect of debris cover on the melting of glacier is not included in the modeling of glacier melt runoff.

Debris thickness mapping of Bara Shigri glacier using remote sensing techniques has been attempted (Schauwecker et al., 2015). Use of optical, thermal and microwave imagery for debris characterization in Bara-Shigri Glacier, Himalayas has been found to be extremely useful (Tiwari et al., 2012). The influence of debris cover and glacial lakes on the recession of glaciers in Sikkim Himalaya has been studied (Smriti Basnett et al., 2013). Spatially variable response of Himalayan glaciers to climate change affected by debris cover has been observed (Scherler et al., 2011). Temporal changes in elevation of the debris-covered ablation area of Khumbu Glacier in the Nepal Himalaya since 1978 have been studied (Nuimura et al., 2011). Geochemical characterization of supraglacial debris via in situ and optical remote sensing methods

has been demonstrated through a case study in Khumbu Himalaya, Nepal (Casey et al., 2012). Decision tree and texture analysis for mapping debris-covered glaciers in the Kangchenjunga area, Eastern Himalaya has been attempted (Racoviteanu and William, 2012).

It is observed that a thin layer of debris cover accelerates melting, but thick layer retards it (Singh et al., 2000). Dusting of snow and ice surfaces by dark materials is known to increase in absorption rate of solar radiation. There is a significant difference in mean seasonal ablation rate between site varying thickness of debris and also in ablation rates at same site over a time. The debris thickness at maximum ablation occurs is known as “effective debris thickness”. There is a “critical thickness”, which is defined as the thickness of the debris layer at which the ablation rate of a debris covered glacier is same as for a debris free glacier. It is observed that an increase in the thickness of the debris cover on a clean ice surface initially increased the rate of ablation, but it led to decrease after the critical thickness was reached. At sites with thinner debris thickness than effective thickness, the reflectivity of surface is high, thus less incoming energy is used for increasing the temperature of debris materials and ice melting. The critical thickness and effective thickness varied from day to day depending up on the total energy available for the melting. During night, a constant ablation was observed for all thickness of the debris.

7.3. Case Study I: Warwan-Bhut sub-basins, Chenab basin

The study area covers glaciers of the Warwan and Bhut sub-basins belonging to the Chenab Basin, Western Himalaya. The sub-basins are located in Jammu and Kashmir between 33°30′–34°21′N lat. and 75°39′–76°28′E long. and 33°15′–33°64′N lat. and 75°72′–76°78′E long. with an area of 4,828.4 sq. km and 2,285.4 sq. km respectively. In the Warwan Basin, the largest glacier covers 51.8 sq. km, (lat./long. 33°45′ 52.43″N/76°07′02.15″E) followed by one with an area of 48.7 sq. km (lat./long. 33°32′14.16″N/76°06′07.25″E). In case of the Bhut Basin, the largest glacier has an area of 49.9 sq. km (lat./long. 33°12′10.21″N/76°43′05.08″E). Most of the glaciers in the two sub-basins have slope in the range 10°–20°. Both the basins lie between altitude 1,100 and 6,500 m. Most of the larger-sized glaciers are covered by rock fragments in the ablation zones, whereas smaller glaciers are debris-free. Majority of the glaciers in the Bhut Basin are moraine-covered than those of the Warwan Basin. The host rocks for the glaciers to rest are gneisses and schist of the Central Crystalline Zone. One major difference between the glaciers of the two basins is that glaciers of the Bhut Basin are mainly south-facing whereas those of the Warwan Basin are north to northwest-facing.

Glacier extent was first adopted from topographical maps and then monitored using satellite images. Mapping from images requires use of elements of visual interpretation, such as unique reflectance of snow and ice, shape of the valley

occupied by the glaciers, the flow lines of ice movement, rough texture of the debris on the ablation zone, and the shadow of the steep mountain peaks and presence of vegetation on the mountains. The SWIR band was used to discriminate cloud and snow as in many cases the glaciers are covered by clouds at the ridges. The snout of a glacier is the most important feature for monitoring, because the movement of the snout helps in recognizing the advance or retreat of the glaciers. Sometimes snouts of many glaciers were not distinct on the images due to debris cover. In such cases various other indicators such as location of origin of streams from the glaciers, presence of distinct geomorphic features in the form of braided streams, lakes, glacio-fluvial sands, etc. helped in the identification of snouts. Additionally, changes of slope or elevation near the snouts observed through DEM from SRTM, also helped in the identification of snouts. The moraine cover was estimated using NDSI technique. The NDSI utilizes the spectral characteristics of snow (Hall et. al., 1995).

NDSI algorithm is applied within the glacier boundary which discriminate snow-ice cover and non snow-ice cover. The threshold value 0.4 has been used to separate snow/ice from debris cover ice (Kulkarni, et al., 2006b; Shukla et al., 2010a; Shukla et al., 2010b). The non snow-ice part of the glaciers corresponds to moraine cover area. Then extracted moraine cover area has been verified using visual interpretation technique. This technique includes the usage of band combination as B2 (0.52-0.59 μm), B4 (0.77-0.86 μm) and B5 (1.55-1.75 μm). Reflectance of rock in band B5 is higher than ice; therefore, debris cover on glacier gives a red tone (Kulkarni, et. al., 2005). The moraine cover for each glacier was estimated using semi-automatic approach with the help of manual correction for study area.

It has been observed that the larger sized glaciers are covered by high percentage of debris cover as they have gentle slopes. Further monitoring of glaciers in Warwan and Bhut sub-basins using satellite images of 2001 to 2011 was carried out. The study indicate that the smaller glaciers (upto 10 sq km) show variation in debris cover upto 10%, whereas larger glaciers (30-40 sq km) show variation in debris cover upto 23%. Loss in glacial area is observed to be ~ 3.4 % for debris free smaller glaciers, whereas it is 1.2-1.5 % for debris-covered smaller glaciers. Larger debris free glaciers show loss in glacial area ~ 0.5 %, whereas large debris covered (12 – 25 % debris cover) glaciers show negligible retreat (Figure 214) for period of 2001 - /2011. More retreat was observed in debris free than in debris cover glaciers.

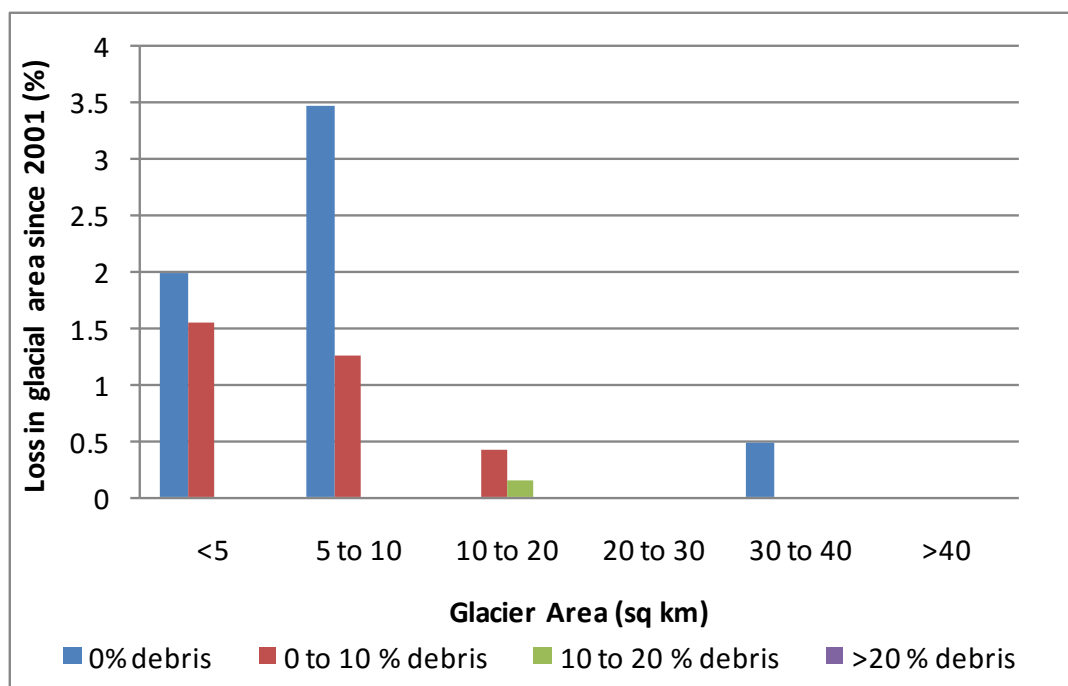


Figure 214: Influence of debris cover on glacier on Loss in glaciers area during the monitoring period 2001/2002 – 2010/2011

7.4. Case Study II: Alaknanda and Bhagirathi sub-basins

The various glacier features are distinctly identifiable on Resourcesat-1 optical data using different band combinations and proper contrast. Outer limits of glacier boundary are conspicuously seen by using FCC with band combination of B2, B3 & B4/B5. Glaciological features comprising accumulation area, ablation area (both ice exposed and debris covered), glacieret & snow field, snout, ice divide, transient snow line, highest and lowest elevation points, de-glaciated valley, glacial lakes, etc. were mapped based on various interpretation keys (Sharma et al 2013). Moraine/debris cover can be identified using visual interpretation key like tone, texture with elongated pattern and association with glaciated region. By using the glacier inventory map layers in GIS environment, systematic observations and measurements are made on the glacial feature and recorded in tabular form in the inventory data sheets created as per modified UNESCO/TTS guidelines with few additional parameters. By measurement in GIS of various stored line features, information for length and width is obtained. Altitude information is extracted from SRTM-DEM using GIS.

Debris cover area with respect to altitude information has been extracted for individual sub-basins. Scatterplot was prepared to understand the variation of debris cover with respect to change in altitude for Ganga basin. AAR (Accumulation area/Total area) and DAR (Debris cover ablation area/Total area) was estimated while ignoring the glacier with negligible debris cover less than 0.1 sq km. Glaciers without ablation and accumulation zone was not considered for the analysis. This exercise was carried out

at sub-basin level. Glacier area, debris and snout altitude was categorized with respect to change in their area. Averaged ablation area (with or without debris) and number of glacier were also categorized in altitude zone to understand the variation of debris with respect to elevation. Alaknanda and Bhagirathi basin are two adjoining basins which have been reported to shown different retreat in Ganga basin in Indian Himalayas (Bahuguna et al., 2014). These basins were selected to understand the possible linkage of debris cover with respective retreat. Change in debris cover area was studied with respect to the elevation of snout of respective glacier. Average debris cover area (sq km) was being categorized into different altitude zone.

Ganga basin has shown mean high accumulation and ablation area with significant area occupied by mean moraine dam lakes and supra glacier lake. Ganga has shown highest debris covered ablation zone with less number of small glacier in comparison to Indus and Brahmaputra basin. Accumulation, Ablation and Debris Cover area cumulatively affect the retreating pattern of a particular basin. This information was further sub-divided into sub-basin scale which showed varying trend for different sub-basins. Alaknanda, Bhagirathi and Karnali was found to be in high negative correlation in comparison to remaining basins. Figure 215 shows that for smaller glaciers the percentage of debris cover is significantly high along with high altitude of snout. The relationship depicts vice-versa pattern for large glaciers. This analysis was further carried out for considering only ablation area as shown in Figure 216. This shows that the glaciers are few in the altitude range of 3000-3500 m but average debris cover area is highest. This also holds true for altitude range of 3500-4000 and lowest towards higher altitude range. The occurrence of maximum debris cover area coincides with the lower to middle altitude range which is prone to maximum melting during the ablation period.

Alaknanda and Bhagirathi sub-basins have been taken further to understand the effect of retreating pattern. Figure 217 shows that Bhagirathi shows a high percentage of debris covered area of glaciers than Alaknanda in the altitude range of 3500-4000 m of snout whereas no class was observed for 3000-3500 m. This indicates that more protection was provided to Bhagirathi sub-basin than Alaknanda sub-basin. A scatterplot of debris cover area for both basins with respect to their snout altitude position shows a relatively higher negative trend for Alaknanda sub-basin (Figure 218). This can lead to an understanding of more retreat of glaciers in Alaknanda sub-basin than Bhagirathi sub-basin. This observation also matches with more retreat for Alaknanda showing 14% than Bhagirathi basin showing 11% retreat based on SOI maps, and 10 % and 1.8% based on satellite images respectively (SAC, 2011a).

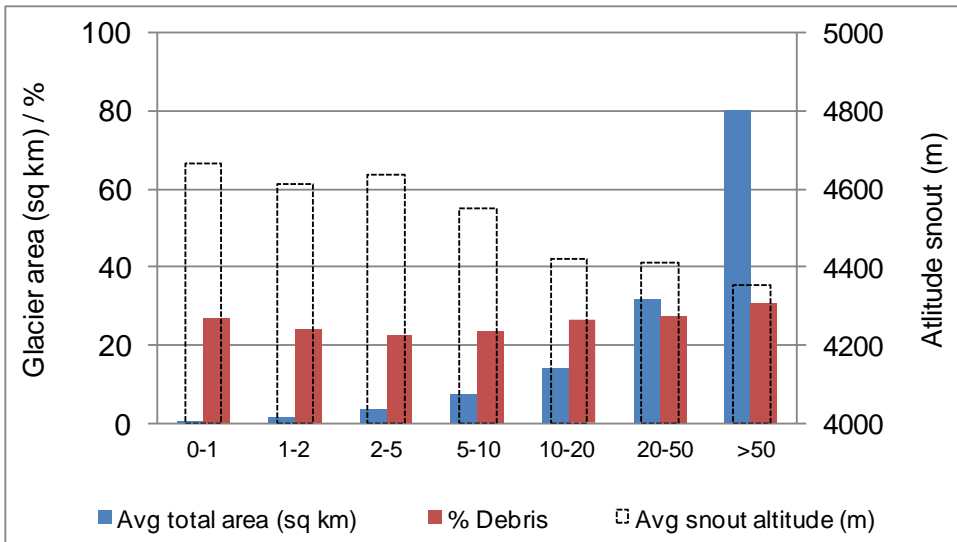


Figure 215: Altitude-wise distribution of total and debris cover area of Ganga basin

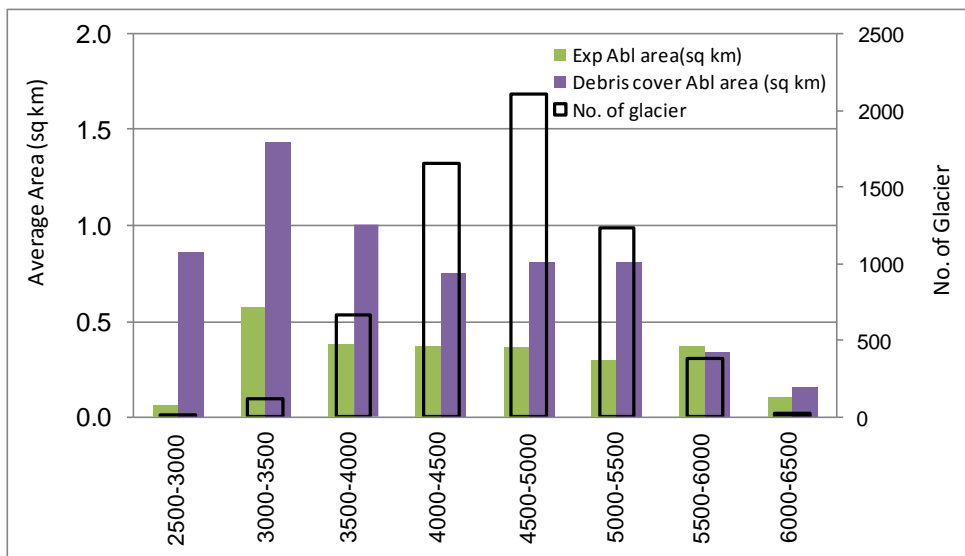


Figure 216: Bar diagram of debris cover and debris free ablation zone of Ganga

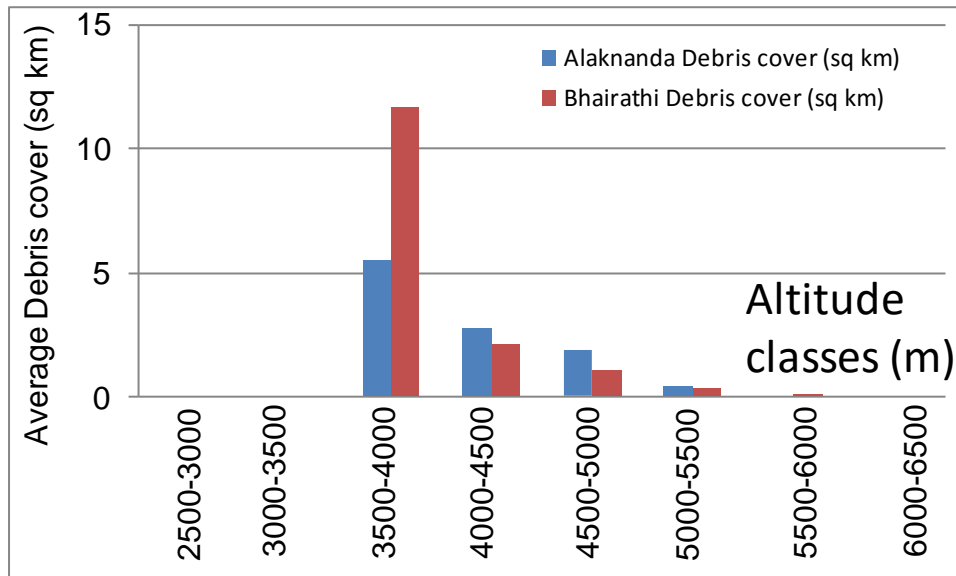


Figure 217: A comparative bar diagram of debris cover glaciated area for Alaknanda and Bhagirathi sub-basin

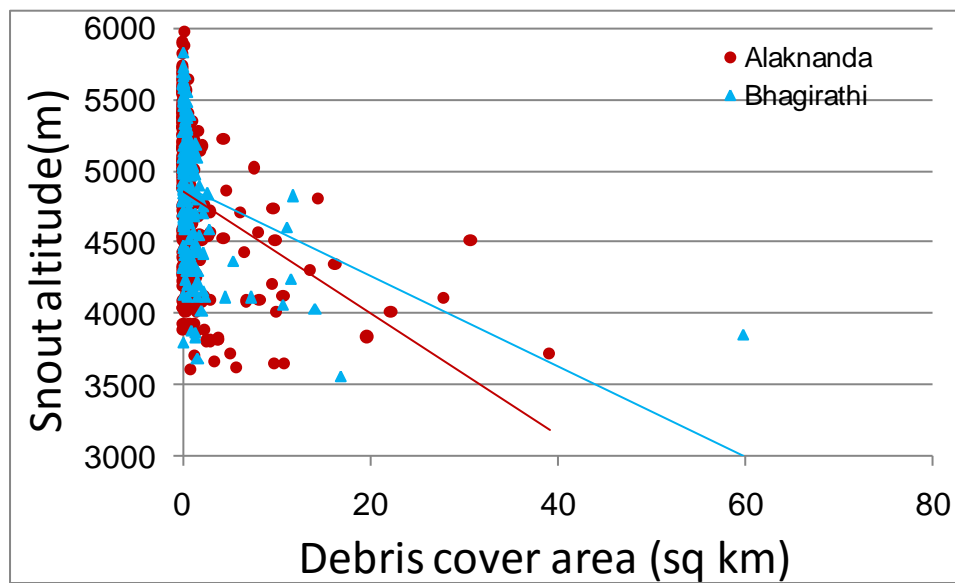


Figure 218: Scatterplot of altitude of snout and debris cover area for both sub-basins

8. Use of Ground Penetrating Radar

8.1. Objective

Estimation of glacier ice thickness using Ground Penetrating Radar in the Himalayan region.

8.2. Scientific Rationale

One of the key issues in Himalayan glaciology is the estimation of glacier ice thickness. Glacier ice thickness is an important parameter to assess the frozen water reservoirs which depends on glacier geomorphology and its areal extent. The ice thickness of a glacier may vary from few meters for small glaciers to few hundred meters for large glaciers and ice sheets. Change in glacier ice thickness can provide an important input to understand the effect of global warming on glaciers. Numerous approaches like seismic method, gravitational method, electrical resistivity method and magnetic method has been used to estimate the depth of glacier in different part of world (Kennett, 1966; Stern, 1978; Merlanti and Pavan, 1998; Shean et al. 2007). Besides these techniques, Ground Penetrating Radar has emerged as a recent technique to estimate the subsurface ice thickness in addition to its role in other sub-surface geological studies. Radio wave penetrate deeper through glacier due to low dielectric constant of ice and gets reflected from bedrock. GPR is a non-destructive technique which provides fast and accurate method and widely used in numerous other applications other than glaciological studies. GPR is used to map geologic conditions that include depth to bedrock, depth to the water table (Wright et al., 1984; Irvin-Flinn, et al., 2006), depth and thickness of soil and sediment strata on land and under fresh water bodies (Beres and Haeni, 1991; Smith and Jol, 1997), and the location of subsurface cavities and fractures in bedrock (Imse and Levine, 1985). It has also shown promising applications in the location of buried objects like pipes, drums, tanks, cables, and boulders, mapping landfill and trench boundaries (Benson et al., 1983), mapping contaminants (Cosgrave et al., 1987; Brewster and Annan, 1994; Daniels et al., 1995; Guy et al., 2000), and conducting archeological investigations (Conyers and Goodman, 1997). Polar ice shelves may contain layers of basal sea ice a few to a hundred of meters of thick (Blindow, 1994), while temperature terrestrial glaciers may contain stratified, debris-rich basal ice tens of meters thick (Arcone et al, 1995; Lawson et al. 1998). Chaohai and Sharma (1988) developed a relationship to estimate ice thickness of glaciers with respect to its areal extent. Ice thickness measurements of Dokriani bamak (glacier) in Himalayan region were carried out with a ground penetrating radar (GPR) pulse EKKO IV Sensor Software, Canada using 12.5 MHz (Gergan et al, 1999). Singh et al, 2010 reported the estimation of snout and moraine thickness of glaciers in Chandra Bhaga basin, however failed to estimate snout thickness (35-40 m) at Samudra tapu glacier using 50 MHz frequency. Airborne survey has been carried out over Antarctica to estimate the ice thickness (Tabacco et al,

2002) whereas it has been used to snow depth and buried objects under snow in Himalayan region (Negi et al, 2008). The current study presents the results of GPR survey for estimating glacier ice thickness of bare ice ablation zone and subsurface features using 16 MHz frequency in the Himalayan region.

8.3. Study Area and Instrument used

Chhota Shigri is a valley glacier and a part of Chandra sub-basin in Chenab basin located in Lahaul-Spiti valley of Himachal Pradesh. The Lahaul and Spiti valley is considered to be a cold desert and does not possess any permanent vegetation due to snow and glacier covered region. Chhota Shigri glacier lies within the crystalline of the Pir-Panjal range. This crystalline axis is comprised mostly of meso- to ketazonal metamorphites, migmatites and gneisses. Figure 219 shows the location of Chhota Shigri glacier (approximately 77.48° - 77.53° N and 32.19° - 32.28° E). GPR operation is marked with red line on ablation zone along with the field photograph of snout. This glacier is oriented roughly NE-SW in its ablation area, and has variety of orientation in accumulation area. Satellite data of AWiFS sensor for year 2007 (10 July, 20 July, 30 July, 04 Aug, 18 Aug, 27 Aug, 01 Sep, 11 Sep, 15 Sep and 05 Oct) along with LISS IV (16 September 2006 and LISS III (27 August 2001) were used to identify different glacier features and glacier boundary. The temperature variation between the maximum and the minimum at equilibrium line (4600 m) were found to be 10.5°C to -5.2°C , whereas near the snout a maximum temperature of 16°C and a minimum of 4°C have been recorded. Field expedition was organized during August 26-September 07, 2010 using Geophysical Survey System Inc. (GSSI) with SIR-3000 control unit and Multiple Low Frequency (MLF) antenna. A 16 MHz frequency was used for the GPR survey on September 02-03, 2010 during this field investigation. The SIR-3000 is a lightweight, portable, single-channel ground penetrating radar system. GSSI's SIR 3000 runs on intuitive and user friendly DAQ GUI, and radar parameters were set up in the field using control unit of GPR.

8.4. Methodology

Ground penetrating radar of low frequency antenna of GSSI was used to estimate the ice thickness of glacier. 16 MHz frequency antenna was used in point mode. A field photograph and schematic diagram of GPR layout has been shown in Figure 220. This antenna extends an arm of 6 m of rod of transmitter and receiver, and connected with the control unit. The GPR survey parameters (like dielectric constant, scan, frequency, scan/unit etc.) were set in the field using SIR 3000. A signal was triggered through transmitter; data collection was confirmed through a beep at control unit. A 50 cm step wise movement of antenna was carried out and same process was repeated throughout the survey. The data was collected along the bare ice ablation zone during 0900-1600 hours in the month of September as glacier is completely free from seasonal snow. Total four profiles were measured with a length of approximately 400 m excluding profile 2. Profile 2 was discarded during the operation due to poor signal. Figure 221 shows the operation of GPR survey using MLF frequency.

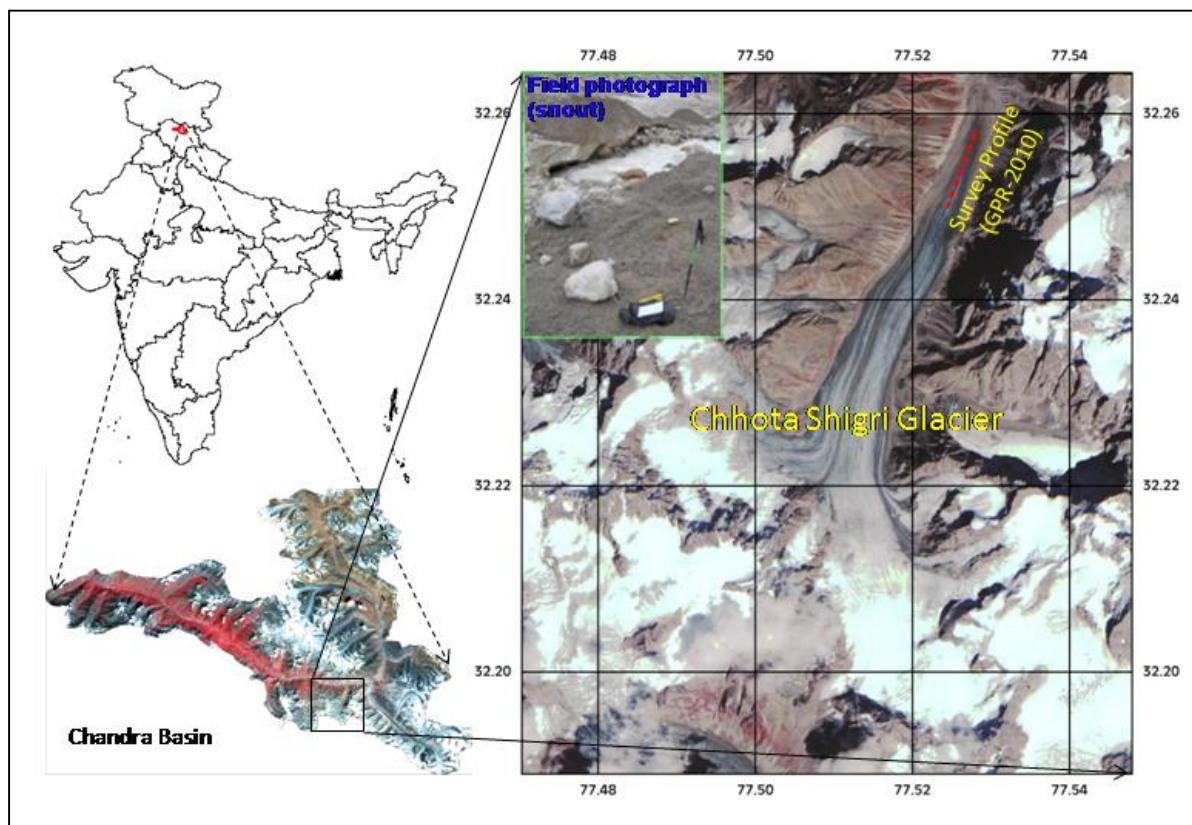


Figure 219: Study area and location of GPR operation (marked with blue line on ablation zone) along with field photograph of snout at Chhota Shigri glacier (Satellite data: LISS IV FCC – 16 September 2006) (Source: Singh et al., 2012)

Figure 222 (a) shows the raw field data and trace window (O scope) at Chhota Shigri glacier. The field data was collected along with 3 transects line along the glacier. The weather gone bad during the fourth profiling exercise and data could not be collected further. RADAN 6.5 software was used to open and process the GPR data. This software is developed by GSSI to display, edit, process and output generation along with advanced processing of dataset. Figure 222 (b) shows the processing steps of GPR data. Correct position was done to rectify the signal received due to direct arrival at receiver through air/ground. This is done while adjusting time-zero in ground coupled bistatic antenna so that the depth scale starts at the ground surface, not several nano second (ns) before. Spatial filtering generates a two-dimensional matrix of phase and amplitude of various spatial waves and allows the user to develop a two dimensional filter to attenuate the noise. Performing the inverse Fourier transformation of the product matrix from the transformed data and the filter yields a data with reduced noise. The advantage of F-K filtering over successive vertical and horizontal one-dimensional frequency filtering is that it enables a better distinction to be made between the signal and the noise. Deconvolution is the filtering method used to remove multiples or "ringing" effect when the radar signal bounces back and forth between an

object and the antenna, causing repetitive reflection patterns throughout the data and obscuring information at lower depths. RADAN uses a method called Predictive Deconvolution. The Hilbert Transform is used to display subtle properties of the earth. The phase information is sometimes more sensitive to important subsurface (dielectric) changes than the amplitude or geometric information. Hilbert Transform will decompose a radar signal represented as a time series into its magnitude (via envelope detection), instantaneous phase, or instantaneous frequency components derivative of phase).

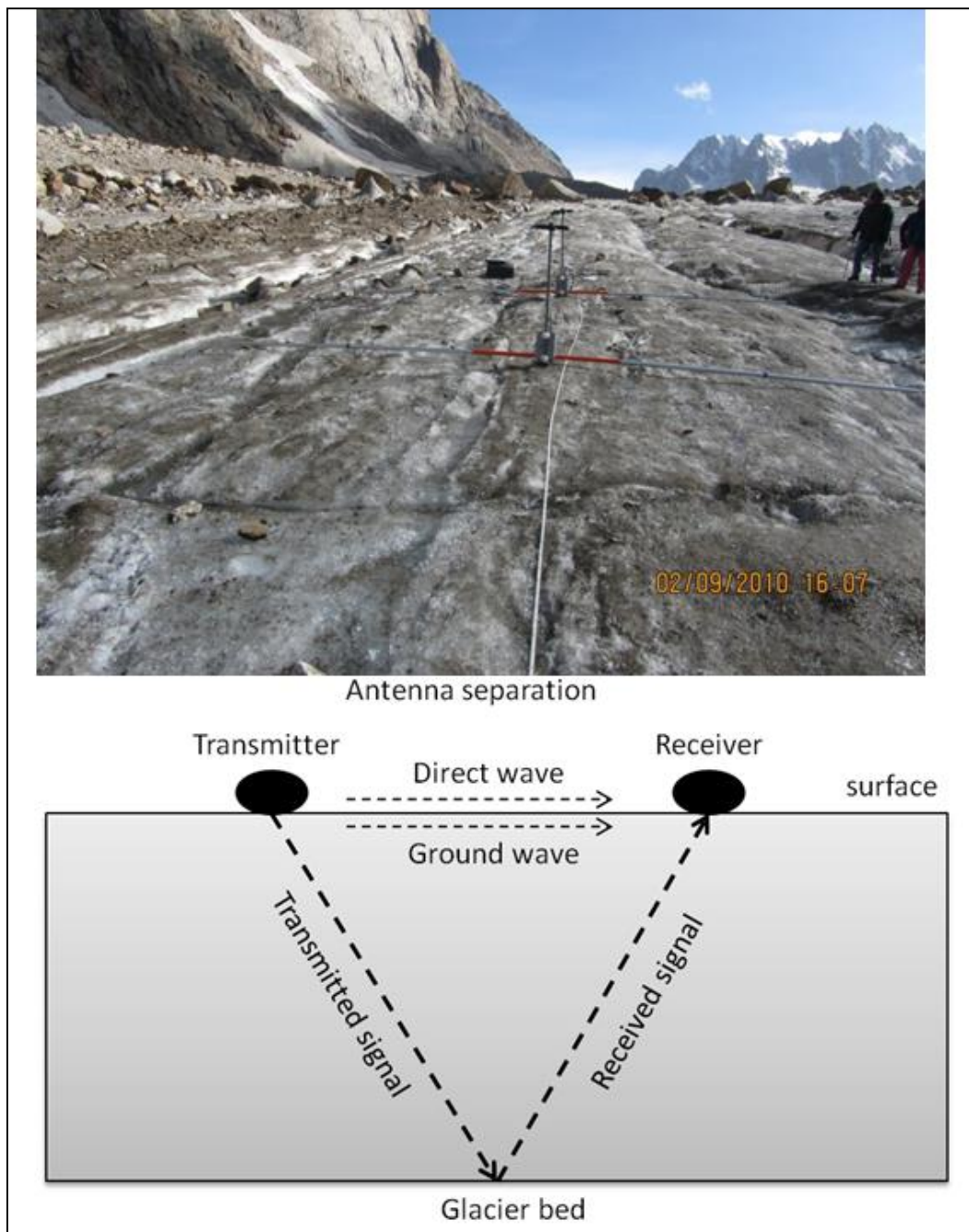


Figure 220: GPR set up on the ablation zone of Chhota Shigri glacier (Source: Singh et al., 2012)



Figure 221: Operation of MLF antenna on ablation zone of Chhota Shigri glacier (Source: Singh et al., 2012)

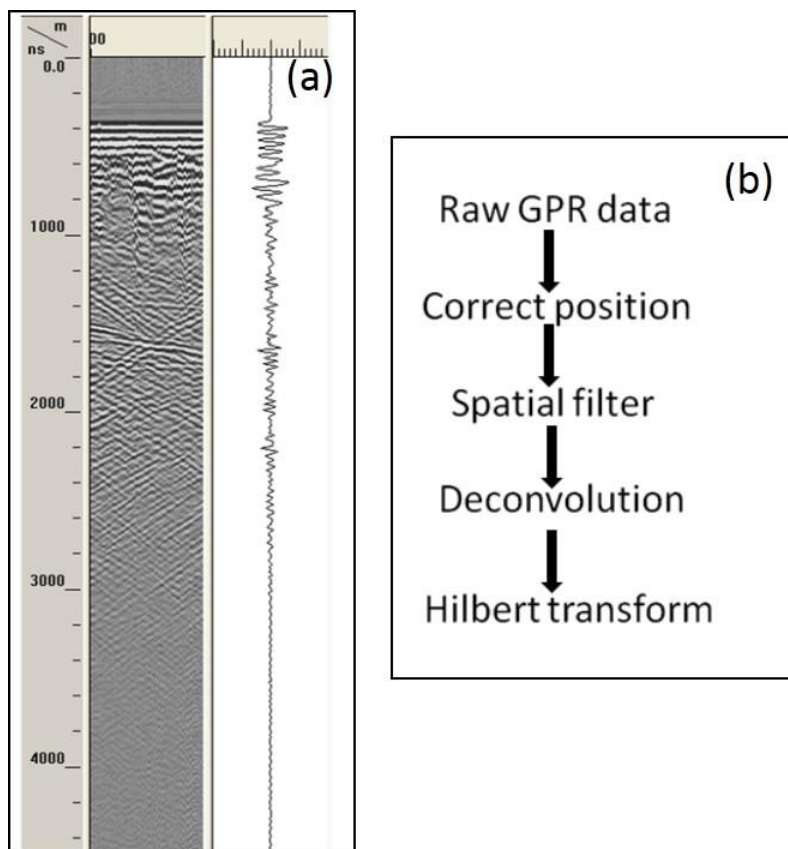


Figure 222: (a) Field data collected through GPR and trace window (Line scan and Wiggle) (b) Processing step of collected GPR data (Source: Singh et al., 2012)

Figure 223 shows the output after incorporating the processing steps as mentioned in Figure 222 (b). In addition, continuous monitoring of AWiFS sensor in ablation season of year 2007 was carried out to determine minimum snow cover data to identify accumulation and ablation zone. However, glacier boundary was delineated using LISS IV data (2006) to calculate accumulation and ablation area in conjunction with LISS III of 2001. Average thickness of glacier was also estimated using empirical relationship developed for the Himalayan region for Chhota Shigri glacier. Figure 224 shows the field survey and output of GPR survey using MLF antenna on Machoi glacier in Dras sector, J&K.

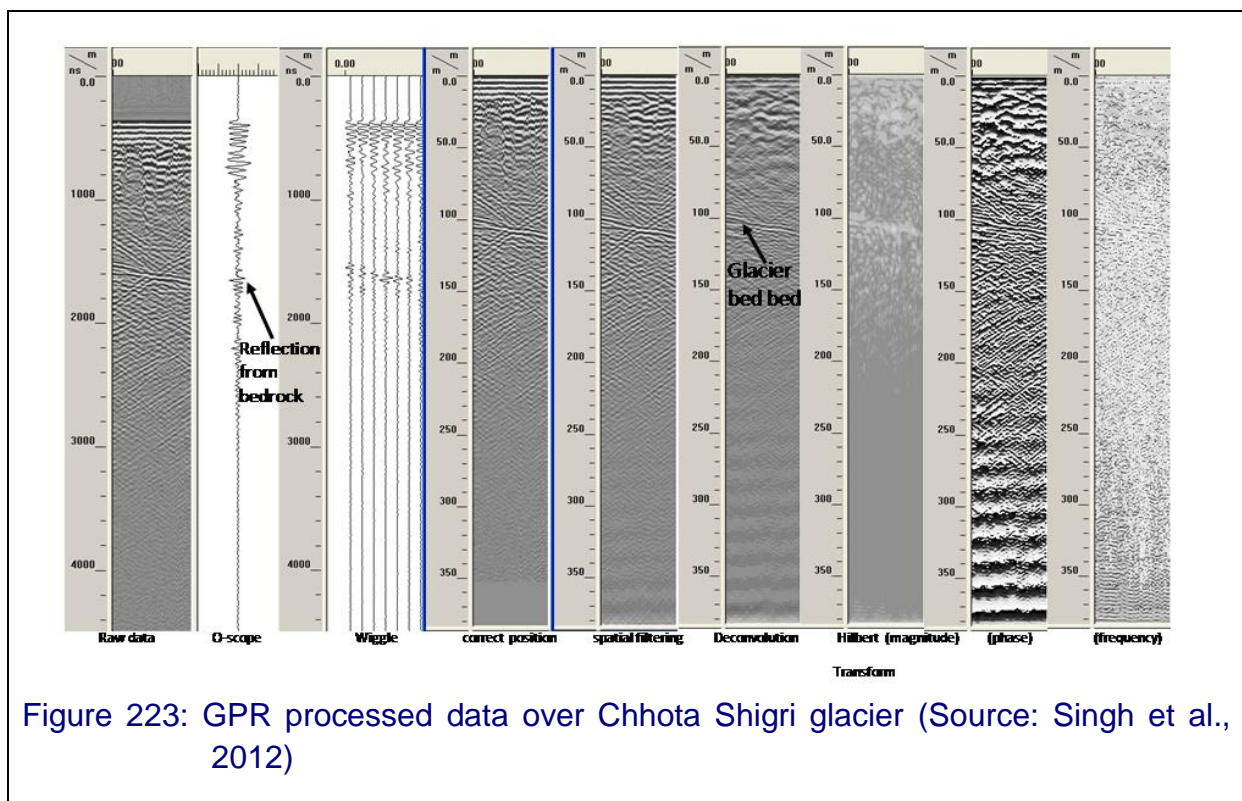
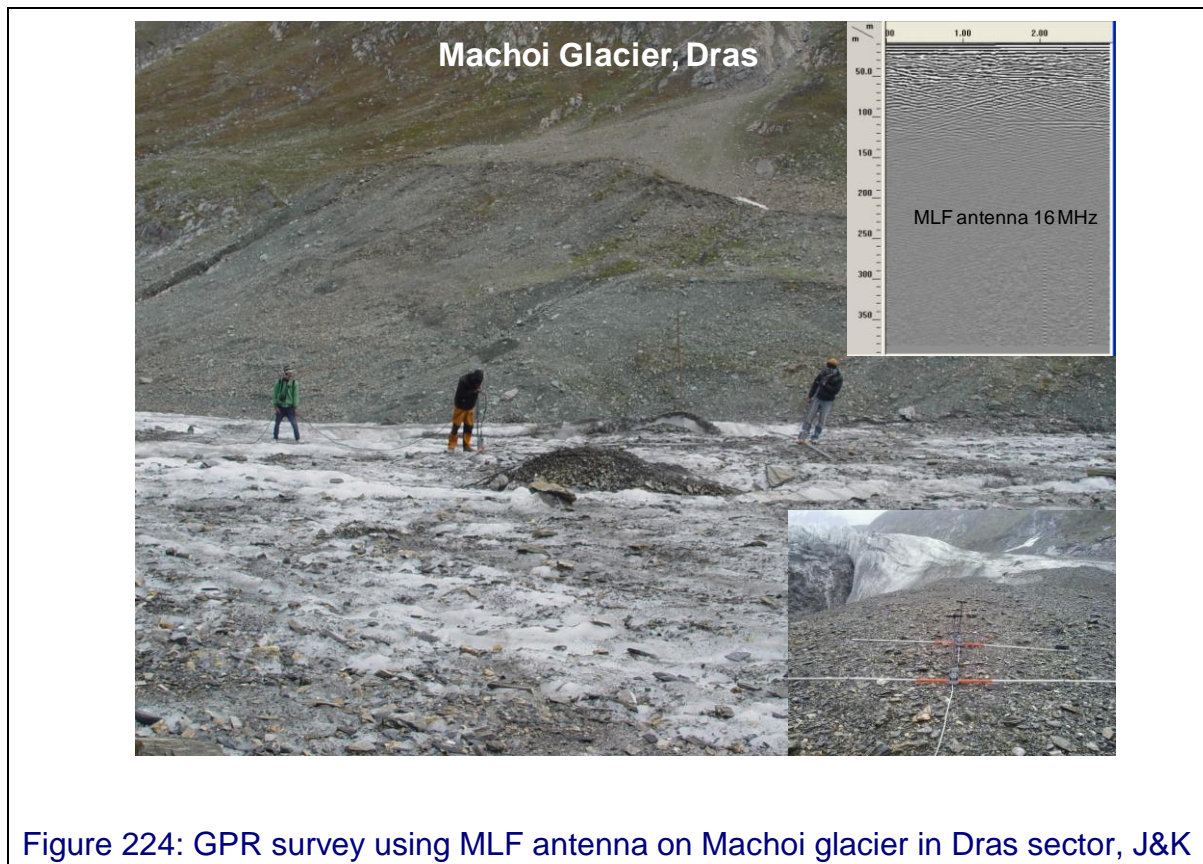


Figure 223: GPR processed data over Chhota Shigri glacier (Source: Singh et al., 2012)

8.5. Results and Discussion

GPR survey depends on many technical/logistics reasons restricting its utilization in Himalayan region. At the same time, it has a constraint of rough terrain, harsh climate and limited time window span (preferably ablation period) to conduct the experiment. Frequency of antenna, dielectric constant of medium (like snow, ice, debris), range to achieve required depth, distance between transmitter/antenna for point mode antenna, sampling of observations are crucial for these investigations.



The MLF frequency of GPR was able to penetrate through ice to interact with bed and retrieve the depth information. Total profiling of GPR survey was approximately 400 m along the glacier. Figure 222 (a) shows the O-scope (raw data) of the survey at Chhota shigri. The processing steps (Figure 222 (b)) were used to remove the noise and improve the data information to estimate the thickness of ice thickness. Figure 223 and Figure 224 show the processed data depicting different glacier sub-surface features at Chhota Shigri and Machoi glacier respectively. Any change in dielectric constant within subsurface medium shows a change in reflection as shown in O-scope of Figure 223. This continuous change in reflection along the bed, which is due to the change in dielectric constant of ice and rock, shows a small dipping bed signature. This change in reflectivity was used to derive the ice thickness information. Vertical resolution at 16 MHz was estimated approximately 2.5 m using pulse width of signal at 16 MHz and velocity of EM waves in glacier ice. GPR profiles have shown the ice thickness varies from 110 m to 150 m at Chota Shigri glacier. An average depth of 130 m using GPR showed the volume of ice approximately 0.0572 km^3 (water equivalent 0.049 km^3) for the surveyed ablation zone section in Chhota Shigri glacier. Non-bed reflection may occur due to the entrained debris layer along a shear plane. A review suggested ice density variations, ice crystallographic anisotropy and chemical variability may also cause internal reflections. Further, a study suggested that during an ablation season, scattering of EM pulses can result from enhanced melting and/or refreezing leading to englacial heterogeneities. Hyperbola shape represents the englacial object signature due to presence of a point source of different dielectric

permittivity like rock. A non-bed reflector was present in profile 3 of survey. There is one vertical structure (possibly crevasse) and in continuation of that melting/refreezing leads to englacial heterogeneities and behaving as different dielectric material. Change in magnitude value (Hilbert transform) clearly shows the presence of subsurface discontinuity, however, phase and frequency (Hilbert transform) could not able to pick up any such variability. Area depth relationship was used to estimate the thickness of glacier (~101 m) using the relationship of Chaohai and Sharma (1988). Total volume of ice and water equivalent of Chhota Shigri glacier was found to be 1.20 and 1.05 km³ respectively.

GPR profile over the ablation zone of Machoi glacier has shown a disturbed subsurface which could be due to the layering of different ice layers. The ice thickness was observed to change from 60 m to 100 m as we move from left to right in upward direction of glacier. A linear bed reflector was also observed in the right side of profile, which may refer to the presence of different lithological layer.

GPR is non-destructive technique which showed potential to estimate ice thickness and identify englacial subsurface features in Chota Shigri and Machoi glacier. A low frequency antenna (16 MHz) was used in the present study and survey have shown that the glacier thickness changed from 110 m to 150 m and from 60 to 100 m as we move upward glacier direction at Chota Shigri and Machoi glaciers. The presence of point reflector (hyperbola signature) and non-bed reflector (due to englacial heterogeneities) could be helpful to understand the subsurface glacier phenomenon. Vertical resolution at 16 MHz was estimated approximately 2.5 m using pulse width of signal and velocity of EM waves in glacier ice. This study presents the application of GPR for ice thickness estimation and identification of subsurface features of glaciers in Himalayan region; however, one has to take care various crucial parameters required for GPR survey especially in Himalayan region.

8.6. Conclusions

GPR is non-destructive technique which showed potential to ice thickness and englacial subsurface features in Chota Shigri glacier. A low frequency antenna (16 MHz) was used in the present study and survey have shown that the glacier thickness changed from 110 m to 150 m across the 400 m profile length as we move towards equilibrium line. Area-depth relationship has shown thickness of glacier ice approximately 101 m averaged over total glacier using Chaohai and Sharma (1988). The presence of point reflector (hyperbola signature) and non-bed reflector (due to englacial heterogeneities) could be helpful to understand the subsurface glacier phenomenon. GPR survey using MLF antenna was also carried out over ablation zone of Machoi glacier in Dras sector, J&K. This study demonstrates and provides an opportunity to develop area-depth relationship for Himalayan region in conjunction with remote sensing based information.

9. Use of Hyperspectral Data for Snowpack Characterization

9.1. Objective

To explore and demonstrate the potential of hyperspectral data for snow pack characterization.

9.2. Scientific Rationale

Hyperspectral imaging is simultaneous acquisition of images in many (usually 100 or more) narrow contiguous spectral bands e.g. Hyperion collects data in 220 channels in spectral range of 400-2500 nm at 10 nm interval or ASD field based spectrometer covers spectral range from 350-2500 nm with 3 nm spectral resolution in VIR and 10 nm spectral resolution in SWIR. Such datasets are extremely useful to develop new algorithms for retrieving various snow and glacier parameters.

Initially, the snow cover mapping process was largely based on the conventional techniques such as manual delineation of snow cover boundaries, segmentation of ratio images and hard or crisp classification. Other analysis techniques such as visual, hybrid (visual and supervised classification) have also been used to estimate the areal extent of snow cover (Kulkarni et al., 2004; Kulkarni et al., 2006b). However, a major difficulty in snow cover monitoring using above techniques is mountain shadow and confusing signature of snow and cloud in the visible and near-infrared region. Because of the above-mentioned reasons, reflectance ratio/index approaches were introduced as they can remove the effects of some sensor radiometric errors and random changes in scene irradiance due to changing effects in the atmosphere and topographical changes across the scene (Dozier, 1989). The spectral region between 350 and 2500 nm is called the reflective part of the spectrum. In the Visible and Near-Infra Red (VNIR) region, the bulk optical properties of ice and water are very similar. This makes reflectance and transmittance of the snowpack depend on the wavelength variation of the refractive index of ice, the grain size distribution of the snow, the depth and density of the snowpack, and the size and amount of those impurities whose refractive indices are substantially different from ice and water (Warren, 1982; Painter and Dozier, 2004). Snow shows very high reflectance in visible region as compared to other objects, this makes appearance of snow as a bright white object on the ground and can be distinctly separated based on its high albedo. However, snow reflectance decreases towards longer wavelength i.e. in NIR and SWIR region (Warren and Wiscombe, 1980; Nolin and Dozier, 1993). Local maxima in the reflectance occur at 1.1, 1.3, 1.8 and 2.2 μm , corresponding to local minima in the absorption coefficient of ice. An approach to estimate spectral reflectance for the Himalayan terrain using the Hyperion data and how it varies by different topography in snow field from Earth

observing-1(EO-1) satellite has been developed. Effect of varying snow physical properties on snow reflectance has also been discussed in the Himalayan region (Singh et al., 2010; 2011, Negi et al., 2006; 2010; 2015; Negi and Kokhanovsky, 2011). It may be seen that large amount of work has been done for snow spectral reflectance studies using the Landsat, AWIFS and other multispectral data sets, however, limited work on use of hyperspectral data for snow pack characterization has been done so far.

9.3. Study Area and Data Used

The study area consists a part of the tributary basin named “Spiti” from the main basin “Satluj”. Spiti basin covers total 597 snow fields which cover an areal extent of 368.37 km² (SAC & MoEF, 2010). Hyperion sensor data onboard NASA’s EO-1 satellite (<http://eo1.usgs.gov>), was selected due to its spatial, spectral and radiometric resolution which is appropriate for Himalayan terrain. Hyperion collects data in 220 unique spectral channels ranging from 357nm to 2576nm with approximately 10 nm bandwidth and 12 bit quantization (EO-1/Hyperion science data user’s guide). The instrument has a spatial resolution of 30m for all bands with the standard swath width 7.7 km. The available data was in 16-bit signed integer radiance values and for each pixel location, 242 spectral channels of 20 data are obtained. Spectral channels from 1–70 are collected from the VNIR and channels 71–242 are collected from the SWIR. Due to low signal for some channels, and to reduce the VNIR-SWIR overlap region, some of these spectral channels are not calibrated. The Uncalibrated channels are set as zero values. The above characteristics of Hyperion sensor provide us to explore the suitable spectral bands for snow study. We have used only the four identified bands of Hyperion data for the snow retrievals i.e. wavelengths 548, 599, 650, and 691 nm. These have corresponding band numbers 20, 25, 30 and 34 for VNIR and wavelengths 1608, 1548, 1648, and 1689 nm have corresponding band numbers 146, 140,150, and 154 for SWIR. One can use the above multi-spectral data easily due to its smaller file size and faster processing in comparison to all 242 bands of hyperspectral data for operational monitoring of snow cover properties.

9.4. Methodology

One of the important concepts in the determination of various objects through remote sensing is that different objects reflect energy differently in various parts of the electromagnetic spectrum. On a satellite image, this reflected energy is normally represented as a binary value, known as digital number (DN) and depends on the calibration parameters and radiometric resolution of the sensor. Whereas the actual spectral reflectance from an object, which is based on fraction of incoming solar radiation, depends on various parameters, such as solar elevation, surface slope and its orientation, surface anisotropy, and atmospheric constituents. Optimum detection of object requires that data be expressed in physical units, such as radiance or

reflectance. Therefore, understanding of the spectral characteristics is necessary for proper interpretation of satellite images. Estimation of reflectance from digital satellite data involves conversion of digital numbers into the radiance values, known as sensor calibration, and then estimation of reflectance from this radiance values. Reflectance also forms an important input in estimating NDSI, which is useful for snow identification under the conditions of cloud cover and mountain shadow. The ENVI v4.4 software was used for the pre-processing of satellite data and atmospheric correction was carried out using Fast Line-of-sight Atmospheric Analysis of Spectral Hypercubes (FLAASH) module based on the MODTRAN-4 radiative transfer code (Figure 225).

In the Himalayan region, during winter time the classification techniques like supervised, unsupervised, etc., are difficult to apply due to mountain shadow and cloud cover (Kulkarni et al., 2002c; 2006b). This problem can be partially solved if the technique based upon the normalized difference snow index (NDSI) is properly developed. The NDSI is estimated for Hyperion sensor data using the following relationship:

$$\text{NDSI} = (\text{Green} - \text{SWIR}) \div (\text{Green} + \text{SWIR})$$

where Green and SWIR are the reflectance of the Green (0.5-0.7 μm) and shortwave infrared (1.5-1.7 μm) bands respectively. Impurities like soil, coal drastically reduces snow reflectance in the visible region. Qualitative and quantitative contamination experiments were planned using these two primary contaminants in the Himalayan region. Numerous avalanche sites exist on Solang-Dhundi route in the Beas basin and disturb the track because of triggering of avalanches during winter period. Snow was qualitatively categorized into clean, low, medium and high contaminated snow under natural conditions. In quantitative experiments, soil and coal contaminants were used in varying quantities under two set of experiments. Study area has minimum human interference to avoid any other environmental effect during the experiments. Position, strength and shape of a spectral curve can provide the information on smoothly varying spectral properties. Relative strength, width and asymmetry of the absorption feature were computed after continuum removal for different wavelength region. Continuum removal isolates the properties of the absorption features from the overall reflectance properties. Continuum depth removal was carried out for varying grain size, contaminated snow (qualitative and quantitative) and metamorphic snow (dry, moist and wet) with respect to the moisture content. Band shape and width of the absorption peak was also estimated. The atmospheric corrected reflectance data was an input to Spectral Hour Glass (SHG) module for the analysis which performs Minimum Noise Fraction (MNF), Data Dimensionality Analysis, End Member selection and Spectral Angle Mapper (SAM) functions.

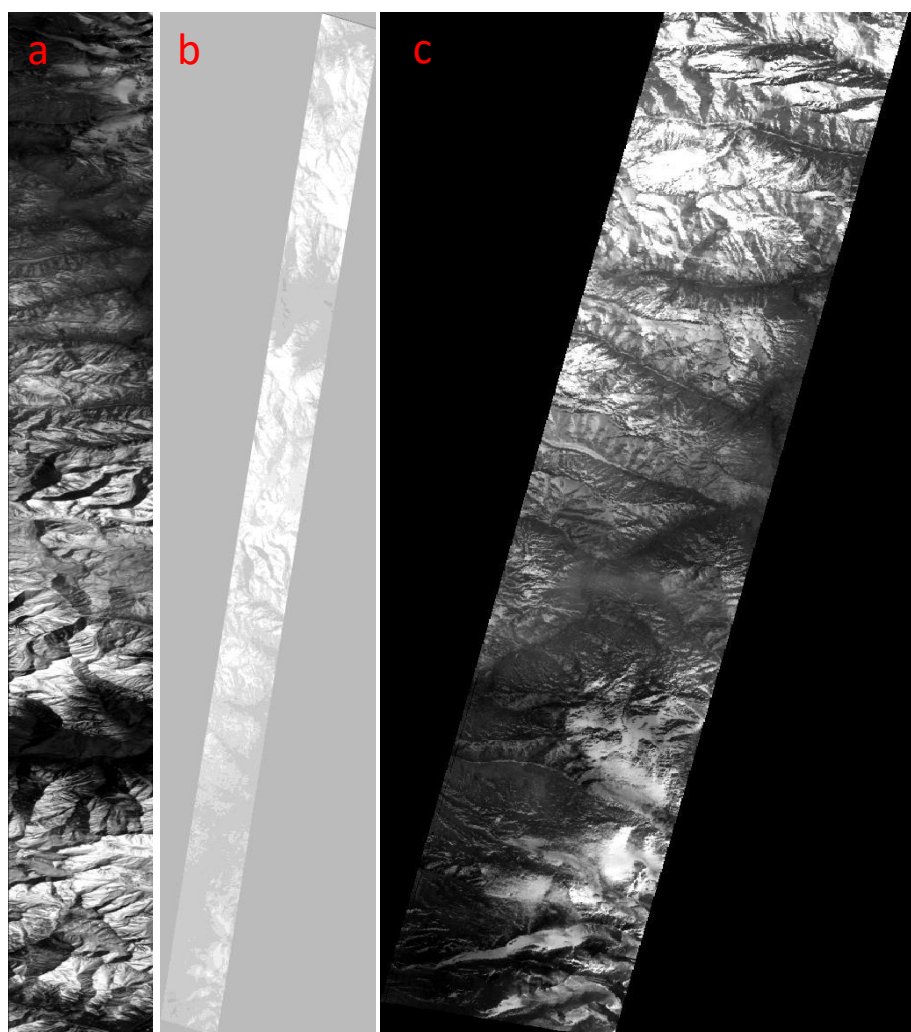


Figure 225: (a) Hyperion total scene in gray scale (b) Geo corrected study area in gray scale (c) Subset geo corrected over study area in gray scale

9.5. Results and Discussion

i) Estimation of NDSI

An image of winter month has been selected to perform NDSI analysis. To estimate the NDSI, 4 wavelength channels (548, 1608), (599, 1548), (650, 1648) and (691, 1689) nm have been taken into consideration. The threshold has been selected based on manual exercise and AWiFS snow product. The major difficulty in the study was to confirm/set a threshold value of NDSI, so that the above model can classify correctly a pixel as snow or non-snow pixel. NDSI could better identify a snow pixel especially in case of shadow due to diffuse radiation which is otherwise difficult to locate manually. NDSI threshold (0.25-0.3) is used for mapping of snow cover above which all pixel will be assigned as a snow pixel. To accurately estimate the threshold value we have taken a comparative analysis of snow cover area (%) for different band ratios and the snow covered area by unsupervised classification. For identifying a pixel as a snow pixel (by NDSI threshold), the range of the percentage snow covered area by

the unsupervised classification (threshold by default=0.968) and by different NDSI thresholds for different wavelengths has been analyzed (Figure 226). It was also compared with the AWIFS data for the same region. The highlight areas (bold) in Table 81 are the matching with unsupervised classification and with AWIFS data, and a threshold value of 0.28 was found to classify snow for all combinations.

Table 81: NDSI threshold and snow cover area for different spectral ratios

R1(548,1608 nm)		R2(599,1548 nm)		R3(650,1648 nm)		R4(691,1689 nm)	
NDSI threshold	Area (sq km)						
0.00	251.25	0.00	266.82	0.00	264.54	0.00	267.36
0.05	241.39	0.05	260.19	0.05	257.30	0.05	259.48
0.10	228.24	0.10	252.85	0.10	247.55	0.10	250.09
0.15	210.98	0.15	242.91	0.15	232.70	0.15	236.17
0.20	192.71	0.20	228.59	0.20	212.33	0.20	215.50
0.25	175.66	0.25	210.25	0.25	191.03	0.25	192.56
0.30	159.04	0.30	191.48	0.30	170.99	0.30	170.72
0.35	143.62	0.35	173.54	0.35	152.12	0.35	150.68
0.40	129.54	0.40	156.24	0.40	135.09	0.40	132.95
0.45	115.85	0.45	140.82	0.45	119.33	0.45	116.14
0.50	101.97	0.50	126.12	0.50	103.80	0.50	99.48
0.55	87.96	0.55	111.86	0.55	88.08	0.55	82.32
0.60	73.30	0.60	97.11	0.60	71.32	0.60	63.33
0.65	56.63	0.65	82.15	0.65	52.54	0.65	41.93
0.70	38.56	0.70	65.89	0.70	31.79	0.70	18.63
0.75	18.71	0.75	47.32	0.75	11.30	0.75	3.22

ii) Snowpack characterization using Hyperspectral data:

Snow reflectance depends on contaminants, grain size and thickness of snow (Figure 227). Snow was categorized into three types of grain as fine, medium and coarse based on crystal gauge observations. NIR bands centered at 1025 nm and 1350 nm shows a reduction in reflectance of approximately 28% with an increase in grain size. SWIR bands show the reduction in reflectance of 8% for finer grain to coarser grain snow. Clean snow gets qualitatively contaminated; reflectance substantially drops in visible region i.e. up to 70 % in blue region from light to heavily contamination. A shift of peak towards longer wavelength (from 575 nm to 735 nm) has also been observed in visible region as the amount of contamination increases in snow. It was also observed that as contamination increases, depth of absorption peak at 1025 nm is influenced.

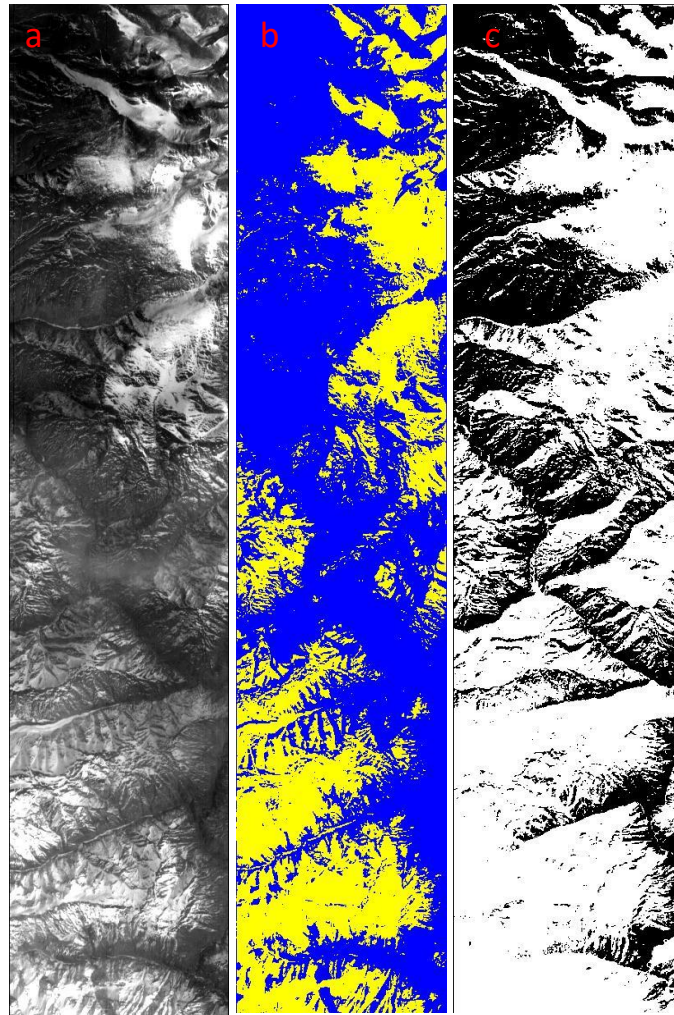


Figure 226: a) Hyperion data of study area in gray scale b) Unsupervised classification of the study area (threshold by default=0.9681) G=snow, B=non-snow c) Best classified threshold (=0.28) among all four band ratios (for Ratio 4)

Depth of absorption peak was computed using continuum depth approach. Estimation of continuum depth brings out all observations at same platform and could able to pick up the change in depth of absorption peak due to varying snow physical properties (Figure 227). The relative strength at 1025 nm, after continuum removal, has shown a decreasing trend for quantitative amount of contamination whereas a reverse pattern of increasing relative strength was observed for grain size (Figure 228).

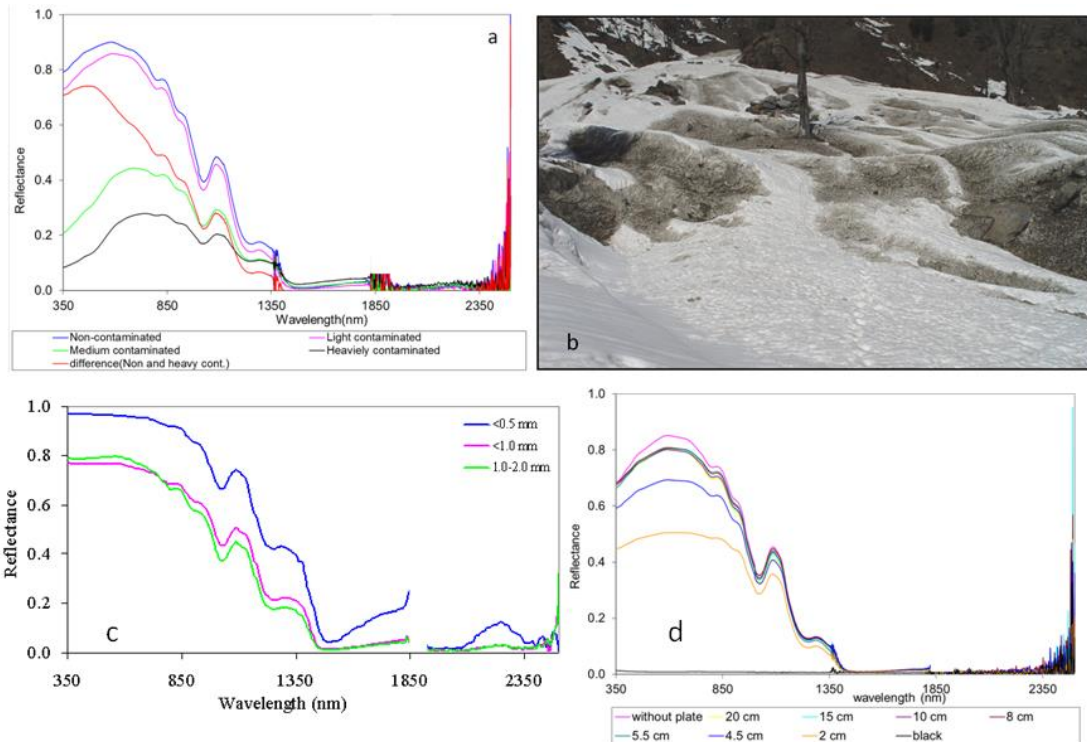


Figure 227: Influence of a&b) contamination; c) grain size and d) optical depth on snow reflectance

It has been observed that as the level of contamination increases, the albedo has been found to be decreasing. Albedo value has been found to be reduced by ~12 % from fine to medium grain size. Present study shows the influence of snow physical properties on snow reflectance and demonstrates the potential of hyperspectral data over multispectral remote sensing to improve our understanding. Reflectance characteristics (in the form of spectral library), hyperspectral analysis (continuum depth, asymmetry, first derivative, peak shift, image processing tools and statistical methods) along with better availability of temporal satellite based hyperspectral data can address the hydrological and climatic applications (like contamination, grain size etc.) for better understanding of climate in snow covered areas of the Himalayan region. This understanding of hyperspectral observations was implemented to classify the hyperspectral satellite data over Himalayan region. Hyperion scene (21 March 2006) of the Himalayan region was atmospherically corrected using FLAASH algorithm and Spectral Hour Glass (SHG) was used to classify the snow. Field based reflectance data was used to select End Members and to classify space based hyperspectral data using Spectral Angle Mapper (SAM) approach in Himalayan region. This study shows the utilization of field and satellite based hyperspectral data analysis in the Himalayan region and demonstrates the possibility of retrieval of snow physical parameters (Figure 229). Continuum depth of moist snow was observed to be 0.70 which increased to 0.52 for wet snow due to variations in grain size.

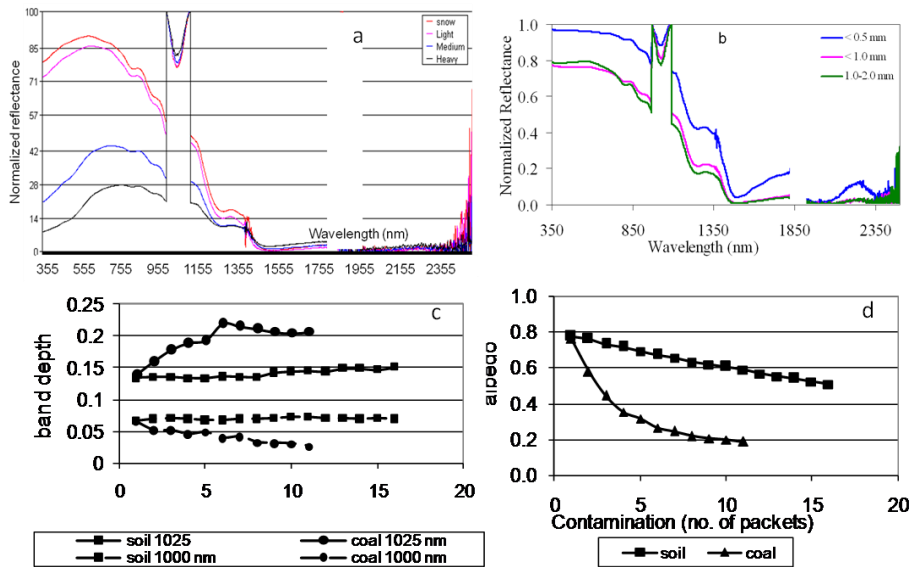


Figure 228: Continuum removal of a) contaminated snow and b) grain size. Estimation of c) band depth and d) albedo for different contamination levels (Source: modified after Singh et al., 2011)

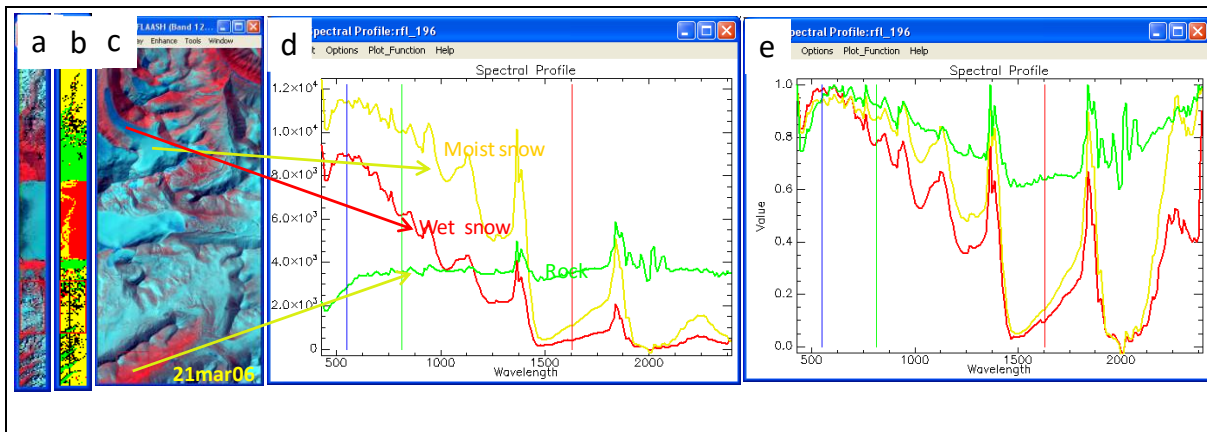


Figure 229: a- Hyperion image; b- Classified output using SAM; c- subset of a; d- Reflectance spectra of objects; e- continuum depth of reflectance spectra

9.5.1. Conclusions

Present study shows the influence of snow physical properties on snow reflectance and demonstrates the potential of hyperspectral data over multispectral remote sensing to improve our understanding. Hyperion data was used for different band combination to evaluate the NDSI to identify snow pixel. It was observed that in four identified ratio, a threshold value of 0.28 was found suitable to identify snow pixel which was also observed to match with unsupervised classification and AWiFS snow product. However, a saturation problem in visible region was also noticed which could be due to calibration issue of sensor. Hyperspectral data also play a crucial role in

snowpack characterization. A increase in continuum depth from moist snow to wet snow was found in field data which was also observed in Hyperion scene in the Himalayan region. Reflectance characteristics (in the form of spectral library), hyperspectral analysis (continuum depth, asymmetry, first derivative, peak shift, image processing tools and statistical methods) along with better availability of temporal satellite based hyperspectral data can address the hydrological and climatic applications (like contamination, grain size etc.) for better understanding of climate in snow covered areas of the Himalayan region. With the planned future missions and improved advanced image processing techniques, space borne hyperspectral data availability will definitely address many issue of Himalayan Cryosphere to improve our understanding for hydrologic and climate applications.

10. Use of SAR Interferometry and Photogrammetry in Glacier Flow Determination and Glacier Mass Balance

10.1. Objective

To use SAR interferometry and photogrammetry techniques in glacier mass balance, glacier velocity and glacier ice thickness estimation.

10.2. Scientific Rationale

Digital Elevation Models (DEMs) can be produced by photogrammetric, interferometric, GPS and digitization of topographic maps based techniques. DEM are extremely useful for deriving various useful parameters for glacier studies. Satellite images combined with DEMs in a GIS provide glacier parameters such as length, termini elevations, median elevations, Equilibrium Line Altitudes (ELA), hypsometry maps, time sequential glacier flow patterns, glacier divides or basin boundaries, glacier outlines etc. DEMs can be used to generate orthoimages particularly for mountainous region where relief distortion is high and thus facilitating quantitative analysis of morphology. The accuracy of DEMs are governed by many factors depending upon the source of DEM. For example, the DEMs derived from optical stereo data depend on accuracy of GCPs, B/H ratio of stereo pair, DEM interpolation algorithms and Image matching algorithms. Synthetic Aperture Radar (SAR) data used in repeat pass interferometric mode, along with its associated signal processing, termed "InSAR", has proven to be extremely useful for estimating topography or displacements of the earth's surface. By measuring the phase differences between two co-registered SAR images, taken with a time lapse and/or a slightly different viewing angle of the sensor, repeat-pass InSAR has been used to generate interferograms and subsequently Digital Elevation Models (DEMs) of the earth's surface. Differencing of the time sequential interferograms known as Differential SAR Interferometry (D-InSAR) is useful to measure surface deformation to millimeter level accuracy. The accuracy of DEM derived from SAR interferometric techniques depends on wavelength, look angle surface roughness and pair of interferometric SAR. Some of the satellite derived DEM widely used are TanDEM-X, SRTM, SPOT5, ASTER, CORONA, ALOS PRISM, CARTOSAT etc.

Suitability of the SRTM DEM and ASTER GDEM for the compilation of topographic parameters in glacier inventories has been assessed (Frey and Paul, 2012). Glacier surface velocity estimation using SAR interferometry technique applying ascending and descending passes in Himalayas has been demonstrated (Kumar et al., 2011). Ice thickness of Gangotri glacier using surface velocities and slope could be estimated

(Gantayat et al., 2014). Elevation changes of glaciers were studied using multitemporal digital elevation models (1992-2008) calibrated by GPS survey in the Khumbu region, Nepal Himalayas (Nuimura et al., 2012). Multi-temporal digital terrain model of the Mt. Everest area from different optical sensors were generated and evaluated (Pieczonka et al., 2011). Bias correction of CartoDEM using IcesatGlas data was done (Rastogi et al., 2015). SAR interferometry and offset tracking approaches for glacier movement estimation in the Himalaya have been attempted (Vijay Kumar et al., 2011).

In absence of direct field measurements, mass balance can be estimated using an indirect method (“geodetic method”) which involves measuring elevation changes over time from various multi-temporal Digital Elevation Models (DEMs) constructed over the glacier surface. Elevations from older DEMs are subtracted from recent DEMs either on a pixel by pixel basis or as average elevation change to obtain elevation difference maps. If elevation changes are computed pixel-by-pixel basis, the elevation difference are multiplied by the pixel area to give the volumetric changes per pixel. If elevation differences are computed over the whole glacier surface, the average elevation change is multiplied with the glacier area to obtain the overall change in volume. The volume change is translated into mass balance change by multiplication with the density of glacier ice. This method yields the changes in the average mass balance expressed as meters water equivalent over the time period considered (Racoviteanu et al., 2008). The geodetic approach has been used in several studies (Surazakov and Aizen, 2006; Surazakov et al., 2007; Narama et al., 2007; Berthier et al., 2004, 2006, 2007; Kaab et al., 2003; Kaab, 2007; Kaab et al., 2012; Kaab et al., 2014; Bahuguna et al., 2004, 2007; Racoviteanu et al., 2007; Rivera and Casassa, 1999; Dedieu et al., 2003; Rabatel et al., 2005; 2008; Hagg et al., 2004; Bolch et al., 2011a; Frey et al., 2013). Bahuguna et al., (2004) attempted to study variations in the glacier extent over a period of time using Digital Elevation Model (DEM) and orthoimages derived from IRS-IC PAN stereo pairs of 1997-98 and topographical map surveyed during 1962-63 in the Janapa Garang and Shaune Garang glaciers of the Baspa basin, India. The Janapa garang and the Shaune garang are observed to have retreat of 596 m and 923 m respectively. Studies carried out by Berthier et al., 2007 for estimating mass balance changes in glaciers covering parts of the Himachal Pradesh in Indian Himalaya using DEMs from 2004 SPOT5 and 2000 SRTM showed significant thinning of the glacier surface of -8 to -10 m at lower elevations including debris-cover tongues, and less thinning in the upper part of the glacier (-2m). The mass calculation values were within the range of field-based mass balance measurements for the same period in the Lahaul-Spiti region (Wagnon et al., 2007).

The remote sensing geodetic method can be utilized to validate other methods of mass balance estimation, with the advantage of being fast and easy to apply. However, it is limited to estimation of mass balance at decadal scales. The accuracy of the geodetic-based mass balance estimation is highly dependent on: i) the interpolation method used to derive a DEM from digitized contour or GPS measurements; ii) errors

introduced by any change in spatial resolution (downscaling or upscaling) used to match various DEMs; iii) biases inherent in the remote sensing-derived DEMs, such as elevation and slope biases; iv) assumptions about the density of the lost or gained mass; v) time of imaging e.g., DEM should be generated for ablation season only. Errors in the source DEMs propagate with each arithmetic operation performed, and may introduce large errors in the output mass balance estimations, necessitating a careful evaluation or validation. Due to these large uncertainties, currently the geodetic method should only be applied for estimating changes in glacier surface and mass balance at decadal or longer time scale (Racoviteanu et al., 2008).

Two of the major parameters used to characterize glacier dynamics are surface velocity and ice thickness. Glacier surface ice velocity can be estimated from satellite data using SAR interferometry, SAR image data intensity tracking or feature tracking from optical data. Although SAR interferometry is a widely used technique for deformation and velocity mapping, it has limitations in highly rugged terrains like the Himalaya and especially for fast-moving glaciers. The visibility of the target glacier is affected in such rugged terrain conditions due to oblique viewing SAR images. Further, high incidence angle requires accurate Digital Elevation Models (DEMs) to correctly orthorectify the measurements. Optical image correlation is another promising technique used to deduce deformation or displacement of a moving object. The principle involved in this technique is that two images acquired at different times are correlated to find out the shift in position of any moving object, which is then treated as displacement in this time interval. Coregistration of Optically Sensed Images and Correlation (COSI-Corr) technique permits remote detection of deformation on the Earth's surface by comparing pairs of optical satellite images acquired on different dates. COSI-Corr technique can map the horizontal component of deformation by sub-pixel correlation of optical images. This technique involves precise image registration, orthorectification and correlation, allowing for the pair wise coregistration with a 1/50 pixel accuracy leading to measurement of horizontal offset with an accuracy on the order of 1/20 of the pixel size. COSI-Corr technique has been utilized for glacier velocity estimation by various investigators (Berthier et al., 2005; Kaab et al., 2003; Kaab, 2005; Scambos et al., 1992; Scherler et al., 2008; Leprince et al., 2008; Tiwari et al., 2014). Tiwari et al., 2014 studied the surface ice velocity of the Chhota-Shigri glacier, Himachal Pradesh by applying sub-pixel image correlation technique (COSI-Corr software of ENVI) on the ASTER time series data (2003–2009). The remote sensing-derived measurements are found to match quite well with the field measurements. In general, the surface ice velocity varies from ~20 m/yr to ~40 m/yr. Velocity variations occur in different parts of the glacier and also from year to year. In all the years considered for this glacier, the mid-ablation zone and the accumulation zone exhibit higher velocities and zones near the snout and equilibrium line altitude have relatively lower velocities. Further, the velocities are found to be relatively higher in the years 2005–2006 and 2007–2008 and lower in the years 2006–2007 and 2008–2009 (Tiwari et al., 2014).

Glacier ice thickness is estimated using laminar ice flow model in which the retrieved surface ice velocity is used as an input. Gantayat et al., 2014 estimated the distribution of ice thickness for a Himalayan glacier using surface velocities, slope and the ice flow law. Surface velocities over Gangotri Glacier were estimated using sub-pixel correlation of Landsat TM and ETM+ imagery. Velocities range from ~ 14–85 m a⁻¹ in the accumulation region to ~20–30 m a⁻¹ near the snout. Depth profiles were calculated using the equation of laminar flow. Thickness varies from ~ 540 m in the upper reaches to ~ 50–60 m near the snout. The volume of the glacier is estimated to be 23.2 ±4.2 km³.

In the present section few case studies related to geodetic mass balance estimation using DEM differencing approach, glacier velocity estimation using COSI-Corr technique and subsequently glacier ice thickness estimation using laminar ice flow model are described.

10.3. Results and Discussion

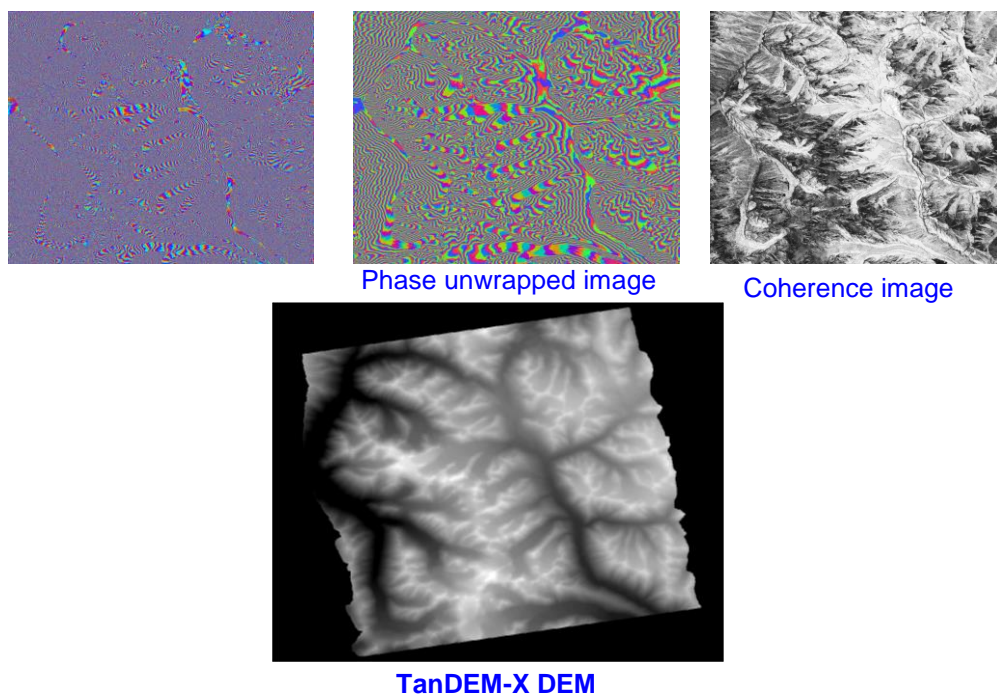
i) Estimation of changes in glacier mass balance using SRTM and TanDEM-X DEM for time frame 2000 - 2011

A procedure of calculating elevation changes on glacier surfaces was demonstrated by generating TanDEM-X DEM (2011) using the standard InSAR technique for parts of Bhaga sub-basin in Himachal Pradesh and subtracting from SRTM DEM (2000). Ten glaciers were studied. A total of about 60.97 km² glacier area has been evaluated for elevation, volume and mass change between 2000 and 2011.

Co-registered TanDEM-X pairs were used to generate TanDEM-X DEM with the help of standard InSAR technique (Figure 230). Evaluation module of SARscape software is used. The generation of DEM consists of following steps:

- Interferogram generation
- Phase unwrapping
- Phase to height conversion
- Geocoding

Figure 231 shows the flow diagram of the various steps followed in finding difference of elevations using two sources of DEMs.



5

Figure 230: DEM generated using TanDEM SAR data

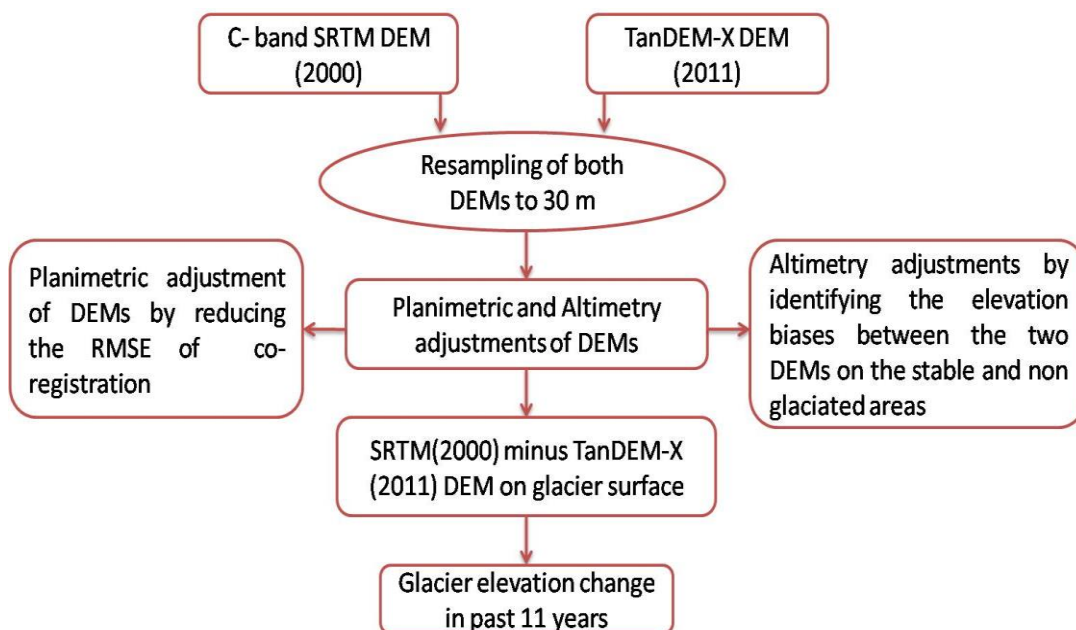


Figure 231: Procedure of calculating elevation changes on glacier surfaces

Change in elevation of 10 glaciers was computed by subtracting TanDEM-X DEM (2011) from SRTM DEM (2000). The glacier is divided into three parts as Terminus, Ablation and Accumulation. Depending on the glacier size, more than 2000 points

were taken from each part for estimation of change. The average elevation changes for each part then considered as the total elevation change for entire glacier.

Change in surface elevation, volume and mass balance was derived for 10 glaciers covering 60.97 km² area. The corrections were applied related to snow cover during 2000. Then slope corrections on SRTM were applied. The elevation profiles show the difference in elevation of glaciers along the central line. Over the last 11 years the glaciers of Bhaga basin display significant decrease in surface elevation and thinning. Figure 232 to 241 show the surface elevation changes observed on the area of glaciers. The average thinning for the total 60.97 km² glacier area of the 10 glaciers studied in the Bhaga basin is 4.37 m in the last decade with a loss of about 0.20 km³ volume of ice. Three glacier zones as Terminus, Ablation zone and accumulation zone are considered for the observation of the thickness change of glaciers of Bhaga basin. The average elevation changes for each zone are then considered as the total elevation change for entire glacier. The thickness change is multiplied with the glacier area to obtain volume change. It is estimated that the total volume loss in the Bhaga sub-basin is 0.2060 km³ during the time frame 2000 – 2011. The volume change is multiplied by the density of ice i.e. 900 kg m³ to estimate the geodetic mass balance. The estimated mean geodetic mass balance is -0.27 m we/year for the 11 years period of investigation.

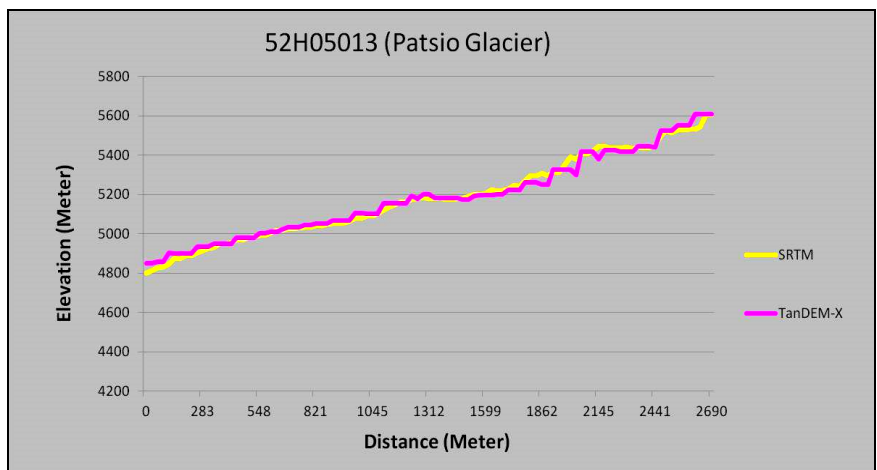
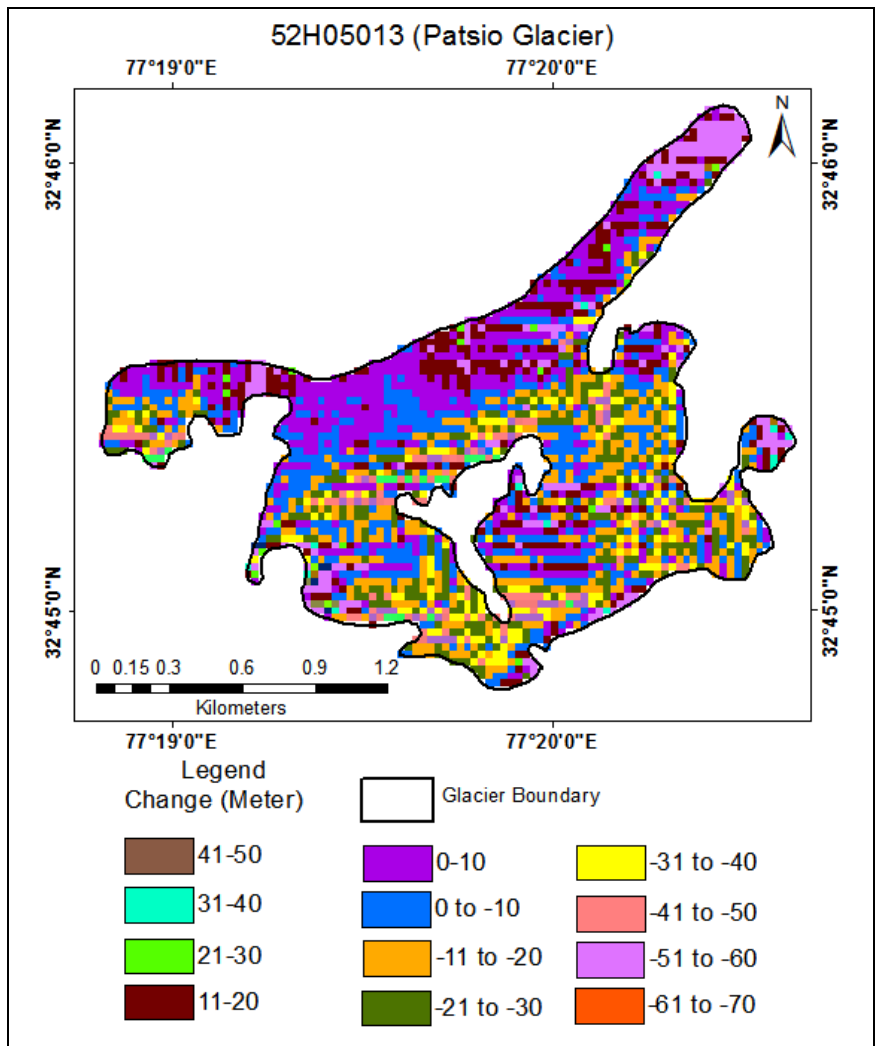


Figure 232: Map of Patsio glacier showing change in elevation (top) and corresponding curves showing difference in elevation along the profile of glacier (bottom)

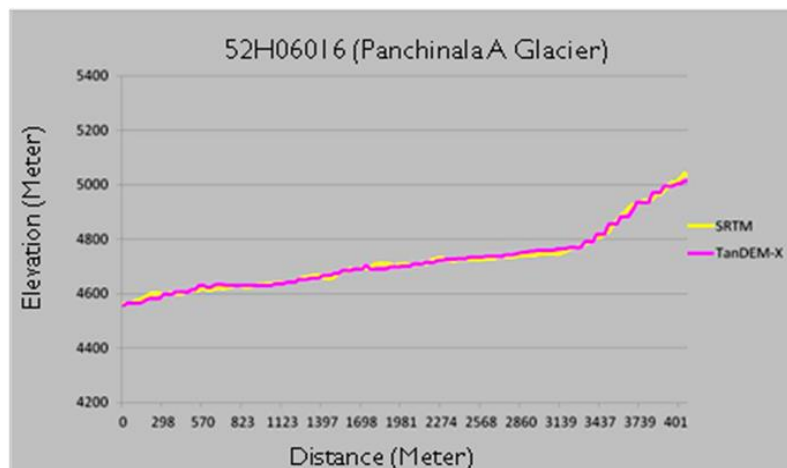
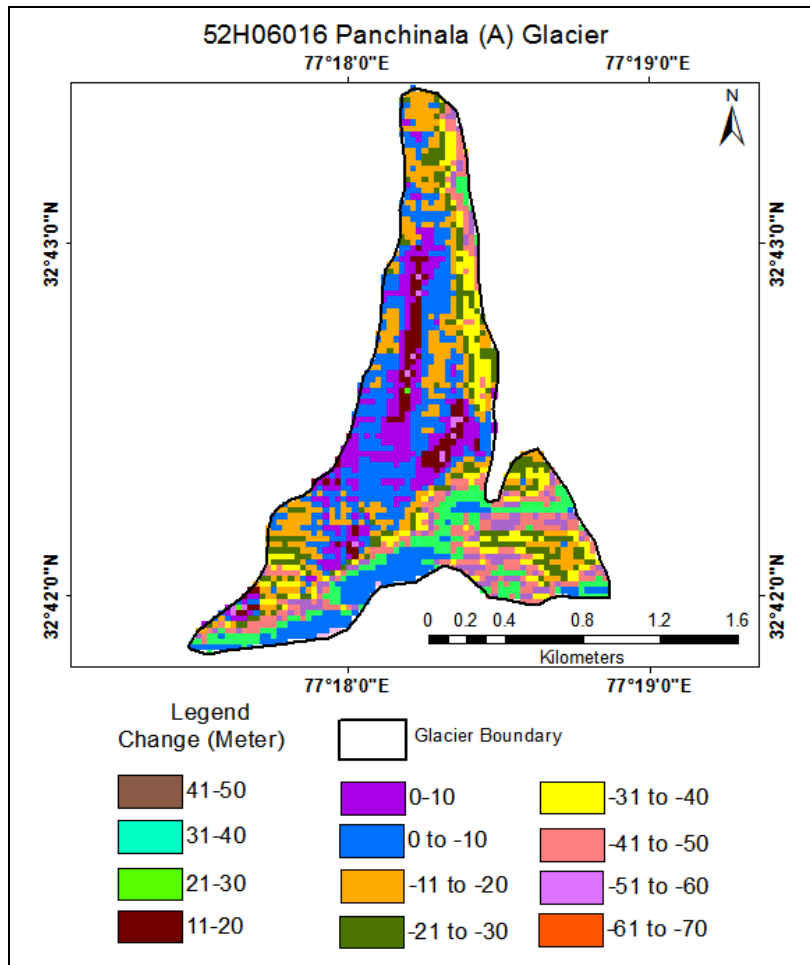


Figure 233: Map of Panchinala A glacier showing change in elevation (top) and corresponding curves showing difference in elevation along the profile of glacier(bottom)

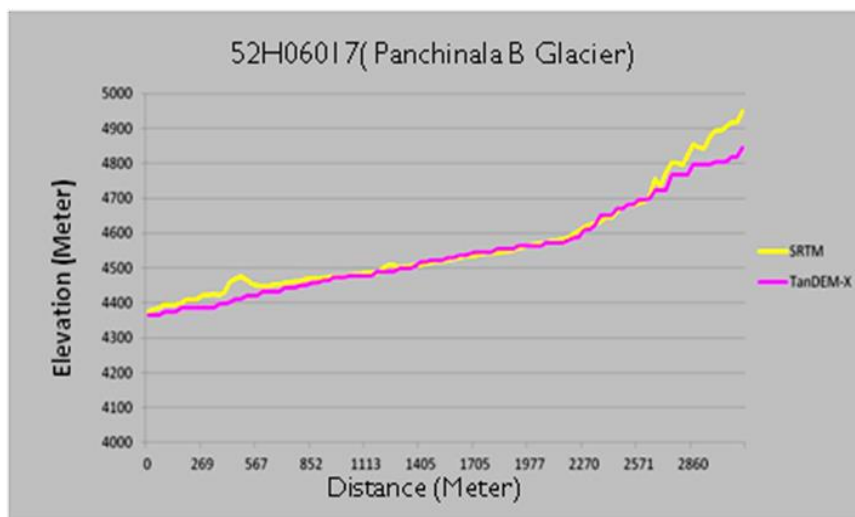
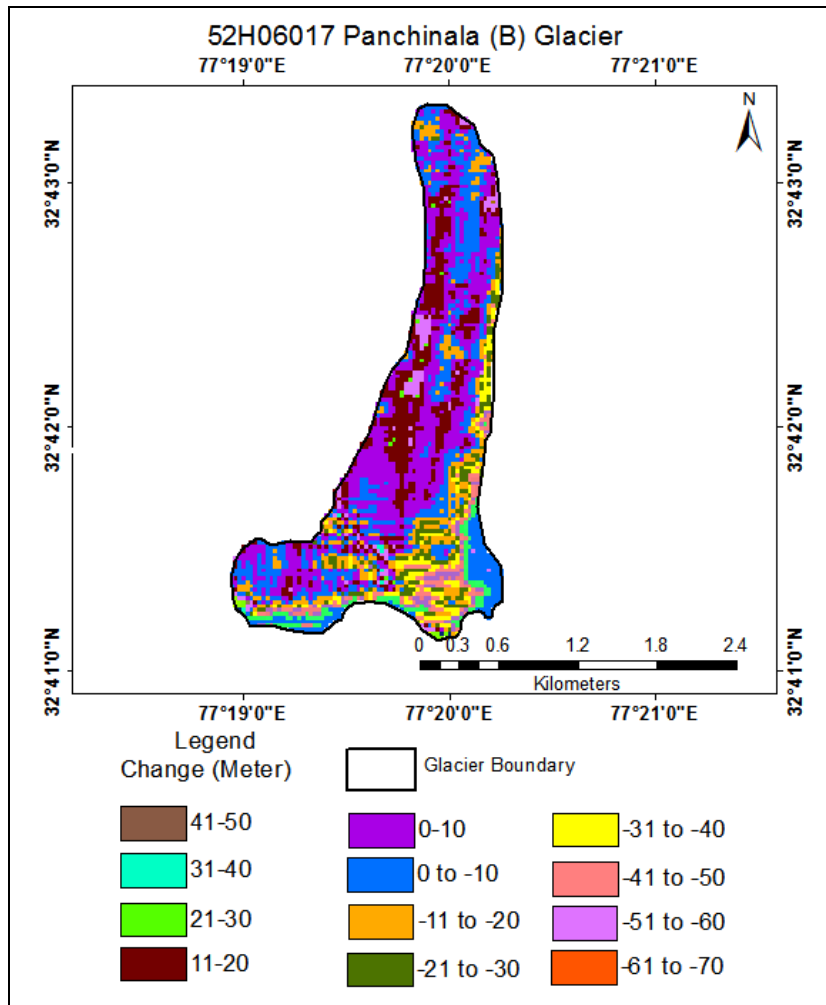


Figure 234: Map corresponding curves showing difference in elevation along the profile of glacier(bottom)of Panchinala B glacier showing change in elevation (top) and

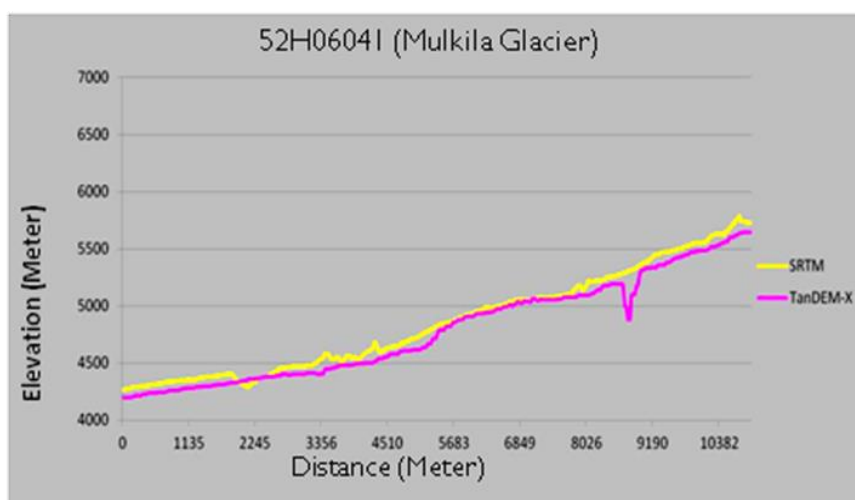
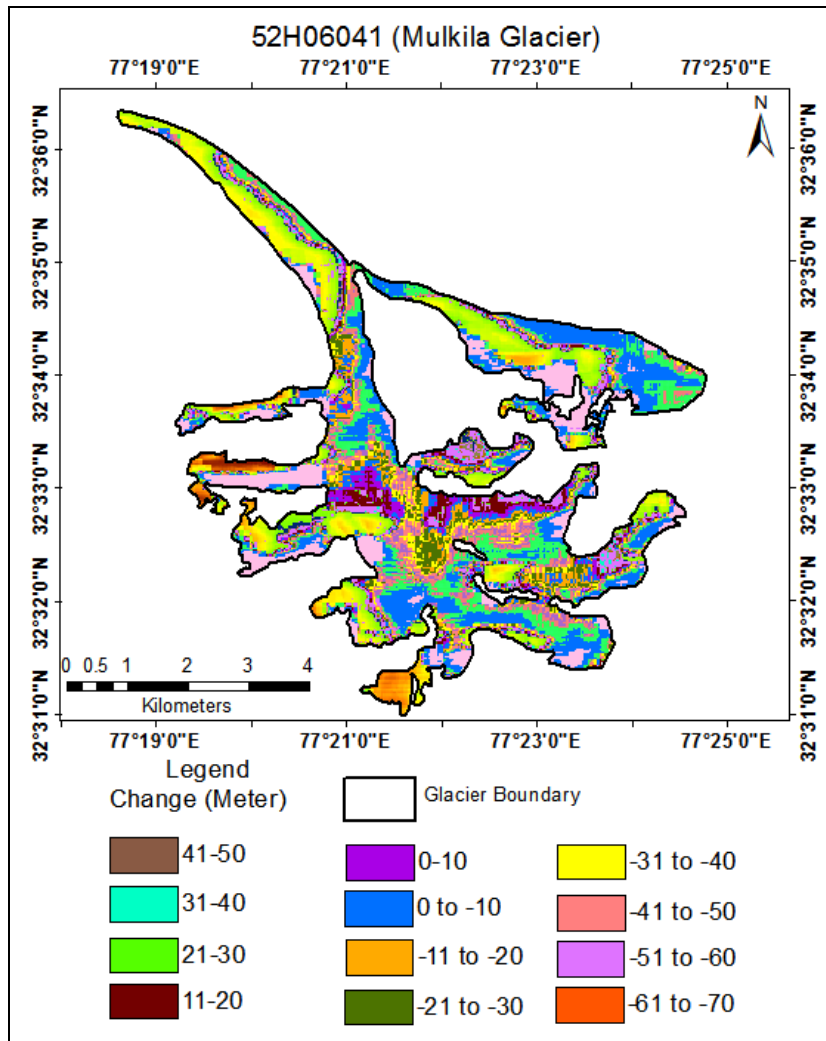


Figure 235: Map of Mulkila glacier showing change in elevation (top) and corresponding curves showing difference in elevation along the profile of glacier(bottom)

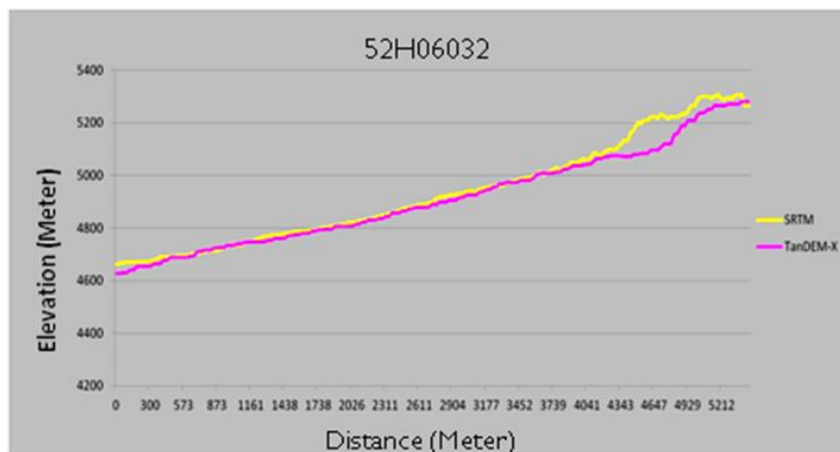
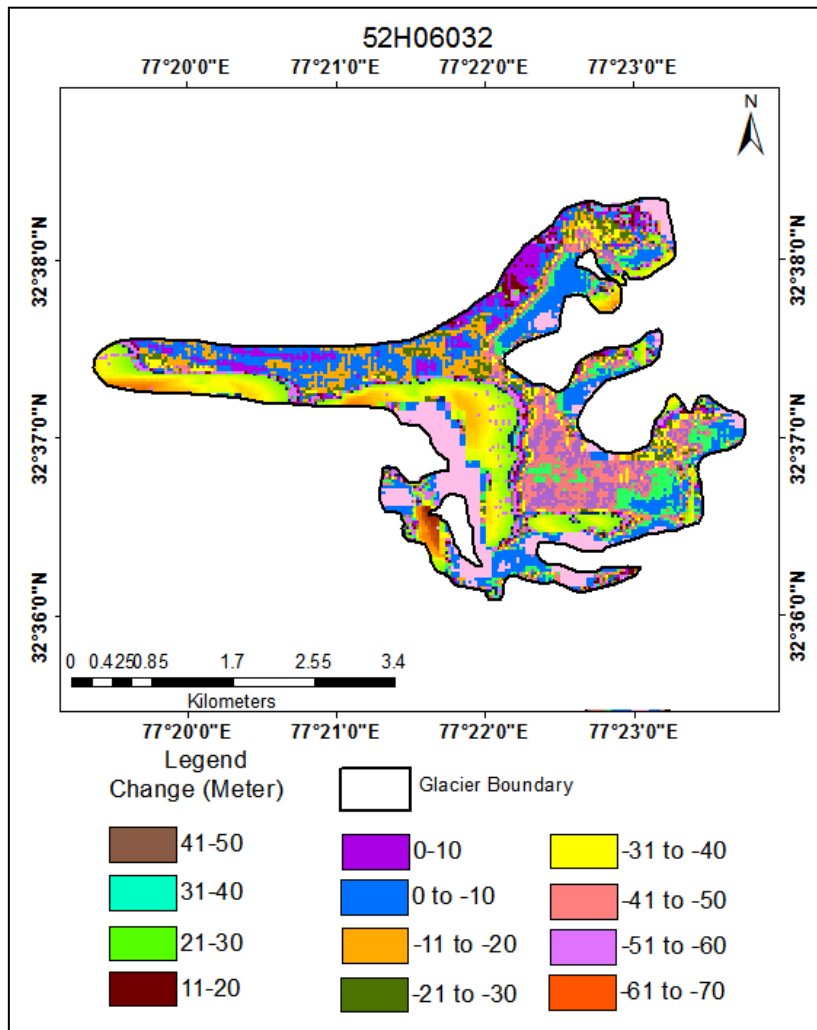


Figure 236: Map of glacier 52H06032 showing change in elevation (top) and corresponding curves showing difference in elevation along the profile of glacier(bottom)

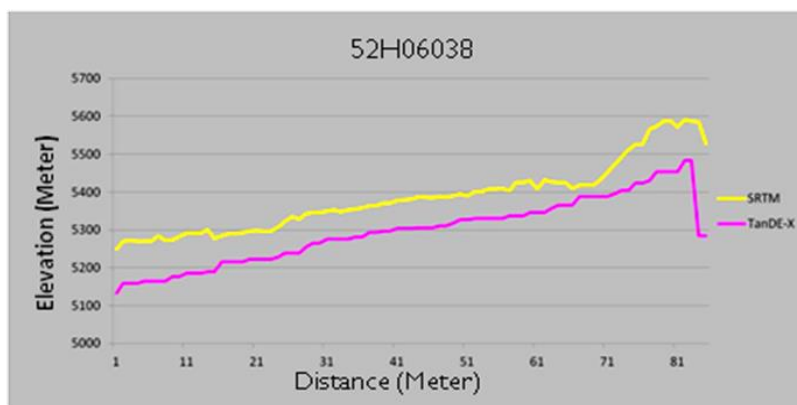
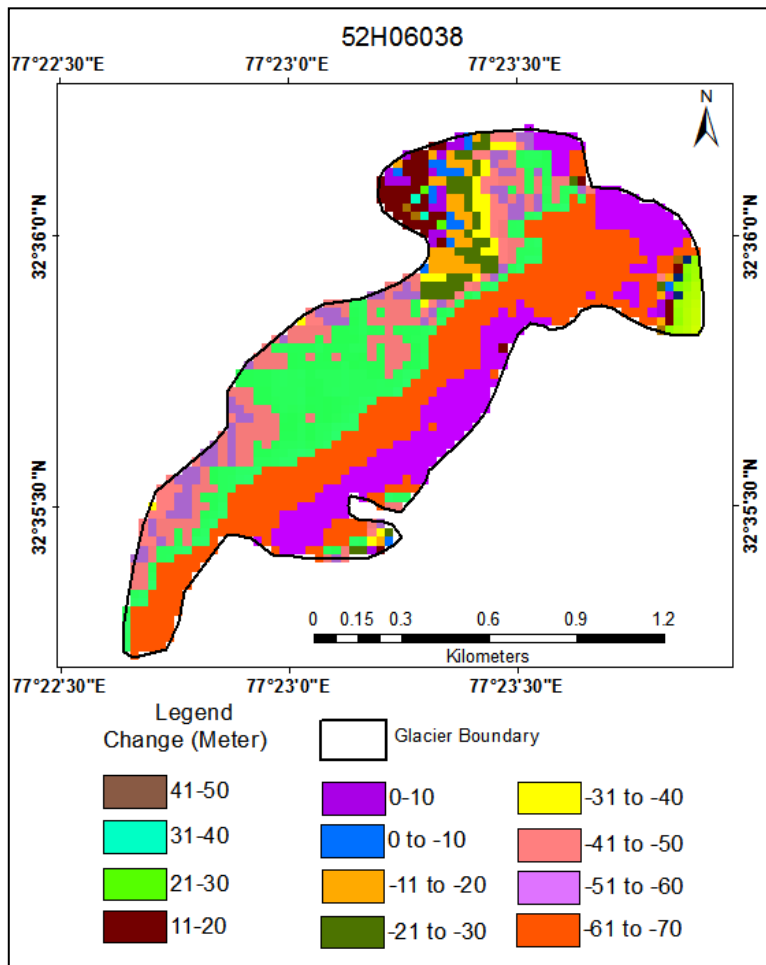


Figure 237: Map of glacier 52H06038 showing change in elevation (top) and corresponding curves showing difference in elevation along the profile of glacier(bottom)

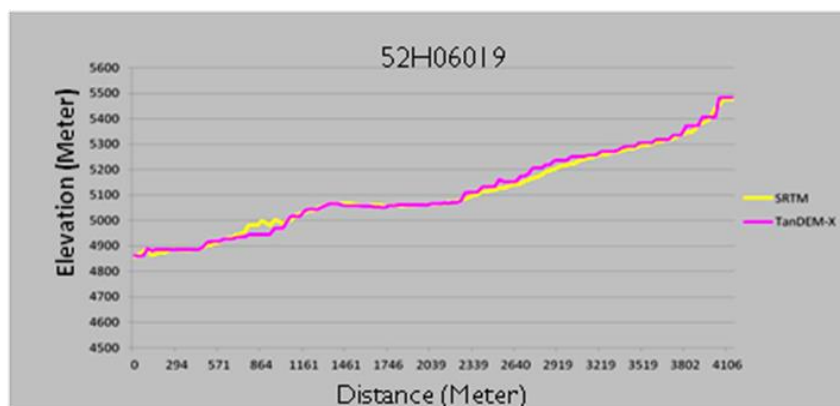
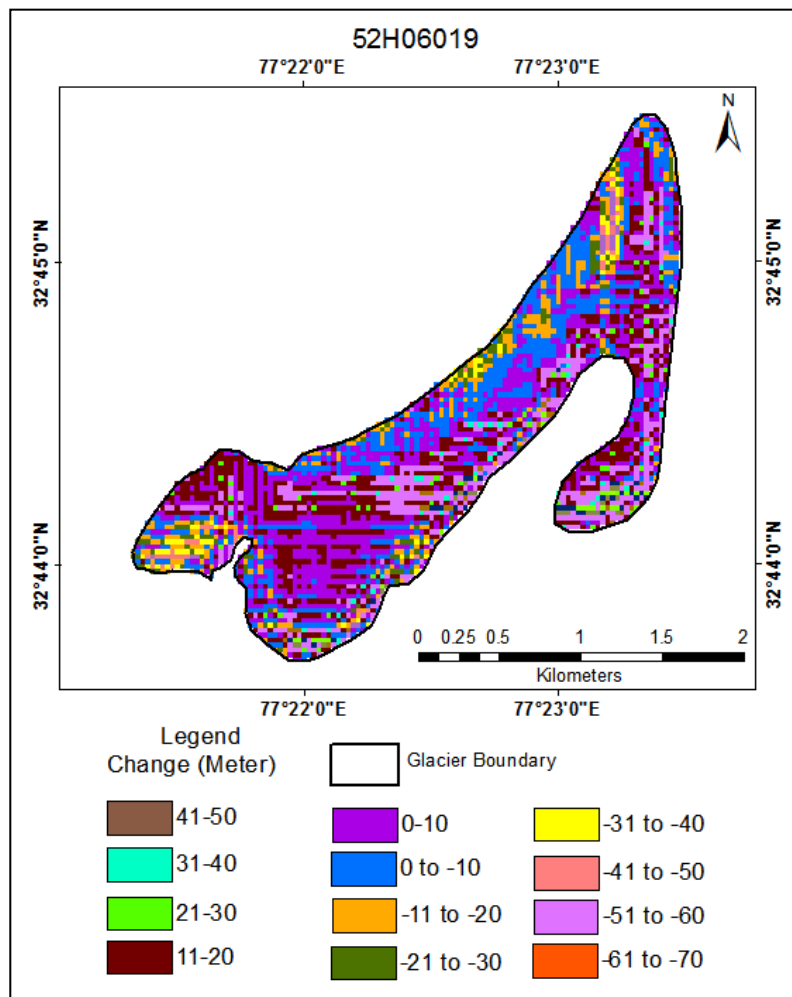


Figure 238: Map of glacier 52H06019 showing change in elevation (top) and corresponding curves showing difference in elevation along the profile of glacier(bottom)

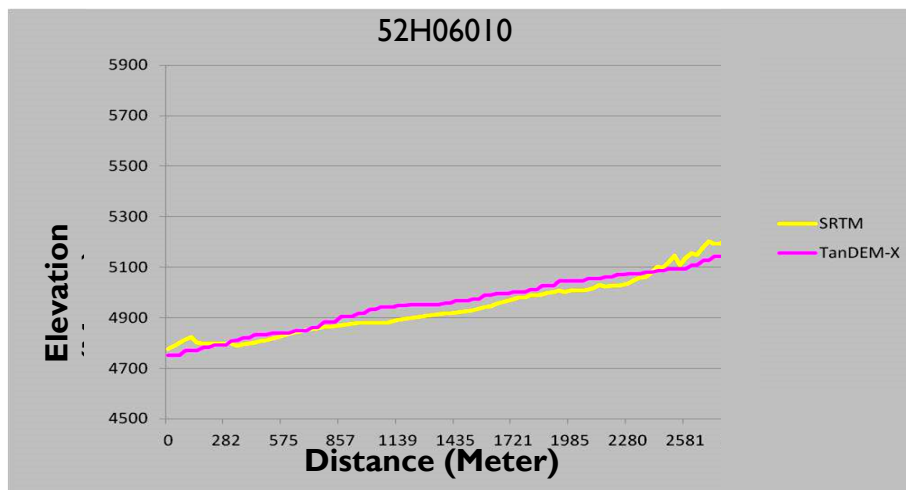
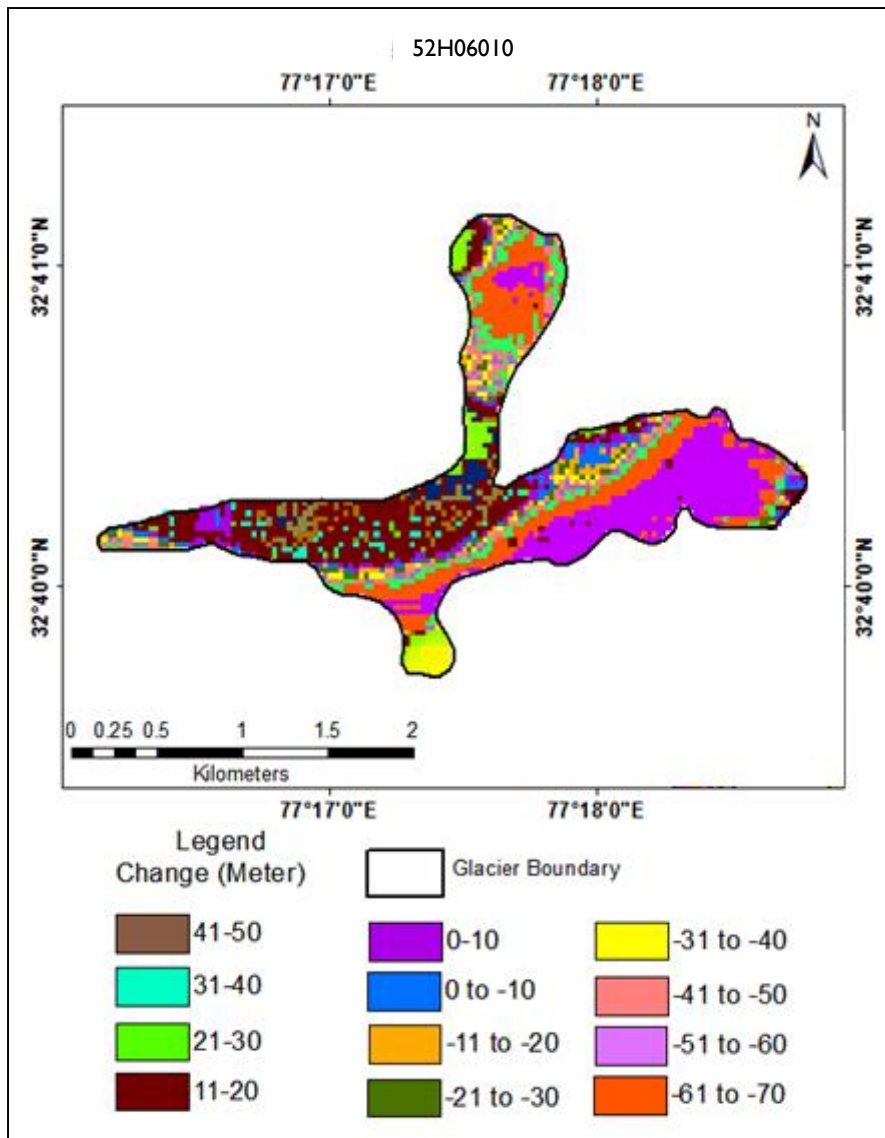


Figure 239: Map of glacier 52H06010 showing change in elevation (top) and corresponding curves showing difference in elevation along the profile of glacier(bottom)

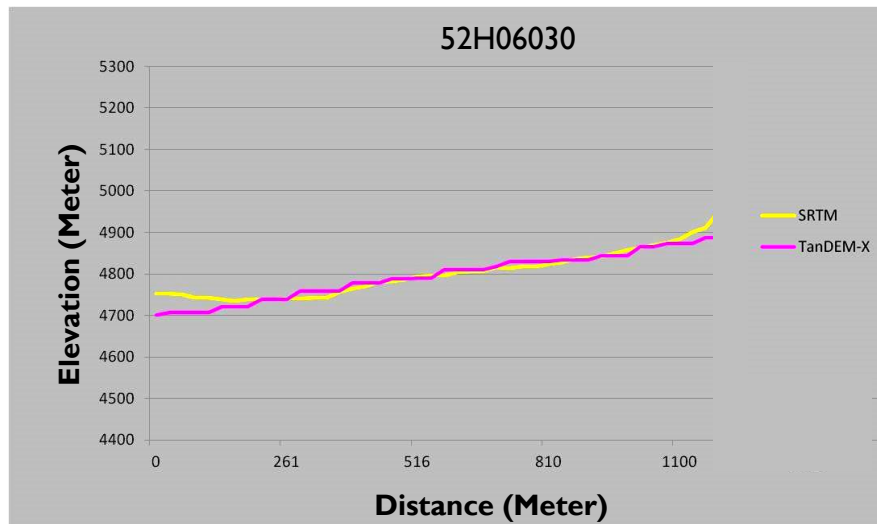
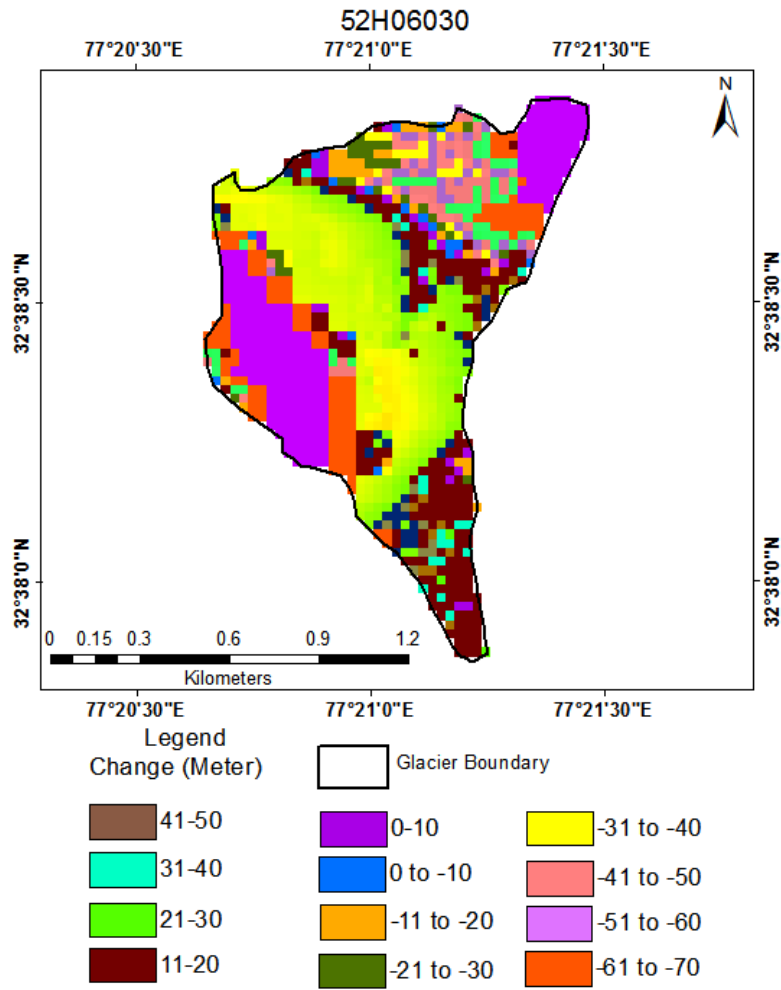


Figure 240: Map of glacier 52H06030 showing change in elevation (top) and corresponding curves showing difference in elevation along the profile of glacier(bottom)

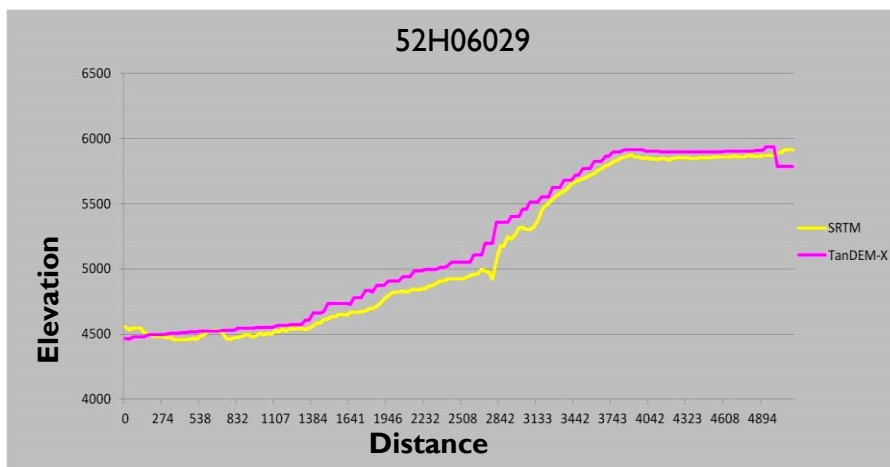
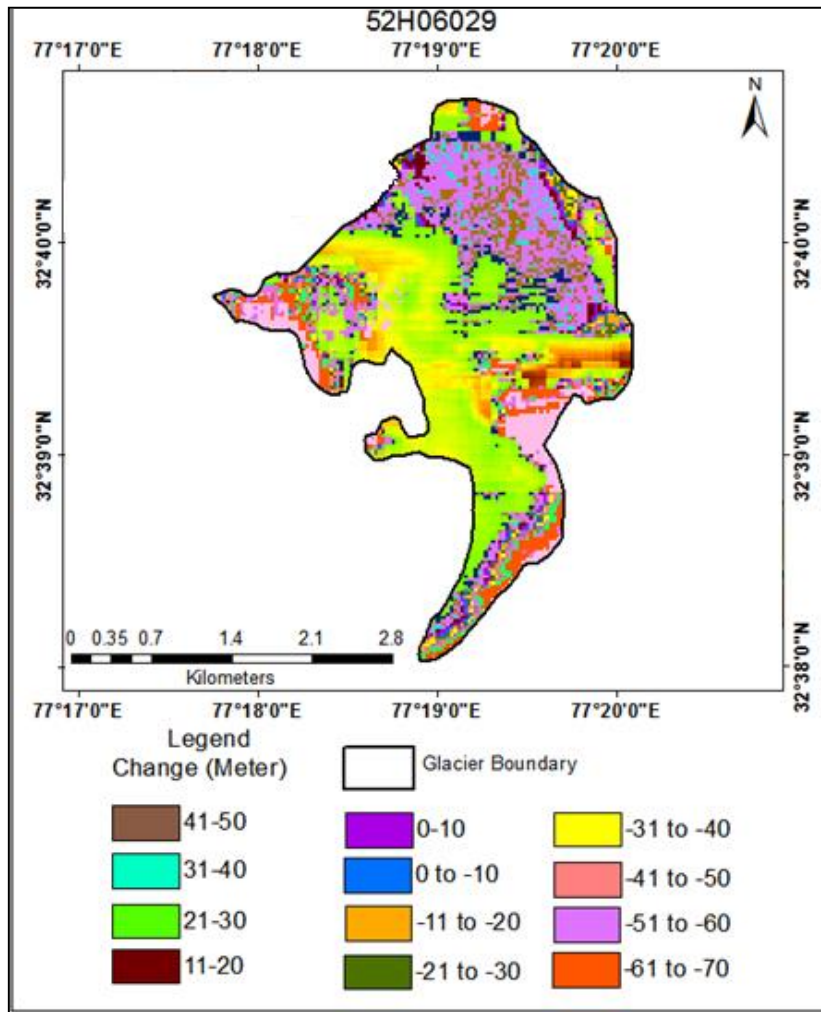


Figure 241: Map of glacier 52H06010 showing change in elevation (top) and corresponding curves showing difference in elevation along the profile of glacier(bottom)

ii) **Estimation of changes in glacier mass balance using DEM derived from topographical map and SRTM DEM for time frame 1962 - 2000**

Elevation changes and specific mass balance were found for a few Himalayan glaciers by comparing a 1962 Toposheet (DEM) with the 2000 SRTM (Shuttle Radar Topographic Mission) DEM data (Figure 242). Before comparing the mass change on glaciers bodies, two DEMs were analyzed on the stable areas surrounding the glaciers where no elevation change was expected. To carry out this analysis on the stable areas adjoining the glacier bodies, the slopes of the adjoining area, like river (gentle slope) and other non-glaciated regions were calculated to remove the biases. Slope classes were made in three degree class interval i.e. 0-3, 3-6, 6-9. Data was generated for about 200 points. For each slope class RMSD between two sources of elevations were calculated (Figure 243). It was observed that RMSD was high on high sloping areas and low in gently sloping areas. For example, deviation was observed less in Class-2 (19.88 m) and deviation was more in class-9 (52.17 m).

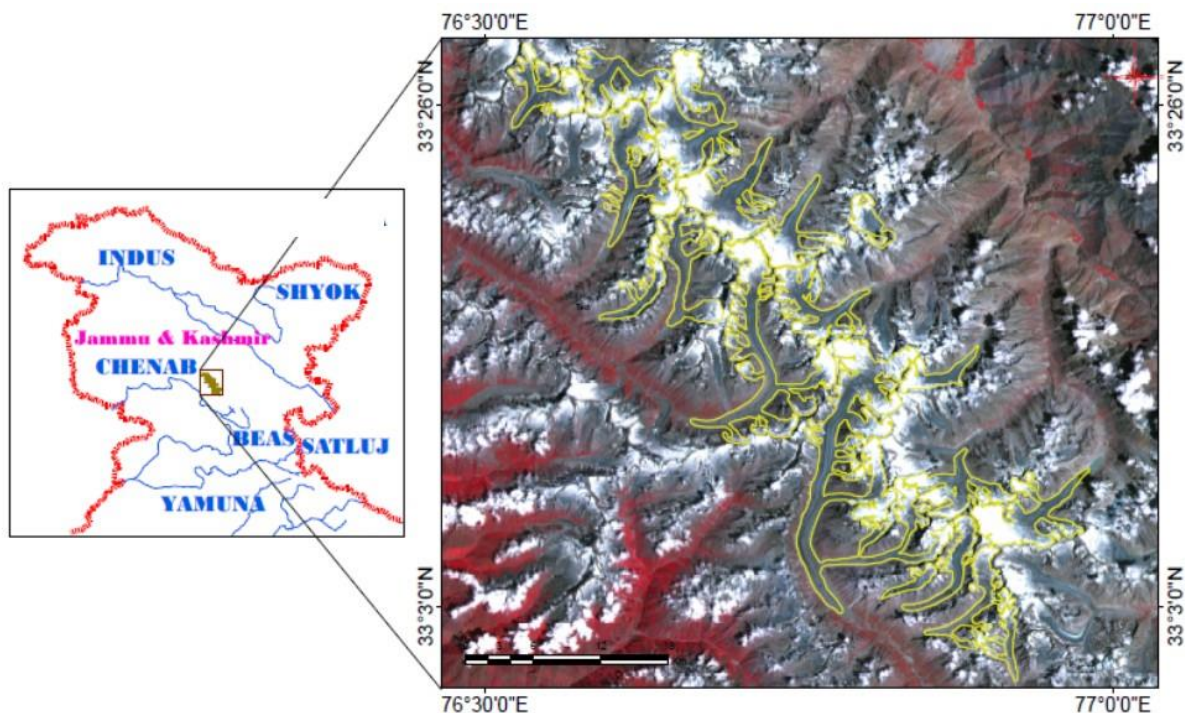


Figure 242: Location map of study area

Then difference in the elevations on the glaciers were found. For each glacier, slope was generated. And finally the RMSD of difference of non-glaciated regions were applied for correction of elevations on glacier surfaces according to slope of each glacier. Figure 244 shows variation of elevation differences observed glacier surfaces with respect to latitudes. It is observed that lowering of surfaces has been observed more on low latitude glaciers than on high latitude glaciers.

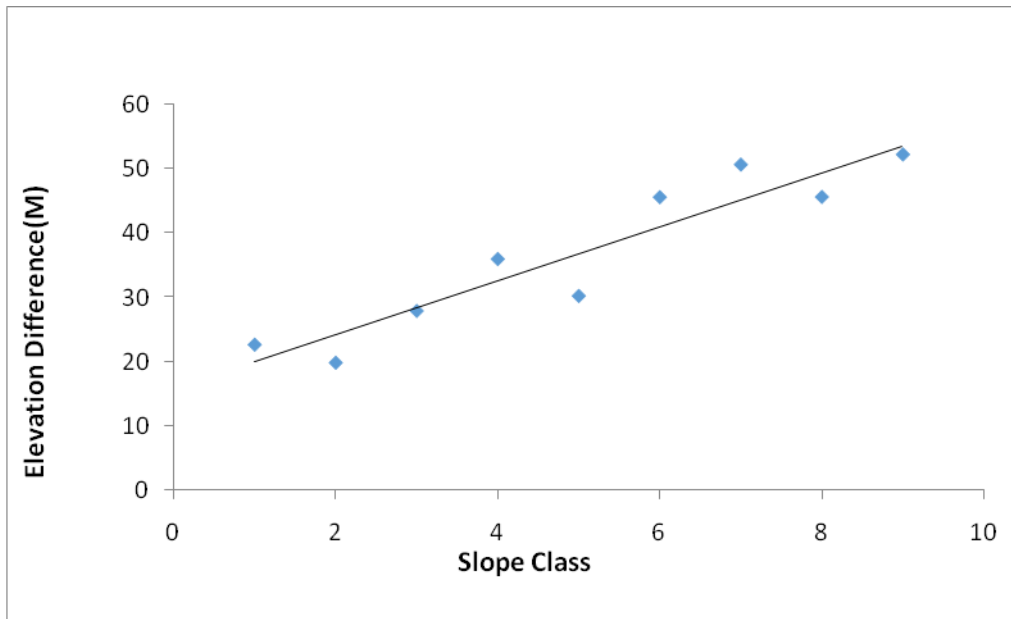


Figure 243: Variation of mean elevation difference on slope categories

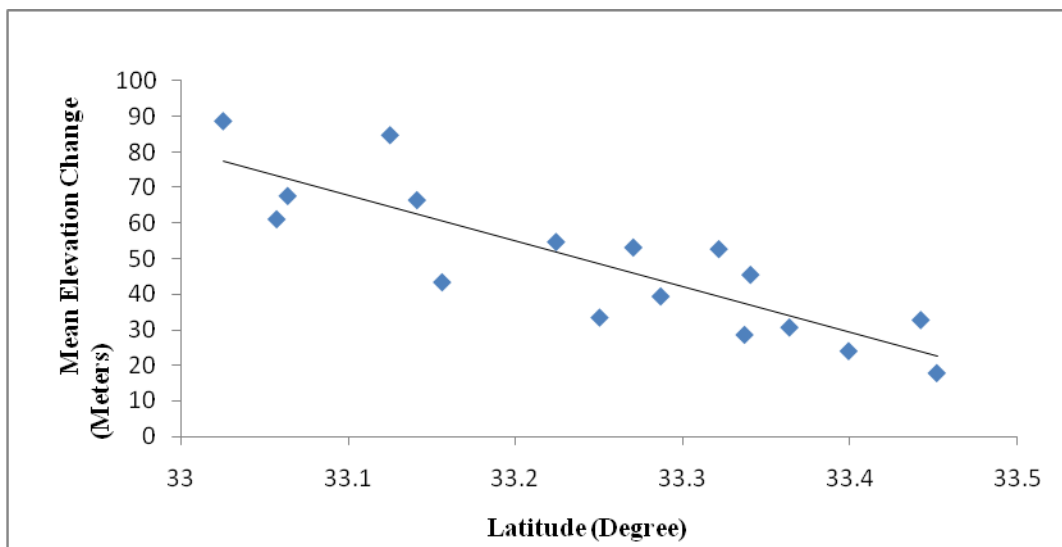


Figure 244: Variation of mean elevation change on glaciers with respect latitude

Glaciers have been identified using topographical maps and satellite images and glaciers numbering have been given according to SOI defined method. Glacier boundaries are then delineated manually. It has been found that all the glaciers in the study area are retreating. Linear and areal changes of glaciers have been calculated from 1962-2000.

Overall, it is concluded that the changes in elevation were computed using DEM derived from topographical maps of 1962 and SRTM DEM of 2000 and results show that average mass balance change for eighteen glaciers in part of Chenab basin is estimated as -70 cm/a water equivalent (w.e.) in 38 years. It is observed that glaciers which lie at lower altitude regions are retreating more than the higher altitude regions. Highest negative mass change has been estimated in low latitude regions (-154.93 cm) and lowest negative mass change has been estimated in high latitude regions (-24.48 cm).

iii) Glacier velocity and ice thickness estimation using COSI-Corr technique

An attempt has been made to estimate glacier surface velocity using optical remote sensing data utilizing newly introduced Coregistration of Optically Sensed Images and Correlation (COSI-Corr) technique. COSI-Corr is a technique that permits remote detection of deformation on the Earth's surface by comparing pairs of optical satellite images acquired on different dates.

COSI-Corr technique can map the horizontal component of deformation by sub-pixel correlation of optical images. This technique involves precise image registration, orthorectification and correlation. In Cosi-Corr, image registration and correlation is achieved with an iterative unbiased processor that estimates the phase plane in the Fourier domain for sub-pixel shift detection. Remote sensing images acquired using pushbroom satellite systems are most suitable for this technique. In pushbroom imaging systems, all optical parts remain fixed during the acquisition, and the scanning is accomplished by the forward motion of the spacecraft. Each line in the image depends on the varying attitudes of the platform. In this case, COSI-Corr corrects the viewing parameters by linearly correcting the camera look directions to compensate for attitude drifts and sensor orientation uncertainties during image acquisition. Viewing geometry of each pixel has to be physically modeled to account for topography and attitude variations. Raw images are wrapped onto the topography within the DEM resolution, and pair wise coregistered with a $1/50$ pixel accuracy, allowing for the measurement of horizontal fault offset with an accuracy on the order of $1/20$ of the pixel size.

COSI-Corr technique was used to study glacier surface displacement and velocity in part of the Chandra sub-basin (Figure 245 and Figure 246) using ASTER data for the period of 2007-2009 (Table 82 and Table 83) and methodology shown in Figure 247. Glacier velocity was further utilized to compute the glacier ice thickness distribution using laminar ice flow equation.

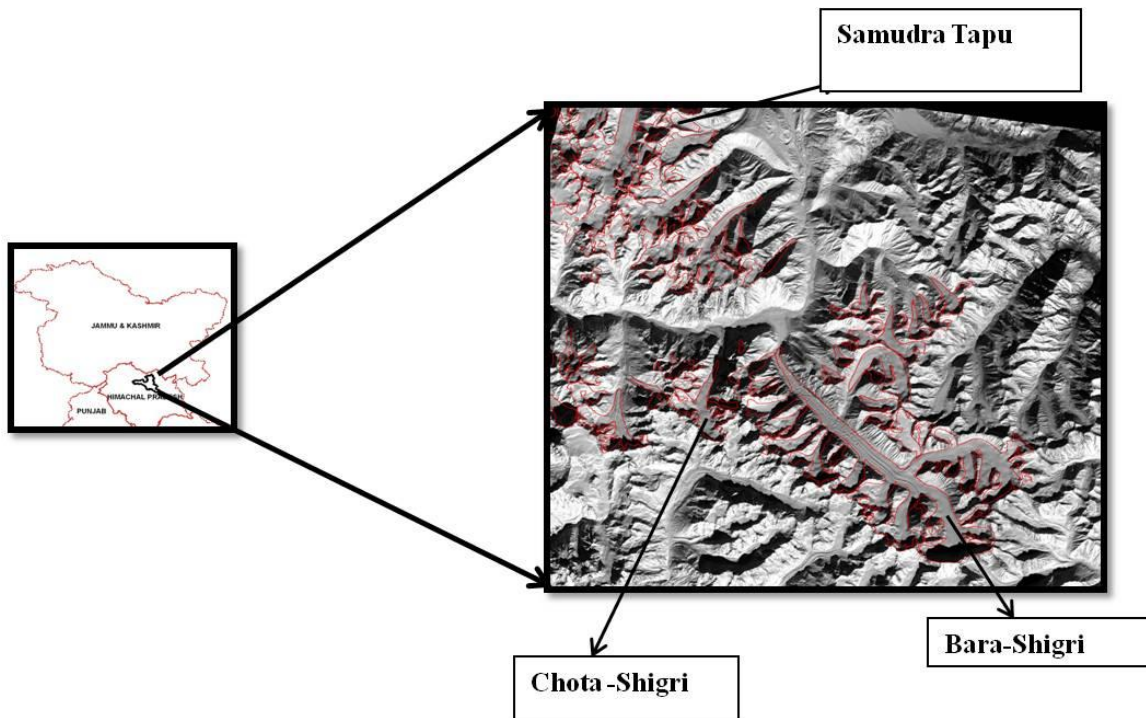


Figure 245: Study area showing major glaciers in Chandra sub-basin, Himachal Pradesh

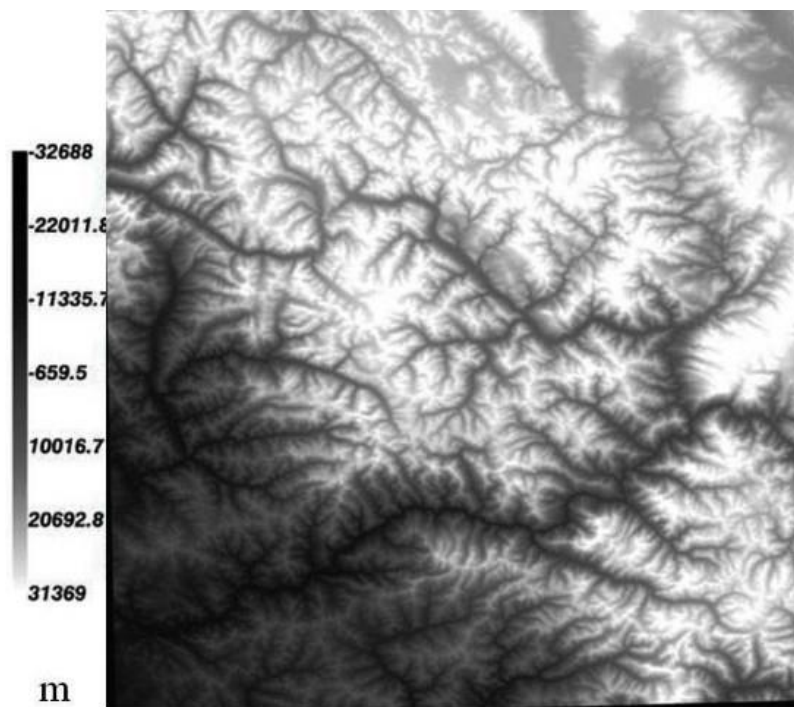


Figure 246: ASTER DEM of the Chandra sub-basin, Himachal Pradesh

Table 82: Characteristics of ASTER Satellite data used

Image No	Granule ID	Acquisition Date	Incidence angle	Sun elevation	Sun Azimuth
1	ASTL1A 0712150535230807180227	15.12.2007	-8.569	32.02364	161.54698
2	ASTL1A 0812010535530812040284	01.12.2008	-8.580	34.06769	162.70681
3	ASTL1A 0909150535330909180130	15.09.2009	-8.589	56.73344	147.21543
4	ASTL1A 0910010535250910040121	01.10.2009	-8.586	51.44754	154.05516

Table 83: Master- Slave and correlation image pair details

S No.	Master Image	Slave Image	Pair Number	Temporal Variation (in year)
1	Hill Shaded Image	Image 1		
2	Image 1	Image 2	Pair-I	0.9611
3	Image 1	Image 3	Pair-II	1.75
4	Image 1	Image 4	Pair- III	1.79

Figure 247 shows processing chain utilized for generation of relative displacement between two images using COSI-Corr. COSI-Corr contains different component for automatic and precise ortho rectification of the image. The processing chain is composed of four fundamental processes: The first process projects each pixel from the satellite focal plane onto a ground reference system. This operation utilizes knowledge from both the imaging system and the ground topography. The second process performs the resampling of the acquired image according to the projection mapping previously calculated. This yields ground-projected images, called orthorectified images. Cumulative uncertainties on both the imaging system and the topography lead to distortions and miss-registrations between the pairs of orthorectified images to be compared. The processing chain is therefore augmented with a third process, optimizing the satellite viewing parameters with respect to some reference frame. This reference frame will be either a shaded version of the topography model or another image previously orthorectified. Miss- registrations to be corrected are measured from the fourth process.

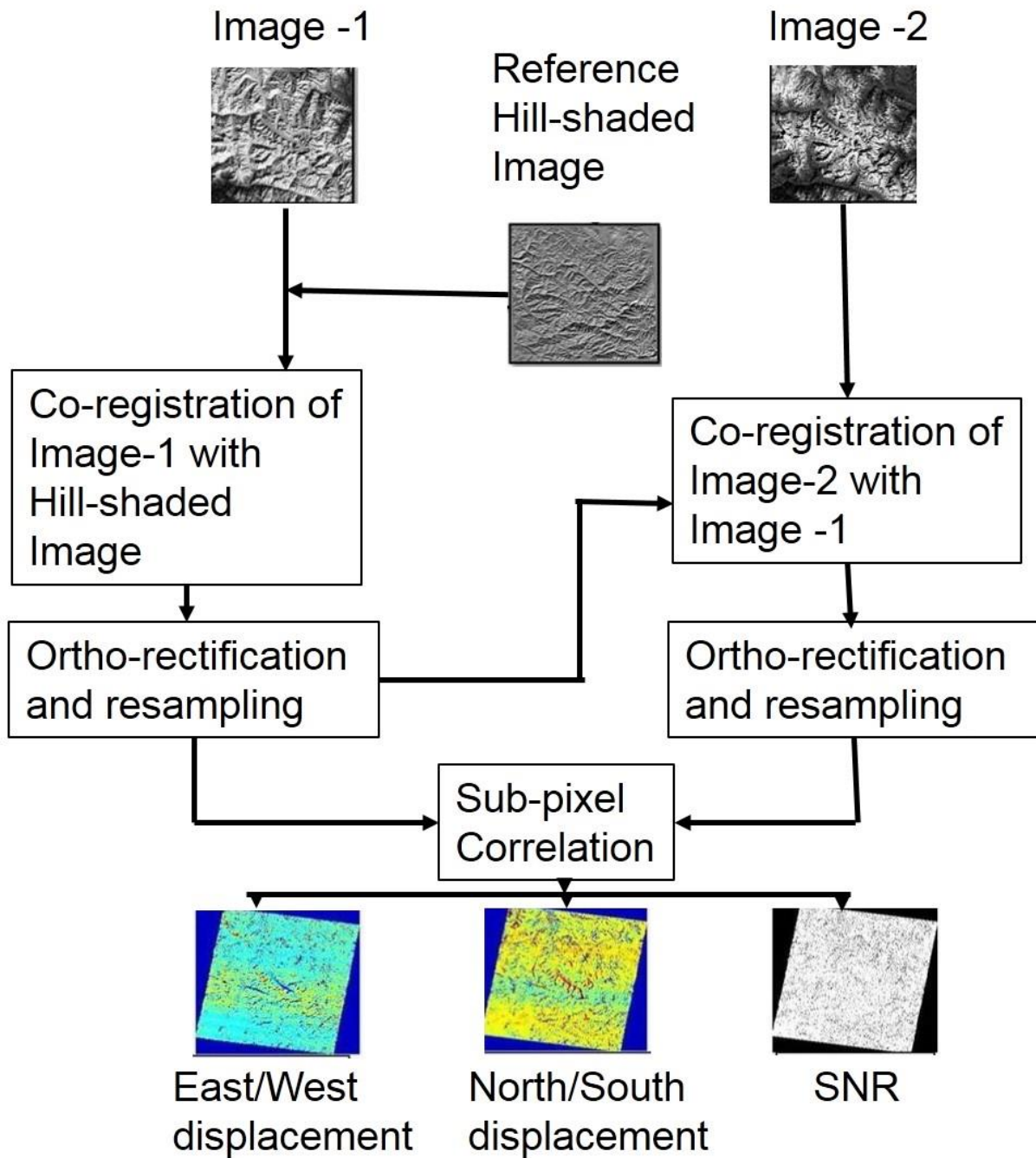


Figure 247: Processing chain for generation of relative displacement between two images using COSI-Corr

Correlation Image gives the displacement in East/ West and North/South direction. Using Post processed Correlation image we can calculate the velocity of Glacier. Velocity in term of Displacement is the total displacement per unit time.

Total Displacement using displacement image in two different directions can be calculated in Band Math using following Formula;

$$\text{Total displacement} = \sqrt{B_1^2 + B_2^2} \dots\dots\dots (i)$$

B_1 =East/West displacement

B_2 =North/South displacement

$$\text{Velocity} = \frac{\text{Displacement}}{\text{time}} \dots\dots\dots (ii)$$

Time = Difference between two Scene in Year or Second.

Using Glacier Velocity, Glacier ice thickness should be calculated with an equation (iii) (Cuffey and Paterson, 2010)

$$U_s = U_b + \left(\frac{2A}{n+1}\right) \tau_b^n H \dots\dots\dots (iii)$$

U_s and U_b are surface and basal velocities

$U_b = 25\% U_s$ (Swaroop et al, .2003)

n = Glen's flow law exponent = 3(assumed) (*Gantayat et.al,2014*)

H = Ice thickness

A = Creep parameter= $3.24 \times (10^{-24})(Pa^{-3})s^{-1}$ (Cuffey and Paterson et al, 2010)

ρ = Ice density = $900 \text{ kg}(m^{-3})$ (Farinotti et al, 2009)

f = Scale factor i.e. the ratio between the driving stress and basal stress along a glacier = 0.8, (Haeberli and Hoelzle et al., 1995)

g = Acceleration due to gravity = $9.8ms^{-1}$

The basal stress is modeled by an equation (iv);

$$\tau_b = f \rho g H \sin\alpha \dots\dots\dots (iv)$$

α = Slope calculated from DEM

τ_b = Basal Stress

From above 2 equations we can conclude equation (v) as;

$$H = \sqrt[4]{\frac{1.5U_s}{Af^3 (\rho g \sin\alpha)^3}} \dots\dots\dots (v)$$

Horizontal Displacement

Horizontal displacement in East-West and North-South directions was derived using sub-pixel correlation techniques with temporal ASTER image pairs. In addition, SNR images were also generated to evaluate the quality of the correlation for the respective image pairs. In general, it was observed that horizontal displacement was found to vary between 20 m and 70 m for both East-West and North-South directions over glaciated regions (Figure 248). SNR was observed to be less than 0.2 over glacier surface which indicate the quality of the estimate displacement values. The displacement for pair - I was observed to vary from ~-64 to -27 m in E-W (Figure 248a) and from ~ 30 to 64 m in N-S (Figure 248b) directions. The displacement for pair -II was observed to vary from ~ -64 to -20 m in E-W (Figure 248d) and from ~ 35 to 69

m in N-S (Figure 248e) directions. The displacement for pair –III was observed to vary from ~ -69 to –59 m in E-W (Figure 248g) and from ~ 20 to 69 m in N-S (Figure 248h) directions.

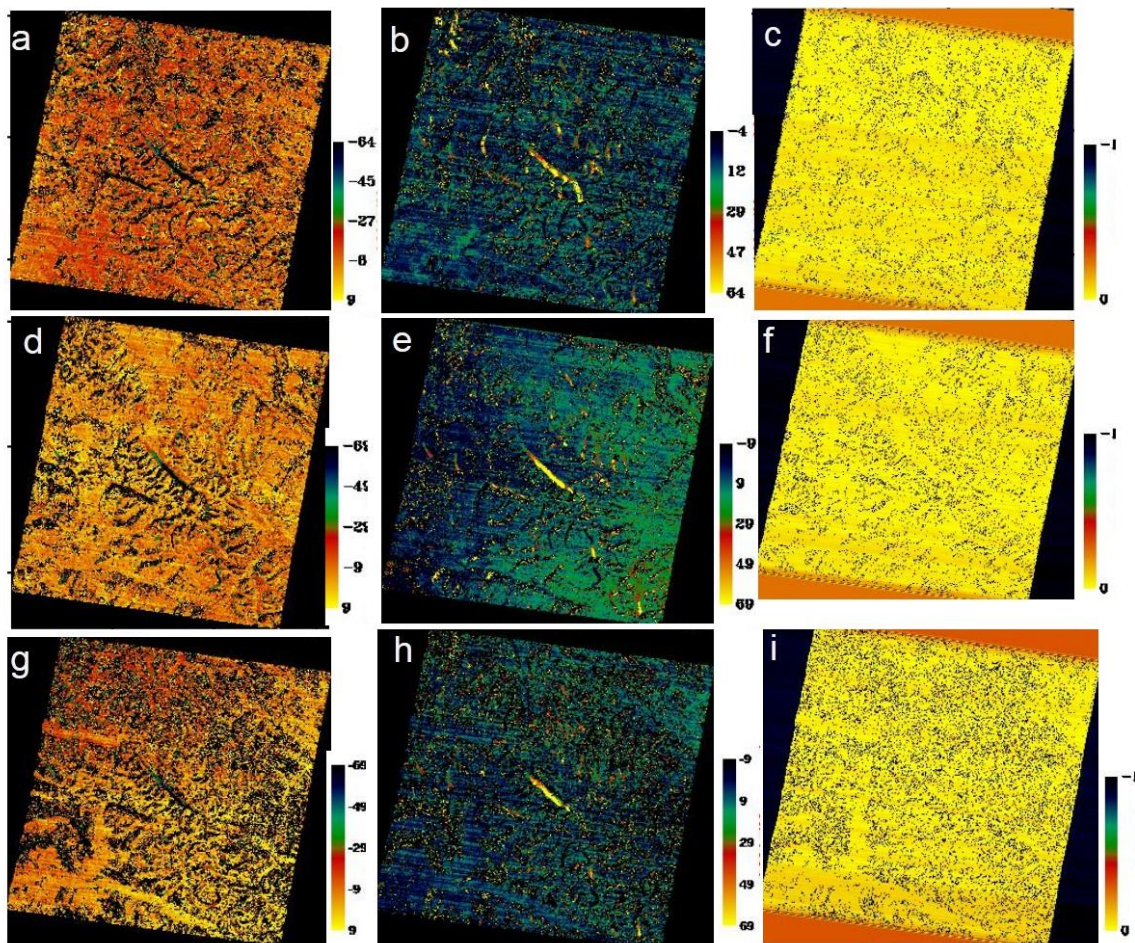


Figure 248: Surface deformation using pair- I (Top), pair-II (Middle) and pair-III (Bottom). Positive towards East and North direction. Eastward component (a, d and g); Northward component (b, e and h); Signal to Noise Ratio (c, f and i)

Flow vectors and streamlines showing general flow pattern is shown in Figure 249 for pair-1, pair-II and pair-III respectively. Length of the arrow indicates the magnitude of the vector. If length of the arrow is small in size, it indicates that the flow field of the displacement is low and if length of the arrow is large in size, it indicates that the flow field of the displacement is high. It is observed that main trunk of Bara Shigri glacier moves in NW direction whereas movements of tributaries are clearly indicating the orientation towards main trunk. Chota Shigri glacier is flowing in NNE direction. Accumulation zone of the glacier have shown relatively less displacement which increases to reach its maximum near equilibrium line, and further reduces towards the end of terminus in the ablation zone.



Figure 249: Glacier surface displacement of the Bara Shigri and Chhota Shigri glaciers, Chandra sub-basin, H.P. (derived from Pair-I, Left Panel; Pair-II, Central Panel; Pair-III, Left Panel)

Glacier velocity estimation

Glacier surface velocity was extracted using displacement vectors. Three velocity fields were produced for the duration year 2007 to 2009 (pairs I, II, III) presenting the velocity field over the active glacier area in part of Chandra sub-basin (Figure 250). Flow velocities was observed to be ~77 to 90 m/yr in the upper part of the ablation zone for Bara Shigri glacier which decreases to ~32 to 50 m/yr on the lower part of the ablation zone.

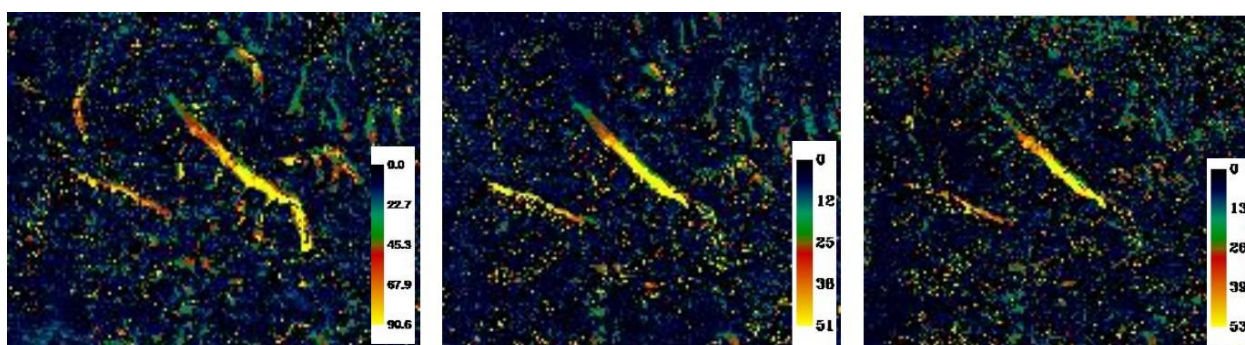


Figure 250: Surface velocity of the Bara Shigri and Chhota Shigri glaciers, Chandra sub-basin, H.P. (Maximum velocity in the higher reaches varies from ~77 to 90 m/yr (derived from Pair-I, Left Panel); ~45 to 51 m/yr (Central Panel, Pair-II and Left Panel, Pair-III); whereas minimum velocity near the snout and glacier boundary varies from ~32 to 50 m/yr (Left Panel); ~22 to 30 m/yr (Central Panel, Pair-II and Left Panel, Pair-III)

Glacier ice thickness estimation

An attempt has been made to estimate glacier ice thickness using glacier surface velocity with the help of equation of laminar flow of ice as described earlier. For glacier thickness estimation, surface velocity from *pair I* was utilized as it has maximum coverage in glaciated region and possess high SNR in comparison with *pair II* and *pair III*. Figure 251 shows the distribution of glacier ice thickness covering Bara Shigri and Chhota Shigri glaciers in Chandra sub-basin. It was found that ice thickness varies

from ~70-400 m from accumulation zone to snout. The spatial variability in the ice thickness can be observed for various zones of the glacier

Glacier ice thickness estimated for the Chhota Shigri glacier was observed to be comparable with GPR measurements in the ablation zone (Singh et al., 2012), however, no ground data was available for Bara Shigri glacier for comparison of results.

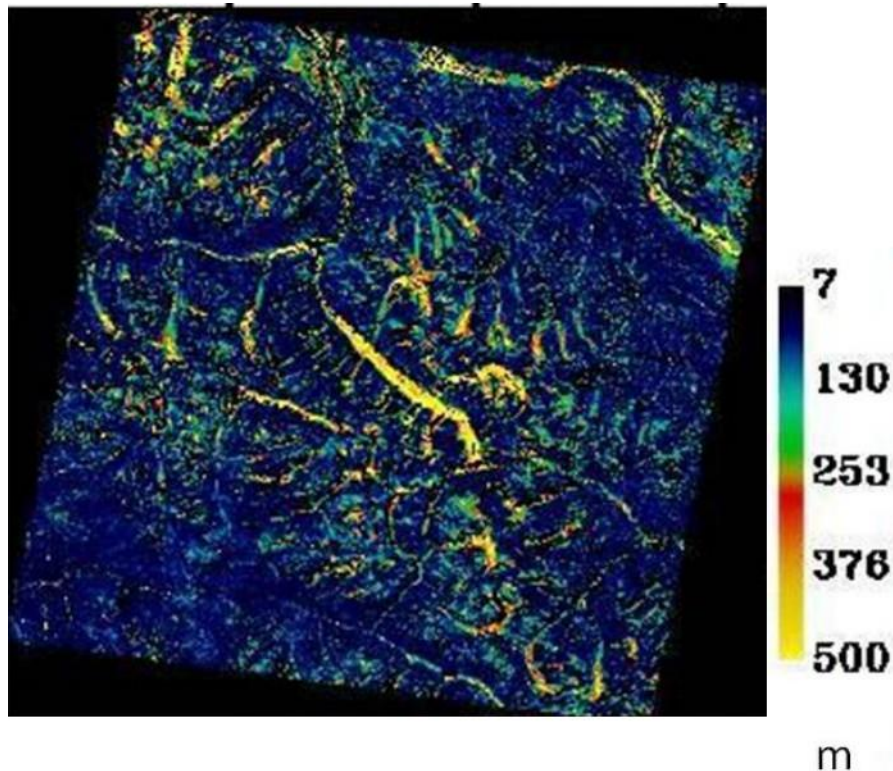


Figure 251: Ice-thickness distribution of glaciers in part of Chandra sub-basin including Bara Shigri. Maximum ice thickness is ~400 m in the central part of the main trunk of Bara Shigri glacier which decreases in the range 200-350 m towards snout

In general, horizontal displacements of two major glaciers in the study area, namely Bara Shigri and Chhota Shigri, were observed to vary between 20 m and 70 m. Further, these displacements were converted to glacier surface velocities using temporal image pairs. It is observed that the upper glacier zones adjoin to the equilibrium line have shown higher velocities of the order of ~77 to 90 m/yr which has reduced to ~32 to 50 m/yr towards the lower part of the ablation zone. Glacier ice thickness was estimated using laminar ice flow model in which the retrieved surface ice velocity was used as an input. It was found that ice thickness varies from ~70-400 m from the snout to the accumulation zone of Bara Shigri glacier. The glacier ice thickness for Chhota Shigri glacier was found to vary between ~ 50-250 m from the snout to the accumulation zone of the Chhota Shigri glacier Sensitivity analysis suggests that slope of the glacier surface significantly affect the glacier thickness estimation. Error in slope estimation can significantly influence the accuracy of glacier ice thickness.

11. Development of Algorithm for Auto Extraction of Debris Cover on Glaciers

11.1. Objective

To develop an algorithm for auto extraction of debris cover on glaciers using optical and thermal data.

11.2. Scientific Rationale

One of the key parameter influencing rates of melting around terminus of glaciers is debris cover over glaciers. Debris cover varies depending upon geomorphology and rock type of surrounding terrain. Therefore, debris cover varies from glacier to glacier, even if these are located in same valley. Supraglacial moraine is a very important glacier feature because its thickness can either enhance or reduce the rate of melting of glacier ice e.g., Figure 252 shows a field photo of debris cover over ice). Morainic materials get deposited in the deglaciated valley as a result of glacier retreats so it is very difficult to differentiate supra glacial moraines from deposited moraine using VNIR data. But the temperature of supraglacial moraine remains less than the deposited moraine. An algorithm based on the thermal infrared data can differentiate both moraines.

11.3. Methodology

An algorithm has been developed to estimate debris cover on glaciers. This is possible due to distinct reflectance characteristics of snow, ice and rock. The reflectance of snow, contaminated snow and ice is higher in visible region of the electromagnetic spectrum. However, in SWIR region reflectance of soil is higher than snow and ice. The emission of EMR from debris cover glacier can be observed using thermal channels. The thermal channels of Landsat TM data have been used to delineate debris cover over glaciers. Different glaciated features were used to collect the reflectance and temperature sample over the Samudra Tapu glacier. To improve the accuracy of extraction, DEM has been used.

11.4. Results and Discussion

Figure 253 shows the image of Samudra tapu glacier of Chandra sub-basin over which data for reflectance and brightness temperature has been generated for development of algorithm. Figure 254 shows the temperature thresholds for various categories of glacier surface. Figure 255 shows the flow chart of the steps followed in generation of algorithm. Reflectance image is subtracted from Thermal image (Figure 256). There are many other features (snow along hill, shadows, moist deglaciated valley) also

having same thermal property of supra glacial debris. In order to eliminate such errors slope image created using DEM is used because supra-glacier debris occur only on the ablation area and most of glacier's ablation area having a slope less than 15° DEM was included in the algorithm to bring more accuracy of debris cover extent (Figure 257). Algorithm was applied on Gangotri, Samudra Tapu (Figure 258) and Kumbhu glacier (Figure 259). Based on the debris cover over ice, accurate extents of glacier ice can be mapped.



Figure 252: Debris covered ice on glacier



Figure 253: Reflectance and temperature samples of different features collected over Samudra Tapu glacier

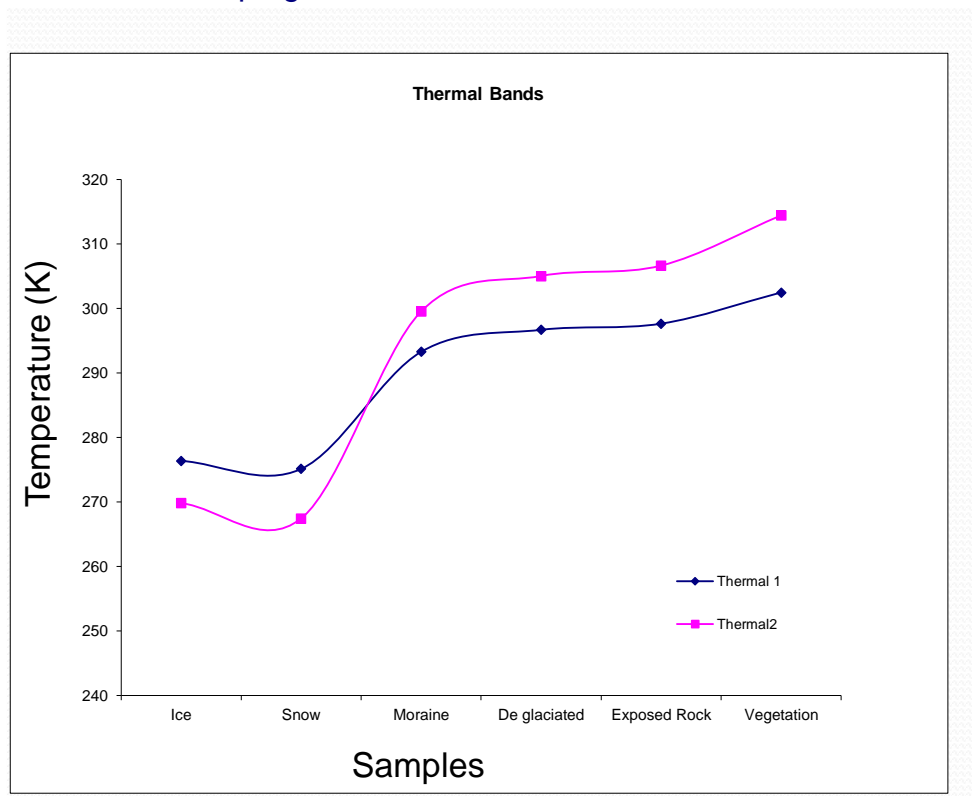


Figure 254: Temperature thresholds for various categories of glacier surface

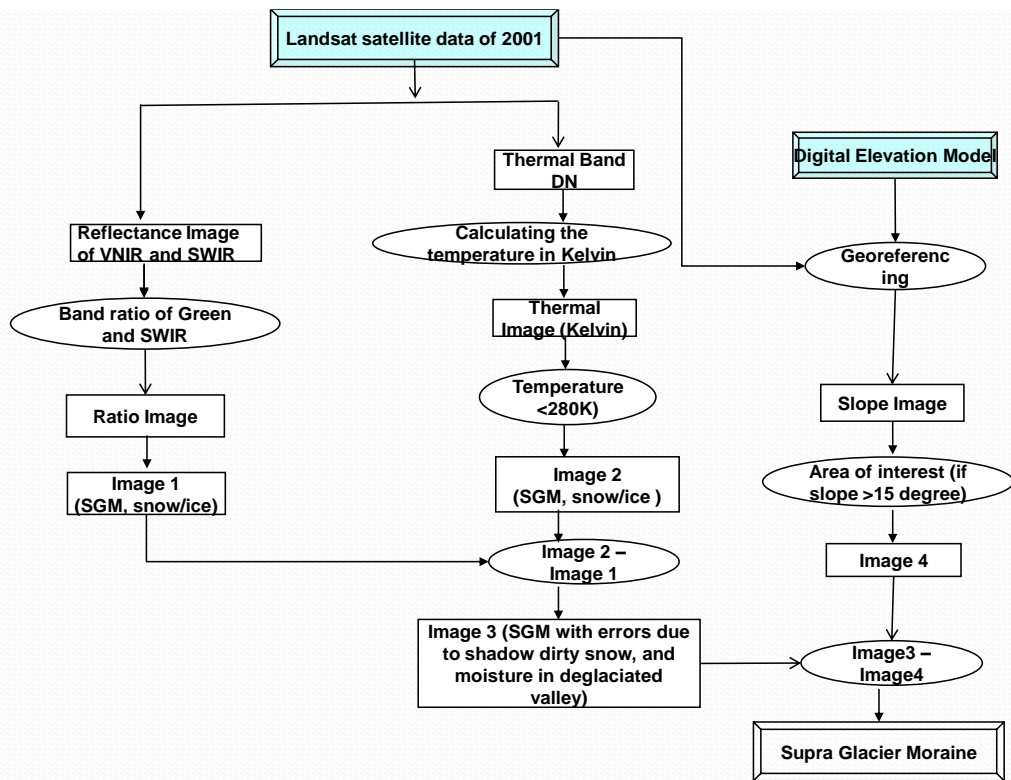


Figure 255: Methodology for developing algorithm for extraction of glacier extents below debris cover

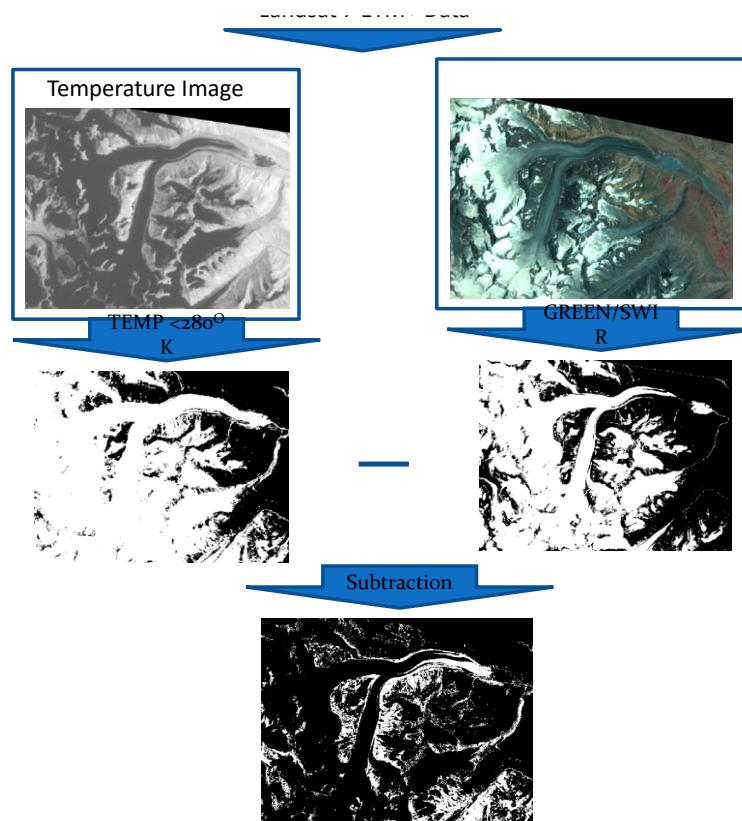


Figure 256: Automatic method for extracting supra glacier debris cover using thermal

data

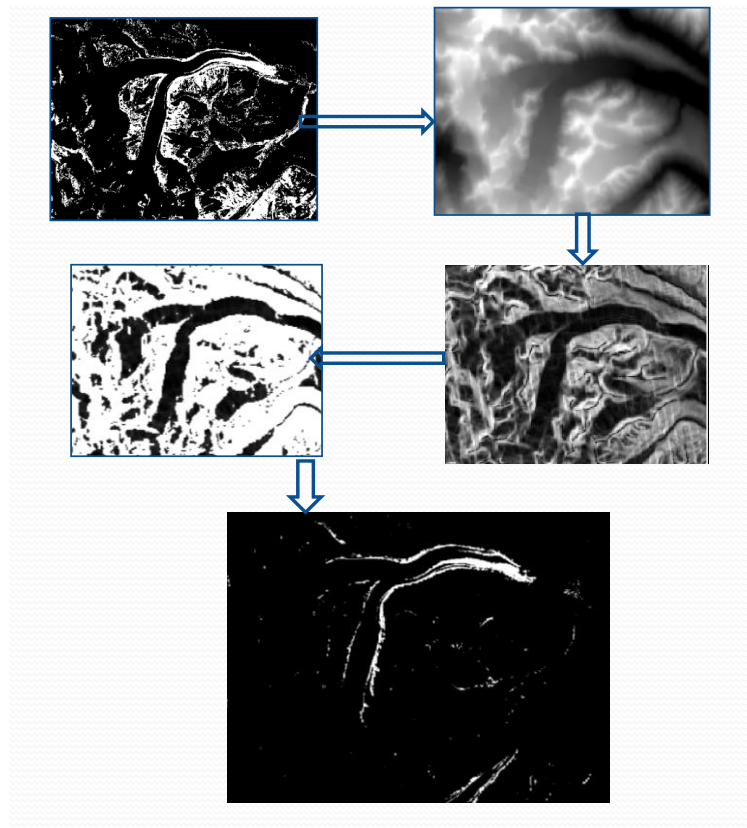


Figure 257: Use of DEM in generation of algorithm for extraction of debris cover

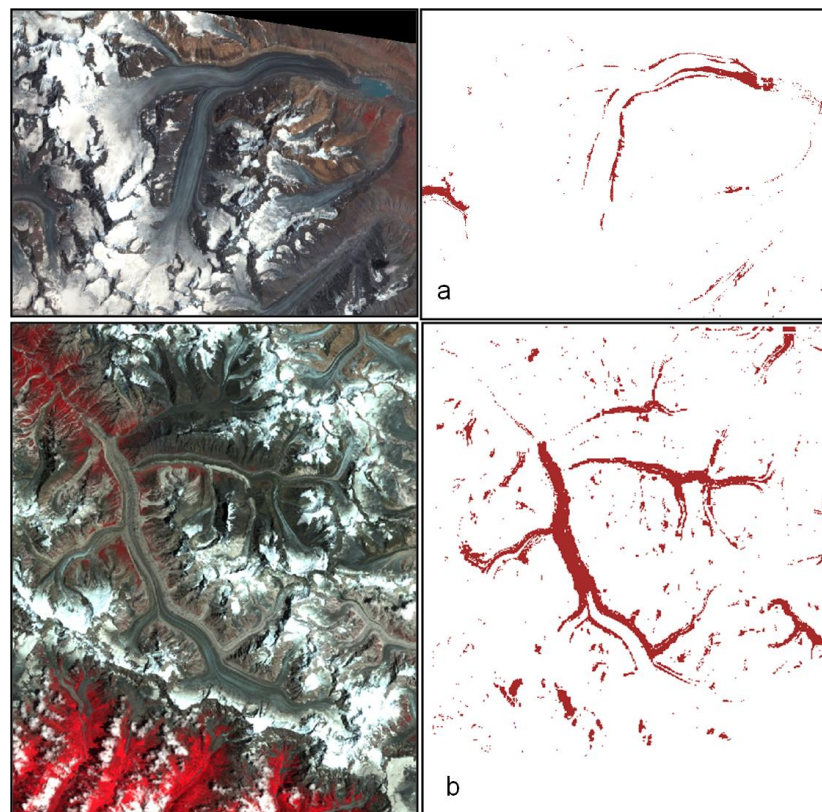


Figure 258: Extraction of debris cover for a) Samudra Tapu and b) Gangotri glaciers

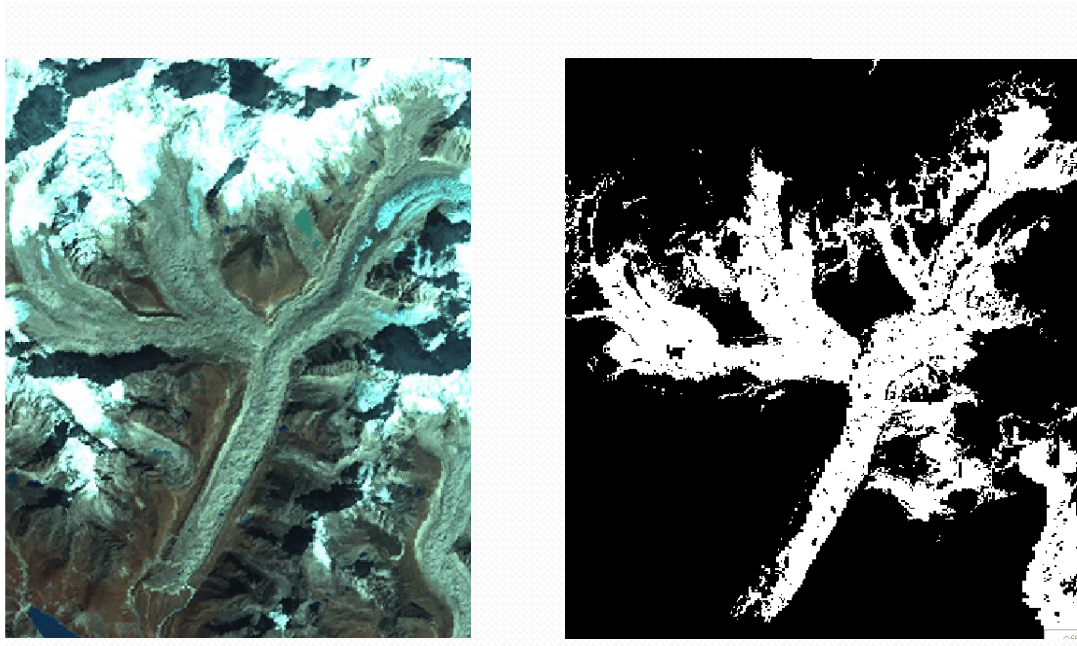


Figure 259: Debris cover over Khumbu glacier, Nepal

12. Glacier Expeditions and Installation of AWS for Field Validation

12.1. Objectives

To collect in-situ data from representative glaciers located in different Himalayan regions, establish high altitude laboratory near selected glacier and installing AWS for catering to the needs of field validation and developing advanced techniques for cryospheric studies.

12.2. Glacier Expeditions

Expeditions were organized in 22 representative glaciers located in different Himalayan regions for collecting ground truth or in-situ data and checking the accuracy of glacier features interpreted using satellite data or validating the satellite data interpretation (Table 84).

Table 84: List of Glacier Expeditions

Sr. no.	Name of glacier	Sub-basin/Basin Glacier valley	State	Year
1	Machoi	Drass	Jammu & Kashmir	2011, 2012, 2013, 2014
2	Hoksar	Jhelum	Jammu & Kashmir	2013, 2014
3	Thajewas	Jhelum	Jammu & Kashmir	2013, 2014
4	Pensilgumpa	Zanskar	Jammu & Kashmir	2013
5	Kolahoi	Liddar	Jammu & Kashmir	2013, 2014
6	Shishram	Liddar	Jammu & Kashmir	2013, 2014
7	Chhota Shigri	Chandra	Himachal Pradesh	2011, 2012, 2013, 2014
8	Batal	Chandra	Himachal Pradesh	2013
9	Patsio	Bhaga	Himachal Pradesh	2013, 2014
10	Miyar	Miyar	Himachal Pradesh	2012, 2013
11	Menthosa	Miyar	Himachal Pradesh	2011, 2012, 2013
12	Gepang-gath	Bhaga	Himachal Pradesh	2012
13	Satopanth	Alaknanda	Uttarakhand	2011, 2012, 2014
14	Bhagirath Kharak	Alaknanda	Uttarakhand	2011, 2012, 2014

15	Chipa near Baling village	Dhauliganga	Uttarakhand	2014
16	Meola	Dhauliganga	Uttarakhand	2012
17	Lapang	Dhauliganga	Uttarakhand	2012
18	Milam	Goriganga	Uttarakhand	2012
19	Jyoling	Dhauliganga	Uttarakhand	2012
20	Naglaphu	Dhauliganga	Uttarakhand	2012
21	Lapa	Dhauliganga	Uttarakhand	2012
22	Changme Khanku	Tista	Sikkim	2012, 2013

Teams from SAC and partner Institutes visited selected glaciers during the time frame 2011-2014. The major tasks during the expeditions was making observations about the geographic location of snout position, observations about glacial landforms, installing stakes on glacier surface for monitoring changes in snow/ice and their positions for glacier mass balance and velocity estimation, black carbon soot measurements, glacier ice/debris thickness estimation, glacier surface roughness estimation, surface/ambient temperature measurements, wind direction and velocity measurements, aerosol optical depth measurements, albedo measurements, snow/ice radiometric measurements etc. However, it may be noted that each expedition had certain specific objectives and accordingly in-situ data were collected. Instruments used are listed in Table 85.

Table 85: Instruments utilized during in-situ data collection and purpose

Instrument	Purpose
GPS (Differential) & GPS	Snout position, Surface elevation profile over glacier ablation zone
Aethalometer	Aerosol (Black Carbon soot)
Sun photometer	Aerosol Optical Depth
Surface profilometer	Surface roughness (Debris zone and exposed ice zone)
Temperature/RH sensor	Near surface air & glacial surface temperature and relative humidity
Digital Camera	Field photographs of glacier features
Instrument controller/Data Logger/Laptop	Data storage/data transfer from various instruments/field observations
Ground Penetrating Radar (GPR)	Snow/Ice Depth
Spectroradiometer	Spectral measurements over snow/ice/debris

Observations made during various glacier expeditions are discussed in respective sections of this report. Figure 260 to Figure 263 show some of the field photographs during glacier expeditions to Chhota Shigri glacier in Chandra sub-basin, Himachal Pradesh during September 08-22, 2014 and Chipa glacier in Dhauliganga sub-basin, Uttarakhand during September 10-22, 2014. Observations for Black Carbon and AOD using Aethalometer and Sun Photometer, measurements of elevation of glacier surface using DGPS, measurement of surface roughness and temperature were carried out. DGPS points were established at Chhota Darra village near Chhota Shigri glacier for monitoring of snout and velocity of glacier ice. Observations using Ground Penetrating Radar (15-80 MHz) for ice thickness estimation, observation of geographical position of snout using GPS, measurements of surface roughness and ground validation of nature of debris cover over the glacier were carried out at Machoi and Chipa glacier near Baling village.



Figure 260: DGPS measurements over the ablation zone of the Chhota Shigri glacier in Himachal Pradesh



Figure 261: Aethalometer measurements over the ablation zone of the Chhota Shigri glacier in Himachal Pradesh



Figure 262: Field observations on Chipa glacier including GPR measurements, Dhauliganga basin, Uttar Pradesh



Figure 263: Establishment of DGPS Base stations and rover near the snout of Chhota Shigri glacier in Himachal Pradesh

12.3. Establishing Glacier Lab and AWS at Chhota Shigri glacier

The in-situ data collection carried out in campaign mode over a glacier is for a very limited duration of 5-15 days. In order to measure various in-situ parameters which are essential for carrying out scientific studies on long term basis, there was a need to establish and setup laboratory in identified high altitude glaciated region for obtaining data on continuous basis. The laboratory setups on a glacier site will be a reference for future development activities. The laboratory at Chhota Shigri has been set up with capability to provide in-situ data for various studies as given below:

- Mass balance using energy balance approach
- Effect of carbon soot on melting of glaciers
- Effect of debris cover on glacier ice-melt
- Determination of Glacier depth
- Snow pack characterization
- Snow and glacier melt run off modeling

Chhota Shigri glacier, located at 32°19'N, 77°31'E at an altitude of ~4000 amsl, is a valley-type glacier that lies on the northern ridge of the Pir-panjal range in the Lahul & Spiti valley of Himachal Pradesh, Indian Himalaya. This glacier lies on left bank of Chandra river. It is located on Manali- Kaza road which passes through Rohtang Pass. The glacier is approx. 70 km from Manali town and 35 km from Koksar village on main Manali-Leh highway. Due to its proximity to road the glacier is ideal for observation and requires approx 3 hrs of trekking to reach the glacier snout from base camp after crossing Chandra river and about 3-4 hours to reach ablation zone. As it is a medium sized glacier (approx. 10 km length), it is more suitable as entire glacier can be approached and studied. Also results from earlier mass balance studies by glaciological methods are available for validation, comparison and continuity of data (Ramanathan, 2011; Azam et al., 2011). The glacier is having narrow stream channel which is ideal for discharge measurements. Published Mass balance measurement data is available for the last 10 years for comparison purpose. Figure 264 shows the location map and AWiFS image showing Chhota Shigri (encircled) and nearby Glaciers.

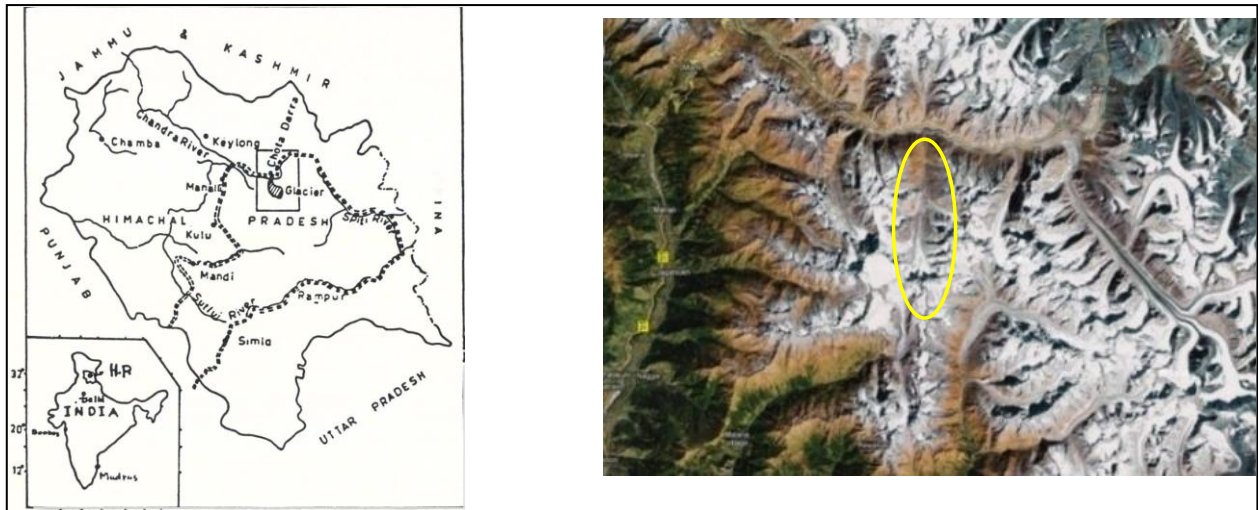


Figure 264: Location map and AWiFS image of Chhota Shigri glacier

Design of the modular laboratory

The modular laboratory was found ideal for installing AWS and Aetholometer at Chhota Darra PWD guest house campus located at the base of Chhota Shigri glacier at altitude of 3851 m for continuous data collection. The modular laboratory of size 10 ft. x 25 ft. dimension has inbuilt residential section with adequate facility for staying two operators. The laboratory is created for data collection and for transmitting data through INSAT. Currently power is provided through portable generator carried to the site. However, 10 KVA power through solar rechargeable batteries is planned. Figure 265 shows a sketch of the pre-fabricated-readymade laboratory installed at Chhota Darra. Figure 266 – 269 are field photos showing outside view, panoramic view, inside view of installed High Altitude Field Laboratory

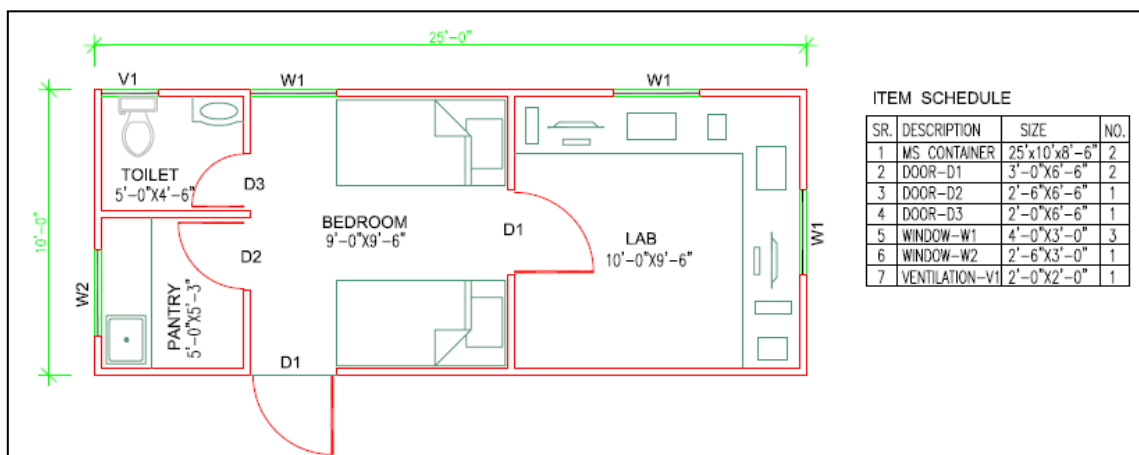


Figure 265: Drawing of Modular Laboratory



Figure 266: Laboratory established at PWD Guest house, Chhota Darra



Figure 267: Panoramic view of Laboratory and PWD Guest house at Chhota Darra



Figure 268: Inside view of Laboratory at Chhota Darra



Figure 269: Inside view of Laboratory at Chhota Darra

Parameters for in-situ measurement

To carry out the identified studies, various parameters and frequency of measurements are given below:

- **Energy balance study:** Hourly measurements of Net Radiations, Albedo, Air Temperature, Relative Humidity, Wind Speed and direction, Atmospheric Pressure, Snow Depth and Snow/Ice surface temperature will be carried out using appropriate instruments.
- **Velocity of glacier:** Four measurements per season using differential GPS at identified marker locations
- **Retreat:** One measurement each for location of snout at the beginning and end of ablation season using differential GPS
- **Snow cover:** One measurement fortnightly for the reflectance of snow and ice using radiometer
- **Moraine cover:** One measurement per season on debris cover part of glacier for surface reflectance
- **Black Carbon Soot:** Daily at 5-minute interval using Aethalometer
- **Runoff:** Four measurements of stream discharge per day

Description of Instruments

- **Aethalometer** for black carbon soot monitoring. The available Portable unit is being carried out by the operator to glacier site periodically to obtain information about the concentration of black carbon in the atmosphere. The portable 7 channel instrument having sensitivity of $0.1 \mu\text{g}/\text{m}^3$ @ 1-minute resolution can operate continuously for up to 4-5 hours on a single battery charge. Multiple batteries with chargers are being used to extend the monitoring period.
- **Pack of handheld sensors.** These are battery operated sensors attached with individual data logger that are carried by the operator to different locations on the glacier to take measurements at regular intervals. The instruments /sensors comprise of Net Radiation Sensor, Albedo Sensor, Air temperature sensor (ventilated), Relative humidity sensor, Wind Speed sensor (ultrasonic), Wind Direction Sensor (ultrasonic).
- **DGPS permanent stations:** These are permanent marker points established as steel sections cemented into the ground at known location the coordinates for which are obtained through long term (24-48 hrs) continuous reading using DGPS. Two such stations are established in the field one near to AWS at Chhota Darra and second station near to snout of Chhota Shigri (Base Camp) including rover as seen in Figure 260 and Figure 263.

- All instruments are maintained & calibrated through annual maintenance contract (AMC) through the suppliers of instruments. Maintenance and calibration is preferably done before the winter season. SAC has provided hands-on-training to scientists / operating staff for data collection using portable instruments.

Establishing Automatic Weather Station

AWS built by M/s ASTRA Systems has been installed at the base of glacier near the field laboratory in PWD Guest house campus (Figure 270). The sensors on AWS are Wind Speed and Wind Direction Sensor, Ambient Temperature and Relative Humidity Sensor, Atmospheric pressure sensor, Albedometer, Net radiation sensor, Ultrasonic Snow Depth Sensor, Soil Temperature sensor, High capacity snow precipitation gauge. Stored data is being transmitted through INSAT series satellite in S-band once in a day and the data is received at SAC and made available through MOSDAC web site.



Figure 270: AWS installed at Chhota Darra near Chhota Shigri glacier, H.P.

13. Geospatial Modeling for Glacier Health Assessment

13.1. Objective

To carry out multi-parameter weighted index analysis for assessing relative health of glaciers and sub-basins.

13.2. Scientific Rationale

The conventional approach to assess the changes in glacier health over time comprise of i) annual mass balance changes, ii) advance / retreat of glacier measured at snout and iii) glacier area changes. Integrated geospatial modeling using various weather/climatic and glaciological parameters can be carried out in a GIS environment. Some of the parameters are e.g., insolation, temperature, precipitation, wind, humidity, glacier dimension, glacier morphology, debris cover, slope, altitude, orientation, hypsometry, glacier-valley morphology, valley geology, valley land use, valley vegetation, etc. Each of these parameters has distinct effect on the health of the glacier. Glacier health indices for each glacier at the end of an annual hydrological cycle can be computed. A comparative analysis of glaciers in a basin over a period of time may bring out relatively fragile glaciers that need more attention and detailed observations.

In this study relative health assessment of glaciers is carried out with the help of multi-sensor, multi-temporal satellite data. Analysis of IRS-P6 AWiFS data of 2004-07 period, SRTM DEM of 2002 and MODIS LST data of 2010-13, using image processing and GIS tools has provided significant information on glacier dimensions, orientation, elevation, morphology related physical and climatic parameters. Synergistic approach is used for the relative health assessment of glaciers and sub-basins. Data synergy involves the combination of independent datasets to extract new or to obtain more accurate information about a parameter being measured (Bingham and Rees, 1997). Many researchers have assessed the health of glaciers using single satellite data sources, but in this research by combining different satellite data sets relative, health of glaciers are identified. An attempt is made to use the multi-parameter weighted index analysis method for assessing relative health of glaciers and sub-basins. Saaty's analytical hierarchy process and weighted analysis method is adopted to analyze the identified glacier parameters and to derive the Composite Glacier Health Index (CGHI) for glaciers (Jyotsna et al., 2014; Swati Tak et al., 2014).

13.3. Study Area

The study area (Figure 271) is the glaciated part of the Ganga Basin in the Himalayas spread across India, Nepal and China (Tibet). In Ganga Basin, there are 6237 numbers of glaciers encompassing 18393 km² of glaciated area (SAC, 2011a; Sharma et.al, 2013).

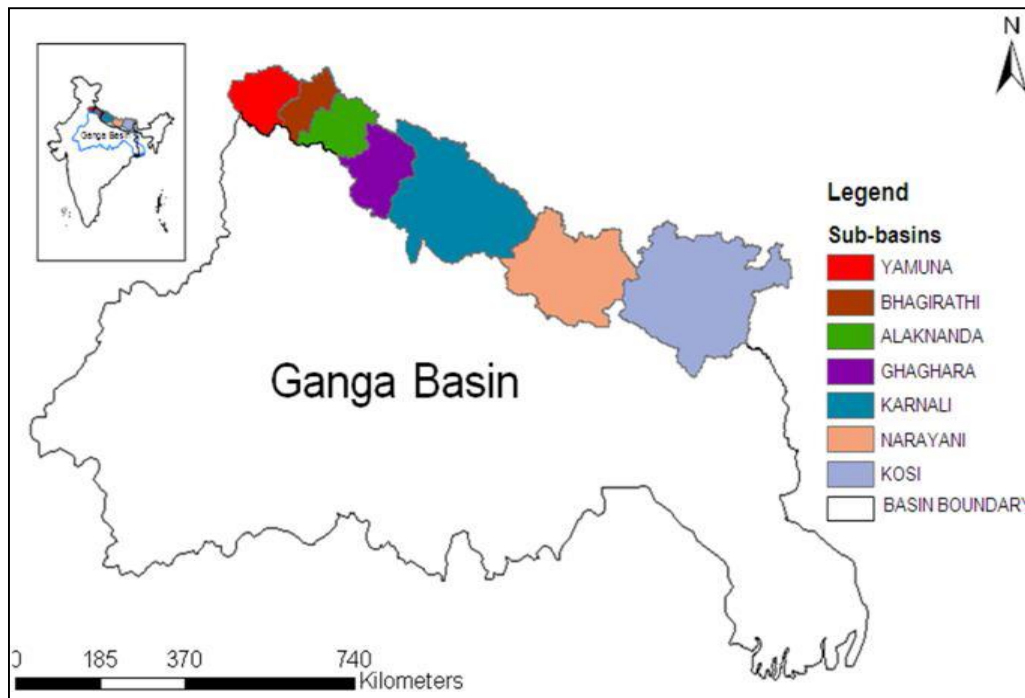


Figure 271: Study area Ganga basin and sub-basins (Source: Jyotsna et al., 2014)

The study area is located between 27° 6' to 31° 21' N latitude and 78° 2' to 88° 5' E longitude (approx.) of Ganga Basin in Himalayas. The total study area sub-set selected to cover the glaciated parts in Ganga Basin is 148588 km². The Ganga basin study area is divided into seven glaciated sub-basins namely Yamuna, Bhagirathi, Alaknanda, Ghaghara, Karnali, Narayani and Kosi as per their relative location from west to east.

Ganga basin is taken as study area because this basin is mostly affected by the anthropogenic activities. Also, for this basin the accumulation–ablation area ratios were low and most of the glaciated areas had varying amounts of debris cover. The thick debris cover plays an important role by stopping the heat from sun rays in reducing the melting of glacier ice. However, the status of these glacier features depends on its altitude and latitudinal distribution. Mass balance is a key parameter for assessing the health of a glacier.

13.4. Methodology

In the current study morphological parameter for glaciers are considered for relative glacier health assessment. Many factors like area–altitude distribution, mass balance, slope and debris cover contribute to variation in rates of retreat (Kulkarni and Karyakarte, 2014; Deota et al., 2011; Singh et al., 2010). Remote sensing-derived outlines combined with DEMs in a GIS provide glacier parameters such as length, termini elevations, median elevations, hypsometry maps and glacier flow patterns at different time steps (Racoviteanu et al., 2008). The details of glacier primary parameters like area, length, orientation, elevation, latitude and derived parameters like percent slope, percent debris cover, percent ice exposed which are responsible for glacier health and used in the present study are discussed below.

i) Length of glacier- The definitions used are: Mean length: The average of the lengths of each tributary along its longest flow lines to the glacier snout. Maximum length: The longest flow line of the whole glacier (Paul et al., 2009). In this study maximum length of glacier is used as one of the physical parameter associated with glaciers morphology. Length is calculated by manually drawing the line from highest point to the lowest point (snout) of the glacier along the major tributary. In glacier inventory datasheets length of glacier is classified into different length classes such as maximum length and Mean length.

ii) Mean Elevation- Glacier advancement and recession are the most significant evidences of change in glacier geometry. In this study mean elevation is taken as one of the important parameter and has higher priority. In general, the most vulnerable glaciers are at relatively low elevations, whereas glaciers at high altitudes are more robust (UNEP, 2010). Elevation information for glacier snout, snowline, and highest glacier elevation is derived from combination of glacier information obtained from Resourcesat-1 AWIFS and elevation obtained from SRTM (DEM).

iii) Total area of glacier- The surface area of a glacier is a very sensitive parameter as it is used in a wide range of applications including global scaling up of glacier area (ICIMOD, 2011) and glacier properties (Paul et al., 2009). In this study total area is one of the important morphological parameter for assessing the relative health of glaciers. In glacier inventory datasheet total area of glacier consist of accumulation area and ablation area. The ablation area is further divided into debris cover area and ablation area exposed. Accumulation includes all processes by which material is added to glacier.

iv) Orientation of glacier- The aspect or orientation of a glacier is a useful parameter for all kinds of modeling (Evans, 2006). Aspect is a circular (directional) parameter and means aspect values must be derived by decomposition into the respective sine and cosine values (Manley, 2008). The calculated orientation values are transformed into

the eight cardinal directions (N, NE, E, SE, S, SW, W, and NW). Each cardinal direction has a range of 45 degrees and ± 22.5 degrees of cardinal direction are measured and assigned values of that cardinal direction.

v) Percent slope- For medium to large glaciers (length >1.5 km), the mean slope and length are expected to play a major role (Venkatesh et al., 2012). Mean slope s is defined as follows:

$$\%S = \frac{h_{\max} - h_{\min}}{\text{length}} * 100$$

Where h_{\max} is the altitude at the top of the glacier, h_{\min} is the altitude at the snout and L is the length of the glacier. The glaciers on steep slopes are generally more unstable as a result of the higher flow velocity; those with maximum slope correspond to icefalls (ICIMOD, 2011). The mean slope is a rough proxy for other parameters like mean thickness (Haerberli and Hoelzle, 1995) and also relates to other dynamic measures such as surface flow speed. Low gradient reduces melting by slowing the transfer of ice from accumulation area to ablation area and further to lower elevation region of higher temperature zone. Gradient is derived from combination of glacier length obtained using Resourcesat-1 AWIFS and altitude from SRTM (DEM).

vi) Percent Debris cover area of the Glacier- Percent debris is derived with the help of ablation area and total area of glacier from the glacier inventory datasheet.

$$\% \text{Debris cover area} = \frac{\text{Debris area}}{\text{Total area of glacier}} * 100$$

In recent studies debris is also important parameter for the health monitoring of glacier. Mapping of debris covered glaciers is important for accurate determination of glacier area and for further applications. Benn et al., (2012) had studied about the relationship between debris thicknesses and melt rate, and predicts an increase in melt rate where debris cover is thin, and an exponentially decreasing melt rate under thicker debris. According to Racoviteanu et al., (2008) a new technique based on thermal sensors takes advantage of the difference in the temperature of the debris overlaying ice versus the temperature of the surrounding moraines. Debris cover is of interest to glaciologists due to its influence on the glacier melt processes. A thick debris cover (> a few centimeters, or “critical thickness”) has been shown to reduce the ablation rates of the ice underneath due to the low thermal conductivity of debris (Zhang et al., 2011a; Brock et al., 2010), whereas a thin debris cover (< a few centimeters) was shown to increase the ice melt rates due to the low albedo of the debris (Takeuchi et al., 2000; Kayastha et al., 2000; Singh et al., 2000).

vii) Latitude- Low latitude glaciers, which include tropical and subtropical glaciers, behave differently from their high latitude counterparts because of different climate and weather patterns. High latitude glaciers typically experience an accumulation season during the winter when precipitation helps to build up a glacier’s ice mass and a melt season during the summer when higher temperatures contribute to glacial mass

loss. Low latitude glaciers are more sensitive to increases in temperature than mid and high latitude glaciers (Rachel, 2012).

viii) Percent Ice Exposed Area of the Glacier- Percent ice exposed area is the bare ice area of the glacier. This is derived by total area and ice exposed area of the glacier. The formula used for the derivation is as follows:

$$\% \text{ Ice Exposed Area} = \frac{\text{Ice Exposed Area}}{\text{Total Area of glacier}} * 100$$

The glacier inventory maps and inventory datasheets prepared based on Indian Remote Sensing Satellite (IRS-P6) AWiFS data of 2004-07 periods, Shuttle Radar Terrain Mapping SRTM-DEM, MODIS land surface temperature and other ancillary data are the main data sets used in deriving the required physical and climatic parameters for the study. Primary physical parameters are taken from the inventory datasheet and with these parameters secondary parameters are derived and land surface temperature is derived from MODIS product. Morphological parameters such as Total area of glacier, Length, Elevation, Orientation, Latitude and Ice exposed area are the primary parameters. Percent debris covers, Percent slope, Temperature are the derived parameters. Each parameter is further grouped into 5 classes based on its range of available values and is assigned with a rank as per its significance for the glacier health. The comparisons of parameters are made using a scale of absolute judgments that represents how much more; one element dominates another with respect to a given attribute. The broad study approach is given in flow diagram Figure 272.

The parameters are compared and assigned importance as per Saaty's (Saaty, 2008) method and comparison matrix is prepared. The matrix is solved by Eigen vector method for deriving the consistency index, Eigen weights and consistency ratio. The consistency ratio less than or equal to 0.1 is acceptable (Saaty, 2008). Larger values require the decision maker to reduce the inconsistencies by revising judgments. Weighted ranks are obtained by multiplying the Eigen weights (Table 86) and rank assigned to each parameter. The composite weights are then obtained by summation of all weighted ranks for a given glacier. These composite values obtained for each glacier are the Composite Glacier Health Index (CGHI) values and are categorized from low to high into five health status classes to identify the relative fragile and healthy glaciers in the Ganga basins.

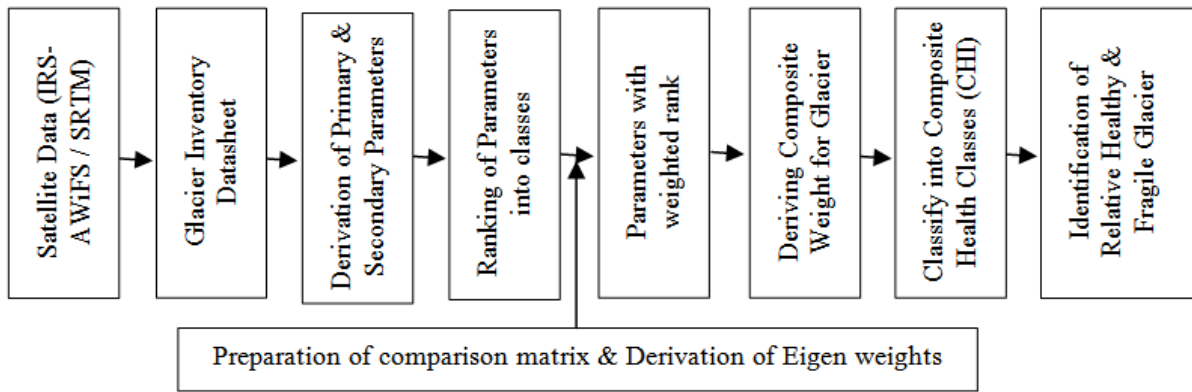


Figure 272: Broad Approach: Relative Glacier Health Assessment (Source: Jyotsna et al., 2014)

Table 86: Eigen weights for relative health assessment parameters (Source: Jyotsna et al., 2014)

Sr.No	Parameter	Eigen Weight	Sr.no	Parameter	Eigen Weight
1	AAR	24.0	5	Glacier Orientation	5.0
2	Glacier Area	18.2	6	Percent Debris Area	9.2
3	Glacier Length	13.0	7	Glacier Elevation	22.8
4	Ice Exposed Area	5.0	8	Glacier Percent Slope	2.9

13.5. Results and Discussion

Morphologically the glaciated area is distributed into accumulation area, ablation area debris and ablation area ice covering 59.1%, 26.3% and 14.5% area respectively in Ganga Basin (Sharma et al, 2013). The eight parameters used in the study are considered significant for glacier health. Each of the eight parameters is ranked as per its significance for the glacier health. Higher rank has been assigned to higher values of AAR, Area, Length, elevation, %debris cover but in case of ice exposed area and %slope these parameters are assigned with lower rank to the higher values of parameter. The eight directions of glacier orientation are also assigned ranks as per their significance. The value of composite weight obtained for each glacier is the Composite Glacier Health Index (CGHI). The CGHI values obtained for these glaciers are values represent the relatively fragile glacier and the higher values represent the relatively healthy glaciers. The percent number of glacier in the five classes are 20.3,18.9, 24.9, 17 and 18.9 percent and occupying glaciated 2.3, 4.3, 10.2, 13.2 and 70.1 percent glaciated area for CGHI class I to V respectively (Table 87)

Table 87: Statistics for %number of glacier and %area of glaciers in Ganga Basin
(Source: Jyotsna et al., 2014)

CGHI	CGHI Range	% No. of Glaciers	% Glaciated Area	Mean Glacier Area
I	<190	20.3	2.3	0.3
II	190 to <260	18.9	4.3	0.7
III	260 to < 330	24.9	10.2	1.2
IV	330 to < 400	17	13.2	2.3
V	>400	18.9	70.1	11

For 6237 glaciers in Ganga basin 20.3% number of glaciers cover 2.3% of area under fragility. Even the cumulative values of CGHI classes I & II at 39.2 % number of glaciers and 6.6 % glaciated area reflect that fragile glaciated area is relatively low. The map showing distribution of relative fragile and healthy glacier in Ganga Basin is given in Figure 273. The sub-basin Level Distribution of Fragile and Healthy Glaciers as percent number of glaciers in each sub-basin and percent area of glaciers in each sub-basin are given below in Figure 274 and Figure 275.

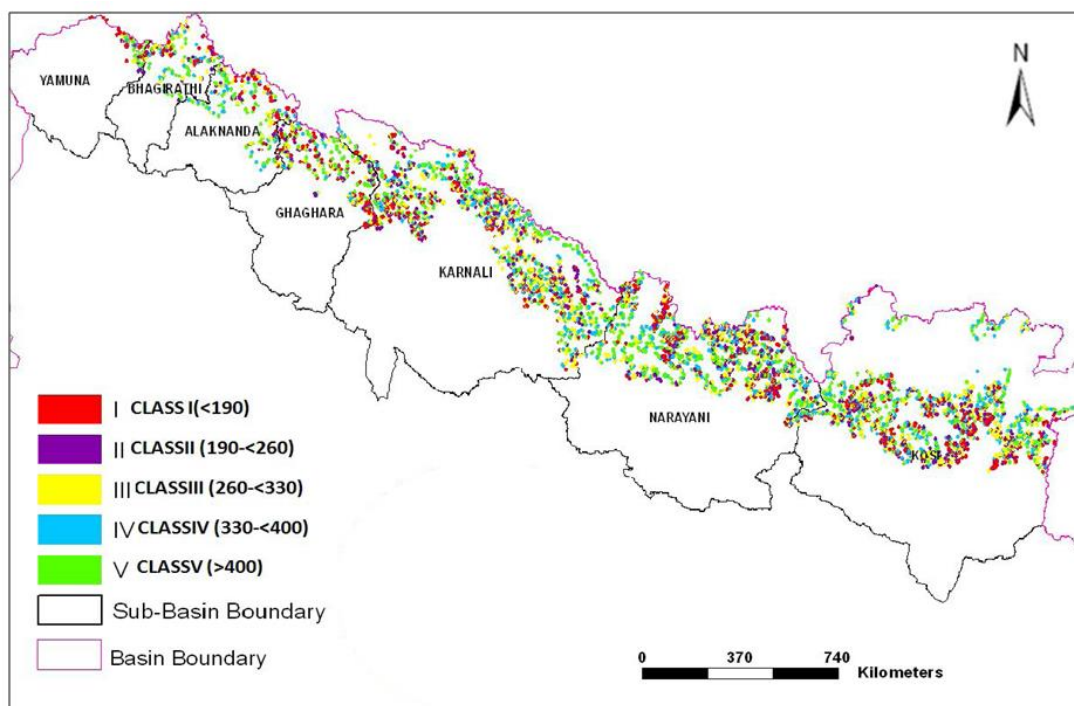


Figure 273: Map showing distribution of relative fragile and healthy glacier in Ganga Basin. Glacier represented as coloured points. Colour assigned as per CGHI class (Source: modified after Jyotsna et al., 2014)

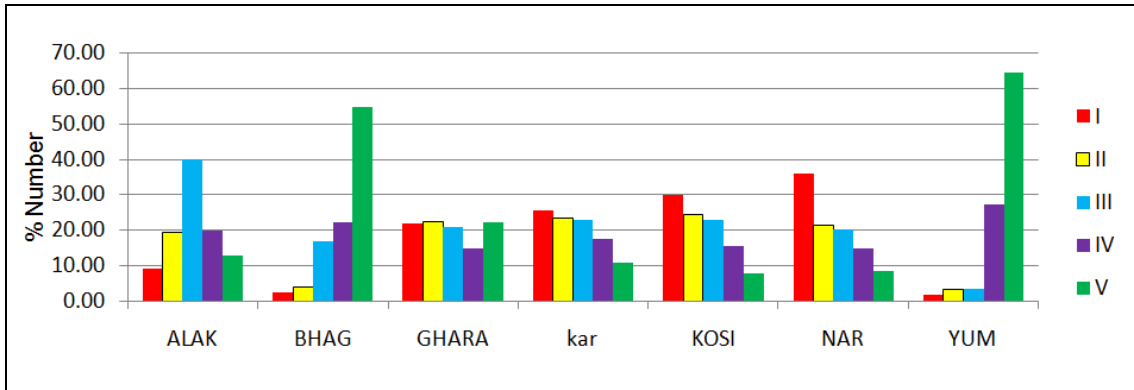


Figure 274: Sub-basin Level Distribution of Fragile and Healthy Glaciers: Percent number of glaciers in each sub-basin Alaknanda (ALAK), Bhagirathi (BHAG), Ghagra (GHARA), Karnali (KAR), Kosi (KOSI), Narayani (Nar), Yamuna (YAM)

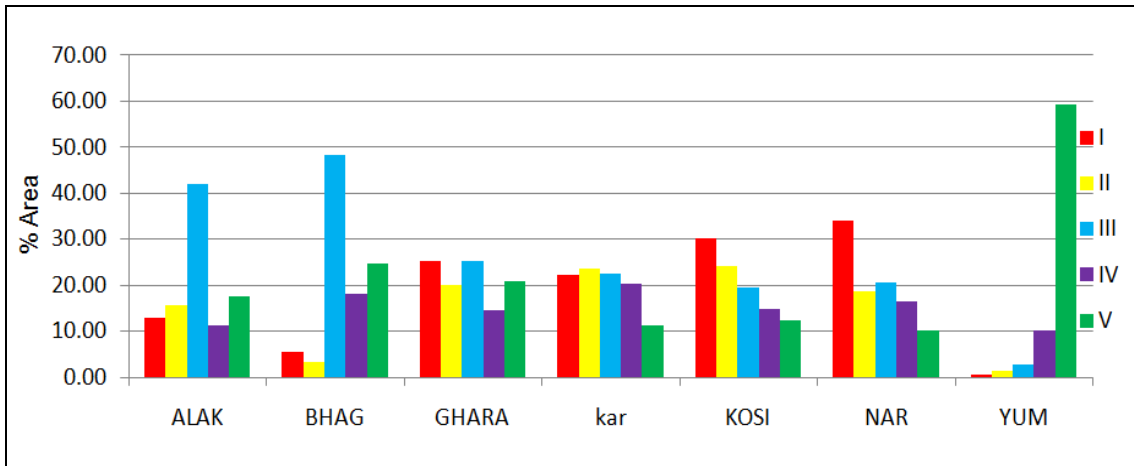


Figure 275: Sub-basin Level Distribution of Fragile and Healthy Glaciers: Percent area of glaciers in each sub-basin Alaknanda (ALAK), Bhagirathi (BHAG), Ghagra (GHARA), Karnali (KAR), Kosi (KOSI), Narayani (Nar), Yamuna (YAM)

The spatial distribution of relatively fragile glaciers is obtained based on the multi-parameter weighted index method by using eight key glacier physical parameters. About 20.3% number of glaciers covers 2.3% area. Apparently the smaller glaciers with mean size of 0.3 km² area in Ganga Basin are relatively fragile.

Remote sensing and GIS based multi-parameter weighted index method is useful to identify spatial distribution of fragile glaciers. The flexibility inherent to this model permits addition of more parameters and thereby has scope for increasing the accuracy of assessment. The climatic parameter not used in this model can be added

to further improve the accuracy. Efforts for systematic validation of results are also required.

14. Impact of Climate Change on Flora of Spiti Valley

14.1. Objective

To understand the impact of snow line on the floral distribution in the valley and its societal impact in Spiti valley, Himachal Pradesh.

14.2. Scientific Rationale

Impact of climate change on the the flora and habitats in regions adjacent to glaciated terrain needs to be studied. Retreating glaciers and dwindling water resources have significant impact on the biodiversity and species richness of the flora. In this context a pilot study to understand the impact of retreating glaciers on the flora of the Spiti valley as well local inhabitants has been taken up. Flora of Spiti valley are extremely important to be conserved not only because of large biodiversity and species richness but also because inhabitants of the area have dependence on these plant resources required for food, health, shelter, fodder, fuel wood and other cultural purposes.

Glacier retreat as well as agro-diversity changes are occurring at an alarming rate since last one decade in the Spiti valley. Water availability is apparently one of the gravest /serious impacts of climatic change in Spiti valley which is mainly dependent on glacier melt water for irrigation and domestic purposes. Natural water resources have decreased up to 27.81% in all the Spiti Villages. Most of the natural springs have dried up and there is insufficient water for irrigation.

Populations of endangered and vulnerable species are gradually diminishing due to great demand for medicinal purposes. Over exploitation, Land scalping, over-grazing and developmental activities are other factors for depletion of this natural wealth. Economically important species of the valley are significantly shifting toward higher altitudinal regimes and making them highly vulnerable. The species of high altitudinal region are under great threats as they have limited opportunity to migrate farther upwards in elevation to find cooler habitat conditions. The climate sensitive species are required to be regularly monitored, protected and modeled by suitable latest modeling tools for their distribution pattern and phenological attributes so that the base line data can be utilized for understanding impact of future climate changes in the area. There is a need for regular monitoring the habitats and communities to understand the dynamics of the habitats and communities and accordingly plan for their management.

14.3. Methodology

Field studies were conducted in the Spiti valley of Lahual and Spiti District in Himachal Pradesh (Figure 276). and analysis of floristic diversity. Plots of 20x20 m were selected in different aspects and habitat. 20 quadrats of 5X5 m for shrubs and 20 quadrats of 1x1 m for herbs were randomly laid within the plot. Communities were identified based on their importance, value-index and calculated as the sum of relative-frequency, relative density and relative abundance. For the collection and analysis of data from these quadrats standard ecological methods (Simpson, 1949; Shannon & Weaver, 1963; Curtis and Intosh, 1950; Grieg-Smith, 1957; Chacko, 1965; Kersaw, 1973; Muller-Dombois and Ellenberge, 1974; Dhar et al., 1997; Samant and Joshi 2004) were followed. During qualitative assessment, surveys and samplings between 3180-4560 m were done in each season and identified with the help of floras and literature available in this field (Polunin and Stainton, 1984; Aswal and Mehrotra, 1994; Chowdhery and Wadhwa, 1984; Dhaliwal and Sharma, 1999; Samant, 1999; Samant and Pangtey, 1993; Samant et al., 2000; Samant and Joshi, 2004; Singh and Rawat, 2000 and Murti, 2001). Socio-economic survey on the impact of retreading glacier, changing weather and cropping pattern was done through interview using formal and informal set of questions.

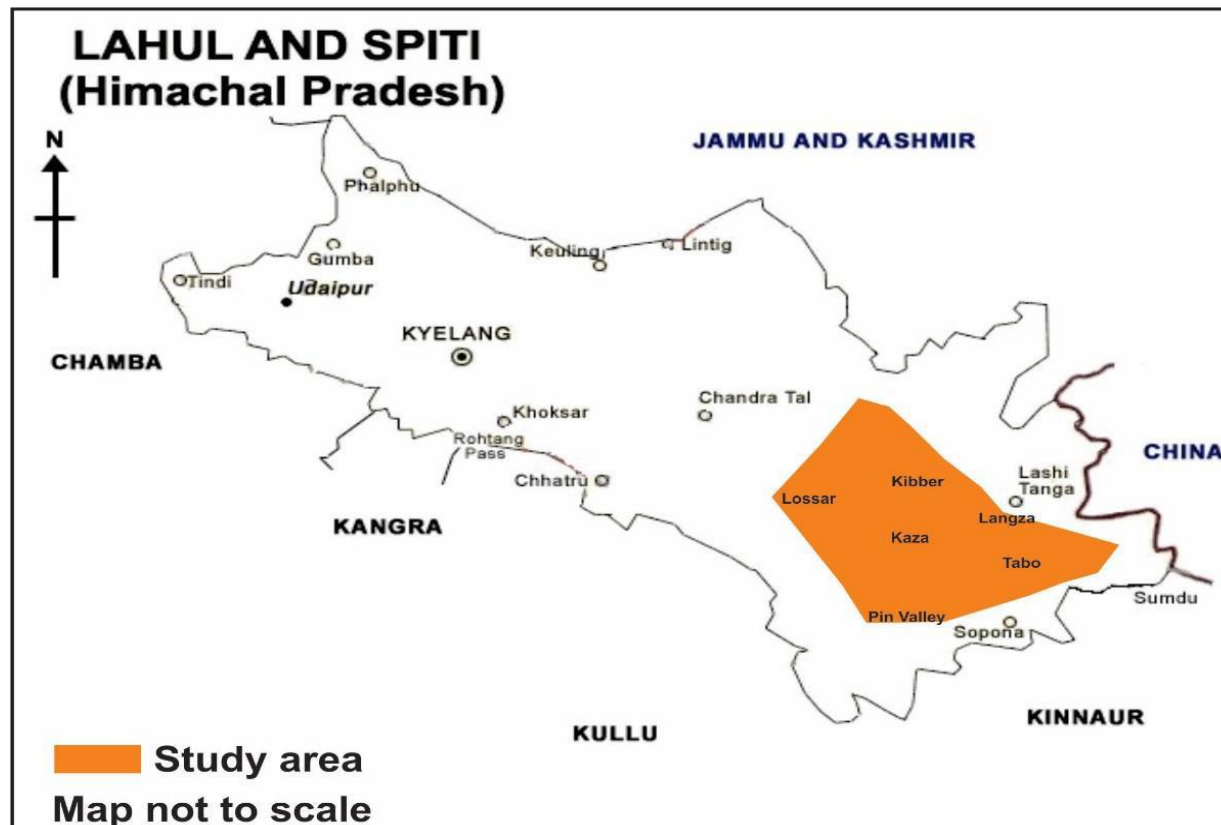


Figure 276 Map showing the study area in Lahul and Spiti district, Himachal Pradesh

14.4. Results and Discussion

The present study was conducted for phyto-diversity assessment in Spiti valley of Himachal Pradesh, India in 84 sites which were distributed between 3000-4560 m above mean sea level. Sites were selected based on different topographical features such as habitat type, altitude, aspect, slope, and different vegetation types. Geo-references for each site/habitat were taken with the help of Global Positioning System (GPS). The number of herbs, shrubs and trees are 369, 24 and 9 respectively. Six species are under shrubs; 3 species are either herbs or shrubs. *Betula utilis* is either a shrub or a tree. The top 9 families of the flora of Spiti are Asteraceae (58 species), Papilionaceae (40 species), Poaceae (30), Brassicaceae (25), Rosaceae (24), Ranunculaceae (23 species), Apiaceae (20 species), Scrophulariaceae (18 species), and Polygonaceae (15 species).

Qualitative analysis of vegetation was carried out between 3180–4560 m. 412 species belonging to 216 genera and 55 families have been collected, identified and photographed. Out of these 362 species belonging to 184 genera and 45 families are dicots, 47 species belonging to 30 genera and 8 families are monocots. The top 10 families of the flora of Spiti are Asteraceae (58 species), Papilionaceae (40 species), Poaceae (30), Brassicaceae (25), Rosaceae (24), Ranunculaceae (23), Apiaceae (20), Scrophulariaceae (18), Polygonaceae (15) and Caryophyllaceae (12). We delineated 41 alpine communities (33 shrub and 8 herb communities) based on relative density for the shrub and herb communities. Amongst these, *Caragana brevifolia* community represented by maximum sites (15 sites); followed by *Hippophae rhamnoides* & *Ephedra gerardiana* (7 each); *Hippophae tibetina* and *Potentilla arbuscula* (4) *Myricaria elegans*, *Lonicera spinosa*, *Astragalus strobiliferus*, *Myricaria germanica* and *Astragalus webbianus* (3 each); *Ephedra intermedia* (2 each) and rest of the communities represented by one site only.

Present study depicts 167 native and 245 non-natives, 37 as endemic, 42 near endemic species in the valley. Increasing number of non-native species is a major concern and hence showing the significance of conservation prioritization in the valley. People in Spiti valley believe in indigenous medicines known as *Amchi* system of medicine which is based on Tibetan System of Medicine. The widely used medicinal plants from high altitude regions are *Aconitum heterophyllum*, *Dactylorhiza hatagirea*, *Ephedra gerardiana*, *Hippophae rhamnoides*, *Inula racemosa*, *Podophyllum hexandrum*, *Rheum webbianum*, etc.

Altitudinal Shift of the plant species

The present study when compared to the earlier studies revealed that the economically important species of the valley are significantly shifting toward higher altitudinal regimes and making them highly vulnerable (Figure 277)



Figure 277: Important species of the valley shifting toward higher altitude

Various ecological parameters studied along altitudinal gradient

- **In 3000-3500m altitudinal range**

Among shrubs the relative density of *Ephedra intermedia* (23.83%) are maximum followed by *Ephedra gerardiana* & *Hippophae rhamnoides* (17.83 & 8.96 %) respectively. Whereas the IVI of *Ephedra intermedia* (65.47) are maximum followed by *Ephedra gerardiana* & *Lectuca orientalis* (35.87 & 29.77). The distribution of species (a/f ratio) in this altitudinal showed that 64.70% species were random and 35.29 % species were contiguous. Among herbs the relative density and IVI are maximum of *Carex melanantha* (3.23% & 6.97) followed by *Koberasia napalensis* & *Carum carvi* (2.90 & 2.65 % and 6.48 & 6.00) respectively. The distribution of species (a/f ratio) in this altitudinal showed that 100% species were of contiguous in nature.

- **In 3500-4000m altitudinal range**

Among shrubs the relative density and IVI are maximum of *Myricaria elegans* (16.66% & 34.57) followed by *Ephedra gerardiana* & *Myricaria saquamosa* (9.57 & 6.72 % and 22.95 & 18.01) respectively. The distribution of species (a/f ratio) in this altitudinal showed that 4.16% species were regular, 58.33% random and 37.5% species were contiguous in nature. Among herbs the relative density and IVI are maximum of *Carex melanantha* (2.88% and 5.74) followed by *Carex borii* & *Euphorbia officinalis* (2.66 &

2.13 % and 5.39 & 4.58) respectively. The distribution of species (a/f ratio) in this altitudinal showed that 100% species were contiguous in nature.

- **In 4000-4500m altitudinal range**

Among shrubs the relative density and IVI are maximum of *Hippophae tibetana* (8.56% & 20.99) followed by *Hippophae rhamnoides* & *Potentilla salesoviana* (8.41 & 7.69 % and 20.78 & 19.65) respectively. The distribution of species (a/f ratio) in this altitudinal showed that 4.16% species were regular, 75% random and 20.83 % species were contiguous. Among herbs the relative density and IVI are maximum of *Carex melanantha* (2.89% and 5.87) followed by *Carum carvi* & *Carex orbicularis* (2.42 & 2.41 % and 5.38 & 5.36) respectively. The distribution of species (a/f ratio) in this altitudinal showed that 100% species were contiguous in nature. Abundance frequency ratio of the Species along altitudinal gradient of shrubs and herbs was observed in different altitudes in Spiti valley. It was reported that the distribution was contiguous in 3000-3500 m range but was regular in 3500-4000 and 4000-4500m

Spiti valley is rich in wild plant resources. The inhabitants of the area have close relationship with surrounding plant resources with reference, to some extent, of their dependence on plant resources for their food, health, shelter, fodder, fuel wood and other cultural purposes. Total 42 villages were surveyed and 316 people of age group 25-88 were interviewed for dependence on local plant resources. In Spiti valley stakeholders use different plant parts in the preparation of indigenous medicines. Study revealed that leaves (49 spp.) are being used most of the times followed by aerial parts (36 spp.), roots & whole plants (29 spp.) and flower (27 spp.) The economic species can be categorized into medicinal (169 species), edible (50 species), fodder (65 species), fuel yielding (21), dye yielding (16 species), oil yielding (11 species), Tannin yielding (8), Wood yielding (7 species), Spices and condiments (7 species), sacred value (7 species), ornamental value (5 species), Soil binder (5), narcotic (2 species) and fiber yielding (2 species).

A comprehensive base line data which has been generated through present study will further enhance the knowledge of the flora, microbial diversity and other ecological aspects of the valley. The study on the niche modeling of the selected ecological and economically important species for keeping the track of the population and their possible distribution in the times to come is urgently required as the anthropogenic activities and habitat destruction and fragmentation and climate change etc. are contributing to the vulnerability of the flora from the region. Maximum species richness & density are distributed below 4000 m and diversity is 3000-3500 m. Some species have wider range of distribution which is present in both altitude range e.g. *Astragalus himalayanus*, *Carex melanantha*, *Causinia thomsonii*, *Gentiana argentea*, *Gentiana moorcroftiana*, *Lomatogonium carinthiacum*, *Nepeta podostachys* etc. The species which are above 4000 m are *Aconitum violacium*, *Rhodila hetrodonta*, *Saxifraga flagellaris*, *Walthemia tomentosa*, *W. glabra*, *Rheum moorcroftiana* etc. shows high rate of acclimatization for the arid environments (Figure 278). The species of high

altitudinal region are under great threats as they have limited opportunity to migrate farther upwards in elevation to find cooler habitat conditions. Species density and diversity index of herbs is decreasing as we go in the higher elevation because of harsh and arid conditions which make survival of the herbs difficult. Whereas species richness is maximum at 3500-4000 m which may be is due to its diverse habitats and suitable bitats. Altitudinal range 3500-4000 m is occupying the maximum number of species.

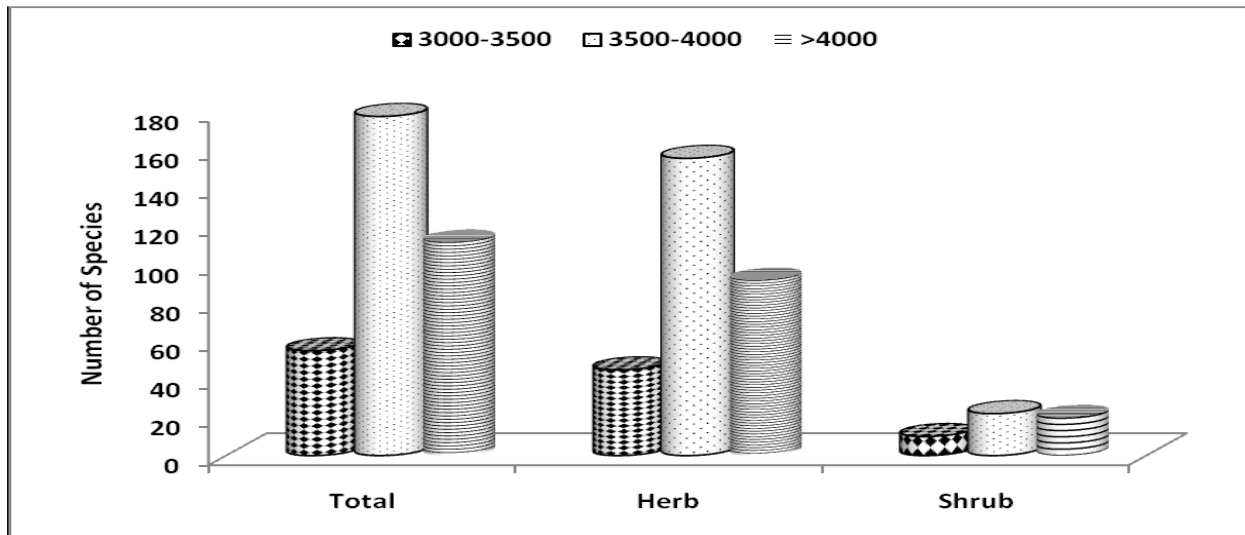


Figure 278: Acclimatization of the herb and shrub to the arid environments

Agriculture/Horticulture and Cropping patternsof Spiti valleys

The data recorded on old crops grown in Spiti valley namely Field Pea, Wheat, Barley, Potato and Mustard shows decrease in their cropping area. Area under these crops 2 decade ago has maximum under barley (55.2%) and minimum under mustard (0.96%). However, in present area under barley reduced 37.72%. Newly introduced crop includes Garden pea (42.66%) and Apple (6.93%) is emerging as major cash value crop therefore other crops agricultural area is shrinking as compare to past. Villages under apple cultivation are Kaza, Lidang, Lara, Shichiling, Poh, Tabo, Hurling, Lari and Dhankar. Maximum apple growing village is Tabo (53.75%) and minimum Lari (35.23%). Garden pea and apple covers 49.59% area out of total cultivated land. (Figure 279).

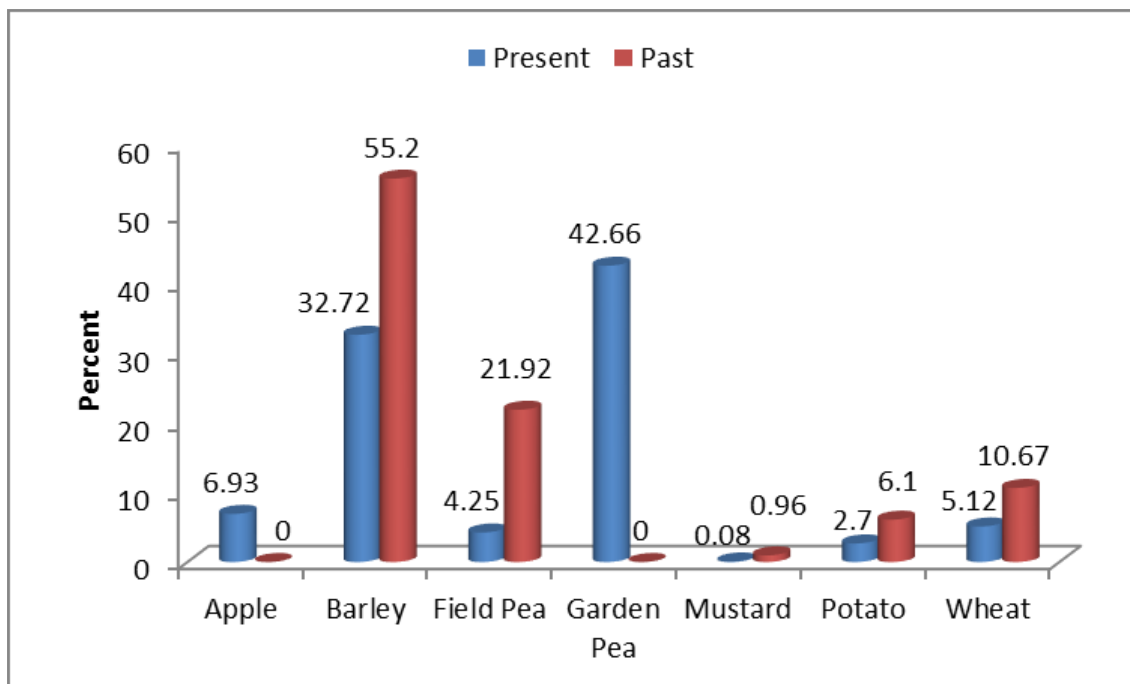


Figure 279: Comparison between Present and past status of various Crops grown in Spiti Valley

All respondents mentioned that apple cultivation has shifted in the higher altitude region. Earlier apple was found only in the lower altitude but now it is found at altitude 3219-3872 m. Another point is the appearance of pests and insects on plants, something that has not happened before in villages of lower valley. The effect of climate on agriculture is related to variability in local climate patterns. Variation in the climate season and shifting to new crops leads attack of pest like powdery mildew in garden pea, farmer is started using chemical or fungicide spray in cash crops which are not common in past. Decrease in potential yield is likely to be caused by shortening of the growing period, decrease in water availability.

Analysis of data gathered on people's perception shows that glacier retreat as well as agro-diversity changes are occurring at an alarming rate since last one decade. Most of the age old group (between age 65-80) are of the view that these are happening since long time back and is not a recent phenomenon. Most of the females of the valley are of the same view. Educational status in the valley showed a significant number of graduates i.e. 49.4% sharing the similar views regarding glacier retreat and agri-horticulture changes.

Water availability is apparently one of the gravest /serious impacts of climatic change in this Spiti valley which is mainly dependent on glacier melt water for irrigation and domestic purposes. The analysis of data collected from 42 villages in the valley revealed 160 that 144 glacier fed natural water resources were feeding in the past, however, only 136 are found to have accessible water at present. Maximum number of natural water resources is found to be present in villages namely Lossar (20),

Dhankar (16), Kibber (15). Followed by Mudh (12) and Burr (10). But there is no significant fall in the number of kuhls in Spiti basin which were used to be 103 in past but left 101 presently. Natural water resources are decreased up to 27.81% all the Spiti Villages. The maximum natural water source (*Kulh*) is reduced in the village Hansa and Kaza up to 40% also minimum reduced in village Jomle (15%).

Regular monitoring using random sampling by quadrat method is suggested in the habitats and communities to understand the dynamics of the habitats and communities and accordingly plan for their management. The climate sensitive species are required to be regularly monitored or modeled by suitable latest modeling tools for their distribution pattern and phenological attributes so that the base line data can be generated for future changes in the area. The information generated on these lines will provide a better insight about the present status of floristic diversity and help in developing adequate strategies and action plan for the management of such biodiversity rich areas. Further, for in-situ conservation of the economically and ecologically important species, regular monitoring of the sites and complete protection of the habitats is suggested. In addition, seed germination protocols developed may be used for mass multiplication of the species and seedlings should be transplanted in comparable habitats so that viable population of the species can be maintained. Furthermore, the effect of retreating glaciers on the biodiversity of the region may be monitored from time to time by suitable modeling tools. The findings would help policy planners, conservationists and local people to devise suitable strategies to protect the economic flora in the valley.

15. Development of Algorithm for Snow Cover/ Snow Depth Products using INSAT-3D Data

15.1. Objective

To develop algorithm for generating snow cover/snow depth product from INSAT 3D Imager data (geostationary platform) and operationalize generation of daily digital snow cover map products.

15.2. Scientific Rationale

Water is one for the most important component on the Earth surface and plays an important role in collection, distribution, analysis and management for hydrological and climatological applications at regional and global scale (Dozier, 1992). About 10% of the earth's surface, $15 \times 10^6 \text{ km}^2$, is covered by polar ice caps and glaciers (the Cryosphere). The glaciers and mountain ice caps cover an area of about 550,000 km^2 on Earth (excluding Antarctica and Greenland) and nearly all of its lies in the North America and Eurasia. Snow covers almost 40 per cent of the Earth's land surface during Northern Hemisphere winter. This makes snow albedo and area an important component of the Earth's radiation balance (Foster and Chang, 1993). The geographical extent of snow cover over the Northern Hemisphere varies from a maximum of $\sim 46 \times 10^6 \text{ km}^2$ in January and February to a minimum of $\sim 4.6 \times 10^6 \text{ km}^2$ in August. About 60 to 65 % of winter snow cover is found in Eurasia and most mid-summer snow cover is found in Greenland (Frei and Robinson, 1999). However, the spatial density of in-situ measurement network is too low to provide an adequate characterization of its distribution (Mognard et al., 2003). The remoteness and hostile environment of snow and glaciated region means investigations by remote sensing methods, preferably from space platform is desirable (Massom 1991). Cryosphere is being monitored from space since the mid-1960s (Foster and Chang, 1993). Large areas in the Himalayas are also covered by snow during wintertime. Area of snow can change significantly during winter and spring. This can affect stream flow during spring and summer of the rivers originating in the Higher Himalayas. The maximum snow cover for the three major river basins, namely the Indus, the Ganga and the Brahmaputra, altogether is approximately 85% of the total geographic area which reduces to approximately 10% during ablation (Singh et al., 2014). In addition, snow pack ablation is highly sensitive to climatic variation. Increase in atmospheric temperature can influence snowmelt and stream runoff pattern (Kulkarni, et al. 2002b). Therefore, mapping of areal extent and reflectance of snow is an important parameter for various climatological and hydrological applications. In addition, extent of snow cover can also be used as an input for avalanche investigation.

Snow was first observed by satellite in eastern Canada from the TIROS-1 satellite in April 1960. Since then, the potential for operational satellite-based mapping has been enhanced by the development of higher temporal-frequency and satellite sensors with higher spatial resolution. Remote sensing technique has been extensively used for snow cover monitoring in the Himalayan region with the help of numerous satellite sensors (Hall et al., 2001; Romanov et al., 2000, 2003; Kulkarni and Rathore. 2003). The discrimination between snow and cloud can be done by using various techniques such as textural analysis, association with shadow and by using multi temporal analysis. Discrimination between cloud and snow is not feasible due to similar high reflectance in VNIR region, however it is possible due to contrasting behavior of them in SWIR region. To overcome the problem of cloud and snow, Normalized Difference Snow Index (NDSI) method was developed (Hall et al., 1995; Kulkarni et al., 2006b). Satellite sensors with better radiometric resolutions, such as MODIS and AWiFS have been used successfully for snow mapping (Hall et al. 2002; Kulkarni et al., 2010; Singh et al., 2014). Information generated from satellite observations has been extensively used for snowmelt runoff modeling (Kulkarni et al. 2002a).

15.3. Study Area and Data Used

INSAT 3D Imager covers the India and neighboring countries from geostationary platform. The entire Hindukush-Karakoram-Himalaya (HKH) region is covered for generating snow cover product. AWiFS derived snow cover product have been used to validate and derive fractional snow cover product over the study area. Auxiliary data such as DEM has been used along with INSAT 3D derived reflectance and thermal data.

15.4. Algorithm Development

Snow strongly reflects in the visible region and absorbs in the SWIR region which makes snow a distinct object on the Earth surface. Figure 280 shows the spectral characterization of snow and other objects. It can be clearly observed that snow is very bright object in visible region due to its high albedo. Snow behaves as a dark object as it moves towards longer wavelength. AWiFS channel collects the radiance in Green (B2), Red (B3), NIR (B4) and SWIR (B5) region and Figure 281 shows the TOA reflectance over the Himalayan terrain. Snow appears quite bright in B2, B3 and B4 whereas it becomes dark in B5. Non-snow area is showing low reflectance in B2, 3 & 4 whereas return comparatively high reflectance in B5. Cloud has persistently shown high reflectance in all bands, however, can be identified based on textural information. The high reflectance in visible region and low reflectance in SWIR region forms a base to estimate Normalized Difference Snow Index (NDSI).

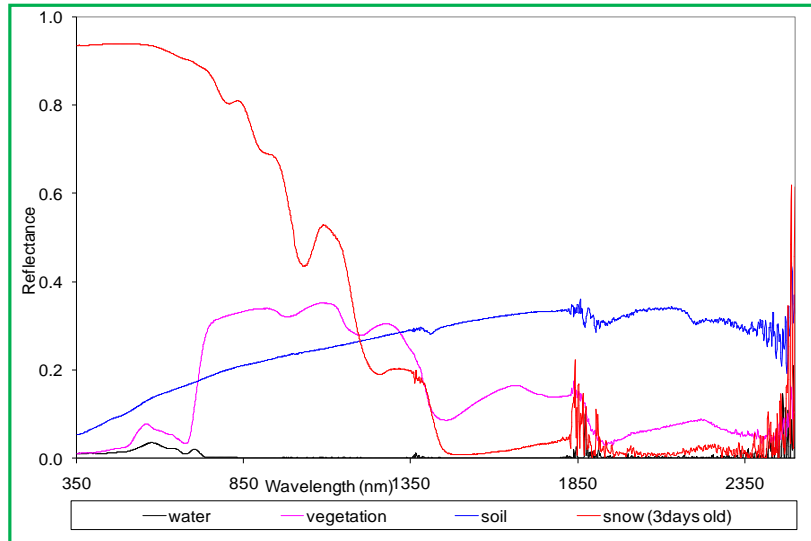


Figure 280: Spectral behaviour of snow and other objects in parts of the Himalayas

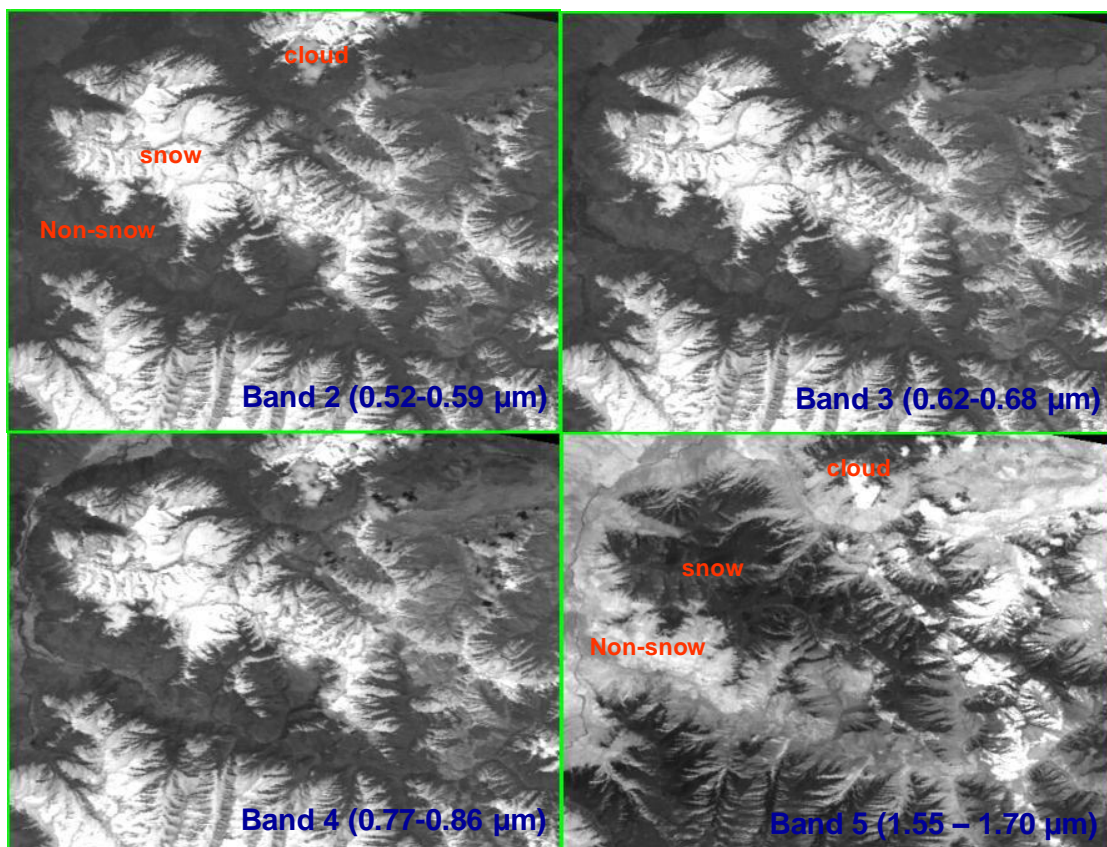


Figure 281: TOA reflectance of AWiFS data over Himalayan region

Normalized Difference Snow Index (NDSI)

The NDSI is useful for the identification of the snow, and for separating snow and most of the clouds. The NDSI is a measure of the relative magnitude of the characteristic reflectance difference of snow between the visible and short-wave IR reflectance. The NDSI is insensitive to a wide range of illumination conditions (Kulkarni et al., 2006b). The NDSI is analogous to the Normalized Difference Vegetation Index (NDVI) (Tucker, 1979 and 1986; Townshend and Tucker, 1984). NDSI can be calculated using normalized difference ratio of visible and SWIR channels for INSAT 3D imager, as given below;

$$NDSI = \frac{visible_{INSAT\ 3D\ B1} - SWIR_{INSAT\ 3D\ B2}}{visible_{INSAT\ 3D\ B1} + SWIR_{INSAT\ 3D\ B2}}$$

Pixels that are approximately 75 % or greater covered by snow have been found to have NDSI values ≥ 0.4 in our field investigation at Dhundi test site in Himachal Pradesh (Negi et. al., 2006, 2010). These NDSI thresholds have been verified from detailed analysis of numerous AWiFS scenes, comparisons with supervised-classification techniques and NDSI technique (Kulkarni et. al. 2004). Pure snow has a high NDSI but NDSI decreases as other features are mixed in a pixel. Snow in mixed pixels has an NDSI that is less than that for pure snow. Pure snow can be distinguished by its high NDSI value (Negi et. al., 2006, 2010). NDSI threshold value was established using visual interpretation and field based spectral data of different targets.

Utilization of INSAT 3A CCD data

INSAT 3A CCD data was also used for the characterization of different land cover classes and cloud. However, a need to recalibrate the INSAT 3A data was felt due to degradation of sensor and AWiFS sensor was used for the same. AWiFS sensor has been routinely calibrated over Chharodi site at Sanand in Gujarat (India) maintaining flat uniform area, stability of surface reflectance, identified area in satellite image and easy accessibility for conducting experiment. The calibration analysis was carried out and the recent calibration data showed less than 2 % degradation for LISS IV and LISS III sensor and 3 % degradation for AWiFS sensor over a period of 3 years (Manjunath and Muralikrishnan, 2008). Three individual scenes from January, February and March months for each sensor were used. Concurrent clear sky satellite overpasses (at 0500 GMT) over India on 23 January 2007, 16 February 2007 and 26 March 2007 for INSAT 3A CCD and AWiFS data were selected. The AWiFS and INSAT 3A CCD have similar spectral channels in visible, NIR and SWIR region but at different spatial resolution of 56 m and 1 km respectively. The study area encompasses spatial extent (22-37° N, 69-94° E) which includes different land cover classes over Northern India such as: snow, agriculture, bare soil, forest, cloud and water bodies. The time for INSAT 3A CCD data was chosen at 10.30 a.m. and the satellite equatorial crossing time for AWiFS was 10.30 a.m. \pm 5 min. In addition, INSAT 3A CCD data on 05 March 2007 was also used in the study to compare the effect of pre-launch and post-launch calibration coefficients. The at-sensor apparent reflectance (TOA reflectance) was computed assuming a lambertian surface and

RSR-weighted exo-atmospheric bandpass irradiances ($E_o(\lambda)$). The INSAT 3A CCD NDSI and NDVI were computed from TOA reflectance before and after cross-calibration.

The average at-sensor radiances for each class were computed for each channel (Visible, NIR and SWIR). Average radiance values of common homogeneous subset of collocated targets were calculated for all INSAT pixels to all respective AWiFS pixels of one object. This accounts for the spatial heterogeneity introduced due to the difference in spatial resolutions of both the sensors. The radiances from both AWiFS and INSAT 3A CCD were subsequently plotted for all the three channels. The linear regression was performed for individual channels between calibrated AWiFS and INSAT 3A CCD at-sensor radiances with pre-launch calibration (Figure 282). The regression analysis between corresponding AWiFS and INSAT 3A CCD channels showed linear relations with high R^2 of 0.96 for visible channel (0.63-0.69 μm) and of 0.92 for NIR (0.77-0.89 μm) channels with 16 datasets. The INSAT 3A CCD SWIR channel showed severe sensor degradation with low R^2 of 0.60. The slope values after cross calibration for Visible, NIR and SWIR channels were found to be 1.839, 1.589 and 2.232, and intercepts as -5.803, -4.950 and -0.481, respectively. The linear relations were further used to compute CCD at-sensor radiances, TOA apparent reflectances, NDVI and NDSI with independent INSAT 3A CCD dataset of 5 march 2007. It was observed that central wavelength difference varies from 5-9 nm for INSAT 3A and AWiFS and is not significant. It rules out any effect of shift in central wavelength on differences in at-sensor radiances between two sensors.

An improvement on dynamic range of reflectance with old calibration (15-75 %) and new calibration coefficient (10-110 %) were found in the visible channel. High reflecting objects such as snow and cloud have shown a significant improvement from old TOA reflectance to new TOA reflectance computation. In agriculture and forest land cover classes, visible channel TOA reflectance has shown a reduction whereas SWIR channel has shown an increase. SWIR channel was also found to be increased for desert and rock land cover classes. This established that the new coefficients of INSAT 3A CCD data for Visible, NIR and SWIR channels can be used to recalibrate and improve the radiometric quantity for routine applications. The Figure 283a showed the INSAT 3A CCD data of 05 March 2007 and Figure 283b showed the scatterplots of TOA apparent reflectance of visible channel and NDSI using old and new calibration coefficients.

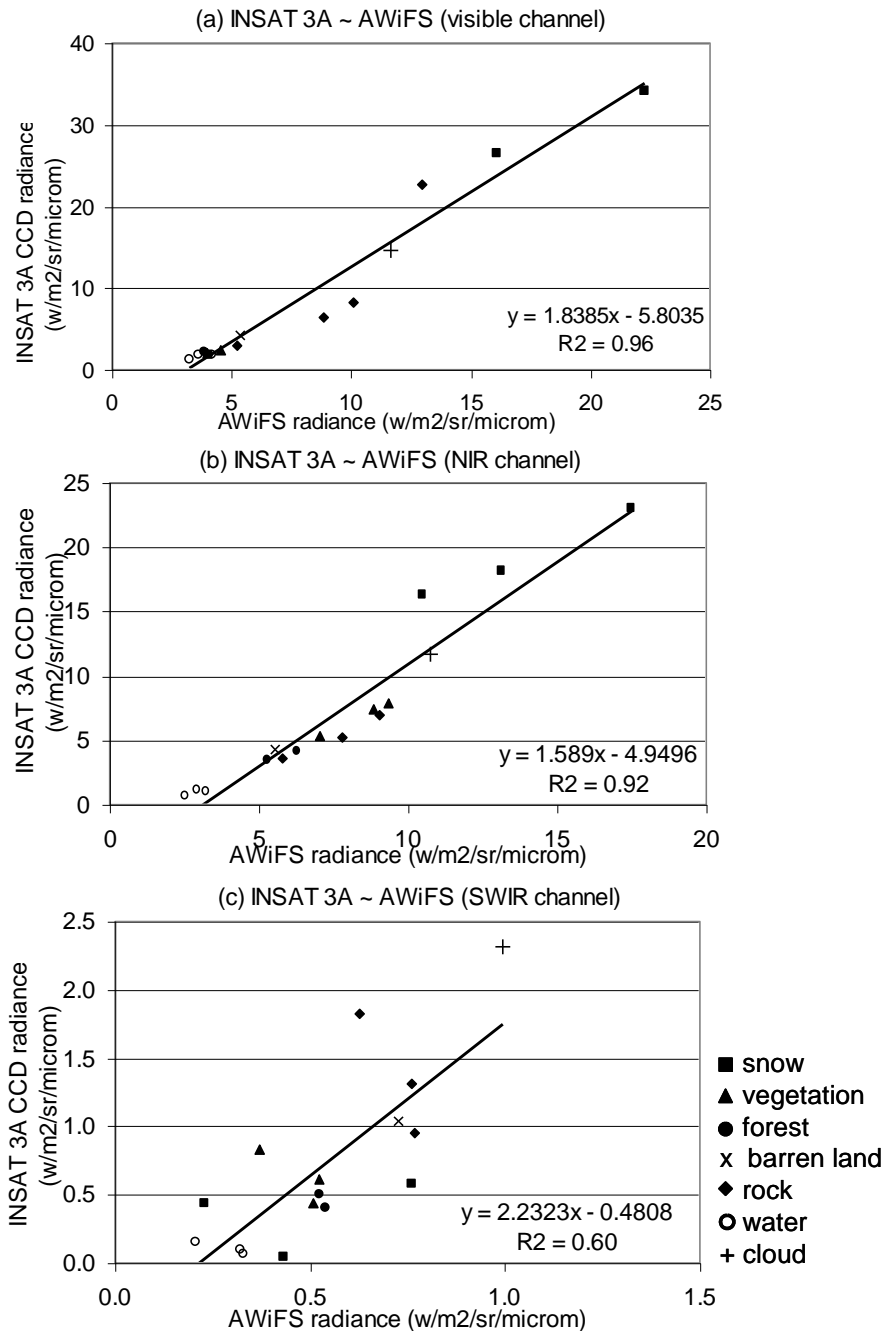


Figure 282: Regression fits between for INSAT 3A CCD and AWiFS at sensor radiances for a) Visible channel, b) NIR channel and c) SWIR channel (Source: Singh et al., 2013)

Figure 284 showed the histogram of NDSI and NDVI for pre-launch and post-launch calibration. The NDSI and NDVI values were computed using both old and new calibrated coefficients. The NDSI and NDVI dynamic ranges have shown an improvement from 0.0 - 0.7 to -0.45 – 0.85 and 0.0 – 0.50 to -0.10 - 0.80, respectively. The NDSI peak has been shifted from 0.1 to -0.25 which showed the dominant presence of non-snow pixels as can be observed in False Colour Composite (FCC) image. Another broad peak of 0.66 was shifted to 0.71 which is

related to snow covered pixels. NDVI values too have shown a peak shifted towards negative side close to 0.0. The dynamic range of NDSI and NDVI was found to be improved in Histograms. This redistribution of NDSI and NDVI values would be helpful further to identify different classes of snow and vegetation pixels. This highlights the importance of post calibration to correct the radiometric quantities for better estimation of various indices for natural resources applications. Thus, these new calibration coefficients will help to improve the monitoring of snow cover and vegetation, and will provide important input to model the long term monitoring of natural resources of Earth environment (Singh et al., 2013a).

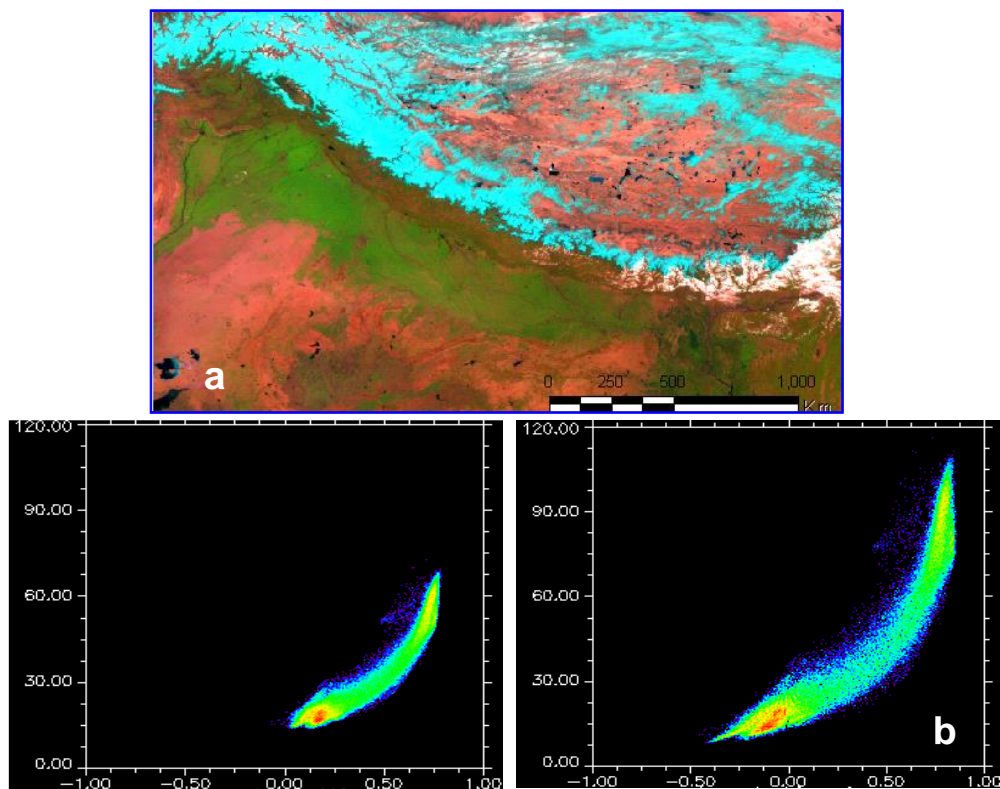


Figure 283: Comparison of INSAT 3A CCD data (05 March 2007) with old and recalibrated coefficients; a. INSAT 3A CCD FCC of 5 March 2000; b. Scatterplots of NDSI (X-axis) and TOA reflectances of red channel (Y-axis) of old and new calibration coefficients (Source: Singh et al., 2013)

INSAT 3A CCD data of 23 January 2007 were also analyzed for different land cover classes. Figure 285 shows the FCC, scatterplot and threshold of SWIR region to separate ice cloud and snow from the snow. However, with the availability of INSAT3D data, seasonal and temporal analysis will be carried out to finalize the suitable threshold of SWIR channel to separate ice cloud and snow in conjunction with NDSI. Separation of cloud will be used as an additional criterion and will be verified with INSAT 3D derived cloud mask product (Figure 285).

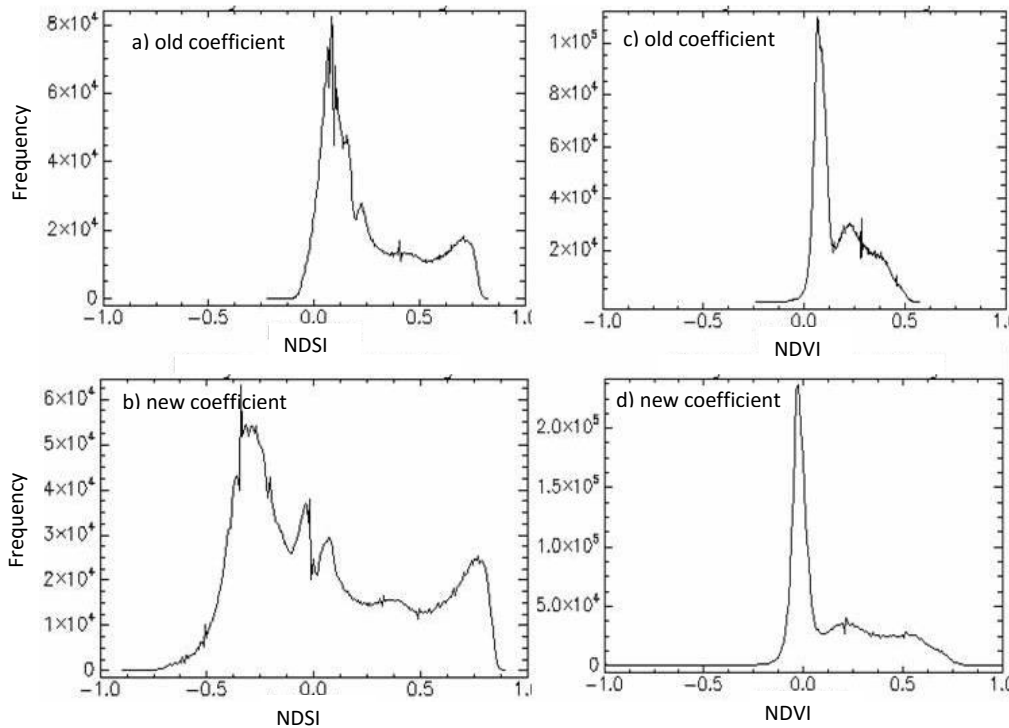


Figure 284: Histograms for NDSI and NDVI from INSAT 3A CCD (5 March 2007 at 0500 GMT) using old and new calibration coefficients (Source: Singh et al., 2013)

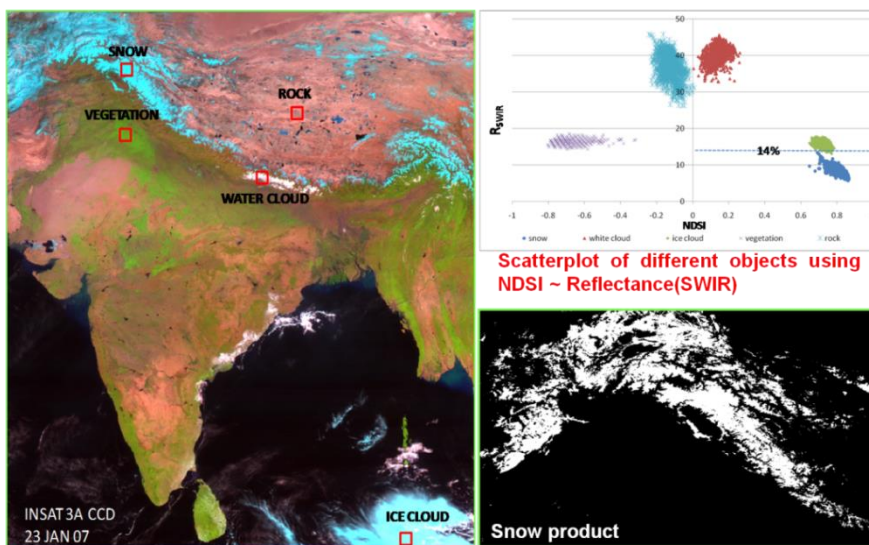


Figure 285: INSAT 3A CCD image of 23 Jan 2007 and SWIR threshold to separate ice cloud from snow product

Snow Cover using INSAT 3D

Snow strongly reflects in visible region and absorbs in SWIR. This peculiar characteristic of snow among various earth objects has been used to develop snow cover mapping algorithm for optical sensors like AWiFS based on Normalized Difference Snow Index (NDSI) approach. While the NDSI can separate snow from

most obscuring clouds, it does not identify or discriminate cirrus clouds from snow due to similar spectral signature. NDSI based algorithm has been developed and validated for AWiFS sensor of Resourcesat. However, INSAT-3D has a broad bandwidth in visible channel whereas SWIR channel collects the radiance in similar bandwidth as in AWiFS. The difference in Visible region of AWiFS and INSAT 3D requires fine tuning of the threshold value for INSAT-3D Imager data.

Visible and SWIR channels of INSAT 3D Imager was used to develop NDSI based approach for snow pixel identification. Thermal data (TIR 1) was used to separate ice cloud and snow based on difference in their temperature. In addition, SWIR reflectance, DEM and Latitude of the study area was also used to remove wrongly classify snow pixels.

$$\text{NDSI} = (\text{Visible}_{\text{INSAT B1}} - \text{SWIR}_{\text{INSAT B2}}) / (\text{Visible}_{\text{INSAT B1}} + \text{SWIR}_{\text{INSAT B2}})$$

Figure 286 shows the operationally generated regional snow cover product, showing in inset the scatterplot of different objects in Visible and SWIR data.

In validation exercise, the product was validated using 4 different approaches (Figure 287).

1. INSAT 3 D snow cover product was validated using archived field spectroradiometer data for varying type of snow and various objects. Snow pixels were well above the NDSI based threshold.
2. AOI of area was selected and accuracy was observed well within 10% except few locations which was due to the inclusion of cloud and sub-pixel heterogeneity during manual mapping of snow.
3. 10 INSAT 3D FCC and derived snow cover product were selected in this exercise. Pure snow subset pixels were selected in FCC which were later verified in the binary product with 100% accuracy.
4. A comparison of INSAT3D snow cover product was carried out with AWiFS derived snow cover product. Snow cover product were accurate within 12% except few dates, caused by the sub-pixel heterogeneity due to coarse resolution of INSAT 3D.

This leads to estimation of fractional snow cover product of INSAT 3D to increase the accuracy of snow cover area. Synchronous INSAT 3D and AWiFS data was used in this exercise covering different level of snow cover area distributed along Himalayan region. Fractional snow cover products of INSAT 3D have been prepared which becomes an input to snow depth estimation in the Himalayan region. However, at present snow depth approach for North America region has been adopted and further improvements and fine tuning for Himalayan region is in progress.

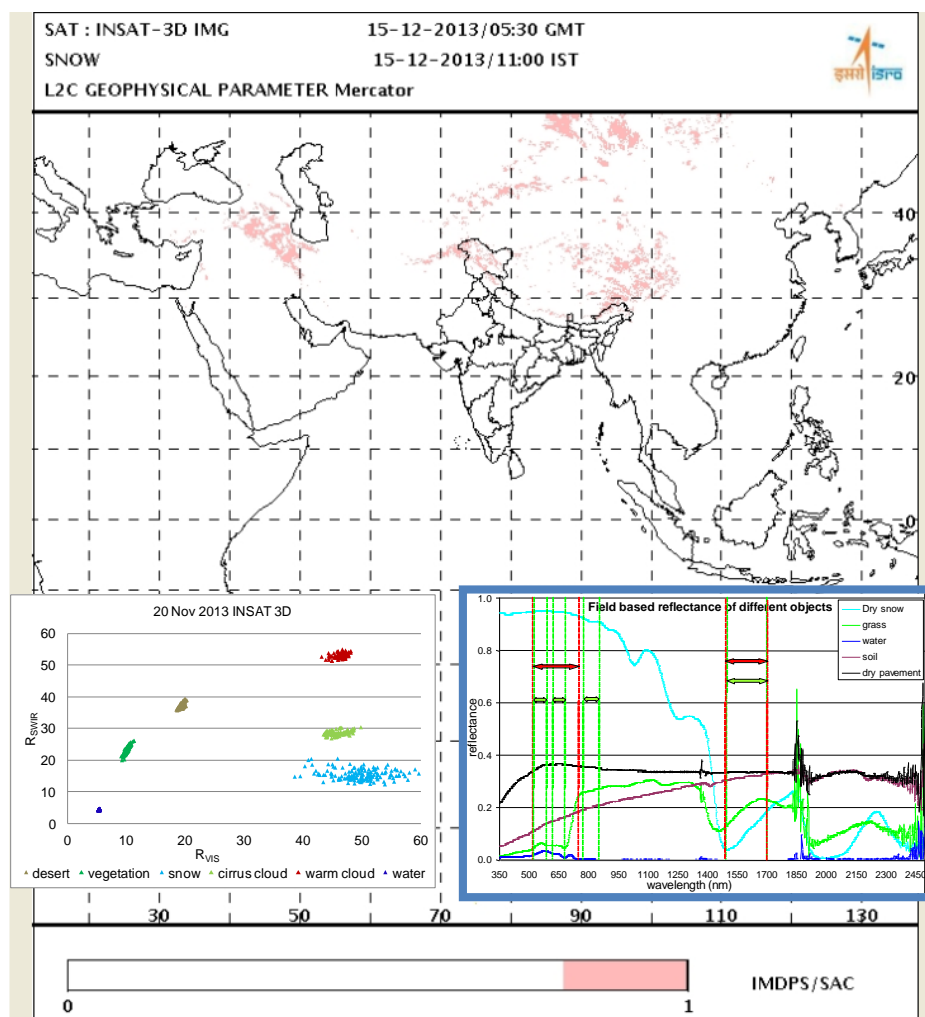


Figure 286: INSAT-3D snow cover product using Imager data. Scatterplot of different objects has been shown using Visible and SWIR region in the inset

15.5. Conclusions

This work presents the approach developed to generate snow cover maps using INSAT 3D Imager data. In present analysis, AWiFS, INSAT 3A CCD, MODIS and ASD spectroradiometer data was used to understand the applicability and Implementation of NDSI based approach to estimate snow cover area. Cross-calibration of INSAT 3A CCD was also carried out in conjunction with AWiFS data which shows improvement over Red and NIR channels, however, depicts severe calibration issue for SWIR channel. NDSI based approach on INSAT-3D data was made operationalized at IMD using Visible, SWIR, Thermal data along with additional input based on DEM and geography of the region. In future, INSAT-3D derived snow cover product will be further improved for different categories of land cover, fractional snow cover, understanding of slope corrected area at coarser resolution, and validation of snow cover product as continuing activity will be further carried out.

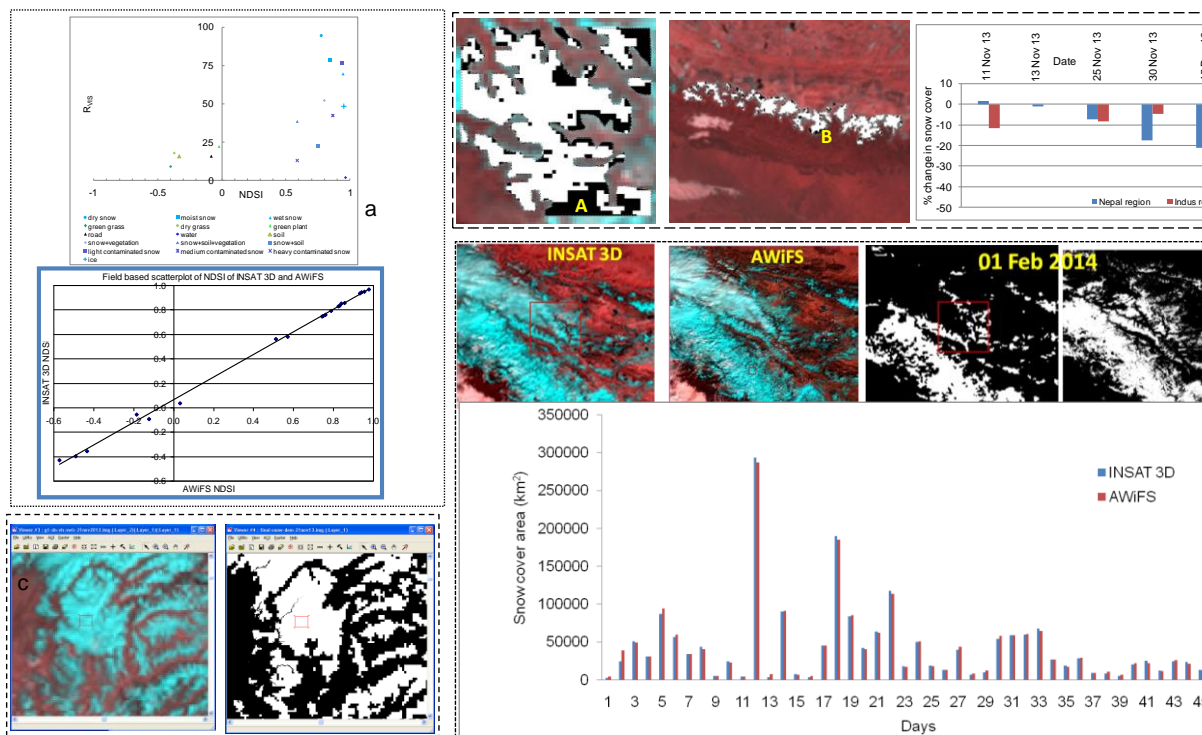


Figure 287: Snow cover product validation using INSAT-3D imager data using a) Field Spectroradiometer data; b) visual AOI extraction of snow cover area; c) pure snow pixels on FCC image; and d) AWiFS snow cover products.

16. Development of Techniques for RISAT-1 SAR Data Analysis for Glacier Studies and Detection of Glacial Lakes Buried under Snow

16.1. Objectives

To develop techniques for RISAT-1 SAR data analysis for glacier studies and detection of glacial lakes buried under snow

16.2. Scientific Rationale

Active microwave sensor based imaging system (Synthetic Aperture Radar-SAR) is independent of cloud and can be operated in day/night. SAR signal is transmitted which interacts with surface and return back to the receiver at satellite system. The received signal is influenced by sensor parameters such as frequency, polarization, incidence angle and target parameters such as dielectric constant and surface roughness (Ulaby et al. 1986, Joseph, 2003). These factors make understanding of radar data more difficult in comparison to optical region.

Surface roughness and dielectric constant are dominant factors in determining the strength of radar signal. A rough surface scatters the energy in all directions and small fraction of that is received at antenna. However smooth surface returns large amount of energy following specular reflections and angle play a important role in collection of energy at antenna. Surface roughness of snow/ice regions depends on the availability of liquid water content at the time of data collection which severely influenced by the atmospheric temperature. Dielectric constant of snow is a function of frequency, snow wetness, temperature and density. Snow has a dielectric constant between 1.2 and 2.0 for density ranging from 0.1 to 0.5 gm/cc. Dielectric constant of snow significantly alters the depth of penetration of radar signal into a snowpack. Backscatter received at SAR antenna is a sum of surface scattering at the air/snow interface, volume scattering within the snowpack, scattering at the snow/soil interface and volumetric scattering from the underlying surface (Hall, 1998). Moraine on glacier surface changes surface roughness which influences the return radar signal. Surface roughness and dielectric constant provides crucial keys to identify the different glaciated features. Optimal antenna-look angle for the mountainous terrain was found between 40° and 60° (MacDonald and Waite, 1971; Rott, 1984). C-band was used to discriminate wet snow from adjoining areas with accuracies more than 80% but failed to separate glacier ice from snow and rock (Shi and Dozier, 1993). The microwave backscattering backscattering properties of most glaciers show significant seasonal variations. Snow is transparent at microwave wavelengths, and depending on

frequency radar penetration depth can reach upto tens of meters in dry snow conditions (Rees 2006; Shi 2008). Backscatter received at SAR antenna is a sum of surface scattering at the air/snow interface, volume scattering within the snowpack, scattering at the snow/soil interface and volumetric scattering from the underlying surface (Hall 1998). SAR data has provided useful information over glaciated terrain irrespective of being complex in nature; however, not much information is available for understanding glacier signature in the Himalayan region (Venkataraman and Singh 2011, Singh et al 2013c). ERS-1 data was studied over 5 lakes in Northern Montana region to understand the different processes of frozen lake and break up date over a decade-scale time frame (Hall et al 1994). Terra SAR-X and Radarsat-2 SAR data was successfully used to map and monitor the glacial lake detection during snow- and ice- free season, emphasizing a need for integrated multi-level approach (Strozzi et al 2012). Lakes at high altitude fluctuate seasonally due to the change in melt rate during accumulation and ablation period. The accessibility of these lakes is restricted in optical spectrum due to the cloud cover in ablation period and snow cover in the accumulation period. Techniques for snow physical parameters extraction including density retrieval using SAR data, validation and applications in part of North Western Himalaya are developed (SASE, 2012; Thakur et al., 2013; 2012).

The recently launched satellite, RISAT-1 C band SAR sensor took off on 26 April 2012 by the ISRO which carries multi-mode SAR system at different resolution and swath, and has enhanced the imaging capacity in microwave region along with other existing satellite system (Kiran Kumar 2013; Misra et al., 2013). RISAT data has been found to be extremely useful for snow and glacier studies (Kundu and Chakraborty, 2015; Chakraborty et al., 2013). This section presents a case study of the use of winter time RISAT-1 SAR MRS data to detect snow buried glacial lakes using multi-temporal images covering Samudra Tapu and Gepang-gath MDLs in Chandra sub-basin, Himachal Pradesh, supported with synchronous AWiFS optical data (Singh et al., 2015).

16.3. Data Used and Methodology

RISAT-1 MRS data over a complete year from winter period (Jan-Feb) to November covering ablation period has been considered in to present study and study area has been shown in Figure 288. The technical specification of the RISAT-1 MRS has are given in Table 88. The synchronous optical AWiFS data was used to validate the existing conditions during SAR data acquisition dates. ERDAS Image processing software has been used to process the RISAT-1 and AWiFS data. Digital number (DN) of RISAT-1 MRS mode was converted into backscattering coefficient for each pixel using meta data. Equation 1 was used to estimate the backscattering coefficient (σ_0) given below;

$$\sigma_0 = 20 \log_{10}(DN_p) - K_{db} + 10 \log_{10}\left(\frac{\sin I_p}{\sin I_{centre}}\right)$$

where, I_p is the incidence angle at the p^{th} pixel, I_{centre} is the incidence angle at centre of scene, K_{db} is the absolute calibration constant, DN is average pixel intensity. Area of interest (AOI) of backscattering coefficients data over various glacier features and MDL was extracted using the aoi tool. Average σ^0 was calculated for temporal RISAT-1 MRS data. Snowfall takes place due to the NW disturbances and region remains under sub-zero temperature conditions during February month in Chandra basin. Snow remains dry in nature which is a mixture of air and ice crystal causing volume scattering losses more prominent during SAR interaction. Depth of penetration of SAR signal depends on the relative permittivity of dry snow which further depends on snow density. Snow density for dry snow generally vary over ranges from 0.1-0.5 gm/cc. The depth of penetration (δ_p) in snow (a loss less medium) was computed using eqⁿ given below;

$$\delta_p = \frac{\lambda \sqrt{\epsilon''}}{2 \pi \epsilon'}$$

where λ is the wavelength and ϵ' & ϵ'' are the real and imaginary components of dielectric constant of dry snow.

16.4. Results and Discussion

i) Glacier Features and Backscattering Response

Himalayan terrain is covered by either cloud or snowpack and glaciers are opportunistically visible for their monitoring in optical data in that short window period. This problem becomes further severe as one move from Central towards Eastern part of the Himalayas. RISAT-1, being a SAR sensor, demonstrates its capability to penetrate through cloud/snowpack providing critical information over glaciated terrain in the Himalayan region throughout the year. It was observed that SAR signal not only

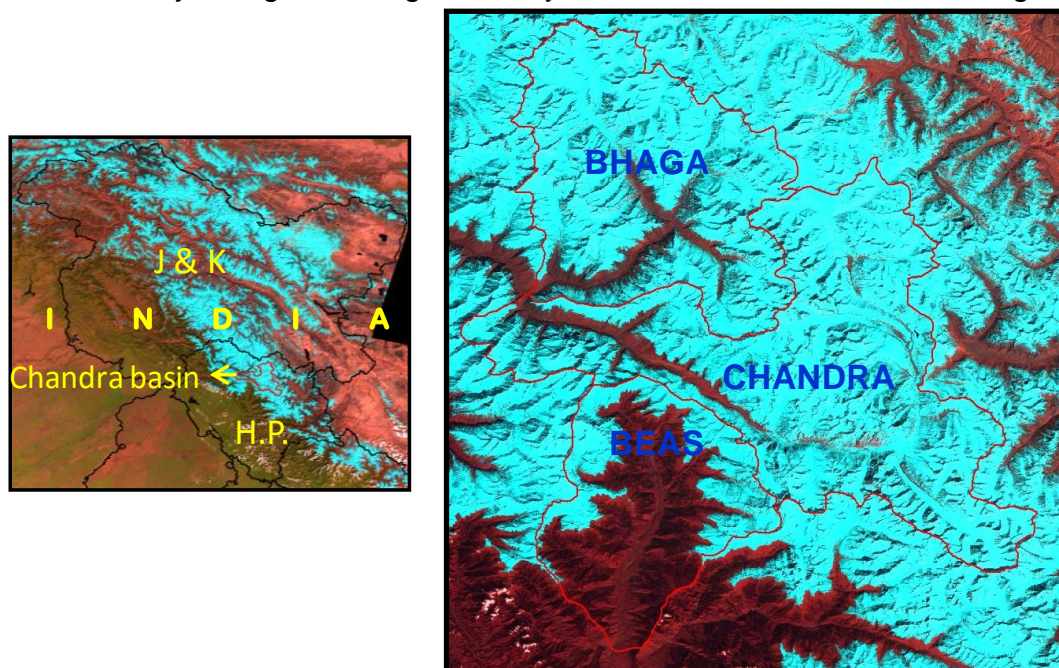


Figure 288: Location map of Chandra and Bhaga sub-basins in the Western Himalayan region

Table 88: Sensor characteristics of RISAT-1 MRS

Sensor specifications	RISAT-1 (MRS)
Frequency	C (5.350 GHz)
Resolution (m)	25 x 25
Swath (Km)	115
Sensitivity (σ^0 in dB)	-17.0
Polarization	Dual

travels through cloud and snowpack but also brings out additional information of the glaciated terrain. Temporal variation in Back Scattering Coefficient (BSC) of different glaciated features of Samudra Tapu glacier has been shown in Figure 289.

BSC response over accumulation zone in glacier significantly changes during transition from winter to ablation month. σ^0 varies from -7.61 to -19.08 dB in accumulation zone for 24 February and 18 August 2013 respectively and an evident change of ~11 dB in BSC was observed. This is due to the varying physical properties of snow and ice due to change in climate conditions which alter the dielectric constant and surface roughness of the medium. During ablation month (18 August 2013), air temperature shoots up making snow wet which acts as a smooth surface, returning low BSC. High BSC in winter months is followed by a slightly low BSC in 29 June 2013 due to increase in wetness and smoothening of snow surface. Snowfall takes place in the higher ridges of glaciers and air temperature also starts falling concurrently. Onset of winter refreezes the wet snow layer and SAR signal gets scattered back returning high BSC, which was observed during 07 October and 01 November 2013 images.

BSC signature over bare ice ablation zone does not vary significantly during winter and ablation month. σ^0 varies from (-14.08 to -14.81 dB) dB in bare ice ablation zone for typical accumulation and ablation months such as 24 February and 18 August 2013 respectively. Two distinct signatures were observed during 4 & 29 June and 7 October 2013. Snow starts melting and becomes wet over the bare ice ablation zone and glacier ice behaves as a smooth surface returning low signature. On the other hand, snowfall take place in the beginning of onset of winter months i.e. 07 October 2013 and lowering air temperature refreezes the overlying snow layer returning slightly high BSC (-8.7 dB) which is very close to BSC (-8.3 dB) in accumulation zone due to similar phenomenon. In November month, snow starts being much colder, and SAR signal penetrates and interacts with glacier ice returning further low BSC in bare ice ablation zone. BSC of debris cover ablation zone and deglaciated valley shows similar signature. Both features lie down at the lower altitude of the glacier. Rocks returns high amount of backscatter due to irregular setting of the medium which was observed in both the features. However, SAR returned slightly low amount of SAR signal probably due to the loss by volume scattering mechanism by overlying snow in winter months.

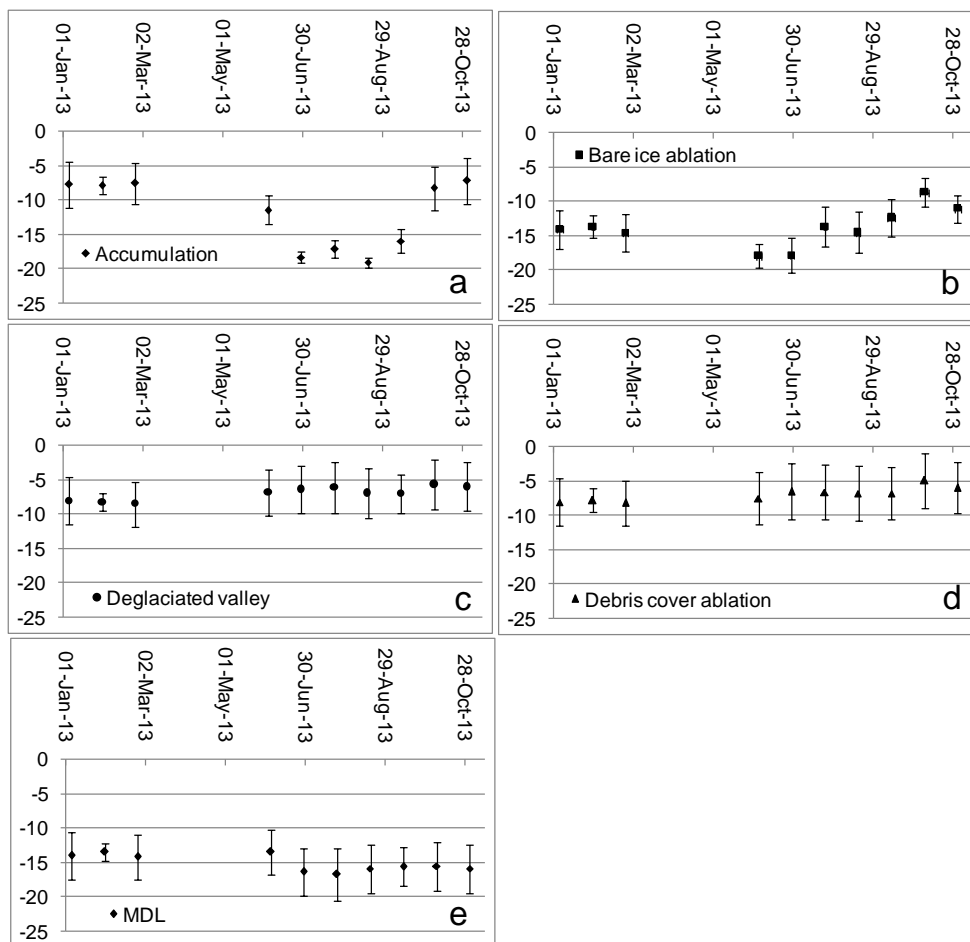


Figure 289: Temporal backscattering signature of various glacial features of Samudra Tapu glacier

Crevasses are large cracks in the glacier developed due to glacier movement over the uneven terrain and curved topography. These cracks are developed due to the shear stress which can run for several hundreds of meters and return high backscattering energy back to the sensor. Figure 290 shows that RISAT-1 MRS SAR (30 January 2013) data, optical image of LISS III and field photograph of visible cracks on the surface of glacier in Chandra basin. Glacier features are completely buried in RISAT-1 image as discussed previously. Optical data (LISS III with alike spatial resolution as MRS) shows the glacier features at the end of ablation period and fractures was less intensely visible on the glacier surface in ablation period. High resolution images could provide better identification with a severe constraint of cloud and snow free data. SAR signal penetrates through the snowpack, interacts with buried crack and returns high amount of backscattering energy (encircled in both RISAT-1 and LISS III image). This demonstrates that how SAR data could see the large opening on the glacier surface which is otherwise not feasible in optical region and is crucial for any human movement on the glacier surface, especially in crucial winter months.

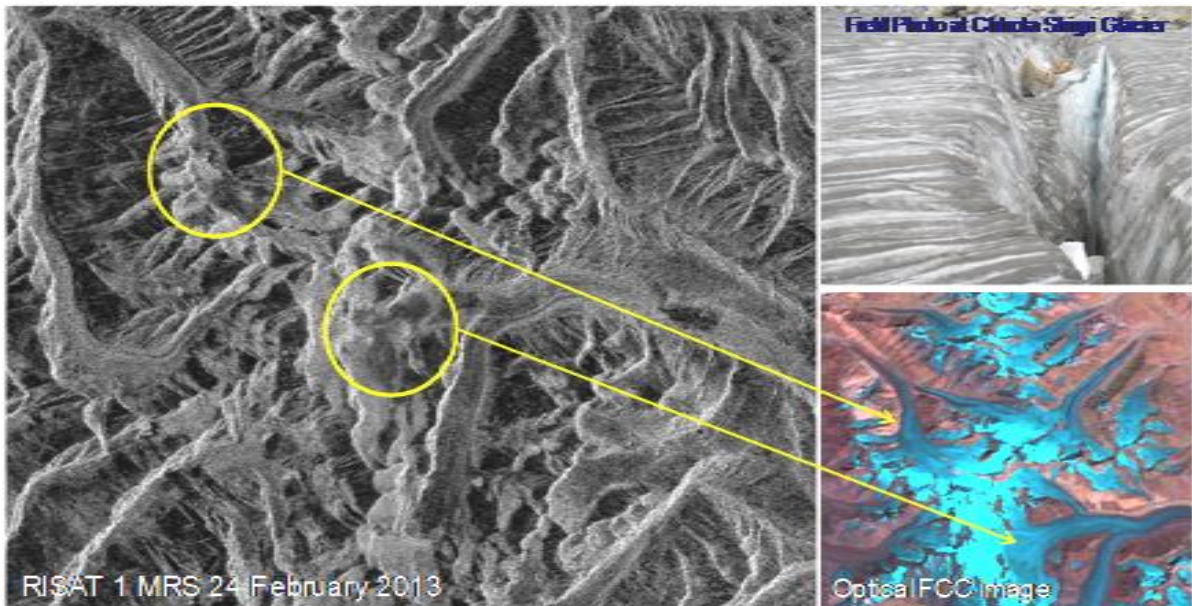


Figure 290: Identification of crevasses under snowpack using RISAT-1 MRS data in part of Chandra sub-basin. Optical image (LISS III) of ablation period (Lower Right) and field photo with crevasses (Upper Right)

Delineation of glacier boundaries in the accumulation area has been a tricky expertise job in optical due to its nadir viewing geometry and snow covered terrain. RISAT-1 SAR data was observed to be useful for identification the delimiting boundaries in accumulation zone of a glacier. SAR data was exploited due to its side looking facility which enhanced the topography of the region. Glacier boundaries along with snow line were delineated over winter image for Samudra tapu and Bara shigri glacier. Snow line were also taken into consideration using AWiFS data of ablation period i.e. 10 Sep 2012 and 10 Sep 2013. It was difficult to delineate the snow line using ablation period image where both glaciers have shown close BSC for accumulation and ablation zone. Snow line can be clearly demarcated based on the contrast in dB between accumulation and ablation zone in winter data. Winter image is found more suitable to delineate snow line due to RISAT-1 penetration capability and high amount of backscattering due to multiple melt-refrozen cycle of previous year underlying snow. The identification of snowline on RISAT-1 image requires more detailed investigation to make it operational in the Himalayan region. These observations shows the potential of RISAT-1 as a complementary information to optical images, however, at the same time leads for a more detailed investigations for sample glaciers in the Himalayan region for confirming snowline on RISAT-1 SAR data along with a extensive validation with AWiFS data.

ii) **Detection of Glacial Lakes buried under Snowpack**

Moraine Dammed Lakes (MDLs) of Samudra Tapu and Gepang-gath glaciers have been chosen in the present study which lies in the Chandra sub-basin of the Lahaul and Spiti region, Himachal Pradesh. Samudra Tapu glacier is the second largest glacier in Chandra sub-basin after Bara Shigri glacier. The snout of the glacier is

located at Lat. 32°30' N and Long. 77°32' E, at an altitude of 4200 m from MSL and about 10 km SW of famous Chandra Tal Lake. Gepang-gath glacier is debris covered glacier with an area of 13.1 sq km, located at Lat. 32°31' N and Long. 77°14' E at an altitude of 4300 m from MSL.

Land cover information was completely opaque in AWiFS data due to cloud cover which is a common phenomenon in the Himalayan terrain, and is clearly visible in RISAT-1 SAR data. This region experiences heavy snowfall during winter months and whole area is buried under thick snowpack. This snow starts melting as one move towards ablation period and glacier features attain a state of minimum snow cover. During this period, snow deposited on the lake is completely melted and the lake is fully exposed. Figure 291 and Figure 292 shows the synchronous capture of RISAT-1 and AWiFS images over Samudra Tapu and Gepang-gath MDLs. It was observed that the lakes were completely snow covered on 03&05 January, 30 January and 24 February 2013 and not visible in AWiFS. However, the lakes were completely visible on RISAT-1 images of similar dates which demonstrates the penetration capability of RISAT-1 C-band through thick snow cover and able to retrieve the buried lake signature.

Lake starts melting as it approaches towards summer which is visible in 08 June and 30 June 2013. AWiFS image has shown distinct signature of melted water on 07 October 2013. In November month, fresh snowfall again took place covering lake with snowpack. Another example of presence of Gepang-gath MDL buried under snow has been shown in Figure 292. These observations show first results of RISAT-1 SAR data penetration to detect the signature of buried lake and validated using optical datasets. Samudra Tapu MDL has shown low backscattering coefficient throughout the year (-15.16 dB). Penetration depth was computed for dry snowpack for varying density (0.1-0.50 gm/cc) at various microwave frequencies such as X, C, S and L. Figure 293 shows schematic diagram of snow deposited on the lake and modeled penetration depth for dry snow.

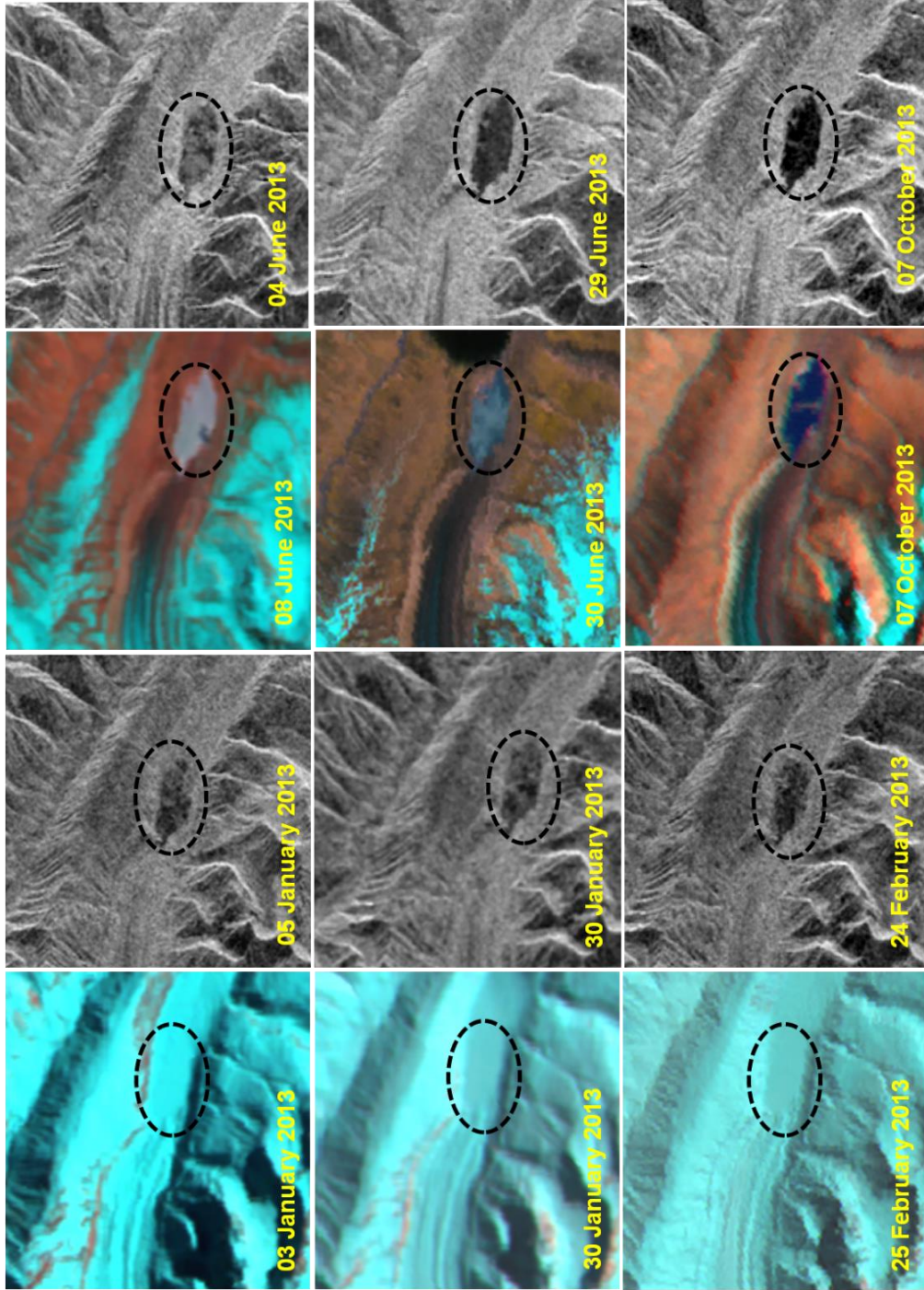


Figure 291: RISAT-1 and AWiFS data over Samudra Tapu MDL during accumulation and ablation seasons. AWiFS data shows MDL completely covered with snow during accumulation (winter), whereas corresponding RISAT-1 SAR data shows presence of MDL buried under snow (Left two panels). MDL is seen in both AWiFS and RISAT-1 SAR datasets during ablation season (Right two panels). The MDL has been shown in dotted black circle. (Source: Singh et al., 2015)

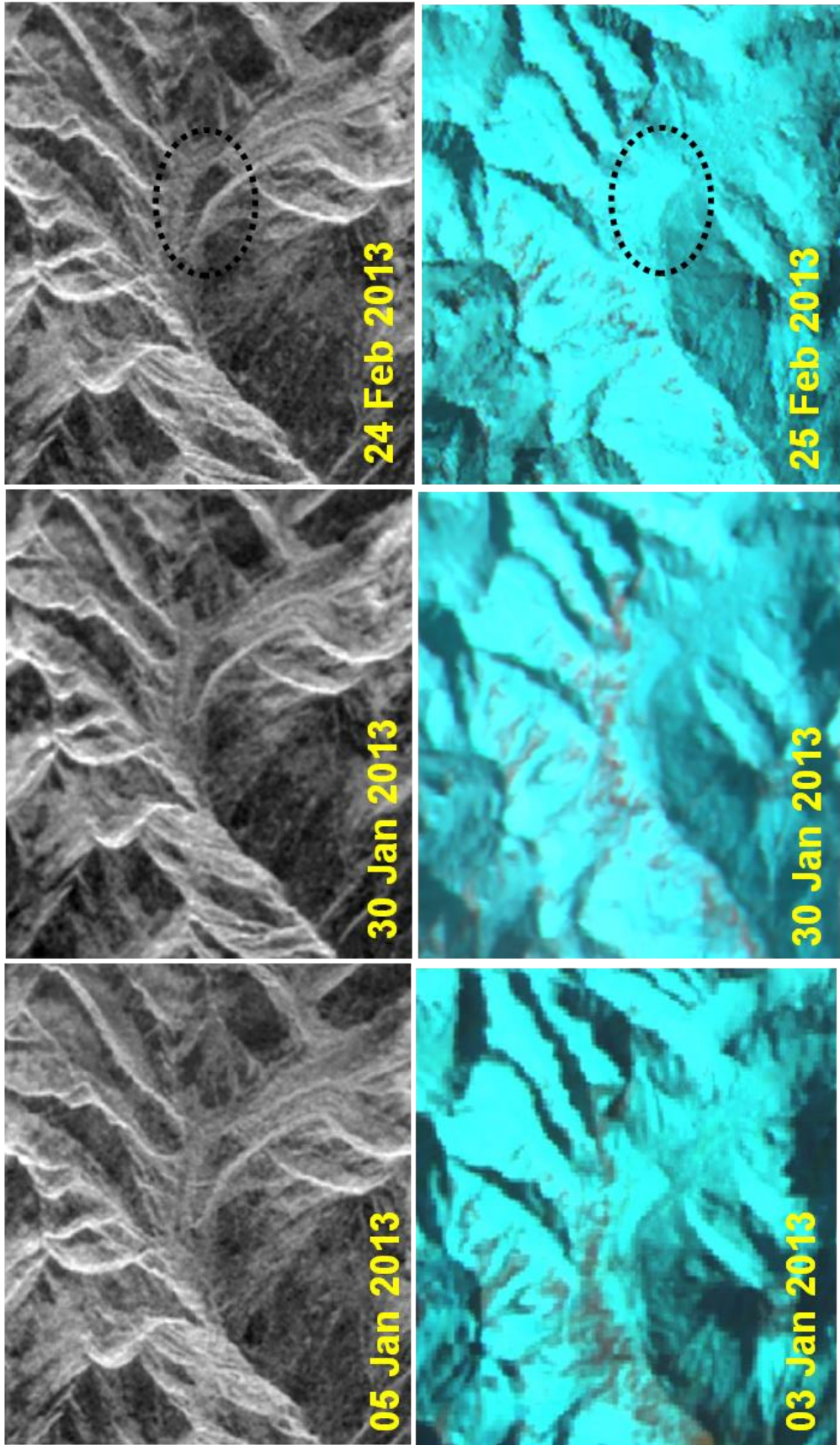


Figure 292: RISAT-1 and AWiFS data over Gepang-gath MDL completely covered with snow during accumulation season (winter). RISAT-1 is able to penetrate and detect the presence of MDL (Upper Panels). The MDL has been shown in dotted black circle. (Source: Singh et al., 2015)

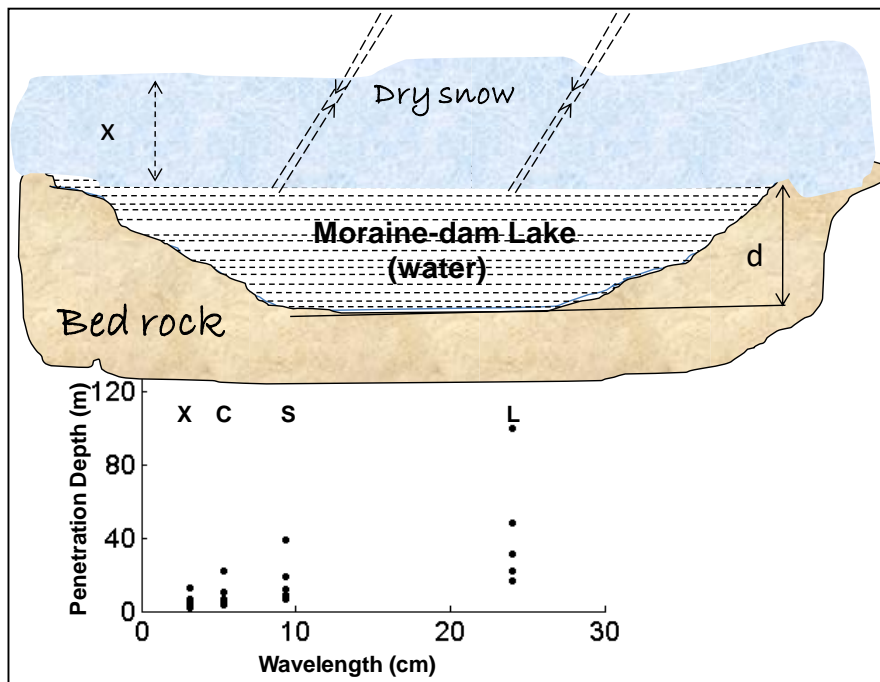


Figure 293: Penetration depth in dry snow for varying dielectric constant (for density range 0.1-0.5 gm/cc) at typical spaceborne SAR sensors frequencies. Schematic diagram shows the thick snowpack over moraine-dam lake during accumulation month (Source: Singh et al., 2015)

It shows that the penetration depth over snow increases as one move towards lower microwave frequencies. This penetration will allow SAR signal to interact with MDL at base of snow covered surface. Penetration depth was observed to vary from 4 to 22 m for 0.1-0.5 gm/cc snow density at C band. These observations were further linked with field snow thickness obtained using Airborne GPR survey data made available by SASE, Chandigarh in that region. Airborne GPR survey conducted on March 2009 and 2010 over Samudra Tapu glacier region has shown snow accumulation of 1.47 and 1.68 m, respectively. The standing snow was further correlated using nearest Patseo observatory data for 30 January and 25 February 2013 with an estimated snow thickness of 1.20 and 2.01 m, respectively (Ganju, 2014) which matches with the modeled thickness. The present analysis shows that RISAT-1 C-band has the capacity to penetrate the thick accumulated snowpack and able to detect the buried lake signature in the Himalayan region. This study demonstrates the advantage of RISAT-1 SAR data over optical data which has limited window period due to presence of snow and cloud for monitoring the expansion of high altitude lakes in the Himalayan region.

17. Monitoring of Moraine-Dammed Lakes for Outburst Potential Assessment

17.1. Objective

To carry out monitoring and mapping of Moraine-Dammed Lakes (MDLs) for outburst potential assessment.

17.2. Scientific Rationale

Himalayan glaciers have been observed to be retreating (SAC, 2011a; Kulkarni, 2010; Kulkarni and Karyakarte, 2014; Kulkarni et al 2007; 2006a; 2011; Brahmhatt et al. 2012a). The pace of retreat is attributed to global warming in the last century. The retreat of glaciers sometimes has given rise to formation of glacial lakes and their expansion. Glacial lakes can be classified according to their topographic position and nature of dam (Tweed and Russel, 1999; Clague and Evans, 2000; Ben and Evans 2010) i.e. sub-glacial lakes, supra glacial lakes, englacial lakes or proglacial lakes. Among various types of glacial lakes, some are formed at the terminus of the glacier due to damming by the moraine brought down by glacier movement across the channel of glacier melt water, if there is a steady rise in the ablation rates of glaciers (Yamada, 1998; Clague and Evans, 2000; Iturrizage, 2005). Large proglacial moraine dam lakes can only form where debris supply at the glacier margin is greater than the capacity of melt stream to transport sediment away and affects glacier mass balance and hydrology (Benn et al., 2001; Hambrey et al., 2008). Adjoining water bodies in the form of moraine-dammed lakes (MDL) considerably accelerates the rate of ablation near the glacier terminus in comparison to ice beneath debris cover (Sakai et al., 2000; Benn et al., 2001).

Himalaya has one of the largest concentrations of glaciers outside Polar regions. A very recent update on number of glaciers, glacier area and number of pro-glacial lakes and debris cover in entire Himalayan region has been given by Sharma et al. (2013) based on glacier inventory carried out using multi-temporal IRS LISS III data. According to these authors, 24.16% of glaciers region in Himalaya is covered with debris. Therefore, the probability of formation and expansion of MDL is high in Himalayas. Some glacier lakes have started to expand at the terminus of glaciers since 1950s and 1960s (Yamda, 1998; Komori, 2008). Moraine-dammed lakes formed in this way could be disastrous if breaching of dam occurs due to heavy rainfall or avalanche or excessive melting of glacier ice. This results into GLOF (Glacial lake outburst flood) caused by MDL which is a common phenomenon in the glaciated terrains. These floods can cause extensive damage to the natural environment and human lives as relatively small lake can cause extremely rapid dramatic flood (Deslognes et al., 1989; Carry, 2008). Many events of outbursts floods are reported in North America, Europe and in the Himalaya (Clarke and Mathews, 1981; Deslognes et al., 1989; Gansser, 1983). Friendship bridge of the China- Nepal Highway and Koshi power station in

Nepal was damaged by GLOF event and caused serious losses during 1981 (Bajracharya et al. 2006). This event may be cyclic and can occur periodically. The first GLOF event was reported in 1926, flood released by Shyok valley, Jammu & Kashmir, destroyed Abuden village and the surrounding area which were at a distance of 400 km from the outburst source (Mason, 1929). On 3rd September 1977, an outburst from a moraine dammed lake occurred in Mingbo valley, Dudh Koshi region, East Nepal. The flood was reported at 70 km downstream from the Mingbo valley (Fushimi et al., 1985). Another burst of moraine dammed lake was reported in Shaune Garang glacier due to sudden release of water from lake in Himachal Pradesh in 1981 and 1988 based on high discharge measured downstream (Sangewar et al., 1999). Recently, a biggest calamity has occurred in Chorabari glacier at Kedarnath, Uttarakhand due to simultaneous bursting of cloud and MDL (Dobhal et al., 2013). Flood and sediment disasters caused by glacial lake outbursts have occurred frequently in recent year in Himalayas of Nepal. Tsho Rolpa glacial lake due to two types of moraine dam failure caused by seepage flow or water overtopping (Shrestha and Nakagawa, 2014). However, no systematic record of floods is available due to outburst of moraine dammed lakes in Indian Himalayas.

Therefore, monitoring of such lakes in Himalayan region has been recognized as the priority area especially from the disaster point of view. Since Glaciers and MDLs are located in very high altitude, cold weather and rugged terrain conditions, making it tedious, hazardous and time consuming task to monitor them by conventional methods. Remote sensing with multi-temporal and multi-sensor capabilities plays a significant role in monitoring of the glacier moraine-dammed lakes. Remote sensing based monitoring of moraine dam lakes in Himalayan region has also been reported earlier (Kulkarni, 1996; Kulkarni et al. 2006a; Randhawa et al. 2005; Dhar et al. 2009; Raj et al. 2013; 2012; Raj, 2010; Basnett et al. 2013; SAC, 2012). A good correlation of glacier retreat with change in pro-glacier lakes for east-central Himalayan region has been shown by Bahuguna (2013). Identification of the potentially dangerous glacial lakes and modelling the burst potential using integration of remote sensing and in-situ data has been attempted in a number of studies (Bolch et al., 2011; Fujita et al., 2013; 2012; Gardelle et al., 2011; Koike and Takenaka, 2012; Komori et al., 2012; Sakai, 2012; Sakai and Fujita, 2010; Tadono et al., 2010; Wang et al., 2012; 2011; Xiaojun et al., 2012; Zhang et al., 2011b).

This study reports occurrence, expansion and outburst probability of two MDLs in western Himalaya monitored using Landsat and IRS images of the year 1976, 1989, 2001, 2006/07 and 2012. Empirical relationship has been used to estimate volume (Akiko Sakai, 2012) and peak discharge (Clague and Mathews, 1973). The objective of this section is to present the evidences of expansion of the lakes which could be taken up for establishing ground based early warning system (Rathore et al. 2015).

17.3. Study Area and Data used

The lakes are located at the mouth or snout of Katkar in Zanskar and Gepang-gath glaciers in Chandra sub-basins (Figure 294). Katkar glacier is shown on an IRS LISS IV data of 5.8m spatial resolution of date Aug. 26, 2008. Various glacial features of Katkar glacier are seen on the image distinctly (Figure 295).

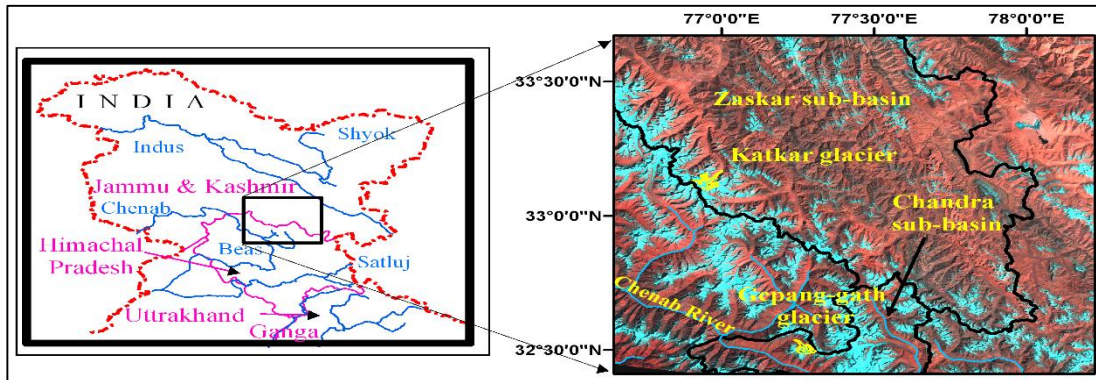


Figure 294: Location map of study area for monitoring glacier lakes (Source: Rathore et al., 2015b)

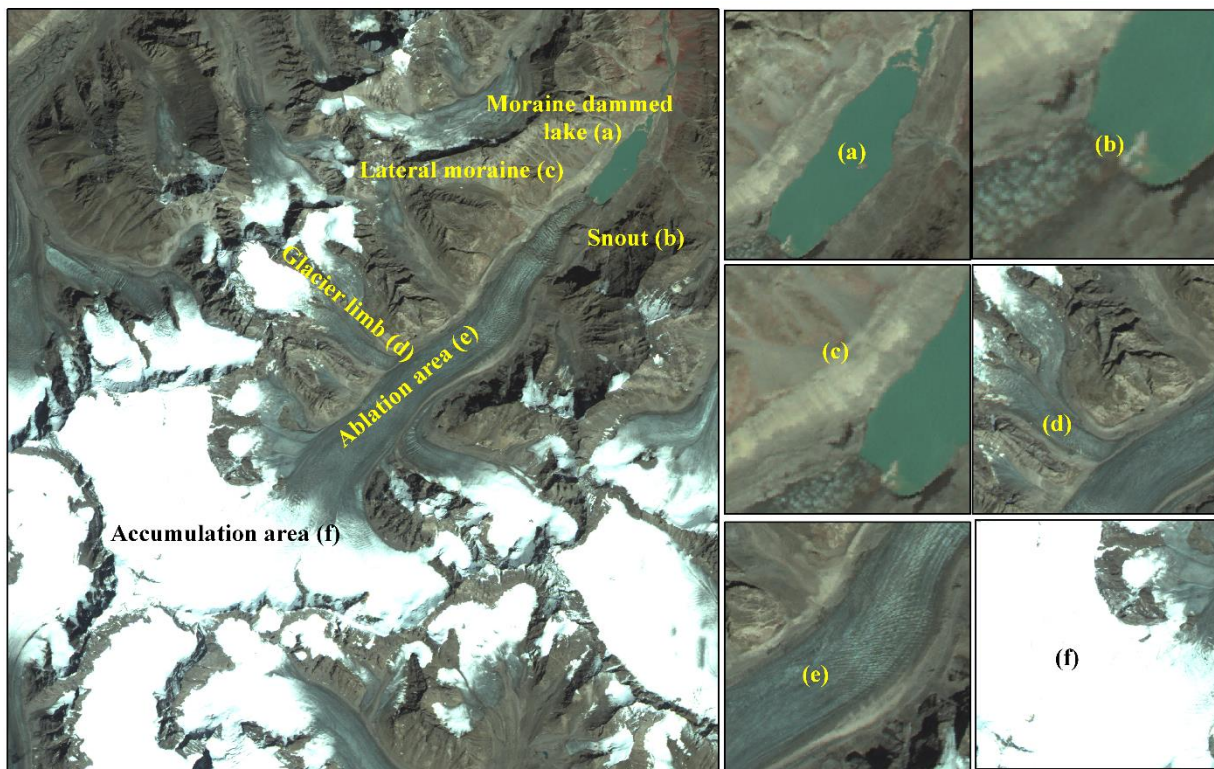


Figure 295: Glacier features of Katkar glacier (a) Moraine dammed Lake (b) Glacier Snout (c) Terminal Moraine (d) Glacier Limb (e) Ablation area (f) Accumulation area (Source: Rathore et al., 2015b)

Both of the glaciers are situated at opposite side of a ridge line of Indus and Chenab basins. Katkar glacier is debris free glacier with an area of 24.4 sq km and having a slope less than 3° near snout with reference to SOI of 1962. Gepang-gath glacier is debris covered glacier with an area of 13.1 sq km and having a slope less than 2° near snout with reference to SOI of 1962. The oldest information about glacial extent is available on Survey of India topographic maps, surveyed in 1962, using vertical air photograph and limited field checks. Toposheets no. 52 C/16 for Katkar glacier and 52 H/2, H/3, H/6 and H/7 for Gepang-gath glacier were used in this study. Multi-temporal mapping of glaciers extent and lakes was carried out using Corona data of 1965, Landsat MSS of 1976, Landsat TM of 1989, IRS LISS III of 2001, 2006, 2007 and IRS LISS IV satellite data of 2008. Landsat of year 2012 & 2014 was used for the latest monitoring of glaciers and MDLs. Altitude information was obtained from the Global Digital Elevation Model (GDEM) version 2 of the Advanced Space borne Thermal Emission & Reflectance Radiometer (ASTER). The spatial resolution of the ASTER GDEM v2 is between 71 & 82 meter with accuracy of 17 m at the 95% confidence level (Aster GDEM team, 2011).

17.4. Methodology

The study was carried out in three stages:

a) Mapping of glaciers and moraine dammed lakes

Firstly, the IRS LISS III and LISS IV data were georeferenced with the SOI topographical maps. Sufficient numbers of distributed Ground Control Points (GCPs) were selected on the satellite data and maps for performing georeferencing. Drainage intersections were given priority as GCPs. Second order polynomial model was used for registration with nearest neighbor approach. Georeferencing was performed at pixel level in conjunction with SOI maps at 1:50000 scale with a positional accuracy of 12.5 meter. Inventory of Himalayan glaciers carried out by Sangewar & Shukla (2009) using SOI Topographical maps with limited field checks. Change in areal extent of Katkar & Gepang-gath glaciers is 4% & 3% respectively with glaciers mapping carried out in this study using SOI maps. The Erdas imagine image processing software was used in the present analysis. Landsat images were reprojected with reference to georeferenced IRS LISS III and LISS IV.

The extents of glaciers and MDL were adopted from SOI topographical maps. Then these extents were digitized and first baseline information corresponding to year 1962 was prepared. This layer was further used in comparing the extents derived from satellite images.

Extents of glaciers and MDLs were extracted from satellite images using elements of visual interpretation as the procedures discussed in various publications (Brahmbhatt et al. 2012a). Standard FCC, combination of bands of multispectral optical data was used for mapping. Image enhancement techniques were sometimes required to enhance the tone

and texture of glaciers. FCC included short wave Infrared (SWIR) band to improve the discrimination of snow and clouds. Moraine dam lakes could be observed due to its typical black/blue tone on image. Position of snout of two glaciers noted and mapped along the central line of glaciers based on the data of 1962/65, 1976, 1989, 2001, 2006, 2012 & 2014. Uncertainty in the changes of snouts position was estimated using standard procedures. Changes in extent of Katkar and Geepang-gath glaciers near their snout and moraine dammed lakes are shown Figure 296 and Figure 297.

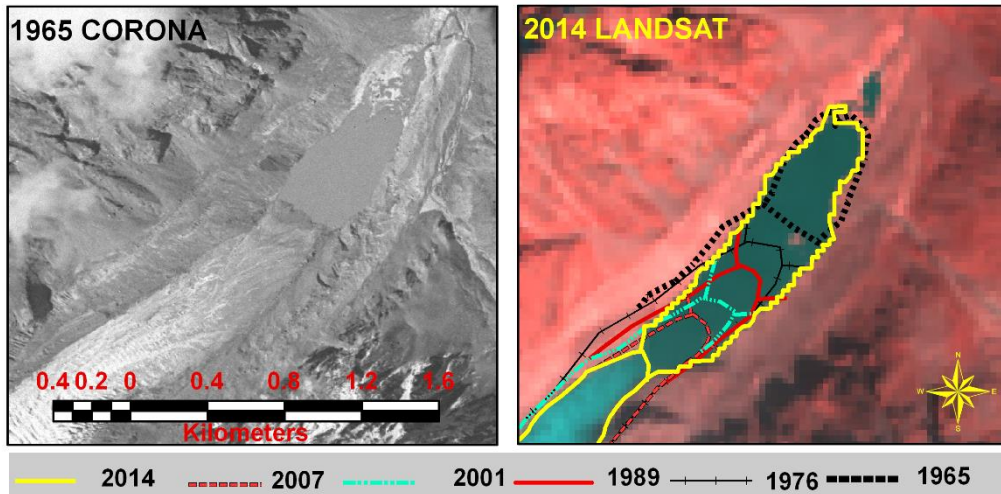


Figure 296: Boundary of the Katkar glacier near its snout and moraine dammed lake during 1965, 1976, 1989, 2001, 2007 and 2014 as mapped using corresponding satellite data (Source: Rathore et al., 2015b)

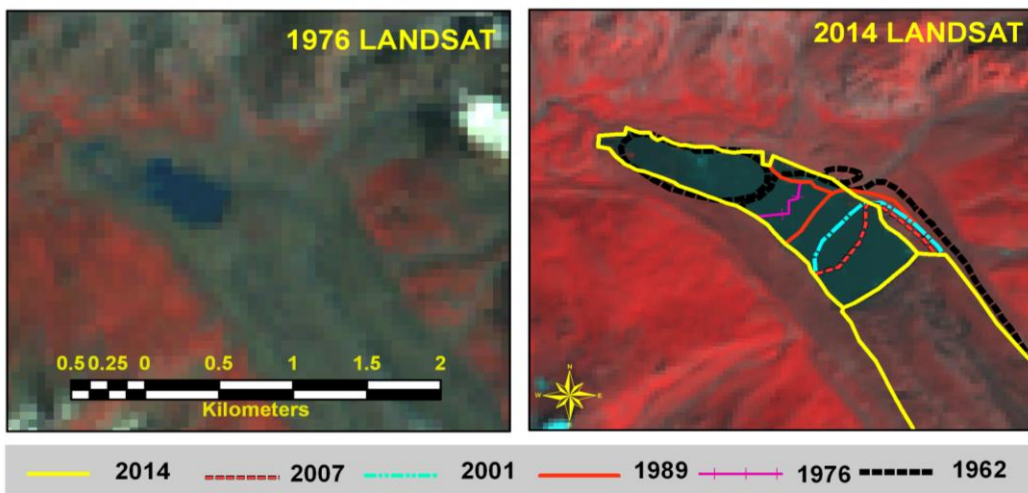


Figure 297: Boundary of the Geepan-gath glacier near its snout and moraine dammed lake during 1965, 1976, 1989, 2001, 2007 and 2014 as mapped using corresponding satellite data (Source: Rathore et al., 2015b)

a) Lake volume and peak discharge estimation

Following Empirical relationship has been given by Akiko Sakai (2012) between areas and volume of glacier lakes based on the work carried out for glacier lakes in Nepal and Bhutan in the Himalayan region.

$$V = 43.24 * A^{1.5307}$$

V is lake volume in 10^6 m^3 and A is surface area of lake in km^2

Volume is validated using area and average depth of lake. Depth of lake is estimated using empirical relation developed by Akiko Sakai (2012) as well as from ASTER DEM. Three dimensional perspective views of the Katkar glacier & MDL are shown in Figure 298, which was used to calculate depth of lake. Depth of both the lakes is found to be more or less same from both the techniques.

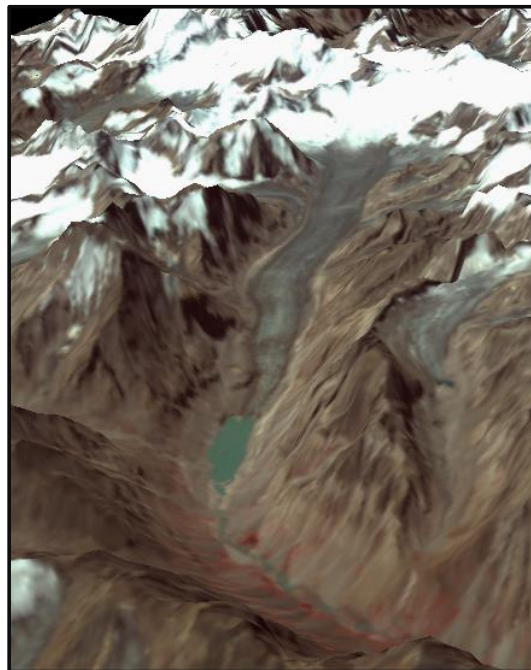


Figure 298: Three-dimensional perspective view of the Katkar glacier and MDL (Source: Rathore et al., 2015b)

Volume of lakes was also estimated using various empirical relations (Table 89). Error is also estimated with respect to area * average depth relationship. It is very much matched with empirical relation given by Akiko Sakai (2012).

Huggel et al. (2002) has also developed similar relationship from glacier lakes located in the Swiss Alps including ice dammed lakes. Peak discharge was estimated using following Empirical relationship developed by Clague and Mathews (1973), where volume is used as an input for peak discharge estimation.

$$Q_{\max} = 75 * (V/1000000)^{0.67}$$

Where Q_{\max} = Peak discharge (m^3/s) and V = lake volume (million m^3).

Table 89: List of models used for estimation of volume of lake (Source: modified after Rathore et al., 2015b)

Sr. No.	References	Empirical relation for volume	Katkar lake			Gepang-gath lake		
			Results Volume 10 ⁶ m ³	Comparison with area-depth relationship	% error	Results Volume 10 ⁶ m ³	Comparison with area-depth relationship	% error
1	Akiko Sakai et al(2012)	$43.24*(A)^{1.5307}$	18.29	1.83	9	30.73	1.27	4
2	Mathematical	Areal extent * Avg. depth	20.12	0	0	32	0	0
3	O'Connoret et al	$3.114*A+.0001685(A)^2$	56.52	-36.40	181	110.33	-78.33	-245
4	Huggel et. al (2002)	$.104*(A)^{1.42}$	15.50	4.62	23	25.09	6.91	22
4	Yao, Xiaojun et al.	$.493*(A)^{.9304}$	29.22	-9.10	45	40.06	-8.06	-25

For development of above mentioned formula, many physical based models were developed to estimate the peak discharge. But due to non-availability of other information it is difficult to develop our own model. Therefore, the relationship developed by Clague & Mathew (1973) is used to estimate peak discharge. Peak discharge of lake in case of outburst was also estimated using various empirical relations. It varies from 196-716 and 287-1012 m³/sec for Katkar & Gepang-gath mdl respectively. Average value of peak discharge lies near to that given by Clague & Mathews (1973).

b) Probability of outburst lake

The extent of a flood caused by the breach of a moraine dam is relevant for further hazard analyses. The present study used the outburst probability model developed by McKillop and Clague (2009) for assessing the dangerous nature of the moraine-dammed lake and the equation proposed by Clague and Mathews for estimating the peak discharge of the lake in case of an outburst. McKillop and Clague (2009) developed the moraine-dammed lake outburst probability model by considering the utility of remote sensing in gathering information and also based on the inventory of 189 moraine-dammed lakes in British Columbia.

$$P = \{1 + \exp - [\alpha + \beta_1(M_hw) + \sum \beta_j(\text{Ice_core}_j) + \beta_2(\text{Lk_area})] + \sum \beta_k(\text{Geology}_k)\}^{-1}$$

Where α is the intercept, β_1 , β_j , β_2 and β_k are the regression coefficients for M_hw (moraine height-to-width ratio), Ice_core (moraine – ice free or ice core), Lk_area (lake area) and Geology (moraine constituents – sedimentary, metamorphic) respectively. The parameters such as moraine height-to-width ratio can be derived using digital elevation data by overlaying the satellite data over the DEM. Presence/absence of an ice-core in the moraine

is established using the following methods proposed by McKillop and Clague (2009); (i) a moraine with a rounded surface with minor superimposed ridges was assumed to be ice-cored; (ii) a moraine with a disproportionately large end in front of a small glacier was suspected to be ice-cored and (iii) a narrow, sharp crested moraine with an angular cross-section was interpreted to be ice-free. The lake area is estimated from the lake boundary layer prepared from satellite data and main rock type forming the moraines is derived from the lithological interpretation of the study area. The regression parameters taken from McKillop and Clague (2009) and the four predictors taken from satellite data of 2014. The M_{hw} value taken from satellite data was used to measure moraine height and width. For further analysis, height of moraine is taken as ~35 & 40 m, width of moraine is ~25 & 40 m and average width is 350 & 500 m for Katkar and Gepang-gath MDLs respectively.

17.5. Results and Discussion

Changes in area and length of Katkar and Geepang-gath glaciers

Areal extent of Katkar glacier was estimated as 24.38 sq km in 1962. Areal extent of glacier continuously decreased from 24.38 to 23.58 sq km during 1962 to 2014. Percent retreat in areal extent of glaciers wrt 1962 is shown in Figure 299. It has been reported that SOI topographical maps estimates higher areal extent of glacier (Bhambri and Bolch, 2009). The length of glacier along central line decreased from 12.56 km to 11.0 km during 1962-2014. Percent retreat in length of glaciers wrt 1962 is shown in Figure 300 According to a study carried by Kamp et al., (2011), glaciers of Chenab sub-basin were retreating at an average rate of less than 20 meter per year (Kulkarni and Karyakarte, these glaciers are not attached with MDL, so we can say that MDL enhances retreat of glacier. The data suggests that rate of retreat decreases from 1962-1976 interval up to 2001 but again increases during 2001-2014. Altitude of glacier snout was 4520 meter in 1962 which was elevated to 4572 meter in 2014.

Gepang-gath glacier is debris covered glacier and located in Chandra sub-basin. Approximately 29% area of glacier is covered by debris. Areal extent of glacier was estimated 13.1 sq km in 1962 which reduced to 12.22 sq km. Areal extent of glacier was observed to be continuously reducing between 1962 and 2014. Percent retreat in areal extent of Gepang-gath glacier is higher than Katkar glacier (Figure 299). Length of glacier along central line was 6.7 km in 1962 which decreased to 5.7 km in 2014. Rate of retreat were observed to be gradually increasing from 1962 to 2014, reaching 31 meter per year during 2001-14. Percent retreat in length of both the glaciers was more or less same (Figure 300). According to a study carried by Sangewar (2011), glaciers of Chenab sub-basin were retreating at an average rate of less than 20 meter per year (Kulkarni and Karyakarte, 2014). These glaciers are not attached with MDL so we can say that MDL enhances retreat of glacier. Width of glacier is around 500 meter. Altitude of glacier snout was 4079 meter in 1962 which elevated to 4132 meter in 2014. Beyond this altitude slope of glacier is less than 5° which support a continuous increase in the rate of change of lake area.

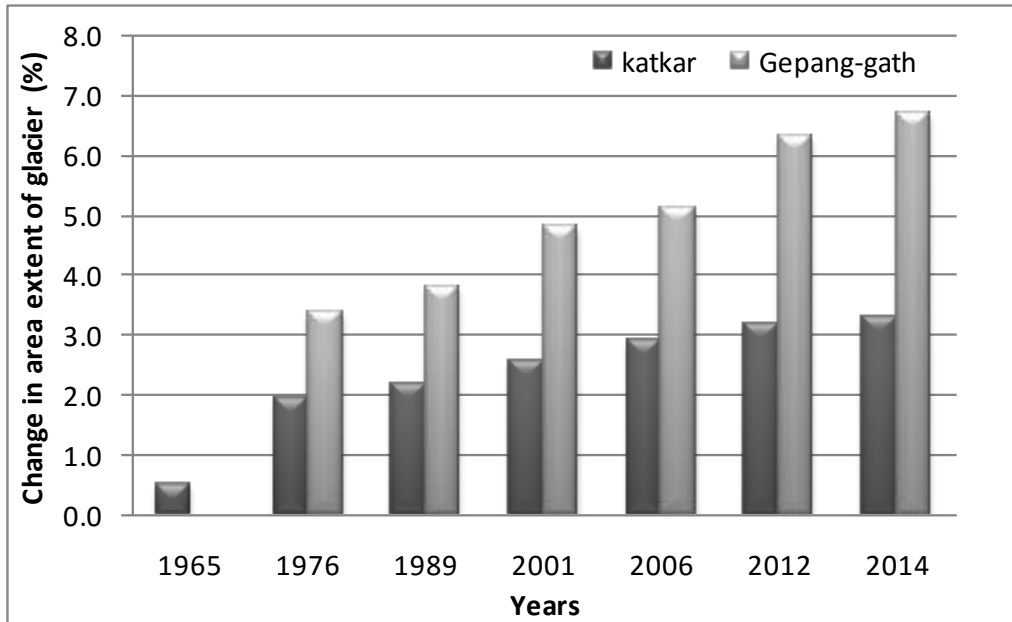


Figure 299: Retreat in areal extent of Katkar and Geepang-gath glaciers w.r.t. 1962 during different time frames upto 2014 (Source: Rathore et al., 2015b)

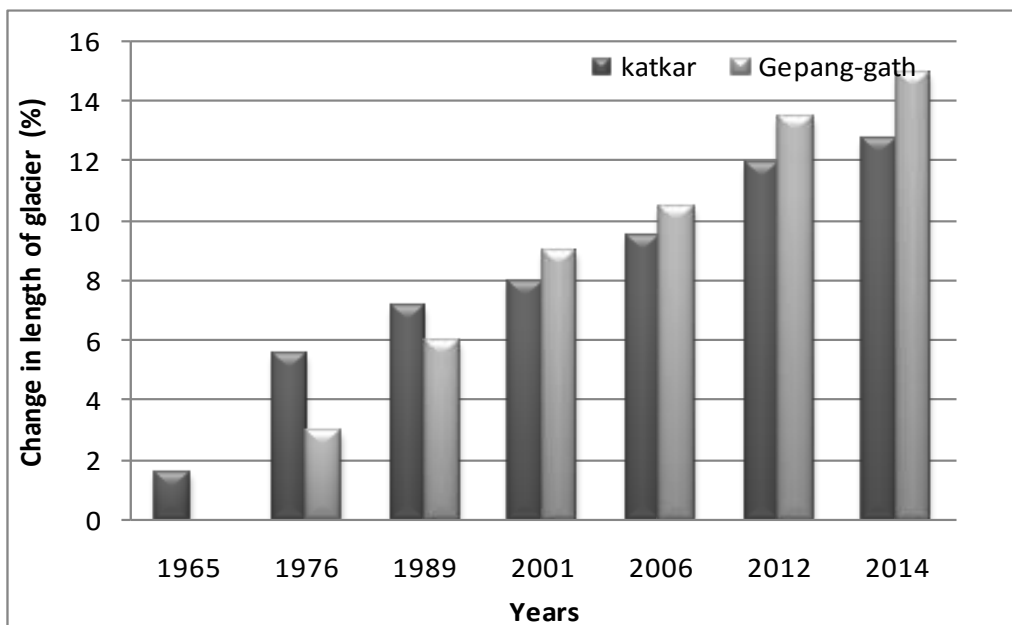


Figure 300: Retreat in length of Katkar and Geepang-gath glaciers wrt 1962 during different time frames upto 2014 (Source: Rathore et al., 2015b)

Changes in the Moraine Dammed Lakes of Katkar and Geepang-gath glaciers

MDL of Katkar glacier was not there during 1962 as per the SOI topographical map. The lake was observed on the corona image of 1965. This shows that this lake was formed between 1962 and 1965. However, supra-glacial lakes, smaller than this, are shown on the

map. This confirms that the lake is not a matter of omission. Glacial lakes are formed, where the inclination of glacier surface is less than 2° (Huggel et. al., 2002). Slope near snout of this glacier was found to be less than 3° which provide suitable terrain condition for the formation of MDL. Area of MDL was observed 21 ha in 1965 which increases to 57 ha in 2014. MDL area increased significantly during 2001 to 14 (Figure 301 and Figure 302). which is also reflected in more retreat over the same period (Figure 299 and Figure 300). Beyond this altitude slope of glacier becomes 9° which reduces the rate of change of lake area. Expansion of MDL of Katkar glacier from 1965 to 1989 is higher than 1989 onwards. It may be due to higher slope toward glacier. 2014 onwards due to higher slope rate of expansion of lake should reduce.

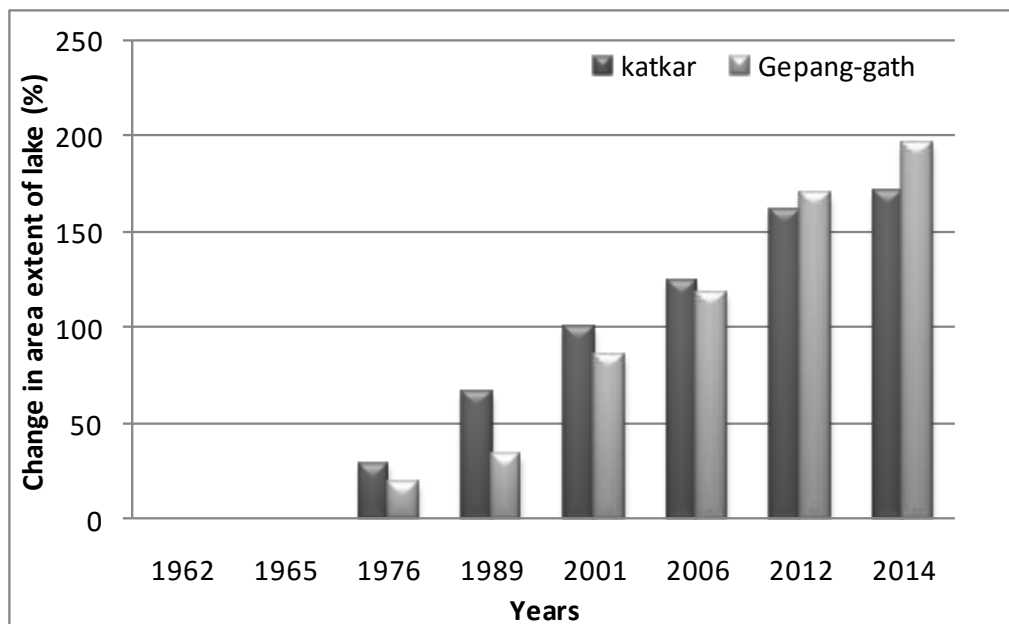


Figure 301: Increase in areal extent of Gepang-gath & Katkar lakes during 1976 to 2014 w.r.t 1962 (SOI Map) and 1965 (Corona Image) respectively (Source: Rathore et al., 2015b)

Maximum depth of MDL was estimated by Akaki Sakai, (2012), 50 meter in 1976 and 73 meter in 2012 which results $5.72 \times 10^6 \text{ m}^3$ and $17.25 \times 10^6 \text{ m}^3$ volume of lake respectively. Depth of lake was found to be 25 m and 35.3 m in 1976 and 2012 respectively using SOI contour approach which was used to estimate the volume. The difference in both approaches for estimating volume was found to be 11%. Peak discharge, using empirical relationship (Clague and Mathews, 1973), was estimated $189 \text{ m}^3/\text{sec}$ in 1965 to $526 \text{ m}^3/\text{sec}$ in 2014 (Table 90). This storage is quite large in comparison to summer discharge as reported 10 cumec for Chhota Shigri glacier in Himachal Pradesh (Kulkarni, 1996).

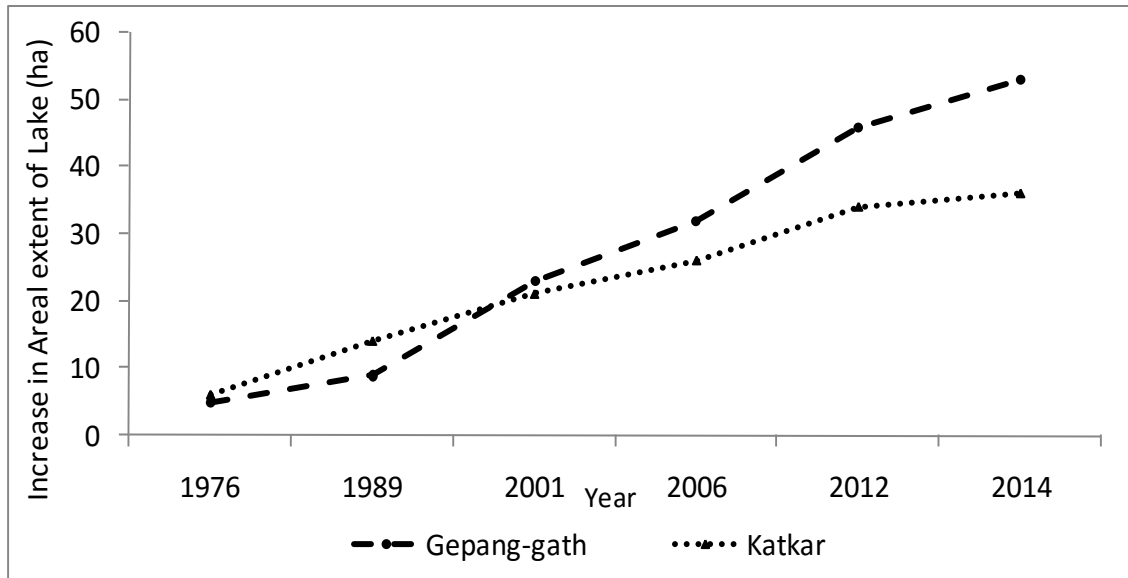


Figure 302: Change in areal extent of Gepang-gath and Katkar lakes during 1976-2014 (Source: Rathore et al., 2015b)

Table 90: List of models used for estimation of peak discharge (Source: modified after Rathore et al., 2015b)

S No.	References	Empirical relation	Results Peak discharge m ³ /sec	
			Katkar lake	Gepang-gath lake
1	Costa & Schuster (1988)	$0.0000055 * (PE)^{0.59}$	196	287
2	Clague & Mathews (1973)	$75 (V)^{0.67}$	526	744
3	Costa (1988)	$113(V)^{0.64}$	726	1012

Expansion of MDL of Gepang-gath glacier from 1965 to 1989 was lower than 1989 onwards. It may be due to lower slope toward glacier. 2014 onwards due to lower slope, areal extent of lake should expand at higher rate.

Lake area was measured 27 ha in 1962 which gradually increases to 80 ha in 2014. Figure 302 shows variation in areal extent of glacier and moraine dammed lake of Gepang-gath glacier. Maximum depth was estimated 50 meter in 1962 and 86 meter in 2014 using Akiko Sakai (2012) approach. Volume of lake was 5.70×10^6 m³ in 1962 which gradually increased to 30.73×10^6 m³ in 2014. Three dimensional perspective views of the Gepang-gath glacier & lake are shown in Figure 298, which was used to calculate depth of lake. Volume was estimated using 22 m and 40 m average depth during 1962 and 2014 respectively using SOI contour. The difference in both approaches for estimating volume was found to be 9%. Peak discharge was estimated 241 m³/sec in 1962 to 744 m³/sec in 2014 using imperial

relation developed by Clague and Mathews (1973). Detail information about glacier retreat, variation in lake area, volume and peak discharge is given in Table 89 and Table 90.

The present analysis shows that increase in lake has accelerated the rate of retreat and the receded vacated area of glacier was occupied by the MDL. The rate of expansion of Gepang-gath lake is higher than Katkar lake (Figure 302). It may be because of lower slope of Gepang-gath glacier as compared to Katkar glacier. Uncertainty in terminus change and accuracy in areal extent of glacier and lake is estimated using empirical relationship developed by Hall et al. (2003) and Wang et al. (2009). Overall accuracy was estimated ± 107 m for SOI maps and Landsat MSS data (1962-1976), ± 113 m for Landsat MSS and TM data, ± 49 m for Landsat TM & IRS LISSIII data, ± 45 m for LISS III data and ± 45 m for LISS III and Landsat ETM data. Changes in areal extent of glacier and MDL were measured with an accuracy of 0.017 km^2 , 0.006 km^2 , 0.002 km^2 , 0.002 km^2 and 0.003 km^2 between each pair of datasets i.e. 1962-1976, 1976-1989, 1989- 2001, 2001-2006/07 and 2006/07-2014 respectively.

By considering the probability model of McKillop and Clague (2009) and incorporating the predictor parameters, the model yields a very low outburst probability of less than 1% for the both the lake (<6% very low; 6–12% low; 12–18% medium; 18–24% high; > 24% very high). The very low outburst probability shows that, if the lake increases its extent in due course of time, it may not cause a dangerous outburst flood. As all the MDLs of Himalayan regions are continuously dewatering so water is being releasing slowly by its outlet channel. So lakes will not outburst by its own but it may outburst due to natural calamity like earth quake, cloud burst or avalanche. In this situation water stored at higher altitude may cause large damage to lower region due to higher kinetic energy. Three glaciers which are located north of Gepang-gath glacier are draining toward lake. These glaciers are having steep slopes as observed by slope map. Slope map is prepared using Aster DEM. So chances of avalanche or landslide are there. Due to this reason lake may outburst and cause damage at Sissu village, which is located 10 km downstream from lake. One glacier which is located at south east side of Katkar glacier is draining toward Katkar lake. But this glacier is not having steep slope. So chances are less for avalanche or landslide. So Katkar lake is not likely to outburst as compared to Gepang-gath due to avalanche or landslide. This is a preliminary assessment their probability to outburst and more field-based studies are needed for proving the hazardous potential.

17.6. Conclusions

In present study, satellite images in conjunction with SOI topographical maps were analyzed for identification and monitoring of crucial MDLs in parts of the Himalayan region over 5 decades. Katkar glacier is a debris free glacier which has shown higher linear retreat in comparison to debris covered (3%) Gepang-gath glacier. In present scenario, Katkar glacier is expected to show lesser rate of increase in lake area in comparison to Gepang-gath glacier as slope of glacier above snout is 9° for Katkar and less than 3° for Gepang-gath. It

is highly probable that increase in lake area for Gepang-gath glacier may gradually further increase. Peak discharge for Katkar glacier has increased from 189 to 505 m³/sec between 1965 and 2014 whereas it varied from 241 to 675 m³/sec between 1962 and 2014 for Gepang-gath glacier. Chances of probability of outburst of both the lakes are very less, however due to landslide or avalanche Gepang-gath lake may outburst & cause damage to lower region. Gepang-gath glacier is required to be monitored regularly as compared to Katkar lake. Similar studies in other parts of the Himalayan terrain are required for assessment of possible GLOF hazards, so that measures to mitigate flash floods from the outburst of MDLs may be planned well in advance.

18. Estimation of Regional Water Mass Variations from Gravity Recovery and Climate Experiment (GRACE) over Himalayan region

18.1. Objective

To estimate regional water mass variations over the Indus, the Ganga and the Brahmaputra basins using Gravity Recovery And Climate Experiment (GRACE) data for the time frame 2003-2012.

18.2. Scientific Rationale

The Earth's global gravity field can be defined by tracking LEO satellites. When the satellites are passing over the mass anomalies, disturbances in the LEO satellites occurs due to attraction of gravity field (Avsar and Ustan, 2012). A joint Mission named as "Gravity Recovery And Climate Experiment (GRACE)", between National Aeronautics and Space Administration and Deutschen Zentrum für Luft- und Raumfahrt (NASA & DLR) was launched on March 17, 2002 from the Plesetsk Cosmodrome in Russia under the NASA Earth System Science Pathfinder Program (ESSP). The satellites were equipped with dual-frequency, K-band microwave ranging (KBR) separated by ~200 km to continuously monitor the variation in distance between the satellites due to varying gravity field of the earth. The satellites also consist with high precision accelerometers (ACC) for measuring the non-gravitational accelerations, highly precise Global Positioning System (GPS) receiver for absolute positioning and star cameras for satellite attitude determination (Tapley et. al, 2005; 2004). The primary goal of GRACE mission was to estimate the time varying gravity field mapping for earth science studies, especially monitoring of hydrological mass redistribution through their integrated gravitational effect (Tapley et al., 2004).

The principle of the GRACE satellite system is based on satellite-to-satellite tracking (SST), both in the high–low mode (SST-hl) and low–low mode (SST-ll) (Liu 2008). In SST-hl mode the LEO satellites are monitored through the GPS satellites which are at higher altitude. The LEO satellite orbit is disturbed due to mass anomalies (Figure 303) and the gravity field can be recovered by the measurements of the non-gravitational acceleration through three-axis accelerometer. SST-ll mode not only provides, the static gravity field with higher resolution but also gives higher temporal resolution with adequate spatial resolutions. In SST-ll mode, the LEO satellites are tracked with reference to each other. In GRACE mission the two GRACE satellites are tracked with the help of K-band microwave ranging instruments. Using the combination of SST-hl and SST-ll mode the accuracy and resolution of the gravity map is enhanced to produce a detailed map of the earth gravity field (Liu 2008). In other words, gravity field changes are sensed by the twin GRACE satellites and GPS networks give the

combined indirect and direct effect of all mass redistributions and mass variability within the Earth and its fluid envelopes (Kusche and Schrama, 2005).

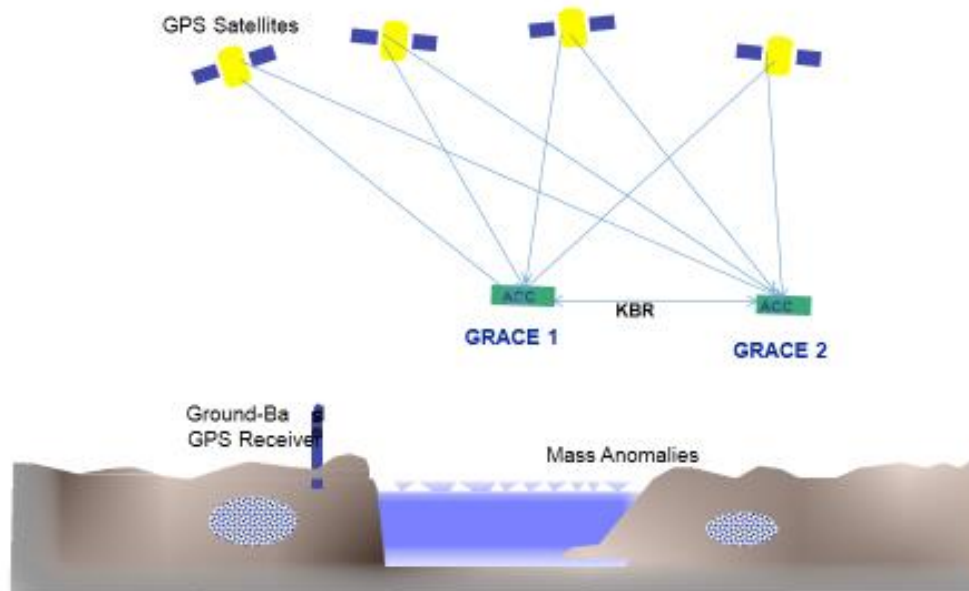


Figure 303: A schematic diagram of GRACE-1 Mission Concept (Source: Agrawal et al., 2014)

The earth's gravity field is measured at approximately monthly intervals with a spatial resolution of a few hundred kilometers (Klees et. al, 2007). These monthly estimates of the Earth's gravity field produced by the GRACE give information about the mass variability at and below the surface of the Earth (Swenson and Wahr, 2006). An estimate of a surface mass anomaly does not represent as a point measurement but rather a spatial average due to coarser resolution (Swenson and Wahr, 2002.). Accuracy of better than 1 cm of equivalent water thickness is expected from such gravity field measurements (Swenson and Wahr, 2002).

Each monthly solution consists of a set of spherical harmonic coefficients complete to degree and order 120. The seasonal gravity variation can be measured by the differencing of the monthly solution by taking one solution as a reference gravity field. The differences in the seasonal gravity field are caused by post glacial rebound, atmospheric and ocean mass transport and redistribution of water, snow and ice on land. To understand the gravity field behavior on the land, GRACE measurements have already been corrected for the major contribution variation due to ocean and atmosphere. Therefore, differences between monthly solutions mainly consists of changes in terrestrial water storage (TWS), i.e. groundwater, soil moisture, rivers, lakes, snow, and ice (Klees et. al, 2007).

GRACE observations has no vertical resolution (Wahr et. al., 2006) and it reflects changes in vertically integrated stored water, which includes variations from snow pack, glaciated areas, surface water, soil moisture and ground water at different depths (Longuevergne et al., 2010). Due to combination of different storage factor, it is not possible to compute

whether the variation in mass is caused due to change in Land surface, subsurface or atmospheric component (Wahr et. al., 2006). The extraction of water from any one of the storage component (e.g., snow packs) requires disaggregating the vertically integrated water storage observation, either by making assumptions or by using different models to eliminate other components. Monitoring of the total water storage as surface and subsurface is essential for understanding of hydrological cycle in climate change environment (Tiwari, et. al., 2009) to understand seasonal behavior, where climate-driven mass transport of water plays a major role towards gravity (Davis et.al, 2008). Time-variable ice loss in Asian high mountains have been estimated from satellite gravimetry (Matsuo and Heki, 2010).

Snow packs and glaciers are a very important component of the Earth's climate system (Su et.al, 2010). In the Himalayan region regional mass anomalies show large variations in terms of snow water equivalent over a season. The accurate estimation of snowpack and its variation is important for various hydrological applications. In this study, the annual mass variability including the rate of mass change were estimated for bringing out the water mass variations in terms of changes in Water Equivalent Heights (WEH) over three major basins of the Himalayan region viz., the Indus, the Ganga and the Brahmaputra basins using GRACE data for the time frame 2003-2012 (Agrawal et al., 2014).

18.3. Study Area

The study area in general extends in the south-east from latitude 25° 39' N and longitude 97° 46' E (approx.) to north-west up to latitude 37° 05' N and longitude 72° 14' E (approx.) covering the Himalayas, Trans-Himalaya and Karakoram regions across four countries viz. India, Nepal, Bhutan and China (Tibet). The study area has been further restricted to the Indus, Ganga and Brahmaputra basins covering the mountainous and piedmont regions (Figure 304). These basins represent the three mighty rivers, which originate from the glaciers of the Himalayan region and are fed by seasonal snow and glacier melt water.

The Indus, Ganga and Brahmaputra basins have a total geographic area of 1.9×10^5 sq km, 0.6×10^5 sq km and 1.2×10^5 sq km respectively, with 0.95 million km² area mapped under glacier inventory (Sharma et al., 2013). The geographical classification of region broadly coincides with the source of precipitation i.e., Southeastern monsoon is more active in eastern Himalayas (decreases westwards) whereas northwestern monsoon is more active in the western Himalayas (decreases eastwards).

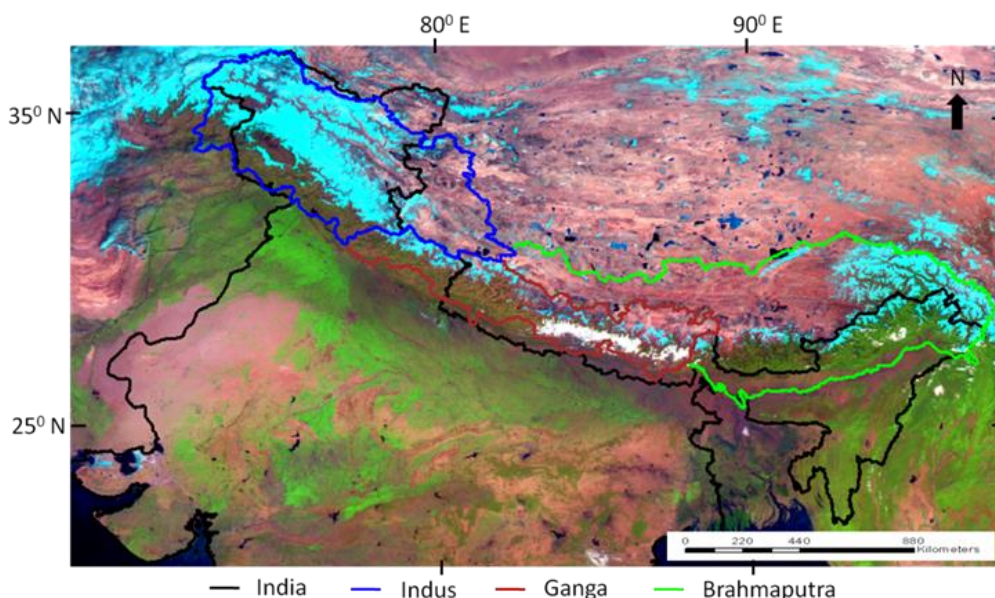


Figure 304: Location of study area consisting three major river basins Indus, Ganga and Brahmaputra in the Himalayas (background image is INSAT 3A-CCD) (Source: Agrawal et al., 2014)

18.4. Data Used

The GRACE data is collected at GRACE Science Data System, which is shared between Jet Propulsion Laboratory (JPL), University of Texas Center for Space Research (CSR) and Deutsches GeoForschungsZentrum (GFZ) (Avsar et.al, 2012). The collected data are processed to generate Level-1B followed by the Level-2 data in the form of harmonic coefficient with a temporal resolution of one month or shorter duration (Longuergne et al., 2010), which can be inverted to estimate changes in mass at the surface. These processed datasets in form of Spherical harmonics produced by different agencies are available online at official data processing repository <http://podaac.jpl.nasa.gov/grace/> (CSR, GFZ, JPL). The different components contributed in the GRACE measurement are analyzed with the help of FES 2004 model for taking care of diurnal and semidiurnal tides, IERS 2003 model for computing solid earth tidal contribution to geo-potential and solid earth pole tide and Ocean pole tide defined based on satellite altimetry data (Liu, 2008). Similarly, datasets are also corrected with variable atmospheric conditions by AOD1B products. The remaining gravity changes are interpreted as monthly vertically integrated stored water of snow packs, ground water and soil moisture in terms of Water Equivalent Height (WEH).

The data is further enhanced with the help of two filtering techniques to reduce the presence of the measurement errors. First filter is designed for removal of correlated errors between spherical harmonic coefficients, which is manifested as stripes oriented towards North-South in GRACE maps (Swenson and Wahr, 2006). Second filter is a Gaussian averaging filter with a half width of 300 Km which reduces random errors in higher degree co-efficient (Wahr et.al, 2006). The data are further translated into global sets of localized surface mass concentrations termed as “mascons”, which omits the direct use of the spherical harmonics

coefficient. The mascons datasets are basically a conversion form of the spherical datasets into a geographical co-ordinate system and such data sets are available with a spatial resolution of $1^0 \times 1^0$ resolution cell. In this study, the monthly mascons data from the CSR processing agency were downloaded for a period of ten years (2003-2012) and analyzed to compute water mass variations over Himalayan basins.

18.5. Methodology

A quantitative analysis of secular and seasonal water mass anomaly was carried out. A weighted least-squares fit was used to estimate the annual cosine (winter-summer) component, the annual sine (spring-fall) component, and a linear trend over a decade of the GRACE derived water mass (Equation 1).

Mathematic model:

$$y(t_i) = a_0 + a_1 \frac{t_i}{12} + a_2 \cos \omega t_i + a_3 \sin \omega t_i + a_4 \cos 2\omega t_i + a_5 \sin 2\omega t_i \quad (1)$$

where,

t_i = Time in month

a_0 = mean model

a_1 = linear trend

a_2 = annual cosine component

a_3 = annual sine component

a_4 = semi annual cosine component

a_5 = semi annual sine component

and, $\omega = \frac{2\pi}{T}$

The model component a_1 gives the secular water mass changes (Figure 305).

The sine terms a_3 indicates positive showing maximum water mass in summer season and negative value indicates maximum water mass in winter. The cosine terms a_2 indicates negative value for the maximum mass in summer season and positive value indicates maximum mass in winter.

The magnitude of the annual mass variability can be computed as (Equation 2).

$$A_{am} = \sqrt{a_2^2 + a_3^2} \quad (2)$$

where, A_{am} = (annual Variability)

The annual water mass variability shows the variations in a year due to the seasonal changes in precipitation, snowfall, evaporation, surface/subsurface movement of water and groundwater extraction.

18.6. Results and Discussion

It is distinctly observed that the northern Indo-Gangetic plains in parts of Punjab, Haryana, and northern Rajasthan are showing high depletion of water mass during 2003-12 (Figure 4.17.3). These results further support the earlier findings of GRACE data analysis for time frame 2002-2008 (Tiwari et al. 2009 and Rodell et al. 2009). It is also observed that the Ganga and the Brahmaputra basins show depletion trend of water mass while the Indus basin shows a mix of negative and positive secular water mass.

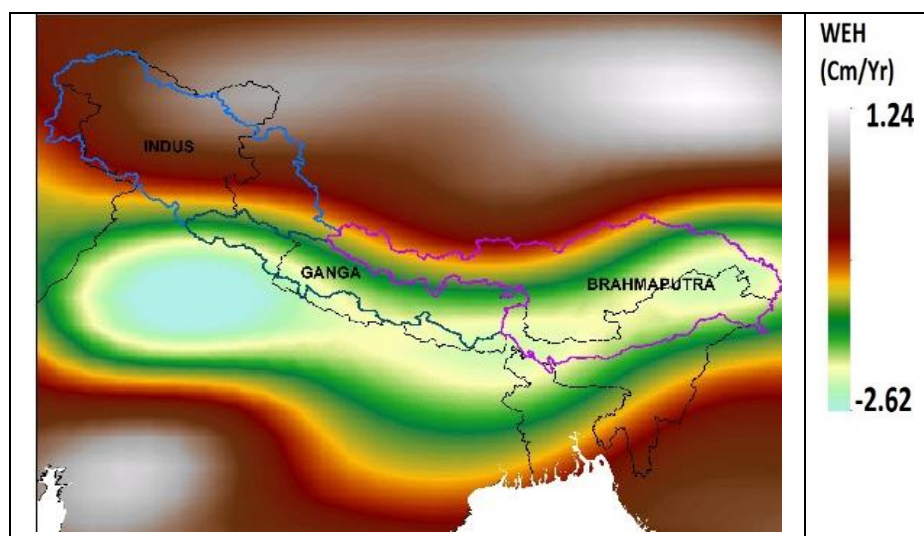


Figure 305: Spatial secular water mass changes (WEH) over the Himalayan and adjoining regions estimated using GRACE data of 2003-12 (Source: Agrawal et al., 2014)

The spatial annual water mass variability over the Himalayan and adjoining regions during time frame 2003-12 shows very low annual water mass variability in the Western Himalaya and Tibetan plateau, while the Central and Eastern Himalaya shows low to high annual water mass variability (Figure 306). The gridded data of Water Equivalent Height (WEH) for Himalayan region were used for statistical analysis and estimation for the secular trends over the Indus, Ganga and Brahmaputra Basins. The temporal profile of spatial averaged WEH over Indus, Ganga and Brahmaputra basins are shown in Figure 307.

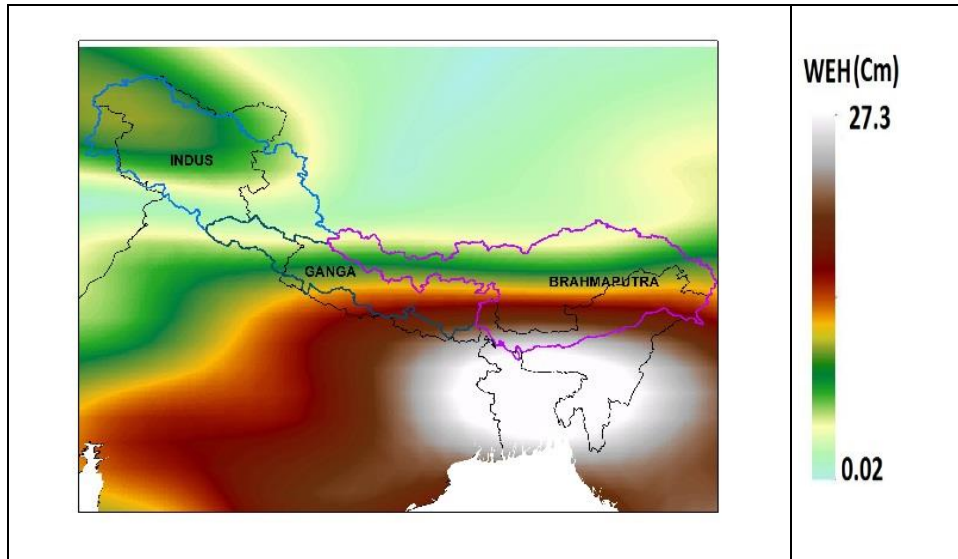


Figure 306: Spatial annual mass variability over the Himalayan and adjoining regions estimated using GRACE data of 2003-12. (Source: Agrawal et al., 2014)

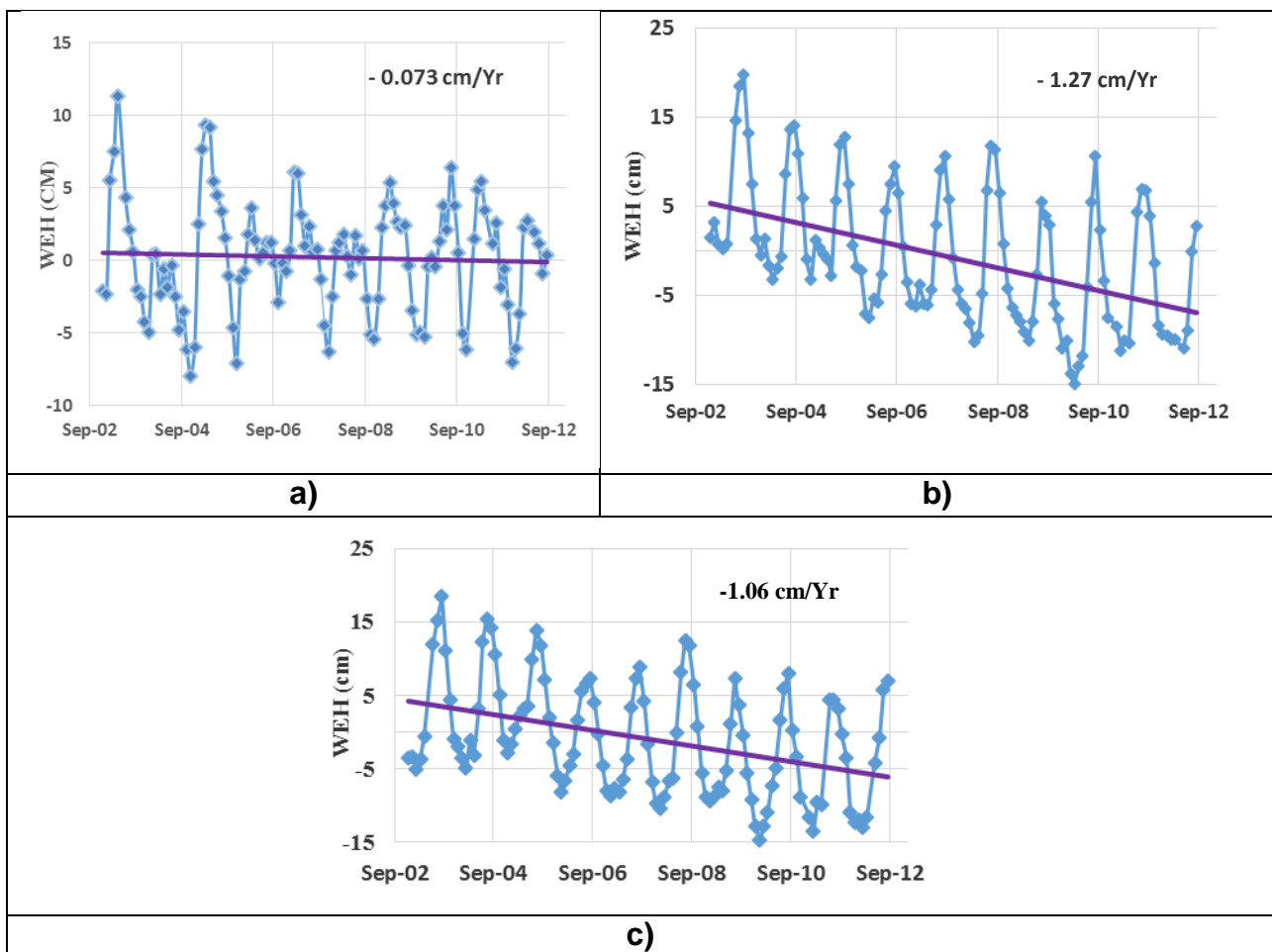


Figure 307: Temporal profile showing secular trend of spatially averaged WEH (2003-2012) over a) Indus, b) Ganga and c) Brahmaputra basin (Source: Agrawal et al., 2014)

The trend analysis over Ganga and Brahmaputra basins have shown an average annual change of -1.28 cm and -1.06 cm in terms of WEH whereas Indus basin has shown a slight annual change of -0.07 cm, which is statistically insignificant at 95% confidence level. It is inferred that there is no water mass change in the Indus basin and there is depleting trend in the Ganga and Brahmaputra basins.

The present analysis has not computed the changes in groundwater extraction, soil moisture and snowpack individually and is presently representing the sum of all these components. GRACE data are also sensitive towards interior strain variation, surface uplift and surface subsidence cover over a large area. Therefore, future work has been planned to quantify these components individually. The next mission GRACE-2 with increased resolution is expected to provide more information on changes in water masses and shall be extremely useful to understand the impact of climate change on the Himalayan Cryosphere and Hydrology.

19. Snow and Glacier Melt Runoff Modeling

19.1. Objective

To develop a distributed snow & glaciers melt runoff model.

19.2. Scientific Rationale

Himalayan region has high concentration of mountain glaciers. Large extent of this region is covered by seasonal snow cover during winter. Runoff generated from melting of these snow & glaciers is one of the important sources of water for the Himalayan Rivers. Only 1% of the world 's water is usable to us. About 97% is salty sea water and 2% is in frozen state as snow and glaciers. As 1% is insufficient to overcome the causes of water scarcity which vary from natural causes such as climate change and draught and human causes such as demand over stripping supply, population growth, water quality and resource allocation. So studies on mountain glaciers and snow are welcomed. The pious peaks of the Himalayas are known as the water towers of Asia providing drops of elixir to quench the parched plains and to satisfy the scorching throats of the living world. They store a significant quantity of fresh water which is found in the concentrated form of seasonal snow cover and glaciers outside the polar realm. Indeed, they have the capacity for supplying 86,000,000 cubic meters of water annually to Asia's seven great rivers. Western Himalayan Rivers combine into the Indus Basin, of which the Indus River is the largest. The Indus begins in Tibet at the confluence of Sengge and Gar river and flows southwest through India and then through Pakistan to the Arabian Sea. It is fed by the Jhelum, the Chenab, the Ravi, the Beas and the Sutlej River, among others. In western Himalayas, the temperature is lesser due to higher altitude as well as latitude and as a consequence the snowline in the western Himalaya is at a lower altitude than the eastern Himalaya. As distance from the sea is greater, both annual and diurnal range of temperature is greater in the western Himalayas. So it receives lesser precipitation than eastern Himalayas (Bose, 2013). As in western Himalayas, the snowmelt commences in March, the snow line starts receding upwards and by the end of June to an altitude of 4,500m (Prasad and Roy, 2005). Changes in climate have drastic repercussions on the entire earth and have affected more dramatically on the Himalayan glaciers. These glaciers are more susceptible to climate change due to their latitudinal and altitudinal position and other interrelated processes. These processes need detailed multidisciplinary investigations and have opened a new venue for estimating the runoff with the help of different models. These models require the fundamental variables which directly affect the melt process. For snowmelt runoff modeling, the two pragmatic approaches are accessible. They are energy balance approach and degree day method. In comparison to the energy balance approach, degree day approach is more practicable and needs minimum parameters for simulating snow & glacier melt runoff. It is widely used due to its being less complicated. The energy exchange at snowpack surface can be explained by four major components. They are shortwave radiation exchange and heat exchange, convective and advective heat transfer. These radiations exchange and heat transfer can

be estimated if information on various parameters as cloud covers, albedo, wind, cloud temperature and dew point temperature are known (Anderson, 1976). Information on these parameters is normally not available; therefore, degree-day approach is used for operational forecasting (Quick and Pipes., 1988). Precipitation and temperature are the major factors for generating runoff in mountainous regions which are covered with snow and glaciers. Precipitation falls either in the form of liquid (rain) at lower latitude and altitude or in the form of solid (snow) at higher latitude and altitude. When rainfall occurs, runoff is estimated by subtracting various types of water losses. In case of snow fall, snow remains static for quite some time and it requires certain amount of temperature to convert it into liquid and then to set the process of runoff. Integrated approach for snowmelt runoff estimation using temperature index model, remote sensing and GIS has been developed (Aggarwal et al., 2014). Present and future glacier melt-water contribution to runoff in a Central Himalayan river basin have been estimated (Prasch et al., 2012). Snowmelt contributions to discharge of the Ganges are also estimated (Siderius et al., 2013). However, missing (in-situ) snow cover data hampers climate change and runoff studies in the Greater Himalayas (Rohrer et al., 2013).

19.3. Study Area

Parbati sub-basin of Satluj basin in Himachal Pradesh has been selected as the study area. It is continuously fed by melting of high altitude snowfields and glaciers. This basin is sub divided in to various watersheds. Tosh watershed is one of the significant and substantial watersheds of Parbati sub-basin, representing similar hydrologic processes as that of the whole Parbati sub-basin and is identified as an intensive study site. Figure 308 shows the study area and river network of Parbati sub-basin and Tosh watershed. Parbati sub-basin covers the area of 1773 km². Elevation range of this catchment is 1110 m to 6597 m. Tosh watershed covers the area of 329 km² which is a part of Parbati sub-basin.

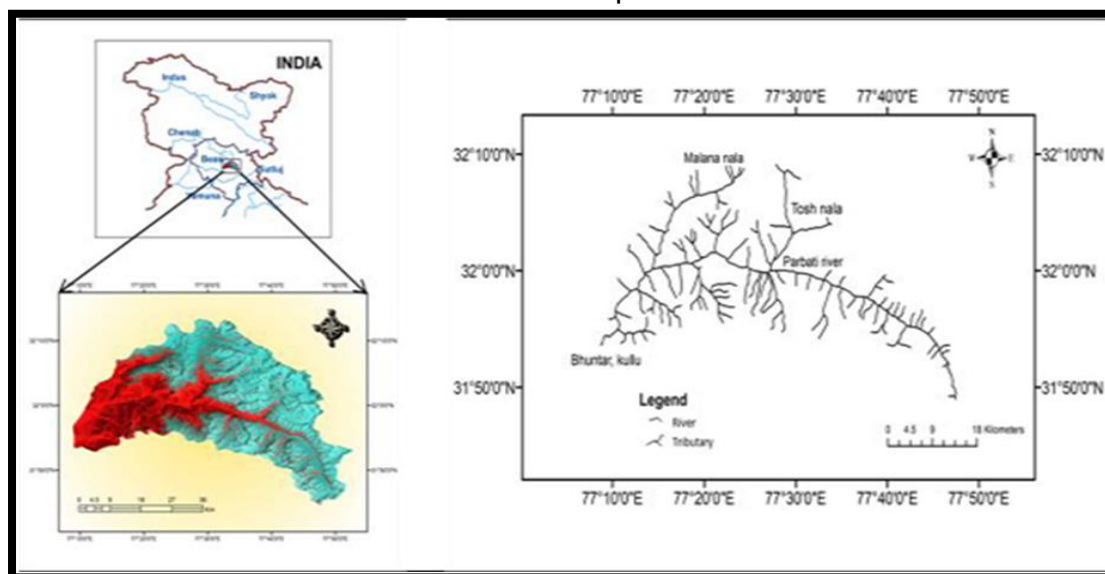


Figure 308: Location map of Parbati sub-basin, Himachal Pradesh

19.4. Data Used

i) Satellite data

The Advanced Wide Field Sensor (AWiFS) data have been used for this study. It provides a spatial resolution of 56 m and covering a swath of 740 Km. to cover this wide swath, the AWiFS camera is split into two separate electro optic modules, AWiFS-A and AWiFS-B. Because of its large swath the repetivity of the AWiFS is 5 days. These data are imported from NRSC (National Remote Sensing Centre), Hyderabad. Reflectance, NDSI images are generated using NDSI algorithm (Kulkarni et al., 2006b). Advanced Space born Thermal emission and Reflection radiometer (ASTER) sensor is one of the five remote sensory devices on board the Terra satellite launched into the Earth's orbit by NASA in 1999. ASTER GDEM (Global Digital Elevation Model) is the global DEM created using ASTER.

ii) Meteorological data

Surface variables like precipitation and temperature are to be highlighted for estimation of runoff in snow & glacier covered area. Indeed, precipitation is said to be any product of the condensation of atmospheric water vapour that falls under gravity while the changes in air temperature in the atmosphere which take place due to dynamic processes should both be taken in to account. These significant parameters which have high contribution in snow & glacier melt runoff have been taken from Bhuntar, Kullu District of Himachal Pradesh for this present study. For clarity, maximum and minimum air temperatures and precipitation data from 2004-2005 available in daily format are converted in to 10-daily format specifically for utilizing and for fulfilling the requirements of the model.

iii) Hydrological data

For the calibration period of the model at Tosh watershed, the discharge data are collected from the U/s of the confluence of both Tosh Nala and Parbati River. For the validation period of the model at Parbati sub-basin, the discharge data are collected from the D/s of the Parbati sub-basin near the dam site. These places are the focal and centric points where total discharge is collected from both the catchments.

19.5. Methodology

Model is designed to simulate and forecast stream flow in mountain basins where snowmelt is a major runoff factor. To develop the model different remote sensing and GIS techniques are used. Catchments are distributed using grid. Model works on NDSI to estimate snow cover and on reflectance to estimate melt factor. Using ARC GIS 9.3, distribution of the Tosh watershed (329 Km²) and Parbati sub-basin (1773 km²) is done by fabricating a grid of the same size and laying it over the catchments. So consequently, the catchments are distributed into a number of small grid cells. In this way, the Tosh watershed and Parbati sub-basin are divided respectively in to 90,236 and 78,411 cells. For Tosh watershed, the area of cells 0.0046 km² while for the Parbati sub-basin is 0.0228 Km². So it can be said that for Tosh watershed area of cell is smaller than the AWiFS resolution and for Parbati

sub-basin area of cell is equal to 3-pixel resolution of the AWiFS. Figure 309 shows distribution of Parbati sub-basin.

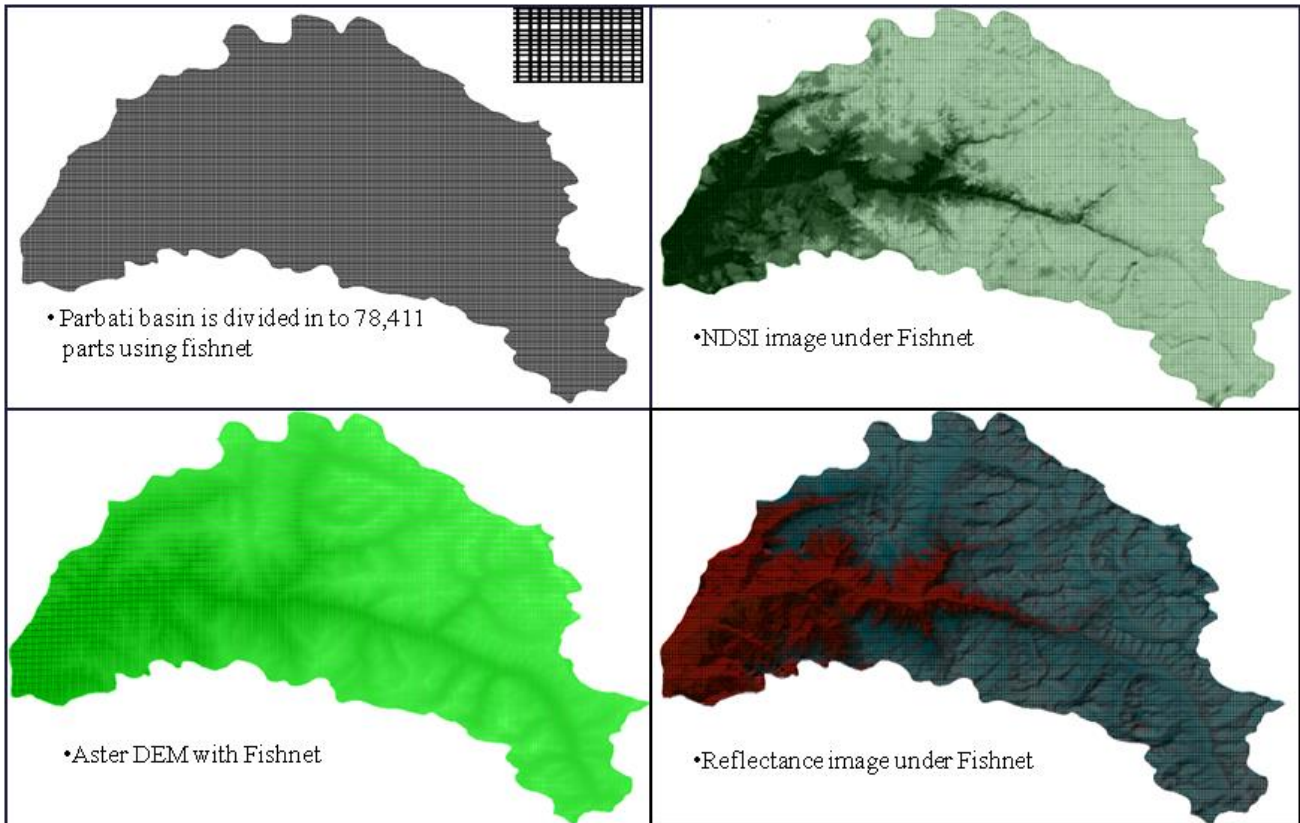


Figure 309: Fishnet map of Parbati sub-basin

From time to time, runoff generated from snow and glacier melt and also from rainfall is computed using the following equation (Martinec et al., 1975):

$$Q = \sum_{i=1}^n \{C1 \{a(T * G)\} + C2 (P * B) + C3 \{(a(T * S))\} 10000/86400\} (1 - K) + Q_{last} * K$$

where, Q = Average 10-Daily runoff (m³/s), C1 = Runoff coefficient for glaciated areas, C2 = Runoff coefficient for non-snow and non-glaciated areas, C3 = Runoff coefficient for seasonal snow covered areas, = Melt-factor (cm °C⁻¹ d⁻¹), T =Average 10-daily degree days (°C. d), G = Grid cell area of glaciers, permanent and 10-daily snow (km²), S = Grid cell area of 10-daily snow (km²), P = Average 10-daily rainfall (cm), B = Grid cell area without snow/glacial cover (km²), Factor 10000/86400 is required for conversion of units from cmkm²d⁻¹ tom³s⁻¹, K= recession coefficient, Q_{last}= last average 10-daily discharge, n= No of cells.

Model Parameters

i) Temperature

Daily maximum and minimum temperature data are used from 2004-2005. From the available maximum and minimum daily temperature data, average daily temperature data are calculated and finally converted in to 10-daily format. Then they are extrapolated to each cell of the grid by overlaying it on Aster DEM using temperature lapse rate (Martinec et al, 1975).

$$T = (T \text{ max} + T \text{ min})/2$$

ii) Snow cover area and Precipitation

Model itself estimates snow cover area using NDSI. Catchments are distributed in to small cells and each cell has its own NDSI value. Principally, NDSI value varies from -1 to 1. The value ≥ 0.4 indicates snow cover area (SCA) while the value < 0.4 indicates snow free area (SFA) Model has capacity to sense whether the cell area is under snow cover or snow free area as shown in table. It takes the threshold values of NDSI that means model senses all the grid cell area which has NDSI value greater than or equal to 0.4, considering as snow cover area (Kulkarni et al., 2006b). Available precipitation data of Bhuntar meteorological station are extrapolated to the mean hypsometric altitudes of the respective grid cell. There are two forms of precipitation: Rain and Snowfall. Critical temperature (T_{crit}) determines whether the measured precipitation is either rain or snow. Model gives an output from each grid cell whether it is snowmelt-runoff, rainfall-runoff or the mixture of both. This model output is dependent on critical temperature, occurrence of an event (rain fall/snowfall) and whether it is SCA or SFA.

iii) Melt factor

Model computes both reflectance based melt factor and field based melt factor (using degree-days). In this study, the melt factor parameter is calculated by model itself by using reflectance value of each cell. Reflectance changes with the changes in density of snow/glacier (Reflectance decreases with increment in density of snow/glacier). The threshold values of reflectance are adjusted with the density of new snow, damp snow, settled snow, depth hoar, wind packed snow, very wet snow and firn and glacier ice. Using below empirical equation (Martinec et al., 1975), melt factor is computed of all cells:

$$a = 1.1 * (\text{density of snow}) / (\text{density of water})$$

iv) Runoff coefficients

Runoff coefficient shows difference between the available water volume (snowmelt + rainfall) and the outflow from the basin. Runoff coefficient of rain indicates the percentage of rainfall converted to runoff. It is found 0 to 0.72 for Toshi watershed and 0 to 0.84 for Parbati sub-basin. Runoff coefficients of snow/glacier indicate the percentage of snowfall converted to runoff. These coefficients are found 0.21 to 0.78 for Toshi watershed and they are 0.13 to 0.69 for Parbati sub-basin. These coefficients have been calibrated using observed runoff on a 10-daily basis.

v) Recession coefficient

Recession coefficient indicates the fraction of discharge contribution from last day 's discharge of snowmelt on a current day. In this study, observed daily discharges are plotted on log-log scale and the slope of the best fit line is determined as the recession coefficient. It is calibrated on 10-daily basis. It varies from 0.73 to 1 for Tosh watershed and 0.64 to 1 for Parbati sub-basin.

Model is developed at the Tosh watershed and executed at Parbati sub-basin for 2004-2005. After applying the model at the Tosh watershed, training of the model is done using the available field data for calibration. The best match simulation is adopted. After this procedure, model is executed at Parbati sub-basin. Model is developed and validated on the 10-daily basis using degree day approach.

19.6. Results and Discussion

Snow and glacier melt runoff modeling at Tosh watershed and Parbati sub-basin has been carried out by integrating space based and in-situ data using degree-day method. Parameters such as melt factor, runoff coefficients and recession coefficient for the model are derived from satellite, topographic and hydro meteorological data. For Tosh watershed and Parbati sub-basin maximum snow cover areas are respectively found 99.82% and 92.53%. Minimum snow cover for both Tosh watershed and Parbati sub-basin are respectively: 23.16% and 13.56%. Mean annual snow cover for both Tosh watershed and Parbati sub-basin are: 80.25 % and 63.06 % respectively. Snow cover in the Tosh watershed and Parbati sub-basin is maximum in winter while it is minimum in monsoon on the 10-daily basis using AWiFS data (Table 91). Geographically, Tosh watershed is situated at higher elevation so in winter it is found that this watershed area is almost covered with snow. As some part of Parbati sub-basin is situated at lower elevation so in winter only this lower elevated part is found without snow. For both the catchments, the least snow cover is found in the season of monsoon.

Table 91: Snow cover pattern for year 2004-2005

No.	Catchment	Minimum SCA(%)	Maximum (SCA)	Annual mean SCA (%)
1	Tosh	23 (17 Aug. 04)	100 (21 Dec. 04)	80
2	Parbati	14 (12, Sep. 04)	93 (19 Jan. 05)	63

Temperature and precipitation are observed to be major factors in contributing runoff. Temperature data suggest that the winter season exists normally and the melt season starts from March and ends in June. Precipitation occurs normally in July, August, September and October. However, some isolated precipitation is also observed in other months as this study area is for mountainous region.

Runoff due to rain is noted high during monsoon while it is very low in winter. Runoff generated from snow and glaciers is noted high in summer and monsoon than winter and autumn. By using grid of smaller size cells, physical processes can be represented easily and the results are found to be accurate and reliable. Indirect way of estimating the melt factor using the threshold values of reflectance is found to be very successful and convenient by using AWiFS satellite data as it calculates melt factor remotely.

Efficiency of the model

Efficiency of model is derived by computing coefficient of determination (R^2) and (%) volume difference (D_v) using below equations Martinec et al., 1975):

$$R^2 = 1 - \frac{\sum_{i=1}^n (Q_i - Q_i')}{\sum_{i=1}^n (Q_i - \bar{Q})} \quad D_v[\%] = \frac{V_R - V_R'}{V_R} \cdot 100$$

where, R^2 = Coefficient of determination, Q_i = Measured 10-daily discharge, Q_i' = Simulated 10-daily discharge, \bar{Q} = Average daily discharge for the simulation year or simulation season, n = Number of 10-daily discharge values, D_v = (%) Volume Difference between the total observed and simulated runoff, V_R = Observed 10- daily runoff volume, V_R' = Simulated 10-daily runoff volume.

Figure 310 shows coefficient of regression and comparison between observed and simulated discharge for both the catchments. It also shows that except monsoon, best match is found between observed and simulated discharge.

Table 92 and Figure 311 comprehensively show that for Tosh watershed, co-efficient of determination (R^2) is derived 0.91, Volume difference (D_v) is derived 8.82%, and coefficient of regression from graph is derived 0.938. For Parbati sub-basin, co-efficient of determination (R^2) is derived 0.92, Volume difference (D_v) is derived 5.44%, and coefficient of regression from graph is derived 0.93.

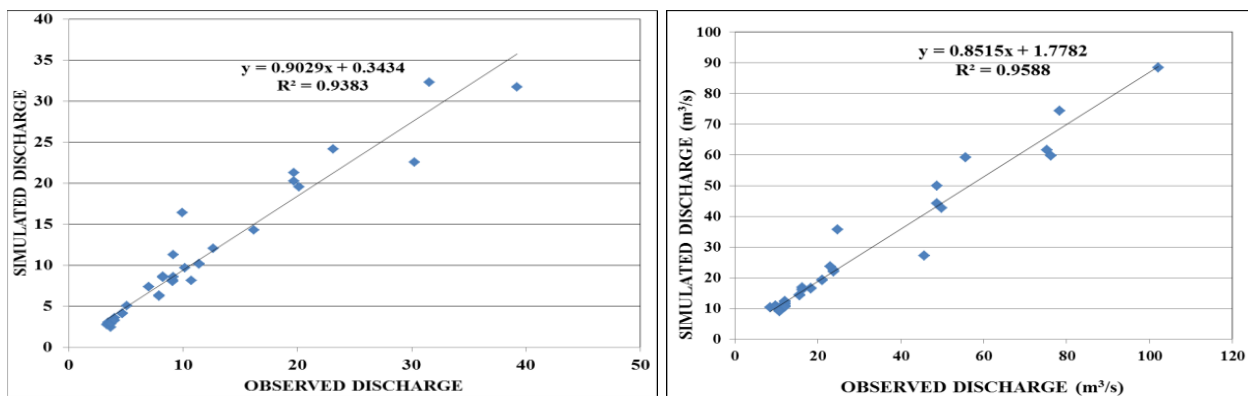


Figure 310 Coefficient of regression for Tosh watershed and Parbati sub-basin

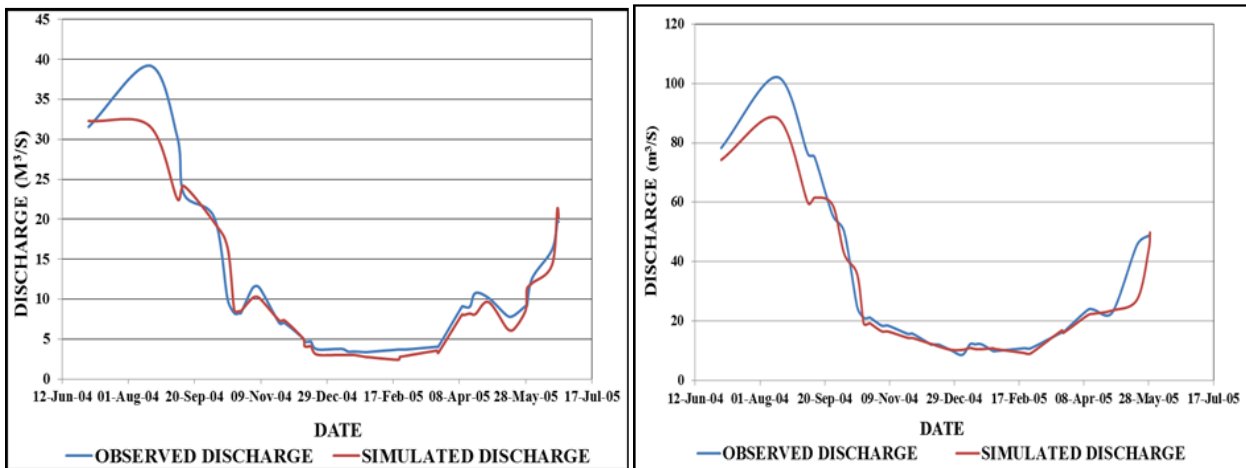


Figure 311: Comparisons of simulated and observed discharge for Tosh watershed and Parbati sub-basin

Table 92: Accuracy criteria of model

catchment	Year	Coefficient of determination (R^2)	Volume difference (Dv)	Coefficient of regression (Graph)
Tosh watershed	2004-05	0.91	8.8	0.94
Parbati sub-basin	2004-05	0.92	5.4	0.96

19.7. Conclusion

The study has developed and demonstrated a distributed hydrological model based on inputs from satellite data as well in-situ measured hydrological data for Parbati sub-basin in Himachal Pradesh. It is observed that simulated discharges are fairly matching with the observed discharges. The coefficient of determinations, % volume differences and coefficient of regressions for Tosh watershed and Parbati sub-basin indicate that the model is efficient and has high potential for application of snow and glacier prediction.

20. Development of Energy Balance Modeling

20.1. Objective

To carry out energy balance modeling for ablation estimation of Gangotri and Chota Shigri glaciers.

20.2. Scientific Rationale

Glacier surface melt rate can be calculated by two different approaches: i) empirical models based on temperature index/ temperature degree day and ii) energy-balance models. Both, process-based models (derived from a surface energy balance) and empirical models, which correlate melt with temperature and to some extent the radiation, have been developed for glacierized regions. Empirical models/approach are normally area specific and difficult to extend to other regions as they are developed under specific conditions (geomorphic settings and physical environment). Empirical model based on air temperature were refined for estimating glacier melt rate (Jones 1997, Hock 2003). These models relate ice melt with temperature but sometimes additional input variables such as incoming shortwave radiations are also incorporated through parameterization based on time and locations. Energy Balance approach are generic in nature offering better accuracy as it involves computations based on basic principles of Physics. Energy Balance approach is based on the computation of the relevant energy fluxes and melt rate is calculated as the sum of the individual fluxes (Pellicciotti et.al., 2005). The energy balance incorporates radiative flux, turbulent flux and the energy flux in the subsurface. This approach requires information on radiation energy, sensible and latent heat flux. These models more properly describe the physical processes at the glacier surface and provides reliable estimate of ablation and melt rates. There has been a large number of studies on energy balance computation on glaciers in different parts of the world, e.g. in the Sierra Nevada (Marks and Dozier, 1992), in Antarctica (Bintanja et al., 1997), in the Alps (Oerlemans and Klok, 2002; Klok and Oerlemans, 2002). Studies have been done to compute glacier ablation in outer tropics using energy balance approach (Wagnon et al. 1999a, 1999b, 2001, 2003). Favier et. al. (2004) computed the annual cycle of the local surface energy balance on the ablation zone of Antizana Glacier 15, Ecuadorian Andes (inner tropics). Moolg and Hardy et. al. (2004) estimated the energy balance of a horizontal glacier surface on Kilimanjaro, tropical East Africa, for the periods March to September 2000 and March 2001 to February 2002 to study the impact of climate variations. Sicart et. al. (2005) examined the surface energy fluxes of the Bolivian Zongo Glacier (South American Andes) for identifying the atmospheric variables that control melting. A distributed surface energy-balance model was developed by Hock and Holmgren (2005) for complex topography of Storglaciaren, a valley glacier in Sweden. Energy and mass balance of Zhadang glacier surface situated in central Tibetan Plateau has been estimated by Zhang et. al. (2013). Though energy balance studies have been carried out in Antarctica, Andes, Alps, inner and outer tropical region, however it has not been used for estimating glacier ablation, mass balance and melt run off in the valley

glaciers of the Himalayas. The difficulties in taking in-situ measurements, required for formulation of energy balance equation in the highly undulating and difficult terrains might have been the main reason for lack of such studies in the Himalaya. The Himalayas have the highest concentration of glaciers outside the polar region and thus holds one of the most important natural resources of water in frozen form. It is important from the point of view of water and energy security of India and many other countries in the region.

To understand the response of Himalayan glaciers to climatic variability, a study was taken to compare energy balance on two of the Himalayan glaciers, one each from Indus and Ganga basins, which have different climatic and physiographic conditions. The salient findings have been reported (Rastogi and Ajai, 2014, 2013a and 2013b).

20.3. Study Area

Gangotri glacier in Uttarakhand and Chhota Shigri glacier in Himachal Pradesh have been taken up as study areas (Figure 312).

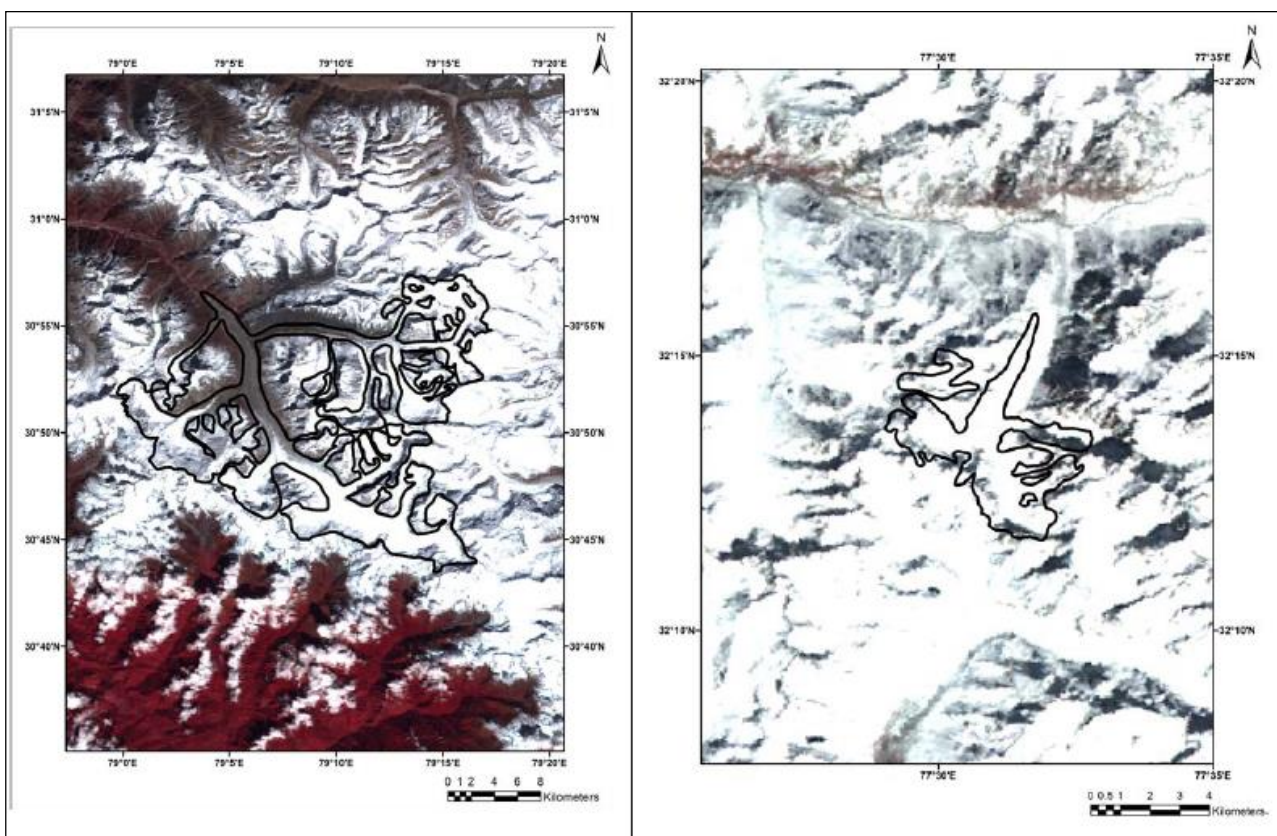


Figure 312: FCC of AWiFS image showing Gangotri glacier, Uttarakhand (Left panel) and Chhota Shigri glacier, Himachal Pradesh (Right Panel) (Source: Rastogi and Ajai, 2014)

The first glacier chosen for this study is Gangotri glacier. Gangotri glacier is one of the largest glaciers in the central Himalaya. It is located in Uttarkashi District, Uttarakhand, India. Gangotri glacier originating from Chaukhamba peaks (7138 amsl) and is about 27 km long with a glacierised area of about 143.58 km². This is a valley type glacier in Ganga basin and the source of a major river system Ganga in northern India. This glacier is bounded between longitude 78° 59' 30" and 79° 17' 45" E and latitude 30° 43' 00" and 30° 57' 15" N. The snout is around 18 km from Gangotri Township. This glacier is having orientation in the north-west direction and is about 2 to 3 km wide. Most of the people depend on these rivers for their water and food supply. Indian population is dependent on it for irrigation and drinking water purposes.

The second glacier chosen for surface energy balance comparison is Chhota Shigri glacier. The Chhota Shigri glacier of Chandra River basin on the northern poles of the Pir Panjal range in the Lahaul and Spiti valley of Himachal Pradesh, is located at a distance of about 36 km SE of Rohtang Pass, in the western Himalaya and bounded by latitudes 32.19-32.28° N and longitudes 77.49-77.55° E. Its reported maximum elevation is 6263 amsl, snout position is nearly at 4050 amsl, and length of glacier is ~ 9 km and width of about 1.5 km in its widest portion. It is included in the upper basin of the Chandra River, contributing to Chenab River, one of the tributaries of the Indus river basin. This valley-type glacier is oriented roughly north-south in its ablation area, but variety of orientations in the accumulation area. This glacier is well developed and easily accessible glaciers of the Chandra river basin. As this glacier falls in the monsoon-arid transition zone that is why it is considered to be a sensitive indicator of northern climate. It lies in high pressure belt that is controlled by the intense heat of summer and severe cold in winter season. It is covered by debris because of weathering effects. The climate of this zone is mainly characterized by extreme winters from October to April.

20.4. Data Used

The input data sources used to compute energy balance components in the present study are described as under:

Satellite data

Surface reflectance and land surface temperature products (at 500m and 1km resolution respectively) of MODIS, onboard TERRA satellite are used in this study. MODIS has 36 spectral bands with spatial resolutions as: 250m (band1 – 2), 500m (band3 – 7), 1000m (band8 – 36) and quantization is 12 bits (Suzanne et. al., 2006).

Meteorological data

Meteorological parameters such as wind speed, air temperature and relative humidity were obtained through a manned observatory of Snow and Avalanche Study Establishment (SASE) located at Bhojbasa in Gangotri sub-basin. Meteorological parameters over the

Chhota Shigri glacier have been taken from an AWS (Automatic Weather Station), installed there at 3850 m above sea level (Figure 270).

Field data

The surface roughness parameter used to calculate turbulent heat fluxes is obtained through doing field measurements using surface profilometer. The surface roughness parameter is estimated by microtopographic method (Figure 313).



Figure 313: Measurement of roughness on glacier with profilometer

20.5. Methodology

The developed methodology is based on following principles of energy balance:

A unit volume of glacier is defined from the surface to a depth where there are no significant heat fluxes. On this volume, for a unit of time, and assuming a lack of horizontal energy transfers, the surface energy balance equation is written as follows, where the fluxes toward the surface are positive (Oke, 1987):

$$R + H + LE + G + P = \Delta Q_m + \Delta Q_s = \Delta Q \quad ..1$$

R is the net all-wave radiation, H is the turbulent sensible heat flux, LE is the turbulent latent heat flux. The conductive heat flux in the snow/ice G can be disregarded as the glacier is isothermal. The heat advected by precipitation P is insignificant compared to the other terms (Wagnon et al., 1999a; 1999b). ΔQ_m is the latent heat storage change due to melting and freezing and ΔQ_s is the net convergence or divergence of sensible heat fluxes within the

volume. The change of the energy ΔQ is stored in the volume or utilized in the melting process. If the top layers of a glacier have a temperature below 0°C , then ΔQ corresponds to a temperature change within the surface layers. If these layers are at 0°C , then ΔQ is available for the melting process (Favier et. al., 2004).

Net Radiation

Solar radiation is the major energy source and is able to change large quantities of liquid water into water vapour. The net radiation is the balance of the incident and reflected short-wave radiation and the incident and emitted long-wave. It can be expressed as-

$$R = (1 - \alpha)G + (L_i - L_o)$$

According to Stefan's Boltzmann law above equation can be expressed as (Sellers et. al., 1997)-

$$R = (1 - \alpha)G + \epsilon_a \sigma T_a^4 - \epsilon_s \sigma T_s^4$$

where α is albedo, G is global radiations, ϵ_a and ϵ_s are air and surface emissivities respectively, σ is Stefan's constant and its value is $5.67 \times 10^{-8} \text{ W/m}^2\text{K}^4$ and T_a , T_s are air and surface temperatures respectively (Singh and Singh, 2001). All these parameters are detailed below:

Albedo

The conversion formula for the total shortwave broadband albedo for MODIS is given as under (Liang, 2000) –

$$\alpha^{\text{MODIS}} = 0.160\alpha_1 + 0.291\alpha_2 + 0.243\alpha_3 + 0.116\alpha_4 + 0.112\alpha_5 + 0.081\alpha_7 - 0.0015$$

where α_1 , α_2 , α_3 , α_4 , α_5 and α_7 are spectral narrowband albedos in 1, 2, 3, 4, 5 and 7 bands respectively.

Global Radiations

For clear sky G can be calculated using the following equation (Samani et. al., 2007):

$$G = (a_s + (b_s * n/N)) R_a$$

where n is actual duration of sunshine (hour), N is maximum possible duration of sunshine or daylight hours (hour), n/N is relative sunshine duration, R_a is extraterrestrial radiation ($\text{M J m}^{-2} \text{ day}^{-1}$), a_s is regression constant, expressing the fraction of extraterrestrial radiations reaching the earth on overcast days ($n=0$), $(a_s + b_s)$ fraction of extraterrestrial radiation reaching the earth on clear days ($n=N$). Commonly used values for a_s and b_s are 0.25 and 0.50 respectively (Singh and Singh, 2001). Equation number (4) for the clear sky radiation reaching the earth on clear sky days ($n=N$) can be written as:

$$G = (a_s + b_s) R_a$$

By substituting values of different parameters, it can be expressed as:

$$G = 0.75 * Ra \text{ in } M J m^{-2} day^{-1}$$

Incoming long wave radiations

They are emitted by the atmosphere, primarily by water vapour, CO₂ and ozone. Wavelength range is 4-120 μm. During higher temperature and more cloudy conditions, long wave radiations are high. It is calculated as (Hock, 2010)-

$$L_i = \epsilon_a \sigma T_a^4$$

where ϵ_a is emissivity of air and T_a .

Outgoing long wave radiations

Long wave radiations are emitted by earth's surface. It is a function of temperature of the ice/snow surface and it can't exceed 316W/m² because ice/snow can't be warmer than zero degrees. It is calculated as-

$$L_o = \epsilon_s \sigma T_s^4$$

where ϵ_s is surface emissivity taken from literature as 0.965 (average value) and T_s is land surface temperature obtained as from Terra-MODIS data.

Sensible and Latent heat fluxes

The transport of heat and moisture in the surface boundary layer of the atmosphere is dominated by turbulent motions and that is why sensible and latent heat fluxes are called turbulent heat fluxes. Bulk aerodynamic method was used to calculate turbulent fluxes of sensible and latent heat. It employs bulk transfer coefficients derived from flux gradient relationships. The bulk transfer coefficients explicitly account for variable stability, surface conditions and measurement heights, and are used for melt estimation. Stability of the surface layer is assessed by calculating the bulk Richardson number, R_b , which relates the relative effects of buoyancy to mechanical forces (Reid and Brock, 2010):

$$R_b = (g * (T_a - T_s) * (z_a - z_{0m})) / (T_m u^2)$$

where T_a and u are the values of air temperature (in °K) and horizontal wind speed (in m/s) respectively at the level of measurement z ; g is the acceleration due to gravity ($g = 9.8 \text{ m s}^{-2}$); T_s is the surface temperature (in °K); T_m is the mean absolute air temperature between the surface and the measurement level z (in °K); z_{0m} is the surface roughness length for momentum transfer. The roughness length is defined as the height above a surface at which the extrapolated horizontal wind speed profile reaches zero.

Assuming that local gradients of mean horizontal wind speed u , mean air temperature T_a and mean vapour pressure are equal to the finite differences between the measurement level and the surface, it is possible to give analytical expressions for the turbulent fluxes. (Oke, 1987):

$$H = \{(\rho C_p k^2 u (T_a - T_s)) / (\ln (z_a/z_{0m}) * \ln (z_a/z_{0t}))\} * (\Phi_m \Phi_h)^{-1}$$

$$LE = \{(\rho L_v k^2 u (q_a - q_s)) / (\ln (z_a/z_{0m}) * \ln (z_a/z_{0q}))\} * (\Phi_m \Phi_v)^{-1}$$

where q_a and q_s are specific humidities at the level of measurement z and surface, respectively. ρ is the air density; C_p is the specific heat capacity for air at constant pressure; k is the von Karman's constant ($k = 0.4$) and L_v is the Latent heat of vapourization ($L_v = 2.476 * 10^6$ J/kg). The surface roughness lengths for heat z_{0t} and humidity z_{0q} were considered equal to z_{0m} .

Ground heat flux

The ground heat flux or the conductive heat transfer within a glacier tends to be small when compared to radiative or turbulent fluxes (Marks and Dozier, 1992). The thermal energy stored by the ground during the summer period, when there is no snow cover over the ground, is released during winter and spring which contributes to the melting of the overlying snowpack. The temperature of the ground surface is reduced due to existing snowpack in comparison to the lower part of the ground, which results in a temperature gradient. Thus the heat is supplied by ground in the upward direction. In case the temperature of snow just above the ground is below 0°C , the ground heat flux raises the temperature and makes it ready for melting. The vertical flux of heat at the snow surface is described as

$$G = -K * \partial T / \partial z$$

where K is the thermal conductivity of snow/ice (in $\text{W m}^{-1} \text{K}^{-1}$), T is the snow/ice temperature, and z is the depth.

Surface energy balance of snowpack

The internal energy change of the glacier ($\Delta Q_m + \Delta Q_s$) is calculated using equation (1). If the left hand side of the equation (1) is positive, energy is available to the snow/ice. This energy is first used to increase the snow/ice temperature until it reaches 0°C ($\Delta Q_s > 0$ and $\Delta Q_m = 0$), and as soon as temperature reaches 0°C , the melting of snow/ice starts ($\Delta Q_m > 0$). If the LHS is negative then the reverse situation is observed, it indicates that the melted water of the glacier refreezes ($\Delta Q_m < 0$) and then snow/ice temperature decreases ($\Delta Q_s < 0$). In equation (1), ΔQ_s is the rate of gain/loss of heat in a vertical column extending from the surface to the depth of snowpack. Therefore considering daily means, ΔQ_s usually remains zero because the gain of heat during the day is compensated by the loss of heat at night. Therefore looking at daily means, the change of the internal energy of glacier is reduced to the latent heat storage change. Now Q ($\text{kJ/m}^2\text{d}$) is converted to mass units using the Latent heat of fusion L_f ($L_f = 333.5$ kJ/kg).

$$M = 0.0031 * Q$$

where M is the depth of melt water (mm/day). Similarly, the sublimation rate can be calculated using following relation:

$$LE = L_s * S$$

where LE is the Latent Heat Flux calculated by equation (18) and L_s is the Latent heat of sublimation ($L_s = 28.3 * 10^5$ J/kg). The ablation (A) can be calculated as:

$$A = M + S$$

20.6. Results and Discussion

For comparison of Energy Balance on Gangotri and Chhota Shigri Glaciers different energy components (Net radiations, Sensible heat flux and Latent heat flux) have been computed on daily basis for November and December, 2011. Total energy available for melting of the glaciers has also been computed by taking the algebraic sum of above mentioned energy fluxes. Different energy fluxes for two glaciers are shown in Figures 314 and Figure 315.

Net Radiations (NR)

The net radiation is the balance of the incident and reflected short-wave radiation and the incident and emitted long-wave radiation. As shown in Figure 4.19.2(a) the monthly average value of net radiations during November, 2011 on Gangotri is 87.26 W/m^2 while on Chhota Shigri is 50.04 W/m^2 . This variation is because incoming shortwave radiation is higher on Gangotri than Chhota Shigri and outgoing longwave radiation is higher on Chhota Shigri than Gangotri. Figure 4.19.3 (a) depicts the similar trend in December, 2011. Monthly average value of net radiations during December, 2011 on Gangotri is 73.25 W/m^2 while on Chhota Shigri is 57.31 W/m^2 .

Sensible Heat Flux (SH)

This is the heat exchange that takes place because of temperature gradient between atmospheric boundary layer and glacier surface. As shown in Figure 4.19.2(b) the monthly average value of Sensible heat flux during November, 2011 on Gangotri is 3.28 W/m^2 while on Chhota Shigri is 14.41 W/m^2 . Sensible heat flux in Chhota Shigri is higher than Gangotri glacier because the wind speed and ambient temperature values are higher in Chhota Shigri than Gangotri glacier. Figure 4.19.3(b) depicts the similar trend in December, 2011. Monthly average value of Sensible heat flux during December, 2011 on Gangotri is 1.45 W/m^2 while on Chhota Shigri is 17.78 W/m^2 .

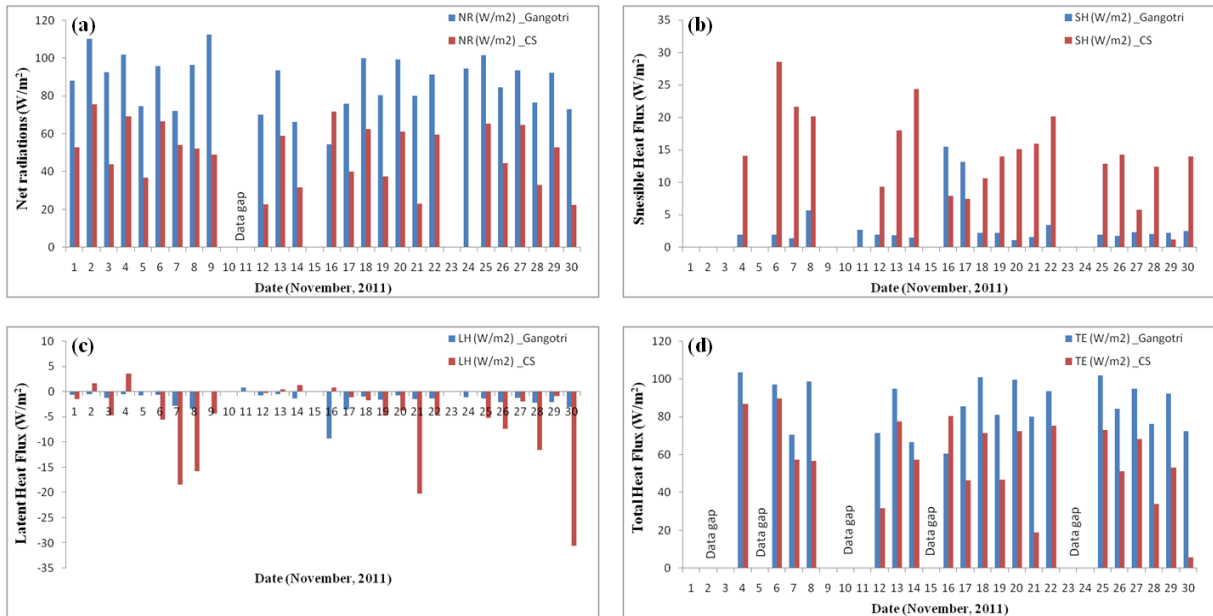


Figure 314 Variation of heat fluxes on Gangotri and CS glacier during November, 2011(a) Daily variation of net radiations; (b) Daily variation of sensible heat flux; (c) Daily variation of latent heat flux; (d) Daily variation of total energy (Source: Rastogi and Ajai, 2014)

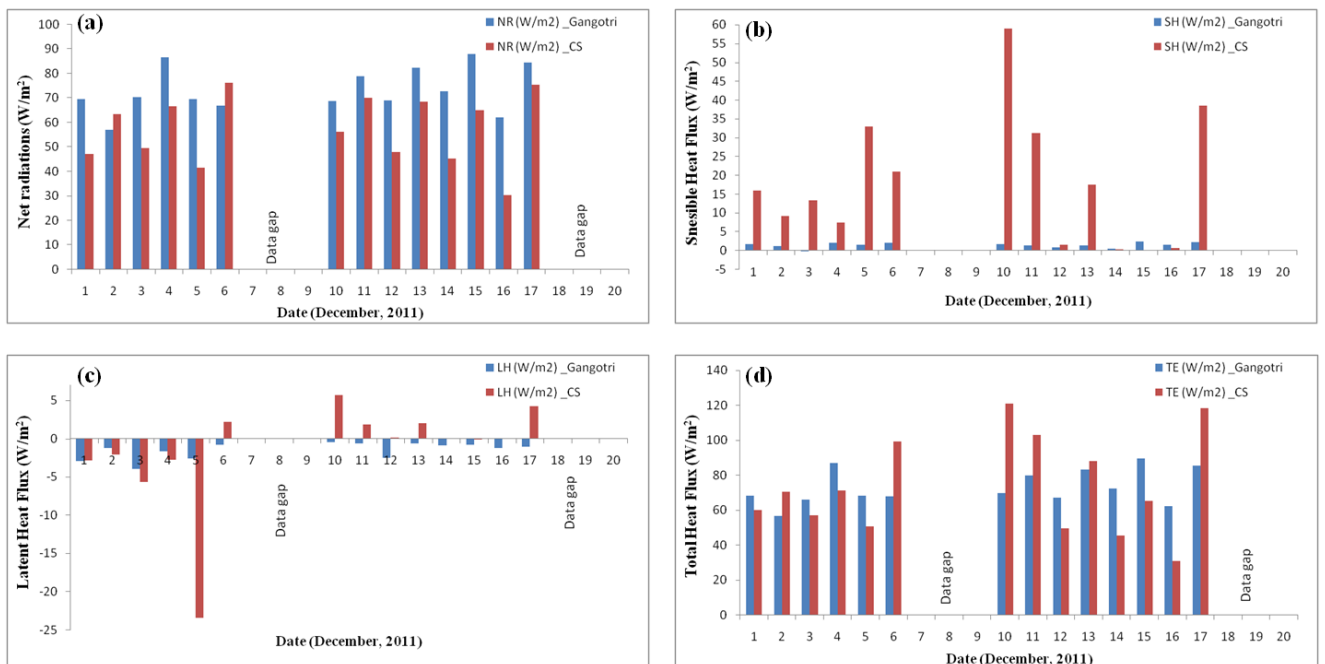


Figure 315 Variation of heat fluxes on Gangotri and CS glacier during December, 2011(a) Daily variation of net radiations; (b) Daily variation of sensible heat flux; (c) Daily variation of latent heat flux; (d) Daily variation of total energy (Source: Rastogi and Ajai, 2014)

Latent Heat Flux (LH)

This is the heat exchange that takes place because of moisture gradient between atmospheric boundary layer and glacier surface. As shown in Figure 314(c) the monthly average value of Latent heat flux during November, 2011 on Gangotri is -1.85 W/m^2 while on Chhota Shigri is -5.48 W/m^2 . Here negative sign of heat flux represents heat sink. Negative values of latent heat flux also indicate that snow/ice surface loses mass by sublimation and also infers that the stratification of the lower atmosphere is moderately stable. Latent heat flux in Chhota Shigri is lesser than Gangotri glacier because the atmosphere in Chhota Shigri is dry than Gangotri glacier. Figure 315(c) depicts the similar trend in December, 2011. Monthly average value of Latent heat flux during December, 2011 on Gangotri is -1.34 W/m^2 while on Chhota Shigri is -1.38 W/m^2 .

Total Energy (TE)

Total heat flux available for melting of the glaciers has also been computed by taking the algebraic sum of above mentioned energy fluxes. As shown in Figure 314(d) the monthly average value of total heat flux during November, 2011 on Gangotri is 85.53 W/m^2 while on Chhota Shigri is 57.64 W/m^2 . Figure 315(d) depicts the similar trend in December, 2011. Monthly average value of Total heat flux during December, 2011 on Gangotri is 74.30 W/m^2 while on Chhota Shigri is 73.35 W/m^2 . Total heat flux on Gangotri glacier is higher than Chhota Shigri because net radiation contribution and latent heat contribution is higher on Gangotri. Thus the melting of ice is higher for Gangotri as compared to Chhota Shigri glacier during the above two months.

Comparison of energy balance model with temperature index model

Temperature index model is simple and has potential to predict mass balances and discharges. It is based on the assumption that melt rates are linearly related to air temperature, which is considered as an integrated index of the total energy available for melt. The factor of proportionality is called degree day factor, DDF ($\text{mm } ^\circ\text{C}^{-1}$ per time step). The melt rate based on this model is given as under (Pellicciotti et al., 2005):

$$\left\{ \begin{array}{ll} M = \text{DDF}_{\text{snow/ice}} T & T > T_T \\ 0 & T \leq T_T \end{array} \right.$$

where M is the melt rate (mm water equivalent per unit of time), T is the mean air temperature of each time step ($^\circ\text{C}$) and T_T is a threshold temperature above which melt is assumed to occur (e.g. 1°C). The degree day factors for the analysis period were optimized for our study area. The results from energy balance model and temperature index model were compared for Gangotri glacier. Comparison of daily average melt rate from energy balance model and temperature index model are shown in Figure 316. The correlation between the melt rates computed from the above mentioned two models shown in Figure 316. It is observed from the Figure 316 that there is a good agreement in daily averaged melt rates as computed from the two models.

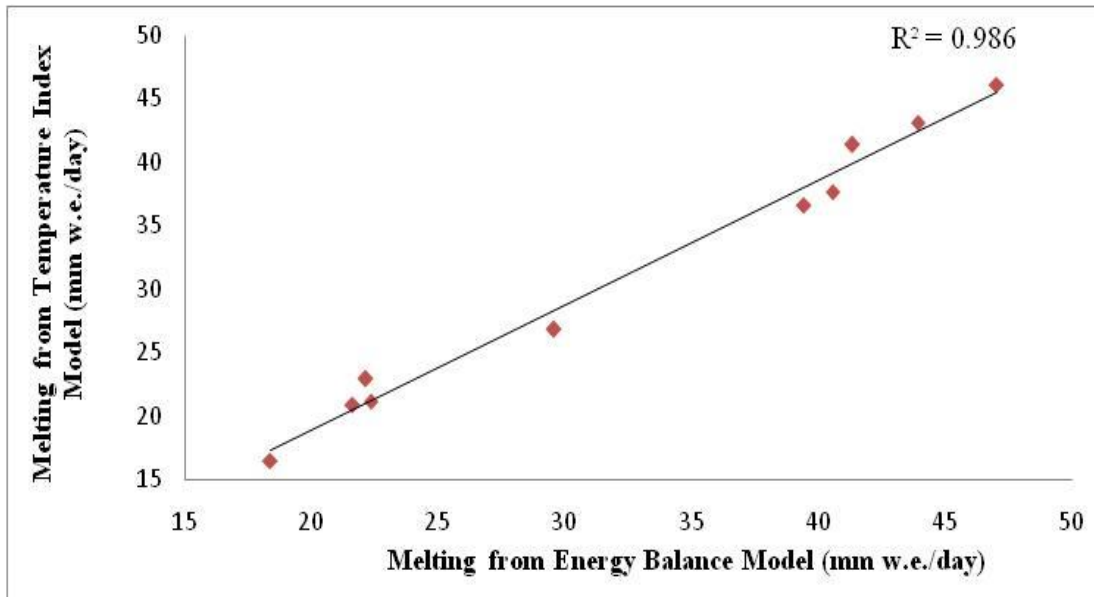


Figure 316: Comparison of melt rate estimated from Energy Balance Model and Temperature Index Model (Source: Rastogi and Ajai, 2013)

21. Analysis of ICESAT/GLAS LASER Altimetry Data for Monitoring Ice Thickness Changes

21.1. Objective

To demonstrate potentials of laser altimetry data for monitoring ice thickness changes.

21.2. Scientific Rationale

Surface elevation and its variation remains an important parameter for studying the global environment and climate change. Till date a large number of earth observation satellites have been launched to retrieve surface elevation data. Satellite radar altimetry have been used for estimation of surface elevation and its change detection since late 1970s (Zwally et al., 1989; Wingham et al., 1998; Johannessen et al., 2005). Due to limitation of large footprint size, the satellite radar altimetry is mainly suitable to the region of low relief glaciers and ice sheets in cryosphere studies. Estimation of surface ice thickness change over in high relief glaciers, requires high resolution altimetry elevation datasets available. In last few years, altimeters like Ice, Cloud and land Elevation Satellite (ICESat) laser altimeter (Zwally et al., 2002) provides high resolution and Cryosat-2 radar altimeter (Wingham et al., 2006) also gives high resolution datasets by implying advanced SAR interferometric altimeter techniques that are comparable to maps (Sauber et al., 2005; Muskett et al., 2008; Nuth et al., 2010).

ICESat which was launched by NASA in January 2003 had a prime objective to estimate ice-elevation changes in Polar Regions. However, the utility of ICESat/GLAS data covered more aspects other than its main objective. Laser altimeter named Geoscience Laser Altimeter System (GLAS) on board ICESat with high resolution footprint of 70m with along-track spacing of 170m provides elevation data with exceptional accuracy. During 2003 to 2009 a large amount of data was acquired by three laser sensors of GLAS.

Glaciers are among the best indicators of terrestrial climate change, contribute to water resources in different parts of world. Varying glacier elevation can provide an insight to fluctuations in climate over these areas. Himalayan glaciers cover over 71,182 km² and monitoring changes in their thickness is a key issue as the melting of glaciers in central Asia may significantly contribute to sea level rise (Sharma et al., 2013). In addition, runoff generated by the melting of the glaciers in the Himalaya is an important source of water for domestic, industrial and recreational activities. Given the size and remoteness of glaciers in Himalayas, in-situ measurements are sparse in these regions and thus satellite imagery is a viable alternate to obtain a comprehensive and frequent monitoring (Berthier et al., 2006). The mostly applied

technique for estimation of changes in elevation over these areas by comparing multi-temporal DEMs, which is generated from satellite photogrammetry (Gardelle et al., 2012).

Himalayan glaciers, however, generally have rough surface and steep regional slopes than the ice sheets for which ICESat was optimized (Sauber et al., 2005). Elevation changes over glaciers from satellite altimetry is computed directly using elevation difference at crossover points between ascending and descending satellite passes. This method gives coarse sampling for computation of elevation changes instead of accurate method (Brenner et al., 2007). In this paper, an attempt has been made to explore the potential of repeat track ICESat altimetry with the help of reference DEM to derive interim glacier elevation changes for four glaciers namely Siachin, Baltoro and Drenmarg in Indus basin and Gangotri in the Ganga basin of Himalayan region.

21.3. Study Area

Three glaciers from Indus basin, namely, Siachen, Drenmarg and Baltoro and one glacier from Ganga basin, Gangotri, have been taken in this study. Figure 317 and Figure 318 shows the location of all four glaciers.

- i. **Gangotri Glacier**, one of the largest glaciers in the central Himalaya, is located in Uttarkashi District, Uttarakhand state of India. This is a valley type glacier in Ganga basin and the source of a major river system Ganga in Northern India. The glacier has an estimated glacier volume of about 27 km³ and it is about 27 km long and 1-2 km wide. The orientation of the glacier is towards North West (NW).
- ii. **Siachen Glacier**, located in the eastern Karakoram Range in the Himalayan Mountains, is the longest glacier in the Karakoram and second-longest in the world's mountain glacier areas. It lies between the Saltoro Ridge immediately to the west and the main Karakoram Range to the east. Including all tributary glaciers, the Siachen Glacier system covers about 700 km² area and 1.3-3.2 km wide. The orientation of the glacier is towards South East (SE).
- iii. **Baltoro Glacier**, located in the Karakoram Range and is the origin of Shigar River which is a tributary of the Indus River. The glacier covers an area of 872 km². It is about 57.6 km long with orientation towards South West (SW) and 1.7-3 km wide. The glacier altitude varies from 3,497 to 6,011 amsl.
- iv. **Drenmarg Glacier** is located in the eastern Karakoram Range in the Himalayan Mountains. The glacier altitude varies from 5,467 to 3,769 amsl. The glacier covers an area of 413.5 km². It is about 25.31 km long with orientation toward South East (SE) and 0.8-1.5 km wide.

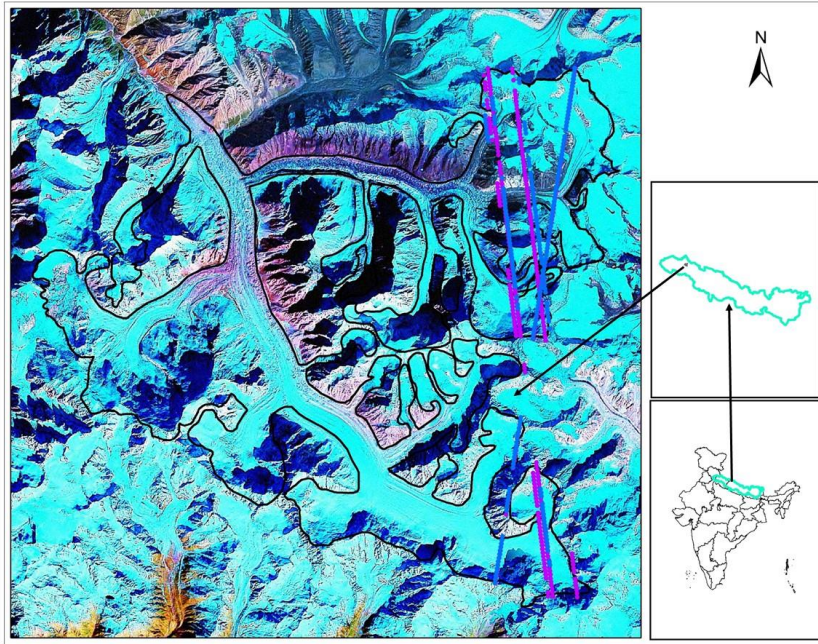


Figure 317: Image showing location of Gangotri glacier lying in Ganga basin of Himalayan region. The straight purple and blue lines indicate ICESat tracks.

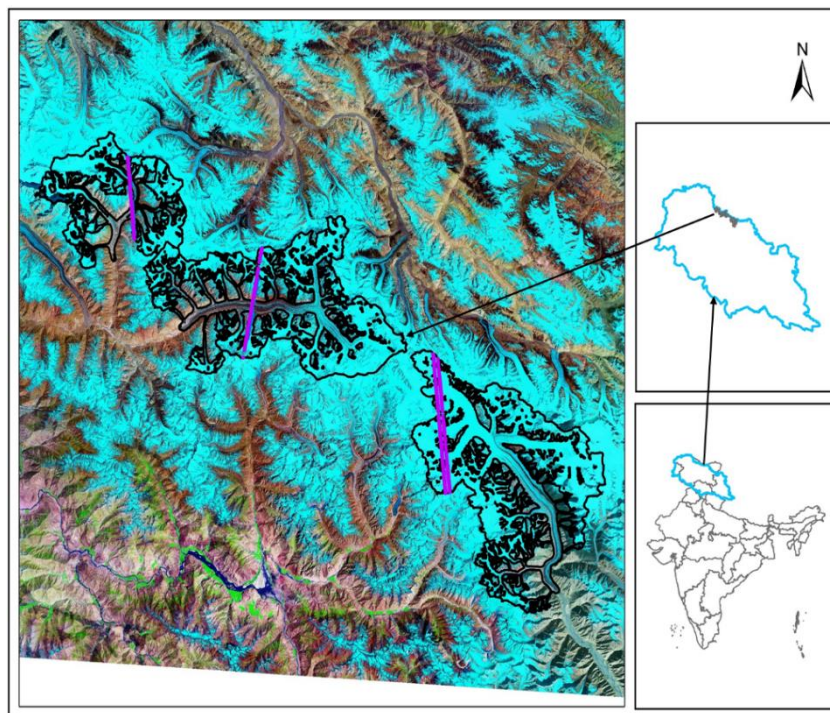


Figure 318: Location of three glaciers lying in Indus basin, the Himalayan- Karakoram region. The straight purple and blue lines indicate ICESat tracks.

21.4. Data Used

a) ICESat/GLAS

ICESat has an onboard laser altimeter system, to collect surface elevations all over the globe with high precision. Since 2003 to the end of its operation in 2009, GLAS has been operating for three annual observation campaigns, each of approximately 35 days. This instrument combines a 3 cm precision 1064-nm laser altimeter with a laser pointing angle determination system (Sirota et al., 2005) and it is used to measure the Earth's surface and it also measure the backscattering profile from thicker clouds, while those at 532-nm use photon-counting detectors and measure the height distributions of optically thin clouds and aerosol layers. A GPS receiver on the spacecraft provides data for determining the spacecraft position, and also the absolute time reference for the instrument measurements and altimetry clock (Abshire et al., 2005). It retrieves surface elevations within 70 m diameter footprints and along track spacing of 170 m. GLAS elevation accuracy is reported to be 15 cm over flat terrain (Zwally et al., 2002). In this study GLA06 product of ICESat has been used between 2003 and 2009 available from the National Snow and Ice Data Centre (NSIDC) (Zwally et al., 2008).

b) DEMs

CartoDEM as well as SRTM DEM has been used to project ICESat repeat tracks onto common locations and to extrapolate elevation changes to unmeasured locations.

Carto DEM

Cartosat-1 Digital Elevation Model (CartoDEM) is a National DEM developed by the Indian Space Research Organization (ISRO), derived from the Cartosat-1. Cartosat-1 has a pair of Panchromatic cameras having an along track stereoscopic capability to acquire two images simultaneously, one forward looking (Fore) at +26 degrees and another rear looking (Aft) -5 degrees with a base-to-height ratio of about 0.63. Its Absolute planimetric accuracy is 15m and absolute vertical accuracy is 8 m and having 5 m relative vertical accuracy (Muralikrishnan et. al., 2011).

SRTM DEM

The SRTM (Shuttle RADAR Topographic Mission) was the first mission using space-borne single pass interferometric SAR which was flown in February 2000. The goal of the mission was to survey the Earth surface and to generate a homogeneous elevation data set of the world with a grid spacing of 3arcsec. The digital topographic map products expected to meet the Interferometric Terrain Height Data (ITHD)-2 specifications sampling with 16 m absolute vertical height accuracy, 10 m relative vertical height accuracy and 20 meter absolute horizontal accuracy (Balmer, 1999). The horizontal datum is the World Geodetic System 1984. The vertical datum is mean sea level as defined by the Earth Gravitational Model geoid (EGM-96). Most of the users commonly ignore the original vertical datum and use SRTM data as referenced to the WGS84 ellipsoid as geoid models (Markus, 2005).

21.5. Methodology

Researchers have used mainly three approaches for estimation of the elevation change using ICESat altimetry (Moholdt et al., 2010). The first approach, which computes elevation changes at crossover points, has very high accuracy. Elevations at crossover points are linearly interpolated from the two closest footprints within 200 m in each track (Brenner et al., 2007). The main drawback of this approach is that the sampling is too coarse. The second approach uses a DEM to correct for the surface slope between the centre points of overlapping footprints (Slobbe et al., 2008) and used over the Greenland ice sheet. This approach takes care of the slope-induced errors; however, it is constrained by the data availability for comparison. It is difficult to compare repeat track ICESat profiles due to the relatively large cross track separation between repeat profiles. In view of the limitations of the first two approaches, the third approach has been used in this study which utilizes near repeat ICESat tracks having small cross-track separation (Moholdt et. al.,2010) shown in Figure 319 and Figure 320.

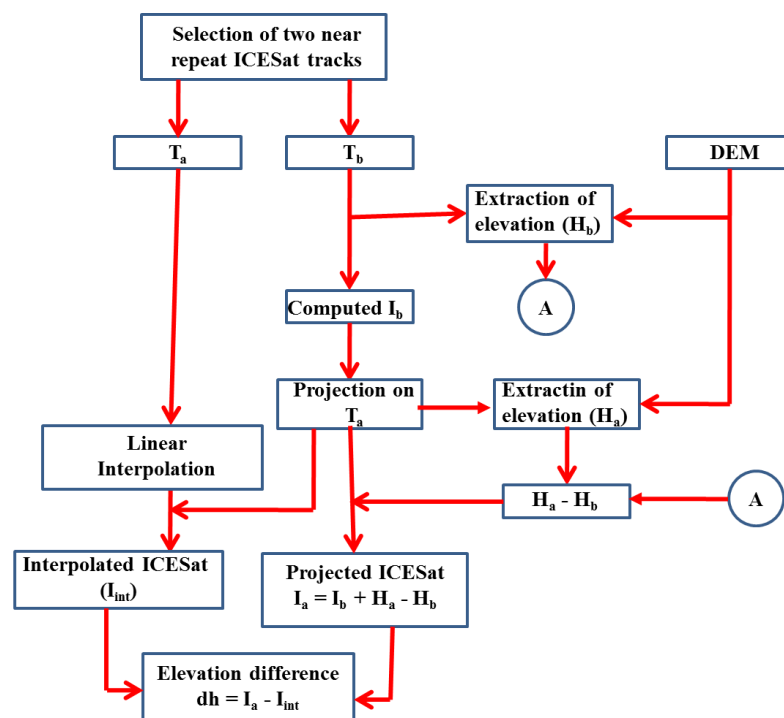


Figure 319: Flowchart showing the near repeat track methodology for elevation change estimation

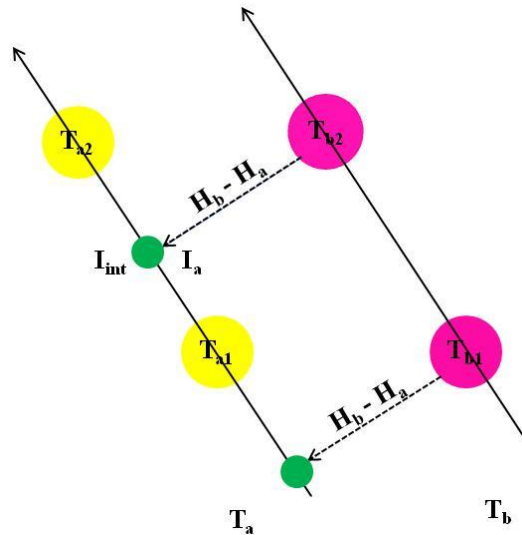


Figure 320: Projection of near repeat tracks on common locations using DEMs. Green dots represent projected location, Pink dots represent secondary track and Yellow dots represent reference track (adopted from Moholdt et al., 2010)

In this approach two near repeat ICESat tracks (T_a and T_b) pertaining to different years and same season has been taken. For every pair of ICESat repeat tracks one track is considered as the reference track and other one is secondary track. The track which is oldest is chosen as the reference track. The second track is projected on the reference track and topographical change at these two locations can be estimated by the change in elevation values of these locations using DEM. The elevation information H_a and H_b has been extracted from the DEM at the ICESat footprints on track T_a and T_b respectively. The difference ($H_a - H_b$) of this elevation information (H_a & H_b) is represented as the unmeasured topography between the near repeat tracks. Here the utility of DEM implies along-track interpolation to restrict the DEM slope correction to the cross-track distance between two repeat-tracks (Moholdt et al., 2010b). Now each footprint on Track T_b is projected perpendicularly on track T_a . The ICESat elevation on the projected points (I_a) over reference track (I_a) can be computed as in equation given below

$$I_a = I_b + H_a - H_b$$

At the same projected points on the reference track T_a , ICESat elevation (I_{int}) is estimated through linearly interpolating the neighbouring footprints (T_{a1} and T_{a2}) along the track. The elevation difference at the projected points (dh) is the change in the elevation between the projected (I_a) and interpolated ICESat elevation (I_{int}) and it can be computed as in equation given below:

$$dh = I_a - I_{int}$$

where,

dh = elevation difference of two different periods

I_a = ICESat elevation at projected location on track T_a

I_{int} = interpolated ICESat elevation on track T_a

I_b = ICESat elevation on track T_b

H_a = extracted elevation from DEM on track T_a

H_b = extracted elevation from DEM on track T_b

21.6. Results and Discussion

The ICESat altimetry data of near repeat tracks (T_a and T_b) have been used to estimate the elevation changes in the glaciers (Figure 321). Here track T_a is considered as the reference track and track T_b as secondary track. The mean elevation changes and mean offsets are computed from the repeat passes of the ICESat for the four glaciers are given in Table 93. Different tracks over Gangotri glacier shows the variations in the thinning/thickening rate in the range of 0.01 to 0.71m/Year by utilizing CartoDEM. Similar variation (-0.20 to 0.84 m/Year) is obtained while using SRTM DEM. The reason behind the variation is due to the pass of the track over different region.

Table 93: Mean elevation change along the ICESat tracks of Gangotri, Siachen, Baltoro and Drenmarg Glacier

S. No	Glacier name	ICESat Tracks		Mean Offset (m)	Elevation change rate (m/Year)	
		Track T_a (Ref.)	Track T_b		Carto-DEM	SRTM
1.	Gangotri	Mar-04	Mar-08	273.77	0.01 ± 2.83	-0.20 ± 2.85
		Mar-05	Apr-07	34.67	0.71 ± 3.24	0.84 ± 4.25
		Feb-04	Feb-08	15.06	0.02 ± 2.54	0.04 ± 2.39
2.	Siachen	Oct-04	Oct-09	5.14	0.23 ± 0.60	0.27 ± 0.56
		Oct-03	Oct-05	24.03	-0.19 ± 1.70	-0.38 ± 0.95
3.	Baltoro	Oct-03	Oct-09	277.95	0.44 ± 1.27	0.66 ± 1.20
4.	Drenmarg	Oct-03	Oct-07	182.68	-1.02 ± 2.21	-1.05 ± 2.64

Considering the second near repeat track on Gangotri Glacier taken as April, 2007 and March, 2005, the mean elevation change rate is observed to be positive which depicts the thickening of glacier surface in a period of two years. The mean separation between the ICESat near repeat tracks in the Siachen glacier is observed as 14.5m.

The first near repeat track on Siachen Glacier was October, 2009 and October, 2004, the mean elevation change rate during this period is observed more or less similar with CartoDEM (0.23 m/Year) and with SRTM (0.27 m/Year). The positive elevation change rate depicts the thickening of glacier surface in a period of five years. The second near repeat track was taken as October, 2005 and October, 2003 and the mean elevation change rate observed with CartoDEM is -0.19 m/Year and with SRTM is -0.39 m/Year. Here the negative elevation change rate depicts the thinning of glacier surface in a period of two years.

The near repeat track on Baltoro Glacier has a temporal separation of six years and the mean elevation change rate during this period observed with CartoDEM is 0.44 m/Year and with SRTM is 0.66 m/Year. The ICESat near repeat track on Drenmarg Glacier having temporal separation of 4 years (October, 2003, October, 2007) and the mean elevation change rate during this period is observed more or less similar with CartoDEM (-1.02 m/Year) and with SRTM (-1.05 m/Year). Figure 4.20.5 shows the average annual 2003-2009 elevation change rates at different locations of different glacier. There are large local dh/dt variations which may attribute to glacier dynamics, wind drift and error in the datasets. The datasets error contains instrumental error of GLAS as well as the relative inaccuracies of DEMs. It has also been observed that the thinning/thickening rate computed using SRTM and CartoDEM are similar. Most of the complexities are likely caused by glacier dynamics and wind posting of snow might also have an impact. The change rates are slightly different in different glaciers which reflect different local climatic conditions, different hypsometry's of the glaciers, and different glacier flow dynamics.

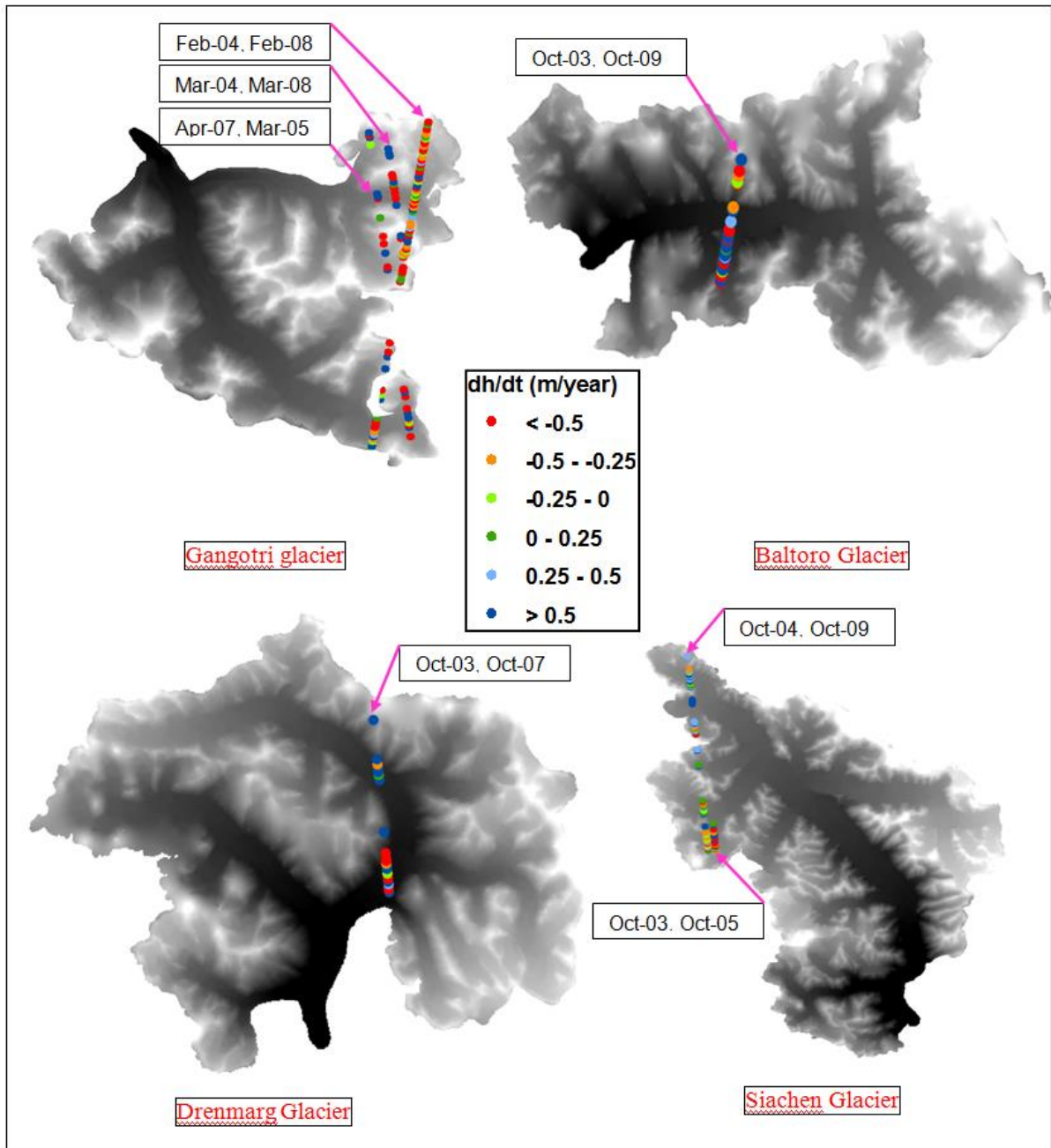


Figure 321: Elevation change rate along ICESat tracks on Siachen, Gangotri, Baltoro and Drenmarg glaciers of the Himalayan region.

21.7. Conclusion

In this study four glaciers in the Himalaya region have been taken up for the estimation of elevation change using ICESat altimetry data and DEMs (CartoDEM and SRTM). Until now, ICESat has mainly been applied in Antarctica and Greenland ice sheets. Here, ICESat laser altimetry proved to be a highly valuable dataset for computing regional scale elevation changes for smaller glaciers with mountainous topography. Its applicability for smaller glaciers in mountainous regions is limited because of the insufficient spatial distribution of tracks. In this study the near repeat track approach has been used to compute elevation changes by estimating unmeasured variation in

local topography with the consideration of reference DEM. This approach takes care of the slope induced error but the relative error in the DEM may play an important role for change detection. To minimize the relative inaccuracies in DEM the near repeat track separation should have minimum value.

This study shows the similar variation with the CartoDEM and SRTM DEM. The thinning rate is observed negative in tracks of Gangotri and Baltoro Glaciers while tracks on Drenmarg glaciers have high thinning rate. Since the observed tracks are very limited over the glaciers, the observed estimates may be biased towards the representation for the entire glacier region. To estimate the mean elevation, change in the glacier region more near repeat tracks distributed spatially are required. However, this procedure can be used for the better estimates in the Himalaya region with the processing of future ICESat-2 mission, which will cover densely with close spacing and dense point coverage using six laser beam configuration. This work can be extended to other Himalayan regions to assess elevation change of glacier ice and to better understand its association with provincial climate changes.

22. Future Plan

Monitoring of Himalayan region using space based observations needs to be continued for improved understanding of Himalayan cryosphere. Ongoing as well future plans to understand Himalayan Cryosphere include analysis of satellite data from existing as well planned Earth Observation Missions of ISRO and other International Missions. Large scale glacier mapping and monitoring shall be carried out. Techniques shall be developed/improved for estimation of snow depth, snow pack characterization, glacier mass balance estimation, glacier velocity determination, snow and glacier melt estimation and early warning of snow and glacier related hazards.

A new project entitled, “**Integrated studies of Himalayan Cryosphere using space based inputs and impact assessment due to climate change**”, has been initiated from Financial Year 2016-17 which is funded by Department of Space. This project is aimed to do a comprehensive integrated study of Hindu Kush-Karakoram-Himalayan region using space based observations for societal benefits and understand impact due to climate change. The major work components currently undertaken are given below:

- i) Glacier characterisation using SAR data which involves understanding of the freeze-melt cycle of glaciers occurring in different climatic regions of Himalayan terrain in spatial and temporal domain using RISAT-1 SAR data. Selected large glaciers from entire Himalaya-Karakoram-Hindukush region have been taken up. This work is aimed to generate multi-temporal glacier facies maps along with their spatial and temporal analysis.
- ii) Snow Cover Mapping component involves sub-basin wise snow cover product generation in GIS environment and analysis of geospatial database. Snow cover products shall be generated at every 5 days and 10 days for hydrological year 2015 to 2018 covering 35 sub-basins of Indus, Ganga and Brahmaputra river basins using IRS (Resourcesat-1 and 2) AWiFS data. This database is in continuation of the earlier phases and thus shall enrich the existing geospatial database of snow cover for long term analysis.
- iii) Development of techniques for estimation of mass balance of glaciers using Altimeric, Geodetic and AAR methods (Photogrammetry, Interferometry, GRACE, Laser Altimetry). Work shall be carried out for selected glaciers for hydrological year 2015-2018.
- iv) Estimation and validation of snow and glacier melt run-off for selected sub-basins in Satluj, Ganga and Chenab basins. The work involves improvement in accuracy of model and spatial and temporal variability of snow and glacier melt runoff in the Himalayan region.

- v) Techniques for retrieving velocity of glaciers using optical and microwave data shall be developed for selected glaciers from sub-basins in western, west-central, central and eastern Himalayan regions;
- vi) Techniques for retrieval of snow depth in the Himalayan region using AWiFS and RISAT-1 SAR data in winters for Beas basin and Bhaga basin shall be developed.

In addition, it is planned to carry out glacier mapping and change detection of selected glaciers on 1:10, 000 scale using high resolution satellite images (~100 glaciers); Mapping and monitoring of glacial and peri-glacial lakes (~ 2,000 - 2, 500 lakes); Development of Himalayan Cryosphere Information System (HKH Region); Evaluating feasibility of geostationary satellite data for Cryosphere studies (Estimation of snow depth Snow cover, snow line and melt runoff studies using INSAT-3D); Retrieval of snow pack characterisation using Hyperspectral data; Monitoring and impact assessment of Black Carbon soot on glaciers; Study of spatial and temporal variability of snow Albedo for assessing radiative transfer over Himalayan snow covered regions; Development of empirical relation for glacier ice thickness using GPR; Energy Balance modelling on snow and glaciers; Development of approach for Glacier health Bulletin; Development of alert system for glacial lakes outbursts; Comparative study of glacier dynamics in Himalayan, Central Asian mountains, Alps and Svalbard regions

References

1. Abshire J B, Sun X L, Riris H, Sirota J M, McGarry J F, Palm S, Yi D H, and Liiva P (2005) Geoscience Laser Altimeter System (GLAS) on the ICESat mission: On-orbit measurement performance *Geophys. Res.Lett.* **32** L21S02 doi:10.1029/2005 GL024028
2. Aggarwal S P, Thakur K P, Nikam B R and Garg, V (2014) Integrated approach for snowmelt runoff estimation using temperature index model, remote sensing and GIS *Current Science* **106**(3) 397-407
3. Aggarwal K C, Kumar V and Dass T (1983) Snowmelt run-off for a catchment of Beas basin. In: *Proc. First National Symp. on Seasonal Snow Cover*, SASE, Manali 28-30 April, 1983 **II** 43-63
4. Agrawal Ritesh, Singh S K, Rajawat A S and Ajai (2014) Estimation of regional mass anomalies from Gravity Recovery and Climate Experiment (GRACE) over Himalayan region. In: *The International Archives of the Photogrammetry, Remote Sensing and Spatial Information Sciences* Volume XL-8 2014 ISPRS Technical Commission VIII Symposium doi:10.5194/isprsarchives-XL-8-329-2014, 329-332
5. Akiko Sakai (2012) Glacial lakes in the Himalayas: a review on formation and expansion processes *Global Environ. Res.* **16** 23–30
6. Akyurek Z and Sorman A U (2002) Monitoring snow-covered areas using NOAAVHRR data in the eastern part of Turkey *Hydrol. Sci.* **47** 243–252
7. Anderson E A (1976) National river forecast system-snow accumulation and ablation model, *NOAA Tech. Memo.NWS Hydro-17*, US Dept. of Commerce, Silver Spring, USA
8. Arcone S A, Lawson D E and Delaney A J (1995) Short-pulse radar wavelet recovery and resolution of dielectric contrasts within englacial and basal ice of Motanuska glacier, Alaska *Journal of Glaciology* **41** 68-86
9. Armstrong R L and Brun E (2008) *Snow Climate*, Cambridge University Press, 222; ISBN 978-0-521-85454-2
10. Arnott W P, Hamasha K, Moosmuller H, Shredian P J and Orgen J A (2005) Towards aerosol light-absorption measurements with a 7-wavelength aethalometer: Evaluation with a photoacoustic instrument and 3-wavelength nephelometer *Aerosol Sci. Technol.*, **39** 17-29

11. Aster GDEM team (2011) Aster digital Global Digital Elevation model version 2 – summary of validations result. *GDEM2, validation report final*, <http://www.ersdac.or.jp/GDEM/ver2validation/summary>
12. Aswal B S and Mehrotra B N (1994) Flora of Lahaul-Spiti (A Cold Desert in North-West Himalaya). Bishen Singh Mahendra Pal Singh, Dehradun
13. Avsar N B and Ustun A (2012) Analysis of regional time variable gravity using GRACE's 10-day solutions *FIG Working Week 2012 Knowing to manage the territory, protect the environment, evaluate the cultural heritage* Rome, Italy, 6-10 May 2012
14. Azam M F, Wagnon P, Ramanathan A L, Vincent C, Sharma P, Arnaud Y, Linda A, Pottakkal J G, Chevallier P, Singh V B and Etienne B (2011) From balance to imbalance: a shift in the dynamic behaviour of Chhota Shigri Glacier (Western Himalaya, India) *Jour. Glacio.* **58**(208) 315-324
15. Bahuguna I M, Rathore B P, Brahmabhatt R, Sharma M, Dhar S, Randhawa S S, Kumar K, Romshoo S, Shah R D, Ganjoo R K and Ajai (2014) Are the Himalayan glaciers retreating? *Current Science* **106**(7) 1008-1013
16. Bahuguna I M (2013) Geomatics in early assessment of Himalayan lakes outburst hazards. *Newsl. ISG* **19**(2) 57–64
17. Bahuguna I M, Kulkarni A V, Nayak S, Rathore B P, Negi H S and Mathur P (2007) Himalayan glacier retreat using IRS 1C PAN stereo data *Int. J. Remote Sensing* **28**(2) 437–442
18. Bahuguna I M, Kulkarni A V and Nayak S R (2004) DEM from IRS-1C PAN stereo coverage over Himalayan glaciated region *Int. J. Remote Sensing* **25**(19) 4029–4041
19. Bajracharya S R, Maharjan S B, Shrestha F (2014) The status and decadal change of glaciers in Bhutan from 1980's to 2010 based on the satellite data *Ann. Glaciol.* **55**(66) 159-166. doi: 10.3189/2014AoG66A125
20. Bajracharya S R, Mool P K and Shrestha B R (2006) The impact of global warming on the glaciers of the Himalaya. *In Proceedings of the International Symposium on Geo-disasters, Infrastructure Management and Protection of World Heritage Sites*, Nepal Engineering College, Ehime College and National Society for Earthquake Technology, Nepal, 25–26 November 2006 231–242

21. Bamler R (1999) The SRTM Mission – A Worldwide 30 m Resolution DEM from SAR Interferometry in 11 Days. In: *Photogrammetric Week '99 D* (Eds.: Fritsch D and Spiller R) WichmannVerlag, Heidelberg, Germany 145-154
22. Basnett S, Kulkarni A V and Bolch T (2013) The influence of debris cover and glacial lakes on the recession of glaciers in Sikkim Himalaya, India *J of Glaciology* **59** 1035-1046 <http://dx.doi.org/10.3189/2013JoG12J184>
23. Benn D I, Bolch T, Hands K, Gulley J, Luckman A, Nicholson L I, Quincey D, Thompson S, Toumi R and Wiseman S (2012) Response of debris-covered glaciers in the Mount Everest region to recent warming, and implications for outburst flood hazards *Earth-Science Reviews* **114** 156–174 doi:10.1016/j.earscirev.2012.03.008
24. Benn D I and Evans D J A (2010) *Glaciers and Glaciation*, Hodder Education, London, 802; ISBN 978-0-340-90579-1
25. Benn D I, Wisemen S and Hands K (2001) Growth and drainage of supraglacial lakes on debris-mantled Ngozumpa glacier, Khumbu Himal, Nepal *J. Glaciol.* **47** 625–638
26. Benson R C, Glaccum R A and Noel M R (1983) Geophysical techniques for sensing buried wastes and waste migration. Environmental Monitoring Systems Laboratory, US Environmental Protection Agency, Contract # 68-03-3050 Las Vegas NV 236
27. Beres M and Haeni F P (1991) Application of Ground-Penetrating-Radar methods in hydrogeologic studies *Groundwater* **29**(3) 375-386
28. Berthier E, Arnaud Y, Kumar R, Ahmad S, Wagnon P and Chevallier P (2007) Remote sensing estimates of glacier mass balances in the Himachal Pradesh (Western Himalaya, India) *Remote Sensing Environ.* **108** 327–338
29. Berthier E, Arnaud Y, Vincent C and Remy F (2006) Biases of SRTM in high-mountain areas: Implications for the monitoring of glacier volume changes. *Geophys. Res. Lett.*, **32**(8) L08502. doi:10.1029/2006GL025862
30. Berthier E, Vadon H, Baratoux D, Arnaud Y, Vincent C, Feigl K L, Remy F and Legresy B (2005) Surface motion of mountain glaciers derived from satellite optical imagery *Rem Sens Environ* **95**(1)14-28
31. Berthier E, Arnaud Y, Baratoux D, Vincent C and Remy F (2004) Recent rapid thinning of the "Mer de Glace" glacier derived from satellite optical images *Geoph Res Lett*, **31** (17)

32. Bhambri R, Bolch T, Kawishwar P, Dobhal D P, Srivastava D and Pratap B (2013) Heterogeneity in glacier response in the upper Shyok valley, northeast Karakoram *Cryosphere* **7** 1385–1398 (doi: 10.5194/tc-7-1385-2013)
33. Bhambri R, Bolch T and Chaujar R (2012) Frontal recession of Gangotri Glacier, Garhwal Himalayas, from 1965 to 2006, measured through high-resolution remote sensing data *Current Science* **102** 489-494
34. Bhambri R, Bolch T, Chaujar R K and Kulshreshtha S C (2011) Glacier changes in the Garhwal Himalaya, India, from 1968 to 2006 based on remote sensing *J Glaciol* **57**(203) 543–556 (doi: 10.3189/002214311796905604)
35. Bhambri R and Bolch T (2009) Glacier mapping: a review with special reference to the Indian Himalayas *Prog. Phys. Geogr.* **33** 672–704
36. Bingham A W and Rees W G (1997) Satellite data synergies for monitoring Arctic ice masses. In: *Proc. 3rd ERS Scientific Symp.* March 17-21,1997 Florence, Italy (SP-414 Vol. 2) ESA, Frascati Italy 867-870
37. Bintanja R, Jonsson S and Knap W (1997) The annual cycle of the surface energy balance of Antarctic blue ice. *J. Geophys. Res.* **102**(D2) 1867–1881
38. Birajdara F S, Venkataramana G, Bahuguna I M and Samant H P (2014) A revised glacier inventory of Bhaga basin Himachal Pradesh, India. In: *ISPRS Annals of the Photogrammetry, Remote Sensing and Spatial Information Sciences*, Volume II-8, 2014, ISPRS Technical Commission VIII Symposium, doi:10.5194/isprsannals-II-8-37-2014, 37-43
39. Blindow N (1994) The central part of the Filchner-Ronne Ice Shelf, Antarctica: internal structures revealed by 40 MHz mono pulse RES *Annals of Glaciology* **20** 365-371
40. Bolch T, Kulkarni A, Kaab A, Huggel C, Paul F, Cogley J G, Frey H, Kargel J S, Fujita K, Scheel M, Bajracharya S and Stoffel M (2012) The state and fate of Himalayan glaciers, *Science* **336**(6079) 310-314 (doi:10.1126/science.1215828)
41. Bolch T, Pieczonka T and Benn D I (2011a) Multi-decadal mass loss of glaciers in the Everest area (Nepal Himalaya) derived from stereo imagery *The Cryosphere* **5** 349–358, www.the-cryosphere.net/5/349/2011/ doi: 10.5194/tc-5-349-2011

42. Bolch T, Peters J, Pradhan B, Yegorov A B, Buchroithner M F and Blagoveshchenskiy V P (2011) Identification of potentially dangerous glacial lakes in the northern Tien Shan *Nat. Hazards* **59**(3) 1691–1714
43. Bolch T *et al.* (2010) A glacier inventory for the western Nyainqentanglha Range and the Nam Co Basin, Tibet, and glacier changes 1976–2009 *Cryosphere* **4** 419–433
44. Bose A (2013) Comparison of Eastern and Western Himalayas. *Indian Geography*, <http://www.importantindia.com/4310/compare-westernand-eastern-himalayas/>
45. Brahmabhatt R M, Bahuguna I M, Rathore B P, Shah R D, Kargel J S and Rajawat A S (2016) Significance of glacio-morphological factors in the glacier retreat: A case study of part of Chenab basin, Himalaya, *J of Mountain Science* (in Press)
46. Brahmabhatt R M, Bahuguna I M, Rathore B P, Singh S K, Rajawat A S, Shah R D and Kargel J S (2015a) Satellite monitoring of glaciers in the Karakoram from 1977 to 2013: an overall almost stable population of dynamic glaciers *The Cryosphere Discussions* **9** 1555- 1592, doi:10.5194/tcd-9-1555-2015
47. Brahmabhatt R M, Rathore B P, Pattnaik S, Jani P, Bahuguna I M, Shah R D and Rajawat A S (2015b) Peculiar characteristics of fragmentation of glaciers: a case study of Western Himalaya, India *Int J Geosciences* **6** 455-463
48. Brahmabhatt, R.M., Nainwal, H.C. and Kulkarni, A.V. (2014) Impact of Accumulation Area Ratio (AAR) on Glacial Change: A Few Examples of Jammu & Kashmir *J Geomatics* **8** 61-65
49. Brahmabhatt R M (2014) Study of Glacio-geomorphic Characteristics and its effect on Glacial Dimensions in parts of Chenab basin using Remote Sensing and Geographic Information System. *Ph. D. Thesis*, H. N. B. Garhwal University (Central University), Garhwal, Srinagar
50. Brahmabhatt R M, Bahuguna I M, Rathore B P, Kulkarni A V, Nainwal H C, Shah R D and Ajai (2012a) A comparative study of deglaciation in two neighboring basins (Warwan and Bhut) of Western Himalaya *Current Science*, **103**(3) 298-304
51. Brahmabhatt R M, Bahuguna I M, Rathore B P, Kulkarni A V, Shah R D, Nainwal H C and Ajai (2012b) Variation of snowline and mass balance of glaciers of Warwan and Bhut basin of Western Himalaya using remote sensing technique *J Ind Soc Remote Sensing* **40**(4) 629-637

52. Brenner A C, DiMarzio J R and Zwally H J (2007) Precision and accuracy of satellite radar and laser altimeter data over the continental ice sheets. *IEEE T. Geosci. Remote*, **45**(2) 321–331 doi:10.1109/TGRS.2006.887172
53. Brewster M I and Annan A P (1994) Ground penetrating radar monitoring of a controlled DNAPL release: 200 MHz radar *Gephysics* **59** 1211-1221
54. Brock B W, Mihalcea C, Kirkbride M P, Diolaiuti G, Cutler M E J, Smiraglia C (2010) Meteorology and surface energy fluxes in the 2005–2007 ablation seasons at the Miage debris-covered glacier, Mont Blanc Massif, Italian Alps. *J. Geophys. Res.* **115** D09106
55. Brown R D (2000) Northern Hemisphere snow cover variability and change, 1915–1997 *J Climate* **13** 2339–2355
56. Butt M J (2012) Characteristics of the snow cover in the Hindukush, Karakoram and Himalaya region using Landsat satellite data *Hydrol Process* **26**(24) 3689-3698
57. Carey M (2008) Disasters, development and glacial lake control in twentieth-century Peru. In: *Mountains Sources of Water, Sources of Knowledge. Advances in Global Change Research* (Ed: Wiegandt E) Springer the Netherlands **31** 181–196
58. Casey K A, Kaab A and Benn D I (2012) Geochemical characterization of supraglacial debris via in situ and optical remote sensing methods: a case study in Khumbu Himalaya, Nepal *The Cryosphere* **6** 85–100
59. Chacko V J (1965) A Manual of Sampling Technique for Forest Surveys. Manager Publications Delhi 172
60. Chakraborty M, Panigrahy S, Rajawat A S, Kumar R, Murthy T V R, Halder D, Chakraborty A, Kumar T, Rode S, Kumar H, Mahapatra M and Kundu S (2013) Initial results using RISAT-1 C band SAR data *Current Science* **104**(4) 490–501
61. Chaohai L and Sharma C K (1988) Report on First Expedition to Glaciers in the Pumqu (Arun) and Poiqu (Bhote-Sun Kosi) River Basins, Xizang (Tibet). China, Science Press, Beijing, China 192
62. Che T, Li X, Jin R, Armstrong R and Zhang T (2008) Snow depth derived from passive microwave remote sensing data in China *Ann. Glaciol.* **49** 145–154

63. Chowdhery H J and Wadhwa B M (1984) Flora of Himachal Pradesh **1-3** Bot. Surv. India, Calcutta
64. Clague J J and Evans S G (2000) A review of catastrophic drainage of moraine dammed lakes in British Columbia. *Quaternary Sci. Rev.* **19** 1763–1783
65. Clarke G K C and Mathews W H (1981) Estimation of magnitude of glacier outburst floods from Dojeck, Yukon Territory, Canada *Can. J. Earth Sci.* **18** 1452–1463
66. Clague J J and Mathews W H (1973) The magnitude of jokulaphs *J. Glaciol.* **12** 501–504
67. Conyers L B and Goodman D (1997) *Ground Penetrating Radar: An Introduction for Archaeologists*, Altamira Press, Walnut Creek, CA 232
68. Copland L, Sylvestre T, Bishop M P, Shroder J F, Seong Y B, Owen L A, Bush A and Kamp U (2011) Expanded and recently increased glacier surging in the Karakoram *Arct. Antarct. Alp. Res.* **43** 503–516
69. Cosgrave T M, Greenhouse J P and Barker J F (1987) Shallow stratigraphic reflections from ground-penetrating-radar. In: *First National Outdoor Action Conference on Aquifer Restoration Ground Water Monitoring and Geophysical Methods*, Las Vegas N V 559-569
70. Cuffey K M and Paterson W S B (2010) *The Physics of Glaciers* Fourth Edition *Academic Press* 704 ISBN 9780123694614
71. Curtis J T and Mc Intosh (1950) The interrelation of certain analytic and phytosociological characters *Ecol.* **31** 434-455
72. Daniels J J, Roberts R and Vendl M (1995) Ground penetrating radar for the detection of liquid contaminants *J. Appl. Geophys.* **33** 195–207
73. Das S K, Dobhal D P and Juyal N (2010) Variability of aerosol optical depth and recent recessional trend in Dokriani Glacier, Bhagirathi Valley, Garhwal Himalaya *Current Science* **99**(12) 1816–1821
74. Davis J L, Tamisiea M E, Elosegui P, Mitrovica J X and Hill E M (2008) A statistical filtering approach for Gravity Recovery and Climate Experiment (GRACE) gravity data, *Journal of Geophysical Research* **113** B04410 doi:10.1029/2007JB005043

75. Dedieu J P, Rabatel A, Vincent C, Valla F, Thibert E and Arnaud Y (2003) Glacier mass balance determination by remote sensing in the French Alps: progress and limitation for time series monitoring In: *Proceedings of Geoscience and Remote Sensing Symposium*, IGARSS '032003; 4; 2602-2604 vol.4
76. Deota B S, Trivedi Y N, Kulkarni A V, Bahuguna I M and Rathore B P (2011) RS and GIS in mapping of geomorphic records and understanding the local controls of glacial retreat from the Baspa Valley, Himachal Pradesh, India, *Current Science* **100**(10) 1555– 1563
77. Deslognes J R, Jones D P and Kiker K E (1989) Estimation of peak discharge from drainage of ice dammed Ape lake, British Columbia *Can. J. Glaciol.* **35** 349–354
78. Dhaliwal D S and Sharma M (1999) Flora of Kullu District. Himachal Pradesh. Dehra Dun: Bishen Singh Mahendra Pal Singh
79. Dhar S, Kulkarni A V, Rathore B P and Kalia R (2009) Reconstruction of the moraine dammed lake, based on field evidences and paleohistory, Samudra Tapu Glacier, Chandra Basin, Himachal Pradesh *J. Indian Soc. Remote Sensing* **38**(1)133–141
80. Dhar U, Rawal R S and Samant S S (1997) Structural diversity and representativeness of forest vegetation in a protected area of Kumaun Himalaya, India Implications for conservation *Biod. Cons.* **6** 1045-1062
81. Dobhal D P, Gupta A K, Mehta M and Khandewal D D (2013) Kedarnath disaster: facts and plausible causes. *Current Science* **105**(2) 171–174
82. Dobhal D P (2010) Climate Change and Glacier Retreat in the Himalaya, India – an Overview. In: *Climate Change at the Third Pole: The Impact of Climate Instability on Himalayan Ecosystems and Himalayan Communities* (Eds: Shiva V and Bhatt V K) p. 67-77
83. Dobhal D P and Mehta M (2010) Surface morphology, elevation changes and Terminus retreat of Dokriani Glacier, Garhwal Himalaya: implication for climate change *Him. Geol.* **31**(1) 71-78
84. Dobhal D P, Gergan J T, Thayyen R J (2008) Mass balance studies of the Dokriani glacier from 1992 to 2000, Garhwal Himalaya, India. *Bulletin of Glaciological Research* **25** 9–17

85. Dozier J (1992) Opportunities to improve hydrologic data *Review of Geophysics* **30**(4) pp 315-331
86. Dozier J (1989) Spectral signature of Alpine snow cover from the Landsat Thematic Mapper *Remote Sens. Environ.* **28** 9-12
87. Dutta S, Ramanathan A L and Linda A (2012) Glacier fluctuation using satellite data in Beas basin, 1972–2006, Himachal Pradesh, India *J. Earth Syst. Sci.* **121**(5) 1105–1112
88. Evans I S (2006) Local aspect asymmetry of mountain glaciations: a global survey of consistency of favored directions for glacier numbers and altitudes *Geomorphology* **73**(1–2) 166–184
89. Favier V, Wagnon P, Chazarin J P, Maisincho L and Coudrain A (2004) One-year measurements of surface heat budget on the ablation zone of Antizana glacier 15, Ecuadorian Andes *J. Geophys. Res.* **109** D18105 doi:10.1029/2003JD004359
90. Flanner M G, Liu X, Zhou C, Penner J E and Jiao C (2012) Enhanced solar energy absorption by internally-mixed black carbon in snow grains *Atmos Chem Phys* **12**(10):4699–721
91. Flanner M G, Shell K M, Barlage M, Perovich D K and Tschudi M A (2011) Radiative forcing and albedo feedback from the Northern Hemisphere cryosphere between 1979 and 2008 *Nat Geosci* **4**(3) 151–155
92. Foster J L and Chang A T C (1993) Snow Cover, In: *Atlas of Satellite Observations related to Global Change* (Eds.: Gurney R J, Parkinson C L and Foster J L), Cambridge University Press, Cambridge 361-370
93. Frey H, Machguth H, Huss M, Huggel C, Bajracharya S, Bolch T, Kulkarni A, Linsbauer A, Salzmann N, Stoffel M (2013) Ice Volume estimates for the Himalaya-Karakoram region: evaluating different methods *The Cryosphere* **7**(5) 4813-4854 doi:10.519/tcd-7-4813-2013
94. Frey H, Paul F and Strozzi T (2012) Compilation of a glacier inventory for the western Himalayas from satellite data: methods, challenges, and results *Remote Sens Environ* **124** 832–843
95. Frey H and Paul F (2012) On the suitability of the SRTM DEM and ASTER GDEM for the compilation of topographic parameters in glacier inventories. *Int. J. Appl. Earth Obs. Geoinf.* **18** 480–490 (doi: 10.1016/j.jag.2011.09.020)

96. Frei A and Robinson D A (1999) Northern Hemisphere snow extent: regional variability 1972-1994 *International J. of Climatology* **19** 1535-1560
97. Fujita K, Sakai A, Takenaka S, Nuimura T, Surazakov A B, Sawagaki T and Yamanokuchi T (2013) Potential flood volume of Himalayan glacial lakes *Nat. Hazards Earth Syst. Sci.* **13** 1827–1839. www.nat-hazards-earth-syst-sci.net/13/1827/2013/ doi:10.5194/nhess-13-1827-2013
98. Fujita K, Nishimura K, Komori J, Iwata S, Ukita J, Tadono T and Koike T (2012) Outline of research project on glacial lake outburst floods in the Bhutan Himalayas *Global Environ. Res.* **16** 3-12
99. Fushimi H, Ikegani K, Higuchi K and Shankar K (1985) Nepal Case Study: Catastrophic Floods, Techniques for Prediction of Runoff from Glacierised Areas, *IASH Publ.* **149** 125–130
100. Ganju R K (2009) Is the Siachen glacier melting? Scientific Correspondence *Current Science* 97(3) 309
101. Gansser A (1983) Geology of the Bhutan Himalaya *Mem. Soc. Sci. Nat.* 149–154
102. Gantayat P, Kulkarni A V and Srinivasan J (2014) Estimation of ice thickness using surface velocities and slope: case study of Gangotri glacier, India *J Glaciology* **60**(220) 277-282
103. Gardelle J, Arnaud Y and Berthier E (2011) Contrasted evolution of glacial lakes along the Hindu Kush Himalaya mountain range between 1990 and 2009 *Global Planet. Change* **75**(1–2) 47–55 (doi: 10.1016/j.gloplacha.2010.10.003)
104. Gardelle J, Berthier E and Arnaud Y (2012) Slight mass gain of Karakoram glaciers in the early twenty-first century *Nature Geoscience* **5**(5) 322-325, doi: 10.1038/NGEO1450
105. Gardelle J, Berthier E, Arnaud Y and Kaab A (2013) Region-wide glacier mass balances over the Pamir-Karakoram-Himalaya during 1999-2011 *The Cryosphere* **7** 1263-1286 <http://dx.doi.org/10.5194/tc-7-1263-2013>
106. Gergan J T, Dobhal D P and Kaushik R (1999) Ground penetrating radar ice thickness measurements of Dokriani bamak (glacier), Garwal Himalaya. *Curr. Sci.* **77** 169–173
107. Greig-Smith P (1957) Quantitative Plant Ecology. Academic Press, New York

108. Groisman P Y, Karl T R and Knight R W (1994a) Observed impact of snow cover on the heat balance and the rise of continental spring temperatures *Science* **263** 198–200
109. Groisman P Y, Karl T R and Knight R W (1994b) Changes of snow cover, temperature and relative heat balance over the Northern hemisphere *J. Climatol.* **7** 1633–1656
110. Gurung D R, Kulkarni A V, Giriraj A, Aung K S, Shrestha B, Srinivasan J (2011) Changes in seasonal snow cover in Hindu Kush-Himalayan region *The Cryosphere Discuss* **5** 755–777
111. Guy E D, Daniels J J, Holt J, Radzevicius S J and Vendl M A (2000) Electromagnetic induction and GPR measurements for creosote contaminant investigation *J Env. Engineering Geophysics* **5**(2) 11-19
112. Haeberli W and Hoelzle M (1995) Application of inventory data for estimating characteristics of and regional climate-change effects on mountain glaciers: a pilot study with the European Alps. *Ann. Glaciol.* **21** 206–212
113. Hagg W, Braun L, Uvarov V N, and Makarevich K G (2004) A Comparison of three Methods of Mass Balance Determination in the Tuyuksu Glacier Region, Tien Shan *J Glaciol* **50**(171), 505-510
114. Hall D K et al. (2003) Consideration of the errors inherent in mapping historical glacier positions in Austria from the ground and space (1893–2001) *Remote Sensing Environ.* **86**(4) 566–577
115. Hall D K, Salomonson V V, Riggs G A, DiGirolamo N and Bayr K J (2002) MODIS snow cover products *Remote Sensing Environ.* **83** 181-194
116. Hall D K, Kelly R E J, Riggs G A, Chang A T C and Foster J L (2001) Assessment of the relative accuracy of hemispheric-scale snow-cover maps *Annals of Glaciology* **34** 24-30
117. Hall D K (1998) Remote sensing of snow and ice using imaging radar; in *Principles and Applications of Imaging Radars*, Third Edition-Vol. 2 (Eds.: Henderson F M and Lewis L A; Editor-in-Chief Ryerson R A) John Wiley & Sons Inc. 677-703
118. Hall D K, Riggs G A and Salomonson V V (1995) Development of methods for mapping global snow cover using moderate resolution image spectroradiometer data *Rem Sens Environ* **54** 127-140

119. Hall D K, Fagre D B, Klasner F, Linebaugh G and Liston G E (1994) Analysis of ERS 1 Synthetic Aperture Radar of frozen lakes in northern Montana and implications for climate studies *Journal of Geophysical Research* **99**(C11) 22,473-22,482
120. Hall D K and Martinec J (1985) Remote Sensing of Ice and Snow, Chapman and Hall, New York, 189p
121. Hambrey M J, Quincey D J, Glasser N F, Reynolds J M, Richardson S J and Clemmets S (2008) Sedimentological, geomorphological and dynamic context of debris mantled glaciers, Mount Everest (Sagarmatha) region, Nepal *Quaternary Sci. Rev.* **27** 2361–2389
122. Hansen J et al. (2005) Efficacy of climate forcings *J. Geophys. Res.* **110** D18104, doi:10.1029/2005JD005776
123. Hansen A D A, Rosen H and Novakov T (1984) The Aethalometer, an instrument for the real-time measurement of optical absorption by aerosol particles *Sci. Total Environ.* **36** 191–196.
124. Hock R (2010) Glacier meteorology energy balance. Summer school in glaciology, 1-10
125. Hock R and Holmgren B (2005) A distributed surface energy balance model for complex topography and its application to Storglaciaren *Journal of Glaciology* **51** 25-36
126. Hock R (2003) Temperature index melt modelling in mountain areas. *Journal of Hydrology* **282** 104-115
127. Huggel C, Käab A, Haeblerli W, Teyssere P and Paul F (2002) Remote sensing based assessment of hazards from glacier lake outbursts: a case study in the Swiss Alps *Can. Geotech. J.* **39** 316–330.
128. ICIMOD (2011) Glacial lakes and glacial lake outburst floods in Nepal, *ICIMOD*, Kathmandu, Nepal, 99
129. Imse J P and Levine E N (1985) Conventional and state of art geophysical techniques for fracture detection. In: *Proc. Nat. Water Well Assoc. Annual Eastern Groundwater Regional Conf.* 2d Portland Maine 18-36

130. IPCC (2013) Summary for Policymakers. In: *Climate Change 2013: The Physical Science Basis. Contribution of Working Group I to the Fifth Assessment Report of the Intergovernmental Panel on Climate Change* (Eds: Stocker, T. F. et al.) Cambridge University Press Cambridge UK
131. IPCC (2007) Summary for policymakers. In: *Climate Change: The Physical Science Basis. Contribution of Working Group I to the Fourth Assessment Report of the Intergovernmental Panel on Climate Change* (Eds.: Solomon S, Qin D, Manning M, Chen Z, Marquis M, Averyt K B, Tignor M and Miller H L) Cambridge University Press, Cambridge, United Kingdom and New York, NY, USA
132. Irvin-Finn T D L, Moorman B J, Williams J L M and Walter F S A (2006) Seasonal changes in ground-penetrating radar signature observed at a polythermal glacier, Bylot Island, Canada *Earth Surf. Process. Land.* **31** 892–909
133. Iturrizaga L (2005) New observations on present and prehistorical glacier dammed lakes in the Shimshal valley (Karakoram mountains) *J. Asian Earth Sci.* **25** 545–555
134. Jain S K, Goswami A and Saraf A K (2010) Snowmelt runoff modeling in a Himalayan basin with the aid of satellite data *Int. J. Remote Sensing* **31**(24) 6603–6618
135. Jain S K, Goswami A and Saraf A K (2008) Accuracy assessment of MODIS, NOAA and IRS data in snow cover mapping under Himalayan conditions *Int. J. Remote Sensing* **29** 5863–5878
136. Johannessen O M, Khvorostovsky K, Miles M W and Bobylev L P (2005) Recent icesheet growth in the interior of Greenland *Science* **310**(5750) 1013–1016 doi:10.1126/science.1115356
137. Jones J A A (1997) *Global Hydrology*. Harlow: Pearson
138. Joseph G., 2003, *Fundamentals of Remote Sensing*, Universities Press (India) 433
139. Jyotsna V, Sharma A K and Sinha V S P (2014) Remote sensing and GIS based weighted model for assessing health of glaciers in Ganga basin, India *Int J of Applied Engineering Research*, ISSN 0973-4562, **9**(2) 171 – 176

140. Kaab A, Nuth C, Treichler D and Berthier E (2014) Brief Communication: Contending estimates of early 21st century glacier mass balance over the Pamir-Karakoram-Himalaya *The Cryosphere* **8** 5857-5874. <http://dx.doi.org/10.5194/tcd-8-5857-2014>
141. Kaab A, Berthier E, Nuth C, Gardelle J and Arnaud Y (2012) Contrasting patterns of early twenty-first-century glacier mass change in the Himalayas *Nature* **488**(7412) 495–498 (doi:10.1038/nature11324)
142. Kääb A (2007) Glacier Volume Changes using ASTER Optical Stereo. A Test Study in Eastern Svalbard *IEEE Trans Geosci Rem Sens* 10.1109/IGARSS.2007.4423724 3994 -3996
143. Kääb A (2005) Combination of SRTM3 and repeat ASTER data for deriving alpine glacier flow velocities in the Bhutan Himalaya *Rem Sens Environ* **94**(4) 463-474
144. Kääb A, Huggel C, Paul F, Wessels R, Raup B, Kieffer H, Kargel J (2003) Glacier Monitoring from ASTER Imagery: Accuracy and Applications. In: *Proceedings of EARSeLLIS-SIG Workshop*, Berne, March 11-13, 2002
145. Kamp U, Byrne M and Bolch T (2011) Glacier fluctuations between 1975 and 2008 in the Greater Himalaya Range of Zaskar, southern Ladakh *J. Mt. Sci.* **8**(3) 374–389 (doi: 10.1007/s11629-011-2007-9)
146. Kasturirangan K, Navalgund R R and Ajai (2013) Observed changes in the Himalaya-Tibetan glacier. In *Working group on Fate of Mountain Glaciers in the Anthropocene*. Vatican City. Pontifical Academy of Sciences, Scripta Varia **118** 1-28 www.pas.va/content/dam/accademia/pdf/sv118/sv118-kasturirangan.pdf
147. Kayastha R B, Takeuchi Y, Nakawo M and Ageta Y (2000) Practical prediction of ice melting beneath various thickness of debris cover on Khumbu Glacier, Nepal, using a positive degree-day factor. In *Debris-Covered Glaciers* (Eds.: Nakawo M, Raymond C F, and Fountain A) IAHS: Wallingford UK, 71–81
148. Kennett P (1966) Reconnaissance gravity and magnetic surveys of part of the Larsen ice shelf and adjacent mainland. *Br. Antarct. Surv. Bull.* **8** 49–62
149. Kersaw K A (1973) *Quantitative and Dynamic Plant Ecology*. Second Edition. Edward Arnold Limited, London
150. Khalid Omar Murtaza and Shakil A Romshoo (2015) Recent Glacier Changes in the Kashmir Alpine Himalayas, India *Geocarto International*, DOI: 10.1080/10106049.2015.1132482

151. Kiran Kumar A S (2013) Significance of RISAT-1 in ISRO's Earth Observation Programme, *Current Science* **104**(4) 444-445
152. Klees R, Zapreeva E A, Winsemius H C, and Savenije H H G (2007) The bias in GRACE estimates of continental water storage variations *Hydrol. Earth Syst. Sci.* **11** 1227–1241
153. Klein A G, Hall D K and Nolin A W (2000) Development of a prototype snow albedo algorithm for the NASA MODIS instrument. In: *57th Eastern Snow Conference*, Sysacuse, NY, USA, 17–19 May 2000, 143–158
154. Klein A G, Hall D K and Riggs G A (1998) Improving snow cover mapping in forests through the use of a canopy reflectance model *Hydrol. Proc.* **12** 1723–1744
155. Klok E J and Oerlemans J (2002) Model study of the spatial distribution of the energy and mass balance of Morteratschgletscher, Switzerland, *J. Glaciol.* **48**(163) 505– 518
156. Koike T and Takenaka S (2012) Scenario analysis on risks of glacial lake outburst floods on the Mangde Chhu River, Bhutan *Global Environ. Res.* **16** 41–49
157. Komori J, Koike T, Yamanokuchi T and Tshering P (2012) Glacial lake outburst events in the Bhutan Himalayas *Global Environ. Res.* **16** 59–70
158. Komori J (2008) Recent expansions of glacial lakes in the Bhutan Himalayas *Quaternary Int.* **184** 177–186
159. Koul M N, Bahuguna I M, Ajai, Rajawat A S, Sadiq Ali and Sumit Koul (2016) Glacier area change over past 50 years to stable phase in Drass Valley, Ladakh Himalaya (India), *American Journal of Climate Chang* **5** 88-102 Published Online March 2016 in SciRes. <http://www.scirp.org/journal/ajcc>
<http://dx.doi.org/10.4236/ajcc.2016.510>
160. Kulkarni A V and Karyakarte Y (2014) Observed changes in Himalayan glaciers, *Current Science*, **106**(2) 237-244
161. Kulkarni A V, Kumar G Vinay, Negi H S, Srinivasan J and Satheesh S K (2013) The effect of black carbon on reflectance of snow in the accumulation area of glaciers in the Baspa basin, Himachal Pradesh, India *The Cryosphere Discussions* **7** 1359–1382

162. Kulkarni A V, Rathore B P, Singh S K and Bahuguna I M (2011) Understanding changes in Himalayan cryosphere using remote sensing technique, *Int J Remote Sensing* **32**(3) 601-615
163. Kulkarni A V, Rathore B P, Singh S K and Ajai (2010) Distribution of seasonal snow cover in central and western Himalaya *Annals of Glaciology* **51**(54) 123-128
164. Kulkarni A V (2010) Monitoring Himalayan Cryosphere using remote sensing techniques *J Ind Inst Sci* **90**(4) 457-469
165. Kulkarni A V, Bahuguna I M, Rathore B P, Singh S K, Randhawa S S, Sood R K and Dhar S (2007) Glacial retreat in Himalaya using Indian remote sensing satellite data *Current Science* **92**(1) 69–74
166. Kulkarni A V, Dhar S, Rathore B P, Govindharaj K and Kalia R (2006a) Recession of Samudra Tapu glacier, Chandra River basin, Himachal Pradesh *J. ISRS* **34**(1) 39–46
167. Kulkarni A V, Singh S K, Mathur P and Mishra V.D. (2006b) Algorithm to monitor snow cover using AWiFS data of Resourcesat for the Himalayan region *Int J Remote Sensing* **27**(12) 2449-2457
168. Kulkarni A V, Rathore B P, Mahajan S and Mathur P (2005) Alarming retreat of Parbati glacier, Beas basin, Himachal Pradesh *Current Science* **88**(11) 1844-1850
169. Kulkarni A V, Mathur P, Singh S K, Rathore B P and Thakur N (2004a) Remote sensing based techniques for snow cover monitoring for the Himalayan region. In: Proceedings International symposium on Snow Monitoring and Avalanches (ISSMA-2004), Manali (12-16 April 2004) 399-405
170. Kulkarni A V, Rathore B P, Alex S (2004b) Monitoring of glacial mass balance in the Baspa basin using accumulation area ratio method, *Current Science*, **86**(1) 185-190
171. Kulkarni A V and Rathore B P (2003) Snow cover monitoring in Baspa basin using IRS WiFS data *Mausam* **54**(1) 335-34
172. Kulkarni A V, Randhawa S S, Rathore B P, Bahuguna, I M and Sood R K (2002a) Snow and glacier melt runoff model to estimate hydropower potential *J ISRS* **30**(4) 220-228
173. Kulkarni A V, Mathur P, Rathore B P, Alex Suja, Thakur N and Manoj Kumar (2002b) Effect of global warming on snow ablation pattern in the Himalayas, *Current Science* **83**(2) 120-123

174. Kulkarni A V, Srinivasulu J, Manjul S S and Mathur P (2002c) Field based spectral reflectance to develop NDSI method for snow cover monitoring *J ISRS* **30** 221-228
175. Kulkarni A V (1996) Moraine-dammed glacial lake studies using remote sensing techniques *Himalayan Geology* **17** 161-164
176. Kulkarni A V (1992) Mass balance of Himalayan glaciers using AAR and ELA methods *Journal of Glaciology* **38**(128) 101-104
177. Kumar V, Venkataramana G and Hogda K A (2011) Glacier surface velocity estimation using SAR interferometry technique applying ascending and descending passes in Himalayas *Int J Applied Earth Observation and Geoinformation* **13** 545–551
178. Kundu S and Chakraborty M (2015) Delineation of glacial zones of Gangotri and other glaciers of Central Himalaya using RISAT-1 C-band dual-pol SAR, *Int J Rem Sen* **36**(6) 1529-1550 DOI: 10.1080/01431161.2015.1014972
179. Kusche J and Schrama E J O (2005) Surface mass redistribution inversion from global GPS deformation and Gravity
180. Lama L, Kayastha R B, Maharjan S B, Bajracharya S R, Chand M B and Mool P K (2015) Glacier area and volume changes of Hidden Valley, Mustang, Nepal from ~1980s to 2010 based on remote sensing. In: *Remote Sensing and GIS for Hydrology and Water Resources (IAHS Publ. 368, 2015)* 57-62 doi:10.5194/piahs-368-57-2015
181. Lamsal D, Sawagaki T and Watanabe T (2011) Digital terrain modelling using Corona and ALOS PRISM data to investigate the distal part of Imja Glacier, Khumbu Himal, Nepal. *Journal of Mountain Science* **8** 390-402
182. Lau W, Kim M K, Kim K M and Lee W S (2010) Enhanced surface warming and accelerated snow melt in the Himalayas and Tibetan Plateau induced by absorbing aerosols *Environ Res Lett* **5**(2) 025204
183. Lawson D E, Strasser J C, Everson E B, Alley R B, Larsen G J and Arcone S A (1998) Glaciohydraulic supercooling: a mechanism to create stratified debris rich basal ice, Field evidences and conceptual model *Journal of Glaciology* **44** 547-562
184. Leprince S, Berthier E, Ayoub F, Delacourt C and Avouac J (2008) Monitoring Earth surface dynamics with optical imagery. *EOS Trans. Am. Geophys. Union* **89** 1–2

185. Liang S (2000) Narrowband to broadband conversions of land surface albedo I algorithms Remote Sensing of Environment **76** 213-238
186. Liu X (2008) Global gravity field recovery from satellite-to-satellite tracking data with the acceleration approach, Ph. D. thesis, Netherlands Geodetic Commission, Publications on Geodesy, 68, Delft, The Netherlands
187. Lohmann U and Feichter J (2001) Can the direct and semi-direct aerosol effect compete with the indirect effect on a global scale? *Geophysical Research Letters* **28**(1) 159-161
188. Longuevergne L, Scanlon B R and Wilson C R (2010) GRACE hydrological estimates for small basins: Evaluating processing approaches on the High Plains Aquifer, USA *Water Resources Research* **46** W11517 doi:10.1029/2009WR008564
189. MacDonald H C and Waite W P (1971) Optimum radar depression angles for geological analysis *Modern Geology* **2** 179-193
190. Manjunath A S and Muralikrishnan S (2008) Geometric and radiometric evaluation of Resourcesat-1 sensors. *Int. J Applied Earth Observation and Geoinformatics* **10** 159-164
191. Manley W F (2008) Geospatial inventory and analysis of glaciers: a case study for the eastern Alaska Range. *US Geol. Surv. Prof. Pap.* 1386-K, K424–K439
192. Markham B L and Barker J L (1987) Radiometric properties of U.S. processed Landsat MSS data *Rem Sens Environ* **22** 39-71
193. Marks D and Dozier J (1992) Climate and energy exchange at the snow surface in the Alpine Region of the Sierra Nevada: 2. Snow cover energy balance. *Water Resour. Res.* **28** 3043-3054
194. Markus N (2005) SRTM and VMAP0 data in OGR and GRASS *GRASS-News* **3** 2-6
195. Martinec J (1975) Snowmelt runoff model for stream flow forecast *Nordic Hydrology* **84** 197-219
196. Maskey S, Uhlenbrook S and Ojha S (2011) An analysis of snow cover changes in the Himalayan region using MODIS snow products and in-situ temperature data *Clim Change* **108**(1–2) 391–400
197. Mason K (1929) Indus floods and Shyok glaciers *Himalayan J* **1** 10–29

198. Massom R (1991) *Satellite Remote Sensing of Polar Regions*. Lewis publication, Boca Raton, Florida 307
199. Matsuo K and Heki K (2010) Time-variable ice loss in Asian high mountains from satellite gravimetry *Earth Planet. Sc. Lett.* **290** 30–36
200. McKillop R J and Clauge J (2009) Statistical remote sensing based approach for estimating the probability of catastrophic drainage from moraine dammed lakes in southwestern British Columbia *Global Planet. Change* **56** 153–171
201. Merlanti F and Pavan M (1998) A geoelectrical survey above an Antarctic ice shelf *Ann. Geofis.* **41** 271–287
202. Ming J, Xiao C, Cachier H, Qin D, Qin X, Li Z and Pu J (2009) Black Carbon (BC) in the snow of glaciers in west China and its potential effects on albedos *Atmospheric Research* **92** 114–123
203. Mir R A, Jain S K, Saraf A K and Goswami A (2014) Glacier changes using satellite data and effect of climate in Tirungkhad basin located in western Himalaya *Geocarto International* **29**(3) 293-313
204. Misra T, Rana S S, Desai N M, Dave D B, Rajeevjyoti, Arora R K, Rao C V N, Bakori B V, Neelakantan R and Vachchani J G (2013) Synthetic Aperture Radar payload on-board RISAT-1: configuration, technology and performance *Current Science* **104**(4) 446-461
205. Mognard N M, Kouraev A V and Josberger E G (2003) Global snow cover evolution from twenty years of satellite passive microwave data. International Geoscience and Remote Sensing Symposium (IGARSS03), Inst. of Electr. and Electron. Eng., Toulouse, France, 21 – 25 July, 2003
206. Moholdt G, Hagen J O, Eiken T and Schuler T V (2010) Geometric changes and mass balance of the Austfonna ice cap, Svalbard *The Cryosphere* **4**(1) 21–34 doi:10.5194/tc-4-21-2010
207. Moolg T and Hardy D R (2004) Ablation and associated energy balance of a horizontal glacier surface on Kilimanjaro *J. Geophys. Res.-Atmos.* **109** 16104–16116 doi:10.1029/2003JD004338 98
208. Muller-Dombois D and Ellenberge H (1974) *Aims and Methods of Vegetation Ecology*. John Willey and Sons, New York.
209. Muralikrishnan S, Narender B, Reddy S and Pillai A (2011) Evaluation of Indian National DEM from Cartosat-1 Data. Summary Report (Ver.1)

210. Murti S K (2001) Flora of Cold Deserts of Western Himalaya. Vol (I) Monocotyledons. Botanical Survey of India, Kolkata.
211. Muskett R R, Lingle C S, Sauber J A, Rabus, B T and Tangborn W V (2008) Acceleration of surface lowering on the tidewater glaciers of Icy Bay, Alaska, USA from InSAR DEMs and ICESat altimetry. *Earth Planet.Sci.Lett.* **265**(3-4) 345–359 doi: 10.1016/j.epse.2007.10.012
212. Nair Vijayakumar S, Suresh Babu S, Krishna Moorthy K, Sharma A K, Marinoni Angela and Ajai (2013) Black carbon aerosols over the Himalayas: direct and surface albedo forcing *Tellus B* **65** 19738 Int. Met. Institute Stockholm Sweden. <http://dx.doi.org/10.3402/tellusb.v65i0.19738>
213. Nair V S, Moorthy K K, Alappattu D P, Kunhikrishnan P K, George S, Nair P R, Babu S S, Abish B, Satheesh S K, Tripathi S N, Niranjana K, Madhavan B L, Srikant V, Dutt C B S, Badarinath K V S and Reddy R R (2007) Wintertime aerosol characteristics over the Indo-Gangetic plain (IGP): Impacts of local boundary layer processes and long-range transport *J. Geophys. Res.* **2** D13205, doi:10.1029/2006JD008099
214. Narama C, Käab A, Kajiura T, and Abdrakhmatov K (2007) Spatial variability of recent glacier area and volume changes in Central Asia using Corona, Landsat, ASTER and ALOS optical satellite data *Geophys Res Abstr* **9**(08178) SRef-ID: 1607-7962/gra/EGU2007-A-08178
215. Negi H S, Chander Shekhar and Singh S K (2015) Snow and glacier investigations using hyperspectral data in the Himalaya *Current Science* **108**(5) 892-902
216. Negi H S, Saravana, G, Rout R and Snehmami (2013) Monitoring of great Himalayan glaciers in Patsio region, India using remote sensing and climatic observations *Current Science* **105**(10) 1383-1392
217. Negi H S, Thakur N K, Ganju A and Snehmami (2012) Monitoring of Gangotri Glacier using Remote Sensing and Ground Observations *J. Earth Syst. Sci.* **121**(4), 855–866
218. Negi H S and Kokhanovsky A (2011) Retrieval of snow albedo and grain size using reflectance measurements in Himalayan basin *Cryosphere* **5**(1) 203-217
219. Negi H S, Singh S K, Kulkarni A V and Semwal B S (2010) Field based spectral reflectance measurements of seasonal snow cover in the Indian Himalaya *Int. J. Remote Sens.* **31** 2393–2417

220. Negi H S, Snehmani, Thakur N K and Sharma J K (2008) Estimation of snow depth and detection of buried objects using airborne Ground Penetrating Radar in Indian Himalaya. *Current Science* **94** 865–870
221. Negi H S, Kulkarni A V, Prajapati R P, Singh S K and Sharma J K (2006) Effect of contamination and mixed objects on snow reflectance using spectroradiometer, Scientific Report number RSAM/SAC/RESIPA/MWRG-GLI/SN25/2006, Space Applications Centre, Ahmedabad, India 24
222. Nuimura T, Fujita K, Fukui K, Asahi K, Aryal R and Ageta Y (2011) Temporal changes in elevation of the debris-covered ablation area of Khumbu Glacier in the Nepal Himalaya since 1978 *Arctic, Antarctic, and Alpine Research* **43** 246-255
223. Nolin A W (2010) Recent advances in remote sensing of seasonal snow. *Journal of Glaciology* **56**(200) 1141–1150
224. Nolin A W and Dozier J (2000) A hyperspectral method of remotely sensing the grain size of snow *Rem Sens Environ* **74** 207-216
225. Nolin A W and Dozier J (1993) Estimating snow grain size using AVIRIS data *Rem Sens Environ* **44** 231-238
226. Nuimura T, Fujita K, Yamaguchi S and Sharma RR (2012) Elevation changes of glaciers revealed by multitemporal digital elevation models calibrated by GPS survey in the Khumbu region, Nepal Himalayas, 1992–2008 *J Glaciol* **58**(210) 648–656 (doi: 10.3189/2012JoG11J061)
227. Nuth C, Moholdt, G, Kohler, J, Hagen, J O and Kääb A (2010) Svalbard glacier elevation changes and contribution to sea level rise *J. Geophys. Res.*, **115** F01008 doi:10.1029/2008JF001223.
228. Oerlemans J and Klok E J (2002) Energy balance of a glacier surface: Analysis of AWS data from the Morteratschglatscher, Switzerland, *Arct. Antarct. Alp. Res.* **34**(123) 115–123
229. Oke T R (1987) *Boundary Layer Climates*, 2nd ed., Routledge, New York 435
230. Painter T H and Dozier J (2004) The effect of anisotropic reflectance on imaging spectroscopy of snow properties *Remote Sens. Environ.* **89** 409-422
231. Pandey A C, Ghosh S and Nathawat M S (2011a) Evaluating patterns of temporal glacier changes in Greater Himalayan Range, Jammu & Kashmir, India *Geocarto Int.* **26**, 321–338.

232. Pandey A C, Ghosh S, Nathawat M S and Tiwari R K (2011b) Area change and thickness variation over Pensilungpa Glacier (J&K) using remote sensing *J. Indian Soc. Remote Sensing* **40**(2) 245-255 doi:10.1007/s12524-011-0134-y
233. Paul F, Barry R G, Cogley J G, Frey H, Haeberli W, Ohmura A, Ommanney C S L, Raup B, Rivera A, Zemp M (2009) Recommendations for the compilation of glacier inventory data from digital sources *Annals of Glaciology* **50**(53) 119-126
234. Pellicciotti F, Brock B, Strasser U, Burlando P, Funk M and Corripio J (2005) An enhanced temperature index glacier melt model including the Shortwave radiation balance: Development and testing for Haut Glacier d'Arolla, Switzerland *Journal of Glaciology* **51** 573-587
235. Pfeffer W T, 18 others and Randolph consortium (2013) The Randolph glacier inventory [v3.0]: a globally complete inventory of glaciers. Colorado, USA (<http://www.glims.org/RGI/randolph.html>)
236. Pepe M, Brivio P A, Rampini A, Rota Nodari F and Boschetti M (2005) Snow cover monitoring in Alpine regions using ENVISAT optical data *Int. J. Remote Sensing* **26** 4661–4667
237. Pieczonka T, Bolch T, Buchroithner M F (2011) Generation and evaluation of multi-temporal digital terrain model of the Mt. Everest area from different optical sensors *ISPRS J. Photogramm. Remote Sens.* **66** 927-940 doi:10.1016/j.isprsipr. 2011.07.003
238. Polunin O and Stainton A (1984) *Flowers of the Himalaya*. Oxford University Press, Delhi
239. Prasad A K, Elaskary Hesham M, Asrar Ghassem R, Kafatos Menas and Jaswal Ashok (2011) Melting of major glaciers in Himalayas : Role of desert dust and anthropogenic aerosols. In: *Planet Earth 2011 – Global Warming Challenges and Opportunities for Policy and Practice* 89-122
240. Prasad V H and Roy P S (2005) Estimation of snowmelt runoff in Beas Basin, India, *Geocarto International* **20**(2)
241. Quick M C and Pipes A (1988) High mountain snowmelt and application to runoff forecasting *Proc. of Workshop on Snow Hydrology*, held at Manali from Nov. 23-26,1988, ppIV1-32

242. Prasch M, Mauser W and Weber M (2012) Quantifying present and future glacier melt-water contribution to runoff in a Central Himalayan river basin *Cryosphere Discuss* **6**(5) 4557–98
243. Rabatel A, Dedieu J P, Thibert E, Letreguilly A, and Vincent C (2008) Twenty-five years of equilibrium-line altitude and mass balance reconstruction on the Glacier Blanc, French Alps (1981-2005), using remote-sensing method and meteorological data. *J Glaciol* **54** 307-314
244. Rabatel A, Dedieu J P, and Vincent C (2005) Using remote-sensing data to determine equilibrium-line altitude and mass-balance time series: validation on three French glaciers, 1994-2002. *J Glaciol* **51**(175) 539-546
245. Rachel C (2012) Assessing the impact of climate change on high mountain glacial watersheds in the Andes and Himalayas, *Sustainability on UT campus: A Symposium* 1-7
246. Racoviteanu A, Arnaud Y, Williams M, and Manley W F (2014a) Spatial patterns in glacier area and elevation changes from 1962 to 2006 in the monsoon-influenced eastern Himalaya *The Cryosphere Discuss.* **8** 3949–3998 doi:10.5194/tcd-8-3949-2014
247. Racoviteanu A, Bolch T, Bhambri R, Bajracharya S, Mool P, Chaujar R K, Kargel J, Leonard G, Furfaro R, Kaab A, Rauenfelder R, Sossna I, Kamp U, Byrne M, Kulkarni A V, Baghuna I M, Berthier E, Arnaud Y, Bishop M P and Shroder J F (2014b) Himalayan glaciers (India, Bhutan, Nepal) Chapter 24. In: *Global Land Ice Measurements from Space* (Eds. Kargel J S, Leonard G J, Bishop M P, Kaab A and Raup B) 20 Springer-Praxis, Heidelberg, 549–582, ISBN 978-3-540-79817-0, e-ISBN 978-3-540-79818-7, doi:10.1007/978-3-540-79818-7
248. Racoviteanu A, William M W (2012) Decision tree and texture analysis for mapping debris-covered glaciers in the Kangchenjunga area, Eastern Himalaya *Remote Sens.* **4**(10) 3078-3109, doi:10.3390/rs4103078
249. Racoviteanu A E, Williams M W and Barry R G (2008) Optical remote sensing of glacier characteristics: a review with focus on the Himalayas *Sensors* **8** 3355-3383 DOI:10.3390/s8053355
250. Racoviteanu A E, Manley W F, Arnaud Y and Williams M (2007) Evaluating digital elevation models for glaciologic applications: An example from Nevado Coropuna, Peruvian Andes *Global Planet Change* **59**(1-4) 110-125

251. Raina V K, Snehmani and Sangewar C V (2015) Glacier Snout Monitoring in the HIMALAYAS. Geological Society of India, ISBN: 978-93-80998-06-0 377
252. Raina V K (2011) Glacial retreat and global warming – A Review *Indian Journal of Geomorphology* **16** 19-28
253. Raina V K (2009) Himalayan Glaciers, A State-of-Art Review of Glacial Studies, Glacial Retreat and Climate Change, MoEF Discussion Paper, Ministry of Environment and Forests, Government of India 56
254. Raina V K and Srivastava D (2008) Glacier Atlas of India. Geological Society of India, Bangalore
255. Raj B K G, Kumar V K and Remya S N (2012) Remote sensing-based inventory of glacial lakes in Sikkim Himalaya: semi-automated approach using satellite data. *Geomat. Natur. Hazards Risk*, **4**(3) 241–253 (doi: 10.1080/19475705.2012.707153)
256. Raj K B G, Remya S N and Kumar K V (2013) Remote sensing based hazard assessment of glacial lakes in Sikkim Himalaya *Current Science* **104**(3), 359–364
257. Raj K B G (2010) Remote sensing based hazard assessment of glacial lakes: a case study from Zanskar basin, Jammu & Kashmir *Geomatics, Nat. Hazards Risks* **1** 339–347
258. Rajawat A S and Sharma A K (2015) Web based Himalayan Glacier Information System, *ISG Newsletter* **22**(1)11-14
259. Ramanathan A L (2011) Status Report on Chhota Shigri Glacier (Himachal Pradesh), Department of Science and Technology, Ministry of Science and Technology, New Delhi *Himalayan Glaciology Technical Report* **1** 88
260. Randhawa S S, Sood R K, Rathore B P and Kulkarni A V (2005) Moraine dammed lakes study in the Chenab and Satluj river basins using IRS data *J. ISRS* **33**(2) 285–290
261. Rankl M, Kienholz C and Braun M (2014) Glacier changes in the Karakoram region mapped by multitemporal satellite imagery *The Cryosphere* **8** 977–989 doi:10.5194/tc-8-977-2014
262. Rastogi G, Agrawal R and Ajai (2015) Bias correction of CartoDEM using IcesatGlas data in hilly regions *GIScience & Remote Sensing* <http://dx.doi.org/10.1080/15481603.2015.1060923>

263. Rastogi G and Ajai (2014) Comparison of energy balance of Gangotri and Chhota Shigri glaciers. In: The International Archives of the Photogrammetry, Remote Sensing and Spatial Information Sciences, Volume XL-8, 2014 ISPRS Technical Commission VIII Symposium, 09 – 12 December 2014, Hyderabad, India doi:10.5194/isprsarchives -XL-8-537-2014 537-542
264. Rastogi G and Ajai (2013a) Modeling energy and mass balance of Chhota Shigri glacier. In: *Climate Change and Himalayan Informatics* (Eds: Sundaresen J, Gupta P, Santosh K M and Ram Boojh) Scientific Publishers (India) ISBN: 978-81-7233-846-6 1-18
265. Rastogi G and Ajai (2013b) Energy balance modeling for ablation estimation of Gangotri glacier, *Journal of Geomatics* **7**(2) 178-185
266. Rathore B P, Singh S K, Bahuguna I M, Brahmbhatt R M, Rajawat A S, Thapliyal A, Panwar A and Ajai (2015a) Spatio temporal variability of snow cover in Alaknanda , Bhagirathi and Yamuna sub-basins, Uttarakhand Himalaya *Current Science* **108**(7) 1375-1380
267. Rathore B P, Singh S K, Brahmbhatt R M, Bahuguna I M, Rajawat A S and Ajai (2015b) Monitoring of moraine-dammed lakes: a remote sensing based case study in the Western Himalaya *Current Science* **109**(10) 1843-1849
268. Rathore B P, Kulkarni A.V., Randhawa S S, Bahuguna I M and Ajai (2011) Operationalization of snow and glacier melt runoff model to compute hydropower potential of 72 watersheds in Chenab basin, Himachal Pradesh, India *J Geomatics* **5**(1) 53-59
269. Rathore B P, Kulkarni A V and Sherasia N K (2009) Understanding future changes in snow and glacier melt runoff due to global warming in Wangar gad sub-basin, India. *Current Science* **97**(7) 1077–1081
270. Ravindra R and Laluraj C M (2012) Status Report Cryosphere Research: Indian Perspective *Proc. Ind Nat Sci Acad* **78**(3) 249-257
271. Rees W G (2006) Remote Sensing of Snow and Ice, Cambridge University, England, CRC Press, Taylor & Francis Group ISBN 9780415298315 312
272. Reid T D and Brock B W (2010) An energy balance model for debris covered glaciers including heat conduction through the debris layer *Journal of Glaciology* **56** 903-916
273. Rivera A and Casassa G (1999) Volume changes on Pio XI glacier, Patagonia: 1975-1995. *Global Planet Change* **22**(1-4) 233-244

274. Rodell M, Velicogna I and Famiglietti J S (2009) Satellite based estimates of groundwater depletion in India *Nature* **460** 999-1002 doi:10.1038/460789a
275. Rohrer M, Salzmann N, Stoffel M and Kulkarni A V (2013) Missing (in-situ) snow cover data hampers climate change and runoff studies in the Greater Himalayas *Science of the Total Environment* **468-469** 560-570
276. Romanov P, Tarpley D, Gutman G and Carroll T (2003) Mapping and monitoring of snow cover fraction over North America *J. of Geophysical Research* **108** D16 8619 14-1 to 14-15
277. Romanov P, Gutman G and Csiszar I (2000) Automated monitoring of snow cover over North America with multispectral satellite data *J. of Applied Meteorology* **39** 1866-1880
278. Rott H (1984) Synthetic Aperture Radar capabilities for snow and glacier monitoring, *Advance Space Research* **4**(11) 241-246
279. Saaty T L (2008) Decision making with the analytic hierarchy process. *Int. J. Services Sciences* **1**(1) 83-98
280. SAC (2012) National Wetland Atlas: High Altitude Lakes of India (Eds.: Panigrahy S., Patel, J.G. and Parihar J S), Space Applications Centre, ISRO, Ahmedabad, India ISBN :978-93-82760-00-9 108
281. SAC (2011a) Snow and Glaciers of the Himalayas (Study carried out under the joint project of Ministry of Environment and Forests and Department of Space, Government of India), Space Applications Centre, ISRO, Ahmedabad, India ISBN 13, 978-81-909978-7-4, 258
282. SAC (2011b) Glimpses of Earth Observations - An Indian Experience, Space Applications Centre, ISRO, Ahmedabad, India ISBN 978-81-909978-4-3, 180
283. SAC & MoEF (2010) Snow and Glaciers of the Himalayas: Inventory and Monitoring (Work carried out by Space Applications Centre, ISRO in collaboration with other Organisations) *Discussion Paper II* Space Applications Centre, ISRO, Ahmedabad and Ministry of Environment and Forests, New Delhi 88
284. SAC (2010) Final Technical Report Snow and Glacier Studies (A joint project of Ministry of Environment and Forests and Department of Space, Government of India), Space Applications Centre, ISRO, Ahmedabad *Technical Report No. SAC/RESA/MESG/SGP /TR/59/2010* 268

285. Sakai A (2012) Glacial lakes in the Himalayas: a review on formation and expansion processes *Global Environ. Res.* **16** 23–30
286. Sakai A and Fujita K (2010) Correspondence. Formation conditions of supraglacial lakes on debris-covered glaciers in the Himalaya *J Glaciol* **56**(195) 177–181 (doi: 10.3189/002214310791190785)
287. Sakai A, Takeuchi N, Fujita K and Nekawo M (2000) Role of supra-glacial ponds in the ablation process of a debris covered glacier in the Nepal Himalaya *IAHS Publication Washington USA* **264** 53–61
288. Samani Z, Bawazir A S, Bleiweiss M, Skaggs A S R and Tran V D (2007) Estimation daily net radiations over vegetation canopy through remote sensing and climatic data. *Journal of Irrigation and drainage engineering* **133** 291-297
289. Samant S S and Joshi H C (2004) Floristic diversity, community patterns and changes of vegetation in Nanda Devi National Park. In: *Biodiversity Monitoring Expedition Nanda Devi 2003*. Bishen Singh Mahendra Pal Singh, Dehradun 39-54
290. Samant S S, Joshi H C and Arya S C (2000) Diversity, nativity and endemism of vascular plants in Pindari area of Nanda Devi Biosphere Reserve-II. *Himal. Bios. Reserv.*, **2**(1&2) 1-29
291. Samant S S (1999) Diversity, nativity and endemism of vascular plants in a part of Nanda Devi Biosphere Reserve in west Himalaya I. *Himalayan Biosphere Reserves (Biannual Bulletin)* **1**(1&2) 1-28
292. Samant S S and Pangtey Y P S (1993) Rediscovery of some rare and endangered shrubs and climbers of Kumaun Himalaya *J. Econ. Tax. Bot.* **17**(3) 509-512
293. Sangewar C V (2011) Remote sensing applications to study Indian glaciers *Geocarto International* **27**(3) 197-206 DOI:10.1080/10106049.2011.617841.
294. Sangewar C V and Shukla S P (2009) Inventory of the Himalayan glaciers – a contribution to the International Hydrological Programme (an updated edition) [Spl. Pub., No. **34**]. Kolkata: Geological Survey of India 588
295. Sangewar C V, Srivastava D and Singh R K (1999) Reservoir within the Shaune Garang glacier, district Kinnaur, Himachal Pradesh. In *Proceedings of the Symposium on Snow, Ice and Glaciers: A Himalayan Perspective, Abstr.*, Geological Survey of India 39–40

296. SASE (2012) Field Survey Report for Project Development of Methodology for Snow Pack Characterization and Glacial Movement Studies Using Multi-Frequency SAR Time Series Data, Under Department of Science & Technology Sponsored Project, Snow and Avalanche Study Establishment, Defence Research and Development Organization (DRDO), Chandigarh. http://www.dst.gov.in/about_us/ar10-11/PDF/17-21.pdf
297. Sauber J, Molnia B, Carabajal C, Luthcke S and Muskett R (2005) Ice elevations and surface change on the Malaspina Glacier, Alaska *Geophys. Res. Lett.* **32** L23S01 doi:10.1029/2005GL023943
298. Scambos T A, Dutkiewicz M J, Wilson J C and Bindschadler R A (1992) Application of image cross-correlation to the measurement of glacier velocity using satellite image data. *Remote Sensing Environ.* **42** 177–186
299. Schauwecker S, Rohrer M, Huggel C, Kulkarni A, Ramanathan A L, Salzmann N, Stoffel M, Brock B (2015) Remotely sensed debris thickness mapping of Bara Shigri Glacier, Indian Himalaya *Journal of Glaciology* **61**(228) 675-688 doi: 10.3189/2015JoG14J102
300. Scherler D, Bookhagen B and Strecker M R (2011) Spatially variable response of Himalayan glaciers to climate change affected by debris cover, *Nature Geoscience*, **4**(3) 156-159
301. Scherler D, Leprince S and Strecker M R (2008) Glacier-surface velocities in alpine terrain from optical satellite imagery – accuracy improvement and quality assessment *Remote Sensing Environ* **112** 3806–3819
302. Schmidt S and Nusser M (2012) Changes of high altitude glaciers from 1969 to 2010 in the Trans-Himalayan Kang Yatze Massif, Ladakh, Northwest India *Arct., Antarct. Alpine Res.* **44** 107
303. Shi J (2008) Active microwave remote sensing systems and applications to snow monitoring. In: *Advances in Land Remote Sensing* (Editor: Liang S) Springer Science + Business Media B.V. 19-49
304. Shi J and Dozier J (1993) Measurements of snow- and glacier- covered areas with single-polarization SAR *Annals of Glaciology* **17** 72-76
305. Shroder J F and Bishop M P (2010) Satellite Image Atlas of Glacier of the World. In: *Asis Professional Paper* 1386-F, F201–F257. Washington, DC: US Geological Survey, US Government Printing Office.

306. Sellers P J, Dickinson R E, Randall D A, Betts A K, Hall F G, Berry J A, Collatz G J, Denning A S, Mooney H A, Nobre C A, Sato N, Field C and Sellers A H (1997) Modeling the exchanges of energy, water, and carbon between continents and the atmosphere *Journal of Glaciology* **51** 25-36
307. Shannon C E and Weaver W (1963) *The Mathematical Theory of Communication*. University of Illinois Press, Urbana.
308. Sharma A K, Rawal D, Vyas A and Rajawat A S (2015) Test Plan Specifications, Himalayan Glacier Information System (HGIS) *SAC Technical Report SAC/EPISA/GSAG/GSD/SN/02/2015*
309. Sharma A K, Singh S K, Kulkarni A V and Ajai (2013) Glacier Inventory in Indus, Ganga and Brahmaputra Basins of the Himalaya *National Academy Science Letters*, ISSN 0250-541X, **36**(5) 497-505, DOI 10.1007/s40009-013-0167-6
310. Shean D E, Head III J W and Marchant D R (2007) Shallow seismic surveys and ice thickness estimates of the Mullins valley debris-covered glacier, McMurdo dry valleys, Antarctica *Antarct. Sci.* **19** 485–496
311. Shrestha B B and Nakagawa H (2014) Assessment of potential outburst floods from the Tsho Rolpa glacial lake in Nepal. *Nat. Hazards* **71**(1) 913–936
312. Shukla A, Arora M K and Gupta R P (2010a) Synergistic approach for mapping debris-covered glaciers using optical–thermal remote sensing data with inputs from Geomorphometric parameters *Remote Sensing of Environ.* **114** (7) 1378-1387
313. Shukla A, Gupta R.P. and Arora M K (2010b) Delineation of debris covered glacier boundaries using optical and thermal remote sensing data *Remote Sensing Letters* **1**(1) 11-17
314. Sicart J E, Wagnon P and Ribstein P (2005) Atmospheric controls of the heat balance of Zongo Glacier (16°S, Bolivia) *J. Geophys. Res.-Atmos.* **110** 12106–12122, doi:10.1029/2004JD005732 98
315. Siderius C, Biemans H, Wiltshire A, Rao S, Franssen W H P, Kumar P et al (2013) Snowmelt contributions to discharge of the Ganges *Sci Total Environ* **468–469**(Suppl.) S93–S101
316. Simpson E H (1949) Measurement of diversity *Nature* **163**(688)
317. Singer F S and Popham R W (1963) Non-meteorological observations from satellites *Astronaut. Aerospace Eng.* **1**(3) 89–92

318. Singh K K, Kulkarni A V and Mishra V D (2010) Estimation of glacier depth and moraine cover study using Ground Penetrating Radar in the Himalayan region *J. Indian Soc. Remote Sensing* **38**(1) 1–9
319. Singh S K, Rajawat A S, Rathore B P, Bahuguna I M and Manab Chakraborty (2015) Detection of glacier lakes buried under snow by RISAT-1 SAR in the Himalayan terrain, *Current Science*, **109**(09) 1728-1732
320. Singh S K, Rathore B P, Bahuguna I M and Ajai (2014) Snow cover variability in the Himalayan-Tibetan region *Int. J. Climatol.* **34** 446–452; doi: 10.1002/joc.3697
321. Singh S K (2013) Applications of Hyperspectral Data for Snowpack Characterization in the Himalayan Region, *Ph. D. Thesis*, Kurukshetra University, Kurukshetra
322. Singh S K, Bhattacharya B K and Kulkarni A V (2013a) Cross Calibration of INSAT 3A CCD Channel Radiances with IRS P6 AWiFS Sensor, *J Earth System Sciences* **122**(4) 957-966
323. Singh S K, Bahuguna I M, Rathore B P and Ajai (2013b) Spatial distribution of glacier mass balance using remote sensing data in the Himalayan region. In: *Climate Change and Himalaya, Natural Hazards and Mountain Resources* (Eds: Sundaresen J, Gupta P, Santosh K M and Ram Boojh) Scientific Publishers (India), ISBN: 978-81-7233-881-7 1-6.
324. Singh S K, Rathore B P and Bahuguna I M (2013c) Understanding the Effect of Various Glacier Features on Backscattering Coefficients using SAR Data in the Himalayan region, *SAC Scientific Report, SAC/EPISA/MPSG/GSD/RISAT /SR/83/2013*, 24 p.
325. Singh, S K, Rathore B P, Bahuguna I M, Ramanathan A L and Ajai (2012) Estimation of glacier ice thickness using Ground Penetrating Radar in the Himalayan region, *Current Science* **103**(1) 68-73
326. Singh S K, Kulkarni, A V and Chaudhary B S (2011) Spectral characterization of soil and coal contamination on snow reflectance using hyperspectral analysis, *J. Earth Syst. Sci.* **120**(2) 321-328
327. Singh S K, Kulkarni A V and Chaudhary, B S (2010) Hyperspectral analysis of snow reflectance to understand the effects of contamination and grain size *Annals of Glaciology* **54**(44) 83-88

328. Singh S K and Rawat G S (2000) Flora of Great Himalayan National Park, Himachal Pradesh. Bishen Singh Mahendra Pal Singh, Dehradun.
329. Singh P and Singh V P (2001) Snow and Glacier Hydrology. The Netherlands: Kluwer Academic, (Chapter 6)
330. Singh P K, Naresh R K S and Yatveer S (2000) Influence of a fine debris layer on the melting of snow and ice on a Himalayan Glacier. In *Debris-Covered Glaciers* (Eds. Nakawo M, Raymond C F and Fountain A) IAHS: Wallingford UK 63–69
331. Sirota J M, Bae S, Millar P, Mostofi D, Webb C, Schutz B and Luthcke S (2005) The transmitter pointing determination in the Geoscience Laser Altimeter System Geophys. Res. Lett. 32 L22S11 doi:10.1029/2005GL024005
332. Slobbe D, Lindenbergh R and Ditmar P, (2008) Estimation of volume change rates of Greenland's ice sheet from ICESat data using overlapping footprints. Remote Sens Environ, **112**(12) 4204–4213
333. Smith D G and Jol H M (1995) Ground penetrating radar: antenna frequencies and maximum probable depths of penetration in Quaternary sediments *J. Appl. Geophys.* **33** 93–100
334. Smriti Basnett, Kulkarni A V and Bolch T (2013) The influence of debris cover and glacial lakes on the recession of glaciers in Sikkim Himalaya, India *Journal of Glaciology* **59**(218) doi: 10.3189/2013JoG12J184 1035-1046
335. Srinivasulu J and Kulkarni A V (2004) A satellite based spectral reflectance model for snow and glacier studies in Himalayan terrain. In: Proc. Indian Academy of Science (Earth and Planetary Science) **113**(1) 117-128
336. Srivastava D (2012) Status Report on Gangotri Glacier, Science and Engineering Research Board, Department of Science and Technology, New Delhi, *Himalayan. Glaciology Technical Report No. 3*, 102
337. Stern T A (1978) Gravity Survey of the Taylor Glacier, Victoria Land, Antarctica, Geology Department, Victoria University of Wellington, New Zealand **8** 1–6
338. Strozzi T, Wiesmann A, Kaab A, Joshi S and Mool P (2012) Glacial lake mapping with very high resolution satellite SAR data *Nat. Hazards Earth Syst. Sci.* **12** 2487–2498

339. Su H, Yang Z L, Dickinson R E, Wilson C R and Niu G Y (2010) Multisensor snow data assimilation at the continental scale: The value of Gravity Recovery and Climate Experiment terrestrial water storage information *J. Geophys. Res.* **115** D10104 doi:10.1029/2009JD013035
340. Surazakov A B, Aizen V B, Aizen E M and Nikitin S A (2007) Glacier changes in the Siberian Altai mountains, Ob river basin (1952 - 2006) estimated with high resolution imagery *Environ Res Lett* 2007, 10.1088/1748-9326/2/4/045017
341. Surazakov A B and Aizen V B (2006) Estimating volume change of mountain glaciers using SRTM and map-based topographic data *IEEE Trans Geosci Rem Sens* 2006 **44**(10) 2991-2995
342. Suzanne W S, Eva E B, Jun L, Menzel W P and Liam E G (2006) MODIS atmospheric profile retrieval algorithm theoretical basis document. Cooperative Institute for Meteorological Satellite Studies, University of Wisconsin-Madison, Version-6
343. Swati Tak, Sharma A K, Rajawat A S, Ajai and Palria S (2014) Assessment of glacier health in Alaknanda Sub-basin of Ganga using remote sensing and GIS techniques *Int J of Adv. Remote Sensing and GIS* **3**(1), 598-605 Article ID Tech-287 ISSN2320 – 0243
344. Swenson S and Wahr J (2006) Post-processing removal of correlated errors in GRACE data *Geophysical Research Letters* **33** L08402, doi:10.1029/2005GL025285
345. Swenson S and Wahr J (2002) Methods for inferring regional surface-mass anomalies from Gravity Recovery and Climate Experiment (GRACE) measurements of time-variable gravity *J. Geophys. Res.* **107**(B9) doi:10.1029/2001JB000576
346. Tabacco I E, Binachi C, Zirizzotti A, Zuccheretti E, Forieri A and Vedova A D (2002) Airborne radar survey above Vostok region, east-central Antarctica: ice thickness and Lake Vostok geometry *Journal of Glaciology* **48** 62-69
347. Tadono T, Takaku J, Kawamoto S, Yamanokuchi T, Fujita K, Nishimura K (2010) Evaluations for potential of glacial lake outburst floods (GLOFS) in the Bhutan Himalaya using PRISM and AVNIR-2 onboard ALOS in: *International Archives of the Photogrammetry, Remote Sensing and Spatial Information Science*, Volume XXXVIII, Part 8, Kyoto Japan 52-55

348. Takeuchi Y, Kayastha R B and Nakawo M (2000) Characteristics of ablation and heat balance in debris-free and debris-covered areas on Khumbu Glacier, Nepal Himalayas, in the pre-monsoon season. In *Debris-Covered Glaciers* (Eds.: Nakawo M, Raymond C F and Fountain A) IAHS: Wallingsford, UK 53–61
349. Tangri A K, Ram Chandra and Yadav S K S (2004) Temporal monitoring of the snout, equilibrium line and ablation zone of Gangotri glacier through remote sensing and GIS techniques: An attempt at deciphering the climatic variability Geol. Surv. Ind. Spl. Pub. **80** 145-153
350. Tapley B D, Ries J C, Bettadpur S, Chambers D, Cheng M, Condi F, Gunter B, Kang Z, Nagel P, Pastor R, Pekker T, Poole S and Wang F (2005) GGM02 – An improved Earth gravity field model from GRACE *J Geod* **79** 467-478 DOI 10.1007/s00190-005-0480-z
351. Tapley B D, Bettadpur S, Ries J C, Thompson P F, Watkins M M (2004) GRACE measurements of mass variability in the Earth system *Science* **305** (503–505)
352. Thakur P K, Garg R D, Aggarwal S P, Garg P K, Snehmani and Shi J (2013) Snow density retrieval using SAR data: algorithm validation and applications in part of North Western Himalaya *The Cryosphere Discuss.* **7** 1927–1960 www.the-cryosphere-discuss.net/7/1927/2013/ doi:10.5194/tcd-7-1927-2013
353. Thakur P K, Aggarwal S P, Garg P K, Garg R D, Snehmani, Pandit A and Kumar S (2012) Snow physical parameter estimation using space based SAR *Geocarto International* **27** 263–288 doi:10.1080/10106049.2012.672477
354. Tiwari R K, Gupta R P and Arora M K (2014) Estimation of surface ice velocity of Chhota – Shigri glacier using sub-pixel ASTER image correlation *Current Science* **106**(6) 853-859
355. Tiwari R K, Gupta R P, Gens R and Prakash A (2012) Use of optical, thermal and microwave imagery for debris characterization in Bara-Shigri Glacier, Himalayas, India. In: *IGARSS 2012. Proceedings of the International Geoscience and Remote Sensing Symposium 22–27 July 2012, Munich IEEE*, 4422–4425 (doi: 10.1109/IGARSS.2012.6350392)
356. Tiwari V M, Wahr J and Swenson S (2009) Dwindling groundwater resources in northern India from satellite gravity observations, *Geophys. Res. Lett.* **36** L18401 doi:10.1029/2009GL039401

357. Townshend J R G and Tucker C J (1984) Objective assessment of Advanced Very High Resolution Radiometer data for land cover mapping *Int J. Remote Sensing* **5** 497-504
358. Tucker C J (1986) Maximum normalized difference vegetation index images for sub-Saharan Africa for 1983-1985 *Int J Remote Sensing* **7** 1383-1384
359. Tucker C J (1979) Red and photographic infrared linear combinations for monitoring vegetation *Remote Sensing of Environment* **8** 127-150
360. Tweed F S and Russell A J (1999) Controls on the formation and sudden drainage of glacier-impounded lakes: implications for jokulhlaup characteristics *Prog. Phys. Geogr.* **23** 79–110
361. Ulaby F T, Moore R K and Fung A K (1986) Microwave remote sensing active and passive III Addison-Wesley publishing Company Reading MA 2162
362. UNEP (2010) High Mountain Glaciers and Climate Change – Challenges to Human Livelihood and Adaptation (Eds.: Kaltenborn B P, Nellesmann C and Vistnes I I) Printed by Birkeland Trykkeri A S Norway ISBN: 978-82-7701-087-8 52
363. Venkataraman G and Singh G (2011) Radar application in snow, ice and glaciers. In: *Encyclopedia of Snow, Ice and Glaciers* (Eds. Singh V P, Singh P and Haritashya U K) doi 10.1007/978-90-481-2642-2 883-903
364. Venkatesh T N, Kulkarni A V and Srinivasan J (2012) Relative effect of slope and equilibrium line altitude on the retreat of Himalayan glaciers *The Cryosphere* **6** 301–311 doi:10.5194/tc-6-301-2012
365. Vijay Kumar, Venkataramana G, Yngvar Larsenb and Hogdab K A (2011) SAR interferometry and offset tracking approaches for glacier movement estimation in the Himalaya. In: IGARSS-2011, 978-1-4577-1005-6/11/\$26.00 ©2011 IEEE, 3175-3178
366. Wagnon P, Kumar R, Arnaud Y, Linda A, Sharma P, Vincent C, Pottakal J, Berthier E, Ramanathan A, Hassnain S I and Chevalier P (2007) Four years of mass balance on Chhota Shigri Glacier, Himachal Pradesh, India, a new benchmark glacier in the western Himalaya *J Glaciol* **53**(183) 603 - 611
367. Wagnon P, Sicart J E, Berthier E and Chazarin J P (2003) Wintertime high-altitude surface energy balance of a Bolivian glacier, Illimani, 6340 m above sea level *J. Geophys. Res.* **108**(D6) 4177 doi:10.1029/2002JD002088

368. Wagnon P, Ribstein P, Francou B and Sicart J E (2001) Anomalous heat and mass budget of Glaciar Zongo, Bolivia, during the 1997/98 El Niño year *J. Glaciol.* **47** 21–28
369. Wagon P, Ribstein P, R E, Francou B and Pouyaud B (1999a) Annual cycle of energy balance of Zongo Glacier, Cordillera Real, Bolivia *Journal of Geophysical Research* **104** 3907-3923
370. Wagnon P, Ribstein P, Kaser G and Berton P (1999b) Energy balance and runoff seasonality of a Bolivian glacier, *Global Planet. Change* **22** 49– 58
371. Wahr J, Swenson S, and Velicogna I (2006) Accuracy of GRACE mass estimates *Geophys. Res. Lett.* **33** L06401 doi:10.1029/2005GL025305
372. Wang W, Yang X, and Yao T (2012) Evaluation of ASTER GDEM and SRTM and their suitability in hydraulic modelling of a glacial lake outburst flood in southeast Tibet *Hydrol. Process.* **26** 213–225. doi:10.1002/hyp.8127
373. Wang W, Yao T, Gao Y, Yang X and Kattel D B (2011) A first order method to identify potentially dangerous glacial lakes in a region of the southeastern Tibetan Plateau *Mt. Res. Dev.* **31** 122–130
374. Wang Y, Hou S and Liu Y (2009) Glacier changes in the Karlik Shan, eastern Tien Shan, during 1971/72–2001/02. *Ann. Glaciol.* **50**(53) 39–45
375. Warren S G (2013) Can black carbon in snow be detected by remote sensing? *J Geophys Res* <http://dx.doi.org/10.1029/2012JD018476>
376. Warren S G (1982) Optical properties of snow *Rev. Geophys. Space Phys.* **20** 67-89
377. Warren S G and Wiscombe W J (1980) A model for the spectral albedo of snow-II: Snow containing atmospheric aerosols *J. Atmos. Sci.* **37** 2734–2745
378. Wingham D J, Francis C R, Baker S, Bouzanac C, Brockley D, Cullen R, Thierry P C, Laxon S W, Mallow U, Mavrocordatoy C, Phalippou L, Ratio G, Rey L, Rostan F, Viau P and Wallis D W (2006) CryoSat: a mission to determine the fluctuations in Earth's land and marine ice fields. *Adv. Space Res.* **37**(4) 841–871 doi: 10.1016/j.asr.2005.07.027
379. Wingham D J, Ridout A J, Scharroo R, Arthern R J and Shum C K (1998) Antarctic elevation change from 1992 to 1996 *Science*, **282**(5388) 456–458, doi:10.1126/science.282.5388 456

380. Wiscombe N J and Warren G S (1981) A model for spectral albedo of snow, I, pure snow. *J. Atmos. Sci.* **37** 2712–2733
381. Wright D L, Olhoeft G R and Watts R D (1984) Ground-penetrating radar studies on Cape Cod. In: *NWAA/EPA Conference on surface and borehole geophysical methods in groundwater investigations* (Eds.: Nielson D M and Curl M) National Water Well Association, Worthington, Ohio 666-680
382. Xiaojun Yao, Shiyin, Liu, Meiping, Sun, Junfenj, Wei, Wanqin, Guo (2012) Volume calculation and analysis of the changes in morainedammed lakes in the North Himalaya: a case study of Longbasaba lake. *J. Glaciol.*, 2012, **58**(210), 753–760
383. Yamada T (1998) Glacier lake and its outburst flood in the Nepal Himalaya *Monograph no. 1 Data Center for Glacier Research, Japanese Society of Snow and Ice*, Tokyo 96
384. Yasunari T J, Bonasoni P, Laj P, Fujita K, Vuillermoz E, Marinoni A, Cristofanelli P, Duchi R, Tartari G, Lau K M (2010) Estimated impact of black carbon deposition during premonsoon season from Nepal Climate Observatory – Pyramid data and snow albedo changes over Himalayan glaciers *Atmos Chem Phys* **10** 6603–6615, doi: 10.5194/acp-10-6603.
385. Zhang G. et al. (2013), Energy and mass balance of Zhadang glacier surface, Central Tibetan Plateau *J Glaciol* **59**(213) 137-148
386. Zhang Y, Fujita K, Liu S, Liu Q, Nuimura T (2011a) Distribution of debris thickness and its effect on ice melt at Hailuogou glacier, southeastern Tibetan Plateau, using in situ surveys and ASTER imagery *J Glaciol* **57** 1147–1157
387. Zhang G, Hongjie X, Kang S, Yi D and Stephen F A (2011b) Monitoring lake level changes on the Tibetan Plateau using ICESat altimetry data (2003-2009) *Remote Sensing of Environment* **115** 1733-1742
388. Zhao H and Fernandes R (2009) Daily snow cover estimation from advanced very high resolution radiometer polar pathfinder data over Northern Hemisphere land surfaces during 1982–2004 *J. Geophys. Res.* **114**, 1–14
389. Zwally H J, Schutz R, Bentley C, Bufton J, Herring T, Minster B, Spinhirne J and Thomas R (2008) GLAS/ICESat L1B Global Elevation Data V028, 20 February 2003 to 21 March 2008. Boulder. CO: National Snow and Ice Data Centre Digital media

390. Zwally H J, Schutz B, Abdalati W, Abshire J, Bentley C, Brenner A, Bufton J, Dezio J, Hancock D, Harding D, Herring T, Minster B, Quinn K, Palm S, Spinhirne J and Thomas R (2002) ICESat's laser measurements of polar ice, atmosphere, ocean, and land. *J. GEODYN.* **34**(3-4) 405–445, doi:10.1016/s0264-3707(02)00042-X
391. Zwally H J, Brenner A C, Major J A, Bindschadler R A and Marsh J G (1989) Growth of the Greenland ice sheet - measurement *Science* **246**(4937) 1587–1589, doi:10.1126/science.246.4937.1587

Annexure-1: Field Photographs



Snow cover in High altitude in Chenab basin, parts of Himachal Pradesh (H.P.)



Snow cover in Bhaga basin, H.P.



Observation of meteorological & physical properties of snow at Dhundi Observatory, Beas basin, H. P.



Observation of radiometric & physical properties of snow at Beas basin, H. P.



Radiometric measurements in glaciated terrain at Patsio glacier, H. P.



Density measurement of snow at Dhundi Observatory, H. P.



Panoramic view of Samudra Tapu glacier in Chandra sub-basin, H.P. showing deglaciated valley, moraine dammed lake, ablation zone, accumulation zone and other geomorphological features



Bare ice and fractures in Ablation zone of Machoi glacier, Dras, J&K



Debris covered ablation zone of Chipa glacier in Alaknanda sub-basin, Uttarakhand



Stream originating from the snout of the Machoi, Glacier, Dras, J&K



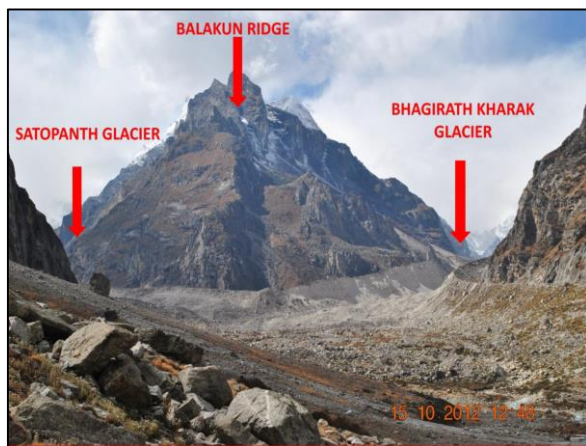
GPS measurement at snout of glacier in Chandra basin, H.P.



A cave like view of Miyar glacier snout in Miyar basin, H.P.



Glacier snout and snow bridge at Machoi glacier, Dras, J&K



Satopanth and Bhagirath Kharak glacial valley separated by Balakun ridge, Alaknanda sub-basin Uttarakhand



Snout of Satopanth glacier, Alaknanda sub-basin, Uttarakhand



Trekking of expedition team members over debris covered ablation zone of Batal glacier, H. P.



Water channels flowing over bare ice of ablation zone in Chota Shigri glacier, H. P.



A view of glacier valley covered with local convection clouds at Samudra Tapu glacier, H. P.



Snowfall during ablation month over Batal glacier, H. P.



Fresh water Lake at Miyar glacier, H. P.



Moraine dammed lake in parts of H.P.



The fragile wall of moraine retaining the lake water in Chandra basin, H.P.



Geomorphological feature *Sirracs*, Dras, J&K



Lateral moraine and Debris cover of glacier in Miyar valley, H.P.



Striations in the deglaciated region of the glacier, Chandra basin H.P.



Downside view of deglaciated terminal moraine deposits in Chandra basin, H.P.



Erratic boulder in Chandra basin, H.P.



Ropeway (Local *Jhula*) to cross the river in Baspa valley, H.P.



Expedition kit & members crossing river as bridge was not usable in Baspa valley, H.P.



Field Lab at Chhota Dara, H.P.



Inside view of Field Lab at Chhota Dara, H.P.



GPR survey over Debris cover Glacier in Dras, J&K



Automatic Weather Station at Chhota Dara, H.P.



Black Carbon (BC) measurement using Aethalometer over Glacier in Dras, J&K



Observations of Energy balance parameters in glaciated region at Chhota Shigri glacier, H.P.



Measuring glaciological mass balance using bamboo sticks, Dras, J&K



Ephedra intermedia- Artemesia maritima community, Basapa Valley, H.P.



Cotoneaster bacillaris community, Basapa Valley, H.P.



Rosa webbiana community, Basapa Valley, H.P.



Caragana brevifolia community, Basapa Valley, H.P.



Hyssopus officinalis- Chrysopogon gryllus- Asperula oppositifolia mixed community, Basapa Valley, H.P.



Snow fall covering tents at Glacier base camp in Chandra basin, H.P.



A view of Kedarnath valley downhill to Chora Bari glacier, Uttarakhand



A view of glacier base camp during glacier expedition of Nardu glacier, Baspa sub-basin, H. P.



Expedition team members at Chhota Shigri glacier, H.P.



Expedition team members at Machoi glacier, Dras, J&K



Expedition team members at Nardu glacier Baspa sub-basin, H. P.

